THE OBSERVATION AND ANALYSIS OF LUNAR OCCULTATIONS OF STARS WITH AN EMPHASIS ON IMPROVEMENTS TO DATA ACQUISITION INSTRUMENTATION AND REDUCTION TECHNIQUES

By

GLENN H SCHNEIDER

A DISSERTATION PRESENTED TO THE GRADUATE SCHOOL
OF THE UNIVERSITY OF FLORIDA IN
PARTIAL FULFILLMENT OF THE REQUIREMENTS FOR THE
DEGREE OF DOCTOR OF PHILOSOPHY

UNIVERSITY OF FLORIDA

1985

This work is dedicated to

Rose Wenig

and

Alice Schneider,

my late, beloved grandmothers.

If the stars should appear one night in a thousand years, how would men believe and adore; and preserve for many generations the remembrance of the city of God which had been shown!

"Emerson", Nature; Addresses, and Lectures

ACKNOWLEDGEMENTS

The debts accrued at the successful completion of any endeavor which spans a number of days requiring four digits to count are many and varied. This work is no exception. Without the input and influence of many people the task which was set before me could never have come to fruition. On two levels, both personal and professional, my thanks go out to all those who helped make this project possible. The task of acknowledging all those who contributed to this study is formidable, and indeed if properly done would fill volumes. To those whom I may fail to personally acknowledge here, I offer my apology, for there are uncountable numbers who have contributed either directly, or indirectly to this study.

To my parents, my grandfather Max Wenig, and grandmothers, Rose Wenig and Alice Schneider, I owe a debt which I can never hope fully to repay. With their love and encouragement, I was raised in an atmosphere which nurtured my intellectual curiosity. I was never denied the opportunity to explore, and to grow in any direction my inquisitiveness had taken me. To them go my most profound gratitude, respect and love.

To my committee chairman, John P. Oliver, go my warmest thanks for first suggesting this course of investigation.

Without his assistance and guidance throughout my years at the University of Florida, this dissertation would never have been. I also thank my other committee members, Heinrich K. Eichhorn, Howard L. Cohen, Haywood C. Smith, and Ralph G. Selfridge, for their help, valuable suggestions, and at times much needed criticisms as this study progressed. To the latter, and to the University's Center for Intelligent Machines and Robotics I offer additional thanks for securing the use of the computational resources required for this investigation. I would also like to thank Ben Adenbaum and Warner Computer Systems, Inc., for granting the use of their facilities during the early stages of this project.

My personal thanks extend to Frank B. Wood, and Kwan-Yu Chen, both of whom often provided much needed information related to this study. In addition, through their efforts I was afforded the unique opportunity to hone my fledgling skills as an instrumentalist by actively working on the development of the South Pole Observatory.

My fellow graduate students proved to be a source of a wealth of information and ideas. To them I offer not only my thanks but the hope that there may indeed be life after graduate school. In particular, I would like to acknowledge the support I received from Roger Ball, Joseph T. Pollock (who have already realized this hope), and Gregory L. Fitzgibbons. To Elaine Reeves, who soon will enter into indentured servitude as a graduate student herself, go my thanks for proof reading the manuscript of this dissertation, and for helping "bag" Pallas.

For their fabrication of the mechanical components required (often on a moment's notice) in support of the occultation program, I am grateful for the work done by Harvey Nachtrieb and the machinists in the Department of Physics. Though still new to the Astronomy Department, Donald McNeil has been an outstanding asset during the latter stages of this project. I offer him my personal thanks, and a tip of the hat for his help with the 1984 annular eclipse, and for Ceres as well.

I would like to thank Marie Lukac of the United States Naval Observatory, David Dunham and the International Occultation Timing Association, and Robert Millis at Lowell Observatory for providing the occultation predictions used in planning the observing programs.

On a number of personal notes I would like to express my gratitude to Alan Nathans for his support and encouragement during my childhood. Also extended are my thanks to the members of the Amateur Observers' Society of New York, for helping to lay the foundation for my future work. To Susan Howard goes my deepest appreciation for her unfailing encouragement during my early years in Florida. I must also thank Laura E. Kay, who is at this very moment spending a long, cold winter at the South Pole, for her prodding and nudging me to finish this thing and get out of Florida.

To William Tillchock (whereever he may be) I say thank you for introducing me to APL, one of the major tributaries of my life. And I thank to Kenneth E. Iverson for inventing what very well may be the most beautiful, aesthetically pleasing, and incomparably useful symbolic notations ever conceived.

Finally, I thank from the bottom of my heart Karla Rahman for her love and understanding during the 25-hour days and 32-day months while this dissertation was being prepared. Though to her I now say "I will", by the time this work is shelved I intend to say "I do".

TABLE OF CONTENTS

LIST OF TABLES

LIST OF FIGURES

Abstract of Dissertation Presented to the Graduate School of the University of Florida in Partial Fulfillment of the Requirements for the Degree of Doctor of Philosophy

THE OBSERVATION AND ANALYSIS OF LUNAR OCCULTATIONS OF STARS WITH AN EMPHASIS ON IMPROVEMENTS TO DATA ACQUISITION INSTRUMENTATION AND REDUCTION TECHNIQUES

By

Glenn H Schneider

August 1985

Chairman: John P. Oliver
Major Department: Astronomy

A program of observation and analysis of lunar occultations was conceived, developed, and carried out using the facilities of the University of Florida's Rosemary Hill Observatory (RHO). The successful implementation of the program required investigation into several related areas. First, after an upgrade to the RHO 76-cm. reflecting telescope, a microprocessor controlled fast photoelectric data acquisition system was designed and built for the occultation data acquisition task. Second, the currently available model-fitting techniques used in the analysis of occultation observations were evaluated. A number of numerical experiments on synthesized and observational data were carried out to improve the performance of the numerical techniques. Among the numerical methods investigated were

solution schemes employing partial parametric adjustment, parametric grouping into computational subsets (randomly and on the basis the correlation coefficients), and preprocessing of the observational data by a number of smoothing techniques for a variety of noise conditions. Third, a turn-key computational software system, incorporating data transfer, reduction, graphics and dislplay, was developed to carry out all the necessary and related computational tasks in an interactive environment.

Twenty-four occultation observations were obtained during the period March 1983 to March 1984. The observational data and the solutions resulting from the subsequent reductions are presented graphically and tabularly for each of the occultation events. Several angular diameter determinations were made. Among those of particular interest were 32 Librae (12.1, +/- 1.9 milliseconds of arc), 1 Geminorum-B1 (5.9, +/- 0.8 milliseconds of arc), and X07598 (5.5, +/- 2.0 milliseconds of arc). The visual/spectroscopic binary 1 Geminorum was discovered to have a fourth, previously undetected, component. Two other stars, X13534 and X13607, were found to be binary with compainions closer than 15 milliseconds of arc. Previously unknown faint companions were discovered for ZC1221 and ZC0126. Times of geometrical occultation for all the events (including the secondary components of the binary systems) were reported as part of a cooperative astrometric project to the International Lunar Occultation Center.

CHAPTER I
INTRODUCTION

Lunar Occultations: A Historical Synopsis

When the moon, as a result of its orbital motion, moves in front of a star as viewed by an Earth-based observer, the light from the star is obscured. Such an event is known as a lunar occultation. At the time of the star's disappearance (or reappearance) the moon's limb is seen to move across the stellar disc. MacMahon (1909) proposed that the angular diameter of the occulted star could be determined by measuring the time interval of lunar limb passage across the star. Immediately thereafter, Eddington (1909) correctly pointed out that this was not possible, as the star's light would be diffracted by the moon's limb, hence the problem could not be approached from the standpoint of simple geometrical optics. He noted that the time-scale of the disappearance phenomenon is essentially unchanged as a function of stellar diameter.

Williams (1939) showed that while the time-scale of the event is not affected by the angular diameter of the star the diffraction intensity as a function of time most certainly is. The time-scale of variation of the diffraction fringes projected on the Earth's surface resulting from a lunar occultation is on the order of tens of milliseconds, thus requiring fast photometric observations. Whitford (1939), reported on observations of occultations of Nu Aquarii and Beta Capricorni using a photocell with a Cesium-Oxygen-Silver cathode on the 100-inch telescope. Neither of these events showed any deviation in the diffraction pattern from a point source, as his instrumental detection limit was approximately 5 milliseconds-of-arc. Yet the foundation for a powerful new technique for the acquisition of fundamental astronomical information, i.e. stellar diameters, was laid.

Over the ensuing three decades additional photoelectric occultation observations were carried out. The first angular diameter measurement was reported by Evans (1951) for the star Antares. This was followed, also by Evans (1959), with the determination of the angular diameter of Mu Geminorum. Over the next two decades other observations had been made, and additional theoretical work on the extraction of information from lunar occultation observations progressed. It was not until the advent of electronic computers and reliable fast photometric equipment that occultation observations could truly begin to be exploited. In a now classic series of papers by Nather and Evans (1970), Nather (1970), Evans (1970 and 1971), and Nather and McCants (1970) the theoretical and observational aspects of lunar occultations are discussed in detail. The methods reported in these papers serve as the foundation for modern investigation of lunar occultations.

Only in the last few years, with the revolution in both microcomputer and opto-electronic technology, have the tools essential to bringing the observation and analysis of lunar occultations come to fruition. The problems are still many, but the instrumental hurdle, at least, may now be cleared.

Information Which May Be Learned From the Analysis of Lunar Occultations

The analysis of the lunar occultation intensity curve, obtained from a fast photoelectric record of an occultation event can yield, in principle, a wealth of information. The degree to which any observation can be exploited depends upon a large number of variables. The geometry of the relative position of the moon and the star, the quality of the sky during the observation (seeing and scintillation), the physical nature of the source, and the response of the instrumental system, to mention only a few, can help or hinder the discovery of information hidden in the intensity curve.

In the case of an occultation of a single star the angular diameter of the star can be determined. Coupled with either a knowledge of the stellar parallax, or the V and R stellar flux (Barnes and Evans, 1976) this angular measurement can be transformed into an actual linear diameter. The observational techniques for direct measurement of stellar diameters are severely limited. Speckle interferometry (Lohman and Weigelt, 1980), Phase Correlation Interferometry (Brown, 1968), and Michelson

Interferometry (Brown, 1980), are the only other currently available techniques. All of these are restricted, instrumentally, to the measurement of diameters of very bright stars.

The size of extended non-stellar sources such as the emission shells of Be stars can be determined (White and Slettebak, 1980) as was investigated in the case of Zeta Tauri (Schmidtke and Africano, 1984). In ideal cases, with multiple observations the brightness distributions of such sources could be found.

The angular optical resolution achievable through occultation observations, on the order of milliseconds-of-arc, often leads to the discovery of stellar duplicity of stars previously thought to be single. An accurate determination of the separation of the components in a binary (Evans, 1971) or multiple system (Evans et al., 1977) can be found from simultaneous observations from more than one site (or a projected separation from a single observation). The individual brightnesses of otherwise "unresolved" binaries, or multiple systems, can be determined.

The field of chronometry is dependent upon, and enhanced enormously by, the precise measurement of the times of occultation events. These event timings lead to an accurate determination of the moon's longitude from which Ephemeris Time is derived. Time intervals are easily obtained with a precision of one part in 10 trillion through the use of atomic clocks. The observation of dynamical phenomena must have a zero point reference to couple dynamical events to atomic time (Van Flandern, 1974). Hence the accumulation of a database of accurate timing measurements of occultation events (dynamical phenomena) is essential in helping provide corrections to Co-ordinated Universal Time (C. U. T.).

The determination of stellar positions, the fundamental concern of the field of astrometry can benefit from occultation observations. The predicted time of an occultation event for a given topocentric location depends upon a knowledge of the moon's actual longitude, the geometry of the point of contact of the lunar limb, and the position in a given co-ordinate system of the star under study. Prediction errors in the times of occultation can lead to an improved knowledge of the positions of stars (Van Flandern, 1975). In some cases, gross errors in the predicted times of occultation can be attributed to positional errors in the stellar catalogs.

Goals of the Program of Occultation Observation

The primary intent of this program was to concentrate the investigation in areas which could have lead to astrophysically significant, or interesting results. While it could not have been determined, a priori, which stars or stellar systems would yield the most useful information, a judicious choice of program objects was called for. Many observational selection effects and instrumental limitations dictated the types of stars for which the occultation method would be fruitful. The general nature of these constraints has been addressed by Taylor (1966) and Ridgway (1977). Hence, in order to be considered for the observing program, candidate stars had to meet a variety of selection criteria. Unfortunately this left only a handful of stars each year to be considered for this investigation.

As a result of the stringent limitations a great deal of attention was paid to improving observational techniques and the development of new microelectronic data acquisition instrumentation. Once implemented, improved instrumentation allowed relaxation, to some degree, of the observational constraints placed on candidate star selection, thereby increasing the number of stars which were available for study. In addition, several non-traditional methods of data reduction were tried, which in some cases proved to be advantageous over the more conventional procedures.

The primary emphasis of the program was to extract as much information as possible from lunar occultation observations. The determination of stellar angular diameters, the discovery of unsuspected stellar duplicity or multiplicity, and the elucidation of the parameters of double or multiple systems were paramount. Of secondary importance, but an item to which no concessions were made during evolution of the program, was the accurate measurement of the times of occultation events. These measurements were reported, as part of an international co-operative project, to the United States Naval Observatory, and the International Lunar Occultation Center.

An outgrowth of the lunar occultation program has been the observation and analysis of occultations of stars by asteroids. Such observations typically yield information about the size and shape of the occulting body, as well as better astrometric positions of the occulted stars. Over two thousand asteroids are known and have been catalogued (Bender, 1979), and several hundred have orbits determined with a sufficient degree of precision to allow topocentric predictions of asteroidal occultations to be carried out well in advance of the anticipated event. Hence, the third aspect of this investigation of high speed occultation photometry extended the observational domain to asteroidal, as well as lunar occultations.

CHAPTER II
INSTRUMENTATION

Optical Equipment

The Seventy-Six Centimeter Telescope

Location and description. All observations, unless otherwise noted, were carried out at the University of Florida's Rosemary Hill Observatory (RHO) in Bronson, Florida, utilizing the seventy-six centimeter Tinsley reflecting telecope. This telescope is located at Latitude of 29 degrees 23 minutes 59.4 seconds North, Longitude 82 degrees 35 minutes 11.0 seconds West, at an altitude of 44 meters above mean sea level, based on the 1927 North American Datum. The primary mirror has a focal ratio nominally of f/4. In its Cassegrain configuration the telescope provides a nominal focal ratio of f/16. Figure 2-1 shows the seventy-six centimeter telescope and the associated optical and electronic equipment employed for the observations of lunar occultations.

The telescope light baffle. Observing immediately adjacent to the bright lunar disk increases the background sky illumination considerably. For a given spectral region there is nothing which can be done to enhance the signal to noise ratio considering noise due to atmospherically scattered light. It was found, however, that the Cassegrain

Figure 2-1. The seventy-six centimeter Tinsley relecting telescope at the University of Florida's Rosemary Hill Observatory.

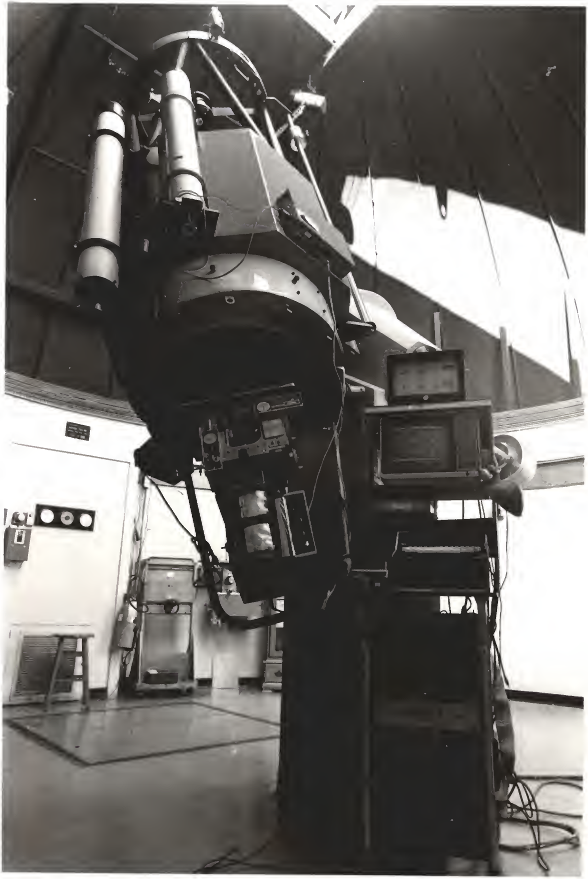

optical baffling for the seventy-six centimeter reflector could be improved upon greatly. A redesign of the optical baffle permitted a reduction in light scattered by the telescope optics and supporting structure. In addition, a tighter baffle system enabled the rejection of off-axis rays, preventing them from reaching the focal plane.

The primary design considerations for a new baffle system were two-fold. First, any baffles and/or field stops would have to be easily removable, so as not to impact on the telescope configuration required by concurrently running observing programs. Second, the unvignetted field of view at the focal plane had to marginally exceed the field obtained with the available diaphragm while minimizing extraneous light. An Astromechanics dual channel photometer was the primary instrument to be used for observing lunar occultations. This instrument has a maximum diaphragm opening corresponding to a field of view with a diameter of thirty two seconds of arc.

Many designs were considered by constructing models of the optical path, and ray tracing paraxial and marginal rays. It became quite obvious early in this investigation that no single tube/field stop design would be satisfactory for the task. The new baffle system would have to consist of two major elements: a tube with concentric annular field stops (rings), and an annular ring placed around the Cassegrain secondary mirror. A schematic representation of the optical path is presented in Figure 2-2.

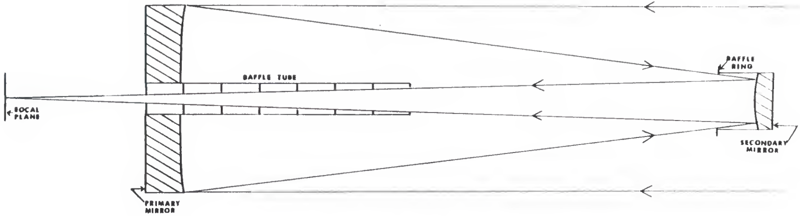

Figure 2-2. A schematic representation of the Cassegrain optical system showing the occultation light baffle tube and ring.

To satisfy the first design objective a system of field stops was built into a baffle tube identical at the mounting base to the existing tube. This would allow easy change-over to either the new or old baffle tube. The Cassegrain secondary ring would be be installed on the already existing locking pins on the secondary mirror baffle, which serve to hold the mirror cover in place. The new baffle tube, with the inner concentric rings removed to show its construction, is shown in Figure 2-3 along with the secondary ring.

Since the position of the focal plane varies with respect to the fixed position of the telescope superstructure and baffle assembly as a function of temperature, some degree of tolerance had to be allowed in the placement and size of field stops in the baffle tube. The system as designed would allow a one minute of arc unvignetted field of view at the focal plane at 15 degrees Celsius. This rather liberal tolerance was felt prudent considering the wide variation of climatic conditions experienced in northern Florida.
Table 2-1 gives the specifications for the spacing and sizes of the inner ring stack. The secondary baffle ring has an outside diameter of 11.375 inches.

To actually perform the ray tracing, the optical path of the telescope had to be determined. Although the blueprints from Tinsley Laboratories claim the primary is an f/4 paraboloid this had to be tested as the engineering specifications did not necessarily represent the state of the completed telescope.

Figure 2-3. The occultation light-baffle tube and ring.

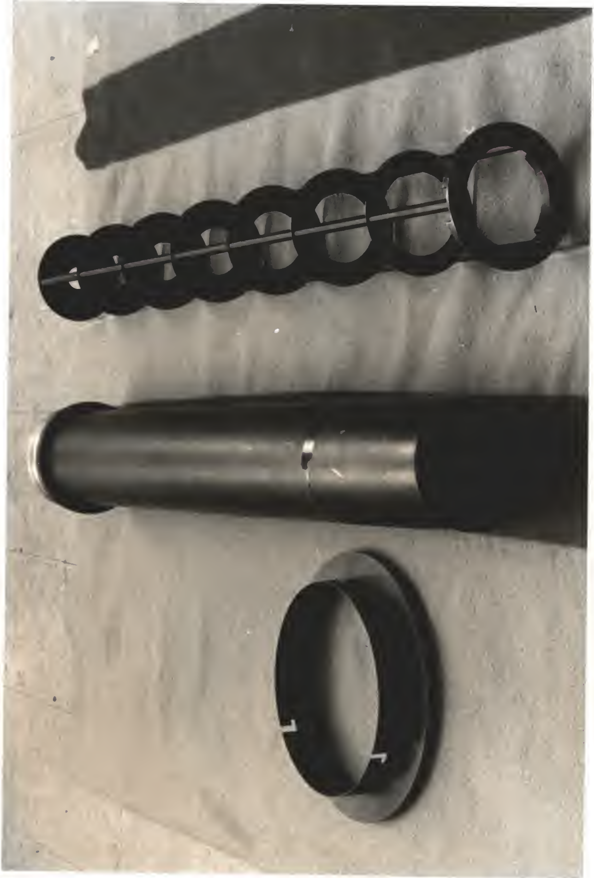

TABLE 2-1
SPECIFICATIONS FOR THE OPTICAL BAFFLE TUBE

Ring	Hole Diameter	Ring	Hole Diameter
1	3.56	5	2.24
2	3.23	6	1.91
3	2.90	7	1.67
4	2.57	8	1.24

Outside diameter or ring 1:	5.000
Outside diameter of rings 2-7:	4.812
Thickness of rings 1-8:	0.0625
Spacing between rings:	5.938
Bevel angle for all 8 holes:	45 degrees

Note: All linear measurements are in inches.

Using photographic plates of regions routinely monitored by the quasar research program, the plate scale of the primary mirror was found to be 67.065 (S.E. 0.06) seconds of arc per millimeter, corresponding to a focal length of 117.505 (S.E. 0.11) inches. The scale was determined by Pollock (1980) by measuring the positions of the quasar 0922+14 (denoted "Q") and the star SAO 098559 (denoted "S") for six plates taken over a period of seven years. Table 2-2 shows the plate measures used in determining the true scale of the primary mirror. The distance to the focal plane from the front surface of the Cassegrain secondary was measured at 15 degrees Celsius. From this the focal length of the Cassegrain system was found to be 1205 centimeters.

The assembled baffle tube is inserted through the central hole in the primary mirror and is screwed into place. The old, wide-field baffle tube is removed by grabbing the outside end and twisting sharply counter-clockwise. This will loosen its seating. When unscrewing the old baffle tube one hand is kept below the lower end of the tube to prevent it from hitting the primary mirror when it is completely released. When screwing the occultation baffle tube into

TABLE 2-2
DETERMINATION OF THE PRIMARY MIRROR FOCAL LENGTH

PLATE DATE	S to Q (mm)	Q to S (mm)	MEAN DIFF (mm)	SCALE "/mm
4/2-3/72	9.212	9.215		
	12.988	12.987		
	9.208	9.217		
	12.982	12.991	3.774	67.01
1/30-31/73	10.024	10.032		
	13.792	13.793		
	10.026	10.028		
	13.796	13.796	3.767	67.14
2/27-28/76	7.940	7.988		
	11.740	11.758		
	7.979	7.985		
	11.750	11.753	3.769	67.10
2/27-28/76	2.782	2.791		
	6.555	6.567		
	2.788	2.790		
	6.560	6.567	3.774	67.01
2/13-14/77	3.995	4.000		
	7.775	7.776		
	4.000	4.005		
	7.769	7.778	3.774	67.01
1/28-29/79	19.972	18.972		
	22.749	22.736		
	18.971	18.975		
	22.735	22.742	3.768	67.12
			MEAN	67.065 (0.06)

position, care must also be taken to assure the tube is not being cross-threaded. To switch back to the old tube (which must be done if using the infra-red photometer available at RHO) the process is reversed. The Cassegrain secondary baffle ring slips over the end of the secondary containment cylinder after it has been aligned with the cylinder's three positioning pins. A small rotation will secure the ring position insets against the pins.

Photoelectric Photometers

The Astromechanics photometer. Unless otherwise stated, the photometer used throughout this investigation was a dual channel instrument manufactured by Astromechanics. This instrument splits the light path into two beams by means of dichroic filters so two wavelengths can be monitored simultaneously. Though the instrument can be used in dual channel mode, observations of lunar occultations obtained thus far at RHO have been observed only in one color. The photometer employs two dry ice cooled photomultiplier tubes (PMT's). The PMT in channel-1 is a 6256S, while channel-2 uses a red sensitive 9684. In most cases 1200 Volts DC was applied to the PMT used. This photometer has a number of different available diaphragms. The linear diameters and angular field sizes of these diaphragms, along with their respective letter designations are listed in Table 2-3.

TABLE 2-3
DIAPHRAGM DESIGNATIONS, LINEAR AND ANGULAR FIELD SIZES

Letter Designation	Diameter (mm)	Field (arc-secs.)
G	1.98	32.5
H	1.52	25.0
I	0.93	15.2
J	0.51	8.3

Optical filters. Occultation observations made with the Astromechanics photometer employed Johnson V and B filters, as well as intermediate bandwidth yellow and blue interference filters. One inch diameter interference filters were obtained from Pomfret Research Optics, and are designated "y" and "b" respectively. The "y" filter, Pomfret part number 20-5400-1, has a peak spectral transmission at 5400 Angstroms and a Full Width at Half Maximum (FWHM) of 100 Angstroms. The "b" filter, Pomfret part number 20-4700-1 has a peak spectral transmission at 4700 Angstroms and a FWHM also of 100 Angstroms. These filters were selected in spectral regions for which M and K stars are relatively free of major absorption features. Of course, late type stars are riddled with a myriad of spectral lines. Hence the choice of these particular filters was somewhat of a compromise. Spectra typical G, K, and M, stars presented by Keenan and McNeil (1976) were examined, and on average were found least plagued with absorption lines at wavelengths of 4716 and 5408 Angstroms. These would have been the ideal central wavelengths for selected filters, but the cost of custom made filters was prohibitive. The filters procured were selected to be as close to these wavelengths as possible from a stock list. The H-Beta line at 4861 Angstroms is outside of the "b" filter passband. While other lines are found at 4716 and 4670 Angstroms, the integrated passband is less subject to absorption losses than adjacent regions. The TiO band at 5448 Angstroms enters into the "y" filter passband, but it is centered close to the lower half-power point.

While an actual set of narrow band filters was not available, a digital spectrum scanner employing Ebert-Fastie optics (Parise, 1978) is part of the standard equipment at RHO. The scanner can be used in a non-scanning mode as a variable-passband tunable filter. This in fact was done with great success in observing the occultation of Zeta Tauri in the passband of its H-Alpha emission.

The portable photometer. A small, lightweight photometer employing a 1P21 photomultiplier tube and built-in Johnson U, B, and V filters was used exclusively for events observed from remote sites. This instrument is discussed in detail by Chen and Rekenthaler (1966).

Data Acquisition Electronics

The SPICA-IV/LODAS System

Design criteria for a new SPICA. The concept of a Small Portable Interactive Computer for Astronomy (SPICA) was first conceived by Dr. John P. Oliver. The first SPICA system was implemented on a KIM-1 computer, and is the precursor to the three generations of SPICAs which have followed. The common thread linking the first SPICA to the latest version, the SPICA-IV, is the use of a 6502 microprocessor. Though each major upgrade to the SPICA systems has involved more hardware an effort has been made in SPICA-IV to retain portability, or at the very least transportability.

The Lunar Occultation Data Acquisition System (LODAS) is the software control program designed to carry out the task of fast photometric data acquisition on SPICA-IV. It is, in actuality, inaccurate to say that LODAS was designed for SPICA-IV, or SPICA-IV for LODAS. The system requirements were such that the hardware and software grew together in a complementary fashion. The major design criteria for SPICA-IV/LODAS are listed in Table 2-4.

TABLE 2-4
DESIGN CRITERIA FOR SPICA-IV/LODAS

1. Data acquisition rates up to and including 1 KiloHertz must be supported.
2. The system must support a minimum of two simultaneous data acquisition channels.
3. Memory space must be provided to hold a minimum of two seconds of data in each channel, at a rate of 1kHz.
4. 12-bit sample resolution should be used, to give a large dynamic range and eliminate last minute gain switching.
5. The system should retain easy transportability.
6. The system must function in the abscence of a disk drive, or a disk operating system.
7. A user friendly command structure and display must be implemented.
8. The control program must reside in Read Only Memory.

In all cases these criteria were met, and in the first three cases they were exceeded.

The SPICA-IV digital electronics. The heart of the SPICA-IV/LODAS system is an Advanced Interactive Microcomputer, model AIM-65, manufactured by Rockwell International. The AIM-65 has proven to be an invaluable design and development tool for the LODAS system as well as for several other astronomical data acquisition systems implemented at the Rosemary Hill Observatory. The AIM-65 is an 8-bit microcomputer with sixteen address lines incorporating a 6502 microprocessor chip. Up to 4-Kilobytes of Random Access Memory (RAM), in the form of paired 1K-by-4 bit chips (i.e. 2114's) can be accommodated on the AIM board. A 6522 Versatile Interface Adaptor (VIA), which is a programmable chip holding 16 bidirectional I/O lines, four control lines, and two timers, serves as an interface to the "outside world" through an expansion connector on back of the AIM board. A standard ASCII keyboard, a 20 character alphanumeric LED display, and a thermal printer are provided for user I/O. The AIM-65 accomodates 24-Kilobytes of ROM space in five 4-Kilobyte Read Only Memory (ROM) sockets, memory mapped in the areas of $B000 to $FFFF. The AIM-65 operating system is normally resident in two ROM's occupying the uppermost 8-Kilobytes of address space.

The SPICA-IV/LODAS system uses three boards manufactured by Micro-Technology Unlimited (MTU) to expand its RAM memory and to support peripheral devices. The first of these is a

16-kilobyte dynamic RAM board, model number K-1016 (MTU, 1979). This board is address assignable only on 8-kilobyte boundaries. Since the AIM-65 board is designed to hold 4-kilobytes of RAM, addressing the RAM board on 8-kilobyte boundaries would leave a 4-kilobyte hole in the system address space. While this in itself is not a problem, it will be seen that all available 64-kilobytes of AIM-65 address space must be used in configuring the system to meet the design criteria. This 4-kilobyte hole would then require a 68-kilobyte address space which the AIM-65 does not support. With this in mind the 2114 RAM chips were removed from the AIM board and the lower 16 kilobytes (address range $0000 to $3FFF) of system RAM reside contiguously on the dynamic RAM board.

A major design consideration was for LODAS to be able to function even if there were a hardware failure of either the disk drive or its controller board. A Shugart model 801, 8-inch floppy disk drive is used for primary data storage. The second MTU board is a Double Density Disk Controller (DDDC), model number K-1013 (MTU, 1980a), used in conjunction with the disk drive. The Channel Oriented Disk Operating System (CODOS) is distributed by MTU along with the DDDC board. The CODOS software provides many utility functions as well as a Service Call Processor and a Visual Memory Terminal driver program (MTU, 1981) which enhance the overall utility of the SPICA system.

The CODOS and its associated programs occupy address space in the range of $5000 to $5FFF, and $8000 to $9FFF. The DDDC board also provides an additional 4-kilobytes of RAM which is mapped in the address range $4000 to $4FFF. Although the disk/CODOS system is an integral part of SPICA-IV/LODAS, it is modular. Both the disk drive and the DDDC board may be removed from the system without impairing the data acquisition capability of the LODAS.

The final MTU board is a bit-mapped dynamic 8-kilobyte "visual" RAM high resolution display, model number K-1008 (MTU, 1980b). The display has a horizontal resolution of 320 dots (40 bytes) and is 192 scan lines in length. Thus 61440 bits may be individually controlled on the display within a 192-by-320 dot matrix. The hi-bit of the lowest byte on the board's address space is displayed on the upper-left of a Video Display Unit. The lo-bit of the highest byte occupies the extreme lower-right corner of the display.
This board is memory mapped for the address space $6000 to $7FFF.

All three MTU boards were designed with on-board voltage regulators to derive +5 Volts from an unregulated +8 Volt supply. Since the SPICA-IV power supply provides regulated +5 Volts, the +8 Volt regulator on each MTU board was bypassed, and regulated +5 Volts distributed to each board. Other than this and the addition of a BNC connector on the visual memory board, the MTU boards are unmodified.

An additional board, referred to as the Analog-to-Digital Converter/Clock (ADCC) board used in the SPICA-IV/LODAS system, was built by Oliver specifically for high speed occultation photometry. However, the devices provided on this board have been conveniently memory mapped and are available for other application programs running in any SPICA system at RHO. An examination of the SPICA-IV/LODAS system memory map, as shown on the LODAS assembly listing in Appendix A , reveals that the system memory space would normally be fully occupied with no addressable locations available for the placement of this board. The AIM-65 reserves the address space $A000 to $AFFF for its own on-board devices, but only a small portion is actually address decoded (Rockwell International, 1978). A minor modification on the AIM-65 board was made to free up normally undecoded address space within this range, and has subsequently been made to all SPICA-III and SPICA-IV computer systems in use at the RHO.

The ADCC was laid out on an MTU prototyping board, K-1020 (MTU, 1980c), and holds a real time clock and three analog-to-digital converters (A-to-D's). All components on the board were wire-wrapped. The clock circuit is based on a National Semiconductor MM-58167 chip which keeps time in month, day-of-month, day-of-week, hour, minute, second, and hundredths of a second. The clock is software readable and writeable, and can generate interrupts at either predetermined intervals or at a specific time/date

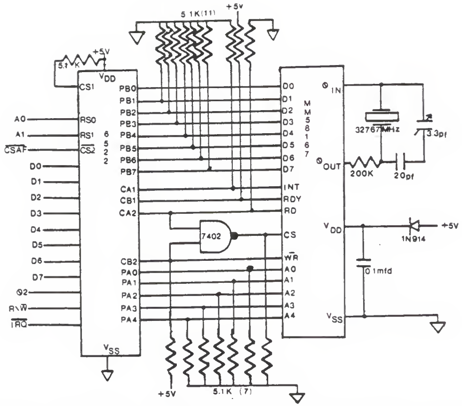

Figure 2-4. Schematic diagram of the SPICA-IV/LODAS clock circuit.

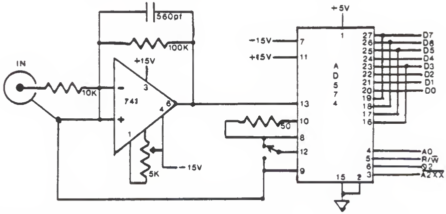

Figure 2-5. Schematic diagram of one of the three SPICA-IV/LODAS analog-to-digital converter circuits.

combination. For ease of operation the clock chip was interfaced to the SPICA-IV system through a 6522 on the protoboard. Thus the LODAS control software commands the clock through the protoboard VIA rather than controlling it directly. A schematic diagram showing the implementation of the clock circuit is presented in Figure 2-4.

The ADCC board also holds three 12-bit Analog Devices AD-574 analog-to-digital converters, each of these memory mapped into two contiguous bytes. A voltage conversion is initiated by writing to the A-to-D's. A digitized representation of the presented input voltage is obtained by reading the two memory mapped data bytes. The settling time for these A-to-D's is 35 microseconds. All three A-to-D's may be used in either a bipolar or unipolar mode, as selected by switches placed on the front-left edge of the ADCC board. In the unipolar mode the dynamic input range of the A-to-D's is zero to 10 Volts. In the bipolar mode the range is -5 to +5 Volts. Since the DC output of the photometer amplifiers used at RHO produce a zero-to-1 Volt negative going signal, buffer amplifiers (AD-741L's) are used between the A-to-D inputs and the actual signal input to the protoboard. Figure 2-5 shows one of the three A-to-D converter circuits. The circuits for all three channels are identical.

Ancillary equipment. Special I/O signals, such as the analog inputs to the A-to-D's, are connected through the system to a 44-pin connector on the back-left edge of the protocard. In addition inputs to each of the A-to-D's may be provided through miniature phone plugs mounted on the front-left side of the ADCC board.

The AIM-65, the three MTU boards and the A-to-D/clock board are mounted on an MTU K-1005 Card File and 5-Slot Motherboard (MTU, 1980d). A Zenith Data Systems 12-inch model ZVM-121-Z monitor is used to display video output. A Radio Shack model CTS-41 cassette recorder is used for secondary data storage.

For operational convenience a remote-control paddle was built. The need for remote control can be critical when observing alone, and obviates the need for continually running up and down telescope access ladders to operate the SPICA-IV keyboard. The paddle holds twelve pushbutton switches, which can select up to twenty-two key closures on the AIM keyboard. It is connected to the SPICA-IV/LODAS through its own cable, and specific functions can be activated by the observer from the telescope.

Power supplies. The DC voltages for the system, except those required by the thermal printer and disk drive, are provided by a Power One, model HBB-512 power supply. This supply can source 5 Volts DC at 3 Amperes, and 12 Volts DC at 1.2 Amperes. The thermal printer is powered by a Power One, model HB-24-1.2 (+24 Volt, 1.2 Ampere) supply. The disk drive employs a Power One, model CP-205 power supply providing 24 Volts DC at 1.5 Amperes, +5 Volts DC at 1 Ampere, and -5 Volts DC at 0.5 Ampere. The CP-205 supply along with the disk drive, is packaged separately from SPICA-IV/LODAS. For use at RHO the disk drive/power supply unit is mounted on the bottom shelf of a rolling equipment cart (see Figure 2-6).

SPICA-IV system configuration. Figure 2-7 indicates the overall system configuration. All major components including peripheral I/O devices are shown. Figure 2-8 is a photograph of the ADCC board. The polarity-mode switches for the A-to-D's are mounted on the top of the board, as is a trim capacitor to adjust the MM-58167 clock rate.

The MTU K-1005 card file holding the digital electronics boards and the HBB-512 power supply, which comprise the major components of the SPICA-IV/LODAS system, are packaged in a small aluminum chassis. All signal and power cables are brought into the system through connectors on the back plate so as not to be obtrusive during operation. A cooling fan, which can be disabled on cold nights, is also mounted on the back plate of the chassis. Figure 2-9 shows the placement and fucntion of each signal and power connector found on the back plate of the chassis. Figure 2-10 shows the assembled SPICA-IV/LODAS system on its rolling cart in operation at RHO.

Portable use. A key element in the system design was the need for relatively low power utilization. The portable aspect of the SPICA system had to be retained in order to use SPICA-IV/LODAS in the field. Observations of lunar grazing or asteroidal occultations often require setting up a

Figure 2-6. The SPICA-IV/LODAS 8-inch floppy disk drive and drive power supply.

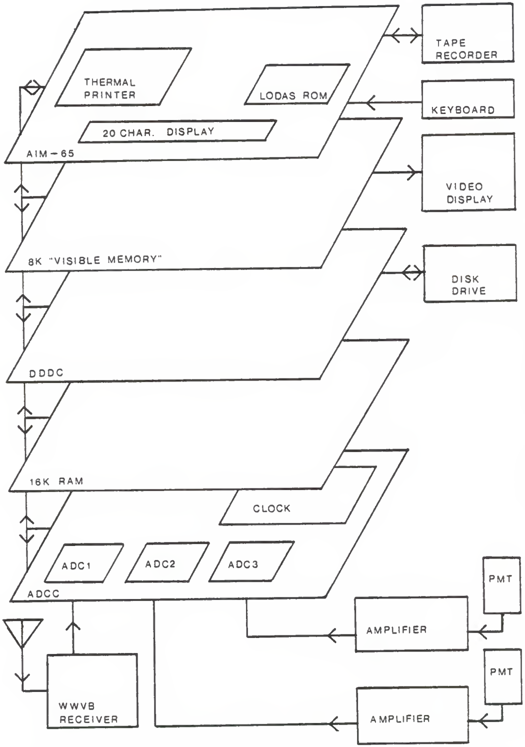

Figure 2-7. The SPICA-IV/LODAS system configuration.

Figure 2-8. The Analog-to-Digital Converter/Clock (ADCC) board.

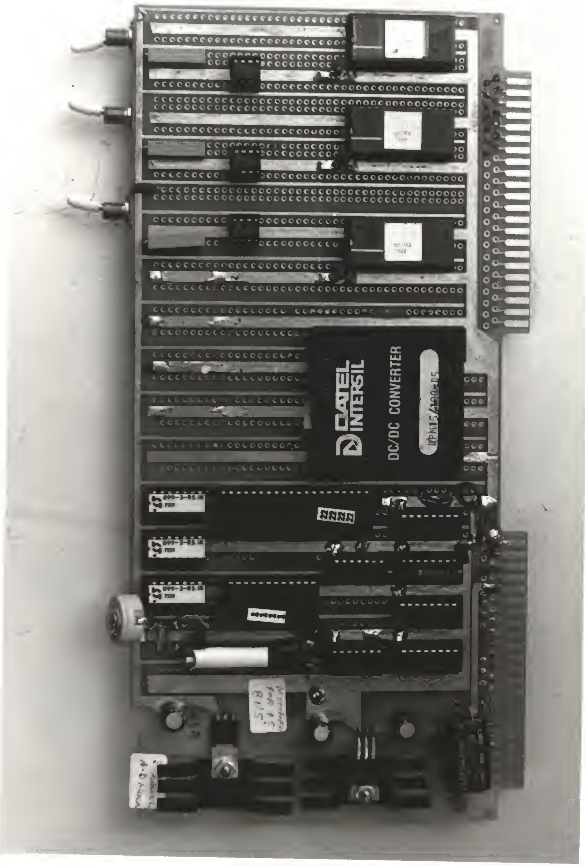
DATEL
INTERSIL
DC/DC CONVERTER

Figure 2-9. SPICA-IV/LODAS backplate and connector layout.

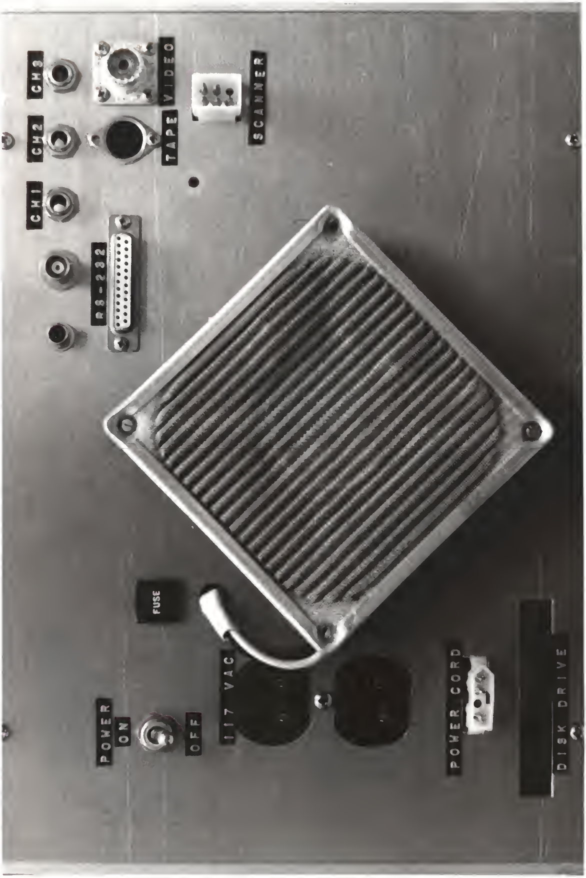
CH3
CH2
CH1
VIDEO
TAPE
SCANNER
RS-232
FUSE
POWER
ON
OFF
117 VAC
POWER CORD
DISK DRIVE

Figure 2-10. The SPICA-IV/LODAS rolling rack and Cassegrain photometric equipment in use at the Rosemary Hill Observatory.

portable photoelectric station in a dark, secluded site where the availability of AC electric power is often non-existent. Thus one reason for using dynamic (as opposed to static) RAM is its lower overall power utilization, drawing higher current only during periods of active write cycles.

For observing at a remote site AC power is required to operate not only the SPICA-IV/LODAS system, but a Kepco model ABC-2500M high voltage power supply, an Astronomical Time Mechanisms model 240V DC electrometer amplifier, and a True Time Instruments WWVB receiver as well. To provide AC power a Nova model 1260-24 DC-to-AC inverter, running on two 12 Volt DC automobile batteries, has sufficient capacity to operate the entire photoelectric station for 35 hours. The AC inverter can supply approximately one Ampere at 120 Volts AC. Thus, to conserve power, the DDDC board and the Shugart 801 disk drive are not used. Data are saved to cassette tape after an observed event. Although the inverter can also provide power for the ZDS 12-inch monitor, this additional load reduces the working life of the portable power supply system considerably. Hence, for field use a Gold Star 12-inch black and white television with an RF modulator that had been built-in is used in its place. Though the power required for the television is no less than that of the ZDS monitor, it can be run directly on 12 Volts DC. The source of 12 Volts can be derived from one of the two batteries supplying the DC-to-AC inverter. In practice, however, the transporting vehicle's 12 Volt car battery is used to power the television as well as the telescope drive corrector, slewing motors, electric dew cap, and ancillary equipment.

Figure 2-11 shows the SPICA-IV/LODAS system in field use while observing the asteroidal occultation of 14 Piscium by Nemausa on September 11, 1983 (Dunham et al., 1984). In this case AC power was available at the observing site. Figure 2-12, taken on November 13, 1984, shows the SPICA-IV/LODAS system when it was powered by the portable supply system while observing the asteroidal occultation of BD +08 471 by Ceres from the middle of the Florida Everglades.

Analog Electronics

The WWVB receiver. Nather and Evans (1970) have pointed out that the reduction of photoelectric observations, in principle, can yield the times of geometrical occultation with an uncertainty of only one or two milliseconds. As Table 2-4 has shown, a primary design criterion of SPICA-IV/LODAS was to have a data acquisition rate of least one point per millisecond. The inherent degree of accuracy in overall system timing depends upon both the AIM-65 phase-2 clock and the clock on the ADCC board. Thus, in order to realize absolute timing accuracy of one millisecond a standard time calibration source must be employed.

This requirement precludes the idea of using High Frequency (HF) transmissions from the National Bureau of Standards' radio station WWV (located in Fort Collins,

Figure 2-11. The SPICA-IV/LODAS, and portable photometer on an 8-inch Schmidt-Cassegrain telescope used to observe the occultation of 14 Piscium by 51 Nemausa. The observation was made on the grounds of the Macon (Georgia) County Museum of Arts and Sciences.

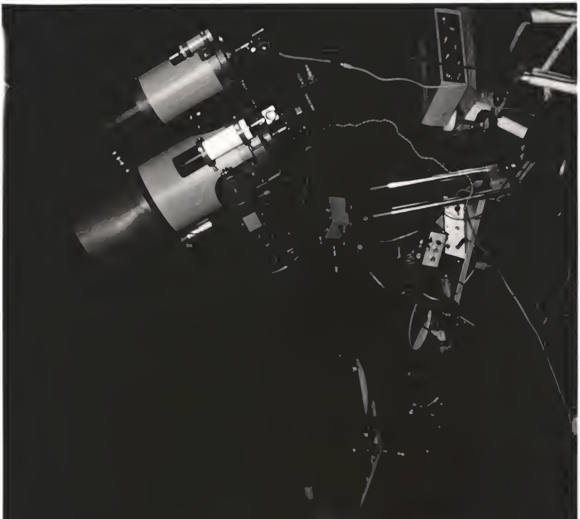

Figure 2-12. The SPICA-IV/LODAS, and portable photometric system used to observe the occultation of BD +08 471 by Ceres from a remote site in the middle of the Florida Everglades. The 14-inch Schmidt-Cassegrain telescope seen in these photographs was on loan from the Tampa Amateur Astronomical Society.

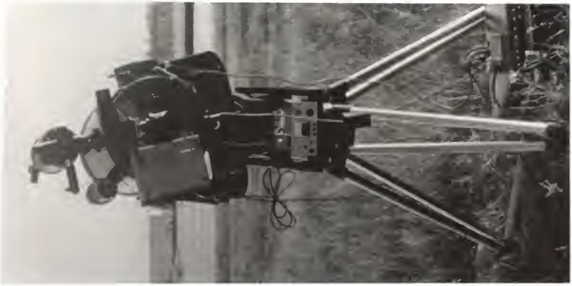

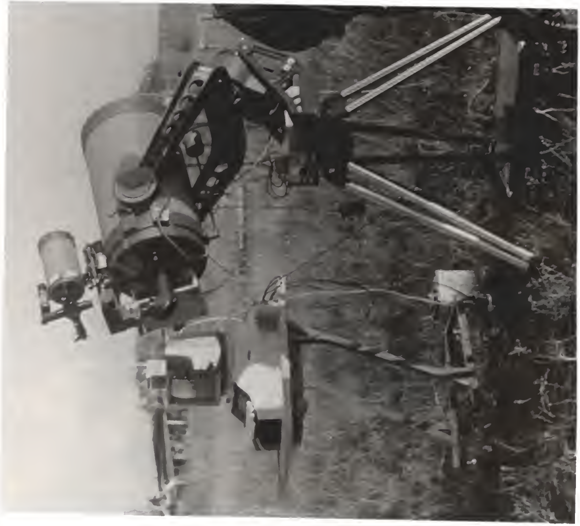

Colorado) as a suitable time base reference. The uncertainty in the HF propagation path arising from variability in ionospheric conditions between Fort Collins and Bronson can lead to timing uncertainties as large as a several milliseconds.

Fortunately, NBS provides a Very Low Frequency Coordinated Universal Time broadcast, via radio station WWVB, which transmits at a standard carrier frequency of sixty kiloHertz (Kamas, 1977). At sixty kiloHertz the mode of propagation is strictly by ground waves; hence, the variability in propagation time is removed (Department of the Army, 1953). The propagation path will simply follow a great circle from transmitter to receiver, amounting to a fixed light-time delay of 7.4 milliseconds at the RHO.

WWVB transmits timing information in a tristated time code. The strength of the carrier wave is modulated by reducing output power for 0.2, 0.5, or 0.8 seconds each second. Encoded in this modulation envelope are the time, date, and current UT1 correction. Each ten-second period and the start of each new minute are identified by encoded framing references.

Detection and interpretation of this signal are precisely what is needed to provide the timing accuracy desired. Several avenues of approach were debated. Rather than having a receiver built, a commercially available unit well suited to the task was procured. The unit, a True Time Instruments model 60-T receiver provides not only a detected carrier output, but a TTL compatible code output as well.

A small modification made to the TTL output, dividing it down to 0.8 Volts, permits feeding the code signal directly into one of the three A-to-D converters available in the SPICA-IV/LODAS system. The digitized time code is sampled simultaneously along with the photometric channels. The receiver is mounted on a 19-inch equipment rack, shown in Figure 2-13, along with a WWV receiver and the high voltage power supply used by the PMT's.

In actual use the LODAS system clock is set manually by the observer to an audio WWV signal. This procedure results in a clock setting accuracy of a few tenths of a second. It is then noted if the clock was set fast or slow. Digitized WWVB second transitions then provide a correction to the nearest millisecond.

The signal strength at RHO rarely exceeds 125 microvolts per meter (True Time Instruments, 1974). An active antenna, model A-60FS, also manufactured by True Time instruments is currently used at the observatory. This is marginal under circumstances of unfavorable reception, and an alternate antenna design is being considered for future use at the observatory. However, it has been found that eighty percent of the time a decodable signal is available while observing. During nights of signal fading, time code is digitized before and after the event as conditions permit and time corrections to the computer's internal clock are interpolated in post-observational reduction.

The receiver introduces a measured electronic delay time of 19 milliseconds from the time of reception of the WWVB

Figure 2-13. The WWV and WWVB receivers, and PMT high voltage power supply.


WWV RECEIVER

carrier to code output. This, however, varies slightly as a function of signal strength. By attenuating the input signal from the antenna it was found the delay is lengthened to 21 milliseconds at a level where the time code cannot be reliably detected. This then sets the limit of the absolute timing determination to +/- 1 millisecond, meeting the occultation program's allowable tolerance. All reductions then have a final correction of 27.4 milliseconds subtracted from the determined time of geometrical occultation, with an additional error of +/- 1 millisecond added to the formal error of the solution.

Radio antennas. For use at the observatory the receiver is mounted in the telescope main-power distribution rack, immediately above the WWV receiver. These two receivers share an antenna cable, so only one receiver can be used at a time. The antenna connector must be switched from the WWV receiver to the WWVB receiver before use. Approximately one minute is required by the WWVB receiver after being powered up to lock onto the time code and produce a readable decoded output. A twenty-five foot cable terminated at one end with a BNC connector and a three conductor phono plug on the other is kept on the rolling cart with the SPICA-IV/LODAS system. The BNC end is connected to the CODE output of the WWVB receiver, and the phono plug end connected to one of the SPICA-IV/LODAS signal inputs. The input channel selected to receive the time code should be switched to unipolar mode.

Because of the frequent lightning strikes, unavoidable on one of the highest hills in Florida, the WWV and WWVB antennas are disconnected at the base of the antenna tower at the end of a night's observing. A PL-259 connector can be found at the tower base to which the WWVB active antenna connects via a plug, and the WWV long wire antenna connects by means of an alligator clip. The WWVB antenna and its 15-foot antenna cable are removed from its 6-foot high mounting stand and stored above the desk on the first floor of the observatory building.

The photometer amplifier. Since millisecond time resolution is desired, the photometer amplifier used must have a response at least as fast at a range of gains useful to the occultation observing program. An Astronomical Time Mechanisms model 240 fast photometric DC electrometer amplifier was choosen. This amplifier described by Astronomical Time Mechanisms (1980) is based on a circuit by Uliver (1976) designed specifically with lunar occultation observations in mind. Amplification is achieved in two stages: first in a current-to-voltage conversion stage; and second in a buffer amplifier. A similar amplifier had been in use at the Rosemary Hill Observatory fourty-six centimeter telescope for several years. Caton (1981) carried out a program of UBV photometry on RS CVn stars using this amplifier. He found eighth magnitude stars could be observed giving a full scale reading with the amplifier switched to the so-called "C" gain. This gain setting employs 10 megOhm feedback resistance in the first amplification stage. Using the seventy-six centimeter telescope would yield a gain of approximately one magnitude over the forty-six centimeter telescope.

The effective time constant of the amplifier is limited by the high precision megohm feedback resistors and the capacitance of the input signal cable (added to a capacitance of 5 pf., the value of the feedback capacitor used on the signal input). In order to observe ninth magnitude stars with a 2 kHz half power response, twice that of the target time resolution, the capacitance of the input signal cable cannot exceed 45 pf. RG-58 A/AU co-axial cable has a capacitance of 28.5 pf./foot. Thus, to achieve this time resolution for stars of ninth magnitude a cable of this type no longer than 18 inches must be used. Rather than RG-58, which is commonly used as a signal cable, the occultation program uses RG-71/U, with a measured capacitance of 13.1 pf./foot.

For practicality, the amplifier is mounted on the side of the photometer cold box as may be seen in Figure 2-9. This allows a short cable run (only eight inches is needed), and is in an extremely convienient place for an observer operating the photometer. Having the amplifier fixed to the photometer also permits the signal cable from the PMT to be securely fastened down thus preventing any possible cable flexure. Such flexure would result in charge redistribution along the signal cable leading to erroneous fluctuations in the observed signal level.

The amplifier coarse gain steps are in increments of 2.5 magnitudes, and fine gain steps in increments of 0.5 magnitudes. After initial use at the telescope the amplifier was modified to provide a 0.25 magnitude gain switch to boost the effective gain at any coarse and fine combination. This was done to provide the observer with a bit more flexibility in chosing the amplification factor used for the purpose of real-time photometric data display.

The output of the amplifier is connected to the SPICA-IV/LODAS system by means of a fifteen foot signal cable terminated on both ends with phono plugs. This cable is kept on the rolling cart along with the WWVB signal cable. One end is connected to the amplifier output marked RECORDER, and the other end is connected to a SPICA-IV/LODAS input switched to unipolar mode.

Limitations of the Occultation Photometric System

Once obtained, the new amplifier was used to assess the limitations of the seventy-six centimeter telescope photometric system and to confirm that stars of reasonable faintness could be observed while preserving a system time constant on the order of a millisecond. Stars over a range of six magnitudes were observed on the moonless night of May 23, 1981 U.T. with the Astromechanics photometer, cooled with dry ice, and a Johnson V filter. Measurements were taken at both the nominal operating voltage of the PMT of 1200 Volts DC, and at the maximum operating voltage of

1600 Volts DC. Five minutes of settling time was allowed after switching voltages before readings were taken. The observations, listed in Table 2-5, give the star name, U.T. of observation, the star's V magnitude, the photometer diaphragm used. For both voltages the amplifier coarse and fine gains, and the signal level due to the star (normalized to a full scale value of 255) are listed. In all cases the dark current and sky background have been subtracted from the star-plus-sky readings. Gain settings were adjusted to give readings as close to 65 percent of full scale as possible.

TABLE 2-5
STELLAR INTENSITY READINGS WITH RHO SPICA-IV/LODAS

				1200 Volts		1600 Volts	
Star Name	U.T.	mV	Dia.	Gain	Star	Gain	Star
Gamma Leo-a	0315	2.6	J	B7	193	B2	173
57 UMa	0338	5.2	J	C7	173	B7	153
88 Leo-a	0401	6.1	J	C9	165	B9	143
88 Leo-b	0413	8.6	J	D10	158	C10	136

The fine gain steps of 0.5 magnitude run from "1" to "11". Hence stars with a V-magnitude as faint as approximately 7 can be observed at a coarse gain setting of "C", at a PMT voltage of 1200 Volts DC. In order to gain one magnitude observations can be made at 25 percent of full scale. With twelve bit digitization this is still roughly one part in one-thousand, or a photometric precision of 0.001 magnitude. Alternatively, a gain can be achieved by increasing the PMT voltage. As can be seen from Table 2-5 increasing the PMT voltage to 1600 Volts provides a gain of approximately 2.4 magnitudes. However, the penalty of increased thermal noise (dark current) must be paid if this option is taken. Fortunately, the RMS amplitude of the dark current for the 1600 Volt observation of 88 Leo-b was only 2 percent of the star signal level.

These observations tend to lead to over-optimistic results, as occultation observations will not be made in dark skies; indeed the telescope will be pointed in the direction of the moon. To assess a "worse case" condition, the star SAO 098723 (mV=8.7) was observed on May 11, 1981 when it was only 0.1 degrees away from the dark limb of a 55 percent illuminated moon. Using the same diaphragm and filter as the observations in Table 2-5, a gain setting of D7 was required to bring the star-plus-sky level up to 67 percent (170 counts out of 255). The sky contribution was 130 counts, so the star signal was only 16 percent of full scale. In order to bring the signal into the range of "C" gains, an additional gain of 0.5 magnitude is needed. This would place the gain of the amplifier at C11. At 1600 Volts the star-plus-sky signal was just above half scale on a gain setting of C7. Hence under bright sky conditions the photometric system would allow detection of stars down to ninth magnitude with timing accuracy of one millisecond. The limit is more stringent for observations with either of the intermediate bandwidth filters, whose integrated bandpass is roughly one-tenth that of the Johnson V filter. In this case the limiting magnitude is reduced to roughly 6.5.

The Lunar Occultation Data Acquisition System Software

Software Design Considerations

The design criteria specified in Table 2-4 were binding not only for the choice of hardware to be used the SPICA-IV system, but applied equally, if not even to a greater extent, to the design of the data acquisition and process control software. The execution of a repetitive task at a precisely defined rate, which must interact in real-time with the "outside-world" is best accomplished by the technique of interrupt processing. Thus, the major process control task of the LODAS software, real-time data acquisition at a rate of at least one-thousand 12-bit samples per second, in at least two channels, was relegated to an interrupt service routine. Yet, some functions of LODAS do not have the need for either repetitive or regularly scheduled execution. For example, scanning the keyboard for user requests, or updating the 20-character alphanumeric display with system status information can be done at the microprocessor's leisure. Hence LODAS actually operates two concurrent programs. A foreground program handling all input to, and output from the observer runs continuously in a relatively quiescent mode, calling upon system services only when required by the observer or program logic. This program is repeatedly interrupted by the aforementioned interrupt service routine, referred to as the background task, on a regularly scheduled basis.

System timing. The limiting factor which played a major role in the development of the LODAS operating concepts was the execution speed of the 6502 microprocessor. The system (i.e. microprocessor) clock rate for the AIM-65, as for all 6502 systems, is 1-megaHertz. A sampling rate of 1-KiloHertz would require the evocation of the interrupt service routine every millisecond. This constrains the process control tasks to a maximum of one-thousand system clock cycles. However, the system cannot spend all of its available clock cycles executing the interrupt service requests. Some percentage of the total system throughput must be allocated to the foreground task. Fortunately, the reaction time of any person is much longer than the cycle time of a 1-MegaHertz computer. This undeniable physiological fact allows a very low bias in time-slicing for the foreground routine. A comfortable allowance of a minimum of 10 percent was deemed more than adequate.

On average, the execution cycle time for a typical machine instruction on a 6502 microprocessor is 3.5 microseconds. This means that approximately three hundred instructions, at most, could be issued in the interrupt service routine before interrupt pile-up would occur. The need for rapid execution speed is clear. For this reason the LODAS software was implemented in 6502 machine language, rather than a more user-oriented, but slower, high level language.

It was found that while the task of data acquisition and storage requires less than a half-millisecond, other interrupt service requests (such as servicing a video "strip chart" display) would demand a total number of machine instructions well in excess of the three hundred maximum. Because of this the interrupt service routine was multi-phased, handling data acquisition and storage in each phase, and pieces of other service requests in successive phases. In breaking the background task into four phases the execution time for any one phase required less than 450-microseconds. Hence, the basic system interrupt rate was defined as 500-microseconds. This allows data to be sampled in successive pairs and averaged together in real-time before being stored. Thus a 1-KiloHertz data sample is actually comprised of two 500-microsecond pair-averaged samples. This not only effectively increases the signal-to-noise ratio of the acquired data by 41 percent, but the stored 1-KiloHertz samples have a Nyquist cut-off frequency of 1-KiloHertz (half the actual data sampling rate) as well.

Memory usage. The area available for storing data in a circulating event buffer is 18-Kilobytes in length. In order to optimize the use of this limited (but sufficient) resource, two 12-bit acquired and averaged data samples are bit-packed into three 8-bit bytes. This packing, accomplished by the interrupt service routine, saves 25 percent over storing the 12-bit data, unpacked, into two 8-bit bytes. The 18-Kilobytes of available RAM are partitioned into three 6-kilobyte regions, each to hold one channel's data. Four seconds of pair-averaged data, acquired at an effective rate of 1-kilohertz, can be stored in each 6-kilobyte region. Hence, the system as built and programmed is capable of holding twice the amount of data originally envisioned, and in an additional data channel as well.

A modified version of the LODAS program, called FASTDAS (Fast Asteroidal Data Acquisition System) partitions RAM into only two data storage areas, thereby gaining 50 percent in the data buffer circulation length. This program has been used in observing asteroidal occultations of stars from remote sites (Dunham et. al, 1984).

The LODAS/E07 program has been assembled to reside in ROM at an address space of $D000. This allows co-residency with AIM-65/FORTH, which is often used on RHO SPICA systems.

<u>Supplementary program documentation</u>. The overall logic flow for the LODAS foreground and background (interrupt service) programs, as well as the program initialization procedure are shown on the operational flow charts presented as Figures 2-13 and 2-14. A fully annotated assembly listing of the LODAS program is contained in Appendix A. This listing reflects LODAS program revision number E07, the seventeenth incarnation of LODAS since its inception. The assembly listing is preceeded by a detailed accounting of the LODAS memory space in terms of I/O addressing, AIM-65 monitor utilization, program variable space, and an overall system memory map. Following the assembly listing is a symbol-table

```
Label                    Description of Program Step
------     ---------------------------------------------------
                        <INITIAL PROGRAM ENTRY>
                                   ↓
COLDST     [Establish Address of Interrupt Service Routine]
                                   ↓
LODAS0     [Print/Display Program Name and Version Number]
                                   ↓
SETVIA      [Initialize T1 for 500 Microsecond Interrupts]
                                   ↓
CLINIT        [Setup Access Control for Internal Clock]
                                   ↓
SETGAP             [Initialize Cold Start Variables]
                                   ↓
            [Interactive Setup of All Control Parameters]
                                   ↓
           [Initialize Video Display for "Glass Recorder"]
                                   ↓
WARMST             [Initialize Action Code to "Quit"]
                                   ↓
SETCTR        [Initialize Flags, Counters and Pointers]
                                   ↓
SETSTL             [Initialize Data Buffer Addresses]
                                   ↓
            [Clear Possible Interrupt Sources: Clock, T1]
                                   ↓
SETBT        [Setup Bit Pattern Table for Video Display]
                                   ↓
            [Clear and Draw Background Pattern on Video]
                                   ↓
MAIN        <Foreground Program: Command Service, Display>
                                   ↓
SCAN               [Scan Keyboard for Command Entry]
                                   ↓
             <"Exit to Monitor" Command Received?>--NO--
                                   ↓                     ↓
             [Clear both VIA Interrupt Flag Registers]   ↓
                                   ↓                     ↓
                     <STOP! EXIT TO AIM-65 MONITOR>      ↓
                                                         ↓
NEWCDE          [Execute User Request: See Table 2-8]←---
                                   ↓
DSPCHK     <MAIN<-NO--<Does LED Display Need Updating?>
                                   ↓
DISTME     <MAIN<---------[Update LED Display]
```

Figure 2-14. LODAS foreground program logic flow chart.

```
Label                    Description of Program Step
------   ----------------------------------------------------
                     <INTERRUPT SERVICE ROUTINE>
                                  ↓
INTRCV        [Save A, X, and Y-Registers on the Stack]
                                  ↓
SNAPCK      <Did a Quit After Delay Just Occur?>--NO--
                                  ↓                   ↓
         <RGET<----[Transfer $0000-$0020 to TAPBUF]   ↓
                                                      ↓
ADCONV                  [Start A-to-D-Conversions]←-------
                                  ↓
            <Was Interrupt Request From Clock?>--YES--------
                                  ↓                         ↓
             <INCMSC<--[Clear Interrupt Flag for T1]        ↓
                                                            ↓
CLCIRQ    [Clear Clock Interrupt, Set Display Update Flag]←-
                                  ↓
           <Tape or Clock Write Requested?>--NO----------
                                  ↓                      ↓
CNTDWN              [Disable Clock Interrupts at VIA]    ↓
                                  ↓                      ↓
         <RGET<---[Clear Tape and Clock Request Flags]   ↓
                                                         ↓
RENHMI       [Reseed T1 Timer in Synchronism with Clock]←-
                                  ↓
          [Enable 500 Microsec. Interrupts, Reset Counter]
                                  ↓
INCMSC              [Increment 500 Microsec Counter]
                                  ↓
             <Has a Millisecond Elapsed?>--NO--
                                  ↓            ↓
                       [Disable T1 Interrupts] ↓
                             -------------
                                  ↓
INTTST                <Data Taking in Progress?>--YES--
                                  ↓                    ↓
         <RGET<----NO-<Has 0.1 Second Elapsed?>        ↓
                                  ↓                    ↓
         <RGET<------------[Read Clock]                ↓
                             ------------------
                                  ↓
SAMPLE    <STPND2<--NO-<Has Time Between Samples Elapsed?>
                                  ↓
SAMPLO    <STEP1, STEP2, STEP3<-<Do 1 of 4 Steps>
                                  ↓
STEP0      [Put A-to-D Readings in Average Registers]
                                  ↓
             <STPND1<--[Update Video Display as Needed]
```

Figure 2-15. LODAS background program logic flow chart.

```
STEP1     [Read A-to-D's, Average with Previous Value]
                              ↓
          [Store Averages in Circulating Data Buffer]
                              ↓
           <STPEND<--[Update Data Buffer Pointer]
                              ↓
STEP2       <STEP2B<--YES--<Is Freeze Flag Clear?>
                              ↓
                    <Has Delay Expired?>--YES-----
                              ↓                  ↓
            <STEP2B<--[Update Delay Counters]    ↓
                                                 ↓
SETSNP     <STPND1<--[Set Snap Flag, Read Clock]←-

STEP2B    [Put A-to-D Readings in Average Registers]
                              ↓
           <STPND1<-------[Read Clock]

STEP3     [Read A-to-D's, Average with Previous Value]
                              ↓
          [Store Averages in Circulating Data Buffer]
                              ↓
                [Update Data Buffer Pointer]
                              ↓
STPEND      [Increment Current Storage-Byte Pointer]
                              ↓
STPND1     [Increment the Interrupt Service Step Count]
                              ↓
STPND2          [Increment the Sample Counter]
                              ↓
RGET        [Restore Y, X and A-Registers from Stack]
                              ↓
              <EXIT INTERRUPT SERVICE ROUTINE>
------  ---------------------------------------------
```

Statements in the flow chart are interpreted as follows:

```
  [Unconditionally Execute Statement In Brackets]

  <LABEL<--[Execute Statement in Brackets and Go To LABEL]

  <LABEL<--NO-<If Proposition Matches YES/NO Go To LABEL>

  <PRIMARY ENTRY OR EXIT POINT>
```

Follow flow lines either unconditionally, or propositionally as is applicable:

```
     [Statement]-------        <Proposition>--YES/NO--
                      ↓   or                         ↓
     ←----------------         ←---------------------
```

Figure 2-15--Continued.

and reference list. The LODAS makes extensive use of internal subroutines and data tables. Tables 2-6 and 2-7 provide a synopsis of these routines and data tables respectively.

Peripheral Input/Output

User (Observer) I/O. The LODAS program was written with ease of operation in mind. An observer at the telescope often has enough problems confronting him or her, and an unfriendly computer need not be among them. After powering up the SPICA-IV, and evoking LODAS, the observer is prompted on the 20-character alphanumeric display to enter the parameters salient to the observing session. The date, data acquisition rate and channel assignments are among these input requests. These parameters may be changed at any time by issuance of a LODAS command. The LODAS commands are actuated by a single keystroke (or for safety, by depressing the CTRL key simultaneously with the command key). The command-key assignments are, in most cases, mnemonic to the command request. A list of LODAS commands is given in Table 2-8. Some of the LODAS commands are acted upon immediately (as in the case of EXIT) and some require additional information from the observer. Examination of Table 2-8 will reveal the proper responses to any LODAS command request prompt. These responses are identical to those required on system initialization when the parameters are first established.

Once the LODAS system initialization is completed the observer is kept abreast of system status on the 20-character

TABLE 2-6
LODAS/E07 SUBROUTINES

Name	Description of Subroutine
CLENUP	Post tape writing clean-up. Reset interrupt count, clear VIA interrupt flags, re-enable 0.1 second interrupts, restore "Action Code".
CLEAR	Clear the 20-character alphanumeric display.
COMENT	Input comment from user, up to 40-characters in length. Display, print, and store in the tape header buffer, (TBUFF).
DECHEX	Convert packed BCD in A-register to hexidecimal.
DISBUF	Output contents of display buffer (DISBUF) to 20-character LED display.
DRSET	Interactive data acquisition rate setting. Get data acquisition rate from keyboard.
FRZSET	Interactive delay time (freeze) setting. Get delay from keyboard. Validity of entry is checked.
GETKEY	Input a character from the AIM-65 keyboard, if no key pressed then wait.
GOCLCK	Reset clock with values stored in MILSEC.
HIOUT	Convert left half-word of A-register to ASCII and store in DISBUF at offset indicated by X-register.
HX1BCD	Convert hexidecimal byte in A-register to 2-byte BCD. Puts MSD into Y-register, and LSD into A-register.
HXASC2	Convert hexidecimal value in A-register to 2-byte ASCII and store in DISBUF at offset indicated in X-register.
HXASC3	Convert two byte hexidecimal value in A, and Y-registers to three byte ASCII and store in DISBUFF at offset indicated by X-register.
KEYCK	Modified AIM-65 keyboard scan routine. Does not exit to monitor on ESC.

Table 2-6. Continued.

Name	Description of Subroutine
LHWOFA	Halfword shift to A-register to the right. Zero out the left halfword of A-register.
OBHXAS	Convert a one-digit hexidecimal number to ASCII.
PACK2	Get two digit BDC number from keyboard, display number, store as packed BCD in A-register.
PNDM	Print and display an in-line message.
RDCLIN	Set up clock to accept a read request.
RDCLK	Read current time from clock and store in MILSEC. A, X, and Y registers unaffected.
ROLACT	Clear the 20-character alphanumeric display and restore old "Action Code".
TICSET	Set up tics, data channel markers and screen lines on video display.
TIMEGO	Start clock running from keyboard command.
TIMSET	Interactive clock setting routine. Get time and date from keyboard. Start clock if commanded. Validity of entry is checked.
TOGPRT	Toggle AIM-65 printer on/off.
TAPINT	Write occultation observation to cassette tape. interrupt request servicing disabled.
TVCLEA	Clear the video display.
TVDISP	Output next hi and lo resolution data points on video display.
TVSET	Interactive set-up of video display parameters. Get channel assignments and display rate from keyboard.
TVSETX	Clear video display and redraw background.
WRCLIN	Set up clock to accept a write request.
WRTAPE	Transfer a contiguous block of data to tape.

TABLE 2-7
LODAS/E07 DATA TABLES

Name	Description of Data Table
CLCTBL	A table of packed BCD numbers from decimal 00 to 99, inclusive. Used by clock and intensity display routines to 20-character LED display.
TVTICS	A bit mapped data table containing the video display background pattern.
TVTBLH	The hi byte of the address of each video display line as mapped on the visual memory.
TVTBLL	The lo byte of the address of each video display line as mapped on the visual memory.

TABLE 2-8
LODAS/E07 KEYBOARD COMMANDS

Key=5 LODAS Cold Start:

This command, if executed from the AIM-65 monitor, will transfer control to the Lunar Occultation Data Acquisition System and begin execution. The system will respond by flashing LODAS R65/E07 on the alphanumeric display and logging this on the printer. Program default parameters will be established, and the observer asked for variable set up parameters. This command is valid only from the AIM-65 monitor and will be ignored once LODAS is in control and running.

Key=6 LODAS Warm Start:

To re-enter LODAS from the AIM-65 monitor while preserving previously set parameters use this command. It is assumed that LODAS was previously cold started, and exited (i.e. to CODOS or the AIM-65 monitor). Warm start will not require resetting the internal clock/calander, selecting data acquisition rates, display channels or the "video strip chart" display rate.

Key=Cc Enter a COMMENT:

This command will allow the observer to enter a comment of up to 40 characters in length (two lines) on the printed observing log. The most recent comment is also retained in the data buffer header to be saved on disk or tape on command. Entering a RETURN in the comment field will terminate comment entry.

Key=Dc Exit To The DISK Operating System (CODOS):

This command will terminate LODAS and boot the Channel Oriented Disk Operating System. If a CODOS system diskette is not in the disk drive, and the drive door closed the system will freeze up. CODOS must be entered in order to save observing data to a data diskette, or load another observing program from the system diskette. Note: To go from CODOS to the AIM-65 monitor strike the ESC key. To go from the AIM-65 monitor to CODOS, after CODOS had been previously booted strike the F3 key.

Table 2-8. Continued.

Key=Fc Save FILE On Cassette tape

Data may be saved on cassette tape instead of a CODOS disk by issuing this command. Be sure the cassette tape recorder is set to RECORD, and that a non-write protected cassette is in the tape recorder. LODAS will ask for a data FILE name. Any name up to five characters in length may be entered. Data transfer to tape will begin immediately after the entry of the file name. As each block is writen the current block count will be presented on the alphanumeric display. When all data has been transferred the message TAPE WRITE COMPLETED will be displayed.

Key=Gc Restart System U.T. Clock To Preset Time: (GO):

If the system clock had previously been set using the U.T. Clock Set command, but not started, this command will start the clock running at the preset time.

Key=Ic INITIATE Data Taking (Integrate/Sample):

Upon receipt of this command LODAS will immediately begin sampling the three Analog to Digital Converters at the preset sample rate. Acquired data will be stored in the all three channels of the 4096 sample circulating data buffers. The Initiate Data Taking command will reset the data buffer pointers to the beginning of the each of the three data storage buffers will overwrite any previously buffered data.

Key=Pc Toggle PRINTER (On/Off):

Each time this command is entered the 20 column printer will toggle from on to off, or off to on. If toggled off command interaction logging will still be displayed on the 20 column alphanumeric display, but will not be printed. The words ON or OFF will be flashed on the 20 character alphaneumeric display to indicate the new status of the printer.

Table 2-8. Continued.

Key=Q QUIT Data Taking:

Upon receipt of this command LODAS will cease data taking after the previously specified delay time. When data taking stops all system status information related to data taking will be saved in the data header buffer for possible subsequent storage to disk or tape.

Key=Rc Select Data Taking RATE:

This command is used to select the data acquisition rate. LODAS will ask for the desired rate, which is to be entered in milliseconds per point. Three digits must be entered. Thus if data is to be taken at five points per millisecond the entry should be 005. Data may be taken at any rate from one to 256 milliseconds per point. An entry of 000 will result in the 256 millisecond per point rate. Data will actually be taken at twice the specified rate and pair averaged before being stored.

Key=Tc Set Delay TIME:

The Delay TIME parameter set by this command affects the system response time to a QUIT command. LODAS will prompt for the desired time delay to be waited before the system will QUIT data taking when commanded to do so. Delay times are entered in units of 100 times the data acquisition rate in milliseconds. Two digits (00-99) must be entered. Thus an entry of 12, with a data acquisition rate of one point per millisecond, will cause LODAS to wait 1.2 seconds before halting data acquisition on a QUIT command.

Table 2-8. Continued.

Key=Uc Set The UNIVERSAL Time Clock/Calendar:

This command will allow the observe to manually reset the internal U.T. Clock. LODAS will first prompt for the the year, month, and day to which the clock should be seeded. Entry must be in the form of a six digit number. For example 850118 will seed the calendar to January 18, 1985. LODAS will then ask for the day of the week, as a single digit number. Day 1 is Sunday and day 7 is Saturday. LODAS will then request the hour and minute to be entered as a four digit number. Thus 1820 will seed the clock to 18 hours and 20 minutes. After these entries are made LODAS will prompt by displaying START=ANY EXIT=CR. If any key other than RETURN is struck, the clock/calendar will immediately start running with the seeded values. If RETURN is hit, the seeded values will be stored and the clock/calendar can be commanded to start running at a later time by issuing a GO command.

Key=Vc Set Up VIDEO Display Parameters:

This command allows the observer to select which of the three input data channels is be displayed on the Hi Resolution Graphics Display, and which is to be displayed on the Lo Resolution Graphics Display. LODAS first asks for the input channel number to be assigned to the A (Hi Resolution) display, and then for the channel number to be assigned to the B (Lo Resolution) display. Valid input channel numbers are 1, 2, and 3. LODAS then requests the video display rate. The display rate is coupled to the the data acquisition rate. Entry is in units of the data acquisition speed divided by two per displayed point. Thus if the data acquisition rate is 5 milliseconds per point (1/200 second), an entry of 002 will result in a point being displayed every 1/50 second. Entries must be three digit numbers in the range 001 to 255. An entry of 000 is interpreted as 256.

Table 2-8. Continued.

Key=Xc   EXIT To The AIM-65 Monitor:

This command will terminate LODAS and return control to the AIM-65 monitor. LODAS may then be restarted with either a COLD or WARM start. This command should be used if CODOS is to be re-entered rather than booted. After exiting to the AIM-65 monitor use the F3 key to re-enter a previously booted CODOS system.

NOTE: A letter designation of "c" postfixing the command key (i.e. KEY=Xc) indicates that the CTRL key must be depressed simultaneously along with the specified key.

alphanumeric display. Figure 2-16 shows the format of this display.

```
=====================================================
   HHMMSS M 000 000 128
   :      : :   :   :
   :      : :   :   Intensity on A-to-D channel #3
   :      : :   Intensity on A-to-D channel #2
   :      : Intensity on A-to-D channel #1
   :      Current (or Last) Command Code
   Universal Time
=====================================================
```

Figure 2-16. Format of the LODAS 20-character alphanumeric system status display.

The A-to-D channel intensities are scaled from zero to 255. With no input on an A-to-D channel the display will read 000 if that channel is set to unipolar mode, or 128 if that channel is set to bipolar mode.

All observer commands, command responses, and the current status display are logged on the 20-character thermal printer whenever a command is issued. The printer can be disabled by an observer command.

<u>The video "strip chart recorder"</u>. Without a doubt, strip chart recorders are the bane of photoelectric observers worldwide. Renowned for clogging up, dripping ink, jamming paper or spewing it forth in voluminous quantities, these devices, while undoubtedly useful, often seem more troublesome than they are worth. Since the LODAS saves all observational data in a digital format on disk or tape there is no need for a printed chart record of the observations.

Yet, a chart recorder is an extraordinarily handy tool (when working) on the observing floor, even if used simply to visually monitor the ongoing photoelectric observations. An ideal chart recorder for use with SPICA-IV/LODAS would provide a graphic display of the event for the observer's immediate inspection, without the necessity of plotting it out on reams of paper. A further ideal would be such a device with no mechanical parts to fail, as they invariably do, while observing.

These ideals were transformed to reality with the introduction of what is now referred to as the video "strip chart recorder". Rather than having the photoelectric and/or timing signals drawn on a paper chart with an inking mechanism, data are displayed on a video monitor. The screen is divided into two halves. The left half, called the hi-res, or A-channel display, has a resolution of 0.25 percent (1 part in 256). The right half, called the lo-res, or B-channel display, has a resolution of roughly 1.5 percent (1 part in 64). Data input to any of the three A-to-D's can be selected to be displayed on either the A or B channels. While observing, typically the A-channel is used to display photometric data, and the B-channel is used to display the WWVB time code. The display rate is software selectable, and can be as fast as one-half the data taking rate, or as slow as 1/256 of the data taking rate. With a millisecond data acquisition rate it is possible to display 500 points per second.

The video "strip chart recorder" is best thought of as either a vertical two-channel programmable storage oscilloscope, or a chart recorder with a fixed paper and moving pen. When the pen hits the bottom of the page, the next point will be plotted on the top of the page as the point previously there is erased.

The LODAS activates the video "strip chart recorder" when an Integrate command is issued, and freezes the display when a Quit command times out. A sample video "strip chart recorder" display is seen in Figure 2-17. The number of short dashes at the top left and top right of the display indicate which A-to-D channels have been assigned to the hi-res and lo-res portions of the screen respectively. The short horizontal dashes (on the same line for both hi and lo-res) indicate where the cursor ("chart pen") was when data acquisition stopped. Tic marks on top and bottom indicate the 25, 50, and 75 percent signal levels for the hi-res display, and the 50 percent level for the lo-res display.

Data archival. Post-event observing data may be stored on either 8-inch floppy disks or on cassette tapes. To save data to disk the observer should command LODAS to enter the disk operating system (CODOS), save the observing data by issuing the command: SAVE filename 0700 4FFF, and then re-enter LODAS (if more observations are to be made) with a warm-start. To save data to cassette tape the LODAS Fc command is used. Approximately 10 minutes are required to save the observing data to cassette tape.

Figure 2-17. The SPICA-IV/LODAS and the video "strip chart recorder" display.


Rockwell
AIM 65
GAIN
08NOV

CHAPTER III
NUMERICAL MODELING OF LUNAR OCCULTATIONS

The Physical Characterization of an Occultation Intensity Curve

When the moon occults a star the lunar limb acts as a diffracting aperture. As the moon's limb approaches the star (as seen topocentrically) the intensity of the starlight is seen to vary as a result of this diffraction. A topocentrically stationary observer sees the diffraction pattern projected onto the Earth's surface moving due to the orbital motion of the moon and rotation of the Earth. The time variation of the intensity of starlight diffracted around the lunar limb under ideal conditions would be characterized by the parameters listed in Table 3-1.

TABLE 3-1
PARAMETERS CHARACTERIZING AN OCCULTATION INTENSITY CURVE

1. The topocentric distance to the limb contact point.
2. The angular velocity of the lunar limb, as measured topocentrically, projected onto a line joining the star and the point of contact on the limb.
3. The peak wavelength, or spectral energy distribution of the star (a function of the photospheric temperature).
4. The unocculted intensity of the starlight.
5. The apparent angular diameter of the star.
6. The brightness distribution of the stellar disc.

The actual observed diffraction pattern, referred to as an occultation intensity curve, is affected by several non-idealized distorting effects. These effects are listed in Table 3-2.

TABLE 3-2
PARAMETERS AFFECTING THE OBSERVED INTENSITY CURVE

1. The contribution of background skylight due to both atmospherically scattered moonlight, and Earthshine along the lunar limb.
2. The local slope of the lunar limb due to surface irregularities.
3. Noise in the observation due to both scintillation and photon statistics.
4. The spectral response characteristics of the optical system (mirrors, windows, lenses, filter, and PMT).
5. Instrumental effects such as PMT dark current and the electrical bandpass of the electrometer amplifier.

The observed occultation intensity curve results from a combination of the effects of the parameters given in both Tables 3-1 and 3-2. The process of "solving" a lunar occultation intensity curve involves isolating or removing the distorting effects and determining the individual parameters intrinsic to the star. The topocentric lunar distance and projected angular velocity (referred to as the R-Rate) can be computed from the moon's orbit. The instrumental parameters can be determined through calibration of the instrumental system. The other intrinsic parameters are determined by a process of fitting an intensity curve, computed from a set of model parameters, to the observed intensity curve. The generation of the computed intensity curve and the fitting procedure will be addressed in detail in this chapter.

The Generation of a Model Occultation Intensity Curve

Monochromatic Point Source Approximation

The process of the formation of a model occultation intensity curve adopted in this study essentially follows the method as outlined by Nather and McCants (1970). As a first approximation, the diffraction of light by a straight-edge from a monochromatic point source is considered. In this approximation the observed intensity of light seen by an observer at a given distance from the geometrical shadow may be expressed as

$$F(U) = (I/2)\{[\tfrac{1}{2} + S(U)]^2 + [\tfrac{1}{2} + C(U)]^2\} \qquad [3\text{-}1]$$

where I is the unocculted intensity of the point source. S(U) and C(U) are the familiar Fresnel integrals:

$$S(U) = \int_0^U \sin(\tfrac{1}{2}\pi t^2)dt \quad \text{and} \quad C(U) = \int_0^U \cos(\tfrac{1}{2}\pi t^2)dt \qquad [3\text{-}2a,b]$$

The quantity, U, is a dimensionless number referred to as the Fresnel number. In performing diffraction calculations it is convenient to work in Fresnel space, where all linear measurements have been normalized to Fresnel numbers. The quantity U is defined as

$$U = X[2/(LD)]^{\frac{1}{2}} \qquad [3\text{-}3]$$

where X is the geometrical shadow to observer distance, L is the wavelength of the light from the source, and D is the straight-edge to observer distance. A typical intensity curve resulting from the defining equations, (3-1, 3-2, and 3-3), as discussed by Borne and Wolf (1970) is shown in Figure 3-1, which also illustrates the geometry of the situation.

It should be noted that at the point of geometrical occultation, when the source, observer, and diffracting straight-edge are co-linear, the diffracted intensity is 0.25 of the intrinsic source intensity. In addition the zeroith order diffraction maximum is approximately 1.37 of the source intensity.

Lunar Limb Effects

While it is true that the lunar limb is not an ideal straight-edge the scale of the occultation phenomenon permits this assumption as a first approximation. The extensive high resolution photographic coverage of the lunar surface obtained by both the Lunar Orbiter probes (Bowker and Hughes, 1971) and subsequent Apollo missions indicate that while the lunar surface is quite irregular it tends to be smoothly undulating rather than possessed of sharp discontinuities. This is presumably due to ceaseless erosional processes caused by the solar wind.

One cannot, however, ignore the possibility of a discontinuity on the lunar surface due to an ill-placed boulder or other protrusional feature, particularly if an occultation is seen at near grazing incidence. The detection and handling of lunar limb irregularites in terms of their

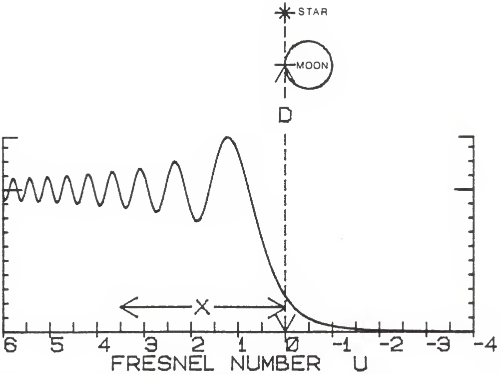

Figure 3-1. Lunar occultation intensity curve for a monochromatic point source.

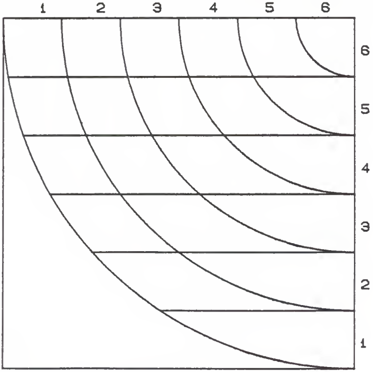

Figure 3-2. Example of a two dimensional grid used to discretely model a stellar quadrant.

distorting effects on the occultation intensity curve are discussed in detail by Evans (1970). Morbey (1972) has compiled an catalog showing the nature of these effects for a variety of surface discontinuities.

The effect upon occultation intensity curves by lunar surface structure along the line of sight was investigated by Murdin (1971) and found to be negligible.

A Monochromatic Extended Source and Limb Darkening

A star, however, is not a true point source, but has a finite angular diameter. If the star is assumed to be spherically symmetric then the visible disc projected onto the plane of the sky will have a circular cross-section. In most cases spherical symmetry is certainly a valid assumption to make. The vast majority of stars which can yield sensible diameters are of late spectral type and hence are not likely to be rotationally distorted out of spheroidicity (Tassoul, 1978). In the special case of occultations of close binaries the tidal distortions and effects of possibly rapid rotation acting on the component stars would cause the spherical symmetry argument to break down.

The computation of the diffraction intensity for an extended circular source is handled by dividing the disc into a series of discrete elements as shown in Figure 3-2. The two dimensional grid used to partition the model stellar disc is linear in one dimension and radial in the other. The partitioning of the model disc into radial zones allows the effects of limb darkening to be modeled discretely. The linear strips are small regions containing surface elements (of variable radial intensity due to limb darkening) at evenly-spaced distances from the lunar limb.

The elemental contribution to the intensity of the entire non-limb darkened disc is simply proportional to the area of that particular surface element. Since spherical symmetry is invoked, only one quadrant of the model stellar disc need be computed. The area to a given radius R, bounded by the intercept of the radius with the lines defining the linear strip boundaries is

$$A = \int_m^n (R^2 - X^2)^{-½} dX \quad = \quad ½[X(R^2 - X^2)^{-½} + R^2 \sin^{-1}(X/R)] \Big|_{X=m}^{X=n} \qquad [3\text{-}4]$$

where m is the X coordinate of the lower bound of the linear strip, and n is the upper bound. Hence, the area of a particular element of the grid bounded by rings of radius R_a and R_b, and strip boundries Sm and Sn (centered approximately at (R,S)) is

$$A(R,S) = ½[X(R_a^2 - X^2)^{-½} + R_a^2 \sin^{-1}(X/R_a)] \Big|_{X=Sm}^{X=Sn} - ½[X(R_b^2 - X^2)^{-½} + R_b^2 \sin^{-1}(X/R_b)] \Big|_{X=Sm}^{X=Sn} \qquad [3\text{-}5]$$

For convenience, the degree of the partitioning of the model stellar grid is referred to as the grid parameter. The grid parameter is the square root of the number of surface elements per quadrant on the model stellar disc. Thus a grid parameter of 6 would refer to a grid containing 36 elements. Since the grid elements are actually represented in a rectangular coordinate system, those elements which fall outside of the stellar disc have zero intensity. Table 3-3 shows the elemental contribution of each surface element as a percentage of the total intensity of the entire model disc. This is a non-limb darkened star with a grid parameter of 6. In this table element (Zone=6, S#=6) is closest to the center of the stellar disc. The total intensity of this quadrant has been normalized to 25 percent.

TABLE 3-3
BRIGHTNESS DISTRIBUTION FOR MODEL STAR WITH GRID PARMETER=6

S#	Zone 1	Zone 2	Zone 3	Zone 4	Zone 5	Zone 6	Sum
6	0.88918	0.89174	0.89697	0.91095	0.99722	0.69444	5.28050
5	0.00000	0.92110	0.94177	0.98906	1.19189	1.08612	5.12993
4	0.00000	0.00000	0.99725	1.07606	1.37182	1.36939	4.81451
3	0.00000	0.00000	0.00000	1.16089	1.53335	1.60326	4.29750
2	0.00000	0.00000	0.00000	0.00000	1.68034	1.80708	3.48743
1	0.00000	0.00000	0.00000	0.00000	0.00000	1.99012	1.99012

The relative attenuation of the zonal intensity due to limb darkening is modeled by a simple linear limb darkening function of the form

$$I(\theta)/I(0) = (1-\Upsilon) + \Upsilon\cos(\theta) \qquad [3-6]$$

where Υ is the limb darkening coefficient, and θ is the angle between the star's radius vector and the line of sight. Table 3-4, which is similar to Table 3-3, shows the relative intensity of the surface elements of a fully limb darkened disc with a grid parameter of 6. The effects of limb darkening coefficients of values 0.0, 0.2, 0.4, 0.6, 0.8 and 1.0 are depicted in Figure 3-3. This figure shows the relative intensity of each linear strip on the model disc from the center of disc to the edge. A grid parameter of 100 was used in this illustration. The maximum variation found in the intensity distributions was for limb darkening coefficients of 0.0 and 1.0, and was only 13 percent.

TABLE 3-4
BRIGHTNESS DISTRIBUTION FOR MODEL STAR WITH
GRID PAREMETER=6 AND A LIMB DARKENING COEFFICIENT OF 1.0

S#	Zone 1	Zone 2	Zone 3	Zone 4	Zone 5	Zone 6	Sum
6	0.52257	0.86735	1.07134	1.21774	1.41985	1.01764	6.11648
5	0.00000	0.54132	0.91601	1.18132	1.59329	1.54643	5.77838
4	0.00000	0.00000	0.58608	1.04663	1.63850	1.83057	5.10177
3	0.00000	0.00000	0.00000	0.68225	1.49142	1.91493	4.08859
2	0.00000	0.00000	0.00000	0.00000	0.98753	1.75766	2.74519
1	0.00000	0.00000	0.00000	0.00000	0.00000	1.16958	1.16958

The observed diffraction intensity of a monochromatic point source of intensity unity at a fixed distance from the observer is dependent only on the distance of the source from the diffracting aperture. In the limit, each surface element is essentially a point source. Those point sources equidistant from the lunar limb (i.e., along the same strip) will result in an observed diffraction intensity whose total intensity is the linear sum of the individual intensities. Hence, the strip itself can be treated as a point source.

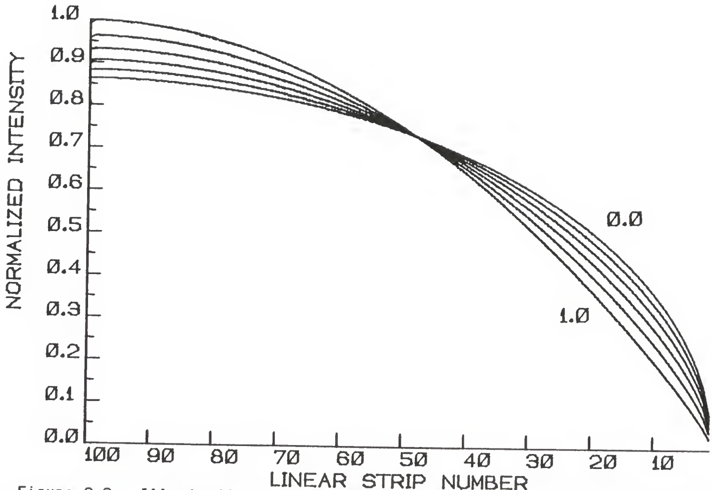

Figure 3-3. Illustration of the relatively small effect of limb darkening upon the brightness distribution of the linear strips. Strip 100 borders the center of the stellar disc, strip 1 borders the surface.

Equation 3-1 may be computed for each linear strip, S. The Fresnel numbers, U_s, for the points of evaluation of each strip will be offset by an amount corresponding to the separation of the center of each strip and the occulting aperture. The intensities, I_s, are the fractional normalized intensities for the corresponding strips. Thus, the intensity curve resulting from a grid of individual elements is computed as the linear superposition of strip intensity curves, $F_s(U_s)$. This is shown graphically in Figure 3-4. The uppermost curve is the linear sum of the individual curves shown. The sum curve is shown at a reduced scale so the details of the component curves can be seen on the same figure. In this example the resultant curve is that of a 10-millisecond-of-arc source, at a distance of 375,000 Kilometers, and an angular velocity of 0.3 seconds-of-arc per second.

Polychromatic Intensity Curves

The monochromatic approximation to the occultation intensity curve is sufficient to model observations taken with a narrow bandwidth filter (less than 50 Angstrom FWHM). In order to model intensity curves over a broader bandwidth individual model curves, of the monochromatic type described above, must be computed for a number of discrete spectral regions, approximating the contiguous spectral energy distribution of the source. Each individual curve, computed for a specific wavelength, is intensity weighted by the

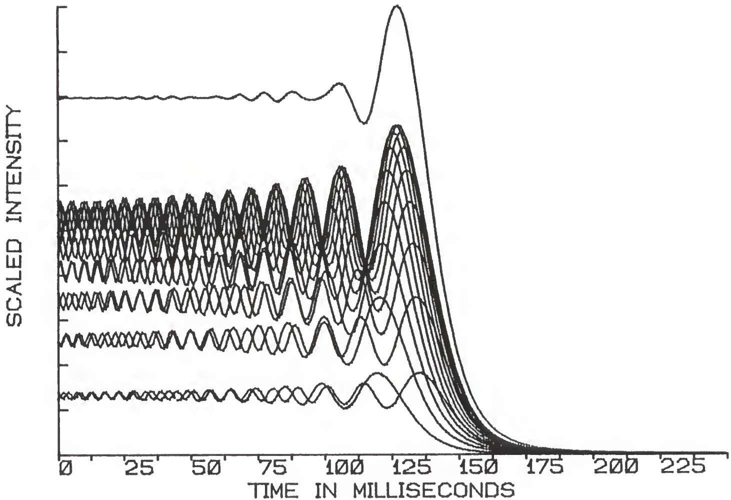

Figure 3-4. Formation of an intensity curve for a monochromatic 10-millisecond-of-arc source by the linear superposition of intensity-weighted point source curves.

relative total power of the source in that particular spectral region.

In the actual case of stellar modeling, a blackbody spectral energy distribution is assumed. The total power radiated by the star for a spectral region centered at a wavelength, λ_i, and of spectral bandwidth 2B is

$$E_i(\lambda_i) = \int_{\lambda_i - B}^{\lambda_i + B} [26729\lambda^5(e^{1.473887/\lambda T} - 1)]^{-1} d\lambda \qquad [3\text{-}7]$$

as given by Allen (1963). The quantity T, is the effective color temperature of the star, and could be sought as one of the parameters to be determined by the model fitting procedure. In practice, however, the effective color temperature is entered into the model based on a best guess predicated on the spectral type of the star under study. Numerical experimentation indicates that this procedure is justified. An error of 5 percent in the pre-determined color temperature of the star (quite a reasonable error estimate for stars of spectral type G and later) resulted in only very minor changes to model intensity curves.

Figure 3-5 illustrates an example of the linear superposition of intensity weighted monochromatic curves to generate a polychromatic intensity curve. As in Figure 3-4 the uppermost curve which is the summation of all other curves is shown in a reduced scale. In this example, the 10-millisecond-of-arc curve generated in Figure 3-3 was modeled as a 4500 degree Kelvin blackbody under the bandpass of a Johnson V filter. For computational purposes, only the

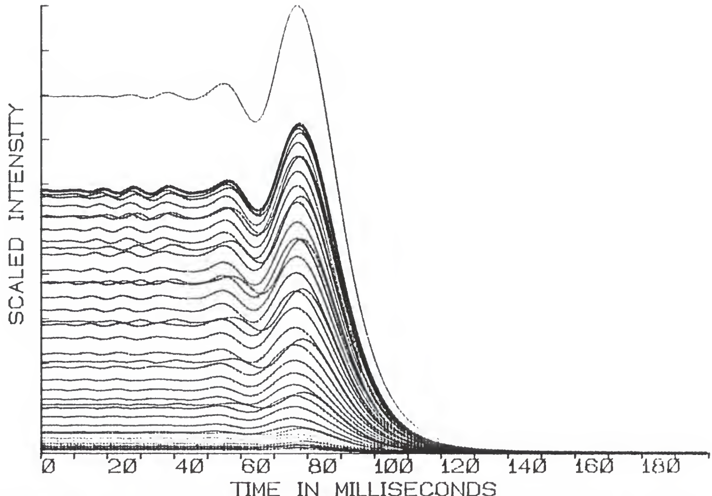

Figure 3-5. Formation of a polychromatic intensity curve for a 10-millisecond-of-arc source by the linear superposition of intensity-weighted monochromatic curves.

fractional contribution of $E_i(\lambda_i)$ is important. Thus, each $E_i(\lambda_i)$ is adjusted subject to the normalization that the sum of $E_i(\lambda_i)$ over all wavelengths considered is set equal to 1.

The Effects of Discrete Modeling

The brightness distribution of the strips generated from the stellar grid and the contribution to the total source intensity from each spectral region considered are discrete or quantized representations of continuous functions. Two related questions arise which must be answered before a computational procedure can be developed from the numerical model. First, how fine must the stellar grid be to adequately represent the disc? Second, how small must each spectral region be in modeling the energy distribution of the source?

To answer these questions a number of numerical models were generated and compared. As to the partitioning of the stellar grid, it was found that as the source diameter was decreased, even a moderately coarse grid was sufficient to produce intensity curves indistinguishable from those generated with a fine grid. This may have been expected as the limiting case of a point source requires a grid with only one element. A source with an angular diameter of 20 milliseconds-of-arc required a grid parameter of 10 (400 points, or 20 strips) to achieve a variation of no more than 0.05 percent in the worst case, when compared with a model generated with a grid parameter of 32 (4096 points, or 64 strips).

The effect of choosing too few strips to represent the disc is easily seen in Figure 3-6. This figure shows a family of model occultation intensity curves for a 10-millisecond-of-arc star, similar to the model shown in Figure 3-4 for a variety of grid parameters (as indicated on the vertical axis). In this example the bandpass provided by the intermediate bandwidth "y" filter was used. Choosing grid parameters of 8 or larger caused no discernible difference in the intensity curves.

The model fitting procedure, which will be discussed, generally would use a grid parameter of 8, sufficient for all but the very largest sources. If the fitting procedure indicated a source larger than 5 milliseconds-of-arc, a re-fit was attempted using the roughly determined parameters and a finer grid parameter.

In order to determine the appropriate spectral width to use in discretely modeling an observed optical passband, model intensity curves were generated for sources of 0, 5, 10, and 20 milliseconds-of-arc with a grid parameter of 20. Each of these were "observed" with a Johnson V filter whose bandpass was modeled in spectral regions of 500, 200, 100, 50, and 10 Angstrom widths. In all cases 50 Angstrom steps across the bandpass were required to achieve a worst case precision of 0.05 percent.

<u>The Effects of Instrumental Optical Response</u>

The instrumental response of the optical system affects the measured spectral energy distribution of the source, and

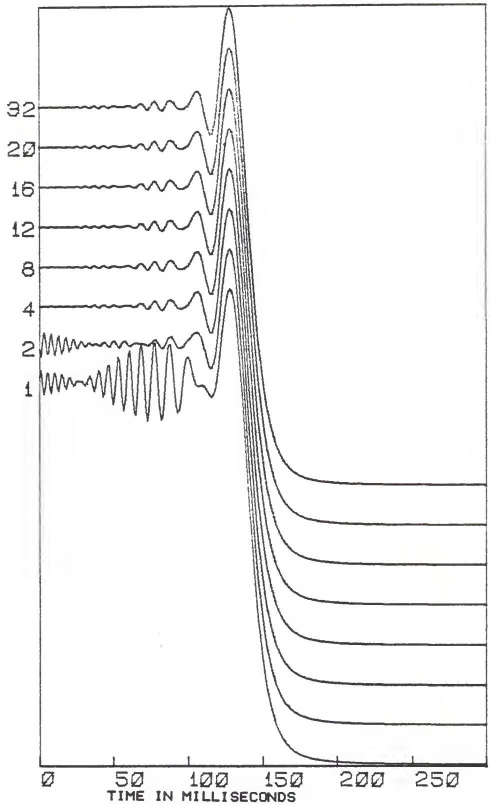

Figure 3-6. The effect of discrete modeling on a 10-millisecond-of arc curve for the grid parameters indicated.

hence must be included in the formation of the model intensity curve. Thus, the relative power in each spectral region from the source, $E_i(\lambda_i)$, computed by Equation 3-7 must be modified by the instrumental response function. The intensity of light measured in a wavelength regime contributes fractionally to the light passing through the integrated bandpass for a given filter. Tables of instrumental response, reflecting the filter function for each of the filters actually used in the observations, were constructed for this purpose. The model un-occulted intensity of the blackbody source, I_i, in a given spectral region, λ_i, corrected for the instrumental response is simply

$$I_i(\lambda_i) = E_i(\lambda_i)R_i(\lambda_i) \qquad [3\text{-}8]$$

where $R_i(\lambda_i)$ is the fractional wavelength-dependent instrumental response. The resulting intensity response function, $I_i(\lambda_i)$, is then normalized such that $\Sigma I_i(\lambda_i)=1$. It is these normalized intensity values which must be used in computing the wavelength dependent intensity curve.

The Polychromatic Extended Source Intensity Curve

The monochromatic point source intensity, F(U), given by Equation 3-1 is a one-dimensional, time-dependent function (since the value of X, the geometrical shadow-to-observer distance is time dependent). A polychromatic intensity curve for an extended source is a three dimensional analog of the one dimensional case, the resultant curve being the linear superposition of intensity weighted curves computed over three variables. The first variable is time, as in the simple case of F(U). The second is spatially dependent upon the angular separation of the strips in the intensity weighted stellar grid. The third is wavelength dependent upon the spectral energy distribution of the adjusted spectral energy distribution.

Computing a net polychromatic curve for an extended source is quite computationally extensive. For example, consider the generation of an intensity curve over 200 milliseconds, with intensity points 1 millisecond apart (scaled in Fresnel space). If a grid parameter of 8 is employed then a grid of 256 points must first be computed. Intensity weighting this grid for limb darkening and summing along the linear axis after replicating quadrants (by applying spherical symmetry) reduces the grid to 16 points. These 16 points must be evaluated for each of the 200 milliseconds under consideration. If the polychromatic model is to span the complete response bandpass of a Johnson V filter in 50 Angstrom steps, then an additional 53 values for each of the 3200 computed points must be determined. This amounts to 640,000 values to be calculated prior to weighting and summation in order to determine the net curve.

Models of Double Stars

Before considering the modeling of occultation intensity curves for double stars, a fundamental distinction must be drawn between binary systems which are widely spaced and those which have small angular separations of the components. Because of the millisecond of arc resolution achievable through the analysis of lunar occultation observations. the more conventionally held concepts of "wide" and "close" binaries are not applicable. In the context of discussing occultation binaries the term "close" does not necessarily refer to contact, or semi-detatched systems. Rather. the reference here is to the apparent angular separation of the components. Occultation binaries which are considered "wide" undergo disappearances which are well separated in time. Specifically, if the intensity curve resulting from the the disappearance of the first star has essentially converged to its post-occultation level before any significant fringing effects are seen due to the disappearance of the second star, then the system is considered "wide". Typically, wide occultation binaries are separated by more than 50 milliseconds of arc. Widely separated double stars (in this sense of the definition) present no additional complications in modeling occultation intensity curves. The disappearance of each star (once detected and noted), can be modeled independently, as their respective intensity curves are not overlapping.

The component stars in close occultation binaries, on the other hand, undergo disappearances closely spaced in time. The observed intensity curve arises from the linear superposition of the diffracted intensity variation for both component stars. Hence the model curve for close double stars is formed by computing the individual curves for the component stars and linearly superimposing them (along with a constant sky background).

A model intensity curve computed for close occultation binaries (referred to as the two-star case) uses the same filter and systemic response matrix, as well as background sky level for both stars. Individual stellar diameters. times of geometrical occultation, pre-occultation stellar intensities, and velocity parameters are employed. The velocity parameters, in principle, would be the same for both stars, if the lunar limb were smooth. However, since the lunar surface undulates, the contact points of geometrical occultation for the individual stars may have different slopes and therefore different projected angular velocities of lunar limb passage. If the individual spectral types of the component stars are known, then different effective photospheric color temperatures should be employed in computing the stellar spectral energy distributions.

The Differential Corrections (DC) Fitting Procedure

A Note on Time

The process of solving a lunar occultation intensity curve requires referencing the observed data points to a zero point in time. Though this time is arbitrary, by convention the time of geometrical occultation has been adopted. In terms of Fresnel numbers, times after geometrical occultation for a disappearance (i.e. when the observer is within the geometrical shadow) have negative values. Unfortunately, the time of geometrical occultation is unknown, and indeed is one of the parameters for which a solution is sought. Thus, throughout the fitting process times are referenced to the time of the first point in the observed data set. Units of time are referred to in milliseconds as this is most commensurable with the time-scale of the occultation phenomenon. All observations to which the fitting procedure has been applied have been made with 1-millisecond sampling. Thus, for convenience, the term "bin number" is often used interchangeably with "time with respect to data sample number zero". After the time of geometrical occultation has been found by the fitting procedure it is referenced to Coordinated Universal Time.

Choosing Initial Parameters for the DC Procedure

The fitting procedure is basically an iterative, non-linear least squares, differential corrections process following the method outlined by Nather and McCants (1970). Initially, a model curve is generated from physical quantities and model parameters listed in Table 3-5.

The choice of initial parameters in some cases is quite obvious. The number of points to be generated in the model must be the same as the length (i.e. number of data points) extracted from the 4096 milliseconds of observational data which is to be fit to a model curve. The selection of this extracted data set must be done by visual inspection, and roughly centering the subset on the apparent time of occultation. The specification of the filter response table

TABLE 3-5
PARAMETERS FOR GENERATING THE INITIAL MODEL

Model Generating and Controlling Parameters

1. The number of points to be generated in the model occultation intensity curve.

2. Specification of the filter/systemic response table.

3. Maximum number of iterations to executed in the corrections procedure.

4. Fraction of computed adjustments to be applied at each iterative adjustment step.

Fixed Physical Parameters

1. The topocentric distance to the lunar limb.

2. The predicted R-rate, based on a smooth limb (seconds of arc per second).

Normally Fixed Physical Parameters

1. The effective color temperature of the stellar photosphere.

2. The stellar limb darkening coefficient.

Adjustable Parameters

1. The stellar angular diameter.

2. The pre-occultation intensity of the star plus the background skylight.

3. The velocity of lunar limb passage.

4. The time of geometrical occultation.

5. The post-occultation intensity of the background skylight.

must obviously match the instrumental set-up used in obtaining the observational data.

The next two parameters are concerned not with the initial model generation, but with control of the adjustment procedure. The number of iterations required for a convergent solution depends strongly on the signal-to-noise ratio of the observations. Experimentation with the numerical and computational processes suggests that a maximum of 10 to 20 iterations is usually sufficient. The fraction of computed adjustments will be discussed in the section on the application of partial parametric adjustments.

The fixed parameters have already been addressed. In principle, there is no reason why the two parameters listed as "normally fixed" could not be treated as adjustable parameters as well. However, the model is rather insensitive to the effects of limb darkening, and as previously indicated stellar temperature (within the normal accuracy determined from the spectral type, and if available luminosity class). Unless there is an astrophysically compelling reason, a limb darkening coefficient of 0.5 is suitable in virtually all cases.

The stellar angular diameter, unless previously determined by another occultation, or in rare cases by interferometric methods, is unknown. As already mentioned an initial guess can be made on the basis of the star's parallax and spectral type, or by application of the Barnes-Evans relation. However, an initial guess of a "middle-of-the-road" value such as 5 milliseconds-of-arc will be adjusted rather quickly even if grossly wrong.

The initial guess for the velocity of lunar limb passage should be the R-Rate, as any variation from the predicted rate would be due to a local slope of the lunar limb. This slope, in fact is derived from the difference between the predicted and observed velocities. The numerical procedure actually works with a linear, rather than an angular rate. Thus the lunar limb distance is used in conjunction with the R-Rate to compute the L-Rate, the linear rate of the motion of the geometrical shadow across the telescope in units of meters per millisecond.

Initial values for the pre and post-occultation intensities can be determined by averaging the intensity of a few hundred milliseconds of data before and after the time of geometrical occultation. The time of geometrical occultation can be estimated from visual inspection of the observed intensity curve.

Parametric Adjustment

Once an initial model curve is computed, each of the adjustable parameters in turn is varied by a small percentage in order to numerically compute the partial derivatives of the intensity curve with respect to each of the parameters. Analytic evaluation of the partial derivatives is obviously impossible as the intensity curve itself is determined from discrete numerical functions. Due to different degrees of sensitivity of the intensity curve to numerical variation of the parameters, and indeed to the values of the parameters themselves, experimentation was required to ascertain an optimal percentage variation to use. This would present no problem if an analytic form for the computation of the derivatives existed. Choosing a variation which is too small results in computational truncation errors and discontinuities in the partial derivatives. Too large a variation results in a loss of computation precision. It was found that for most ranges in the values of the parameters that a numerical variation (multiplicative factor) of 1.001 was applicable for the intensities and time of geometrical occultation. The partial derivative of the intensity curve proved better behaved with a variation of 1.005 for the velocity parameter, and 1.02 for the stellar diameter.

Since the diameter can go to zero for a point source, numerical limits must be put on the variation procedure to assure no computational singularites arise. This is also true, conceptually for the velocity parameter as well (and in the unrealistic case of no background sky contribution the post-occultation intensity). However, this would be important only for true grazing incidence which is virtually never seen. Hence, as the angular diameter or the projected velocity (or both) approach zero the variation of these parameters in computing the numerical partial derivatives should be increased accordingly.

Once the partial derivaties have been computed a matrix of residual equations of the form

$$O_j - C_j = \sum_{i=1}^{n} \frac{\delta C_j}{\delta P_i} \Delta P_i \qquad [3\text{-}9]$$

can be established. The P_i's are the varied parameters, n is the number of parameters in the model (normally 5), the C_j's are the computed intensity values, and the O_j's are the observed values. The ΔP_i's are the adjustments to be applied to each of the parameters. These adjustments are determined by solving the residual equations by the method of least squares and is discussed in a general formulation by Brown (1955).

Eichhorn and Clary (1974) have suggested that when the adjustment parameters derived from non-linear equations of condition are not significantly larger than the adjustment residuals, then the second order terms should be included in the adjustment residuals. However, as can be seen, Equation 3-9 has been linearized, and hence does not include higher order terms to represent the non-linear equations. This was done primarily for a practical reason. The numerical evaluation of the first derivatives of the non-linear, non-analytic equations alone is already computationally extensive. The actual computer time required to arrive at a solution is discussed in the section on computational procedures. The additional computations required for the inclusion of the higher order terms in the solution were computationally prohibitive with the computer resources available.

As a result of this linearization the derived adjustments are not completely correct. Thus, the adjustments must be applied to the parameters, and the process repeated until convergence is achieved. Fortunately, the least squares process is sufficiently robust that convergent solutions (with less than 1 percent change in successive adjustment attempts) were usually achieved for all parameters in less than a dozen iterations of the adjustment procedure.

The DC Fitting Procedure for Close Double Stars

A procedure analogous to the single star DC fitting process previously discussed is followed in the case of a close double star. In this case, refered to as the DC2 procedure, if the limb darkening coefficients of the stars, and photospheric temperatures are held constant, then the model is parameterized by nine adjustable quantities. These are listed in Table 3-5 as "Adjustable Parameters" numbers 1 through 4 (for each star) and the background skylight intensity (item 5). Hence, Equation 3-9 is the same as in the single star case, with $n=9$ instead of $n=5$.

The choice of initial parameters for the two-star fitting procedure is similar to that of the single star case, though "good guesses" for the starting values of some parameters are more difficult to select than for the fitting of a single star model. Since the observed curve is actually the linear combination of the two single star curves, the approximate times of geometrical occultation and the individual pre-occultation stellar intensities are not easily determined by visual inspection. Though the DC procedure is quite forgiving for even wildly disparate initial parameters, the required computation time for convergence can be reduced by giving some thought to the starting parameter selection.

To serve as a guide to selecting the initial time and intensity parameters, a family of model curves was generated for a series of monochromatic double stars considered as point sources. The curves covered the range of stellar separation in Fresnel space from U = -2.5 to U = +2.5 in steps of 0.2, and a range of magnitude differences of 0.0 to 2.5 in steps 0.5 magnitudes. By comparing these against the observed intensity curve, a reasonable match could usually be found. The parameters used to generate the selected model curve were then applied to the particular two-star DC solution under consideration.

The task of generating the simple monochromatic two-star models from point sources was relegated to a desk-top microcomputer (Commodore SP9000). The computation of the Fresnel intensity curves (Equation 3-1), by the numerical integration of the Fresnel integrals (Equations 3-2a and b), and the production of the 306 graphs of the two-star intensity curves required 25 hours. However, this only had to be done once, and a compendium for future guidance in parameter selection was created. Figure 3-7 is a sample of a

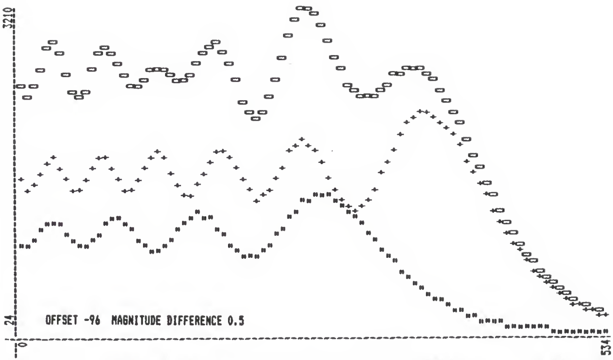

Figure 3-7. Linear superposition of two monochromatic point source curves separated by U=-0.96. The sources differ in brightness by 0.5 magnitudes.

two-star curve extracted from this compendium. In this case the star which disappeared first is the fainter star (by 0.5 magnitudes), and leads the brighter star by -0.96 Fresnel units. The individual curves, as well as the composite curve, are shown.

Validation of the Fitting Procedures

To validate the fitting procedures (and check on the function of the computer programs, which are discussed in Chapter 4), a number of model intensity curves were generated, treated as observations, and subjected to the fitting process. The model curves which served as synthetic observations were generated with a very fine grid of 4096 points. All the synthetic observations were created assuming a lunar distance of 375,000 kilometers, a stellar temperature of 4500 degrees Kelvin, and an R-Rate of 0.3 seconds of arc per second. Both monochromatic (5500 Angstoms) and polychromatic model curves were synthesized. The latter were modeled under the bandpass of a Johnson-V filter, with discrete spectral regions only 20 Angstroms wide.

For single stars, diameters of 0, 8 and 20 milliseconds of arc were considered. Double stars models used all combinations of 0, 8 and 20 milliseconds of arc with temporal separations of 2 and 20 milliseconds. The synthetic curves were subjected to the DC and DC2 procedures, respectively. The fitting programs employed a grid parameter of 8, and in the polychromatic cases each spectral region within the V filter bandpass was 50 Angstroms wide. The initial parametric guesses for the adjustable parameters were deliberately chosen to be far from the correct values. In every case the DC fitting process converged rapidly (in three to five iterations) to the correct values in all the adjustable parameters. The same, unfortunately, could not be said for the nine parameter DC2 fitting procedure. The DC2 process would usually recover the synthetic model parameters, but only after many (often greater than thirty) iterations. Worse, however, was that on several occasions the adjustment process would either fail to converge to a solution, or fall into a local minimum in parameter space, unreflective of the true parameter set. This was a problem that had to be addressed.

While these tests showed that the numerical (and computational) processes were indeed correct, they were overly optimistic as indicators of the the ease of recovering the parameters of the synthetic curves, both in terms of the formal errors attached to the solutions, and the small number of iterations required (for the DC procedure). This overoptimism resulted from the fact that observational noise (due to both seeing effects and scintillation) were not included in the initial synthetic models.

The effects on the DC and DC2 procedures from the introduction of noise to the synthetic observational curves were then considered. Synthetic noise could have been generated stochastically. However, this would have required making assumptions about both the distribution function (in terms of relative amplitudes) of the noise, and the temporal variation in the stochastic noise on time-scales shorter than the length of the synthetic data set. Rather than make such assumptions, noise which was actually observed, as extracted from a pre-occultation observational record, was applied to the synthetic curves.

The character of the observational noise would be different for each observed occultation, and in fact is a function of the local seeing and scintillation effects and photometric signal-to-noise ratio (as will be discussed in Chapter 5). Thus, ideally, it would have been preferable to consider all of the above synthetic cases under a variety of observed noise conditions. However, due to the limited system throughput on the computer employed in this investigation, a compromise had to be made.

The noise characteristics of the occultation observation of ZC0835 were found to be nicely representative in terms of the noise figures and power spectra seen in most of the observational records. The distribution function of the observational noise obtained from this observation was applied to the synthetic models, and the noisy models then re-reduced by DC and DC2, with the same initial starting parameters used in the first trials.

Once again, the model parameters were essentially recovered; however, three effects were noticed. First, and somewhat expected, the formal errors of the solution were significantly worse than in the "clean" synthetic cases.

Second, the number of iterations required for the DC model to converge was increased by roughly a factor of four. And third, for the corresponding trials where DC2 solutions were previously obtained, the DC2 procedure would not asymptotically converge to recovering the solution parameters. Rather, after initial movement toward convergence, oscillation about some set of final values would set in. The amplitudes of these oscillations were often as great as 100 percent of the mean values about which the parameters were oscillating. This effect was also seen, but to a much smaller degree, in the DC solutions.

While this behavior (except for the recalcitrant DC2 solutions) was not unacceptable it lead to a number of numerical experiments in an attempt to improve the basic DC and DC2 fitting procedures.

Numerical Experiments to Improve the Fitting Procedure

Two types of improvements were sought to enhance both the utility of the fitting procedures and the statistical significance of the numerical results. First, from a practical standpoint, it was desired to reduce the amount of computation time required to achieve a convergent solution. Second, the DC procedure, (and usually DC2 as well), could successfully recover the physical parameters intrinsic to the intensity curve in question; it was of interest to see if the formal errors of the solution parameters could be reduced.

Addressing the first point, it was noticed that the fitting process would approach convergent solutions rather rapidly in most cases. But, on occasion, rather than smoothly approaching the true parametric values (i.e., those used to generate the synthetic curves), the numerical values of the adjustable parameters would oscillate about some undetermined, final values. This effect was usualy small for the five parameter DC fitting process but often was quite pronounced for the nine parameter DC2 routine.

Since the residual equations had been linearized, as previously discussed, the adjustments applied at the end of each iteration step tended to overcompensate for the fact that the higher order terms had been omitted. Thus, as the solution was approached, the adjustments to the parameters computed from the residual equations would overcorrect the interim values of the adjustable parameters, and thereby lead to the noted oscillations.

The uppermost set of graphs in Figure 3-8 shows the progress of the DC fitting process as the adjustable parameters approached their final values through twenty iterations of parametric adjustments. From left to right the parameters presented are the angular diameter, pre-occultation intensity, post-occultation intensity, time of geometrical occultation and L-Rate. The correct values (those used in generating the synthetic curve) are indicated by the dashed lines. This example is from the DC fitting of an 8 millisecond of arc star, with observational noise added to the synthetic curve as specified in the previous section.

Figure 3-8. An example of the convergence of the DC fitting process applied to "noisy" data for twenty iterations. The set of graphs labeled "A" correspond to the solution obtained using full parametric adjustments. The "B" and "C" graphs were obtained with a partial adjustment factor of 0.5. The "B" solutions were from a fit to the raw data, while the "C" solutions were from a fit to data which were Fourier smoothed. The dashed lines are the true intrinsic parametric values. The thin vertical lines represent a 1 percent variation from the true values, except in the case of the angular diameter where these lines show 50 percent variations. The thick vertical lines represent the one sigma uncertainties in the solution parameters.

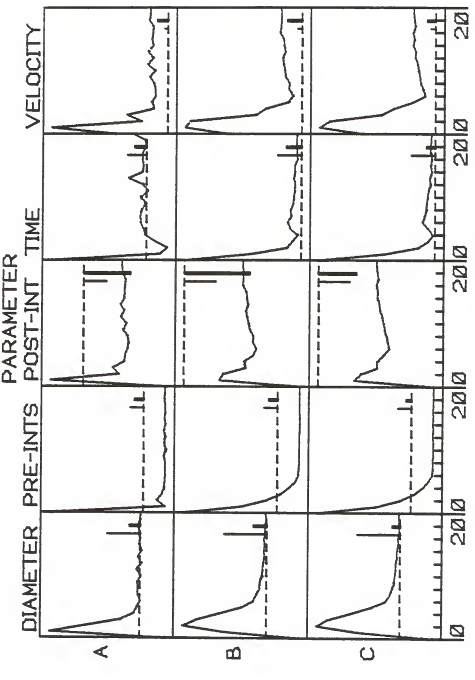

PARAMETER
DIAMETER
PRE-INTS
POST-INT
TIME
VELOCITY
A
B
C
0
20
ITERATION NUMBER

In this case, the noise was taken from the residual amplitude distribution function for the occultation observation of ZC1221 (see Figure 5-19). The mean value of this distribution function is skewed negatively by 1.706 percent. (The physical reasons for this skewing, and the Poisson character of some of the observed residual distributions are addressed in Chapter 5.)

The negative bias (or offset) in the noise was not corrected before application to the synthetic curve. Hence, there was an expectation that the pre-occultation and post-occultation intensities would be underestimated, and the L-Rate overestimated by this amount. This expectation was indeed borne out, within the one sigma uncertainties of the final parametric solution values.

The model generating parameters, and parameters for the best solution determined by the DC procedure, are presented in Table 3-6. The table indicates that the best solution, as determined by the smallest value of the sum of the squares of the residuals, was achieved on the fourteenth iteration. The parenthetical values are the one sigma uncertainties in the formal errors of the solutions. It should be noted that while the best solution required fourteen iterations, after only four iterations the interim values for all the adjustable parameters were not significantly different from the later determined best parametric solutions.

<u>Application of Partial Parametric Adjustments</u>

To reduce the degree of oscillation about the finally determined values of the solution parameters, the DC process, starting with the same initial values, was run again with one minor change. Rather than applying the full corrections derived from the linearized residual equations, only partial corrections were made at each iteration step. The initial tests of the partial corrections procedure applied a fractional correction factor, denoted ξ, of 0.5 (i.e. only half of the computed adjustments were applied to each of the interim values of the parameters at the end of each iteration step. If the adjustments at the end of each step had been absolutely correct (which they were not) then the solutions would be approached asymptotically. In that case, after n-iteration steps the current value of a given parameter, P_i, would be

$$P_{i,n} = P_{i,s} + [(1 - \xi^n)\cdot(P_{i,0} - P_{i,s})] \qquad [3\text{-}10]$$

where $P_{i,0}$ is the initial guess for the i^{th} parameter, and $P_{i,s}$ is the true value of the i^{th} parameter.

Thus, after ten iterations the interim solution parameters would converge to better than 0.1 percent of their true values. Of course, ξ need not be given a value of 0.5. If a larger value is used the true parameter values are approached more quickly, but larger amplitude oscillations set in after initial convergence has begun.

The middle set of graphs in Figure 3-8 shows a typical historical run of the solution parameters with a partial adjustment of $\xi = 0.5$. As may have been expected, the best solution was obtained on the last iteration. By that time, however, the variations in the parameters from one iteration to the next were insignificant. Table 3-6 shows that the parametric solutions obtained for the DC fitting with partial adjustments (ξ=0.5) were essentially identical to those obtained using the full parametric adjustments (ξ=1.0). This was found to be the case for the fitting of all other synthetic curves as well.

As a result of this numerical experiment a new procedure was adopted in the differential corrections process. Full parametric adjustments were made at each correction step until oscillation of the parameters began to show up. It was found that an increase in the sum of the squares of the residuals was a good indicator of the onset of oscillation. After that, only fractional adjustments (ξ<1.0) were applied.

Parametric Grouping into Computational Subsets

The application of partial parametric corrections to the DC2 procedure was quite successful in reducing the degree of oscillation of the solutions and obtaining convergent solutions for those cases where none were previously achieved. The number of iterations required to obtain acceptable convergence in the DC2 fitting process was greater than in the case of single star DC fitting, but not unacceptably so. This was expected, as the number of degrees of freedom had been increased by the inclusion of an additional four adjustable parameters. In principle, as long as the intrinsic parameters were recoverable, no further modifications to the DC2 process were required.

TABLE 3-6
COMPARATIVE SAMPLE OF DC FITTING TO SYNTHETIC CURVE

PARAMETERS FOR SYNTHETIC INTENSITY CURVE

Distance (km):	375000	Diameter (ms. of arc):	8.0
# of Points (msec):	200	Time (milliseconds):	101.0
Temperature:	4500	Pre-Event Intensity:	1495.4
Limb Darkening	0.5	Post-Event Intensity:	498.5
Filter:	Johnson V	L-Rate (meters/s.):	545.4
Grid Parameter:	8		

METHOD OF DC SOLUTION

Smoothing	Raw	Raw	150 Hertz
ξ	1.0	0.5	0.5

SOLUTIONS

Iterations	14	20	20
Diameter	8.10 (1.28)	8.12 (1.28)	8.10 (0.75)
Time (msec)	101.2 (0.65)	101.2 (0.65)	101.2 (0.38)
Pre-Event	1471.3 (10.3)	1471.2 (10.3)	1471.2 (6.3)
Post-Event	489.4 (10.4)	489.2 (10.4)	489.2 (6.1)
Velocity	572.8 (18.6)	571.4 (18.8)	572.6 (10.7)

It was of interest, however, to evaluate a computational procedure discussed by Wilson (1976), and to determine its applicability to fitting lunar occultation intensity curves by non-linear least squares, differential corrections. In determining his solution to the light curve of the eclipsing binary TX UMa, Wilson encountered similar difficulties. The approach he suggested, of dividing the adjustable parameters into two subsets which were adjusted independently, was tried. When coupled with the procedure of using only partial parametric adjustment, this parametric subgrouping method was found to yield convergent solutions, but not as rapidly as by adjusting all nine parameters simultaneously.

The variations in the methods of DC2 fitting were compared by attempting solutions to a variety of synthetic curves. Table 3-7 is an example of the comparative results obtained after twenty iterations of an illustrative case studied. The synthetic parameters for generating the two-star model curve are given in the table. This was a case for which full parametric adjustment ($\xi=1.0$) in the DC2 fitting process could yield no convergent solution. In both cases shown where the Wilson method was tried (for $\xi=0.5$ and $\xi=1.0$) the process was still heading toward convergence where the DC2 process, with $\xi=0.5$, had already obtained convergent solutions. As can be seen, after 20 iterations, the formal errors of the solution parameters are much better in the case of partial adjustments with the DC2 procedure. Figure 3-9 (similar to Figure 3-8) shows the history of the

TABLE 3-7

COMPARATIVE SAMPLE OF DC2 FITTING TO SYNTHETIC CURVE

PARAMETERS FOR SYNTHETIC INTENSITY CURVE

Distance (km):	375000	Diameter Star 1	5.00
# of Points (msec):	201	Diameter Star 2:	10.00
Temperature Star 1:	4500	Intensity Star 1:	1000.00
Temperature Star 2:	5000	Intensity Star 2:	800.00
Limb Darkening (1 & 2):	0.5	Time Star 1:	90.00
Grid Parameter:	8	Time Star 2:	101.00
Iterations:	40	L-Rate Star 1:	400.00
Monochromatic, 5500 Angstroms		L-Rate Star 2:	545.41
		Sky Background:	400.00

INITIAL PARAMETRIC "GUESSES" (STARTING VALUES)

Diameter Star 1:	8.262	Diameter Star 2:	0.206
Intensity Star 1:	1200	Intensity Star 2:	500
Time Star 1:	95	Time Star 2:	105
L-Rate Star 1:	500	L-Rate Star 2:	600
Background:	600		

SOLUTIONS

Method ξ	Grouped 1.0	Grouped 0.5	Ungrouped 0.5
Diameter 1	6.40 (0.14)	6.48 (1.08)	5.00 (0.00)
Diameter 2	6.98 (0.18)	6.8 7 (0.21)	10.00 (0.00)
Intensity 1	1166.5 (11.1)	1176.6 (141.7)	1000.00 (0.00)
ntensity 2	631.6 (7.2)	629.1 (7.0)	800.00 (0.00)
Time 1	91. (0.4)	91.3 (1.5)	90.00 (0.00)
Time 2	103.7 (0.1)	103.9 (0.2)	101.00 (0.00)
L-Rate 1	392.2 (2.7)	391.7 (10.1)	400.00 (0.00)
L-Rate 2	494.0 (2.0)	489.4 (2.4)	545.41 (0.00)
Background	394.5 (8.8)	394.1 (2.4)	400.00 (0.00)
Comment:	Rejected	Rejected	Accepted

Note: No convergent solution for ungrouped, ξ=1 case.

Figure 3-9. An example of the convergence of the DC2 fitting process applied to synthetic data for twenty iterations. The set of graphs labeled "A" correspond to the solutions obtained using full parametric adjustments. The "B" and "C" graphs were obtained with a partial adjustment factor of 0.5. The "B" solutions were from a fit via the parameter grouping method, while the "C" solutions were obtained by adjusting all parameters simultaneously. The dashed lines are the true intrinsic parametric values.

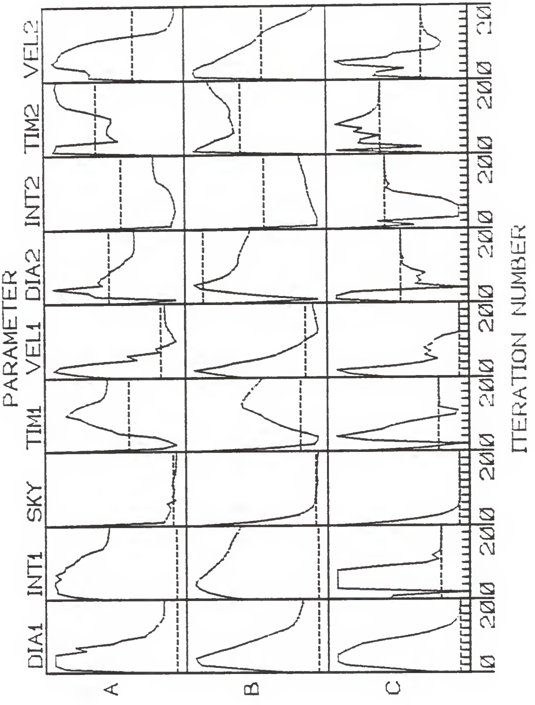

PARAMETER
DIA1
INT1
SKY
TIM1
VEL1
DIA2
INT2
TIM2
VEL2
A
B
C
ITERATION NUMBER
0
200

interim solutions for these three cases. Similar results were seen in all the synthetic trials considered.

Uniqueness of the Solution

The iterative differential correction process cannot absolutely guarantee, in a rigorous sense, that the set of solution parameters obtained is unique. To verify that the set of solution parameters is correct one must first confirm that they are physically meaningful, within the context of the observation. Clearly, solutions with astrophysically improbable implications (i.e. stars with diameters of hundreds of milliseconds of arc, or negative lunar L-rates), must be viewed with obvious suspicion and rejected. Fortunately, such occurences have been found to be very rare.

Meyer (1975) states that while a mathematically rigorous statement of the uniqueness of the solution is not possible, reasonable certainty in the validity of a set of solution parameters can still be obtained. If the parameters are indeed physically meaningful, the non-linear differential corrections procedure should be re-run several times with initial guesses of the adjustable parameters of widely differing values in parameter space. If the adjustable parameters converge to the same solution, then one can be quite confident that the solution has not been misguided by being "stuck" in a local minimum in parameter space.

This seems to exact the penalty of having to repeat the computational process several times. This however, is not necessarily true. Quite often, after only one or two iterations of subsequent runs of the DC or DC2 procedures. with widely differing starting values, it is apparent that the parameters are being adjusted toward the same final values.

The basic DC method was adopted for the initial iterative adjustments in the case of single stars. The application of partial parametric corrections were employed in the two-star DC2 fitting process and in the the final iteration steps for the DC single star fitting procedure. The validity of the solutions was checked by multiple runs of the initial corrections steps with very different starting values.

Smoothing of the Observational Data

As previously mentioned, the second area where improvements to the basic fitting procedure seemed possible was in obtaining more realistic error estimates of the solution parameters. The formal errors of the solution parameters were derived from the variance-covariance matrix of the final set of residual equations. These errors reflect the magnitude of the squares of the residuals. If the residual amplitudes were smaller, then the error estimates would have been tighter as well.

Observationally, this problem is addressed by trying to improve the signal-to-noise ratio. This can be done by rejection of erroneous background light through a good optical baffle (see Chapter 1) and selection of a filter well suited to the spectral energy distribution of the star under study. Once data are acquired, the characteristics of the noise in the raw observational record are fixed; however, this does not preclude the possibility of the raw data being preprocessed before being submitted to the fitting procedure. The question which naturally arises is: can the data be preprocessed in such a manner as to effectively improve the signal-to-noise ratio, without degrading the underlying occultation record itself?

The time scale of variation of an occultation intensity curve is typically 10 to 50 milliseconds. This suggests that some type of time dependent smoothing might be applied to the data, which were acquired at a pair-averaged rate of one sample per millisecond. To see if this inference was indeed true the previously generated synthetic intensity curves, with noise added as before, were subjected to several different smoothing algorithms. The smoothed, synthetic observations were then re-fit by DC and DC2, as appropriate to the model in question.

N-point unweighted smoothing. Each of the synthetic curves previously considered was first smoothed by a simple N-point unweighted moving average. Values of N=3 and N=8 were considered, corresponding to sampling frequencies of 330 and 125 Hertz respectively. This method of smoothing has the advantage of reducing the effect of spurious single-sample values within the smoothing window, at the expense of losing information associated with level transitions which are fast compared to the smoothing length.

The application of N-point smoothing to the synthetic intensity curves resulted in solutions determined by the DC and DC2 procedures that were significantly worse in some of the parameters than those obtained in the unsmoothed trials. In every case the angular diameters of the stars were overestimated. In the case of 8-point smoothing, the determined angular diameters were typically too large by factors of 2 to 5. The times of geometrical occultations were shifted, by a smaller degree, to times earlier than used in generating the synthetic models. The L-rate was consistently low, but only to a small degree; however, the formal error attached to the determined L-rate in some cases was even worse than in the unsmoothed trials. Only the recovery of the true values of the pre-occultation and post-occultation signal levels were unhampered by N-point smoothing. Since the determination of the primary parameters of astrophysical interest (the stellar angular diameter, and time of geometrical occultation) were impeded by N-point unweighted smoothing, this approach was deemed untenable.

N-point weighted, exponential smoothing. At this point, the idea of applying a moving average to the observed (or synthetic) data was not yet abandoned. A weighted moving average was used to smooth the set of trial synthetic (noisy) curves. The weighting function chosen was an exponential in order to provide a numerical analog to observationally increasing the time constant of the instrumental system. The electrometer amplifier employed (see Chapter 1) uses a passive filter network to set the 1/e folding time of the amplifier response. Hence, investigating the use of an exponentially decaying weighting function would mimic the effect of observing with various instrumental time constants.

To be commensurable with the trials attempted in the investigation of unweighted smoothing, decay constants were chosen to provide an effective FWHM in the smoothing function of 330 and 125 Hertz. The results of the DC and DC2 fitting were similar to, though not quite as bad, as fitting to the data which were smoothed with the unweighted functions. Here, too, the effect of increasing the smoothing width resulted in an overestimation of the stellar angular diameter.

Both N-point smoothing techniques proved unusable as methods to preprocess the data in an attempt to reduce the residual amplitudes. These smoothing methods, however, were useful in the visual inspection of the observed intensity curves. It is difficult for the eye to see structure in noisy data, and N-point smoothing helped bring out details which would otherwise would have been visually obscured. Figure 3-10 is a 200 millisecond extract from the observing record of the occultation of ZC1222, centered roughly on the time of geometrical occultation. Eight-point (125 Hertz) unweighted smoothing was applied to these data, and the smoothed curve is superimposed on the raw data.

Smoothing by forward and inverse Fourier transformation. Since the background noise was superimposed on the synthetic (and observational) data, the simple N-point smoothing

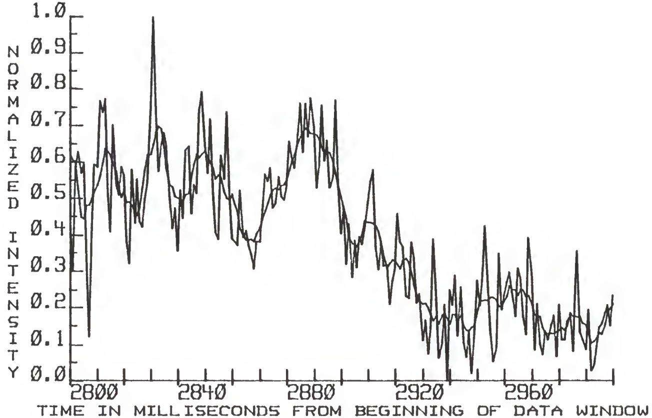

Figure 3-10. Eight-point unweighted smoothing applied to the occultation observation of ZC1222.

algorithms acted with equal effect in not only smoothing out the noise, but the underlying occultation intensity curve as well. What was needed was a method of smoothing only the background noise, while leaving the character of the intensity curve itself effectively undistorted.

Examination of the raw occultation data records seemed to indicate that the temporal characteristics of the variation in background noise were, generally, quite a bit faster than the 10 to 50 millisecond time-scale of variation typical of the intensity curves. This implied that a numerical analog to active low-pass filtering of the data might improve the effective signal-to-noise ratio and subsequently the statistical certainty of the recovered solution parameters.

To see if this implication was true, the power spectra of synthetic "clean" intensity curves had to be compared with the power spectra of actual observed background noise. Several additional synthetic curves were generated and Fourier transformed into the frequency domain. In addition to the synthetic curves already available, point source and 10 milliseconds of arc sources were modeled applying the spectral response of the intermediate bandwidth "y" (as well as the Johnson-V) filter which would actually be used in the observations. The synthetic curves consisted of 1024 data points, evenly spaced in time by one-millisecond. Actually, 2048 data points, spaced one-half millisecond apart were generated and pair averaged to model more appropriately the implemented data acquistion scheme. The length of these synthetic data sets allowed the examination of their power spectra up to a frequency of 512 Hertz.

Figure 3-11 shows three representative power spectra. Only the first 150 integral frequency components (roughly up to 150 Hertz) are shown. At frequencies higher than this, the power spectra continue to smoothly decay. The amplitude of the power contributions for each of the frequency components has been normalized so that the total power associated with all frequency components up to 512 Hertz is unity.

It was found that as either the source diameter or the spectral bandwidth of the optical filters was increased, the power contributions of the higher frequency components diminished. More importantly, in every case, the power associated with the frequency components higher than 150 Hertz contributed less than 0.001 percent to the total power of the intensity curve. The power spectra scale in frequency linearly with the R-rate. The power spectra shown were for R-rates of 0.3 seconds of arc per second, which is a typical value for most occultations.

Examination of the power spectra of the pre-occultation star+sky intensity (shown for each event in Chapter 5) show that, in general, at frequencies above about 150 Hertz the background noise dominates the observational occultation records. But, in almost all cases, at low frequencies it is the signature of the occultation curve itself which is

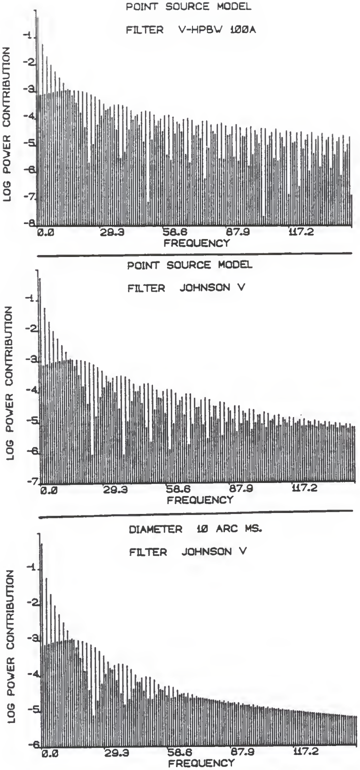

Figure 3-11. Power spectra of three representitive synthetic occultation intensity curves.

dominant. This is exemplified quite nicely in the comparative power spectra shown for the occultation of ZC0835 (Figure 5-124). These findings were significant. They implied that better DC solutions might be obtained by subjecting the observational data to Fourier smoothing. Here, Fourier smoothing means transforming the raw data into the frequency domain, removing the high frequency components characteristic of only the background noise (i.e. greater than 150 Hertz), and inversely transforming the frequency-truncated data back into the spatial domain.

Whenever such transformations are applied, careful consideration must be given to the inverse transformation process. Since these numerical transformations do not operate on infinite data sets, spurious results can be obtained due to edge effects. The endpoints of the transformed functions (i.e. ends of the observational data sets) appear as discontinuites in the numerical functions, and often cause "ringing", or high frequency oscillation, to be seen in the re-transformed data. This effect can be seen in Figure 3-12. The upper curve shows the synthetic curve of a 10 millisecond of arc star observed with a Johnson-V filter. This is the curve whose power spectra is shown as the bottom graph in Figure 3-11. The "ringing" effects of inverse transformation, after the high frequency components have been removed from the data in the frequency domain, are shown in Figure 3-12.

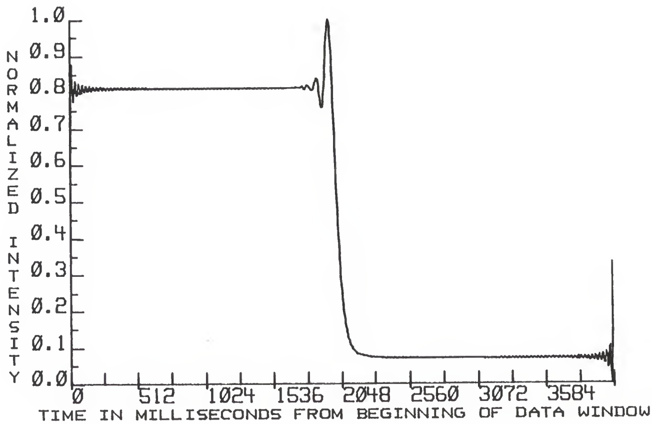

Figure 3-12. An example of "ringing" brought about by the inverse transformation of a finite Fourier smoothed data set.

The "ringing" effects due to data windowing are often effectively suppressed by the judicious application of an apodizing function, as discussed by Bracewell (1965). In practice, however, the intensity curves fit by the DC and DC2 processes are small subsets of the observational data (typically 200 milliseconds out of 4096). The ringing effects, which are pronounced near the ends of a transformation window become unimportant near the middle of the data window (as exemplified by Figure 3-12). Hence, if 200 data points are to be fit by the DC or DC2 procedure, 1024 data points, roughly centered on the time of geometrical occultation are Fourier smoothed. The data to be fit are then extracted from the Fourier smoothed intensity curve.

This process of Fourier smoothing was applied to all of the aformentioned synthetic curves, for which DC and DC2 solutions had already been obtained. In every case the parameters intrinsic to the synthetic curves were recovered with virtually identical values, but with significantly tighter error estimates. The last set of entries in Table 3-6 reflects this for the DC solution of a Fourier smoothed "noisy" synthetic curve of an 8 millisecond of arc star.

The technique of Fourier smoothing was adopted as a viable data preprocessing method to improve the statistical significance of the solution parameters. This method was not applied blindly, but rather was used in conjunction with the more conventional technique of fitting to the raw data. If cases had arisen where fitting to smoothed and unsmoothed data from the same observation yielded significantly different results, further investigation would have been needed. Fortunately, in all the observations reduced and analyzed this problem never arose.

CHAPTER IV
COMPUTATIONAL DATA REDUCTION PROCEDURES

A Choice of Programming Languages: The APL Decision

The data uploading and preprocessing programs, data reduction algorithms, graphics display software, and all numerical experimentation employed in this investigation were implemented and carried out in APL. APL, an understatedly modest acronym for A Programming Language, is a powerful algebraic notation which was invented by Iverson (1962). An interpreter for this notation was developed by International Business Machines and first released as programming product XM/6 (Falkoff and Iverson, 1968 and 1970), more commonly referred to as APL\360. Since that time, numerous releases of APL interpreters and translators have become available for virtually every mainframe and mini-computer as well as for quite a few microcomputers. Brenner (1982) has recently developed an operating philosophy for a version of APL which would be executable in the parallel processing environment realized in the new generation of "supercomputers".

APL is a concise and totally self-consistent implementation of an array algebra, and is capable of dealing with multidimensional arrays with far greater ease than most other notations and computer languages can deal with simple scalar quantities. A rich variety of intrinsic (referred to as primitive) functions enable easy array manipulation. A number of operators which act on the primitive functions create, in effect, new functions and enhance the power of this notation dramatically. In addition, APL allows for the creation of "user defined functions" extending the scope of its inherent capabilities only to the limits of the imagination of the user. Excellent treatments of APL as a computer language, including the practical limitations of the notation as implemented on finite machines, are addressed by Pakin and Polvka (1975) and by Gillman and Rose (1974).

It has been found by Schneider and Brown (1976) that the time required for program development and debugging in APL is typically ten to twenty-five times less than in FORTRAN or similar languages. This same study notes that the number of actual lines of "program code" required to carry out equivalent tasks in APL and FORTRAN is reduced by at least the same amount, and in exceptional cases by as much as one hundred times. Furthermore, the transportability of APL programs from one computer to another is accomplished with a degree of success far in excess of any other computer language. A pro-forma APL standard presented by Falkoff and Orth (1979) has been almost universally agreed upon and was adhered to assiduously in the course of this investigation. The most novel aspect of APL is perhaps the notion that the expression of a problem in APL notation is its solution. No extraneous statements heavily laden with arcane syntax as required by virtually all other computer languages are needed. Given the above, the decision to employ APL in the numerical computations and associated data processing in this project was an easy one to make. It remains a mystery to this investigator why any researcher involved in data processing would make any other choice.

The discussion of the algorithms developed for the solution of lunar occultation intensity curves refers both to the APL functions which have implemented these algorithms (Appendices C, D, and E) and to the underlying equations which have already been presented. This duality in presentation is made to guide the reader unfamiliar with APL notation to an understanding of both the overall data reduction scheme and the computer programs.

Downloading and Uploading of Observational Data

Once the observational data are saved as a contiguous memory image on a CODOS disk file, these data must be transferred to the computer which will be used to perform the computational data reduction. The numerical computations performed on the observations during the course of this investigation were carried out, for the most part, on four mainframe computers. Warner Computer Systems, Inc. (New York) provided access to their Xerox Sigma-9 computer where the initial computational algorithms and basic reduction procedures were developed and tested. A small amount of numerical experimentation was carried out on the Northeast

Regional Data Center's Amdahl 470/V6 and IBM 4341. The latter was done when the MVS operating system was first established and computing was free for a limited time. The majority of computing and the final reduction of all observations was done on the Harris-500 computer operated by the University of Florida's Center for Intelligent Machines and Robotics.

The process of moving data from CODOS disk files onto any of the above mainframes was accomplished by a data transfer program called OCCTRANS. This program (listed in Appendix B) is a 6502 machine language program written to run on a SPICA-IV system equipped with an RS-232 serial port. A SPICA-IV computer, similar to the SPICA-IV/LODAS with the addition of a 6850 asynchronous communications adapter interface (ACIA), which also serves as a backup system for the RHO SPICA-IV/LODAS, was used for this purpose. The communication protocols in terms of baud rates, number of start and stop bits, parity, character prompting, and handshaking are different for each of these machines. As a result OCCTRANS must be modified slightly to establish the proper communications interface for different mainframe computers. The version of the OCCTRANS program listed in Appendix B is for communication with the HARRIS-500 computer.

This program converts the CODOS file which contains the file header and three channel data buffers to ASCII before it is sent to the mainframe computer. Data are transferred in blocks whose size is appropriate to the length of the input buffer on the receiving computer. Data are received directly into APL via a very simple receiving program called READ, given in the listing of the APL workspace OCCPREP (Appendix C). The OCCTRANS and READ programs "talk" to each other, handshaking and transferring the data. The data, once transferred into the APL OCCPREP workspace, exist as a text vector of length 37376.

This vector is then submitted as the right argument to the function TRANSLATE. TRANSLATE unpacks the ASCII representation of the 12-bit observing data and header information and stores this information as global variables in the workspace. The variables CH1, CH2, and CH3, each numeric vectors of length 4096, hold the contiguous intensity readings taken on each of the three data channels. These data have been "unfolded" from each channel's circulating buffer so that the first element in each vector is the first sample taken in the wraparound data windows. The time and date of the last data sample, the "foldpoint" (sample pointer to the position of the last sample taken in the circulating buffer), and the last comment entered by the observer before saving the data to CODOS disk are also saved in the workspace. The function TRANSLATE and subordinate functions are shown in the OCCPREP workspace listing.

The Occultation Reduction Workspace (OCCRED)

The APL workspace OCCRED (OCCultation REDuction) listed in Appendix D contains the complete set of functions and global variables needed to reduce a lunar occultation observation. This workspace listing should be consulted in order to elucidate the discussion of the computational procedures which follow.

Global Variables Used by OCCRED

Parameters for the reduction run of the occultation solution are established interactively by the function INPUT. INPUT is monadic and takes as a right argument the global vector of raw observational data (i.e. CH1, CH2, or CH3) created by the function TRANSLATE. The entry of each parameter is prompted for conversationally, and on completion INPUT leaves the established parameters as global variables in the active workspace. A convention of using underscored variable names for parameters passed globally between APL functions is used throughout this and other supporting APL workspaces. Table 4-1 lists the global variables created by INPUT and briefly describes their content. The listing of the function INPUT should be consulted for the physical units of the numerical values. The use of these variables is addressed in the explanation of the differential corrections procedure.

Typically, a maximum of about 250 points (except in the case of very low R-Rates which occur for occultations of near-grazing incidence) is appropriate. The global variables listed in Table 4-2 also reside in the OCCRED workspace and are required by the differential corrections procedure. The names of the filter response matrices are the only global variables employed whose names are not underscored. The FREN vector is explained in the discussion of the FRESNEL function.

TABLE 4-1
GLOBAL VARIABLES CREATED BY THE APL FUNCTION INPUT

Name	Shape	Type	Description
BIN	Scalar	NUM	Estimated Bin Number of Geometrical Occultation.
COMN	VAR	TEXT	Any Applicable Comments of Special Note
DATE	VAR	TEXT	U. T. Date of the Observation
FILT	VAR	TEXT	Name of Filter Matrix to Use
LIMS	2 6		Parametric Limitation Matrix, First Row Are Upper Limits, Last Row are Lower Limits, Values are Limits for PV Elements [6] to [11]
NAME	VAR	TEXT	Name or Catalog Number of the Star
OBS	VAR	NUM	Subset of Observational Data to be Used
PV	14	NUM	The Parameter Vector Indexed as follows: [1] Central Wavelength of Passband [2] Lunar Limb Distance [3] Number of Observation Points Extracted for Solution. [4] Effective Stellar Temperature [5] Square Root of the Number of GRID Points per Stellar Quadrant [6] Stellar Angular Diameter [7] Pre-Event Signal Level [8] Post-Event Signal Level [9] Time of Geometrical Occultation [10] L-Rate [11] Limb Darkening Coefficient [12] Maximum Number of Iterations for DC [13] Spectral Width of Filter Matrix [14] Fraction of Adjustments to Apply

Notes: An Index Origin of 1 is used in this table.
VAR indicates a variable length vector.

TABLE 4-2
GLOBAL VARIABLES RESIDENT IN THE OCCRED WORKSPACE

Name	Shape	Type	Description
NARROWV	5,2	NUM	"y" filter fractional response, normalized, 100 Angstrom steps
VFILTER	53,2	NUM	Johnson V filter fractional response, normalized, 50 Angstrom steps
VFILT	6,2	NUM	Johnson V filter fractional response, normalized, 500 Angstrom steps
NARROWB	5,2	NUM	"b" filter fractional response, normalized, 100 Angstrom steps
BFILTER	42,2	NUM	Johnson B filter fractional response, normalized, 50 Angstrom steps
BFILT	5,2	NUM	Johnson B filter fractional response, normalized, 500 Angstrom steps
FREN	4001	NUM	Diffraction intensity values ordered in decreasing Fresnel units

The Computational Differential Corrections Procedure

The primary function, which sets up and controls the flow of program logic for the solution of occultation intensity curves, is the differential corrections routine called DC. Minor modifications to DC can be made prior to its execution depending upon the nature of the parametric model. For example, the limb darkening coefficient of the stellar atmosphere can be treated as a free parameter. As noted earlier, however, in most cases the model is rather insensitive to changes in limb darkening; hence, it is usually held fixed. Because of the relatively long amounts of CPU time required for computation, "fine-tuning" of the DC procedure to fit the needs of a given observation is felt warranted. A general computational approach may seem more aesthetically pleasing from a programming point of view but is somewhat less efficient computationally. Fortunately, the interactive nature of APL allows variations in the basic DC procedure to be implemented without any special effort. Indeed, alternate execution paths through DC and several subordinate functions are realized by simply turning certain executable statements into comments and vice-versa.

Several global variables are created in the process of determining the occultation solution. In most cases these globals provide information on the solution after completion of the reduction run. A few computational parameters are passed between functions by global variables (though in most cases variables are passed as functional arguments).

The DC solution, in its basic form, is passed the parameter vector as an argument called P. DC[3] begins by establishing two global variables and one local variable. As execution proceeds, the variable <u>SOLS</u> accumulates the adjusted parameter vectors after each iteration step. When execution of DC is completed, <u>SOLS</u> provides an historical record of the various parameter combinations used at each step on the way to arriving at the final solution. The variable <u>SSE</u>, similarly, is an historical record of the sum-of-squares of the residuals from the O-C's after each correction step. DI is a vector containing the fractional variation to be applied to each of the parameters in numerically computing the partial derivatives of the intensity curve. The index position of each entry in this vector corresponds to the index position of the associated parameters in PV. As an example, the intensity curve is fairly insensitive to a small variation in stellar diameter for small diameter sources, hence, DI[6] is typically assigned the moderately large value of 1.02.

DC[4] sets up the iteration counter ITER and the parameter variation control vector CVEC. The first element in CVEC, at any time, determines which parameter is to be varied next in the corrections process. DC[5] computes the spectral response function, R. This response function, corresponding to Equation 3-8, is dependent upon both the spectral energy distribution of the source and the instrumental spectral response function. In order to compute the spectral energy distribution of the source Equation 3-7 is evaluated by the function BBDY.

BBDY takes two arguments. The right argument, L, is a two element vector. L[1] specifies the blackbody temperature, and L[2] specifies the number of terms (i.e. width of each spectral region in Angstroms) to be used in the numerical integration of Equation 3-7. The left argument, W, is a vector giving a list of wavelengths for which the blackbody function is to be computed. BBDY normalizes the integrated blackbody function and returns a vector conformable in length to W, whose elements give the fractional contribution to the total blackbody power distribution function for the wavelength regions evaluated.

The arguments passed to BBDY are computed by DC[5]. The temperature is taken from the local parameter vector P[4] and the spectral width computed from the first difference of the wavelength specifications of the first two entries in the filter matrix specified by FILT. The wavelengths for evaluation are taken directly from the same filter matrix. After the blackbody distribution function is computed, each wavelength regime is attenuated by an amount representing the filter function also given by the FILT matrix. The modified spectral energy distribution function is the spectral response function, R.

The model strip brightness distribution of the projected quadrant of the stellar disc, as previously discussed, is computed in DC[6]. The computation of the non-limb-darkened grid, which represents surface elements on the stellar disc, is handled by the function GRID. GRID takes a scalar right argument specifying the square root of the number of grid points to be computed for each quadrant on the model stellar disc. DC[6] is passed this value from the parameter vector. GRID carries out the analytic solution (Equation 3-5) for the integration of Equation 3-4 for each projected surface element. The result is a normalized matrix where each element gives the fractional brightness contribution of a projected surface element in the grid coordinate system whose origin is centered at the upper right corner of the matrix, as shown in Figure 3-2. Only one quarter of the stellar disc is computed, as spherical symmetry is assumed.

The stellar grid is then limb darkened by the function LDARKEN. LDARKEN takes two arguments. The right argument is the stellar grid quadrant as computed by GRID. The left argument is the limb darkening coefficient to be applied. The linear limb darkening law given in Equation 3-6 is applied. The limb darkened quadrant is renormalized and passed as the resulting matrix.

Since spherical symmetry is assumed, the hemispherical strip brightness distribution is computed by DC[6] by doubling the values and summing the matrix along the last coordinate axis. Again applying symmetry, the vector resulting from the previous step when rotated and concatenated onto itself yields the total strip brightness distribution. The normalized limb-darkened strip brightness distribution is stored in the variable S̲.

DC[7], labeled L0, is the entry point for the outer iterative loop of the differential corrections procedure. This point is re-entered after all parameters have been varied and parametric corrections have been applied to all parameters on the basis of the partial derivatives of the residual matrix. DC[5] establishes a matrix, X, which will hold the numerical partial derivatives of the intensity curve.

DC[8] calculates the computed intensity curve on the basis of the current parameters in P. To do this, the normalized polychromatic intensity curve must be computed from the linear superposition of monochromatic curves. This is carried out by the function WIDE.

WIDE takes two arguments. The parameter vector is passed as the right argument. The left argument, R, is the previously computed spectral response function. WIDE first calculates the individual monochromatic curve (as an approximation to each spectral region), then sums these curves. The normalized monochromatic curves, which are dependent upon the stellar diameter, velocity parameter and limb darkening coefficient, are computed prior to summation by WIDE[6]. In the case where the limb darkening coefficient is not held constant, the stellar grid brightness distribution must be recomputed at this step. Then WIDE[5] would be "uncommented" and the variable S recomputed in the same manner as it had been in DC[6].

The computation of the series of normalized monochromatic curves which eventually forms the polychromatic curve is carried out in Fresnel space. Thus, the parameters given in physical units of kilometers, milliseconds-of-arc, Angstroms and so on, are converted by the function FNOS into Fresnel numbers. At each step through the iterative WIDE function, one monochromatic curve is computed. FNOS takes as its right argument the parameter vector with the first element replaced by the wavelength, in Angstroms, of the particular monochromatic curve sought in the current iteration step. FNOS returns a matrix of Fresnel numbers corresponding to the points of evaluation in time and space for the wavelength and parameter vector specified. The columns of this matrix correspond to the strip segments, S, uniformly separated in space in accordance with the stellar diameter and number of strips. The rows of the matrix correspond to the temporally separated points determined from the data acquisition rate (i.e. one millisecond per point) and the velocity parameter. The zero point references are the center of the stellar disc for the columns, and the time of geometrical occultation for the rows.

It is a simple matter to compute the normalized diffraction intensity for a given Fresnel number by numerically integrating Equations 3-2a and 3-2b and applying Equation 3-1. If this were done for each pass through the WIDE function, both the Fresnel sine and cosine integrals would each have to be numerically integrated approximately 50 million times for a typical DC solution. This is, needless to say, prohibitive. Rather, the diffraction intensities, as a function of Fresnel numbers, in the range of Fresnel numbers from -20 to +20 were computed by the function FRESNEL once and stored as a global vector called FREN in the workspace. FRESNEL performed the numerical integration by rectangular approximation to a precision of approximately one part in 5000. Diffraction intensities are stored in FREN in serial order starting with the intensity for a Frenel number of -20 and incremented by 0.01.

Once the Fresnel numbers are computed by FNOS, the corresponding intensities are found by linear interpolation of the FREN vector by the function NPOL. The right argument of NPOL is the array of Fresnel numbers and the result, conformable in shape to the argument array, is an array of corresponding intensities. It was found that simple linear interpolation would produce values correct to one part in 2000 in the worst case.

The matrix product of the intensity array with the strip brightness distribution yields the normalized monochromatic curve. WIDE[6] then applies the response function for the wavelength evaluated to each point in the curve and accumulates a sum of successive curves. The iterative process is completed when all spectral regions have been computed. The execution of WIDE results in a normalized intensity curve with the spectral response function included.

It should be noted that, in principle, WIDE could have been defined non-iteratively; however, the amount of memory space required was far in excess of that available.

DC[8] scales the polychromatic wideband curve for the parametric value of the signal level (in counts) and adds the parametric value of the sky background. The model curve is then stored in the global variable COMP and subtracted from the selected subset of the raw observations, OBS, to obtain the residuals which are stored in the local variable Y. The sum-of-squares of these residuals for the iteration just completed (or from the initial parametric guesses in the case of iteration zero) is accumulated in the variable SSE as part of the iterative solution history. The current local parameter vector P is saved in a vector of tentative solutions called SOL.

It may be noted that DC[8] displays both the current parametric values and the sum of the squares of the errors of the just completed iteration step. This output, in general, is somewhat superfluous. However, the Harris-500 computer on which most computations were performed was unreliable and often would crash before a DC run would go to completion. Having this information displayed periodically allowed the procedure to be restarted after the computer was brought back up. At that time, the last iteration values which had been displayed were used as new starting parameters.

The inner iterative loop labeled L1 is entered at DC[9]. During the process of computing numerical partial derivatives of the intensity curve, numerical singularities may occur for domains in which the intensity curve is insensitive to variation of a particular parameter. This problem is particularly acute as the angular diameter of the star approaches zero. Hence DC[9] determines what value of dD (variation in diameter) should be used in computing the numerical partial derivative dI/dD. The values were chosen after some computational experimentation. For source diameters less than 1-millisecond of arc, a variation factor of 1.4 is used in the source diameter. Sources larger than 1-millisecond of arc but less than 2-milliseconds of arc have their diameters varied by a factor of 1.2. Sources larger than 2-milliseconds of arc but less than 3-milliseconds of arc are varied by a factor of 1.08, and sources with any angular diameter larger than this are varied by 2-percent.

DC[10] begins the process of parametric variation and adjustment. CVEC is rotated by one to point to the successive parameters in each pass through the L1 procedure. The parameter is then varied by the amount specified by DI and resaved back in the P vector. In order to prevent further numerical singularities due to the finite computational precision of the computer, the varied parameters are never allowed to be fuzzed to zero but are limited to a minimum value of 10^{-12}.

DC[11] recomputes the intensity curve in the same manner as DC[8] using the varied parametric value. The initial model curve, COMP, is subtracted from this resultant curve and the residuals stored in the vector D.

DC[13] computes the partial derivative of the intensity curve as a function of the just-varied parameter. Each partial derivative, as it is computed, is saved as a column in the matrix X. The P vector is restored to its previous value which was tentatively retained in SOL. The variation procedure and computation of partial derivatives is continued until all the parameters whose adjustments are sought have been handled.

In the case where a previous DC run resulted in a particularly recalcitrant solution (i.e. divergent, or non-convergent through oscillation) the parameter grouping method previously discussed may be employed. In this case partitioning of the adjustment set, as suggested by the commented DC[12], may be executed in place of DC[13] (with appropriate alterations to DC[15]). Here only a subset of the parameters (two or three in a five parameter model) are varied at a time before the L1 process is completed.

The adjustment procedure is terminated by DC[14] when the number of iterations reaches the maximum set in the parameter vector. When this occurs the termination procedure, labeled L2, is executed.

Once all the partial derivatives under consideration in the current iteration of the L1 procedure have been computed, the adjustments to the parameters are found by DC[15]. A least squares fit of the form given by the Taylor series in Equation 3-9 is performed, and the adjustments are applied within the constraints allowed by the limitations matrix, LIMS, to the parameters in the P vector. The amount of adjustment to the parametric values is determined by P[14]. An initial run would have P[14]=1, while a final solution would probably have a smaller value of P[14], (e.g., 0.5).

The iterative solution history accumulated in the variable SOLS is updated by DC[16] and the next iteration of the L0 procedure entered.

The L2 procedure at DC[18] is entered on completion of all iterations through the L0 loop. The solution history giving the iteration number, ranking of the solution in terms of the sums-of-squares of the residuals and the successively tried parameter vectors are displayed.

The variance/covariance array of the final adjustments, computed from the residual vector Y, and the partial derivative matrix X are computed by DC[19]. The standard errors of the estimates are found from the variance/covariance array, and displayed. The algorithms for these computations are taken from Smillie (1976). The DC function concludes by assigning the last partial derivative matrix to the global variable <u>PDER</u>. On completion DC leaves a number of global variables in the workspace reflecting the final solution and the history of the DC run. A summary of these variables is given in Table 4-3.

In most cases the last iteration has the lowest ranking, that is, it is the solution which has the smallest sum-of-squares of the residuals. If the variations in successive solutions were small, so that near-asymptotic convergence had been reached, then no further execution is required.

The last iteration, however, need not produce the lowest ranked solution. Meyer (1975) points out that non-linear least squares solutions are not necessarily monotonic. In this case the best solution should be extracted and DC re-executed with an iteration maximum of zero specified in

TABLE 4-3
GLOBAL VARIABLES CREATED BY THE APL FUNCTION DC

Name	Shape	Type	Description
COMP	PV[3]	NUM	Computed Intensity Curve
COV	5 5	NUM	Variance/Covariance Matrix for the Last Adjustments Made by DC
ER	5	NUM	Standard Errors of the Estimates
PDER	PV[12],5	NUM	Partial Derivatives of the Computed Intensity Curve
SOL	14	NUM	Last Adjusted Parameter Vector Used by DC
SOLS	1+PV[12],14	NUM	Solutions Matrix, a Chronological History of Successively Adjusted Parameter Vectors
SSE	1+PV[12]	NUM	Chronological History of the Sum-Square-Errors of OBS-COMP for Successive COMP's Generated.

the parameter vector. If the DC procedure is not invoked directly, but controlled by the function START, then this is done automatically. This is normally done in all reduction runs.

The solution history must be examined to determine if the last computed set of parameters is sufficiently near convergence as to not require any further adjustment. This evaluation is left to human judgement rather than to a preprogrammed algorithmic decision. If it is desired to continue the DC process then the best solution may be extracted from SOLS and these parametric values used in establishing a new PV. DC may then be re-executed with the adjusted parameters as the new starting values. It may be desirable to reduce the iteration maximum on subsequent runs of DC.

The DC procedure will attempt to fit any data presented to a model occultation curve. Thus the raw observed data may be preprocessed before being submitted to DC without any variation in the operation of the computational DC procedure. This was done in the numerical experimentation performed to evaluate the effects of removing high frequency components in the observed data by foward and inverse Fourier transformation, as well as applying simple N-point and exponential and smoothing to the observational data.

The Two-Star Differential Corrections Procedure (DC2)

Global parameters for DC2. The APL function DC2 is a two star analog to DC. The numerical procedures discussed in Chapter 3 have been implemented and are carried out by DC2. Where DC was defined monadicaly, DC2 is defined dyadically. The right argument is a parameter vector, identical in shape and analagous in content to that which would be passed to DC. This parameter vector, PV, would hold the initial parametric guesses for one of the component stars (arbitrarily referred to as star 1) in the two-star system. Here, the pre-event signal level PV[7], is the out-of-occultation signal level of the first star only. The post-event signal level, PV[8], refers to the background sky level, not the star 2 plus sky level.

The left argument passed to DC2 is a similar parameter vector, which will be denoted PV2, and holds the parameter specifications for the second star. The shape and content are similar to PV with a few minor exceptions. The pre-event signal level, PV2[7] refers to the out-of-occultation signal level of star 2 only. PV[8] is an unused element in the parameter vector, as the background sky level is assumed constant throughout the event. Therefore, the background sky level specified for star 1 is used for star 2 as well.

Some of the elements in PV2 are redundant, as they are identical to those in PV (i.e., the lunar limb distance, number of data points extracted for solution, etc.). Structuring PV2 in a manner similar to PV, however, allowed the same previously defined subordinate functions to be employed with no modifications.

The APL function INPUT2, listed in Appendix D, is used to interactively establish the two parameter vectors used by DC2. In addition to the global variables created by the APL function INPUT (see Table 4-1), INPUT2 creates the variables PV[2] and LIMS2. The latter of these is the parametric adjustment limitations matrix for star 2, and has the same arrangement of elements as the LIMS matrix.

The APL function DC2. The function DC2, given in Appendix-D, was developed from DC and has a great resemblance to the one-star function. The variable names and algorithmic procedures, where applicable, were retained from the DC function and include the second star. Variables related to star 2 have names which are postfixed with a "2": P2, DI2, R2, X2, SOLS2, and SOL2. They have the same meaning in algorithmic context as the related variables for star 1.

As can be seen, the structure and content of DC2 resembles DC closely. The version of the DC2 function shown retains the capability of either using the Wilson parameter grouping method or solving for all nine parameters simultaneously. The function as shown uses the latter approach. To implement the parameter grouping method those function lines which are preceded by double comment symbols should be uncommented and those lines which are followed by double comments should be turned into comments.

The function shown here defines the same strip brightness vector, S (on DC2[7]), to be used for both stars. If different limb darkening coefficients or grid parameter specifications are desired for the two stars, a separate strip brightness distribution, S2, for star 2 should be computed as well. This information must be passed to WIDE which currently uses S for computing the model intensity curve. The simplest approach is to create a function identical to WIDE, called WIDE2, which refers to S2 instead of S. WIDE2 would then be called, instead of WIDE, in the computation of the polychromatic model curve for star 2.

The interim model for the two-star (with sky background) curve, and the two individual one-star curves (under adjustment) which comprise it are computed by function lines DC2[9], DC2[14], and DC2[20], respectively. These are equivalent to DC[8] and DC[14] in the one-star case.

The adjustment procedure has been partitioned into two sections labeled L1 and L1B. L1 handles the variation of the model parameters of star 1 for the numerical computation of the partial derivatives. L1B is the same for star 2. In L1B, PV2[8] is skipped as it does not enter into the model. In the usual fitting process, the labeling of L1B has no significance as it is not a line that is entered conditionally. If the parametric grouping code is activated, however, this becomes an entry point for the parametric adjustment of the subset of parameters associated only with star 2. In that case, the computation of the adjustments after the computation of the partial derivatives for each star is handled by DC2[16] and DC2[17], respectively.

After the iterative adjustment process is completed, DC2 concludes in the same manner as DC. Four additional columns are added to the historical synopsis matrix <u>SOLS</u> (defined on DC2[29]) which are not present on the <u>SOLS</u> matrix created by DC. These contain, for each iteration, the interim values of the adjustable parameters for star 2. The variance/ covariance array, <u>COV</u>, is a 9-by-9 matrix, rather than a 5-by-5. Similarly, the vector of error estimates of the solution parameters, <u>ER</u>, is of length 9. These two variables are computed on DC[30]. The 9 column matrix, <u>PDER</u>, contains the numerical partial derivatives of each of the parameters evaluated for every point of observation.

Preprocessing of the Observational Data

Before submitting the raw observational data to either DC or DC2, Fourier smoothing (as discussed in Chapter 3) may be applied. The dyadic APL function FTSMOOTH carries out the Fourier smoothing. The raw observational data, stored globally in the workspace under the name CH1, must be resident. The right argument is a two element vector. The first element is the bin number of the time of geometrical occultation. In the case of a one star event the variable BIN, created by INPUT, should be used. For a two-star event the mean of BIN and BIN2 is more appropriate. The second element is the number of points centered on the specified time to be included in the Fourier smoothed data set. The left argument, a scalar, is the cutoff frequency (in Hertz) used in the Fourier smoothing. FTSMOOTH will store the result in the global variable OBS since the smoothed data is to be treated by DC or DC2 as if it were raw observational data.

FTSMOOTH uses the subordinate functions FFT and FFTI. These functions, listed in Appendix E, are also resident in the APL workspace OCCPLOTS and are discussed in Chapter 5.

Presentation of the Results of the DC Run

The APL function OUTPUT, coresident in this workspace, produces a formatted report detailing computational results of the occultation solution. The information presented by OUTPUT was transcribed for presentation in the section describing the observational results. OUTPUT makes use of the global variables created by both INPUT and DC. The information presented by the OUTPUT function is listed in Table 4-4.

The APL function OUTPUT2 produces a similar report for the results obtained from a DC2 fit. In addition to the information presented for DC fitting, the parameters and derived quantities salient to the two-star model are given. These additional items are listed in Table 4-5.

A number of APL functions have been assembled to present a graphical depiction of the solution and other salient information relating to the fitting process. These functions are discussed in detail in Chapter 5.

TABLE 4-4
INFORMATION PRESENTED BY THE APL FUNCTION OUTPUT

General Information

1. Name of the star
2. U. T. Date of the occultation
3. Any significant comments to head the output

Input Parameters

1. Central wavelength of the passband (Angstroms)
2. Topocentic lunar limb distance (kilometers)
3. Effective photospheric color temperature (Kelvins)
4. Limb darkening coefficient

Model Parameters

1. Number of data points used in the solution
2. Number of grid points on the model stellar grid
3. Number of discrete spectral regions modeled
4. Width of each of the spectral regions (Angstoms)
5. Number of iterations of the DC adjustment procedure

Solutions

1. Stellar angular diameter (milliseconds-of-arc)
2. Bin number of geometrical occultation
3. Pre-event (star-plus-sky) signal level (counts)
4. Post-event (limb-plus-sky) signal level (counts)
5. Observed lunar shadow velocity (kilometers/second)
6. Predicted lunar shadow velocity (kilometers/second)
7. Local slope of the lunar limb (degrees)

Statistics of the Solution

1. The variance/covariance matrix
2. The correlation matrix
3. The sum of the squares of the residuals
4. Sigma (one standard error)
5. The normalized standard error
6. The photometric (Signal-plus-Noise)/Noise ratio
7. The (Change in Intensity)/Background Intensity
8. The change in magnitude

Tabulation of the Observation and the Solution

1. Time from start of solution subset (milliseconds)
2. Observed Intensity (counts)
3. Computed Intensity (counts)
4. Observed-Computed Intensity (counts)

TABLE 4-5
TWO-STAR QUANTITIES PRESENTED BY THE APL FUNCTION DC2

Solutions
1. Stellar angular diameters for each of the components
2. Bin numbers of geometrical occultation for each star
3. Intensity (in counts) of each star
4. L-Rate determined for each component
5. Local limb slopes at the contact points
6. Background sky intensity
Derived Quantities
1. Temporal separation of the stars
2. Intensity-weighted mean L-Rate
3. Projected spatial separation based on:
a) Predicted R-Rate
b) Determined weighted-mean R-Rate
4. Brightness ratio of the components
5. Magnitude difference of the stars

CHAPTER V
THE OCCULTATION OBSERVATIONS AND RESULTS OF THEIR ANALYSIS

Presentation Format

To facilitate the discussion of the occultation observations and the results of their subsequent analysis, the observations, their solutions, and related information are presented in both tabular and graphical form. The order of presentation is chronological, based on the time and date of the observations, beginning with the occultation of ZC0916 (1 Geminorum).

Format and Content of the Tables

The occultation summary table. A synopsis of each event is presented on a table referred to as an occultation summary table. Table 5-9 is an example of an occultation summary table. Each of these tables, headed by the name of the occulted star is divided into six sections. The first of these sections, labeled "Stellar and Observing Information", conveys both the primary characteristics for classifying the star and information with regard to the instrumental configuration employed while making the observation. The primary reference given for the star is either its Robertsons' (1940) Zodiacal Catalog (ZC) number or United States Naval Observatory (USNO) Extended Catalog (X) number. The Smithsonian Astrophysical Observatory (SAO), Bonner

Durchmusterung (DM), and other pertinent catalog numbers or star names are also given. Following these are the Right Ascension and Declination of the star, precessed to the equinox and equator of the date of observation. Also listed are the star's apparent V magnitude, spectral type, and luminosity class (if known). The instrumental specifications include the filter (designated V, B, "y", or "b"), the diaphragm (designated by the letter codes given in Table 2-3), the amplifier gain setting, and the PMT voltage.

The second section, labeled "Lunar Information", presents the lunar geometry and characteristics which are unique to each occultation event. These data refer to the time of geometrical occultation. The percentage of the lunar disc illuminated (by area) as seen at RHO is given first. This is followed by the moon's elongation from the sun and altitude above the horizon. The topocentric distance to the contact point of the lunar limb is given next. The predicted topocentric linear rate at which the lunar shadow crossed the observatory, and the apparent angular rate of the moon's limb relative to the occulted star are the last entries in this section.

The third section is labeled "Event Information". The U.T. date and predicted time of geometrical occultation are given first. This is followed by the USNO "Value" and "Observability" codes (V/O), as defined by Van Flandern (1973). The Hour Angle (HA) of the star at the time of the event, in units of degrees, minutes, and seconds is given next. A negative hour angle indicates a pre-transit event. The selenocentric geometry of the occultation, defined by the position angle, cusp angle, contact angle, and Watts angle, (Van Flandern, 1973) of the star concludes this section. Both the lunar and event information presented are derived from data supplied by Lukac (1983, and 1984).

The fourth section, labeled "Model Parameters", presents the fixed computational model parameters and assumed stellar characteristics used in the final differential corrections solution. Listed first is the number of data points (milliseconds of data) extracted from the observation data buffer that were used in the reduction. The number of grid points used to represent the stellar disc of the star, the number of discrete spectral regions employed to model the stellar blackbody function, the instrumental spectral response, and the width (in Angstroms) of those spectral regions are listed next. The instrumental spectral response function used in all cases corresponds to the filter employed. These response functions are given in Appendix D. The assumed stellar limb darkening coefficient and effective photospheric temperature (based on the star's spectral and luminosity classes) are the last entries in this section.

The fifth section, labeled "Solutions", shows the principal computational results obtained from the model fitting procedure. Each solution parameter also has its formal standard error presented alongside in parentheses. The stellar diameter (in milliseconds of arc), and time of geometrical occultation (in milliseconds) relative to the sample number of the first intensity point taken in the extracted observational subset used in the reduction, are given first. Listed next are the out-of-occultation intensity levels, in raw "counts" (with a full scale value of 4095), before and after the disappearance. The observed topocentric linear velocity of the lunar shadow and the lunar limb slope derived from this velocity are given next. If a decodable WWVB time signal was obtained for the occultation event, the Universal Time of geometrical occultation is presented and is the last entry in this section.

The sixth, and final section of the Occultation Summary tables, labeled "Photometric Noise Information", contains information useful in assessing the photometric quality of the sky during the event. The sum of the square of the residuals is given in raw counts, as is the standard error (Sigma) of the residuals. The absolute unscaled values of these numbers depend both on the number of samples used in the reduction and on the arbitrary full scale intensity value used. To aid in the intercomparison of different observations, a normalized standard error, adjusted for both the size of the data sample and full scale intensity, is also given. The signal-plus-noise to noise (S+N/N) ratio during the time of the observation subset is presented. Out-of-occultation, the S+N/N would be essentially constant over time intervals short enough not to affect the integrated transparency function of the sky.

The amplitude of scintillation noise, which is the dominant noise source for bright stars, varies linearly with the signal level. Scintillation noise affects only the intensity of the source and not that of the background sky. Photon shot noise, which varies as the square root of the intensity, is normally much less important in the observation of bright stars. Yet during an occultation disappearance the intensity of the source itself is diminished rapidly. The photon arrival statistics are even worse for fast photometry when the arrival time between photons can approach the sample interval. Fortunately, this is in the region of the occultation curve which is well into the asymptotic falloff and is insensitive to these effects.

The sky, however, is typically bright due to scattered moonlight. The noise statistics of this background tend to have a Poisson distribution. Henden and Kaitchuck (1982) discuss a method of observationally determining the noise associated with this background. Due to the stellar disappearance at the time of occultation the dominant noise source changes rapidly from being scintillation dominated Gaussian noise, to background dominated Poisson noise. Hence, the S+N/N ratio would also change. A proper computation of the S+N/N ratio must allow for the switchover in dominant noise sources, and in fact must consider both of them. The scintillation noise is easily measured, and the noise due to the background is determined as suggested by Henden and Kaitchuck (1982). The noise sources are then added in quadrature to determine the final figure presented as the S+N/N ratio.

The time-averaged sky background is, for the purpose of considering the noise sources in an occultation event, simply a zero offset. This offset level varies enormously for different events, depending on the lunar phase and the position angle of the event geometry. Thus, an indication of the quality of the degree of detection is the ratio of the change in intensity (the pre-occultation and post-occultation signal levels) compared to the background sky level. This ratio, listed in this section, is independent of the superimposed scintillation noise. This change in intensity, expressed as a stellar magnitude difference, is the last entry in an Occultation Summary table.

An additional section is inserted into the occultation summary tables, in the case of solutions of "close" binary stars. The derived quantities which are listed in Table 4-5 are presented in this additional section.

Variance-covariance, correlation, and dI/dP_i. The formal errors of the solution parameters, as listed in the occultation summary tables, are derived from the variance-covariance matrix of the residual matrix. In the case where high correlations exist between the model parameters, the formal errors of these parameters are often insufficient for judging the quality of the solution

(Bevington, 1969). This is the case for occultation observations where some of the physical parameters describing the occultation intensity curve have a high degree of coupling. The degree of coupling is a function of the scintillation noise, expressed as the photometric S+N/N, the dynamic range of the signal decrease (change in magnitude), and the timescale of the event (projected lunar velocity) in comparison to the data acquisition rate. Thus, the correlation between the parameters is of interest. The correlation coefficients indicate the degree of sensitivity of a solution parameter to a change in the other parameters. The variance-covariance and correlation matrices for the determined solution parameters are presented on tables of numerical and statistical significance. Table 5-6 is an example of this type of table.

As previously discussed, the regions of sensitivity to variation of the intensity curve with respect to changes in each of the parameters are reflected by the partial derivatives of the intensity curve (dI/dP_i). It is noted here, however, that while a list of the partial derivatives tabulated at each point of evaluation is too lengthy to present for each observation, the range of values for each of the partial derivatives are given at the bottom of these tables.

Observed and computed intensity values. A list of the actual observations, computed intensities, and their residuals, are also tabulated. The data presented on these tables are for the subset of observations used in the DC solution. As an example of this type of table see Table 5-6. The first entry corresponds to the first data point in the DC solution subset. These tables are organized in a vertical fashion, and are read from top to bottom within each column of figures.

Format and Content of the Graphs

The graphical representation of the occultations are also of a standard form and are produced by APL functions in the workspace OCCPLOTS listed in Appendix E. As may be seen, the generating functions employ subordinate functions to draw axes, labels, plot points, and perform similar tasks. These functions are not shown here but are discussed by Selfridge (1983). For clarity, each graph will be referred to by the name of its APL generating function. The information presented on each type of graph is discussed here.

Graph of the entire event, RAWPLOT. The first type of graph shows the entire 4096 milliseconds of acquired data for each event. These graphs are produced by the APL function RAWPLOT, an example of which is Figure 5-1. On each RAWPLOT the horizontal axis gives the time of each acquired data point, in milliseconds, relative to the time of the first intensity value (time 0000). The right hand vertical axis gives the actual number of recorded counts scaled from zero to 4096 for each millisecond of observed data. The left hand vertical axis indicates the counts normalized on a scale from zero to one. The plotting device used to draw these graphs (a Houston Instruments digital incremental plotter) has a resolution of 0.01 inches. Hence, trying to depict all 4096 points on the RAWPLOT would result in several retraces along each step in the horizontal direction. Thus, RAWPLOT displays only every fourth point (1024 in all) of the acquired data.

A cursory examination of a RAWPLOT will give a preliminary indication of the quality of the photometric data. The scatter in the data from point to point results from high frequency scintillation noise. Longer period variation in overall signal intensity comes about from the slower variation in the atmospheric transparency. The approximate time of geometrical occultation relative to time zero can be seen where the intensity data takes a sudden downward step. The relative amount of background light from sky and lunar limb brightness can be seen by noting the post-event intensity above the zero count level. The contribution to the total intensity due to the starlight is noted by comparing the intensity of the signal before and after geometrical occultation.

The integration plot, INTPLOT. The second type of graph, produced by the APL function INTPLOT, is an integration plot of the entire 4096 milliseconds of observed data. These graphs are typified by Figure 5-3. This type of plot was first suggested by Dunham et al. (1973), and may be used to examine the occultation record for evidence of stellar duplicity. The mean intensity taken over all observed data points is computed and this mean is then subtracted from each observed point. A running sum is then produced from this difference. When plotted against time, a single star disappearance will ascend to a maximum and descend back to zero. A double star, however, will give itself away by the presence of a change in slope in the ascending or descending branches of the curve. Some such detections, as in the case of 1 Geminorum, are obvious. If, however, the second star is of considerably lesser brightness, the detection might be quite subtle, as is evidenced in the INTPLOT of ZC0126. In these cases the change in inflection can be enhanced by choosing a subset of the data, centered on the time of disappearance of the suspected second star to be processed by the INTPLOT function over a shorter time interval. Several of these shorter INTPLOT figures have been generated and included.

Graphic depiction of the best fit, FITPLOT. Graphs such as Figure 5-13, generated by the APL function FITPLOT, each show the best theoretical fit to the observation for the subset of contiguous data points used in the reduction. This fit is superimposed on the observed data. The bottom horizontal axis, as in the case of RAWPLOT, gives the time in milliseconds relative to time zero. The recorded counts are once again presented on the right hand vertical axis. The left hand vertical axis has been normalized such that zero corresponds to the smallest intensity in the data subset, and one to the largest. The relative time of geometrical occultation is indicated by a dashed vertical line. This time corresponds to an intensity level which is 25 percent above the post-occultation intensity with respect to the pre-occultation intensity. A second dashed line appears in the case of two-star solutions. The computed pre-occultation intensity level (due to starlight, skylight, and lunar limb brightness) is indicated by a short horizontal line extending to the right from the left hand vertical axis. The computed post-occultation intensity level (due only to skylight and lunar limb brightness) is indicated by a short horizontal line extending to the left from the right hand vertical axis.

Across the top of the graph is an additional horizontal axis, scaling the event linearly. This axis gives the distance, in meters, of the projection (along the Earth's surface) of the geometrical shadow from the telescope. The zero reference is taken at the point of geometrical occultation. Negative values along this axis correspond to pre-occultation intensities.

Noise statistics of the observation, NOISEPLOT. The fourth type of graph (of which Figure 5-6 is an example) is generated by the APL function NOISEPLOT and shows the noise figure of the event throughout the entire 4096 milliseconds of data. The observed intensity values are subtracted from the computed values and the residuals binned into fifty classes. Each class width is two percent of the range of the residuals. The binned residuals are plotted against the number of residuals per bin. The horizontal axis indicates the value of the residuals as a percentage of the mean value. The vertical axis indicates the number of residuals per bin. A dashed vertical line shows where the mean of the distribution falls. The one sigma width of the distribution is shown as a horizontal error bar centered on the line representing the mean value.

The non-linear least squares, differential correction procedure, employed to obtain the occultation solution parameters, assumes that the residuals are randomly distributed. Thus, the noise figure should be essentially Gaussian. Often, the distribution function of the residuals, taken across the entire data set, seems to have a small negative-going Poisson tail. This results from an increase in background light during the 4096 milliseconds of data acquisition. The two major sources contributing to a time varying background are: Earthshine along the lunar limb (dominant for events of small solar elongation), and the radial brightness distribution of the lunar aureole (dominant for events occuring at large solar elongations). The background sky intensity determined as one of the solution parameters reflects the light-level at the time of the event, and typically, is somewhat higher than the background observed earlier in the observation. The Poisson tail arising in the residual distribution functions due to these effects is usually inconsequential, as the effect is very small over the short timescale of the occultation itself.

Power spectra, POWERPLOT. While the character of the distribution function of the residual amplitudes is important in confirming that the fundamental assumption of stochastic noise implicit in the reduction process is true, so too is the distribution of the power components associated with the observed data. The question of an optimum data acquisition rate, effective system time constant for the analog electronics, and their relation to scintillation noise and the power spectrum of an occultation observation is discussed in Chapter 3. Figures generated by the APL function POWERPLOT contain three power spectra for each occultation, and show the relative power contributions for all frequency components up to 500 Hertz.

Figure 5-7 is an example of a POWERPLOT. The lower power spectrum in a POWERPLOT results from a discrete Fourier transformation of 1000 millisecond observations centered on the time of geometrical occultation. These may be compared with the middle spectrum, which for the same event shows the pre-occultation power spectrum derived from 1024 millisecond observations typically centered 1500 milliseconds from the time of geometrical occultation. The 512 millisecond separation in time between the endpoints of the pre-occultation and occultation power spectra are sufficiently separated in time so diffraction fringing effects will not corrupt the pre-occultation data. Also, in this short time interval the atmospheric conditions cannot appreciably change and thereby affect the character of the seeing or scintillation. The upper power spectrum is that of the computed occultation curve, also centered on the time of geometrical occultation. In a few cases the data acquisition process was halted too late to to preserve 1024 milliseconds of pre-occultation data. In these cases the out-of-occultation data subset is shorter, and hence, the power spectrum is generated to correspondingly lower frequencies.

The horizontal axes give the frequency components in Hertz. The power spectra are plotted on a logarithmic (base 10) scale. Each decade is marked along the vertical axes. All three power spectra, on each POWERPLOT, are normalized to the same logarithmic power scale. Most of the Fourier transformations were carried out using the APL functions FFT and FFTI (listed in Appendix E), supplied by Selfridge (1984). These are "fast" Fourier transformations and require data to be transformed to have a number of elements evenly divisible by a power of two. In cases where this was not possible or practical, the discrete Fourier transformation functions FT and INVFT were used. These functions are discussed in detail by Schneider (1981).

Examination of the three power spectra for each event will reveal which frequency components are important to the occultation intensity curve and which are primarily associated with the background (i.e. scintillation) noise. It can be seen in all cases that the frequency components in excess of about 150 Hertz are generally unimportant in the occultation curve itself. These graphs also allow one to quickly spot any induced artificial noise, such as a 60Hz component (which could result from improper electrical shielding or loss of a ground or other source of AC pickup in the analog electronics).

Sensitivity of solution to variation of parameters, PDPLOT. Of interest in the final solution to an occultation observation is the sensitivity of the computed curve to variations in the solution parameters. In the computational process of determining differential corrections, numerical partial derivatives of the intensity curve at each observed point are computed for each parameter considered in the model. These derivatives, dI/dP_i, are retained for the best determined theoretical fit. Where each of these derivatives is at a maximum corresponds to an area of the computed intensity curve of high sensitivity to perturbations in the corresponding parameter.

Graphs, such as Figure 5-14, generated by the APL function PDPLOT, show dI/dP_i for the variation of the solution parameters. The partial derivative curves are labeled as follows: PREI = Pre-event Intensity ; POST = Post-event Intensity ; TIME = Time of Geometrical Occultation ; DIAM = Angular Diameter of Stellar Disk ; and VELO = Velocity of Lunar Shadow Passage. In the case of two-star solutions the labeling of the derivative curves are postfixed with a "1" or "2" as is appropriate. Each curve has been normalized from -1 to 1, with the line corresponding to $dI/dP_i = 0$ drawn in. The actual values of dI/dP_i differ by orders of magnitude for the five parameters. Thus, the relative degree of sensitivity of the intensity curve is not easily seen. The maximum and minimum values for dI/dP_i are given in the tables of supplementary statistical information.

Discussion of Individual Occultation Events

ZC0916 (1 Geminorum)

Historical notes. Few binary stars have a detectable duplicity both visually and spectroscopically due to observational selection effects. Fortunately, though only a handful of such stars are known, they do exist and 1 Geminorum is among them. 1 Gem is an interesting star, with perhaps an equally interesting history. It was first discovered to be a spectroscopic binary by Campbell and Moore (1907) from radial velocity data obtained from plates taken at Lick Observatory. A period of 9.590 days was first given to the spectroscopic variation by Young (1919) from 77 plates taken in Victoria and Ottawa, Canada.

Though there had never been any previous visual detection of duplicity, Kuiper (1948) found 1 Gem to be double while using the star to focus the 82-inch telescope at McDonald Observatory. Using a Cassegrain spectrograph, he found the two visual components to be late giants of similar spectral type. Since that time many observations of the visual pair have been carried out with 58 listed by Worley (1984) through 1981.12. Most of these, until 1976, are visual micrometer observations. More recent observations by McAlister (Worley, 1984) have been via speckle interferometry.

Heintz found a period for the visual pair of 13.17 years, as reported by Muller (1961). The orbital elements he determined, along with the associated Thiele-Innes constants, were listed by Finsen and Worley (1970).

Abt and Kallarakal (1963) first elucidated the nature of the 1 Gem system. They determined that the fainter visual component, 1 Gem B, was the spectroscopic binary. They further determined the spectroscopic period to be 9.6595 days, with a mass function of 0.139 solar masses. In addition, the AB visual system was given a period of 11.00 years, with an eccentricity of 0.255 and a total mass of 3.16 solar masses.

Griffin and Radford (1976) rexamined the 1 Gem B spectroscopic binary in the light of photoelectric radial velocity measurements. Their findings, while not substantially different from Abt and Kallarakal, do indicate a period of 9.59659 days (closer to Young's value), and a circular orbit as well. Additionally, they indicate that the dips exhibited in their photoelectric radial velocity data are of "very unequal depth", from which they suggest that the B component is of "substantially earlier spectral type than A" (1976, p. 191).

If a fourth component in this system does indeed exist, as the occultation observation seems to indicate, then the question of final determination of spectral types may still be open.

The observation. On 22 March 1983, a lunar occultation of the KOIII/G8III-VII (Abt and Kallarakal, 1963) visual-spectroscopic binary star 1 Geminorum (BS 2134, HR 2134, HD 41116, KUI 23) was observed under favorable circumstances from RHO. The specifics of the observation are given on Table 5-1. The RAWPLOT of the occultation

TABLE 5-1
THE OBSERVATION OF THE LUNAR OCCULTATION OF ZC0916

STELLAR AND OBSERVING INFORMATION

Star: ZC0916	(1 Geminorum, SAO 077915, DM +23 1170)		
RA: 060305	DEC: +231556	mV: 4.30	Sp: G5
Filter: V	Diaphragm:	Gain: C11+	Voltage: 1000

LUNAR INFORMATION

Surface Illumination:	50 percent
Elongation from Sun:	90 degrees
Altitude Above Horizon:	48 degrees
Lunar Limb Distance:	367212 kilometers
Predicted Shadow Velocity:	716.3 meters/sec.
Predicted Angular Rate:	0.4024 arcsec/sec.

EVENT INFORMATION

Date:	March 22, 1983	UT of Event:	02:44:34
USNO V/O Code:	19	HA of Event:	+464840
Position Angle:	114.0	Cusp Angle:	66S
Contact Angle:	-21.8	Watts Angle:	112.5

observation is shown Figure 5-1, and a subset of these data (renormalized to full scale) showing the occultation in detail is presented in Figure 5-2. The stepped disappearance, well separated in time, is quite obvious. The brighter star (the A component of the visual system) underwent disappearance first. Examination of either the

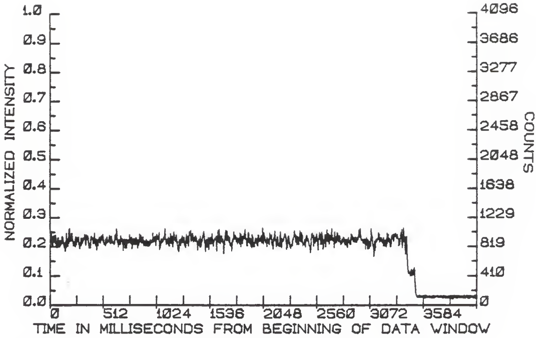

Figure 5-1. RAWPLOT of the occultation of ZC0916.

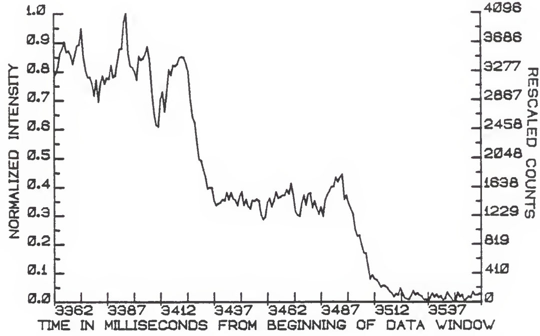

Figure 5-2. Detail of the ZC0916 double disappearance.

complete or detailed integration plots. Figures 5-3 and 5-4, shows no evidence of any disappearances other than those of the A and B visual components.

Reduction and analysis of the 1 Geminorum A observation. The diffraction curves resulting from the occultations of the A and B components were sufficiently separated to allow treating each of these independently. It can be seen from the extracted data set that the B star is so far into the asymptotic falloff of the A star curve that the A star contribution is negligable.

Inspection of the A star curve immediately reveals irregularites unanticipated in the disapearance of a single star, but of the sort commonly seen in the occultation of a close double star. Attributing this to rapid atmospheric variations is difficult, as the sky was well behaved through the other 3900 milliseconds of data taken.

Despite the fact that there was an appearance of duplicity, an attempt was first made to fit the A curve to a single star model with the single-star DC program. Though liberal constraints were applied to the differential corrections, no solution could be obtained. An attempt was then made to fit the data to a two-star model, using the DC2 program.

The initial run of the two-star model allowed for the variation of nine parameters: the diameters of the two suspected stars, their times of geometrical occultation, their unocculted intensity, the local slopes of the lunar

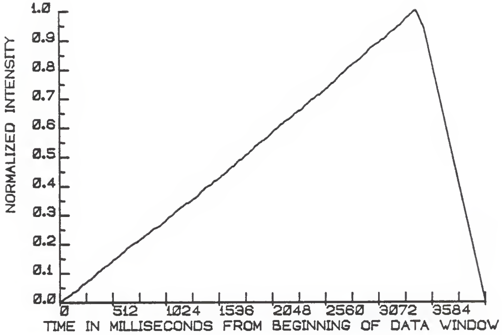

Figure 5-3. Integration plot of the ZC0916 event.

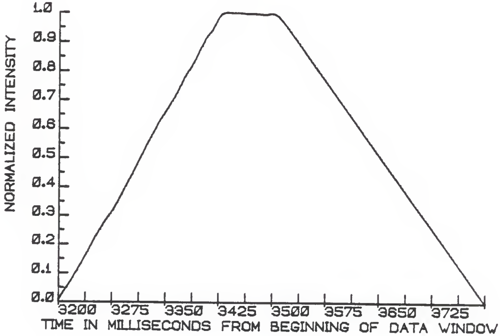

Figure 5-4. Integration plot detailing the double disappearance.

limb (actually the projected component of the lunar velocity vector) at the contact points of geometrical occultation, and the background skylight. The slopes were presumed to be independent as the to-be-determined separation might be sufficiently large to allow this.

One hundred milliseconds of data were used in the reduction of 1 Gem A, as indicated in Table 5-2.

TABLE 5-2
TWO-STAR SOLUTION OF THE OCCULTATION OF 1 GEMINORUM A

MODEL PARAMETERS

Number of Data Points:	101
Number of Grid Points:	4096
Number of Spectral Regions:	5
Width of Spectral Regions:	50 Angstroms
Limb Darkening Coefficient:	0.5
Effective Stellar Temperature:	5400 K

SOLUTIONS

	Brighter Star	Fainter Star
Stellar Diameter (ams):	0.73 (2.42)	0.00 (FIXED)
Time: (Relative):	54.82 (0.37)	34.02 (2.46)
Pre-Event Signal:	372.60 (5.6)	120.30 (12.1)
Velocity (m/sec):	752.3 (9.0)	621.6 (76.1)
Lunar Limb Slope (deg):	-8.89 (0.57)	+14.9 (6.3)

Background Sky Level:	429.8 (6.8)
Separation in Time (milliseconds):	20.80 (2.49)
Projected Spatial Separation (ams):	8.41 (1.01)

PHOTOMETRIC NOISE INFORMATION

Sum-of-Squares of Residuals:	116250
Sigma (Standard Error):	36.54
Normalized Standard Error:	0.5797
Photometric (S+N)/N Ratio:	2.725
Total Intensity/Background:	1.147
Change in Magnitude:	0.149

The data set initially was chosen to include sufficient diffraction fringing effects on the leading edge, and truncated so as not to include significant effects from the 1 Gem B curve. Additional reduction runs containing earlier data points in the sample did not significantly alter the solutions. The solution obtained by the DC2 procedure indicated that both stars were essentially point sources, but a large formal error was attached to the diameter of the fainter star. This is understandable when one notes that the fainter star contributes only 1/3 of the total light to the A curve. Hence, the solution is, unfortunately, insensitive to the diameter of the fainter star. With this in mind the program was re-run, but this time holding the diameter of the second star fixed as a point source. It was found, as might have been anticipated, that the resulting solutions were changed insignificantly, though the formal errors were widened slightly in most of the parameters.

The parametric solutions are also presented in Table 5-2. The difference in time between the geometrical occultations for the two A stars was 20.8 (+/- 2.5) milliseconds. This corresponds to a separation of 8.37 (+/- 1.00) milliseconds of arc projected along a line in the direction of the moon's topocentric motion. The observational evidence is quite strong that there almost certainly is a detection of a fainter star in the 1 Gem A occultation record.

The best two-star solution obtained for the 1 Gem A observation is depicted graphically on the FITPLOT, Figure 5-5. The sensitivity of this solution to variations

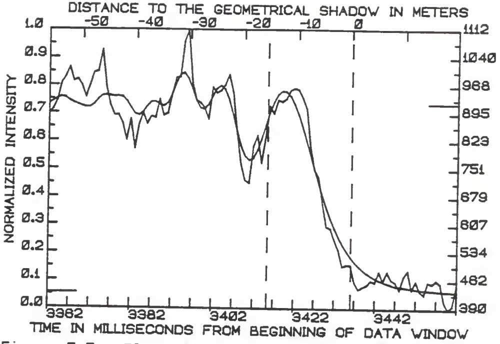

Figure 5-5. FITPLOT of the 1 Gem A two-star solution.

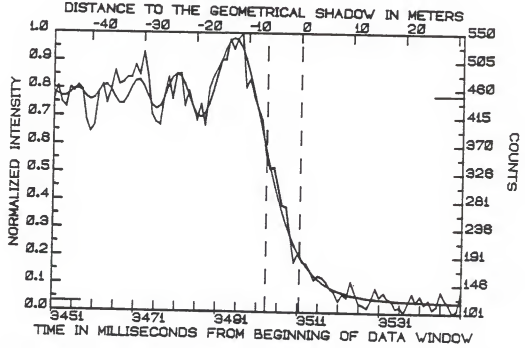

Figure 5-6. FITPLOT of the 1 Gem B two-star solution.

of each of the parameters (i.e., the first derivatives of the intensity curve) is shown on the PDPLOT, Figure 5-7.

Reduction and analysis of the 1 Geminorum B observation. A similar approach was taken for the solution of 1 Gem B. Here, however, DC2 was modified to determine dynamically if a one, or two-star solution would represent a better choice. This decision was made at the end of each differential correction step. It was felt, in the light of the fact that the fainter component of 1 Gem B had never been detected, that a one star solution would be more appropriate. Nevertheless, the model would invariably return to re-entering the additional parameters necessary for a two-star solution. Forcing a one star model resulted in a quasi-convergent solution; that is, the parameters exhibited large amplitude oscillations about some mean values, rather than asymptotically approaching final values. The formal errors and the sum square error of this "solution", and a visual inspection of the best obtainable fit were significantly worse than the two-star model. The two-star solutions for 1 Gem B is presented in Table 5-3, and graphically in Figure 5-6.

Note here that the fainter, previously undetected, spectroscopic component of 1 Gem B is almost ten times fainter than the brighter star. This led to a complete insensitivity of the solution to the diameter of the fainter star. Its detection, however, is quite evident, and the fit is made possible only with the change in level provided by

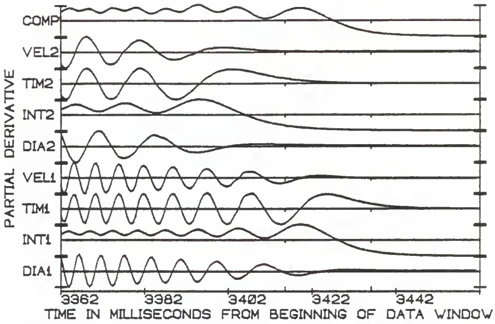

Figure 5-7. PDPLOT of the 1 Gem A two-star solution.

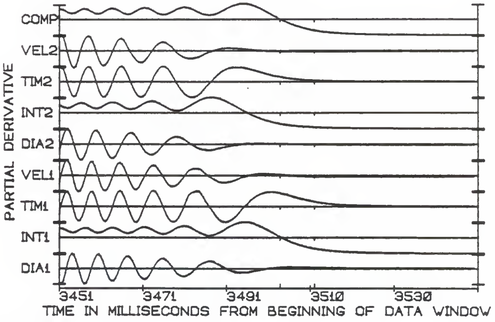

Figure 5-8. PDPLOT of the 1 Gem B two-star solution.

the occultation of the fainter B star component. The PDPLOT for the 1 Gem B solution is presented as figure 5-8.

TABLE 5-3.
TWO-STAR SOLUTION OF THE OCCULTATION OF 1 GEMINORUM B

MODEL PARAMETERS

Number of Data Points:	101
Number of Grid Points:	4096
Number of Spectral Regions:	5
Width of Spectral Regions:	50 Angstroms
Limb Darkening Coefficient:	0.5
Effective Stellar Temperature:	5400 K

SOLUTIONS

	Brighter Star	Fainter Star
Stellar Diameter (ams):	5.89 (0.84)	Point Source
Time: (Relative):	61.00 (0.45)	52.69 (3.05)
Pre-Event Signal:	301.30 (15.1)	33.50 (15.0)
Velocity (m/sec):	773.5 (9.0)	787.5 (72.6)
Lunar Limb Slope (deg):	-11.1 (1.1)	+12.3 (5.8)

Background Sky Level:	115.9 (3.3)
Separation in Time (milliseconds):	8.31 (3.08)
Projected Spatial Separation (ams):	3.34 (1.24)

PHOTOMETRIC NOISE INFORMATION

Sum-of-Squares of Residuals:	348100
Sigma (Standard Error):	18.754
Normalized Standard Error:	0.0857
Photometric (S+N)/N Ratio:	12.68
Total Intensity/Background:	2.89
Change in Magnitude:	1.15

A discussion of the 1 Geminorum results. The distribution function of the residuals of the four-star fit to the observed data is shown in the NOISEPLOT, Figure 5-9. The power spectra of the observed and computed four-star fit, as well as the power spectrum of the pre-occultation signal, can be seen on the POWERPLOT, Figure 5-10.

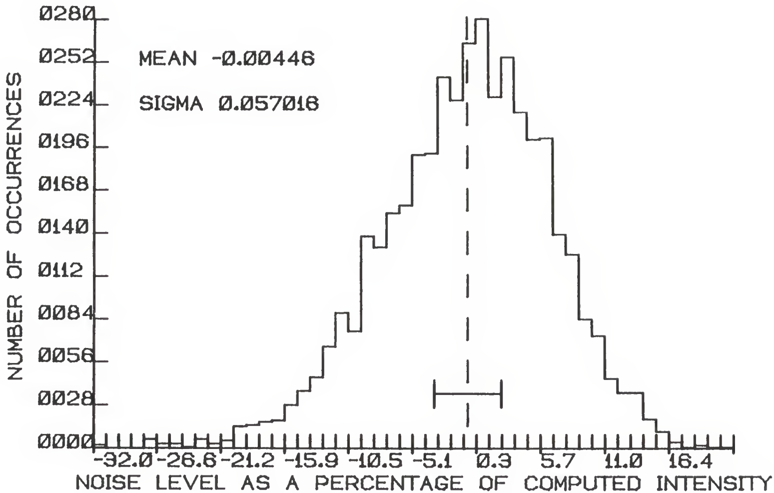

Figure 5-9. NOISEPLOT of the ZC0916 occultation.

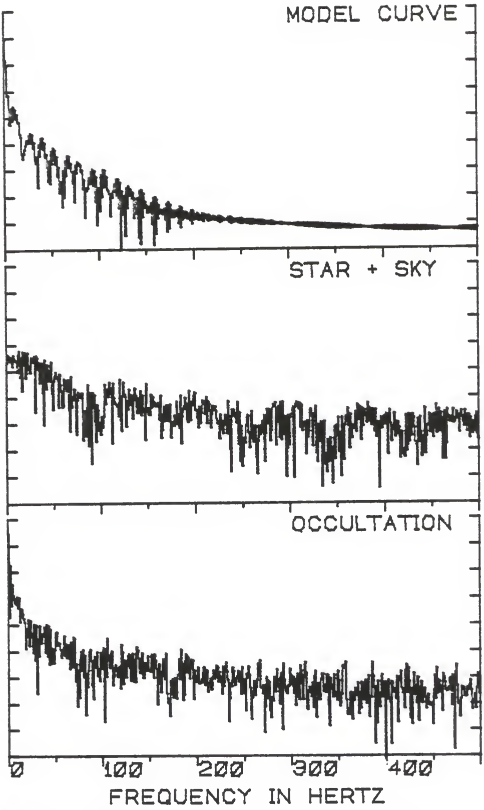

Figure 5-10. POWERPLOT of the ZC0916 occultation.

For purposes of clarity in this discussion the brighter component of 1 Gem A is referred to as A1 and the fainter as A2. Similarly denoted is the brighter member of 1 Gem B as B1 and its unseen spectroscopic companion as B2. The intention in doing so is not necessarily to imply that the A stars are actually a physical pair (i.e., that they orbit about one another, as the B stars do), but the question does of necessity arise.

There are, then, three possibilities if the existence of 1 Gem A2 is accepted: first, that it is a member of a physical pair with A1; second, that it is not, but rather is in an independent orbit about the barycenter of the 1 Gem system; or third, that it is simply, by chance, a bright star in the same field. The third possibility is highly unlikely, as the projected separation of the A components is only 8.4 milliseconds of arc.

One must ask, before addressing the question as to whether the first or second case is the correct one, why the A2 star has not made its presence known through its spectral lines or its possible effect on the radial velocity curve of 1 Gem A1. Table 5-4 shows the relative brightnesses and magnitudes of the four component stars in the 1 Gem system, on the basis of the occultation observation.

The derived individual magnitudes come from a total systemic V magnitude of 4.18 (Eggen, 1965). With the A2 star 1.23 (+/- 0.02) magnitudes fainter than the B1 star, and contributing only 15 percent of the total light of the system, it is quite understandable that its spectral signature does not make itself readily apparent.

TABLE 5-4
1 GEM: COMPONENT CONTRIBUTION TO TOTAL SYSTEM INTENSITY

Star	Intensity	%Total	mV	ΔmV
A1	372.6	45.02	5.05 (+/- 0.02)	
A2	120.3	14.53	6.27 (+0.12,-0.10)	1.22
A1+A2	492.9	59.55	4.74	
B1	301.3	36.40	5.28 (+0.06,-0.05)	
B2	33.5	4.05	7.66 (+0.64,-0.40)	2.40
B1+B2	334.8	40.45	5.19	0.43

As to its effect on the long period radial velocity curve of 1 Gem A, it need have none if A1 and A2 are a physical pair with an inclination near zero degrees. It would, however, be presumptuous to assume, a priori, that this is the case. If A2 has an independent orbit about the barycenter of the system, one still might see an effect in the long period radial velocity curve of the AB system. To resolve this question one will have to look carefully at the available radial velocity data, with an eye to the idea that a fourth component most probably exists. This is a matter for future investigation. It is of interest to note that in their exposition of 1 Geminorum, Abt and Kallarakal conclude that "the astrometric and spectroscopic observations are consistent with a multiple system in which the primary is a K0III star that may be single" (1963, p. 144), while Griffin and Radford state that the system is "at least triple" (1976, p. 189). In either case the previous observations do not rule out the existance of this newely discovered component.

In principle an occultation observation itself can provide a constraint on the orbit of a visual binary. The position angle, ρ, and angular separation θ, are inseparable from a single occultation observation alone. Only a projected separation, along a line in space can be found. However, given an orbit with its associated errors, the intersection of that line with the orbit provides an independent, highly accurate (though only solitary) observation. Unfortunately, with the addition of a fourth member in the 1 Gem system the situation is not quite as clear cut.

If 1 Gem A is assumed to be a physical pair, that is to say a hierarchy 2 quadruple system a la Evans (1968), then the visual observations of the AB pair would have been made not with respect to the AB positions, but with respect to the centers-of-light (CL's) of the A and B component systems respectively. In the case of 1 Gem B the difference is negligible, but not necessarily so for 1 Gem A.

Figure 5-11 shows the chords both in time and space containing the A and B stars. The figure is oriented so the topocentric radial direction of approach of each star to the smooth lunar limb is vertical. Thus, the stars lie somewhere along the horizontal chords. The intersection of the horizontal chords with the time scale on the left is simply the relative times of geometrical occultation. The bottom

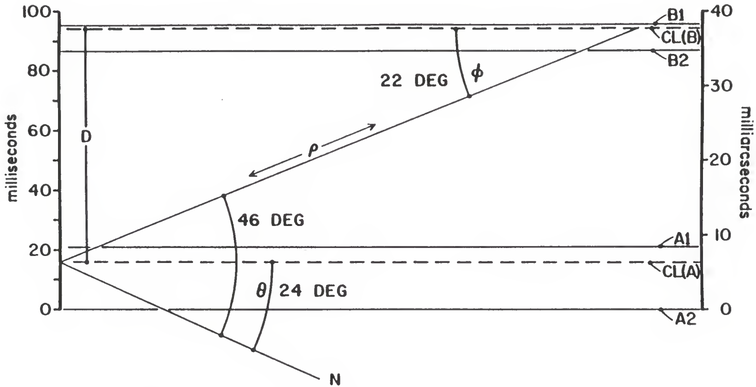

Figure 5-11. Each of the four component stars lie along the horizontal chords labeled A1, A2, B1, B2. These chords are tangent to a line which is tangent to the lunar limb. Their separation, both in time and space are given along the vertical axes. The centers-of-light of the A1-A2 and B1-B2 chords are shown as dashed lines, and their measured separation is indicated by D. The angles shown, and the line labeled ρ are explained in the text.

line is both the chord of A2 (which disappeared first) and the smooth lunar limb at the time of A2's geometrical occultation. The top line corresponds to B1's disappearance, which happened last. From the measured intensities of each of the four stars, the CL's of the A1,A2 and B1,B2 pairs were computed as the intensity and time-weighted-means of the respective components. Hence, the time of geometrical occultation of the CL of the A system is

CL(A)=[(54.82x372.6)+(34.02x120.3)]/(372.6+120.3)

and is similarly found for the B1,B2 stars. The absolute times in terms of the total data window and reduced to Universal Time are given in Table 5-5. The dashed lines shown on Figure 5-11 are the chords of the CL's of the A and B pairs. The direction to North is 24 degrees westward of the horizontal (which is tangent to the smooth lunar limb).

TABLE 5-5
TIMES OF GEOMETRICAL OCCULTATIONS

	A-VISUAL COMPONENT		B VISUAL COMPONENT	
Relative	Times:	3382 msec		3450 msec
	+	=	+	=
Star 2	34.02	3416.02	52.69	3502.69
CL	49.87	3431.87 (0.77)	60.16	3510.16 (0.61)
Star 1	54.82	3436.82	61.00	3511.00
U.T.'s:				
Star 2	02:44:33.3258 (0.0027)		02:44:33.4125 (0.0032)	
CL	02:44:33.3417 (0.0013)		02:44:33.4200 (0.0013)	
Star 1	02:44:33.3466 (0.0012)		02:44:33.4208 (0.0013)	

The projected separation in time between CL(A) and CL(B) was 78.29 (+/- 0.98) milliseconds. Since the projected radial approach rate was 0.4024 seconds of arc per second, then the projected angular separation, D, is 31.5 (+/- 0.39) milliseconds of arc. Next, it is logical to inquire if this is consistent with the 1 Gem orbit derived from visual-micrometer measurements and with recent speckle interferometric observations.

Using the Thiele-Innes constants for Heintz's orbit, as catalogued by Finsen and Worley (1970), the predicted ρ and θ for the date of the occultation observation, 1983.219, were found to be 0".0855 and 68.1436 degrees respectively. Since this orbit was derived from observations predating 1962, it was of interest to determine how well more recent observations of ρ and θ compared to those predicted using Heintz's orbit. For this purpose a compendium of fifty-eight observations up to and including 1981.120 were obtained from Worley (1984). Prior to 1976, most observations were micrometer measurements. Since that time the majority reported were speckle interferometric observations made by McAlister. It was immediately noticed that over the last decade the θ residuals were running negative and increasingly so with time.

In order to define any secular changes quantitatively in both the ρ and θ residuals, the O-C's for all observations were fit via least squares, along with the dates of the corresponding observations, to seven different curves. The curve which fit best, in terms of the sum of the squares of the residuals as well as the Pearson product-moment correlation coefficient, was a third order polynomial.

Figure 5-12 shows the observed and computed residuals for both ρ and θ.

There is no intention to suggest that there is any physical meaning to any of the particular coefficients. Rather, the fitting was done to provide a reasonable method of extrapolation, on the basis of the O-C's for the orbit, for corrections to be applied to predicted values of ρ and θ for the date of the occultation observation. In doing so corrections of $-22\overset{\circ}{.}099$ for θ, and $+0\overset{''}{.}004547$ for ρ were found. The corrected quantities are denoted $\theta' = 46\overset{\circ}{.}04$ and $\rho' = 0\overset{''}{.}090047$.

The position angle of the occultation along the lunar limb was at a PA = $114\overset{\circ}{.}0$. Thus, the angle measured eastward between the line defining the smooth lunar limb (tangent to PA = 114°) and the θ' direction joining the A and B CL's is $\phi = \theta' - (PA - 90^{\circ})$, or in this case $22\overset{\circ}{.}04$. The projection of θ' along the line defining the topocentric radial direction of approach is simply $D' = \rho' \sin\phi$, or 33.8 milliseconds of arc. This is in good physical agreement with the observed projected separation of 31.5 milliseconds of arc, the difference being only 7.3 percent.

With regard to 1 Gem B, the positional information derived from this observation will probably not contribute much to the knowledge of the short period spectroscopic binary. Here, as in the case of 1 Gem A, the derived separation (8.31 (+/- 3.08) milliseconds, or 3.32 (+/- 1.24) milliseconds of arc) is a projection along the

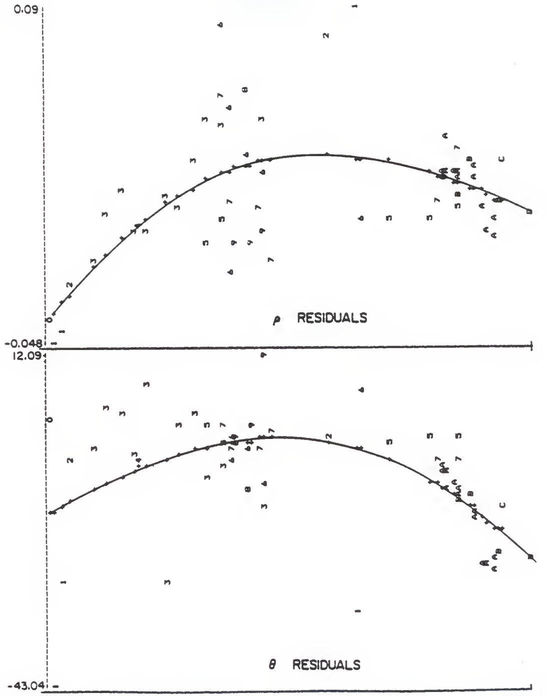

Figure 5-12. The θ and ρ residuals based on Heintz's determination of the 1 Geminorum visual orbit are shown for 58 observations as listed by Worley. The best fit to the residuals (a third order polynomial) is also shown. The numbers or letters indicate the following observers:

0-Kuiper	1-Wilson	2-Muller	3-Van Beisbroeck
4-Finsen	5-Heintz	6-Couteau	7-Worley
8-Van Den Bos	9-Baize	A-McAlister	B-Tokovinin
C-Morel	D-Extrapolation to 1983.219		

radial direction of lunar approach. Since the inclination of the orbit (as well as the orientation of the major axis of the projected orbital ellipse) is unknown, the relative positions of the individual components cannot be determined. Since, however, the fainter star disappeared first, it must have been essentially to the west of B1. Knowing the lunar PA of the event, one can then say that the B1 star was at a position angle greater than 24^{o}, but less than 204^{o}, measured eastward from North of the B2 star. Finally, it is noted from Griffin's period and (T0) = MJD 2440443.129 that this observation occured at phase 0.15 (+/- 0.03) of the short period radial velocity curve.

Concluding remarks on 1 Geminorum. The complete solution to the occultation of all four stellar components is presented graphically in Figure 5-13. Tables 5-7 and 5-8 give the supplemental statistics of the A and B component solutions, including the variance/co-variance and correlation matrices and the numerical ranges of the partial derivatives.

As a result of this observation there is now strong evidence pointing to the existence of a fourth component in the 1 Geminorum system. While this previously undetected component is more than three times fainter than 1 Gem A1, and almost six times fainter than the combined light of 1 Gem A1 and 1 Gem A2, supporting evidence might be found by a careful examination of speckle interferometric and radial velocity observations.

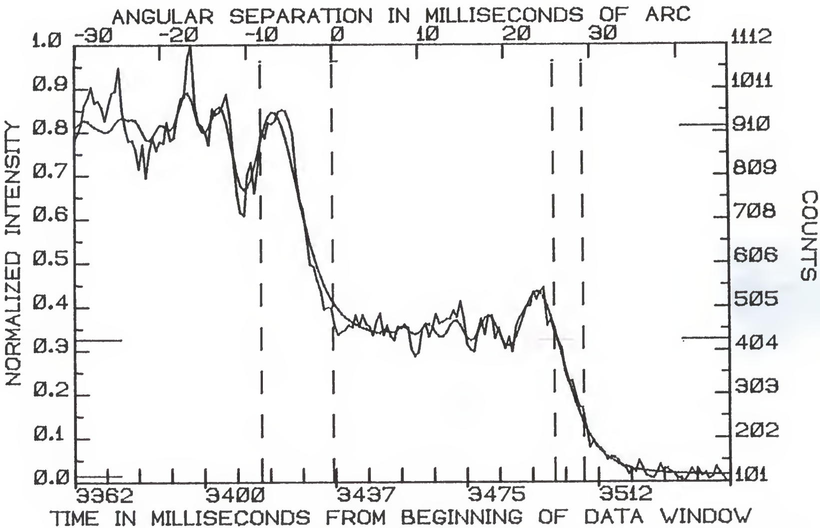

Figure 5-13. The double, two-star solution for 1 Geminorum showing the projected angular separation of the four stellar components.

TABLE 5-6
ZC0916: OBSERVATIONS, COMPUTED VALUES, AND RESIDUALS FROM BIN 3362

NUM	OBS	COMP	RESID	NUM	OBS	COMP	RESID	NUM	OBS	COMP	RESID
0	891	920.3	-29.3	63	909	826.2	82.8	126	401	420.7	-19.7
1	905	925.5	-20.5	64	808	789.1	18.9	127	461	435.8	25.2
2	928	933.0	-5.0	65	750	752.2	-2.2	128	480	457.4	22.6
3	974	937.5	36.5	66	731	716.5	14.5	129	493	481.8	11.2
4	990	934.9	55.1	67	663	682.9	-19.9	130	507	505.3	1.7
5	1015	927.7	87.3	68	603	651.7	-48.7	131	507	524.6	-17.6
6	978	921.2	56.8	69	598	623.4	-25.4	132	540	537.3	2.7
7	983	917.4	65.6	70	568	598.0	-30.0	133	524	541.9	-17.9
8	967	913.8	53.2	71	542	575.5	-33.5	134	541	538.2	2.8
9	936	910.2	25.8	72	500	555.8	-55.8	135	550	526.5	23.5
10	968	910.6	57.4	73	504	538.6	-34.6	136	462	508.0	-46.0
11	1001	918.2	82.8	74	503	523.7	-20.7	137	477	484.2	-7.2
12	1004	930.4	73.6	75	460	510.9	-50.9	138	447	456.6	-9.6
13	1060	939.9	120.1	76	441	499.9	-58.9	139	429	426.9	2.1
14	963	942.3	20.7	77	448	490.5	-42.5	140	411	396.3	14.7
15	916	940.2	-24.2	78	452	482.5	-30.5	141	356	366.1	-10.1
16	890	938.8	-48.8	79	464	475.6	-11.6	142	332	337.1	-5.1
17	891	939.5	-48.5	80	459	469.8	-10.8	143	334	309.9	24.1
18	869	937.3	-68.3	81	487	464.8	22.2	144	304	284.9	19.1
19	825	926.8	-101.8	82	462	460.5	1.5	145	273	262.4	10.6
20	881	909.6	-28.6	83	487	456.9	30.1	146	271	242.4	28.6
21	803	894.2	-91.2	84	466	453.8	12.2	147	226	224.7	1.3
22	866	889.9	-23.9	85	460	451.1	8.9	148	181	209.3	-28.3
23	896	899.1	-3.1	86	440	448.8	-8.8	149	196	196.0	0.0
24	867	914.5	-47.5	87	474	446.9	27.1	150	182	184.6	-2.6
25	888	925.5	-37.5	88	490	445.1	44.9	151	179	174.8	4.2
26	884	926.0	-42.0	89	440	454.5	-14.5	152	168	166.5	1.5
27	933	919.2	13.8	90	463	450.2	12.8	153	152	159.4	-7.4
28	890	915.2	-25.2	91	437	446.7	-9.7	154	160	153.4	6.6
29	896	923.4	-27.4	92	429	447.3	-18.3	155	157	148.4	8.6
30	945	945.5	-0.5	93	461	452.4	8.6	156	150	144.1	5.9
31	989	974.0	15.0	94	456	458.1	-2.1	157	139	140.4	-1.4
32	991	996.3	-5.3	95	465	459.5	5.5	158	133	137.3	-4.3
33	1081	1001.9	79.1	96	457	454.4	2.6	159	119	134.7	-15.7
34	1112	987.6	124.4	97	409	446.2	-37.2	160	131	132.5	-1.5
35	975	959.8	15.2	98	390	441.4	-51.4	161	125	130.6	-5.6
36	931	930.1	0.9	99	400	444.7	-44.7	162	151	128.9	22.1
37	924	910.4	13.6	100	453	454.5	-1.5	163	133	127.5	5.5
38	911	907.4	3.6	101	467	464.1	2.9	164	116	126.3	-10.3
39	880	920.4	-40.4	102	436	466.1	-30.1	165	113	125.2	-12.2
40	965	941.9	23.1	103	458	458.3	-0.3	166	109	124.3	-15.3
41	950	961.3	-11.3	104	489	445.4	43.6	167	122	123.5	-1.5
42	956	969.1	-13.1	105	467	435.7	31.3	168	141	122.8	18.2
43	971	959.7	11.3	106	470	435.8	34.2	169	126	122.2	3.8
44	998	933.1	64.9	107	478	446.2	31.8	170	133	121.7	11.3
45	951	894.3	56.7	108	478	461.3	16.7	171	124	121.2	2.8
46	845	851.3	-6.3	109	498	472.7	25.3	172	121	120.8	0.2
47	765	812.8	-47.8	110	482	474.0	8.0	173	108	120.4	-12.4
48	723	786.0	-63.0	111	519	464.4	54.6	174	111	120.1	-9.1
49	716	774.9	-58.9	112	480	448.4	31.6	175	102	119.8	-17.8
50	810	780.5	29.5	113	419	433.8	-14.8	176	117	119.5	-2.5
51	840	800.4	39.6	114	406	427.4	-21.4	177	132	119.3	12.7
52	768	830.2	-62.2	115	402	432.1	-30.1	178	118	119.1	-1.1
53	835	864.6	-29.6	116	449	446.0	3.0	179	129	118.8	10.2
54	917	898.3	18.7	117	479	463.6	15.4	180	115	118.7	-3.7
55	896	926.6	-30.6	118	443	478.4	-35.4	181	122	118.5	3.5
56	932	946.4	-14.4	119	483	484.8	-1.8	182	107	118.3	-11.3
57	928	955.8	-27.8	120	485	480.8	4.2	183	113	118.2	-5.2
58	936	954.3	-18.3	121	432	467.6	-35.6	184	136	118.1	17.9
59	958	942.6	15.4	122	457	449.3	7.7	185	123	117.9	5.1
60	962	922.0	40.0	123	431	431.3	-0.3	186	114	117.8	-3.8
61	959	894.4	64.6	124	409	418.6	-9.6	187	101	117.7	-16.7
62	937	861.8	75.2	125	436	414.7	21.3	188	106	117.7	-11.7

TABLE 5-7
ZC0916-A: SUPPLEMENTAL STATISTICAL INFORMATION

VARIANCE/CO-VARIANCE MATRIX

DIA1	INT1	SKY	TIM1	VEL1	DIA2	INT2	TIM2	VEL2
7.252E¯16	1.089E¯07	-3.372E¯08	-7.128E¯10	1.145E¯11	-4.455E¯16	-7.542E¯08	-4.008E¯09	4.455E¯11
1.089E¯07	2.168E02	-7.115E01	-7.307E¯01	1.006E¯02	-5.269E¯07	-1.382E02	-1.042E01	1.721E¯01
-3.372E¯08	-7.115E01	8.015E01	-1.066E00	1.625E¯02	3.342E¯09	-7.622E00	-8.203E¯01	1.364E¯02
-7.128E¯10	-7.307E¯01	-1.066E00	1.653E¯01	-2.539E¯03	2.342E¯09	1.647E00	1.059E¯01	-1.426E¯03
1.145E¯11	1.006E¯02	1.625E¯02	-2.539E¯03	4.981E¯05	2.443E¯11	-2.340E¯02	-1.560E¯03	1.798E¯05
-4.455E¯16	-5.269E¯07	3.342E¯09	2.342E¯09	2.443E¯11	2.793E¯14	7.473E¯07	1.687E¯09	7.033E¯11
-7.542E¯08	-1.382E02	-7.622E00	1.647E00	-2.340E¯02	7.473E¯07	1.806E02	6.895E00	-1.059E¯01
-4.008E¯09	-1.042E01	-8.203E¯01	1.059E¯01	-1.560E¯03	1.687E¯09	6.895E00	3.644E00	-6.270E¯02
4.455E¯11	1.721E¯01	1.364E¯02	-1.426E¯03	1.798E¯05	7.033E¯11	-1.059E¯01	-6.270E¯02	1.333E¯03

CORRELATION MATRIX

	DIA1	INT1	SKY	TIM1	VEL1	DIA2	INT2	TIM2	VEL2
DIA1	1.000000	0.999072	-0.671816	-0.585661	0.558796	-0.912874	-0.914834	-0.920960	0.915395
INT1	0.999072	1.000000	-0.699525	-0.554781	0.527477	-0.894776	-0.897445	-0.916912	0.912597
SKY	-0.671816	-0.699525	1.000000	-0.204687	0.235867	0.327547	0.321180	0.442498	-0.451776
TIM1	-0.585661	-0.554781	-0.204687	1.000000	-0.999386	0.840396	0.852153	0.738899	-0.722321
VEL1	0.558796	0.527477	0.235867	-0.999386	1.000000	-0.820977	-0.833559	-0.721219	0.704793
DIA2	-0.912874	-0.894776	0.327547	0.840396	-0.820977	1.000000	0.998321	0.897421	-0.881929
INT2	-0.914834	-0.897445	0.321180	0.852153	-0.833559	0.998321	1.000000	0.918134	-0.904073
TIM2	-0.920960	-0.916912	0.442498	0.738899	-0.721219	0.897421	0.918134	1.000000	-0.999412
VEL2	0.915395	0.912597	-0.451776	-0.722321	0.704793	-0.881929	-0.904073	-0.999412	1.000000

NUMERICAL RANGES OF THE PARTIAL DERIVATIVES

	DIA1	INT1	SKY	TIM1	VEL1	DIA2	INT2	TIM2	VEL2
MAXIMUM	3.873E08	1.370E00	1.000E00	3.944E01	3.461E03	7.970E07	1.368E00	1.061E01	7.781E02
MINIMUM	-4.265E08	1.256E¯02	1.000E00	-4.040E01	-3.280E03	-8.731E07	5.914E¯03	-1.073E01	-8.901E02

TABLE 5-8

ZC0916-B: SUPPLEMENTAL STATISTICAL INFORMATION

VARIANCE/CO-VARIANCE MATRIX

DIA1	INT1	SKY	TIM1	VEL1	DIA2	INT2	TIM2	VEL2
3.177E-15	1.735E-06	3.511E-08	-2.830E-08	4.962E-10	-3.090E-14	-1.717E-06	-2.992E-07	6.647E-09
1.735E-06	1.087E03	1.819E01	-1.768E01	3.129E-01	-1.826E-05	-1.075E03	-1.818E02	3.960E00
3.511E-08	1.819E01	1.092E01	-6.807E-01	1.290E-02	-4.826E-07	-2.842E01	-4.273E00	8.348E-02
-2.830E-08	-1.768E01	-6.807E-01	3.536E-01	-6.496E-03	3.113E-07	1.789E01	2.874E00	-6.016E-02
4.962E-10	3.129E-01	1.290E-02	-6.496E-03	1.272E-04	-5.625E-09	-3.179E-01	-4.903E-02	9.850E-04
-3.090E-14	-1.826E-05	-4.826E-07	3.113E-07	-5.625E-09	3.602E-13	1.829E-05	3.039E-06	-6.581E-08
-1.717E-06	-1.075E03	-2.842E01	1.789E01	-3.179E-01	1.829E-05	1.080E03	1.795E02	-3.899E00
-2.992E-07	-1.818E02	-4.273E00	2.874E00	-4.903E-02	3.039E-06	1.795E02	3.540E01	-7.862E-01
6.647E-09	3.960E00	8.348E-02	-6.016E-02	9.850E-04	-6.581E-08	-3.899E00	-7.862E-01	1.839E-02

CORRELATION MATRIX

	DIA1	INT1	SKY	TIM1	VEL1	DIA2	INT2	TIM2	VEL2
DIA1	1.000000	0.999990	0.933433	-0.999828	0.999732	-0.999963	-0.999952	-0.999879	0.999831
INT1	0.999990	1.000000	0.932503	-0.999806	0.999719	-0.999955	-0.999943	-0.999810	0.999758
SKY	0.933433	0.932503	1.000000	-0.939145	0.940034	-0.935804	-0.936137	-0.933788	0.932952
TIM1	-0.999828	-0.999806	-0.939145	1.000000	-0.999987	0.999946	0.999952	0.999594	-0.999486
VEL1	0.999732	0.999719	0.940034	-0.999987	1.000000	-0.999892	-0.999902	-0.999434	0.999307
DIA2	-0.999963	-0.999955	-0.935804	0.999946	-0.999892	1.000000	0.999999	0.999767	-0.999689
INT2	-0.999952	-0.999943	-0.936137	0.999952	-0.999902	0.999999	1.000000	0.999754	-0.999674
TIM2	-0.999879	-0.999810	-0.933788	0.999594	-0.999434	0.999767	0.999754	1.000000	-0.999993
VEL2	0.999831	0.999758	0.932952	-0.999486	0.999307	-0.999689	-0.999674	-0.999993	1.000000

NUMERICAL RANGES OF THE PARTIAL DERIVATIVES

	DIA1	INT1	SKY	TIM1	VEL1	DIA2	INT2	TIM2	VEL2
MAXIMUM	2.949E08	1.369E00	1.000E00	3.263E01	2.357E03	2.997E07	1.369E00	3.716E00	2.180E02
MINIMUM	-3.150E08	5.562E-03	1.000E00	-3.334E01	-2.073E03	-2.797E07	3.607E-03	-3.788E00	-2.009E02

The contention that the lack of any detectable spectral features from the spectroscopic component of 1 Gem B is due to a considerably lower intrinsic luminosity seems consistent with the V magnitude found for this component.

ZC1221 (9 Cancri)

The moderately bright (mV=6.24) M3-III star ZC1221 (9 Cancri) was occulted under favorable conditions on March 24, 1983. Table 5-9 gives a synopsis of the occultation observation. The RAWPLOT, Figure 5-14, shows the raw observational data. Data acquisition was halted approximately 800 milliseconds before the end of the data window.

A careful examination of the integration plot, Figure 5-15, indicates a slight downward deflection at 2300 milliseconds. This change in integrated level, due possibly to the presence of a second star, is rather subtle. In order to more easily see this level change, an integration plot approximately 1200 milliseconds in length, centered roughly at the suspected time of secondary disappearance and excluding the primary occultation, was plotted and is shown in Figure 5-16. From the cusp seen at 2280 milliseconds, it is evident that a secondary event did occur.

The best fit to the primary occultation event, shown graphically in Figure 5-17, places the relative time of geometrical occultation close to 3426 milliseconds. Thus, the fainter star disappeared 1146 milliseconds before the brighter one. The angular velocity of lunar limb passage was

TABLE 5-9
ZC1221: LUNAR OCCULTATION SUMMARY

STELLAR AND OBSERVING INFORMATION

Star: ZC1221, (9 Cancri, SAO 079940, DM +23 1887)
RA: 080518 DEC: +224106 mV: 6.24 Sp: M3-III
Filter: V Diaphragm: I Gain: C7+ Voltage: 1000

LUNAR INFORMATION

Surface Illumination:	72 percent
Elongation from Sun:	116 degrees
Altitude Above Horizon:	78 degrees
Lunar Limb Distance:	361038 Kilometers
Predicted Shadow Velocity:	657.2 meters/sec.
Predicted Angular Rate:	0.3756 arcsec/sec.

EVENT INFORMATION

Date:	March 24, 1983	UT of Event:	00:44:56
USNO V/O Code:	17	HA of Event:	-114426
Position Angle:	110.4	Cusp Angle:	83S
Contact Angle:	-11.0	Watts Angle:	97.4

MODEL PARAMETERS

Number of Data Points:	201
Number of Grid Points:	1600
Number of Spectral Regions:	53
Width of Spectral Regions:	50 Angstroms
Limb Darkening Coefficient:	0.5
Effective Stellar Temperature:	3300K

SOLUTIONS

Stellar Diameter (ams):	2.70 (2.41)
Time: (relative to Bin 0):	3425.8 (0.6)
Pre-Event Signal:	2931.6 (16.7)
Background Sky Level:	1578.0 (18.5)
Velocity (meters/sec.):	691.0 (16.3)
Lunar Limb Slope (degrees):	-0.47 (1.35)
U.T. of Occultation:	00:44:55.877 (0.012)

PHOTOMETRIC NOISE INFORMATION

Sum-of-Squares of Residuals:	5663500
Sigma (Standard Error):	168.28
Normalized Standard Error:	0.12432
Photometric (S+N)/N Ratio:	9.044
(Change in Intensity)/Background:	0.85782
Change in Magnitude:	0.67251

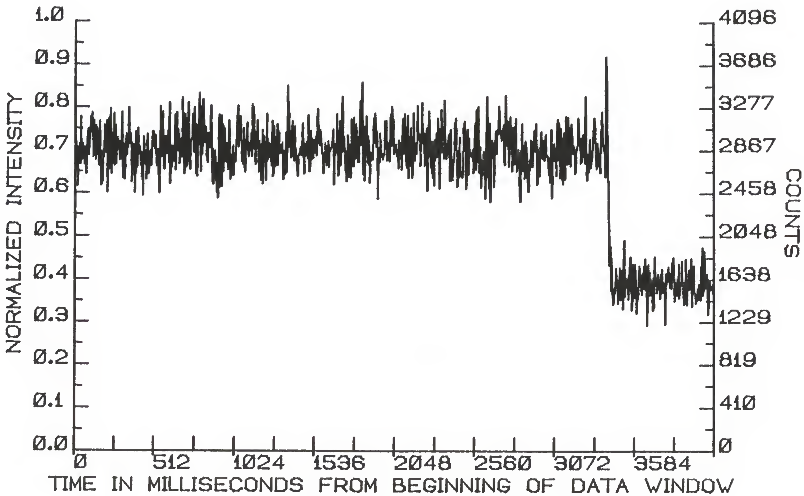

Figure 5-14. RAWPLOT of the occultation of ZC1221.

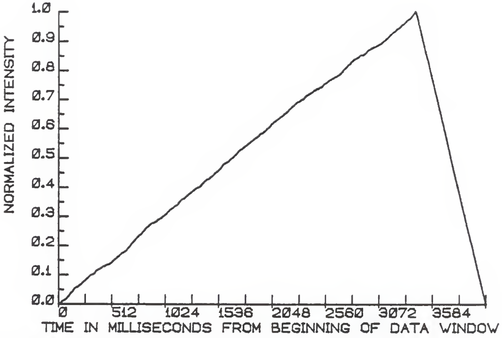

Figure 5-15. INTPLOT of the occultation of ZC1221.

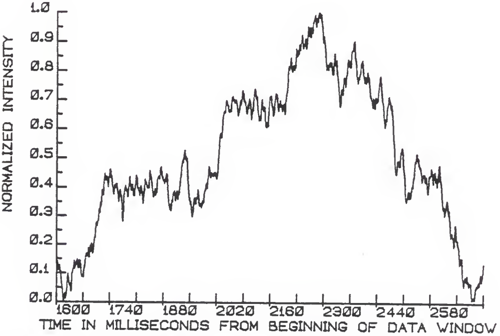

Figure 5-16. Detailed integration plot of ZC1221 showing the secondary event.

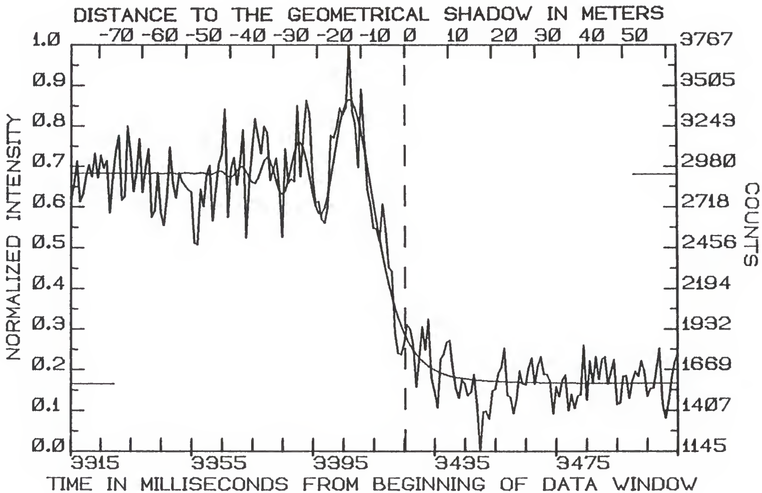

Figure 5-17. FITPLOT of the occultation of ZC1221.

found to be 0.3881 seconds of arc per second. The projected separation between the two stars, therefore, was 0.44 seconds of arc.

The actual change in mean signal level due to the fainter star's disappearance, as determined from the 500-millisecond samples before and after the secondary event, was 29.5 counts. This is only 0.022 of the intensity of the brighter star. Hence, the fainter star is approximately 4 magnitudes fainter in V than the brighter star. While there is always the possibility of a second star coincidentally being in the field of view under study, in an 15.2 arcsecond diaphragm (such as was employed for this observation) the likelihood of such a coincidence is only one part in 10000. Thus, it is extremely likely that ZC1221 is a double star, with a previously undetected component having a V magnitude of approximately 10.4.

Since the secondary event was well separated in time from the primary (i.e., "wide" in the sense of an occultation binary), the disappearance of the fainter star did not enter into the solution of the primary event. The solution to the occultation intensity curve of ZC1221 yielded a sensible angular diameter of 2.70 milliseconds of arc. Figure 5-18 shows the sensitivity of the solution intensity curve to variations in the solution parameters. The diameter determination is most sensitive at the time of the first order fringe maximum, though still highly sensitive at the zeroith and first order minima. As can be seen in

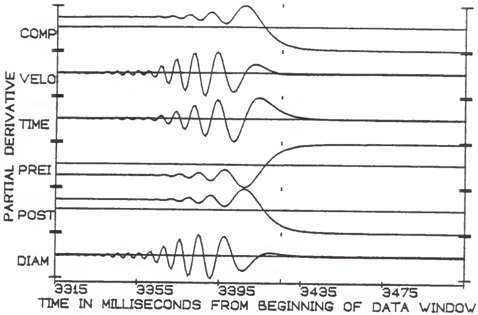

Figure 5-18. PDPLOT of the occultation of ZC1221.

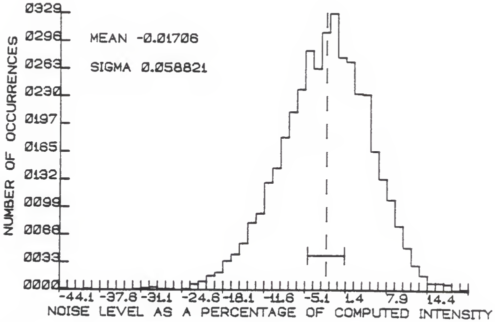

Figure 5-19. NOISEPLOT of the occultation of ZC1221.

Figure 5-18, the best fit to the observed data, in this region, is quite good.

Figure 5-19 shows the residuals of the fit to the 4096 milliseconds of the observation. The Gaussian nature of the residuals (with a slight Poisson tail) is typical of a good fit and a well behaved sky background. The mean deviation from the observed intensity (a measure of the overall observational noise) is only 5.8 percent.

The contiguous subset of observed intensity data, the computed intensity, and the resulting residuals are given in Table 5-10. The variance-covariance and correlation matrices of the adjusted solution parameters, and the dynamic ranges of the partial derivatives of the intensity curve are presented in Table 5-11.

The POWERPLOT, Figure 5-20, of this event clearly shows that the high frequency components of the noise in the raw data arise from scintillation and photon statistics and are not inherent in the occultation signal.

It is of interest to note if the diameter determined by the occultation observation is reasonable in light of what is known about this and similar stars. The distance of ZC1221, as taken from its parallax given by Schlesinger and Jenkins (1940), is roughly 250 parsecs. This is also indicated by an absolute magnitude of -0.7, assumed from its spectral type and luminosity class. Typical characteristics of giant stars are tabulated by Mihalas and Binney (1981). Working from these tables one would expect the linear diameter of an

TABLE 5-10
ZC1221: OBSERVATIONS, COMPUTED VALUES, AND RESIDUALS FROM BIN 3315

NUM	OBS	COMP	RESID	NUM	OBS	COMP	RESID	NUM	OBS	COMP	RESID
0	2770	2935.4	-165.4	67	2958	2963.2	-5.2	134	1441	1601.6	-160.6
1	2868	2935.6	-67.6	68	3036	2888.3	147.7	135	1145	1599.9	-454.9
2	3016	2935.5	80.5	69	2855	2825.4	29.6	136	1403	1598.4	-195.4
3	2753	2935.3	-182.3	70	2528	2799.7	-271.7	137	1405	1597.0	-192.0
4	2801	2935.3	-134.3	71	3095	2823.0	272.0	138	1354	1595.8	-241.8
5	2914	2935.4	-21.4	72	2873	2890.1	-17.1	139	1531	1594.7	-63.7
6	2991	2935.5	55.5	73	2900	2981.2	-81.2	140	1548	1593.7	-45.7
7	2918	2935.5	-17.5	74	2887	3069.2	-182.2	141	1645	1592.7	52.3
8	3065	2935.4	129.6	75	3377	3128.4	248.6	142	1685	1591.9	93.1
9	2910	2935.2	-25.2	76	2918	3141.7	-223.7	143	1811	1591.1	219.9
10	3054	2935.3	118.7	77	3175	3104.5	70.5	144	1506	1590.3	-84.3
11	2971	2935.8	35.2	78	3411	3025.2	385.8	145	1492	1589.6	-97.6
12	3018	2935.7	82.3	79	3328	2921.4	406.6	146	1391	1589.0	-198.0
13	2683	2935.2	-252.2	80	2919	2815.6	103.4	147	1485	1588.4	-103.4
14	2917	2935.1	-18.1	81	2747	2729.3	17.7	148	1665	1587.8	77.2
15	3080	2935.6	144.4	82	2754	2679.0	75.0	149	1579	1587.3	-8.3
16	3183	2935.8	247.2	83	2641	2673.9	-32.9	150	1574	1586.9	-12.9
17	2763	2935.4	-172.4	84	2617	2714.6	-97.6	151	1684	1586.5	97.5
18	2787	2935.3	-148.3	85	2722	2795.0	-73.0	152	1746	1586.2	159.8
19	3245	2935.7	309.3	86	3185	2903.4	281.6	153	1577	1585.8	-8.8
20	3071	2935.6	135.4	87	3167	3025.7	141.3	154	1696	1585.5	110.5
21	2820	2935.0	-115.0	88	3239	3147.3	91.7	155	1754	1585.1	168.9
22	2943	2935.4	7.6	89	3363	3255.4	107.6	156	1638	1584.8	53.2
23	3162	2936.5	225.5	90	3319	3340.0	-21.0	157	1639	1584.5	54.5
24	2815	2936.4	-121.4	91	3363	3394.5	-31.5	158	1598	1584.2	13.8
25	2975	2934.7	40.3	92	3767	3416.0	351.0	159	1387	1584.0	-197.0
26	3095	2934.0	161.0	93	3344	3404.5	-60.5	160	1560	1583.8	-23.8
27	2655	2935.9	-280.9	94	3259	3362.6	-103.6	161	1497	1583.6	-86.6
28	2693	2938.0	-245.0	95	2975	3294.6	-319.6	162	1603	1583.4	19.6
29	2941	2937.1	3.9	96	3482	3205.8	276.2	163	1636	1583.2	52.8
30	2689	2933.8	-244.8	97	3172	3101.6	70.4	164	1408	1583.0	-175.0
31	2601	2932.9	-331.9	98	2833	2987.6	-154.6	165	1512	1582.8	-70.8
32	2782	2936.0	-154.0	99	2741	2868.7	-127.7	166	1423	1582.6	-159.6
33	3106	2939.2	166.8	100	2582	2748.9	-166.9	167	1502	1582.4	-80.4
34	2872	2938.2	-66.2	101	2579	2631.6	-52.6	168	1508	1582.3	-74.3
35	2779	2934.1	-155.1	102	2505	2519.5	-14.5	169	1830	1582.2	247.8
36	2942	2932.3	9.7	103	2737	2414.2	322.8	170	1475	1582.0	-107.0
37	2883	2935.2	-52.2	104	2575	2317.0	258.0	171	1728	1581.9	146.1
38	2857	2939.2	-82.2	105	2335	2228.3	106.7	172	1587	1581.8	5.2
39	2831	2939.1	-108.1	106	2307	2148.4	158.6	173	1755	1581.6	173.4
40	2815	2935.3	-120.3	107	1916	2077.0	-161.0	174	1610	1581.5	28.5
41	2488	2932.9	-444.9	108	1777	2013.7	-236.7	175	1735	1581.4	153.6
42	2478	2935.4	-457.4	109	1769	1958.0	-189.0	176	1751	1581.3	169.7
43	2834	2939.9	-105.9	110	1839	1909.3	-70.3	177	1577	1581.2	-4.2
44	2723	2940.3	-217.3	111	1965	1866.8	98.2	178	1655	1581.1	73.9
45	2927	2934.8	-7.8	112	1933	1829.9	103.1	179	1736	1581.0	155.0
46	2989	2929.2	59.8	113	1837	1798.0	39.0	180	1446	1581.0	-135.0
47	2631	2931.0	-300.0	114	1559	1770.4	-211.4	181	1456	1580.9	-124.9
48	2819	2941.1	-122.1	115	1747	1746.6	0.4	182	1627	1580.8	46.2
49	3003	2951.0	52.0	116	1947	1726.0	221.0	183	1632	1580.7	51.3
50	3063	2950.0	113.0	117	1799	1708.3	90.7	184	1488	1580.6	-92.6
51	3357	2935.5	421.5	118	1998	1693.1	304.9	185	1599	1580.6	18.4
52	2654	2917.2	-263.2	119	1621	1679.9	-58.9	186	1658	1580.5	77.5
53	2967	2910.7	56.3	120	1535	1668.5	-133.5	187	1629	1580.4	48.6
54	3039	2924.7	114.3	121	1426	1658.6	-232.6	188	1728	1580.4	147.6
55	2862	2953.2	-91.2	122	1739	1650.0	89.0	189	1660	1580.3	79.7
56	3007	2977.6	29.4	123	1769	1642.6	126.4	190	1498	1580.3	-82.3
57	3221	2979.6	241.4	124	1845	1636.1	208.9	191	1548	1580.2	-32.2
58	2523	2953.3	-430.3	125	1859	1630.4	228.6	192	1551	1580.2	-29.2
59	2863	2911.3	-48.3	126	1687	1625.5	61.5	193	1676	1580.1	95.9
60	3093	2877.5	215.5	127	1552	1621.1	-69.1	194	1807	1580.1	226.9
61	3293	2873.5	419.5	128	1489	1617.2	-128.2	195	1455	1580.0	-125.0
62	3174	2905.9	268.1	129	1602	1613.8	-11.8	196	1359	1580.0	-221.0
63	3067	2961.9	105.1	130	1580	1610.8	-30.8	197	1465	1579.9	-114.9
64	3243	3015.5	227.5	131	1505	1608.1	-103.1	198	1615	1579.9	35.1
65	3204	3039.9	164.1	132	1526	1605.7	-79.7	199	1719	1579.8	139.2
66	2892	3020.9	-128.9	133	1640	1603.5	36.5	200	1775	1579.8	195.2

TABLE 5-11
ZC1221: SUPPLEMENTAL STATISTICAL INFORMATION

VARIANCE/CO-VARIANCE MATRIX

DIAM	PREI	POST	TIME	VELO
2.463E¯16	3.103E¯08	-2.809E¯08	-7.701E¯10	2.575E¯11
3.103E¯08	2.781E02	8.816E00	-1.967E00	4.594E¯02
-2.809E¯08	8.816E00	3.423E02	-2.411E00	5.674E¯02
-7.701E¯10	-1.967E00	-2.411E00	3.342E¯01	-7.973E¯03
2.575E¯11	4.594E¯02	5.674E¯02	-7.973E¯03	2.643E¯04

CORRELATION MATRIX

	DIAM	PREI	POST	TIME	VELO
DIAM	1.000000	0.797793	-0.744069	0.077028	-0.081285
PREI	0.797793	1.000000	-0.191055	-0.535414	0.531644
POST	-0.744069	-0.191055	1.000000	-0.721129	0.723939
TIME	0.077028	-0.535414	-0.721129	1.000000	-0.999988
VELO	-0.081285	0.531644	0.723939	-0.999988	1.000000

NUMERICAL RANGES OF THE PARTIAL DERIVATIVES

	MAXIMUM	MINIMUM
DIAM	2.730E09	-2.742E09
PREI	1.358E00	1.324E¯03
POST	9.987E¯01	-3.578E¯01
TIME	1.200E02	-1.243E02
VELO	4.841E03	-5.026E03

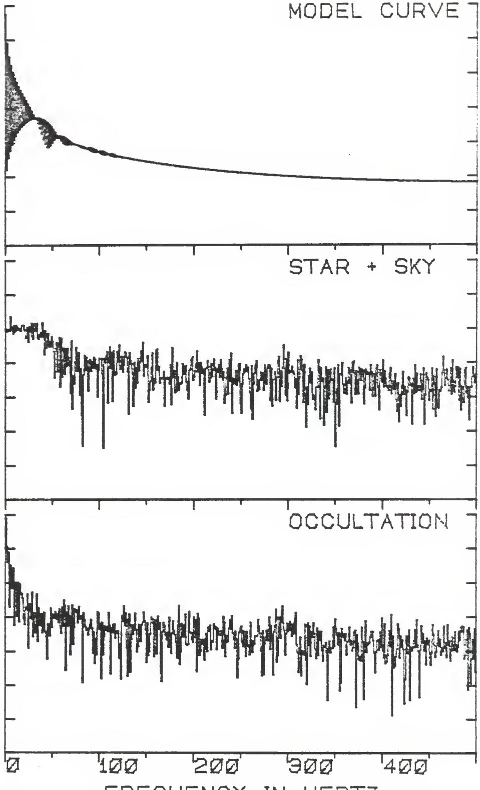

Figure 5-20. POWERPLOT of the occultation of ZC1221.

M3-III star to be on the order of 50 solar diameters. At a distance of 250 parsecs this corresponds to an angular diameter of 1.9 milliseconds of arc. Hence, the observationally determined diameter seems entirely reasonable and in accord with the previously known stellar data.

A rather good internal precision of the time of geometrical occultation, with a formal error of only 0.58 milliseconds, was achieved in the reduction process. However, the radio signal carrying the WWVB time code was unusually noisy, leading to a large one sigma error in the Coordinated Universal Time of 0.012 seconds. The Coordinated Universal Time of geometrical occultation was determined to be 00:44:55.877 (+/- 0.012 seconds).

ZC1222

As indicated on the occultation summary for the G0 star ZC1222 (Table 5-12), this event occured only one half hour after the previously discussed occultation of 9 Cancri. The photometric conditions for these two events were nearly identical. This is evidenced by an intercomparison of the normalized standard errors, and the photometric (S+N)/N ratios of the two events (noting that ZC1222 is both a magnitude fainter and considerably bluer than ZC1221). The event was extremely well placed, being at a zenith distance of only 8 degrees.

The RAWPLOT of the event is shown in Figure 5-21. The integration plot over the entire data window (Figure 5-22), as well as an examination of other detailed integration plots

TABLE 5-12
ZC1222: LUNAR OCCULTATION SUMMARY

STELLAR AND OBSERVING INFORMATION

Star: ZC1222, (SAO 079948, DM +22 1854)
RA: 080535 DEC: +223024 mV: 7.22 Sp: G0
Filter: V Diaphragm: I Gain: C10 Voltage: 1200

LUNAR INFORMATION

Surface Illumination:	72 percent
Elongation from Sun:	116 degrees
Altitude Above Horizon:	82 degrees
Lunar Limb Distance:	360913 Kilometers
Predicted Shadow Velocity:	336.9 meters/sec.
Predicted Angular Rate:	0.2467 arcsec/sec.

EVENT INFORMATION

Date: March 24, 1983		UT of Event:	01:14:46
USNO V/O Code:	26	HA of Event:	-042030
Position Angle:	150.8	Cusp Angle:	42S
Contact Angle:	-49.6	Watts Angle:	137.8

MODEL PARAMETERS

Number of Data Points:	201
Number of Grid Points:	256
Number of Spectral Regions:	53
Width of Spectral Regions:	50 Angstroms
Limb Darkening Coefficient:	0.5
Effective Stellar Temperature:	5900 K

SOLUTIONS

Stellar Diameter (ams):	Point Source	
Time: (relative to Bin 0):	2923.3	(2.1)
Pre-Event Signal:	2117.4	(20.7)
Background Sky Level:	1305.0	(44.8)
Velocity (meters/sec.):	431.7	(12.5)
Lunar Limb Slope (degrees):	+19.34	(1.67)
U.T. of Occultation:	01:14:46.177	(0.004)

PHOTOMETRIC NOISE INFORMATION

Sum-of-Squares of Residuals:	13498450
Sigma (Standard Error):	259.7927
Normalized Standard Error:	0.31979
Photometric (S+N)/N Ratio:	4.12699
(Change in Intensity)/Background:	0.62251
Change in Magnitude:	0.52547

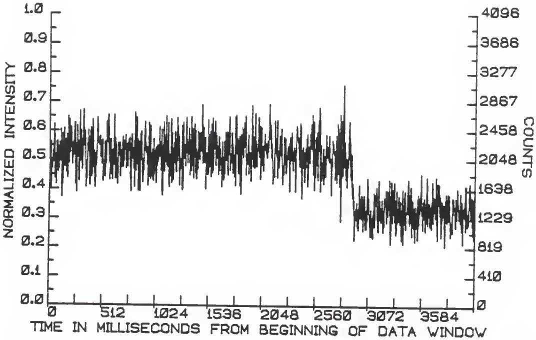

Figure 5-21. RAWPLOT of the occultation of ZC1222.

Figure 5-22. INTPLOT of the occultation of ZC1222.

of data subsets, show no compelling evidence of "wide" stellar duplicity.

The best model fit to the observations indicated that the star was a point source (or at least below the detection threshold of approximately 1 millisecond of arc). This was as expected, considering the spectral type and apparent V magnitude of the star. The graphic depiction of the fit is shown in Figure 5-23. The observational data, the solution curve intensities and the residuals are given in Table 5-13. The formal statistics of the solution parameters (variance-covariance, correlation matrices, and range of partial derivatives) can be found in Table 5-14. The PDPLOT, showing the sensitivity of the model intensity curve to the variation of the solution parameters, is presented as Figure 5-24.

The internal formal error of the time of geometrical occultation was not quite as good as one might have expected, if that expectation were based solely on the noise statistics of the observation. It should be noted that the determined L-rate for this event (431.7 meters/second) is 63 percent slower than the L-rate determined for the ZC1221 event (691.0 meters/second). Under identical photometric conditions this would widen the uncertainty in the time of geometrical occultation by the same amount. Fortunately, in the intervening half hour between these two events, the signal strength of the WWVB time code improved dramatically. The one sigma error of the WWVB time reference was a reasonable

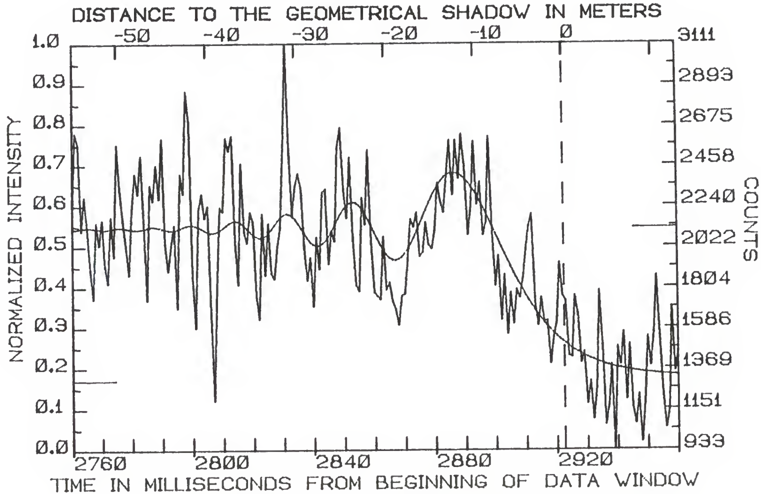

Figure 5-23. FITPLOT of the occultation of ZC1222.

TABLE 5-13
ZC1222: OBSERVATIONS, COMPUTED VALUES, AND RESIDUALS FROM BIN 2760

NUM	OBS	COMP	RESID	NUM	OBS	COMP	RESID	NUM	OBS	COMP	RESID
0	2145	2115.9	29.1	67	1851	2134.5	-283.5	134	2245	2291.5	-46.5
1	2634	2115.9	518.1	68	2020	2156.3	-136.3	135	2365	2261.6	103.4
2	2574	2117.4	456.6	69	2126	2175.3	-49.3	136	2081	2229.8	-148.8
3	2107	2119.9	-12.9	70	2559	2189.1	369.9	137	2151	2196.5	-45.5
4	2287	2122.6	164.4	71	3111	2195.8	915.2	138	2611	2162.1	448.9
5	2125	2124.3	0.7	72	2540	2194.7	345.3	139	2100	2127.0	-27.0
6	1903	2124.6	-221.6	73	2186	2185.5	0.5	140	1814	2091.4	-277.4
7	1745	2123.1	-378.1	74	2344	2169.0	175.0	141	1975	2055.6	-80.6
8	2151	2120.4	30.6	75	2413	2146.9	266.1	142	1628	2019.9	-391.9
9	2031	2117.4	-86.4	76	2335	2121.1	213.9	143	1871	1984.6	-113.6
10	2164	2115.3	48.7	77	2019	2094.3	-75.3	144	1553	1949.8	-396.8
11	1918	2114.6	-196.6	78	1840	2069.0	-229.0	145	1775	1915.8	-140.8
12	1830	2115.8	-285.8	79	1964	2047.7	-83.7	146	1606	1882.6	-276.6
13	2182	2118.6	63.4	80	1703	2032.5	-329.5	147	1796	1850.4	-54.4
14	1971	2121.9	-150.9	81	2073	2024.8	48.2	148	1747	1819.3	-72.3
15	2571	2124.7	446.3	82	1903	2025.6	-122.6	149	1848	1789.4	58.6
16	2335	2126.0	209.0	83	2310	2034.8	275.2	150	1998	1760.6	237.4
17	2166	2125.3	40.7	84	2329	2051.8	277.2	151	2128	1733.2	394.8
18	2032	2122.8	-90.8	85	1931	2075.3	-144.3	152	2193	1707.0	486.0
19	1873	2119.3	-246.3	86	2107	2103.7	3.3	153	1727	1682.1	44.9
20	2213	2116.0	97.0	87	2049	2134.7	-85.7	154	1598	1658.5	-60.5
21	2415	2113.7	301.3	88	2551	2166.1	384.9	155	1749	1636.1	112.9
22	2303	2113.4	189.6	89	2660	2195.5	464.5	156	1620	1615.0	5.0
23	2508	2115.4	392.6	90	2329	2220.8	108.2	157	1624	1595.1	28.9
24	2155	2119.1	35.9	91	2174	2240.4	-66.4	158	1391	1576.3	-185.3
25	1738	2123.3	-385.3	92	2500	2252.9	247.1	159	1534	1558.7	-24.7
26	2353	2127.0	226.0	93	2067	2257.3	-190.3	160	1611	1542.2	68.8
27	2267	2128.8	138.2	94	1819	2253.5	-434.5	161	1935	1526.7	408.3
28	2460	2128.3	331.7	95	1783	2241.7	-458.7	162	1759	1512.3	246.7
29	2279	2125.1	153.9	96	2283	2222.4	60.6	163	1730	1498.7	231.3
30	2602	2120.3	481.7	97	2138	2197.0	-59.0	164	1434	1486.1	-52.1
31	2040	2115.0	-75.0	98	2541	2166.8	374.2	165	1425	1474.3	-49.3
32	1894	2110.5	-216.5	99	2047	2133.4	-86.4	166	1759	1463.3	295.7
33	2026	2108.4	-82.4	100	1780	2098.7	-318.7	167	1662	1453.0	209.0
34	2139	2109.3	29.7	101	1759	2064.5	-305.5	168	1396	1443.4	-47.4
35	1694	2113.2	-419.2	102	1741	2032.4	-291.4	169	1456	1434.6	21.4
36	2412	2119.5	292.5	103	2074	2004.0	70.0	170	1175	1426.3	-251.3
37	2307	2126.8	180.2	104	1790	1980.7	-190.7	171	1299	1418.6	-119.6
38	2859	2133.4	725.6	105	1831	1963.4	-132.4	172	1095	1411.4	-316.4
39	2696	2137.6	558.4	106	1734	1952.9	-218.9	173	1263	1404.8	-141.8
40	1866	2138.2	-272.2	107	1687	1949.5	-262.5	174	1787	1398.6	388.4
41	1589	2134.9	-545.9	108	1603	1953.4	-350.4	175	1492	1392.8	99.2
42	2215	2127.9	87.1	109	1759	1964.4	-205.4	176	1066	1387.5	-321.5
43	2303	2118.6	184.4	110	1767	1981.9	-214.9	177	1165	1382.5	-217.5
44	2175	2108.7	66.3	111	1951	2005.4	-54.4	178	1388	1377.9	10.1
45	2239	2100.3	138.7	112	2169	2033.9	135.1	179	933	1373.6	-440.6
46	1667	2095.2	-428.2	113	2126	2066.5	59.5	180	1483	1369.6	113.4
47	1197	2094.8	-897.8	114	2203	2102.0	101.0	181	1385	1365.8	19.2
48	1801	2099.4	-298.4	115	1967	2139.4	-172.4	182	1562	1362.4	199.6
49	2232	2108.6	123.4	116	1991	2177.6	-186.6	183	1200	1359.2	-159.2
50	2211	2120.9	90.1	117	2152	2215.5	-63.5	184	1496	1356.1	139.9
51	2607	2134.5	472.5	118	2031	2252.0	-221.0	185	1161	1353.3	-192.3
52	2535	2146.8	388.2	119	2011	2286.3	-275.3	186	1071	1350.7	-279.7
53	2615	2155.7	459.3	120	2102	2317.7	-215.7	187	1227	1348.3	-121.3
54	2055	2159.5	-104.5	121	2361	2345.3	15.7	188	974	1346.0	-372.0
55	1821	2157.2	-336.2	122	2263	2368.8	-105.8	189	1183	1343.9	-160.9
56	2466	2148.9	317.1	123	2204	2387.8	-183.8	190	1535	1341.9	193.1
57	2104	2135.5	-31.5	124	2399	2401.8	-2.8	191	1380	1340.0	40.0
58	2043	2118.8	-75.8	125	2590	2410.9	179.1	192	1557	1338.3	218.7
59	2207	2101.3	105.7	126	2296	2415.0	-119.0	193	1864	1336.7	527.3
60	2156	2085.4	70.6	127	2592	2414.2	177.8	194	1540	1335.1	204.9
61	1763	2073.7	-310.7	128	2385	2408.6	-23.6	195	1224	1333.7	-109.7
62	1635	2068.0	-433.0	129	2623	2398.4	224.6	196	1048	1332.4	-284.4
63	2198	2069.3	128.7	130	2450	2384.0	66.0	197	1146	1331.1	-185.1
64	1871	2077.8	-206.8	131	2083	2365.8	-282.8	198	1697	1329.9	367.1
65	2145	2092.8	52.2	132	2228	2344.0	-116.0	199	1351	1328.8	22.2
66	1881	2112.4	-231.4	133	2583	2319.1	263.9	200	1455	1327.8	127.2

TABLE 5-14
ZC1222: SUPPLEMENTAL STATISTICAL INFORMATION

VARIANCE/CO-VARIANCE MATRIX

DIAM	PREI	POST	TIME	VELO
2.849E¯15	1.373E¯07	-5.788E¯07	7.215E¯10	1.217E¯11
1.373E¯07	4.349E02	7.193E01	-1.093E01	5.701E¯02
-5.788E¯07	7.193E01	2.154E03	-4.181E01	2.091E¯01
7.215E¯10	-1.093E01	-4.181E01	4.480E00	-2.315E¯02
1.217E¯11	5.701E¯02	2.091E¯01	-2.315E¯02	1.587E¯04

CORRELATION MATRIX

	DIAM	PREI	POST	TIME	VELO
DIAM	1.000000	0.288964	-0.968314	0.871718	-0.865589
PREI	0.288964	1.000000	-0.040942	-0.210200	0.221926
POST	-0.968314	-0.040942	1.000000	-0.965427	0.962118
TIME	0.871718	-0.210200	-0.965427	1.000000	-0.999923
VELO	-0.865589	0.221926	0.962118	-0.999923	1.000000

NUMERICAL RANGES OF THE PARTIAL DERIVATIVES

	MAXIMUM	MINIMUM
DIAM	8.475E08	-8.332E08
PREI	1.366E00	2.803E¯02
POST	9.720E¯01	-3.664E¯01
TIME	3.576E01	-3.819E01
VELO	6.809E03	-7.093E03

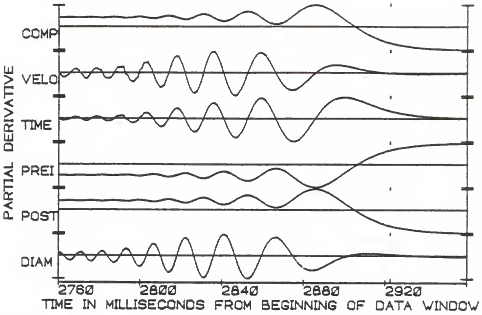

Figure 5-24. PDPLOT of the occultation of ZC1222.

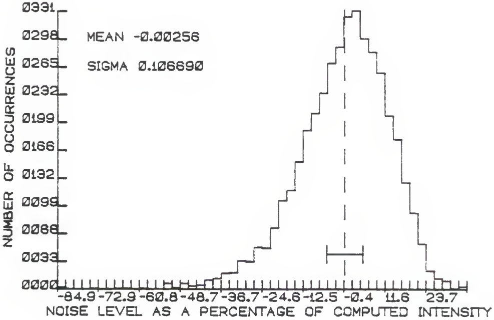

Figure 5-25. NOISEPLOT of the occultation of ZC1222.

3.1 milliseconds. The Universal Time of geometrical occultation was found to be 01:14:50.125 (+/- 0.004 seconds).

The distribution function of the residuals over the 4096 milliseconds of the observation can be seen in Figure 5-25. As expected, this distribution function is quite similar in character to that seen for the ZC1221 occultation. The POWERPLOT for this event is presented as Figure 5-26.

X07589

The occultation of X07589 on April 18, 1983, was observed with the moon only 25 percent illuminated, at a solar elongation of 59 degrees (as noted in Table 5-15). The Earthshine on the shadowed portion of the lunar disk was quite bright, easily detectable to the unaided eye and, of course, photometrically. Examination of the 4096 millisecond plot of the raw data, presented in Figure 5-27, reveals unquestionably that the moon's limb entered the photometeric field of view approximately 2200 milliseconds from the beginning of the data window. For most occultation observations the increase in background signal level due to sunlight reflected off the lunar limb is such a small contributing source that it can be ignored. However, this is not the case for small lunar elongations, when Earthshine can be a major variable source of background light. This is evidenced, in this case, by the inverted nature of the integration plot for X07589 (Figure 5-27) prior to the time of occultation. Stellar duplicity would produce a cusp,

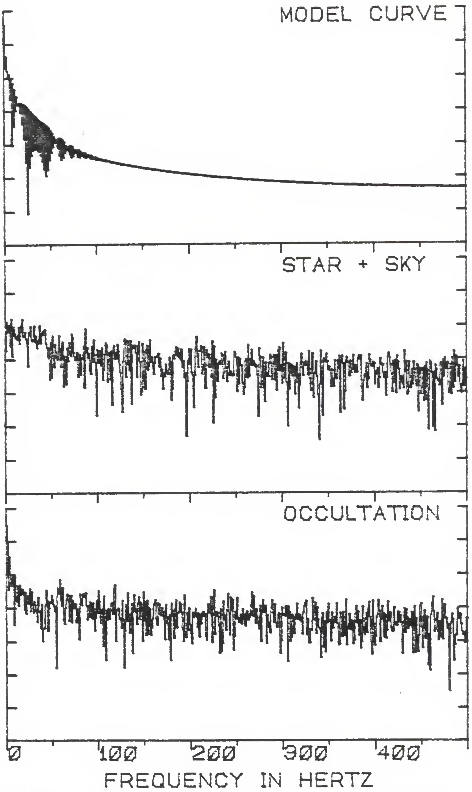

Figure 5-26. POWERPLOT of the occultation of ZC1222.

TABLE 5-15
X07589: LUNAR OCCULTATION SUMMARY

STELLAR AND OBSERVING INFORMATION

Star: X07589 (SAO 077552, DM +23 1042)
RA: 054609 DEC: +230959 mV: 8.6 Sp: M0
Filter: V Diaphragm: I Gain: C10+ Voltage: 1200

LUNAR INFORMATION

Surface Illumination:	25 percent
Elongation from Sun:	59 degrees
Altitude Above Horizon:	36 degrees
Lunar Limb Distance:	368613 kilometers
Predicted Shadow Velocity:	843.5 meters/sec.
Predicted Angular Rate:	0.4720 arcsec/sec.

EVENT INFORMATION

Date: April 18, 1983		UT of Event:	01:35:12
USNO V/O Code:	26	HA of Event:	+601759
Position Angle:	95.7	Cusp Angle:	83S
Contact Angle:	-4.3	Watts Angle:	95.9

MODEL PARAMETERS

Number of Data Points:	201
Number of Grid Points:	256
Number of Spectral Regions:	53
Width of Spectral Regions:	50 Angstroms
Limb Darkening Coefficient:	0.5
Effective Stellar Temperature:	5900K

SOLUTIONS

Stellar Diameter (ams):	Point Source
Time: (relative to Bin 0):	3983.3 (2.1)
Pre-Event Signal:	1977.9 (34.8)
Background Sky Level:	1129.0 (36.1)
Velocity (meters/sec.):	1341.3 (95.8)
Lunar Limb Slope (degrees):	-25.5 (6.5)
U.T. of Occultation:	01:35:12.172 (0.051)

PHOTOMETRIC NOISE INFORMATION

Sum-of-Squares of Residuals:	24078840
Sigma (Standard Error):	346.9787
Normalized Standard Error:	0.40873
Photometric (S+N)/N Ratio:	3.44663
(Change in Intensity)/Background:	0.75192
Change in Magnitude:	0.60879

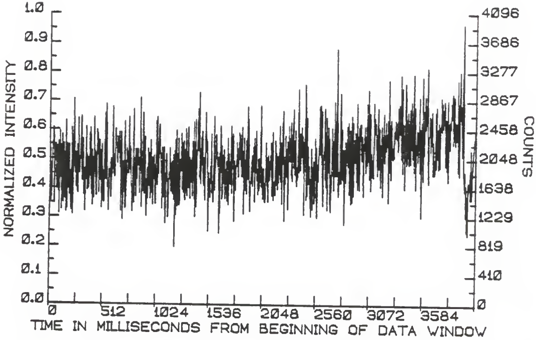

Figure 5-27. RAWPLOT of the occultation of X07589.

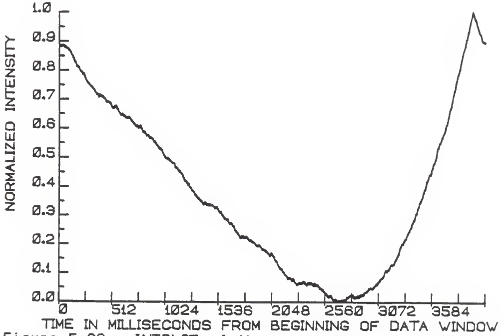

Figure 5-28. INTPLOT of the occultation of X07589.

deflecting the curve in a downward direction. The intrusion of increasing Earthshine midway through the data window caused a decrease in the integrated intensity (subtracted from the mean) for data taken before the moon's limb entered the diaphragm.

Fortunately, since the star was held close to the center of the field-of-view (as called for by standard observing procedures), the increase in background illumination was very close to linear over the short timescale of the occultation event. The lunar angular velocity for this event was 0.4720 seconds of arc per second. Thus, in the 200 milliseconds of data extracted for the DC solution, the lunar limb traversed an angular distance of only about 100 milliseconds of arc. This is only 1/150 of the diameter of the field-of-view given by the diaphragm employed in the observation. (See Table 2-3).

The assumption of linearity in the increase in background light is indeed proven correct by examination of the integration plot. The non-linear change in intensity (due to Earthshine) begins at roughly 2200 milliseconds. The slope of the descending branch of the integration plot changes here. The time at which the change in intensity due to contributed Earthlight is greatest, is at the minumum of the integration plot, at approximately 2700 milliseconds. While still increasing, the change in Earthlight is essentially linear by millisecond 3600, where the slope of the integration plot remains constant until the decrease caused by the occultation itself sets in.

The result of a linear increase in background light causes an effective tilt in the observed occultation intensity curve. Rather than modeling the slope of this tilt as an additional free parameter in the DC solution, a simpler approach was taken. A linear least squares fit was done to both the pre-occultation and post-occultation observations, each containing 100 samples of data bordering the solution data subset. The characteristic slopes obtained were found to be in good agreement and were averaged. The occultation data were then "detilted" by the appropriate amount before being submitted to the DC solution process.

The only time this method of removing increasing moonlight from the occultation data set would not be valid are in the cases of near-grazing incidence, or if the star were near the eastern or western extreme of the field-of-view. In either of these cases, the increase of moonlight at the time of occultation would be non-linear.

In this case, within the linear portions of the integration plot examined in detail, there was no indication of a secondary stellar component.

The solution to the intensity curve is presented graphically on Figure 5-29. The geometry of this event led to a rather rapid L-rate, and as a result the intensity variation of the solution curve is a bit obscured in Figure 5-29. A detailed depiction of the region of interest

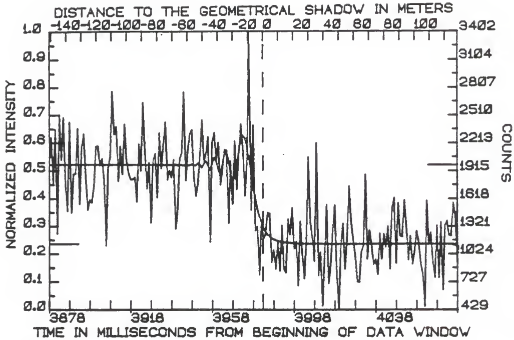

Figure 5-29. FITPLOT of the occultation of X07589.

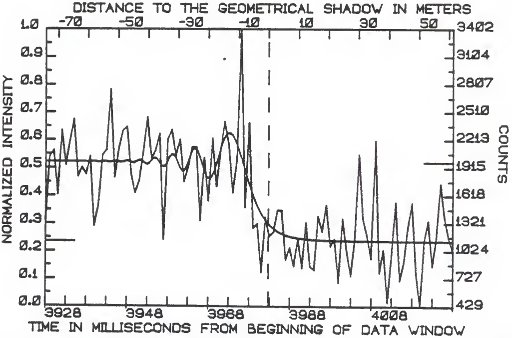

Figure 5-30. 100 millisecond detailed FITPLOT for X07589.

(covering only 100 milliseconds of the observation) is presented in Figure 5-30.

The diameter of X07589 was below the detection threshold, and hence, was indistinguishable from a point source. The PDPLOT for the solution curve is presented as Figure 5-31. The observational data subset used in the solution determination and the computed intensity values, and their residuals are listed in Table 5-16. The variance-covariance and correlation matrices, and the ranges of the partial derivatives are given on Table 5-17.

No attempt was made to fit the non-linear increase in the sky background as the moon entered the diaphragm. Hence, the noise statistics for this event, as well as the distribution function (Figure 5-32) of the noise, reflect only the first 1600 milliseconds of pre-occultation data and detilted occultation data. Even the early part of the pre-occultation record contains an increase in the background level. This is evidenced by the skewed nature of the NOISEPLOT, Figure 5-32.

The power spectra of the event, the star-plus-sky signal, and the solution intensity curve are shown on Figure 5-33. The observed power spectra (occultation and star-plus-sky) reflect the actual observation with the increasing sky background included.

A formal internal error for the time of geometrical occultation of only 1.1 milliseconds was obtained for this event. As had been seen from previous experience, the signal

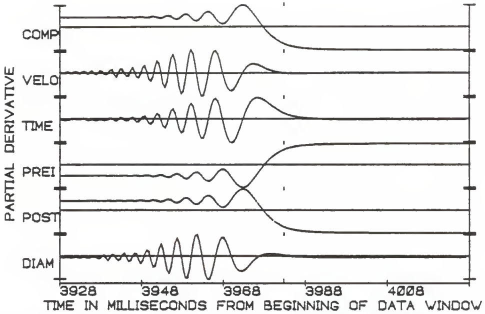

Figure 5-31. PDPLOT of the occultation of X07589.

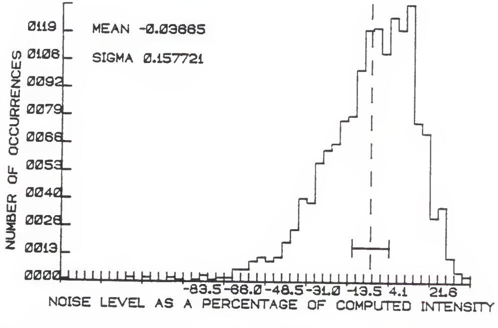

Figure 5-32. NOISEPLOT of the first 1600 milliseconds of data taken for the occultation observation of X07589.

TABLE 5-16
X07589: OBSERVATIONS, COMPUTED VALUES, AND RESIDUALS FROM BIN 3878

NUM	OBS	COMP	RESID	NUM	OBS	COMP	RESID	NUM	OBS	COMP	RESID
0	2023	1981.0	41.8	67	1816	1986.4	-170.4	134	474	1131.8	-657.8
1	2270	1981.1	289.3	68	2115	1978.7	136.8	135	996	1131.6	-136.1
2	1774	1981.0	-207.1	69	2310	1977.0	333.0	136	1551	1131.4	419.6
3	2352	1981.3	371.2	70	2354	1990.0	363.5	137	711	1131.3	-420.7
4	1244	1980.9	-736.9	71	1853	1974.4	-121.3	138	902	1131.2	-229.0
5	2514	1980.9	532.6	72	1649	1974.4	-325.8	139	1282	1131.0	150.6
6	2035	1981.1	53.9	73	1773	1999.4	-226.2	140	1545	1130.9	414.3
7	2482	1980.9	500.7	74	2092	1979.1	112.6	141	785	1130.8	-346.1
8	1765	1980.7	-215.6	75	2455	1954.3	501.0	142	429	1130.7	-701.4
9	1486	1980.7	-495.0	76	2011	1994.2	16.6	143	1129	1130.6	-1.8
10	2434	1980.8	453.4	77	2098	2020.5	77.8	144	1348	1130.6	217.8
11	1467	1980.8	-514.1	78	2278	1965.4	312.4	145	865	1130.5	-265.6
12	1878	1980.8	-102.5	79	1153	1926.5	-773.1	146	1168	1130.4	38.0
13	1888	1980.8	-93.0	80	2217	1987.4	229.5	147	1750	1130.3	619.6
14	2367	1980.8	386.5	81	2322	2058.0	264.5	148	1386	1130.3	255.2
15	1562	1980.8	-418.9	82	2040	2020.6	19.4	149	1170	1130.2	39.8
16	2166	1980.7	185.7	83	2217	1916.6	299.9	150	1014	1130.2	-116.6
17	2310	1980.9	329.1	84	1767	1884.8	-117.7	151	728	1130.1	-402.0
18	1846	1980.8	-135.3	85	1918	1974.3	-56.7	152	724	1130.1	-406.4
19	1498	1980.6	-482.6	86	2140	2092.3	47.8	153	1047	1130.0	-82.8
20	1606	1980.7	-375.1	87	2131	2118.3	12.4	154	1112	1130.0	-18.3
21	1580	1980.6	-400.4	88	1356	2024.4	-668.2	155	1871	1130.0	741.3
22	1748	1980.7	-233.0	89	2023	1886.3	136.4	156	971	1129.9	-159.1
23	2176	1980.7	195.6	90	1564	1805.8	-241.5	157	1274	1129.9	144.5
24	2179	1980.5	198.3	91	2232	1835.7	396.1	158	1123	1129.9	-7.0
25	1971	1980.5	-9.2	92	1717	1958.4	-241.0	159	909	1129.8	-220.4
26	2043	1980.4	62.5	93	2099	2112.9	-14.0	160	964	1129.8	-165.8
27	1821	1980.6	-159.2	94	2411	2235.8	175.6	161	804	1129.8	-326.3
28	1114	1980.7	-866.8	95	2173	2288.3	-115.4	162	1243	1129.7	113.3
29	1945	1980.8	-35.3	96	1650	2262.2	-612.7	163	971	1129.7	-159.1
30	2064	1980.4	83.6	97	1991	2171.7	-180.7	164	1238	1129.7	108.4
31	2767	1980.4	786.1	98	3402	2041.4	1360.2	165	1098	1129.7	-32.0
32	2302	1980.7	321.4	99	1496	1895.5	-399.4	166	1321	1129.7	191.6
33	2384	1980.3	403.3	100	2400	1752.7	647.0	167	866	1129.6	-263.9
34	1809	1980.4	-171.3	101	1271	1624.3	-353.1	168	1520	1129.6	390.7
35	2178	1980.5	197.2	102	1318	1515.7	-197.9	169	1625	1129.6	495.2
36	1882	1980.2	-98.0	103	802	1427.5	-625.2	170	924	1129.6	-205.2
37	2412	1980.5	431.3	104	1386	1358.0	27.8	171	1571	1129.6	441.3
38	2024	1980.5	43.8	105	1185	1304.6	-119.2	172	1218	1129.5	88.9
39	1896	1980.4	-84.5	106	1230	1264.0	-34.0	173	1207	1129.5	77.4
40	1823	1980.3	-157.0	107	1468	1233.3	235.1	174	1603	1129.5	473.0
41	1826	1980.7	-154.8	108	1460	1210.4	249.6	175	1322	1129.5	192.5
42	1847	1980.2	-132.8	109	932	1193.1	-261.6	176	957	1129.5	-172.9
43	1586	1980.6	-394.6	110	1063	1180.1	-117.0	177	1216	1129.5	86.7
44	2203	1980.3	222.2	111	865	1170.2	-305.6	178	916	1129.5	-213.8
45	1918	1980.3	-62.2	112	1163	1162.7	0.5	179	1052	1129.5	-77.2
46	2645	1980.3	664.3	113	842	1156.8	-315.1	180	1269	1129.4	139.3
47	2123	1980.1	143.0	114	1329	1152.2	177.0	181	1160	1129.4	30.9
48	1729	1980.5	-251.8	115	860	1148.6	-288.8	182	923	1129.4	-206.6
49	2007	1980.2	27.0	116	824	1145.7	-321.4	183	809	1129.4	-320.0
50	1365	1980.1	-615.4	117	1400	1143.3	256.5	184	465	1129.4	-664.5
51	2034	1980.6	53.7	118	1234	1141.4	92.9	185	1592	1129.4	463.0
52	2103	1980.0	122.9	119	1520	1139.9	380.0	186	1127	1129.4	-2.4
53	1633	1980.8	-347.5	120	1078	1138.7	-60.2	187	1254	1129.4	124.1
54	2319	1979.7	339.2	121	1154	1137.6	16.3	188	935	1129.4	-194.3
55	1944	1980.8	-36.4	122	691	1136.7	-446.2	189	775	1129.4	-354.8
56	2200	1979.7	220.3	123	1373	1135.9	237.2	190	1329	1129.3	199.8
57	2436	1981.0	454.5	124	1033	1135.2	-102.6	191	772	1129.3	-357.7
58	1820	1979.9	-159.8	125	760	1134.6	-374.5	192	1365	1129.3	235.9
59	1923	1980.7	-58.1	126	1140	1134.2	5.5	193	641	1129.3	-488.6
60	1848	1981.2	-133.0	127	2063	1133.8	929.5	194	1332	1129.3	203.0
61	2038	1978.4	59.3	128	1377	1133.3	243.4	195	1380	1129.3	250.5
62	1297	1984.1	-686.9	129	1190	1132.9	57.3	196	1227	1129.3	98.1
63	1505	1976.8	-472.0	130	947	1132.7	-185.8	197	1221	1129.3	91.6
64	2050	1982.4	67.9	131	2210	1132.4	1077.9	198	1578	1129.3	449.1
65	2108	1982.4	125.4	132	791	1132.2	-341.3	199	1451	1129.3	321.7
66	2759	1975.5	783.9	133	1038	1131.9	-93.5	200	923	1129.3	-206.8

TABLE 5-17
X07589: SUPPLEMENTAL STATISTICAL INFORMATION

VARIANCE/CO-VARIANCE MATRIX

DIAM	PREI	POST	TIME	VELO
1.143E¯16	-4.465E¯08	-5.040E¯09	1.273E¯09	-1.521E¯10
-4.465E¯08	1.212E03	2.450E01	-5.787E00	4.580E¯01
-5.040E¯09	2.450E01	1.303E03	-5.392E00	3.745E¯01
1.273E¯09	-5.787E00	-5.392E00	1.196E00	-8.278E¯02
-1.521E¯10	4.580E¯01	3.745E¯01	-8.278E¯02	9.180E¯03

CORRELATION MATRIX

	DIAM	PREI	POST	TIME	VELO
DIAM	1.000000	-0.994887	0.113292	0.727451	-0.778838
PREI	-0.994887	1.000000	-0.210486	-0.654490	0.711548
POST	0.113292	-0.210486	1.000000	-0.587384	0.523549
TIME	0.727451	-0.654490	-0.587384	1.000000	-0.996928
VELO	-0.778838	0.711548	0.523549	-0.996928	1.000000

NUMERICAL RANGES OF THE PARTIAL DERIVATIVES

	MAXIMUM	MINIMUM
DIAM	8.781E08	-8.462E08
PREI	1.366E00	3.206E¯04
POST	9.997E¯01	-3.656E¯01
TIME	1.469E02	-1.496E02
VELO	1.601E03	-1.799E03

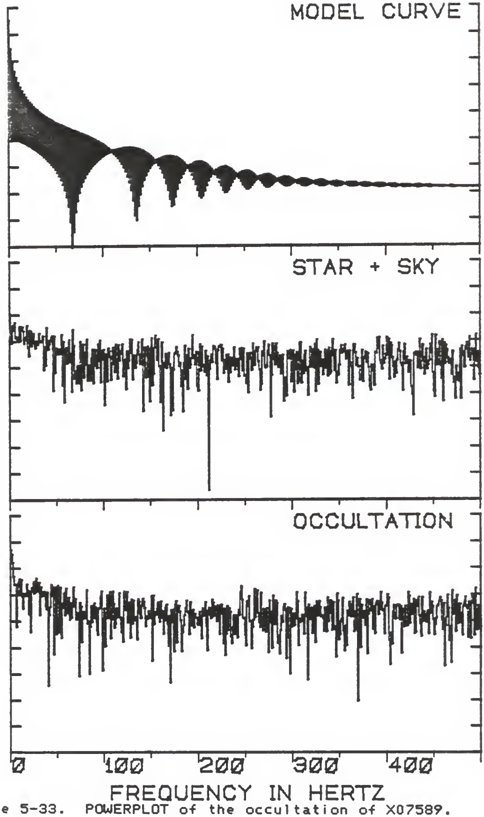

Figure 5-33. POWERPLOT of the occultation of X07589.

strength of the WWVB radio signal during and shortly after evening twilight tends to be quite low. As a result, no WWVB time code was available at the time of the event. Fortunately, the signal strength had improved sufficiently thirty seven minutes later to reliably detect the digital time code. The crystal controlled clock circuit of the SPICA-IV/LODAS system has been found to have a cumulative timing error of at most two seconds per day. Taking this as a worst case condition, the time of the event reckoned from the SPICA-IV/LODAS clock and synchronized to WWVB a half hour after occultation would have a one sigma error of approximately 0.025 seconds. The Universal Time of geometrical occultation was 01:35:12.17 (+/- 0.03 seconds).

X07598

Thirty five minutes after the previously discussed occultation of X07589, the star X07598 was occulted by the moon. The RAWPLOT of the digital photoelectric record obtained is presented in Figure 5-34. The integration plot, Figure 5-35 leads to no indication of "wide" stellar duplicity.

The near grazing geometry of this event (see Table 5-18) led to a predicted R-rate of only 0.0855 seconds of arc per second. Hence, the time-scale of the diffraction phenomena for this event was roughly four times slower than a more typical event. While this was known beforehand, a solution was attempted by fitting only 200 milliseconds of data. Even though a solution was found, the resulting model curve did

TABLE 5-18
X07598: LUNAR OCCULTATION SUMMARY

STELLAR AND OBSERVING INFORMATION

Star: X07598 (SAO 077559, DM +22 1032)
RA: 054627 DEC: +225501 mV: 7.5 Sp: K0
Filter: V Diaphram: I Gain: C8+ Voltage: 1200

LUNAR INFORMATION

Surface Illumination:	25 percent
Elongation from Sun:	59 degrees
Altitude Above Horizon:	28 degrees
Lunar Limb Distance:	369285 kilometers
Predicted Shadow Velocity:	153.1 meters/sec.
Predicted Angular Rate:	0.0855 arcsec/sec.

EVENT INFORMATION

Date:	April 18, 1983	UT of Event:	02:12:03
USNO V/O Code:	47	HA of Event:	+692638
Position Angle:	172.1	Cusp Angle:	7S
Contact Angle:	-80.3	Watts Angle:	172.3

MODEL PARAMETERS

Number of Data Points:	401
Number of Grid Points:	256
Number of Spectral Regions:	53
Width of Spectral Regions:	50 Angstroms
Limb Darkening Coefficient:	0.5
Effective Stellar Temperature:	5100 K

SOLUTIONS

Stellar Diameter (ams):	5.45	(2.04)
Time: (relative to Bin 0):	2645.1	(3.8)
Pre-Event Signal:	2253.0	(21.9)
Background Sky Level:	1139.3	(38.9)
Velocity (meters/sec.)	136.3	(4.4)
Lunar Limb Slope (degrees):	+13.5	(1.6)
U.T. of Occultation:	02:12:00.519	(0.004)

PHOTOMETRIC NOISE INFORMATION

Sum-of-Squares of Residuals:	47842640
Sigma (Standard Error):	345.8419
Normalized Standard Error:	0.31053
Photometric (S+N)/N Ratio:	4.22027
(Change in Intensity)/Background:	0.97752
Change in Magnitude:	0.74030

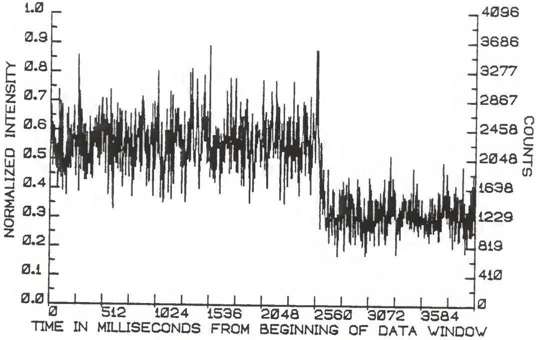

Figure 5-34. RAWPLOT of the occultation of X07598.

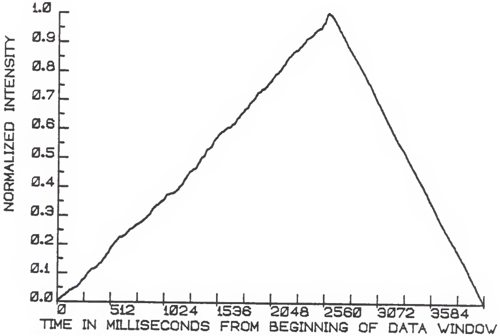

Figure 5-35. INTPLOT of the occultation of X07598.

not span a large enough portion of the intensity curve to be warranted as significant. The observation was re-reduced considering 400 milliseconds of data centered on the estimated time of geometrical occultation.

The solution obtained from the 400 millisecond data set is presented graphically in the FITPLOT, Figure 5-36. Except for the anomalous depression in the zero order diffraction maximum, the fit is quite good. This depression is not too troublesome, remembering that the time-scale is elongated by a factor of roughly four. It is unfortunate that variation in atmospheric transparency took its toll at this point, but it was not unduly critical in the determination of the solution.

The observational data used in the solution, the computed intensities and their residuals are given in Table 5-19. The usual supplementary statistical information is listed in Table 5-20.

An angular diameter for this K0 (mV=7.5) star of 5.45 (+/- 2.04) milliseconds of arc was determined. There is no apparent reason to doubt the validity of the solution in terms of numerical or computational problems as evidenced by either the PDPLOT (Figure 5-37), the distribution function of the residuals as given in the NOISEPLOT (Figure 5-38), or the comparative power spectra (Figure 5-39). A further attempt was made to check the validity of the numerical solution in this case by attempting a refit to the data by a four parameter model, holding the stellar diameter fixed as a

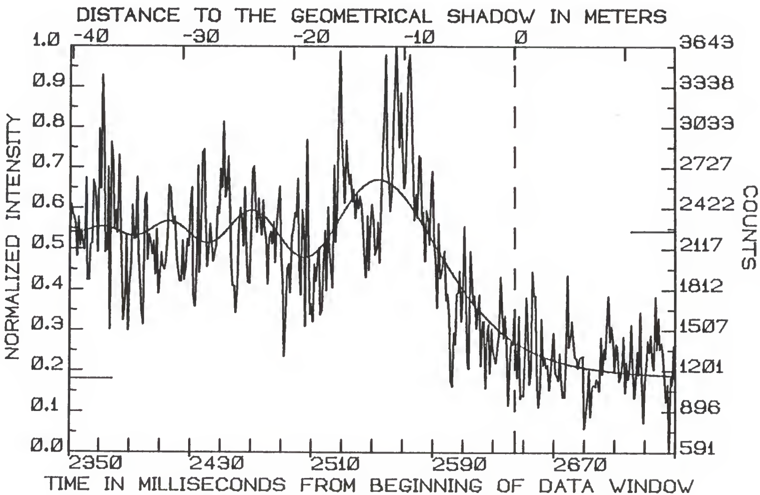

Figure 5-36. FITPLOT of the occultation of X07598.

TABLE 5-19
X07598: OBSERVATIONS, COMPUTED VALUES, AND RESIDUALS FROM BIN 2350

NUM	OBS	COMP	RESID	NUM	OBS	COMP	RESID	NUM	OBS	COMP	RESID
0	2240	2244.0	-4.0	67	2576	2325.6	250.4	134	2155	2292.4	-137.4
1	2449	2242.7	206.3	68	2396	2323.9	72.1	135	2319	2277.3	41.7
2	2383	2241.9	141.1	69	2303	2321.0	-18.0	136	2016	2261.8	-245.8
3	2355	2241.5	113.5	70	2357	2316.9	40.1	137	2324	2246.1	77.9
4	2305	2241.6	63.4	71	2077	2311.8	-234.8	138	2439	2230.4	208.6
5	2066	2242.2	-176.2	72	1979	2305.6	-326.6	139	2585	2214.6	370.4
6	2356	2243.3	112.7	73	1879	2298.6	-419.6	140	2086	2199.1	-113.1
7	2143	2244.9	-101.9	74	1875	2290.7	-415.7	141	1876	2183.8	-307.8
8	2263	2247.0	16.0	75	2181	2282.1	-101.1	142	1311	2168.9	-857.9
9	2156	2249.5	-93.5	76	1890	2272.8	-382.8	143	1631	2154.5	-523.5
10	2115	2252.4	-137.4	77	1975	2263.2	-288.2	144	1975	2140.8	-165.8
11	2649	2255.6	393.4	78	2191	2253.2	-62.2	145	2009	2127.9	-118.9
12	1885	2259.0	-374.0	79	2139	2243.1	-104.1	146	1792	2115.7	-323.7
13	1885	2262.5	-377.5	80	2437	2233.0	204.0	147	2219	2104.5	114.5
14	2146	2266.2	-120.2	81	2578	2223.0	355.0	148	2256	2094.4	161.6
15	2159	2269.8	-110.8	82	1784	2213.4	-429.4	149	2391	2085.3	305.7
16	2632	2273.2	358.8	83	1691	2204.2	-513.2	150	2357	2077.4	279.6
17	2575	2276.4	298.6	84	1879	2195.7	-316.7	151	2647	2070.7	576.3
18	2451	2279.2	171.8	85	2743	2187.9	555.1	152	1981	2065.3	-84.3
19	2099	2281.6	-182.6	86	1942	2181.0	-239.0	153	1775	2061.2	-286.2
20	3023	2283.5	739.5	87	2290	2175.1	114.9	154	2411	2058.4	352.6
21	2571	2284.8	286.2	88	2843	2170.3	672.7	155	2324	2057.0	267.0
22	3423	2285.5	1137.5	89	2867	2166.6	700.4	156	1539	2056.9	-517.9
23	2995	2285.4	709.6	90	2391	2164.2	226.8	157	2938	2058.2	879.8
24	2095	2284.7	-189.7	91	1988	2163.1	-175.1	158	2305	2060.9	244.1
25	2107	2283.3	-176.3	92	2087	2163.4	-76.4	159	1628	2065.0	-437.0
26	2735	2281.2	453.8	93	2307	2165.0	142.0	160	1709	2070.4	-361.4
27	1512	2278.3	-766.3	94	2196	2167.9	28.1	161	1573	2077.0	-504.0
28	2919	2274.9	644.1	95	2027	2172.2	-145.2	162	2006	2085.0	-79.0
29	2772	2270.9	501.1	96	2081	2177.8	-96.8	163	1878	2094.1	-216.1
30	2280	2266.5	13.5	97	2138	2184.6	-46.6	164	2012	2104.4	-92.4
31	2407	2261.6	145.4	98	2431	2192.5	238.5	165	2127	2115.9	11.1
32	2240	2256.5	-16.5	99	2383	2201.6	181.4	166	1627	2128.3	-501.3
33	2825	2251.2	573.8	100	2721	2211.6	509.4	167	1658	2141.8	-483.8
34	2407	2245.9	161.1	101	2576	2222.4	353.6	168	2018	2156.1	-138.1
35	1920	2240.6	-320.6	102	3079	2234.0	845.0	169	2257	2171.3	85.7
36	1584	2235.6	-651.6	103	2506	2246.2	259.8	170	1807	2187.3	-380.3
37	1743	2230.8	-487.8	104	2559	2258.8	300.2	171	2431	2203.9	227.1
38	2219	2226.6	-7.6	105	2813	2271.8	541.2	172	2111	2221.1	-110.1
39	1506	2222.8	-716.8	106	2499	2284.9	214.1	173	1960	2238.8	-278.8
40	1833	2219.8	-386.8	107	1991	2298.0	-307.0	174	1831	2256.9	-425.9
41	2015	2217.5	-202.5	108	1847	2310.9	-463.9	175	2748	2275.4	472.6
42	2445	2216.0	229.0	109	1836	2323.6	-487.6	176	2172	2294.1	-122.1
43	2195	2215.4	-20.4	110	1640	2335.8	-695.8	177	2431	2312.9	118.1
44	2195	2215.8	-20.8	111	1835	2347.5	-512.5	178	3136	2331.9	804.1
45	2655	2217.0	438.0	112	2300	2358.4	-58.4	179	3607	2350.8	1256.2
46	2105	2219.2	-114.2	113	2427	2368.4	58.6	180	2967	2369.7	597.3
47	1864	2222.4	-358.4	114	2347	2377.6	-30.6	181	2711	2388.3	322.7
48	1664	2226.4	-562.4	115	2144	2385.6	-241.6	182	2463	2406.8	56.2
49	1550	2231.2	-681.2	116	2579	2392.5	186.5	183	2935	2424.9	510.1
50	2471	2236.8	234.2	117	2112	2398.1	-286.1	184	2744	2442.6	301.4
51	2530	2243.0	287.0	118	1872	2402.4	-530.4	185	2605	2459.8	145.2
52	2036	2249.7	-213.7	119	1863	2405.4	-542.4	186	2680	2476.6	203.4
53	2223	2256.9	-33.9	120	2191	2406.9	-215.9	187	2475	2492.7	-17.7
54	2191	2264.4	-73.4	121	2714	2407.1	306.9	188	2567	2508.2	58.8
55	2079	2272.0	-193.0	122	2736	2405.8	330.2	189	2352	2523.1	-171.1
56	2179	2279.6	-100.6	123	2435	2403.0	32.0	190	2528	2537.1	-9.1
57	1928	2287.1	-359.1	124	2243	2398.8	-155.8	191	2421	2550.4	-129.4
58	2261	2294.3	-33.3	125	2495	2393.3	101.7	192	2512	2562.9	-50.9
59	1785	2301.0	-516.0	126	2345	2386.4	-41.4	193	2459	2574.4	-115.4
60	1911	2307.2	-396.2	127	2222	2378.3	-156.3	194	2298	2585.1	-287.1
61	2091	2312.7	-221.7	128	2479	2368.9	110.1	195	2032	2594.9	-562.9
62	1996	2317.4	-321.4	129	2257	2358.4	-101.4	196	1909	2603.7	-694.7
63	1967	2321.1	-354.1	130	2207	2346.8	-139.8	197	2368	2611.5	-243.5
64	2024	2323.9	-299.9	131	1857	2334.4	-477.4	198	1963	2618.4	-655.4
65	2205	2325.6	-120.6	132	2203	2321.0	-118.0	199	2338	2624.2	-286.2
66	2597	2326.2	270.8	133	2248	2307.0	-59.0	200	2451	2629.0	-178.0

TABLE 5-19. CONTINUED.

NUM	OBS	COMP	RESID	NUM	OBS	COMP	RESID	NUM	OBS	COMP	RESID
201	2332	2632.8	-300.8	268	1771	1700.5	70.5	335	1296	1236.9	59.1
202	2079	2635.6	-556.6	269	1523	1686.6	-163.6	336	1225	1234.5	-9.5
203	2116	2637.4	-521.4	270	1641	1673.0	-32.0	337	1297	1232.3	64.7
204	2321	2638.2	-317.2	271	1775	1659.6	115.4	338	1303	1230.1	72.9
205	2017	2637.9	-620.9	272	1239	1646.5	-407.5	339	1310	1227.9	82.1
206	2465	2636.7	-171.7	273	1576	1633.6	-57.6	340	774	1225.8	-451.8
207	2897	2634.4	262.6	274	1574	1621.1	-47.1	341	886	1223.8	-337.8
208	3099	2631.3	467.7	275	1073	1608.8	-535.8	342	983	1221.8	-238.8
209	3580	2627.1	952.9	276	1487	1596.8	-109.8	343	1201	1219.9	-18.9
210	2739	2622.0	117.0	277	1551	1585.0	-34.0	344	860	1218.1	-358.1
211	2650	2616.1	33.9	278	1185	1573.5	-388.5	345	1077	1216.2	-139.2
212	2404	2609.2	-205.2	279	1519	1562.3	-43.3	346	1095	1214.5	-119.5
213	2555	2601.5	-46.5	280	1359	1551.3	-192.3	347	1087	1212.8	-125.8
214	3047	2593.0	454.0	281	1299	1540.6	-241.6	348	1139	1211.1	-72.1
215	3363	2583.6	779.4	282	1263	1530.1	-267.1	349	1121	1209.5	-88.5
216	3643	2573.5	1069.5	283	1397	1519.9	-122.9	350	1056	1207.9	-151.9
217	3221	2562.6	658.4	284	1464	1509.9	-45.9	351	1451	1206.4	244.6
218	2885	2551.1	333.9	285	1912	1500.1	411.9	352	1178	1204.9	-26.9
219	3296	2538.8	757.2	286	1695	1490.6	204.4	353	1367	1203.5	163.5
220	2889	2525.9	363.1	287	1450	1481.4	-31.4	354	1294	1202.1	91.9
221	2575	2512.4	62.6	288	1620	1472.4	147.6	355	1599	1200.7	398.3
222	2619	2498.3	120.7	289	1380	1463.6	-83.6	356	1768	1199.4	568.6
223	3123	2483.7	639.3	290	945	1455.0	-510.0	357	1423	1198.1	224.9
224	3487	2468.6	1018.4	291	1243	1446.6	-203.6	358	1534	1196.8	337.2
225	3583	2452.9	1130.1	292	1420	1438.5	-18.5	359	1440	1195.6	244.4
226	3267	2436.9	830.1	293	1399	1430.5	-31.5	360	1207	1194.4	12.6
227	2691	2420.4	270.6	294	1603	1422.8	180.2	361	1405	1193.2	211.8
228	2337	2403.5	-66.5	295	1331	1415.3	-84.3	362	1387	1192.1	194.9
229	2531	2386.3	144.7	296	1151	1408.0	-257.0	363	1127	1191.0	-64.0
230	2351	2368.8	-17.8	297	1615	1400.8	214.2	364	1152	1189.9	-37.9
231	2821	2351.0	470.0	298	995	1393.9	-398.9	365	1251	1188.9	62.1
232	2802	2332.9	469.1	299	1022	1387.1	-365.1	366	1457	1187.9	269.1
233	2307	2314.7	-7.7	300	1015	1380.6	-365.6	367	1042	1186.9	-144.9
234	2393	2296.2	96.8	301	1353	1374.2	-21.2	368	1269	1185.9	83.1
235	2030	2277.5	-247.5	302	1757	1368.0	389.0	369	1141	1185.0	-44.0
236	2407	2258.8	148.2	303	1476	1361.9	114.1	370	1224	1184.1	39.9
237	2361	2239.9	121.1	304	1103	1356.1	-253.1	371	1548	1183.2	364.8
238	2151	2220.9	-69.9	305	1208	1350.3	-142.3	372	1258	1182.3	75.7
239	2595	2201.8	393.2	306	1949	1344.8	604.2	373	1002	1181.5	-179.5
240	2702	2182.8	519.2	307	1778	1339.4	438.6	374	1107	1180.7	-73.7
241	2153	2163.7	-10.7	308	1767	1334.1	432.9	375	1348	1179.9	168.1
242	2059	2144.6	-85.6	309	1085	1329.0	-244.0	376	1171	1179.1	-8.1
243	1680	2125.5	-445.5	310	930	1324.0	-394.0	377	1645	1178.3	466.7
244	2311	2106.5	204.5	311	1082	1319.2	-237.2	378	1152	1177.6	-25.6
245	1903	2087.6	-184.6	312	1594	1314.5	279.5	379	817	1176.9	-359.9
246	1938	2068.7	-130.7	313	1243	1310.0	-67.0	380	1111	1176.2	-65.2
247	2039	2050.0	-11.0	314	1303	1305.6	-2.6	381	1247	1175.5	71.5
248	2104	2031.3	72.7	315	1224	1301.3	-77.3	382	1431	1174.8	256.2
249	1737	2012.8	-275.8	316	1247	1297.1	-50.1	383	1343	1174.1	168.9
250	1783	1994.5	-211.5	317	1061	1293.0	-232.0	384	1471	1173.5	297.5
251	1615	1976.3	-361.3	318	1178	1289.1	-111.1	385	1277	1172.9	104.1
252	1127	1958.2	-831.2	319	1343	1285.2	57.8	386	1215	1172.3	42.7
253	1087	1940.4	-853.4	320	1487	1281.5	205.5	387	1759	1171.7	587.3
254	1490	1922.8	-432.8	321	1186	1277.9	-91.9	388	1365	1171.1	193.9
255	1404	1905.3	-501.3	322	1169	1274.4	-105.4	389	1600	1170.5	429.5
256	1787	1888.1	-101.1	323	1131	1271.0	-140.0	390	1364	1170.0	194.0
257	1797	1871.1	-74.1	324	1334	1267.7	66.3	391	1415	1169.4	245.6
258	1955	1854.3	100.7	325	1112	1264.4	-152.4	392	1336	1168.9	167.1
259	1577	1837.8	-260.8	326	1007	1261.3	-254.3	393	1124	1168.4	-44.4
260	1737	1821.5	-84.5	327	1007	1258.3	-251.3	394	973	1167.9	-194.9
261	2287	1805.5	481.5	328	1255	1255.3	-0.3	395	1103	1167.4	-64.4
262	1857	1789.7	67.3	329	1920	1252.5	667.5	396	591	1166.9	-575.9
263	1275	1774.2	-499.2	330	1381	1249.7	131.3	397	1149	1166.4	-17.4
264	1222	1758.9	-536.9	331	1458	1247.0	211.0	398	1102	1166.0	-64.0
265	2100	1743.9	356.1	332	1576	1244.3	331.7	399	1392	1165.5	226.5
266	1935	1729.2	205.8	333	1411	1241.8	169.2	400	1157	1165.1	-8.1
267	1705	1714.7	-9.7	334	1307	1239.3	67.7				

TABLE 5-20
X07598: SUPPLEMENTAL STATISTICAL INFORMATION

VARIANCE/CO-VARIANCE MATRIX

DIAM	PREI	POST	TIME	VELO
1.447E¯16	3.947E¯08	-9.496E¯08	-1.637E¯09	3.319E¯12
3.947E¯08	4.785E02	8.940E01	-2.714E01	2.714E¯02
-9.496E¯08	8.940E01	1.517E03	-6.788E01	6.483E¯02
-1.637E¯09	-2.714E01	-6.788E01	1.463E01	-1.444E¯02
3.319E¯12	2.714E¯02	6.483E¯02	-1.444E¯02	1.891E¯05

CORRELATION MATRIX

	DIAM	PREI	POST	TIME	VELO
DIAM	1.000000	0.394094	-0.908842	0.681148	-0.667250
PREI	0.394094	1.000000	0.024095	-0.389071	0.405659
POST	-0.908842	0.024095	1.000000	-0.921565	0.914093
TIME	0.681148	-0.389071	-0.921565	1.000000	-0.999822
VELO	-0.667250	0.405659	0.914093	-0.999822	1.000000

NUMERICAL RANGES OF THE PARTIAL DERIVATIVES

	MAXIMUM	MINIMUM
DIAM	3.271E09	-3.408E09
PREI	1.346E00	2.314E¯02
POST	9.769E¯01	-3.458E¯01
TIME	1.910E01	-1.897E01
VELO	1.805E04	-1.822E04

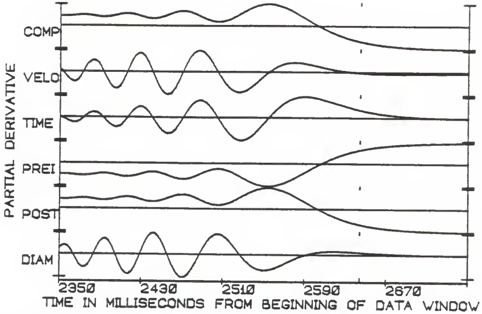

Figure 5-37. PDPLOT of the occultation of X07598.

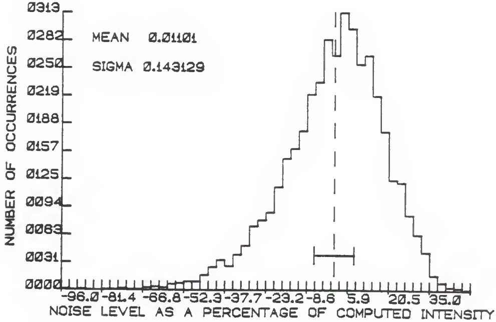

Figure 5-38. NOISEPLOT of the occultation of X07598.

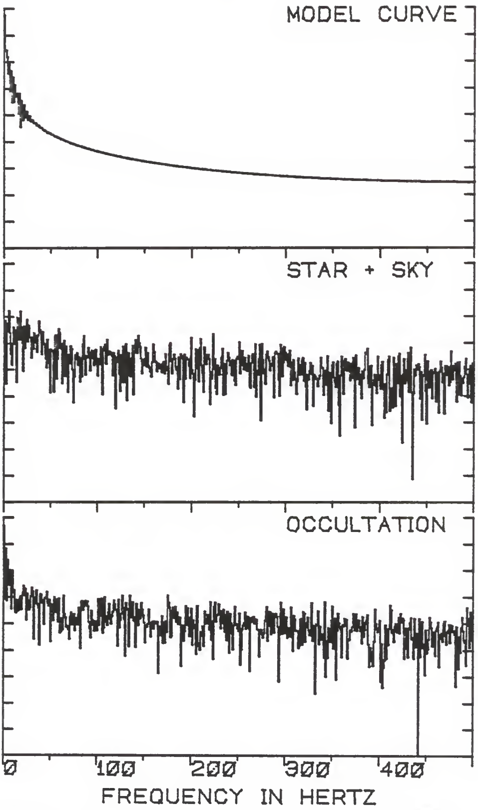

Figure 5-39. POWERPLOT of the occultation of X07598.

point source. No convergent solution could be forced on a point source model. The determined angular diameter does indeed seem to be real.

Because of the relatively slow disappearance (due to the small R-rate) the internal formal error in the time of geometrical occultation was not very well determined (+/- 4.4 milliseconds). The Coordinated Universal Time of geometrical occultation was found to be 02:12:04.713 (+/- 0.0049 seconds).

X13534

The occultation of the K0 star X13534 on April 21, 1983 U. T., (as noted in the occultation summary, Table 5-21) was the first of two events observed on that night. Interestingly enough, these two events both gave rise to the discovery of previously unknown "close" companions. Other than the recognition of 1 Geminorum A1 (ZC0916-A1), these two were the only such discoveries made in the reduction and analysis of the twenty-two observations where "close" duplicity could have been uncovered.

Even from the plot of the raw occultation data (Figure 5-40), one can note a diminution of the positive-going signal spiking (due to scintillation noise) immediately before occultation. While this is only marginally noticeable on the presented RAWPLOT, this was seen quite easily when examined at the four-times greater resolution obtained by using a high resolution graphics display terminal. This diminution in the noise spiking (as

TABLE 5-21
X13534: LUNAR OCCULTATION SUMMARY

STELLAR AND OBSERVING INFORMATION

Star: X13534, (SAO 080497, DM +21 1939)
RA: 085323 DEC: +203905 mV: 8.4 Sp: K0
Filter: V Diaphragm: I Gain: C8 Voltage: 1200

LUNAR INFORMATION

Surface Illumination:	58 percent
Elongation from Sun:	100 degrees
Altitude Above Horizon:	58 degrees
Lunar Limb Distance:	364349 kilometers
Predicted Shadow Velocity:	661.7 meters/sec.
Predicted Angular Rate:	0.3746 arcsec/sec.

EVENT INFORMATION

Date: April 21, 1983		UT of Event:	02:46:31
USNO V/O Code:	15	HA of Event:	+342042
Position Angle:	143.4	Cusp Angle:	53S
Contact Angle:	-30.0	Watts Angle:	126.7

TWO-STAR MODEL PARAMETERS

Number of Data Points:	201
Number of Grid Points:	256, 256
Number of Spectral Regions:	53
Width of Spectral Regions:	50 Angstroms
Limb Darkening Coefficients:	0.5, 0.05
Effective Stellar Temperatures:	5100 K, 5100 K

SOLUTIONS

Sky Level: 1336.5 (39.2)

	STAR 1	STAR 2
Stellar Diameter (ams):	Point Source	Point Source
Time (relative to Bin 0):	2389.2 (2.2)	2372.3 (7.2)
Stellar Intensity:	649.5 (100.2)	229.9 (98.7)
Velocity (meters/sec.):	666.9 (49.4)	559.0 (116.3)
Lunar Limb Slope (degrees)	-3.58 (4.28)	-16.3 (10.1)
U.T. of Occultation:	02:46:29.632 (0.003)	:29.594 (0.008)

Table 5-21. Continued.

TWO-STAR DERIVED QUANTITIES

Temporal Separation (milliseconds):	16.9	(7.6)
Intensity Weighted Mean L-Rate (meters/sec):	634.7	(48.4)
Intensity Weighted Mean R-Rate (arcsec/sec):	0.359	(0.027)
Projected Spatial Separation,		
Based on Predicted R-Rate:	6.32	arc-ms
Based on Weighted Mean R-Rate:	6.07	(2.74) arc-ms.
Brightness Ratio (Brighter/Fainter):	2.82	(1.289)
Magnitude Difference:	1.13	(+0.66, -0.41)
mV of Star 1:	8.73	(0.14)
mV of Star 2:	9.86	(0.37)

PHOTOMETRIC NOISE INFORMATION

Sum-of-Squares of Residuals:	17673786
Sigma (Standard Error):	297.269
Normalized Standard Error:	0.33803
Photometric (S+N)/N Ratio:	3.9583
(Change in Intensity)/Background:	0.6580
Change in Magnitude:	0.5490

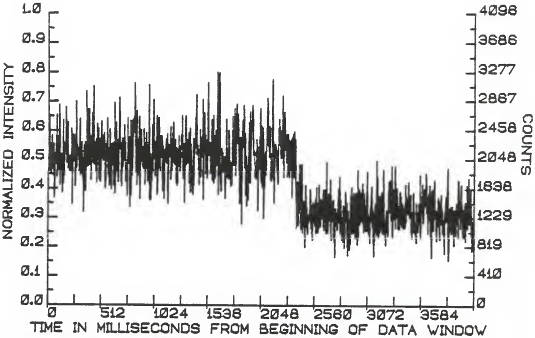

Figure 5-40. RAWPLOT of the occultation of X13534.

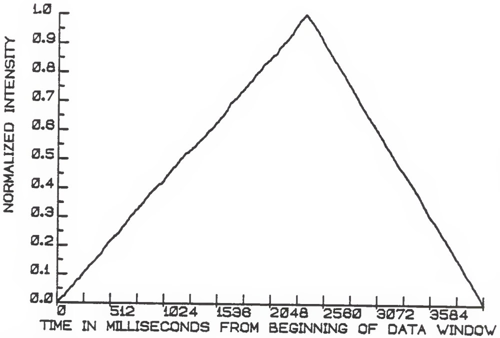

Figure 5-41. INTPLOT of the occultation of X13534.

it so appears when plotted at this scale) was actually due to a reduction in the zero order diffraction fringe maximum brought about by a second star.

The presence of a second star was uncovered by the DC2 fitting process. No "wide" stellar components are indicated by the integration plot, Figure 5-41. An initial attempt to fit the observational data to a one star model failed, and the divergence of the fitting procedure indicated that a two-star model was the appropriate one to use. The FITPLOT of the two-star solution is presented as Figure 5-42. The times of geometrical occultation of the individual components are noted by the dashed vertical lines. The arbitrary zero point reference on the linear distance scale coincides with the point of geometrical occultation of the brighter star.

Neither of the two stars had resolvable stellar diameters, and hence, led to point source solutions. The projected spatial separation of the components was found to be 6.07 (+/- 2.74) milliseconds of arc based on an intensity weighted mean of the determined R-rates of 0.3593 (+/- 0.0274) seconds of arc per second.

The fainter of the two stars underwent disappearance first. The brightness ratio of the components (brighter/fainter) was 2.82 (+/- 1.29). Hence, the difference in stellar magnitudes between the components is 1.13 (+0.66, -0.41). If the systemic apparent V magnitude is taken as 8.4 (as given by the DM catalog), the individual

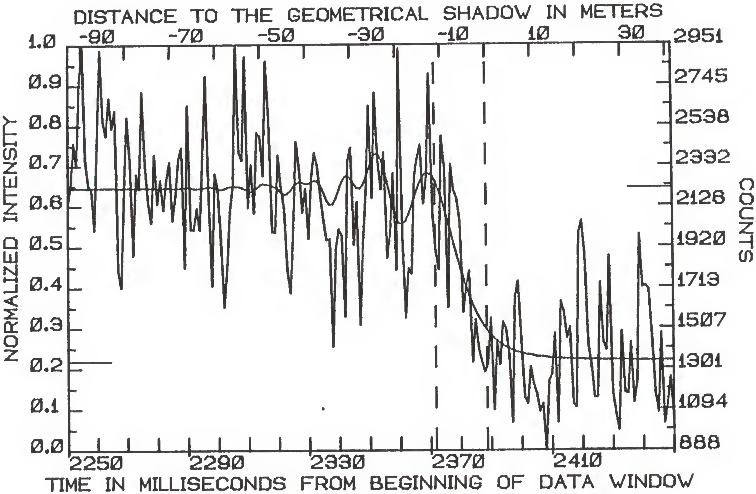

Figure 5-42. FITPLOT of the occultation of X13534.

components would have corresponding V magnitudes of 8.73 (+/- 0.13), and 9.86 (+/- 0.37).

The observations, extracted from the raw data used in the DC2 fit, the computed intensities and the resulting residuals are given in Table 5-22. The sensitivity of the determined two-star intensity curve to variations in the solution parameters is presented in Figure 5-43. A small amount of numerical "noise" is seen in the early part of the partial derivative curves for the velocity parameters. However, the noise amplitude is quite small, and as can be seen, is not in the region of the solution where such noise would be important in the parameter determinations. The numerical ranges of the partial derivatives, and supplemental statistical information are listed in Table 5-23.

The 6.5 percent shift of the mean of the residual amplitude distribution (Figure 5-44), over the 4096 milliseconds of the acquired data, was due to a small increase in background illumination over the event window. This can be seen if the RAWPLOT is examined carefully. The same gradual increase gives rise to the obvious Poisson tail in the distribution function. The slope of the increase is sufficiently small to be negligible on the time-scale of the data extracted for the DC2 solution (less than 1/20 of the entire data window).

The POWERPLOT for this occultation event is presented as Figure 5-45. The Coordinated Universal Times of geometrical occultation for the two component stars were found to be

TABLE 5-22
X13534: OBSERVATIONS, COMPUTED VALUES, AND RESIDUALS FROM BIN 2250

NUM	OBS	COMP	RESID	NUM	OBS	COMP	RESID	NUM	OBS	COMP	RESID
0	2137	2218.7	-81.7	67	2572	2233.3	338.7	134	1334	1633.7	-299.7
1	2223	2218.4	4.6	68	1995	2229.9	-234.9	135	1551	1598.2	-47.2
2	2451	2218.1	232.9	69	1993	2224.0	-231.0	136	1403	1566.6	-163.6
3	2330	2218.5	111.5	70	2387	2212.5	174.5	137	1337	1538.6	-201.6
4	2767	2218.6	548.4	71	2217	2196.8	20.2	138	1284	1513.9	-229.9
5	2941	2218.6	722.4	72	2116	2185.1	-69.1	139	1325	1492.3	-167.3
6	2365	2218.4	146.6	73	1800	2185.7	-385.7	140	1554	1473.4	80.6
7	2235	2218.1	16.9	74	1685	2200.9	-515.9	141	1093	1456.9	-363.9
8	2213	2218.6	-5.6	75	2017	2223.5	-206.5	142	1431	1442.6	-11.6
9	2004	2218.7	-214.7	76	2455	2241.9	213.1	143	1321	1430.1	-109.1
10	2443	2218.4	224.6	77	2314	2248.4	65.6	144	1537	1419.3	117.7
11	2925	2218.1	706.9	78	2093	2244.5	-151.5	145	1503	1409.9	93.1
12	2566	2218.3	347.7	79	2215	2238.7	-23.7	146	1368	1401.7	-33.7
13	2488	2218.3	269.7	80	1960	2239.3	-279.3	147	1027	1394.6	-367.6
14	2679	2218.6	460.4	81	2269	2247.3	21.7	148	1665	1388.5	276.5
15	2526	2219.0	307.0	82	2399	2255.2	143.8	149	1743	1383.1	359.9
16	2617	2218.4	398.6	83	2333	2251.8	81.2	150	1447	1378.4	68.6
17	1802	2217.7	-415.7	84	2179	2230.4	-51.4	151	1157	1374.3	-217.3
18	1715	2217.8	-502.8	85	2057	2194.3	-137.3	152	1123	1370.7	-247.7
19	2207	2218.6	-11.6	86	1951	2156.4	-205.4	153	1310	1367.5	-57.5
20	2579	2219.2	359.8	87	1960	2132.6	-172.6	154	1221	1364.8	-143.8
21	2359	2219.2	139.8	88	1414	2133.9	-719.9	155	1173	1362.3	-189.3
22	1879	2218.2	-339.2	89	1905	2161.1	-256.1	156	1083	1360.1	-277.1
23	2291	2217.2	73.8	90	2009	2203.9	-194.9	157	1123	1358.2	-235.2
24	2215	2217.6	-2.6	91	1975	2246.4	-271.4	158	888	1356.5	-468.5
25	2712	2218.9	493.1	92	1568	2273.7	-705.7	159	1235	1354.9	-119.9
26	2341	2219.5	121.5	93	2353	2278.4	74.6	160	1270	1353.5	-83.5
27	2150	2219.3	-69.3	94	2423	2262.9	160.1	161	1476	1352.3	123.7
28	2044	2218.5	-174.5	95	1930	2238.0	-308.0	162	1028	1351.2	-323.2
29	2388	2217.4	170.6	96	2146	2217.8	-71.8	163	1641	1350.1	290.9
30	2139	2217.0	-78.0	97	1524	2214.3	-690.3	164	1591	1349.2	241.8
31	2259	2218.2	40.8	98	1939	2232.7	-293.7	165	1455	1348.4	106.6
32	2107	2219.9	-112.9	99	2191	2270.2	-79.2	166	1509	1347.7	161.3
33	2259	2219.9	39.1	100	2638	2317.4	320.6	167	1121	1347.0	-226.0
34	2351	2218.7	132.3	101	2167	2360.9	-193.9	168	1103	1346.4	-243.4
35	2054	2217.5	-163.5	102	2703	2388.4	314.6	169	1983	1345.8	637.2
36	2179	2217.3	-38.3	103	2360	2391.0	-31.0	170	2048	1345.3	702.7
37	2363	2217.5	145.5	104	2211	2366.2	-155.2	171	1881	1344.9	536.1
38	2426	2218.5	207.5	105	2399	2317.1	81.9	172	1421	1344.4	76.6
39	1815	2220.5	-405.5	106	1863	2252.0	-389.0	173	1318	1344.0	-26.0
40	2642	2221.2	420.8	107	1986	2181.7	-195.7	174	1151	1343.6	-192.6
41	2008	2219.0	-211.0	108	2292	2117.1	174.9	175	1156	1343.3	-187.3
42	2007	2216.0	-209.0	109	1803	2067.3	-264.3	176	1733	1342.9	390.1
43	2116	2215.1	-99.1	110	2927	2038.1	888.9	177	1433	1342.6	90.4
44	2006	2217.1	-211.1	111	1984	2031.7	-47.7	178	1395	1342.3	52.7
45	2391	2219.6	171.4	112	1558	2046.6	-488.6	179	1870	1342.0	528.0
46	2791	2221.4	569.6	113	1811	2078.5	-267.5	180	1176	1341.8	-165.8
47	2168	2222.7	-54.7	114	1783	2121.4	-338.4	181	1071	1341.6	-270.6
48	1725	2222.7	-497.7	115	2271	2168.7	102.3	182	987	1341.4	-354.4
49	2290	2219.4	70.6	116	2367	2214.1	152.9	183	1488	1341.2	146.8
50	2216	2213.4	2.6	117	2439	2252.2	186.8	184	1178	1341.0	-163.0
51	1951	2209.6	-258.6	118	2136	2279.0	-143.0	185	1171	1340.8	-169.8
52	1616	2212.4	-596.4	119	2274	2292.1	-18.1	186	1431	1340.7	90.3
53	1811	2219.8	-408.8	120	2799	2290.7	508.3	187	1126	1340.5	-214.5
54	2099	2225.9	-126.9	121	2093	2275.1	-182.1	188	1234	1340.3	-106.3
55	2232	2227.5	4.5	122	1893	2246.6	-353.6	189	1979	1340.2	638.8
56	2951	2226.2	724.8	123	1804	2207.3	-403.3	190	1711	1340.1	370.9
57	2403	2224.7	178.3	124	2483	2159.5	323.5	191	1720	1340.0	380.0
58	2361	2221.4	139.6	125	2328	2105.6	222.4	192	1699	1339.8	359.2
59	2887	2214.3	672.7	126	1612	2047.9	-435.9	193	1463	1339.7	123.3
60	2119	2205.1	-86.1	127	2338	1988.5	349.5	194	1179	1339.6	-160.6
61	2338	2200.7	137.3	128	2207	1929.3	277.7	195	1077	1339.5	-262.5
62	2091	2206.2	-115.2	129	2165	1871.6	293.4	196	1478	1339.4	138.6
63	2502	2219.4	282.6	130	2047	1816.5	230.5	197	1023	1339.3	-316.3
64	2487	2232.1	254.9	131	1587	1764.9	-177.9	198	1123	1339.2	-216.2
65	2279	2238.0	41.0	132	1720	1717.0	3.0	199	1255	1339.2	-84.2
66	2867	2237.0	630.0	133	1795	1673.3	121.7	200	1039	1339.1	-300.1

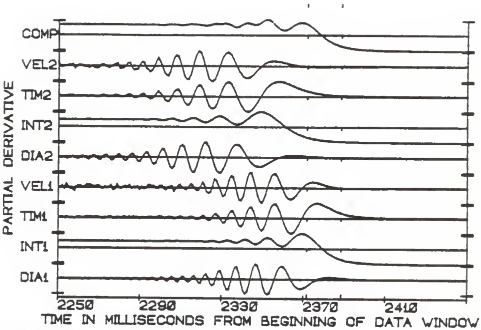

Figure 5-43. PDPLOT of the occultation of X13534.

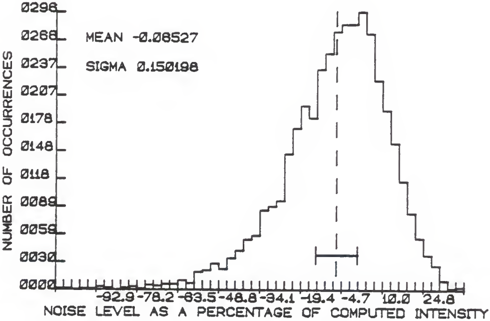

Figure 5-44. NOISEPLOT of the occultation of X13534.

TABLE 5-23
X13534: SUPPLEMENTAL STATISTICAL INFORMATION

VARIANCE/CO-VARIANCE MATRIX

DIA1	INT1	SKY	TIM1	VEL1	DIA2	INT2	TIM2	VEL2
9.337E-15	7.941E-07	1.002E-07	-1.242E-08	3.111E-10	-5.816E-16	-4.969E-07	-1.049E-07	2.256E-09
7.941E-07	1.004E04	-9.829E02	-7.696E01	1.395E00	-2.472E-07	-8.753E03	-3.588E02	4.855E00
1.002E-07	-9.829E02	1.534E03	-2.512E01	4.864E-01	-2.458E-08	-5.334E02	-2.237E01	3.215E-01
-1.242E-08	-7.696E01	-2.512E01	4.834E00	-9.390E-02	2.047E-09	1.003E02	2.763E00	-3.390E-02
3.111E-10	1.395E00	4.864E-01	-9.390E-02	2.443E-03	-1.222E-12	-1.867E00	-4.641E-02	5.681E-04
-5.816E-16	-2.472E-07	-2.458E-08	2.047E-09	-1.222E-12	1.670E-14	-1.190E-07	4.962E-08	-1.290E-09
-4.969E-07	-8.753E03	-5.334E02	1.003E02	-1.867E00	-1.190E-07	9.749E03	3.322E02	-4.455E00
-1.049E-07	-3.588E02	-2.237E01	2.763E00	-4.641E-02	4.962E-08	3.322E02	5.241E01	-7.408E-01
2.256E-09	4.855E00	3.215E-01	-3.390E-02	5.681E-04	-1.290E-09	-4.455E00	-7.408E-01	1.351E-02

CORRELATION MATRIX

	DIA1	INT1	SKY	TIM1	VEL1	DIA2	INT2	TIM2	VEL2
DIA1	1.000000	0.973216	-0.199990	-0.936817	0.931709	-0.556013	-0.962973	-0.986138	0.986958
INT1	0.973216	1.000000	-0.263947	-0.944109	0.938969	-0.420862	-0.986250	-0.989304	0.988643
SKY	-0.199990	-0.263947	1.000000	-0.067580	0.082593	0.548542	0.103520	0.149732	-0.149551
TIM1	-0.936817	-0.944109	-0.067580	1.000000	-0.999876	0.244568	0.984623	0.970768	-0.970057
VEL1	0.931709	0.938969	0.082593	-0.999876	1.000000	-0.232740	-0.981974	-0.966960	0.966221
DIA2	-0.556013	-0.420862	0.548542	0.244568	-0.232740	1.000000	0.318093	0.417146	-0.421728
INT2	-0.962973	-0.986250	0.103520	0.984623	-0.981974	0.318093	1.000000	0.992630	-0.991806
TIM2	-0.986138	-0.989304	0.149732	0.970768	-0.966960	0.417146	0.992630	1.000000	-0.999974
VEL2	0.986958	0.988643	-0.149551	-0.970057	0.966221	-0.421728	-0.991806	-0.999974	1.000000

NUMERICAL RANGES OF THE PARTIAL DERIVATIVES

	DIA1	INT1	SKY	TIM1	VEL1	DIA2	INT2	TIM2	VEL2
MAXIMUM	1.293E08	1.367E00	1.000E00	5.625E01	2.712E03	1.981E09	1.365E00	1.669E01	1.224E03
MINIMUM	-3.059E09	3.027E-03	1.000E00	-5.948E01	-2.837E03	-5.252E08	2.639E-03	-1.781E01	-1.174E03

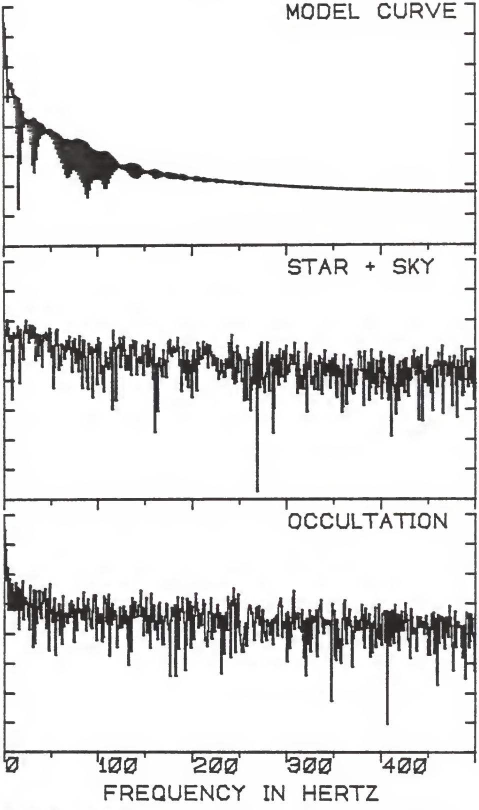

Figure 5-45. POWERPLOT of the occultation of X13534.

02:46:29.594 (+/- 0.008 seconds) and 02:46:29.632 (+/- 0.003 seconds), for the fainter and brighter components respectively.

X13607

The second occultation observed on the night of April 21, 1983, that of the F5 star X13607, occurred approximately one hour and forty eight minutes after the X13534 event. Because of the relatively early spectral type and moderate faintness (mV=8.2) of this star, a Johnson B filter had initially been chosen for the observation. However, a check on the sky brightness several minutes before the predicted time of disappearance showed that a significantly better S+N/N ratio could be obtained with a Johnson V filter. The event, as indicated in the occultation summary, Table 5-24, occured with the lunar surface 59 percent illuminated. In addition, the selenocentric angle of the contact point was only 16 degrees from the southern cusp. This small cusp angle, along with the past first-quarter moon, made the sky rather bright and significantly brighter in B than V.

The RAWPLOT of the observation is shown in Figure 5-46, and the integration plot in Figure 5-47. There is no indication in either of these figures of any "wide" secondary components. A preliminary look at the subset of data selected for solution (200 milliseconds, beginning at millisecond 2395), which can be seen in Figure 5-48, rather obviously shows an unusual diffraction intensity variation. This was recognized as being attributable to a previously

TABLE 5-24
X13607: LUNAR OCCULTATION SUMMARY

STELLAR AND OBSERVING INFORMATION

Star: X13607, (SAO 080527, DM +20 2244)
RA: 085559 DEC: +201558 mV: 8.2 Sp: F5
Filter: V Diaphragm: I Gain: C7+ Voltage: 1200

LUNAR INFORMATION

Surface Illumination:	59 percent
Elongation from Sun:	100 degrees
Altitude Above Horizon:	35 degrees
Lunar Limb Distance:	366061 kilometers
Predicted Shadow Velocity:	347.5 meters/sec.
Predicted Angular Rate:	0.1958 arcsec/sec.

EVENT INFORMATION

Date:	April 21, 1983	UT of Event:	04:33:56
USNO V/O Code:	25	HA of Event:	+603457
Position Angle:	180.2	Cusp Angle:	16S
Contact Angle:	-67.4	Watts Angle:	163.2

TWO-STAR MODEL PARAMETERS

Number of Data Points:	201
Number of Grid Points:	256, 256
Number of Spectral Regions:	53
Width of Spectral Regions:	50 Angstroms
Limb Darkening Coefficients:	0.5, 0.05
Effective Stellar Temperatures:	5100 K, 5100 K

SOLUTIONS

Sky Level: 1429.3 (38.2)

	STAR 1	STAR 2
Stellar Diameter (ams):	Point Source	Point Source
Time (relative to Bin 0):	2542.2 (3.4)	2488.7 (6.9)
Stellar Intensity:	481.5 (53.1)	202.5 (49.1)
Velocity (meters/sec.):	410.9 (29.7)	524.8 (100.7)
Lunar Limb Slope (degrees)	-16.1 (4.28)	-24.3 (16.6)
U.T. of Occultation:	04:33:58.827 (0.007)	:58.773 (0.009)

Table 5-24. Continued.

TWO-STAR DERIVED QUANTITIES

Temporal Separation (milliseconds):	53.4	(7.7)
Intensity Weighted Mean L-Rate (meters/sec):	436.8	(37.6)
Intensity Weighted Mean R-Rate (arcsec/sec):	0.246	(0.021)
Projected Spatial Separation,		
Based on Predicted R-Rate:	10.46	arc-ms
Based on Weighted Mean R-Rate:	13.15	(2.19) arc-ms.
Brightness Ratio (Brighter/Fainter):	2.38	(0.634)
Magnitude Difference:	0.94	(+0.34, -0.26)
mV of Star 1:	8.58	(0.09)
mV of Star 2:	9.52	(0.20)

PHOTOMETRIC NOISE INFORMATION

Sum-of-Squares of Residuals:	13265444
Sigma (Standard Error):	257.541
Normalized Standard Error:	0.37652
Photometric (S+N)/N Ratio:	3.6558
(Change in Intensity)/Background:	0.4785
Change in Magnitude:	0.4246

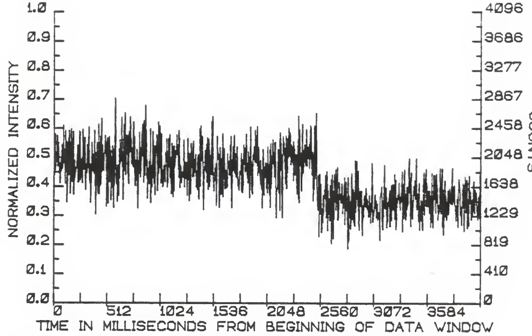

Figure 5-46. RAWPLOT of the occultation of X13607.

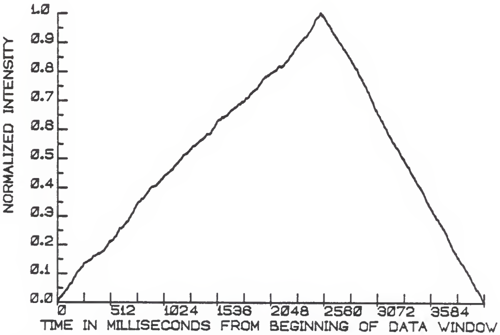

Figure 5-47. INTPLOT of the occultation of X13607.

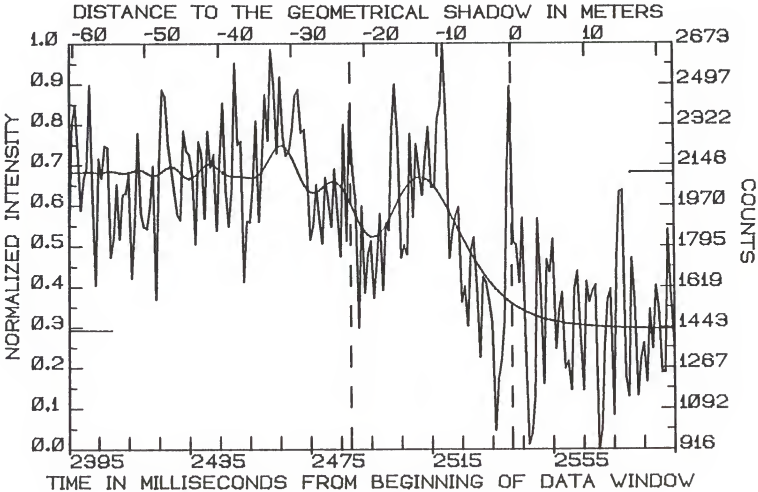

Figure 5-48. FITPLOT of the occultation of X13607.

unknown "close" stellar companion. Indeed, this was the case and was verified by the DC2 fit to the observed intensity curve.

Because of the early spectral type of the star (or properly the composite spectra of the two stars), an angular diameter determination was not expected, and indeed, the diameters of both components were found to be below the detection threshold.

The fainter of the two stars was occulted 53.4 (+/- 7.7) milliseconds before the brighter. The projected separation of the individual stellar components was found to be 13.2 (+/- 2.1) milliseconds of arc. This was determined using an intensity weighted mean R-rate of 0.2462 (+/- 0.02123) seconds of arc per second.

The determined ratio of component brightnesses (brighter/fainter) was 2.38 (+/- 0.63), or 0.94 (+0.34, -0.26) in terms of a stellar magnitude difference. Assuming an apparent V magnitude of 8.2 (as listed in the SAO catalog), the individual V magnitudes of the component stars are 8.58 (+/- 0.09) and 9.52 (+/- 0.20), respectively.

The observational data used in the DC2 fitting process, as well as the solution intensities and the residual values, are listed in Table 5-25. Table 5-26 gives the usual supplemental statistics, including the numerical ranges of the solution curve's partial derivatives which are depicted in Figure 5-49.

TABLE 5-25
X13607: OBSERVATIONS, COMPUTED VALUES, AND RESIDUALS FROM BIN 2395

NUM	OBS	COMP	RESID	NUM	OBS	COMP	RESID	NUM	OBS	COMP	RESID
0	1845	2116.3	-271.3	67	2647	2183.6	463.4	134	1832	1743.7	88.3
1	2330	2115.2	214.8	68	2499	2204.9	294.1	135	1621	1721.9	-100.9
2	2404	2114.3	289.7	69	2198	2221.3	-23.3	136	1313	1701.1	-388.1
3	2207	2114.2	92.8	70	2529	2230.4	298.6	137	1662	1681.5	-19.5
4	1950	2114.9	-164.9	71	2271	2230.5	40.5	138	1639	1662.9	-23.9
5	2082	2116.0	-34.0	72	2186	2221.0	-35.0	139	1563	1645.5	-82.5
6	2135	2116.7	18.3	73	2203	2202.9	0.1	140	1463	1629.2	-166.2
7	2495	2116.6	378.4	74	2296	2177.6	118.4	141	1000	1613.9	-613.9
8	2007	2115.6	-108.6	75	2448	2147.9	300.1	142	1218	1599.7	-381.7
9	1628	2114.5	-486.5	76	2474	2116.7	357.3	143	1300	1586.5	-286.5
10	2176	2113.9	62.1	77	2287	2087.0	200.0	144	1467	1574.3	-107.3
11	2090	2114.5	-24.5	78	2299	2061.5	237.5	145	2092	1563.0	529.0
12	2231	2115.9	115.1	79	2121	2042.2	78.8	146	2488	1552.6	935.4
13	2222	2117.5	104.5	80	1822	2030.3	-208.3	147	1815	1543.0	272.0
14	1748	2118.3	-370.3	81	1883	2025.8	-142.8	148	1800	1534.1	265.9
15	1830	2117.6	-287.6	82	2059	2027.9	31.1	149	1637	1526.0	111.0
16	2062	2115.5	-53.5	83	1919	2035.2	-116.2	150	1915	1518.5	396.5
17	1827	2112.8	-285.8	84	1807	2045.6	-238.6	151	1363	1511.7	-148.7
18	2019	2111.0	-92.0	85	2091	2056.8	34.2	152	939	1505.4	-566.4
19	2023	2111.1	-88.1	86	1993	2066.4	-73.4	153	985	1499.6	-514.6
20	2104	2113.6	-9.6	87	1879	2072.4	-193.4	154	1145	1494.3	-349.3
21	1658	2117.8	-459.8	88	2127	2073.2	53.8	155	1913	1489.5	423.5
22	1891	2122.0	-231.0	89	1943	2068.0	-125.0	156	1614	1485.0	129.0
23	2287	2124.5	162.5	90	1752	2056.3	-304.3	157	1199	1481.0	-282.0
24	1943	2123.8	-180.8	91	2321	2038.5	282.5	158	1738	1477.2	260.8
25	1879	2119.5	-240.5	92	1819	2015.5	-196.5	159	1683	1473.8	209.2
26	1871	2112.9	-241.9	93	2382	1988.8	393.2	160	1824	1470.7	353.3
27	1961	2106.1	-145.1	94	2126	1959.9	166.1	161	1350	1467.9	-117.9
28	2143	2101.9	41.1	95	1990	1930.7	59.3	162	1518	1465.2	52.8
29	1567	2102.0	-535.0	96	1443	1903.0	-460.0	163	1595	1462.8	132.2
30	2143	2107.3	35.7	97	1968	1878.5	89.5	164	1264	1460.6	-196.6
31	2474	2116.5	357.5	98	1595	1858.5	-263.5	165	1296	1458.6	-162.6
32	2446	2126.9	319.1	99	1759	1844.1	-85.1	166	1171	1456.7	-285.7
33	2238	2135.3	102.7	100	1815	1836.0	-21.0	167	1607	1455.0	152.0
34	2137	2138.8	-1.8	101	1573	1834.4	-261.4	168	1686	1453.4	232.6
35	2034	2135.8	-101.8	102	1739	1839.2	-100.2	169	1417	1451.9	-34.9
36	1935	2126.6	-191.6	103	1935	1850.0	85.0	170	1171	1450.6	-279.6
37	1909	2113.6	-204.6	104	1606	1866.0	-260.0	171	1643	1449.4	193.6
38	2295	2100.2	194.8	105	1897	1886.3	10.7	172	1554	1448.2	105.8
39	2208	2090.1	117.9	106	1863	1909.8	-46.8	173	1600	1447.1	152.9
40	2191	2086.1	104.9	107	2301	1935.3	365.7	174	1626	1446.2	179.8
41	2103	2089.5	13.5	108	2496	1961.6	534.4	175	916	1445.2	-529.2
42	1805	2099.6	-294.6	109	2263	1987.5	275.5	176	1001	1444.4	-443.4
43	2250	2113.9	136.1	110	1744	2012.2	-268.2	177	1362	1443.6	-81.6
44	2198	2129.1	68.9	111	1800	2034.6	-234.6	178	1566	1442.9	123.1
45	1916	2141.7	-225.7	112	1759	2054.1	-295.1	179	1610	1442.2	167.8
46	2293	2149.2	143.8	113	2281	2070.0	211.0	180	1064	1441.5	-377.5
47	2136	2150.3	-14.3	114	1920	2081.9	-161.9	181	1747	1440.9	306.1
48	2193	2145.4	47.6	115	2239	2089.7	149.3	182	2028	1440.4	587.6
49	1863	2136.2	-273.2	116	2122	2093.1	28.9	183	2035	1439.9	595.1
50	2173	2125.0	48.0	117	2015	2092.3	-77.3	184	1230	1439.4	-209.4
51	2415	2114.2	300.8	118	2179	2087.5	91.5	185	1143	1438.9	-295.9
52	2041	2105.6	-64.6	119	2311	2078.7	232.3	186	1742	1438.5	303.5
53	1882	2100.1	-218.1	120	2047	2066.5	-19.5	187	1559	1438.1	120.9
54	2047	2097.4	-50.4	121	2047	2051.2	-4.2	188	1147	1437.7	-290.7
55	2589	2096.5	492.5	122	2343	2033.1	309.9	189	1307	1437.3	-130.3
56	2234	2096.4	137.6	123	2407	2012.7	394.3	190	1373	1437.0	-64.0
57	2250	2095.8	154.2	124	2673	1990.5	682.5	191	1207	1436.7	-229.7
58	1642	2094.2	-452.2	125	2343	1966.9	376.1	192	1520	1436.4	83.6
59	1903	2092.1	-189.1	126	1743	1942.2	-199.2	193	1351	1436.2	-85.2
60	1899	2090.4	-191.4	127	1858	1916.8	-58.8	194	1625	1435.9	189.1
61	2064	2090.8	-26.8	128	1926	1891.1	34.9	195	1524	1435.7	88.3
62	2339	2094.9	244.1	129	1962	1865.3	96.7	196	1245	1435.4	-190.4
63	1901	2103.9	-202.9	130	1552	1839.7	-287.7	197	1249	1435.2	-186.2
64	2156	2118.3	37.7	131	1623	1814.6	-191.6	198	1864	1435.0	429.0
65	2453	2137.6	315.4	132	1448	1790.2	-342.2	199	1571	1434.8	136.2
66	2253	2160.2	92.8	133	1775	1766.5	8.5	200	1379	1434.6	-55.6

TABLE 5-26

X13607: SUPPLEMENTAL STATISTICAL INFORMATION

VARIANCE/CO-VARIANCE MATRIX

DIA1	INT1	SKY	TIM1	VEL1	DIA2	INT2	TIM2	VEL2
3.525E-15	1.020E-06	-3.654E-07	-2.014E-08	1.835E-10	-3.092E-16	-6.285E-07	-3.836E-08	5.245E-10
1.020E-06	3.147E03	-1.339E03	-1.590E01	1.258E-01	-1.161E-06	-1.750E03	-1.013E02	1.259E00
-3.654E-07	-1.339E03	1.491E03	-4.583E01	3.431E-01	-1.759E-07	-1.438E02	-7.691E00	1.125E-01
-2.014E-08	-1.590E01	-4.583E01	1.162E01	-8.876E-02	5.810E-08	5.996E01	3.166E00	-4.302E-02
1.835E-10	1.258E-01	3.431E-01	-8.876E-02	8.903E-04	-5.205E-10	-4.600E-01	-2.339E-02	3.404E-04
-3.092E-16	-1.161E-06	-1.759E-07	5.810E-08	-5.205E-10	2.483E-14	1.970E-06	-3.218E-08	6.905E-10
-6.285E-07	-1.750E03	-1.438E02	5.996E01	-4.600E-01	1.970E-06	2.637E03	5.894E01	-7.362E-01
-3.836E-08	-1.013E02	-7.691E00	3.166E00	-2.339E-02	-3.218E-08	5.894E01	4.707E01	-5.940E-01
5.245E-10	1.259E00	1.125E-01	-4.302E-02	3.404E-04	6.905E-10	-7.362E-01	-5.940E-01	1.003E-02

CORRELATION MATRIX

	DIA1	INT1	SKY	TIM1	VEL1	DIA2	INT2	TIM2	VEL2
DIA1	1.000000	0.997229	-0.722289	-0.383576	0.395768	-0.823021	-0.857099	-0.878964	0.873699
INT1	0.997229	1.000000	-0.771404	-0.313878	0.326433	-0.781473	-0.818742	-0.856130	0.850179
SKY	-0.722289	-0.771404	1.000000	-0.358492	0.346085	0.220042	0.276065	0.452869	-0.442802
TIM1	-0.383576	-0.313878	-0.358492	1.000000	-0.999903	0.810498	0.781205	0.576135	-0.582599
VEL1	0.395768	0.326433	0.346085	-0.999903	1.000000	-0.818431	-0.789639	-0.584063	0.590396
DIA2	-0.823021	-0.781473	0.220042	0.810498	-0.818431	1.000000	0.997529	0.808705	-0.808388
INT2	-0.857099	-0.818742	0.276065	0.781205	-0.789639	0.997529	1.000000	0.843111	-0.842422
TIM2	-0.878964	-0.856130	0.452869	0.576135	-0.584063	0.808705	0.843111	1.000000	-0.999927
VEL2	0.873699	0.850179	-0.442802	-0.582599	0.590396	-0.808388	-0.842422	-0.999927	1.000000

NUMERICAL RANGES OF THE PARTIAL DERIVATIVES

	DIA1	INT1	SKY	TIM1	VEL1	DIA2	INT2	TIM2	VEL2
MAXIMUM	8.667E08	1.366E00	1.000E00	2.565E01	3.330E03	3.602E08	1.365E00	1.376E01	1.082E03
MINIMUM	-8.669E08	1.038E-02	1.000E00	-2.732E01	-3.404E03	-3.644E08	1.628E-03	-1.458E01	-1.112E03

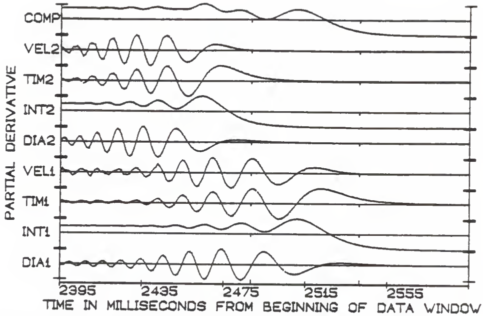

Figure 5-49. PDPLOT of the occultation of X13607.

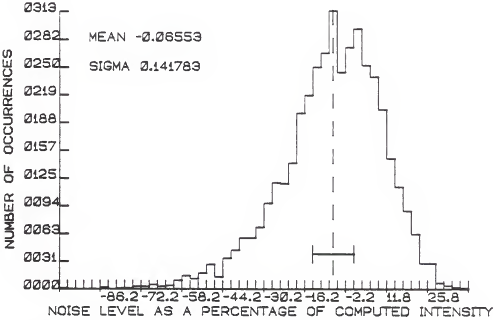

Figure 5-50. NOISEPLOT of the occultation of X13607.

The NOISEPLOT of the 4096 milliseconds of observational data (Figure 5-26), as well as the mean offset and one sigma values, are nearly identical to those obtained for the earlier occultation of X13567. This was expected as both stars were nearly the same apparent V magnitude, and the observing conditions were essentially identical.

Finally, the power spectra of the observation centered on the event, the pre-occultation and star-plus-sky signals, and the two-star model curve are shown in the POWERPLOT, Figure 5-51.

Since the WWVB time signal was of lower quality for this event, the Coordinated Universal Times of geometrical occultation were not quite as well determined as for the X13534 event. The fainter star underwent disappearance at 04:33:58.773 (+/- 0.009 seconds). The brighter component followed this at 04:34:58.827 (+/- 0.007 seconds).

ZC1462

The occultation of the K0 star ZC1462 on April 22, 1983, was observed under rather poor conditions, as detailed in the following excerpt from the observing log regarding that event: " ... seeing poor, often worse than 8 or 10 seconds of arc. Occasional image blooming causes the star to become invisible in the photometer viewing optics. ... " Despite the bad photometric conditions, a digital photoelectric record of the occultation was obtained and is presented in the RAWPLOT, Figure 5-52.

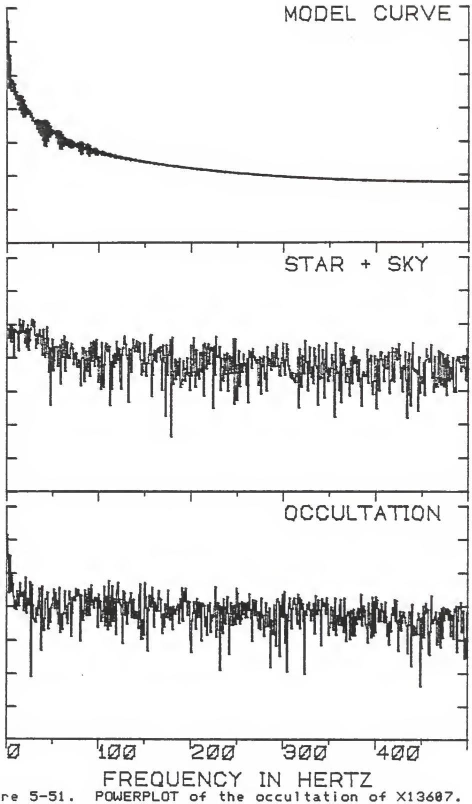

Figure 5-51. POWERPLOT of the occultation of X13607.

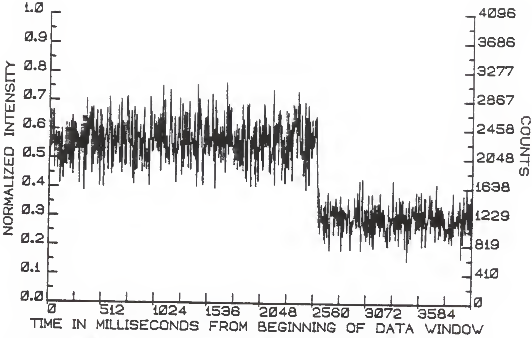

Figure 5-52. RAWPLOT of the occultation of ZC1462.

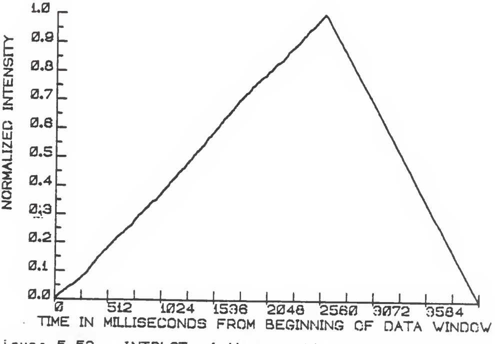

Figure 5-53. INTPLOT of the occultation of ZC1462.

The integration plot, Figure 5-53, shows no evidence of stellar duplicity. Though there is an apparent change in slope at approximately 1800 milliseconds, it is a gradual change in level, rather than a sharp discontinuity typical of a second star. In addition, the original slope of the integration curve returns at approximately 2200 milliseconds. This behavior is due only to variations in atmospheric transparency.

The formal solution to the observed intensity curve is shown on the FITPLOT, Figure 5-54. As may be seen from the figure, or from the occultation summary, Table 5-27, the best fit to the raw data calls for a source diameter of roughly 9 milliseconds of arc. This anomalously large angular diameter is quite unexpected considering the relative faintness of this star, and is believed to be spurious.

The power spectrum of the star-plus-sky signal determined from 1000 millisecond data samples taken between 1.5 ond 0.5 seconds preceeding the determined time of geometrical occultation is shown on Figure 5-56. Contributions to the background noise due to the low frequency power components are quite important. Indeed, in the range of 10 to 70 Hertz these are dominant over the power spectral signature of the solution curve by one to two orders of magnitude, respectively. It is precisely, however, in this power spectral region that

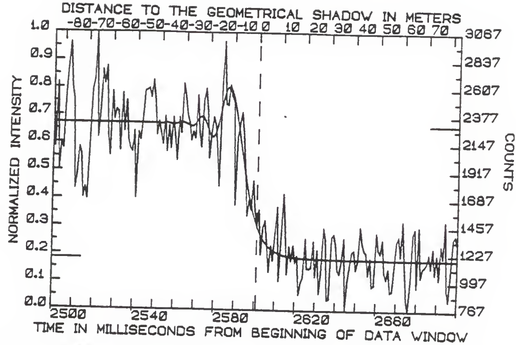

Figure 5-54. FITPLOT of the occultation of ZC1462 to the raw data.

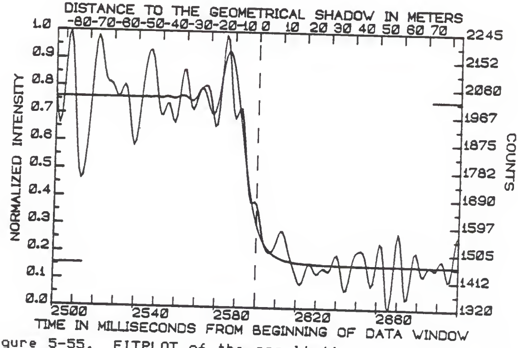

Figure 5-55. FITPLOT of the occultation of ZC1462 to the Fourier transformed data.

TABLE 5-27
ZC1462: LUNAR OCCULTATION SUMMARY

STELLAR AND OBSERVING INFORMATION

Star: ZC1462 (SAO 098862, DM +17 2156)
RA: 095639 DEC: +163225 mV: 7.38 Sp: K0
Filter: V Diaphragm: I Gain: C7 Voltage: 1200

LUNAR INFORMATION

Surface Illumination:	70 percent
Elongation from Sun:	114 degrees
Altitude Above Horizon:	37 degrees
Lunar Limb Distance:	366100 kilometers
Predicted Shadow Velocity:	809.68 meters/sec.
Predicted Angular Rate:	0.4969 arcsec/sec.

EVENT INFORMATION

Date:	April 22, 1983	UT of Event:	05:13:38
USNO V/O Code:	15	HA of Event:	+562152
Position Angle:	124.6	Cusp Angle:	77S
Contact Angle:	-7.0	Watts Angle:	104.1

MODEL PARAMETERS

Number of Data Points:	201
Number of Grid Points:	256
Number of Spectral Regions:	53
Width of Spectral Regions:	50 Angstroms
Limb Darkening Coefficient:	0.5
Effective Stellar Temperature:	5100K

SOLUTIONS	Raw Fit	Fourier Fit
Stellar Diameter (ams):	9.27 (3.69)	9.02 (2.44)
Time: (relative to Bin 0):	2601.5 (1.1)	2601.1 (0.7)
Pre-Event Signal:	2307.9 (25.1)	2299.8 (16.8)
Background Sky Level:	1187.6 (25.3)	1184.9 (16.3)
Velocity (meters/sec):	831.4 (78.6)	833.9 (50.4)
Lunar Limb Slope (degrees):	-6.57 (5.56)	-6.29 (3.57)
UT of Occultation:	05:13:37.1989 (0.0014)	37.1985 (0.0011)

PHOTOMETRIC NOISE DATA	Raw Fit	Fourier Fit
S-O-S of Residuals:	11526000	1253100
Sigma (Standard Error):	240.07	79.154
Normalized Standard Error:	0.2143	0.1420
Photometric (S+N)/N Ratio:	5.6663	8.0434
Intensity Change/Background:	0.94324	0.94092
Change in Magnitude:	0.72132	0.72002

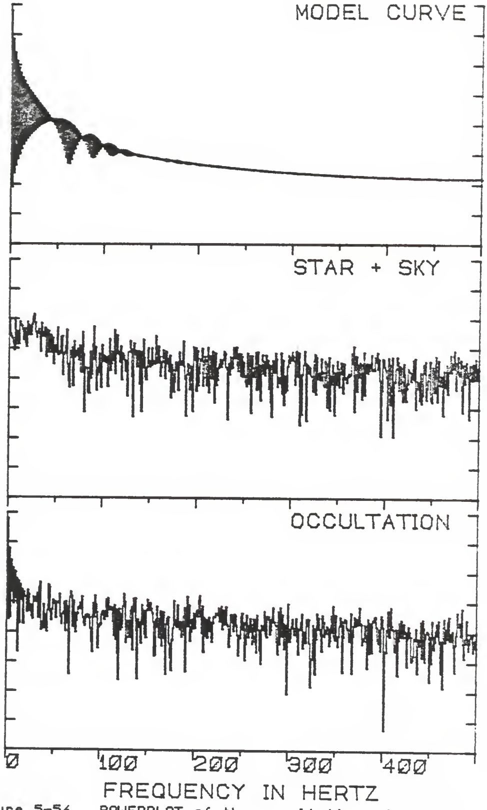

Figure 5-56. POWERPLOT of the occultation of ZC1462.

the signature of the occultation curve is most important. Hence, the observed data are corrupted by intensity variations due to atmospheric noise which mimic the variations seen in an occultation curve.

This effect is seen rather dramatically in the second FITPLOT presented (Figure 5-55). Here, the observed data were Fourier transformed and all power components of frequency higher than 150 Hertz removed. After inverse transformation, the Fourier smoothed data were fit by the DC procedure. The solutions obtained in a fit to the smoothed data, as expected, are nearly identical to the fit to the raw data. What is obvious from visual inspection is that the undulating character of the data, in terms of both frequency and amplitude, is very similar to the fringing effects expected due to the occultation.

It is therefore apparent that the noise characteristics of the sky, at the time of this event, were such that the formal solution of the angular diameter is highly suspect, and in fact most probably erroneous. Under these conditions, with present reduction and analysis techniques, it is almost certainly impossible to ascertain the true angular diameter of the star. Though a formally determined diameter is presented here, a strong "caveat emptor" is placed on the result.

The observations extracted from the raw data set (as well as the computed intensity curve and the residuals) are listed in Table 5-28. The variance-covariance and correlation matrices of the formal solution are given in Table 5-29. Also found on this table are the ranges of the numerical values of the partial derivatives of the intensity curve, as depicted on the PDPLOT, Figure 5-57.

The photometrically poor conditions for occultation photometry are further noted by an examination of the NOISEPLOT of the 4096 milliseconds of observational data presented in Figure 5-58. The mean signal level does correspond with the peak of the distribution function of the residuals, but the distribution function itself is highly skewed. The mean signal level over the entire data window is more than 2 percent down from the mean level during the 201 milliseconds centered on the time of the event, and the one sigma level of the distribution function is approximately 11.5 percent.

A final note on observations, such as this one, taken under photometrically noisy conditions is warranted. In this case, the noise associated with the raw data has a one sigma level of 21.4 percent of the mean intensity. This by itself is not sufficient to dismiss the possibility of obtaining a meaningful solution from the observed intensity curve. What is

TABLE 5-28
ZC1462: OBSERVATIONS, COMPUTED VALUES, AND RESIDUALS FROM BIN 2500

NUM	OBS	COMP	RESID	NUM	OBS	COMP	RESID	NUM	OBS	COMP	RESID
0	2682	2311.0	371.0	67	2321	2298.5	22.5	134	1458	1194.5	263.5
1	2111	2311.1	-200.1	68	2173	2293.2	-120.2	135	1361	1194.1	166.9
2	2648	2311.0	337.0	69	2250	2297.6	-47.6	136	858	1193.7	-335.7
3	1923	2311.0	-388.0	70	2193	2313.8	-120.8	137	870	1193.4	-323.4
4	2155	2311.0	-156.0	71	2553	2338.1	214.9	138	1379	1193.1	185.9
5	2095	2311.0	-216.0	72	2244	2361.7	-117.7	139	1403	1192.8	210.2
6	2555	2311.0	244.0	73	2117	2373.5	-256.5	140	1324	1192.6	131.4
7	2800	2311.0	489.0	74	2503	2365.0	138.0	141	1104	1192.3	-88.3
8	2979	2311.0	668.0	75	2607	2334.8	272.2	142	1074	1192.1	-118.1
9	2619	2311.0	308.0	76	2423	2290.0	133.0	143	1183	1191.9	-8.9
10	2507	2311.0	196.0	77	2029	2243.6	-214.6	144	1370	1191.7	178.3
11	1767	2311.0	-544.0	78	2226	2210.8	15.2	145	778	1191.5	-413.5
12	1882	2311.0	-429.0	79	2371	2204.0	167.0	146	1014	1191.3	-177.3
13	2111	2311.0	-200.0	80	2311	2229.1	81.9	147	1143	1191.2	-48.2
14	2050	2311.0	-261.0	81	2095	2284.2	-189.2	148	1257	1191.0	66.0
15	1691	2311.0	-620.0	82	1797	2360.7	-563.7	149	1269	1190.9	78.1
16	1779	2311.0	-532.0	83	2639	2445.5	193.5	150	1109	1190.8	-81.8
17	1683	2310.9	-627.9	84	2996	2524.4	471.6	151	1182	1190.6	-8.6
18	2115	2311.0	-196.0	85	2478	2584.9	-106.9	152	1464	1190.5	273.5
19	2583	2311.0	272.0	86	2471	2618.1	-147.1	153	1336	1190.4	145.6
20	2671	2311.0	360.0	87	2641	2619.4	21.6	154	1271	1190.3	80.7
21	3067	2311.0	756.0	88	2543	2588.7	-45.7	155	1247	1190.2	56.8
22	2194	2311.0	-117.0	89	2496	2529.3	-33.3	156	1065	1190.1	-125.1
23	2387	2311.0	76.0	90	1643	2446.6	-803.6	157	1203	1190.0	13.0
24	2755	2311.0	444.0	91	2203	2347.3	-144.3	158	968	1190.0	-222.0
25	2641	2311.1	329.9	92	2313	2238.3	74.7	159	986	1189.9	-203.9
26	2783	2311.0	472.0	93	2411	2125.6	285.4	160	1415	1189.8	225.2
27	2216	2311.0	-95.0	94	2218	2014.3	203.7	161	1278	1189.7	88.3
28	2043	2311.2	-268.2	95	1920	1908.3	11.7	162	1241	1189.7	51.3
29	2573	2311.1	261.9	96	1553	1810.0	-257.0	163	1357	1189.6	167.4
30	2343	2311.0	32.0	97	1691	1721.1	-30.1	164	1087	1189.5	-102.5
31	2426	2311.1	114.9	98	1608	1642.2	-34.2	165	1032	1189.5	-157.5
32	2403	2311.3	91.7	99	1844	1573.2	270.8	166	1119	1189.4	-70.4
33	2083	2311.2	-228.2	100	1599	1513.6	85.4	167	924	1189.4	-265.4
34	2559	2311.0	248.0	101	1475	1462.8	12.2	168	936	1189.3	-253.3
35	2247	2311.2	-64.2	102	1605	1419.8	185.2	169	1139	1189.3	-50.3
36	2498	2311.4	186.6	103	1229	1383.6	-154.6	170	1343	1189.2	153.8
37	2175	2311.4	-136.4	104	1457	1353.2	103.8	171	1387	1189.2	197.8
38	2102	2311.2	-209.2	105	1515	1327.9	187.1	172	1219	1189.1	29.9
39	2075	2311.3	-236.3	106	1318	1306.9	11.1	173	1516	1189.1	326.9
40	2246	2311.5	-65.5	107	1090	1289.3	-199.3	174	1139	1189.1	-50.1
41	1692	2311.6	-619.6	108	1308	1274.8	33.2	175	868	1189.0	-321.0
42	2237	2311.4	-74.4	109	1183	1262.6	-79.6	176	767	1189.0	-422.0
43	2175	2311.3	-136.3	110	1407	1252.5	154.5	177	1027	1188.9	-161.9
44	2339	2311.7	27.3	111	1631	1244.0	387.0	178	1403	1188.9	214.1
45	2582	2312.2	269.8	112	1015	1236.8	-221.8	179	1451	1188.9	262.1
46	2591	2311.8	279.2	113	1331	1230.8	100.2	180	965	1188.8	-223.8
47	2604	2310.9	293.1	114	1739	1225.7	513.3	181	1467	1188.8	278.2
48	2527	2311.2	215.8	115	1460	1221.4	238.6	182	1047	1188.8	-141.8
49	2673	2313.0	360.0	116	1073	1217.7	-144.7	183	1121	1188.8	-67.8
50	2503	2314.2	188.8	117	1301	1214.5	86.5	184	1139	1188.7	-49.7
51	2217	2312.7	-95.7	118	1182	1211.8	-29.8	185	1166	1188.7	-22.7
52	2331	2309.7	21.3	119	1309	1209.4	99.6	186	1242	1188.7	53.3
53	2233	2309.1	-76.1	120	1167	1207.3	-40.3	187	1126	1188.7	-62.7
54	2140	2312.4	-172.4	121	1224	1205.5	18.5	188	1291	1188.6	102.4
55	2369	2316.9	52.1	122	902	1204.0	-302.0	189	1075	1188.6	-113.6
56	2080	2317.9	-237.9	123	999	1202.6	-203.6	190	1231	1188.6	42.4
57	2294	2314.1	-20.1	124	1045	1201.4	-156.4	191	1033	1188.6	-155.6
58	2107	2308.6	-201.6	125	1367	1200.4	166.6	192	1315	1188.6	126.4
59	2367	2306.1	60.9	126	1119	1199.4	-80.4	193	1209	1188.5	20.5
60	2202	2308.7	-106.7	127	1115	1198.6	-83.6	194	1515	1188.5	326.5
61	2010	2314.8	-304.8	128	1125	1197.8	-72.8	195	954	1188.5	-234.5
62	2367	2320.9	46.1	129	1345	1197.1	147.9	196	856	1188.5	-332.5
63	2237	2324.3	-87.3	130	1051	1196.5	-145.5	197	1117	1188.5	-71.5
64	2647	2323.3	323.7	131	1273	1195.9	77.1	198	1367	1188.4	178.6
65	2539	2317.7	221.3	132	913	1195.4	-282.4	199	1401	1188.4	212.6
66	2390	2308.4	81.6	133	1079	1194.9	-115.9	200	1325	1188.4	136.6

TABLE 5-29
ZC1462: SUPPLEMENTAL STATISTICAL INFORMATION

VARIANCE/CO-VARIANCE MATRIX

DIAM	PREI	POST	TIME	VELO
3.207E¯16	6.839E¯08	-2.060E¯08	-4.716E¯09	3.890E¯10
6.839E¯08	6.296E02	2.217E01	-6.631E00	3.594E¯01
-2.060E¯08	2.217E01	6.404E02	-7.124E00	3.994E¯01
-4.716E¯09	-6.631E00	-7.124E00	1.306E00	-7.414E¯02
3.890E¯10	3.594E¯01	3.994E¯01	-7.414E¯02	6.182E¯03

CORRELATION MATRIX

	DIAM	PREI	POST	TIME	VELO
DIAM	1.000000	0.959624	-0.441850	-0.367280	0.348224
PREI	0.959624	1.000000	-0.176967	-0.603263	0.586464
POST	-0.441850	-0.176967	1.000000	-0.669212	0.683702
TIME	-0.367280	-0.603263	-0.669212	1.000000	-0.999770
VELO	0.348224	0.586464	0.683702	-0.999770	1.000000

NUMERICAL RANGES OF THE PARTIAL DERIVATIVES

	MAXIMUM	MINIMUM
DIAM	4.426E09	-3.867E09
PREI	1.278E00	6.941E¯04
POST	9.993E¯01	-2.781E¯01
TIME	1.127E02	-8.438E01
VELO	1.411E03	-1.846E03

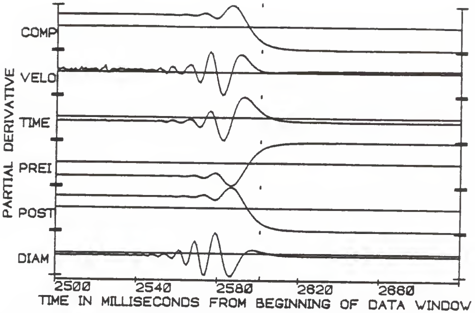

Figure 5-57. PDPLOT of the occultation of ZC1462.

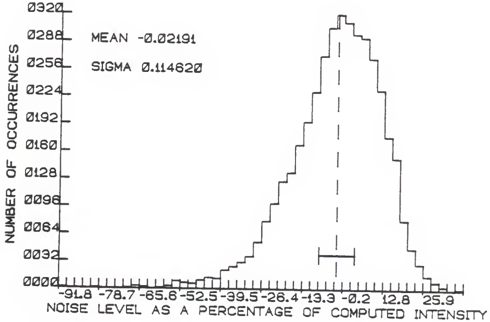

Figure 5-58. NOISEPLOT of the occultation of ZC1462.

important is whether the noise is dominant in the low or high frequency regime. To further verify that this is indeed true, a computational test was performed. A model intensity curve was needed for the test. For convenience, the solution curve for this occultation was used. To this model curve, noise (whose characteristics are described by the distribution function shown in Figure 5-58) was applied. The addition of this noise was subject to a temporal distribution such that the power components in the low frequency domain (less than 70 Hertz) were not highly dominant. In two trial attempts, the DC procedure had no trouble recovering the model parameters. In addition, the same noise distribution as used in the first trial was applied to a point source, and a point source solution was obtained.

Fortunately, the time-scale and zero reference of the occultation event were found through this, and additional numerical experimentation, to be moderately insensitive to this type of predominantly low frequency noise. Thus, the determination of the time of geometrical occultation of 05:13:37.199 (+/-0.001) Coordinated Universal Time is fairly reliable.

X18067

The K0 star X18067 (mV=7.9) was occulted on June 18, 1983, under clear, photometrically steady skies. The fast photoelectric digital record of this event, shown in Figure 5-59, was obtained by John P. Oliver and

Martin England who (as noted in the occultation summary, Table 5-30) employed a Johnson V filter for the observation.

The integration plot of the observational data (Figure 5-60) hints at a possible "wide" stellar duplicity approximately 150 milliseconds before the obvious disappearance. To ascertain if this drop (also seen on the RAWPLOT) was real, a detailed integration plot was produced containing the data from 3100 to 3625 milliseconds. To aid in the visual interpretation of the graph, the integrated data were subjected to 5-point unweighted smoothing before being plotted. It is apparent in Figure 5-61 that a real, sharp change of slope does occur at approximately millisecond 3265.

The mean intensity (averaged over 125 milliseconds) prior to this was 2515 counts, and afterward, 2488 counts. This drop of 27 counts represents a lowering of the signal intensity by approximately 0.011 magnitudes. This seems like a rather small amount. However, as will be seen, the formal error of the pre-occultation intensity found by the DC fitting process at the time of the primary event was only roughly 0.007 magnitudes. Hence, the one sigma certainty of detection of a "wide" component is 64 percent better than the determination of the mean star-plus-sky level. Therefore, one can

TABLE 5-30
X18067: LUNAR OCCULTATION SUMMARY

STELLAR AND OBSERVING INFORMATION

Star: X18067 (SAO 119227, DM +05 2587)
RA: 120641 DEC: +043627 mV: 7.9 Sp: K0
Filter: V Diaphragm: I Gain: B10+ Voltage: 1200

LUNAR INFORMATION

Surface Illumination:	53 percent
Elongation from Sun:	93 degrees
Altitude Above Horizon:	48 degrees
Lunar Limb Distance:	370414 kilometers
Predicted Shadow Velocity:	364.91 meters/sec.
Predicted Angular Rate:	0.2032 arcsec/sec.

EVENT INFORMATION

Date:	June 18, 1983	UT of Event:	02:16:54
USNO V/O Code:	26	HA of Event:	+354352
Position Angle:	63.8	Cusp Angle:	40N
Contact Angle:	+61.5	Watts Angle:	40.6

MODEL PARAMETERS

Number of Data Points:	201
Number of Grid Points:	4096
Number of Spectral Regions:	53
Width of Spectral Regions:	50 Angstroms
Limb Darkening Coefficient:	0.5
Effective Stellar Temperature:	5100K

SOLUTIONS

Stellar Diameter (ams):	Point Source	
Time: (relative to Bin 0):	3422.1	(1.5)
Pre-Event Signal:	2459.2	(16.8)
Background Sky Level:	1738.6	(20.8)
Velocity (meters/sec.):	365.6	(10.7)
Lunar Limb Slope (degrees):	-1.83	(1.68)
U.T. of Occultation:	02:16:52.406	(0.007)

PHOTOMETRIC NOISE INFORMATION

Sum-of-Squares of Residuals:	6146800
Sigma (Standard Error):	175.316
Normalized Standard Error:	0.24332
Photometric (S+N)/N Ratio:	5.1099
(Change in Intensity)/Background:	0.41441
Change in Magnitude:	0.37643

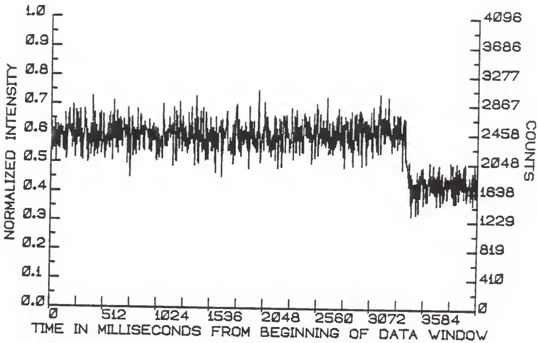

Figure 5-59. RAWPLOT of the occultation of X18067.

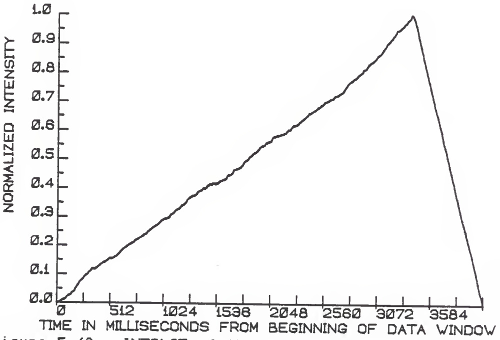

Figure 5-60. INTPLOT of the occultation of X18067.

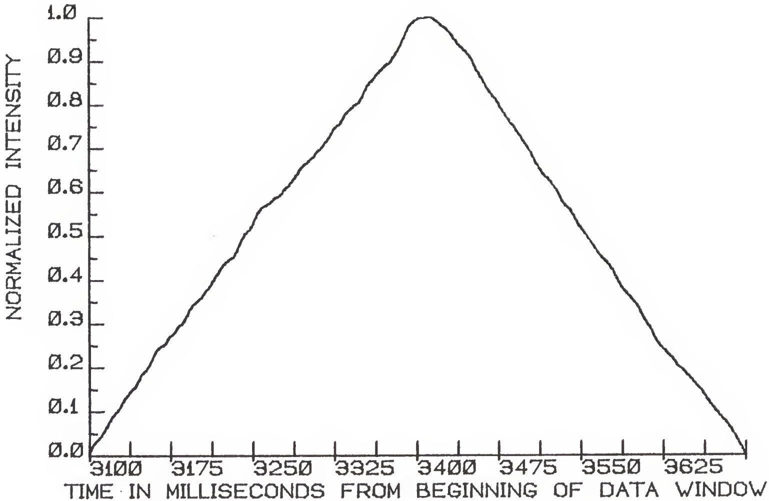

Figure 5-61. Detailed INPLOT with 5-point un-weighted smoothing, showing the X18067 secondary event.

ascribe a confidence level to the detection of a "wide" secondary component of 90 percent.

The best solution for the observation of the primary occultation of X18067 (depicted graphically in Figure 5-62) found the star to be a point source. This was not unexpected as X18067 has been classified as a main sequence star, thus giving it a distance modulus of approximately 2.0, and an anticipated diameter of 0.85 solar radii. At this distance the corresponding angular diameter would be only 1/25 millisecond of arc, well below the detection threshold of roughly one millisecond of arc.

From the determined R-rate of 0.2036 (+/- 0.0059) seconds of arc per second, the "wide" secondary component was found to have a projected separation of 32 milliseconds of arc. The uncertainty in this is somewhat conjectural. In this case it is safe to assume that the time of secondary disappearance can be determined by inspection of the detailed integration plot to an accuracy of roughly 10 milliseconds. This gives an uncertainty of approximately 2 milliseconds of arc in the projected separation.

The subset of the observational data used in the fitting procedure, the computed intensities, and the resulting residuals are listed in Table 5-31. The supplementary statistical information, including

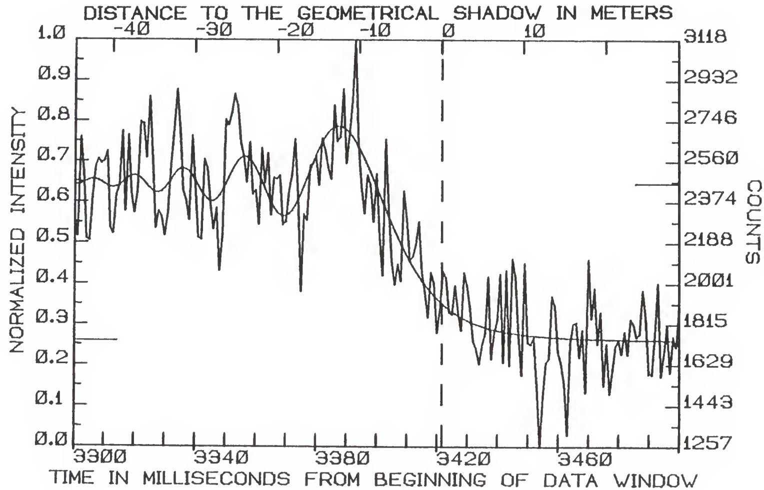

Figure 5-62. FITPLOT of the occultation of X18067.

TABLE 5-31
X18067: OBSERVATIONS, COMPUTED VALUES, AND RESIDUALS FROM BIN 3300

NUM	OBS	COMP	RESID	NUM	OBS	COMP	RESID	NUM	OBS	COMP	RESID
0	2297	2452.3	-155.3	67	2479	2330.9	148.1	134	1635	1811.4	-176.4
1	2216	2452.4	-236.4	68	2497	2317.4	179.6	135	1723	1806.7	-83.7
2	2672	2455.4	216.6	69	2270	2311.0	-41.0	136	1775	1802.4	-27.4
3	2512	2460.8	51.2	70	2284	2311.9	-27.9	137	2036	1798.4	237.6
4	2207	2467.3	-260.3	71	2421	2320.1	100.9	138	1657	1794.7	-137.7
5	2197	2473.2	-276.2	72	2496	2335.1	160.9	139	1779	1791.3	-12.3
6	2398	2476.5	-78.5	73	2663	2356.3	306.7	140	1831	1788.1	42.9
7	2534	2476.4	57.6	74	2407	2382.8	24.2	141	2049	1785.1	263.9
8	2572	2472.5	99.5	75	1967	2413.5	-446.5	142	1641	1782.4	-141.4
9	2550	2465.3	84.7	76	2320	2447.2	-127.2	143	2067	1779.9	287.1
10	2561	2456.4	104.6	77	2292	2482.8	-190.8	144	1627	1777.5	-150.5
11	2607	2447.9	159.1	78	2543	2519.0	24.0	145	2119	1775.3	343.7
12	2256	2441.8	-185.8	79	2552	2554.7	-2.7	146	2039	1773.3	265.7
13	2231	2439.7	-208.7	80	2579	2588.8	-9.8	147	1768	1771.4	-3.4
14	2405	2442.5	-37.5	81	2452	2620.4	-168.4	148	1583	1769.6	-186.6
15	2448	2450.0	-2.0	82	2669	2648.7	20.3	149	2096	1768.0	328.0
16	2699	2460.9	238.1	83	2613	2673.0	-60.0	150	1734	1766.5	-32.5
17	2333	2473.3	-140.3	84	2535	2692.8	-157.8	151	1723	1765.0	-42.0
18	2681	2484.8	196.2	85	2479	2707.9	-228.9	152	1755	1763.7	-8.7
19	2415	2492.8	-77.8	86	2821	2717.9	103.1	153	1536	1762.5	-226.5
20	2324	2495.7	-171.7	87	2653	2722.8	-69.8	154	1257	1761.3	-504.3
21	2427	2492.5	-65.5	88	2671	2722.7	-51.7	155	1484	1760.2	-276.2
22	2744	2483.5	260.5	89	2895	2717.7	177.3	156	1639	1759.2	-120.2
23	2734	2469.9	264.1	90	2551	2708.1	-157.1	157	1658	1758.2	-100.2
24	2575	2453.8	121.2	91	2679	2694.3	-15.3	158	1946	1757.3	188.7
25	2858	2437.9	420.1	92	2835	2676.5	158.5	159	1899	1756.5	142.5
26	2566	2425.0	141.0	93	3118	2655.2	462.8	160	1689	1755.7	-66.7
27	2255	2417.3	-162.3	94	2639	2630.9	8.1	161	1640	1754.9	-114.9
28	2335	2416.3	-81.3	95	2449	2603.9	-154.9	162	1546	1754.2	-208.2
29	2309	2422.6	-113.6	96	2322	2574.8	-252.8	163	1311	1753.6	-442.6
30	2220	2435.5	-215.5	97	2499	2543.9	-44.9	164	1727	1752.9	-25.9
31	2317	2453.4	-136.4	98	2456	2511.7	-55.7	165	1819	1752.3	66.7
32	2539	2474.0	65.0	99	2284	2478.6	-194.6	166	1825	1751.8	73.2
33	2703	2494.4	208.6	100	2505	2444.9	60.1	167	1665	1751.3	-86.3
34	2891	2511.8	379.2	101	2218	2411.0	-193.0	168	1791	1750.8	40.2
35	2704	2523.8	180.2	102	2040	2377.1	-337.1	169	1505	1750.3	-245.3
36	2427	2528.5	-101.5	103	2663	2343.6	319.4	170	2115	1749.9	365.1
37	2384	2525.2	-141.2	104	2348	2310.6	37.4	171	1843	1749.4	93.6
38	2292	2513.9	-221.9	105	2108	2278.3	-170.3	172	1984	1749.0	235.0
39	2679	2495.9	183.1	106	1999	2246.9	-247.9	173	1727	1748.7	-21.7
40	2452	2473.1	-21.1	107	2094	2216.6	-122.6	174	1872	1748.3	123.7
41	2212	2448.0	-236.0	108	2015	2187.3	-172.3	175	1536	1748.0	-212.0
42	2203	2423.4	-220.4	109	2427	2159.3	267.7	176	1728	1747.7	-19.7
43	2571	2402.1	168.9	110	2299	2132.5	166.5	177	1498	1747.4	-249.4
44	2530	2386.4	143.6	111	2108	2107.0	1.0	178	1611	1747.1	-136.1
45	2364	2378.0	-14.0	112	2127	2082.8	44.2	179	1718	1746.9	-28.9
46	2251	2378.1	-127.1	113	2180	2059.8	120.2	180	1743	1746.6	-3.6
47	2347	2386.7	-39.7	114	2285	2038.2	246.8	181	1680	1746.4	-66.4
48	2063	2403.2	-340.2	115	2059	2017.9	41.1	182	1783	1746.1	36.9
49	2217	2426.1	-209.1	116	1966	1998.8	-32.8	183	1676	1745.9	-69.9
50	2753	2453.6	299.4	117	1848	1980.8	-132.8	184	1841	1745.7	95.3
51	2729	2483.1	245.9	118	2056	1964.1	91.9	185	1819	1745.5	73.5
52	2782	2512.4	269.6	119	2007	1948.4	58.6	186	1756	1745.2	10.8
53	2872	2538.8	333.2	120	1779	1933.8	-154.8	187	1772	1745.0	27.0
54	2818	2560.4	257.6	121	1887	1920.2	-33.2	188	1973	1744.8	228.2
55	2647	2575.3	71.7	122	2062	1907.5	154.5	189	1850	1744.7	105.3
56	2586	2582.4	3.6	123	2031	1895.8	135.2	190	1592	1744.5	-152.5
57	2464	2581.2	-117.2	124	1872	1884.9	-12.9	191	1585	1744.3	-159.3
58	2648	2571.9	76.1	125	1863	1874.7	-11.7	192	1768	1744.1	23.9
59	2409	2554.7	-145.7	126	1995	1865.3	129.7	193	2008	1744.0	264.0
60	2428	2531.2	-103.2	127	1874	1856.6	17.4	194	1579	1743.8	-164.8
61	2271	2502.7	-231.7	128	1787	1848.6	-61.6	195	1680	1743.7	-63.7
62	2623	2471.1	151.9	129	2055	1841.1	213.9	196	1808	1743.6	64.4
63	2459	2438.2	20.8	130	2000	1834.2	165.8	197	1596	1743.4	-147.4
64	2599	2406.0	193.0	131	1888	1827.8	60.2	198	1762	1743.3	18.7
65	2315	2376.4	-61.4	132	1741	1821.9	-80.9	199	1711	1743.2	-32.2
66	2488	2351.0	137.0	133	1703	1816.5	-113.5	200	1895	1743.1	151.9

range of the partial derivatives presented on the PDPLOT (Figure 5-63) are given in Table 5-32.

A cursory examination of the raw intensity plot reveals that while the expected high frequency scintillation and photon noise sources are present, there is virtually no variation in atmospheric transparency on longer time-scales. This led to a rapidly convergent solution with very low formal statistical errors. The distribution function of the observational noise is shown in Figure 5-64. The usual occultation power spectra are displayed in Figure 5-65.

The Coordinated Universal Time of geometrical occultation was determined to be 02:16:52.406 (+/- 0.007 seconds).

ZC2209 (32 Librae)

The bright (m_V=5.92) star ZC2209 was occulted on June 22, 1983. ZC2209 is of spectral type K0 and has been classified as a giant (luminosity class III). The occultation event was observed by John P. Oliver, Martin England, and Howard L. Cohen with the instrumental configuration specified in Table 5-33. The observing log indicates that clouds appeared seven minutes after the event. Oliver, however, has indicated that prior to this the transparency of the sky was quite good and the seeing steady and calm. The post-event cloud cover was of the low patchy cumulus type, which is common in north Florida during the summer. Therefore, the onset of

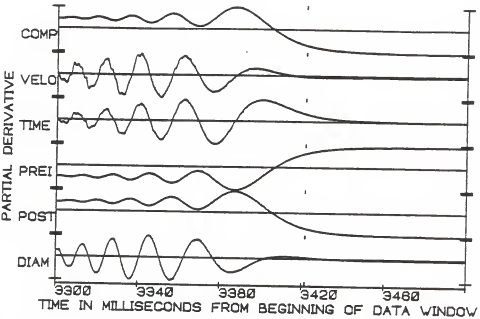

Figure 5-63. PDPLOT of the occultation of X18067.

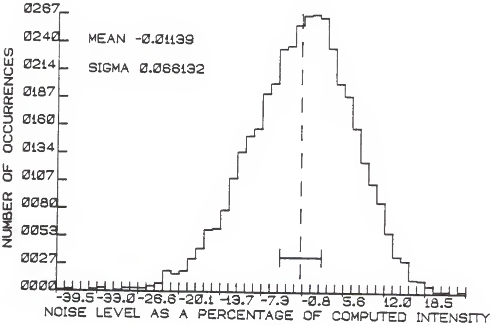

Figure 5-64. NOISEPLOT of the occultation of X18067.

TABLE 5-32
X18067: SUPPLEMENTAL STATISTICAL INFORMATION

VARIANCE/CO-VARIANCE MATRIX

DIAM	PREI	POST	TIME	VELO
1.008E¯14	2.581E¯07	-3.101E¯07	-1.077E¯08	9.371E¯11
2.581E¯07	2.874E02	1.917E01	-7.082E00	4.368E¯02
-3.101E¯07	1.917E01	4.509E02	-1.010E01	5.972E¯02
-1.077E¯08	-7.082E00	-1.010E01	2.379E00	-1.439E¯02
9.371E¯11	4.368E¯02	5.972E¯02	-1.439E¯02	1.171E¯04

CORRELATION MATRIX

	DIAM	PREI	POST	TIME	VELO
DIAM	1.000000	0.701669	-0.797370	0.254354	-0.231840
PREI	0.701669	1.000000	-0.130101	-0.498781	0.518495
POST	-0.797370	-0.130101	1.000000	-0.781331	0.766733
TIME	0.254354	-0.498781	-0.781331	1.000000	-0.999731
VELO	-0.231840	0.518495	0.766733	-0.999731	1.000000

NUMERICAL RANGES OF THE PARTIAL DERIVATIVES

	MAXIMUM	MINIMUM
DIAM	3.274E08	-3.212E08
PREI	1.366E00	6.222E¯03
POST	9.938E¯01	-3.659E¯01
TIME	3.393E01	-3.612E01
VELO	6.036E03	-6.035E03

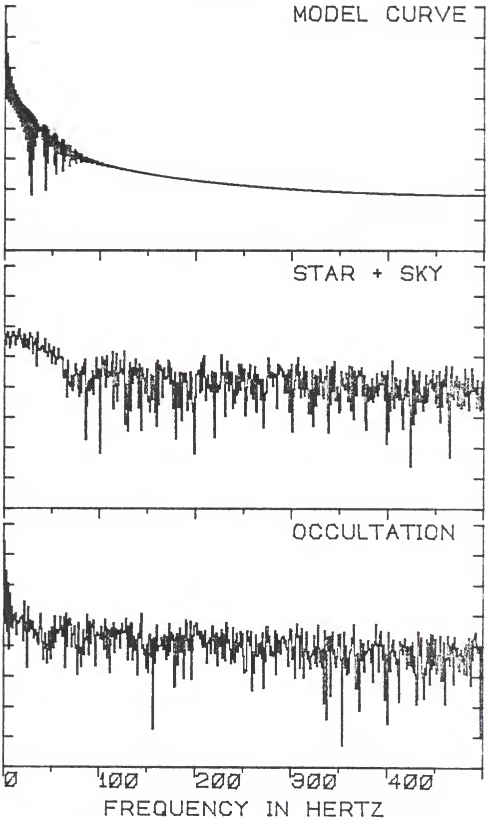

Figure 5-65. POWERPLOT of the occultation of X18067.

TABLE 5-33
ZC2209: LUNAR OCCULTATION SUMMARY

STELLAR AND OBSERVING INFORMATION

Star: ZC 2209, (32 Librae, SAO 159280, DM -16 4089)
RA: 152719   DEC: -163935   mV: 5.92   Sp: K0-III
Filter: V   Diaphragm: I   Gain: B8   Voltage: 1000

LUNAR INFORMATION

Surface Illumination:	90 percent
Elongation from Sun:	143 degrees
Altitude Above Horizon:	44 degrees
Lunar Limb Distance:	386528 kilometers
Predicted Shadow Velocity:	625.71 meters/sec.
Predicted Angular Rate:	0.3339 arcsec/sec.

EVENT INFORMATION

Date:	June 22, 1983	UT of Event:	03:12:54
USNO V/O Code:	76	HA of Event:	+033323
Position Angle:	111.6	Cusp Angle:	85S
Contact Angle:	+8.3	Watts Angle:	98.8

MODEL PARAMETERS

Number of Data Points:	201
Number of Grid Points:	256
Number of Spectral Regions:	53
Width of Spectral Regions:	50 Angstroms
Limb Darkening Coefficient:	0.5
Effective Stellar Temperature:	5100 K

SOLUTIONS

Stellar Diameter (ams):	12.18	(1.86)
Time: (relative to Bin 0):	631.2	(0.8)
Pre-Event Signal:	3020.2	(12.2)
Background Sky Level:	2025.8	(12.2)
Velocity (meters/sec.):	673.7	(45.5)
Lunar Limb Slope (degrees):	-10.88	(4.16)
U.T. of Occultation:	03:12:53.356	(0.007)

PHOTOMETRIC NOISE INFORMATION

Sum-of-Squares of Residuals:	2494300
Sigma (Standard Error):	111.68
Normalized Standard Error:	0.11231
Photometric (S+N)/N Ratio:	9.904
Intensity Change/Background:	0.49086
Change in Magnitude:	0.43359

cloud cover after the event did not adversley affect the observation.

The digital photoelectric record obtained is presented in Figure 5-66. As can be seen, the sky was quite well behaved throughout the 4096 milliseconds of data acquisition. The observation is seen early in the data window. One of the observers, who was using the LODAS system for the first time, nearly forgot to stop the data acquisition process after the event. The integration plot of the occultation record (Figure 5-67) shows no indication of stellar duplicity.

The solution to the observed intensity curve is depicted graphically in Figure 5-68. As indicated, a rather large angular diameter (12.18 +/- 1.86 milliseconds of arc) was determined by the differential corrections fitting procedure. Assuming the spectral type and luminosity classification for ZC2209 are correct, they would indicate a distance on the order of 115 parsecs; hence, the diameter found is an order of magnitude larger than one would expect. This disparity remains unresolved, as the fit is rather good and difficult to dismiss. Examination of the PDPLOT (Figure 5-69) clearly indicates that the region of sensitivity of the observed curve to variations in all the parameters was well considered and that numerical noise was minimal.

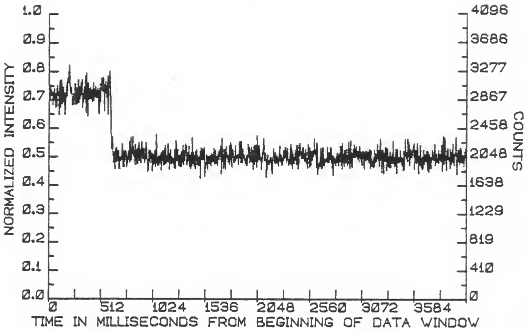

Figure 5-66. RAWPLOT of the occultation of ZC2209.

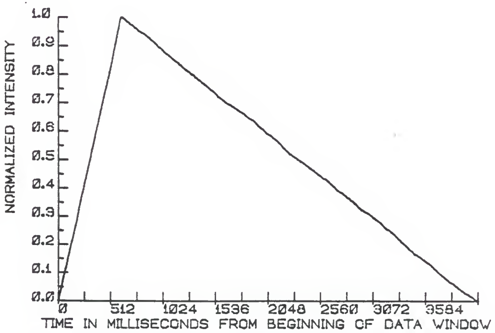

Figure 5-67. INTPLOT of the occultation of ZC2209.

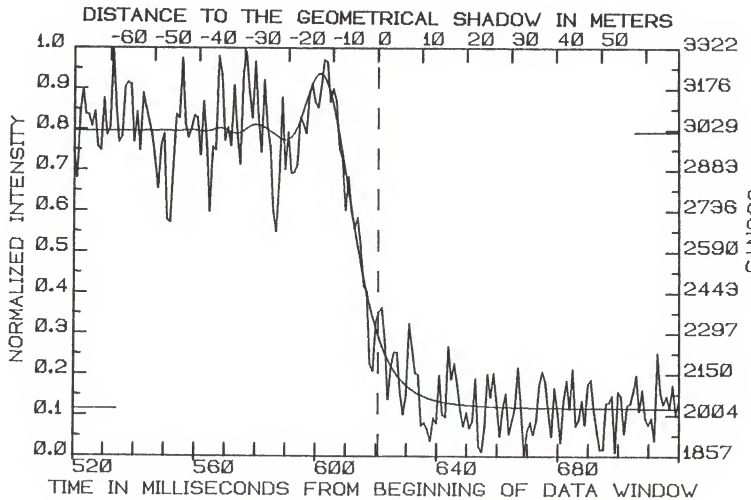

Figure 5-68. FITPLOT of the occultation of ZC2209.

The distribution function of the residuals shown in the NOISEPLOT (Figure 5-70) is obviously Gaussian in nature. The mean observed intensity is down only 0.1 percent from the computed intensity, with a one sigma width in the distribution function of only 4 percent. In addition, the photometric (S+N)/N ratio of the observation was 9.9. Hence, the photometric noise characteristics of the sky were very well behaved.

The POWERPLOT (Figure 5-71) for this event shows the relative power contributions up to a limiting frequency of 250 Hertz. While the power components of the occultation signal and star-plus-sky background are normally examined to higher frequencies, this was not possible for this observation. Since only roughy 500 milliseconds of data prior to the event were retained in the data acquisition process, the power spectrum of the star-plus-sky background will have a Nyquist cutoff frequency of 250 Hertz. It is apparent, however, that the frequency components in the observed curve due to the occultation signal are dominant over the background noise in the region of importance in the occultation solution (i.e., the low frequency domain).

Hence, the angular diameter determined from the solution of the observed occultation intensity curve is unaffected by both the spatial and temporal characteristics of the background noise, and is not spurious due to any possible numerical problems. The

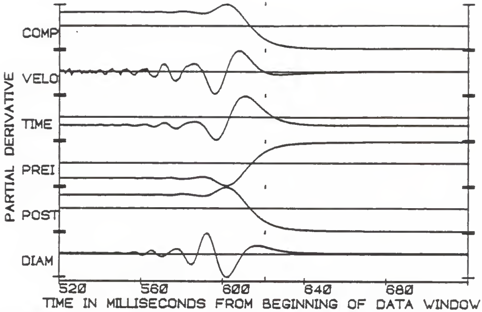

Figure 5-69. PDPLOT of the occultation of ZC2209.

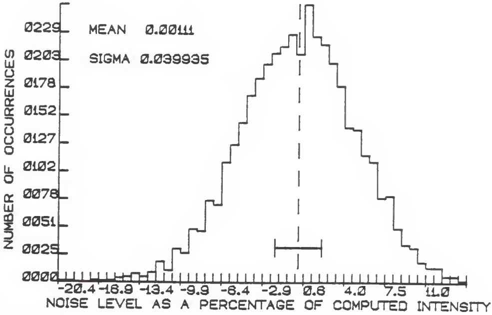

Figure 5-70. NOISEPLOT of the occultation of ZC2209.

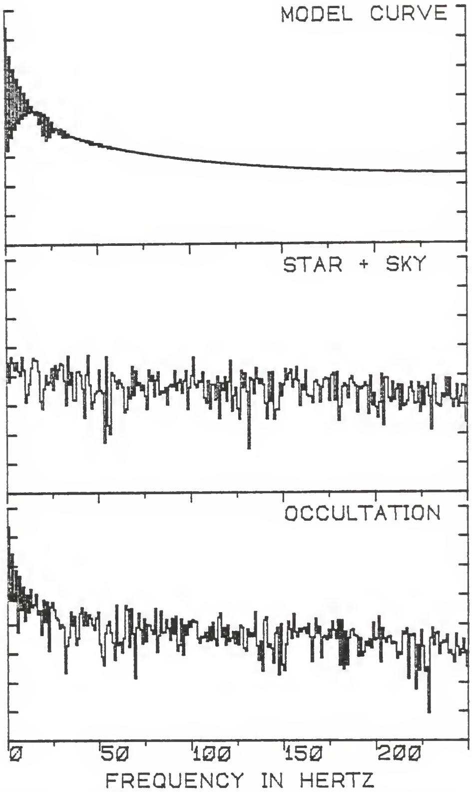

Figure 5-71. POWERPLOT of the occultation of ZC2209.

reason for the disparity between the anticipated small angular diameter and the larger diameter inferred from the observation could lie in an erroneous spectral classification. However, this tentatve suggestion is put forth without much force, and the question at this time remains open.

The Coordinated Universal Time of geometrical occultation for this event was found to be 03:12:53.356 (+/- 0.007 seconds). The observed and computed intensity values (and the residuals) are given in Table 5-34. The variance-covariance and correlation matrices, and the numerical ranges of the partial derivatives are listed in Table 5-35.

ZC3214

As noted in the occultation summary, Table 5-36, the occultation of ZC3214 was observed on November 13, 1983. The photoelectric record of the event is shown in Figure 5-72. As can be seen in this RAWPLOT, the transparency of the sky was quite steady on time-scales of a few tenths of a second. This is reflected in the very flat nature of the integration plot (Figure 5-73). Examination of the integration plot shows no indication of any secondary events.

ZC3214 is an A0 star, with an apparent V magnitude of 6.6. Thus, it was not suprising when the solution, depicted graphically in Figure 5-74, failed to reveal a

TABLE 5-34
ZC2209: OBSERVATIONS, COMPUTED VALUES, AND RESIDUALS FROM BIN 520

NUM	OBS	COMP	RESID	NUM	OBS	COMP	RESID	NUM	OBS	COMP	RESID
0	2949	3023.0	-74.0	67	2661	3007.6	-346.6	134	1894	2036.4	-142.4
1	2853	3023.0	-170.0	68	2848	3000.2	-152.2	135	1874	2035.8	-161.8
2	3089	3023.0	66.0	69	3145	2994.2	150.8	136	1959	2035.3	-76.3
3	3176	3023.0	153.0	70	2884	2991.0	-107.0	137	2151	2034.8	116.2
4	3085	3022.9	62.1	71	3019	2992.1	26.9	138	2068	2034.3	33.7
5	3082	3022.9	59.1	72	2870	2999.0	-129.0	139	2155	2033.9	121.1
6	3042	3023.1	18.9	73	2873	3012.8	-139.8	140	2050	2033.5	16.5
7	3093	3023.1	69.9	74	2900	3033.7	-133.7	141	1929	2033.1	-104.1
8	2969	3023.1	-54.1	75	3074	3061.0	13.0	142	2028	2032.7	-4.7
9	2954	3023.0	-69.0	76	3050	3093.1	-43.1	143	2080	2032.4	47.6
10	3142	3023.0	119.0	77	3015	3127.5	-112.5	144	1937	2032.1	-95.1
11	3009	3023.1	-14.1	78	3147	3161.2	-14.2	145	1983	2031.8	-48.8
12	3034	3023.2	10.8	79	3195	3191.1	3.9	146	2031	2031.6	-0.6
13	3322	3023.3	298.7	80	3127	3214.3	-87.3	147	2175	2031.3	143.7
14	3119	3023.2	95.8	81	3109	3228.2	-119.2	148	2033	2031.1	1.9
15	2983	3023.1	-40.1	82	3184	3231.1	-47.1	149	1857	2030.9	-173.9
16	3003	3023.1	-20.1	83	3281	3222.0	59.0	150	1948	2030.7	-82.7
17	3182	3023.2	158.8	84	3271	3200.7	70.3	151	1979	2030.5	-51.5
18	3199	3023.4	175.6	85	3127	3167.7	-40.7	152	1936	2030.3	-94.3
19	3191	3023.4	167.6	86	3177	3124.2	52.8	153	1986	2030.1	-44.1
20	2984	3023.3	-39.3	87	3132	3071.9	60.1	154	2111	2030.0	81.0
21	3094	3023.2	70.8	88	2959	3012.5	-53.5	155	2161	2029.8	131.2
22	2954	3023.3	-69.3	89	2925	2948.2	-23.2	156	2125	2029.7	95.3
23	3160	3023.5	136.5	90	2737	2880.7	-143.7	157	2020	2029.5	-9.5
24	3109	3023.7	85.3	91	2859	2812.1	46.9	158	1930	2029.4	-99.4
25	3060	3023.7	36.3	92	2736	2743.8	-7.8	159	2101	2029.3	71.7
26	3011	3023.3	-12.3	93	2675	2677.2	-2.2	160	2023	2029.2	-6.2
27	2924	3023.1	-99.1	94	2712	2613.4	98.6	161	1907	2029.0	-122.0
28	2816	3023.2	-207.2	95	2611	2553.1	57.9	162	2055	2028.9	26.1
29	2971	3023.8	-52.8	96	2470	2496.9	-26.9	163	2127	2028.8	98.2
30	3012	3024.6	-12.6	97	2449	2445.1	3.9	164	2027	2028.7	-1.7
31	2705	3024.8	-319.8	98	2188	2397.7	-209.7	165	2168	2028.6	139.4
32	2694	3024.2	-330.2	99	2163	2354.9	-191.9	166	1966	2028.6	-62.6
33	2899	3023.2	-124.2	100	2343	2316.4	26.6	167	1987	2028.5	-41.5
34	3084	3022.4	61.6	101	2374	2282.1	91.9	168	2056	2028.4	27.6
35	3071	3022.6	48.4	102	2391	2251.6	139.4	169	1971	2028.3	-57.3
36	3285	3023.7	261.3	103	2273	2224.7	48.3	170	2115	2028.3	86.7
37	3052	3025.3	26.7	104	2060	2201.0	-141.0	171	2130	2028.2	101.8
38	3000	3026.5	-26.5	105	2179	2180.1	-1.1	172	2021	2028.1	-7.1
39	3034	3026.7	7.3	106	2228	2161.9	66.1	173	1949	2028.1	-79.1
40	3080	3025.8	54.2	107	2228	2146.0	82.0	174	1882	2028.0	-146.0
41	3071	3024.1	46.9	108	2089	2132.2	-43.2	175	1882	2027.9	-145.9
42	2936	3022.1	-86.1	109	2006	2120.1	-114.1	176	2047	2027.9	19.1
43	3131	3020.9	110.1	110	2075	2109.5	-34.5	177	2048	2027.8	20.2
44	2985	3021.0	-36.0	111	2334	2100.3	233.7	178	2073	2027.8	45.2
45	2733	3022.9	-289.9	112	2245	2092.3	152.7	179	1873	2027.7	-154.7
46	2967	3026.3	-59.3	113	2156	2085.3	70.7	180	2089	2027.7	61.3
47	2955	3030.1	-75.1	114	2147	2079.2	67.8	181	2071	2027.6	43.4
48	3293	3032.8	260.2	115	1966	2073.9	-107.9	182	1939	2027.6	-88.6
49	3227	3033.1	193.9	116	1976	2069.2	-93.2	183	2039	2027.5	11.5
50	2989	3030.3	-41.3	117	1956	2065.1	-109.1	184	2045	2027.5	17.5
51	3037	3025.1	11.9	118	1913	2061.4	-148.4	185	2087	2027.5	59.5
52	2971	3019.2	-48.2	119	1994	2058.2	-64.2	186	2147	2027.4	119.6
53	3188	3014.7	173.3	120	1976	2055.4	-79.4	187	2019	2027.4	-8.4
54	3019	3013.5	5.5	121	2145	2052.9	92.1	188	2094	2027.3	66.7
55	2902	3016.3	-114.3	122	2006	2050.6	-44.6	189	1994	2027.3	-33.3
56	3235	3022.6	212.4	123	1998	2048.7	-50.7	190	1969	2027.3	-58.3
57	3307	3030.7	276.3	124	2252	2046.9	205.1	191	1994	2027.2	-33.2
58	3168	3038.4	129.6	125	2133	2045.3	87.7	192	1916	2027.2	-111.2
59	3070	3044.1	25.9	126	2190	2043.9	146.1	193	2227	2027.2	199.8
60	3272	3046.6	225.4	127	2114	2042.6	71.4	194	2087	2027.1	59.9
61	3076	3045.9	30.1	128	2024	2041.4	-17.4	195	2043	2027.1	15.9
62	2947	3042.4	-95.4	129	1965	2040.4	-75.4	196	2071	2027.1	43.9
63	3207	3037.0	170.0	130	2015	2039.4	-24.4	197	2031	2027.1	3.9
64	3043	3030.4	12.6	131	1959	2038.6	-79.6	198	2112	2027.0	85.0
65	2969	3023.1	-54.1	132	1983	2037.8	-54.8	199	2011	2027.0	-16.0
66	2737	3015.4	-278.4	133	2134	2037.1	96.9	200	2053	2027.0	26.0

TABLE 5-35
ZC2209: SUPPLEMENTAL STATISTICAL INFORMATION

VARIANCE/CO-VARIANCE MATRIX

DIAM	PREI	POST	TIME	VELO
8.149E¯17	2.649E¯08	2.525E¯10	-2.870E¯09	1.899E¯10
2.649E¯08	1.476E02	9.753E00	-3.250E00	1.445E¯01
2.525E¯10	9.753E00	1.478E02	-3.257E00	1.454E¯01
-2.870E¯09	-3.250E00	-3.257E00	6.850E¯01	-3.114E¯02
1.899E¯10	1.445E¯01	1.454E¯01	-3.114E¯02	2.066E¯03

CORRELATION MATRIX

	DIAM	PREI	POST	TIME	VELO
DIAM	1.000000	0.996428	-0.137148	-0.647710	0.645788
PREI	0.996428	1.000000	-0.109177	-0.661815	0.659550
POST	-0.137148	-0.109177	1.000000	-0.663632	0.665138
TIME	-0.647710	-0.661815	-0.663632	1.000000	-0.999983
VELO	0.645788	0.659550	0.665138	-0.999983	1.000000

NUMERICAL RANGES OF THE PARTIAL DERIVATIVES

	MAXIMUM	MINIMUM
DIAM	3.608E09	-4.206E09
PREI	1.212E00	1.209E¯03
POST	9.988E¯01	-2.122E¯01
TIME	6.867E01	-3.459E01
VELO	1.120E03	-1.217E03

TABLE 5-36
ZC3214: LUNAR OCCULTATION SUMMARY

STELLAR AND OBSERVING INFORMATION

Star: ZC3214 (SAO 164756, DM -18 6037)
RA: 215551   DEC: -175835   mV: 6.6   Sp: A0
Filter: V   Diaphragm: I   Gain: C5+   Voltage: 1200

LUNAR INFORMATION

Surface Illumination:	54 percent
Elongation from Sun:	95 degrees
Altitude Above Horizon:	20 degrees
Lunar Limb Distance:	402184 Kilometers
Predicted Shadow Velocity:	694.7 meters/sec.
Predicted Angular Rate:	0.3563 arcsec/sec.

EVENT INFORMATION

Date: November 13, 1983		UT of Event:	03:35:44
USNO V/O Code:	28	HA of Event:	540443
Position Angle:	31.0	Cusp Angle:	51N
Contact Angle:	+28.4	Watts Angle:	51.8

MODEL PARAMETERS

Number of Data Points:	201
Number of Grid Points:	256
Number of Spectral Regions:	53
Width of Spectral Regions:	50 Angstroms
Limb Darkening Coefficient:	0.5
Effective Stellar Temperature:	10800 K

SOLUTIONS

Stellar Diameter (ams):	Point Source	
Time: (relative to Bin 0):	2255.7	(0.8)
Pre-Event Signal:	2481.5	(18.6)
Background Sky Level:	1484.8	(18.3)
Velocity (meters/sec.):	732.3	(20.4)
Lunar Limb Slope (degrees):	-9.22	(1.68)
U.T. of Occultation:	03:35:43.107	(0.018)

PHOTOMETRIC NOISE INFORMATION

Sum-of-Squares of Residuals:	6385000
Sigma (Standard Error):	178.68
Normalized Standard Error:	0.17927
Photometric (S+N)/N Ratio:	6.5781
(Change in Intensity)/Background:	0.67124
Change in Magnitude:	0.5576

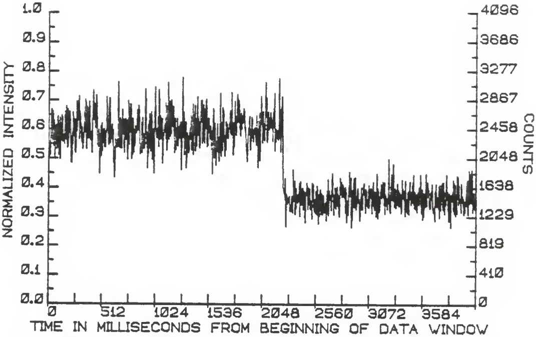

Figure 5-72. RAWPLOT of the occultation of ZC3214.

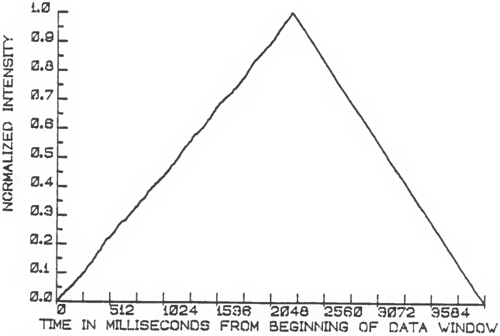

Figure 5-73. INTPLOT of the occultation of ZC3214.

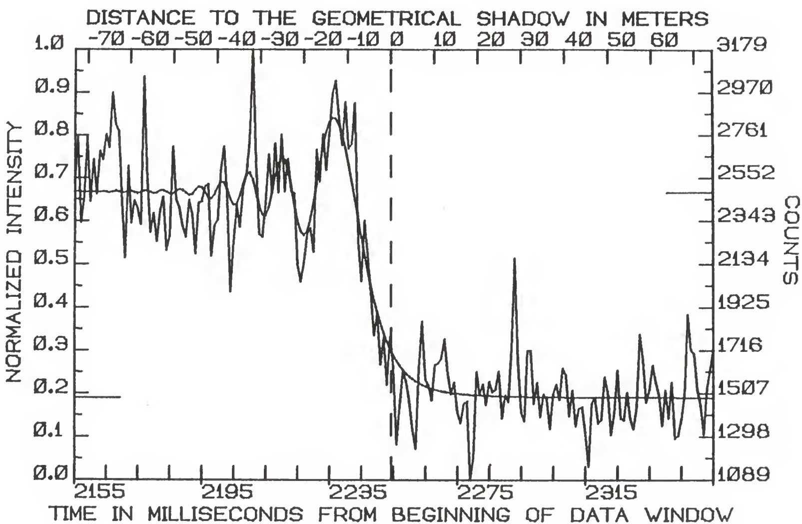

Figure 5-74. FITPLOT of the occultation of ZC3214.

measurable angular diameter. The fit of the model intensity curve to the observations appears to be quite good. This is reflected in the low formal errors of the solution parameters and is seen by visual inspection of the FITPLOT even as far out as the fourth order diffraction minimum.

As evidenced by the PDPLOT, Figure 5-75, the portions of the intensity curve most sensitive to parametric variation were well covered in the solution process. The model intensity curve was fit to the data presented in Table 5-37. The usual supplemental statistical information is compiled in Table 5-38.

The NOISEPLOT of the observation is presented as Figure 5-76. As noted, the RMS background noise through the 4096 milliseconds of the observation was approximately 8 percent. The power spectra of the occultation event, the star-plus-sky signal, and the best fit model curve are shown on the POWERPLOT, Figure 5-77.

As in the case of the occultation of ZC1221, a fine determination of the time of geometrical occultation, made possible by the small (0.8 millisecond) error of the formal solution, was thwarted by a noisy WWVB radio signal. The Coordinated Universal Time of geometrical occultation was 03:35:43.929 (+/- 0.018 seconds).

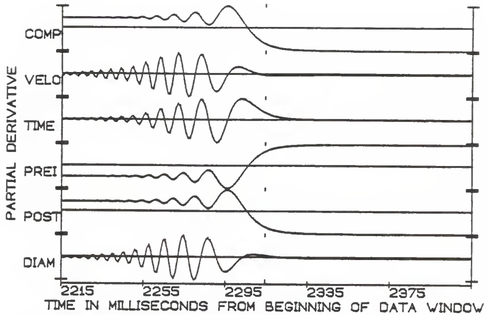

Figure 5-75. PDPLOT of the occultation of ZC3214.

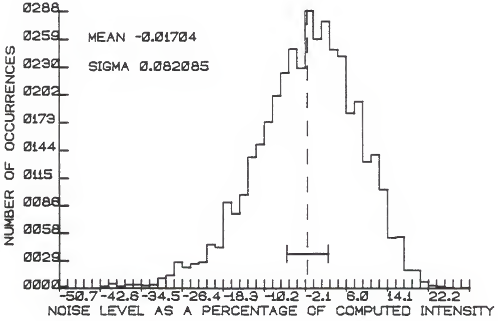

Figure 5-76. NOISEPLOT of the occultation of ZC3214.

TABLE 5-37
ZC3214: OBSERVATIONS, COMPUTED VALUES, AND RESIDUALS FROM BIN 2215

NUM	OBS	COMP	RESID	NUM	OBS	COMP	RESID	NUM	OBS	COMP	RESID
0	2527	2484.1	42.9	67	2646	2590.3	55.7	134	1387	1493.1	-106.1
1	2756	2485.3	270.7	68	2491	2511.5	-20.5	135	1499	1492.6	6.4
2	2335	2484.4	-149.4	69	2478	2423.6	54.4	136	1465	1492.2	-27.2
3	2454	2483.1	-29.1	70	2134	2345.4	-211.4	137	1723	1491.8	231.2
4	2752	2484.3	267.7	71	2050	2292.6	-242.6	138	2165	1491.5	673.5
5	2436	2485.7	-49.7	72	2142	2274.9	-132.9	139	1667	1491.2	175.8
6	2643	2484.3	158.7	73	2276	2294.9	-18.9	140	1416	1490.9	-74.9
7	2472	2482.8	-10.8	74	2309	2349.0	-40.0	141	1373	1490.7	-117.7
8	2683	2484.4	198.6	75	2195	2428.6	-233.6	142	1717	1490.4	226.6
9	2643	2486.2	156.8	76	2690	2522.4	167.6	143	1716	1490.1	225.9
10	2766	2484.4	281.6	77	2534	2618.5	-84.5	144	1456	1489.9	-33.9
11	2701	2482.1	218.9	78	2767	2706.0	61.0	145	1560	1489.6	70.4
12	2968	2483.9	484.1	79	2591	2776.4	-185.4	146	1392	1489.4	-97.4
13	2815	2487.2	327.8	80	2763	2824.0	-61.0	147	1503	1489.2	13.8
14	2781	2485.9	295.1	81	2960	2845.7	114.3	148	1478	1489.1	-11.1
15	2433	2481.5	-48.5	82	3027	2841.6	185.4	149	1335	1488.9	-153.9
16	2164	2481.4	-317.4	83	2848	2813.4	34.6	150	1503	1488.8	14.2
17	2612	2486.7	125.3	84	2713	2764.3	-51.3	151	1552	1488.6	63.4
18	2333	2489.2	-156.2	85	2923	2698.6	224.4	152	1476	1488.5	-12.5
19	2443	2484.4	-41.4	86	2694	2620.7	73.3	153	1631	1488.3	142.7
20	2405	2478.9	-73.9	87	2717	2534.9	182.1	154	1595	1488.2	106.8
21	2327	2481.4	-154.4	88	2920	2445.1	474.9	155	1396	1488.1	-92.1
22	3047	2489.0	558.0	89	2244	2354.5	-110.5	156	1523	1488.0	35.0
23	2540	2491.0	49.0	90	2052	2265.9	-213.9	157	1349	1487.9	-138.9
24	2289	2483.9	-194.9	91	2343	2181.3	161.7	158	1434	1487.8	-53.8
25	2380	2477.1	-97.1	92	2181	2102.0	79.0	159	1440	1487.7	-47.7
26	2243	2480.2	-237.2	93	1999	2028.9	-29.9	160	1315	1487.6	-172.6
27	2384	2489.8	-105.8	94	1789	1962.4	-173.4	161	1152	1487.5	-335.5
28	2460	2493.7	-33.7	95	1894	1902.6	-8.6	162	1459	1487.4	-28.4
29	2200	2486.1	-286.1	96	1647	1849.3	-202.3	163	1487	1487.3	-0.3
30	2265	2475.9	-210.9	97	1779	1802.3	-23.3	164	1361	1487.3	-126.3
31	2705	2475.9	229.1	98	1549	1761.0	-212.0	165	1379	1487.2	-108.2
32	2448	2487.5	-39.5	99	1785	1725.0	60.0	166	1586	1487.1	98.9
33	2407	2498.0	-91.0	100	1634	1693.8	-59.8	167	1515	1487.0	28.0
34	2318	2494.6	-176.6	101	1261	1666.7	-405.7	168	1306	1487.0	-181.0
35	2266	2479.3	-213.3	102	1443	1643.3	-200.3	169	1411	1486.9	-75.9
36	2445	2467.4	-22.4	103	1611	1623.2	-12.2	170	1620	1486.9	133.1
37	2373	2472.7	-99.7	104	1568	1605.8	-37.8	171	1386	1486.8	-100.8
38	2185	2492.6	-307.6	105	1470	1590.9	-120.9	172	1378	1486.8	-108.8
39	2434	2509.4	-75.4	106	1331	1578.1	-247.1	173	1511	1486.7	24.3
40	2436	2506.4	-70.4	107	1240	1567.1	-327.1	174	1384	1486.7	-102.7
41	2507	2483.2	23.8	108	1627	1557.5	69.5	175	1335	1486.6	-151.6
42	2521	2457.2	63.8	109	1860	1549.3	310.7	176	1439	1486.6	-47.6
43	2174	2450.5	-276.5	110	1575	1542.3	32.7	177	1795	1486.5	308.5
44	2322	2471.4	-149.4	111	1546	1536.1	9.9	178	1670	1486.5	183.5
45	2348	2507.6	-159.6	112	1474	1530.8	-56.8	179	1463	1486.4	-23.4
46	2588	2534.1	53.9	113	1645	1526.1	118.9	180	1523	1486.4	36.6
47	2705	2530.7	174.3	114	1654	1522.1	131.9	181	1644	1486.4	157.6
48	2437	2496.3	-59.3	115	1677	1518.6	158.4	182	1563	1486.3	76.7
49	2003	2450.2	-447.2	116	1771	1515.4	255.6	183	1498	1486.3	11.7
50	2239	2419.9	-180.9	117	1607	1512.7	94.3	184	1351	1486.3	-135.3
51	2413	2425.2	-12.2	118	1503	1510.3	-7.3	185	1523	1486.2	36.8
52	2315	2466.3	-151.3	119	1560	1508.1	51.9	186	1387	1486.2	-99.2
53	2503	2523.9	-20.9	120	1416	1506.2	-90.2	187	1560	1486.2	73.8
54	2563	2569.4	-6.4	121	1363	1504.5	-141.5	188	1287	1486.1	-199.1
55	2728	2579.7	148.3	122	1455	1502.9	-47.9	189	1303	1486.1	-183.1
56	3179	2547.7	631.3	123	1468	1501.6	-33.6	190	1379	1486.1	-107.1
57	2628	2485.6	142.4	124	1089	1500.4	-411.4	191	1495	1486.0	9.0
58	2281	2418.5	-137.5	125	1195	1499.3	-304.3	192	1892	1486.0	406.0
59	2265	2373.3	-108.3	126	1612	1498.3	113.7	193	1718	1486.0	232.0
60	2427	2368.5	58.5	127	1503	1497.4	5.6	194	1698	1486.0	212.0
61	2668	2407.3	260.7	128	1552	1496.7	55.3	195	1527	1485.9	41.1
62	2477	2477.7	-0.7	129	1451	1496.0	-45.0	196	1449	1485.9	-36.9
63	2722	2557.5	164.5	130	1564	1495.3	68.7	197	1311	1485.9	-174.9
64	2482	2622.4	-140.4	131	1513	1494.7	18.3	198	1526	1485.9	40.1
65	2765	2653.5	111.5	132	1527	1494.1	32.9	199	1623	1485.9	137.1
66	2487	2641.8	-154.8	133	1614	1493.6	120.4	200	1721	1485.8	235.2

TABLE 5-38
ZC3214: SUPPLEMENTAL STATISTICAL INFORMATION

VARIANCE/CO-VARIANCE MATRIX

DIAM	PREI	POST	TIME	VELO
5.694E¯16	5.662E¯08	-4.205E¯08	-1.344E¯09	4.047E¯11
5.662E¯08	3.371E02	7.832E00	-2.875E00	6.537E¯02
-4.205E¯08	7.832E00	3.262E02	-2.672E00	5.986E¯02
-1.344E¯09	-2.875E00	-2.672E00	5.657E¯01	-1.283E¯02
4.047E¯11	6.537E¯02	5.986E¯02	-1.283E¯02	4.051E¯04

CORRELATION MATRIX

	DIAM	PREI	POST	TIME	VELO
DIAM	1.000000	0.845265	-0.692455	-0.164543	0.173361
PREI	0.845265	1.000000	-0.200047	-0.660013	0.666554
POST	-0.692455	-0.200047	1.000000	-0.592852	0.585544
TIME	-0.164543	-0.660013	-0.592852	1.000000	-0.999958
VELO	0.173361	0.666554	0.585544	-0.999958	1.000000

NUMERICAL RANGES OF THE PARTIAL DERIVATIVES

	MAXIMUM	MINIMUM
DIAM	1.811E09	-1.802E09
PREI	1.365E00	1.019E¯03
POST	9.990E¯01	-3.655E¯01
TIME	9.068E01	-9.686E01
VELO	3.942E03	-3.974E03

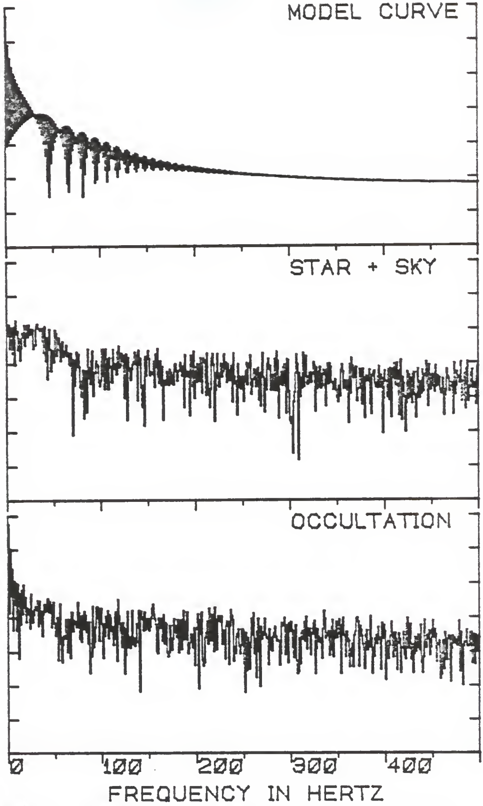

Figure 5-77. POWERPLOT of the occultation of ZC3214.

X31590

The rather slow occultation disappearance of the K0 star X31590 is apparent on the plot of the 4096 milliseconds of raw observational data shown in Figure 5-78. The relative faintness of the star (mV=8.7) and the high sky brightness, due to a 72 percent illuminated moon, resulted in a final photometric S+N/N of only 2.55. Fortunately, the seeing was unusually good, and the photometer J diaphragm (as noted in the occultation summary, Table 5-39) was selected.

The integration plot of the event, Figure 5-79, shows no indication of any disappearances other than that of X31590 itself.

The graphical depiction of the solution is shown in Figure 5-80. Three hundred and fifty milliseconds of data (given in Table 5-40) were included to be fit by the DC process. This rather lengthy data set was necessary due to the somewhat lengthened time-scale of the event. Not unexpectedly, given the poor S+N/N ratio and the faintness of the star, no detectable stellar disc was found.

The partial derivatives of the intensity curve, with respect to each of the solution parameters, are shown graphically in Figure 5-81. The numerical ranges of these derivatives are listed, along with the other usual supplemental statistics, in Table 5-41.

TABLE 5-39
X31590: LUNAR OCCULTATION SUMMARY

STELLAR AND OBSERVING INFORMATION

Star: X31590, (SAO 165704, DM -10 6166)
RA: 222634 DEC: -095159 mV: 8.7 Sp:K0
Filter: V Diaphragm: J Gain: C7 Voltage: 1200

LUNAR INFORMATION

Surface Illumination:	72 percent
Elongation from Sun:	116 degrees
Altitude Above Horizon:	50 degrees
Lunar Limb Distance:	397056 kilometers
Predicted Shadow Velocity:	574.2 meters/sec.
Predicted Angular Rate:	0.2983 arcsec/sec.

EVENT INFORMATION

Date: November 15, 1983		UT of Event:	01:51:29
USNO V/O Code:	33	HA of Event:	+071416
Position Angle:	75.6	Cusp Angle:	78S
Contact Angle:	-24.5	Watts Angle:	99.4

MODEL PARAMETERS

Number of Data Points:	351
Number of Grid Points:	256
Number of Spectral Regions:	50
Width of Spectral Regions:	53 Angstroms
Limb Darkening Coefficient:	0.5
Effective Stellar Temperature:	5100 K

SOLUTIONS

Stellar Diameter (ams):	Point Source
Time: (relative to Bin 0):	2401.3 (5.3)
Pre-Event Signal:	2396.0 (16.5)
Background Sky Level:	1999.5 (29.4)
Velocity (meters/second):	229.6 (14.1)
Lunar Limb Slope (degrees):	+33.2 (1.4)
U.T. of Occultation:	01:02:40.701 (0.014)

PHOTOMETRIC NOISE INFORMATION

Sum-of-Squares of Residuals:	22911940
Sigma (Standard Error):	225.8576
Normalized Standard Error:	0.654175
Photometric (S+N)/N Ratio:	2.54997
(Change in Intensity)/Background:	0.19834
Change in Magnitude:	0.19645

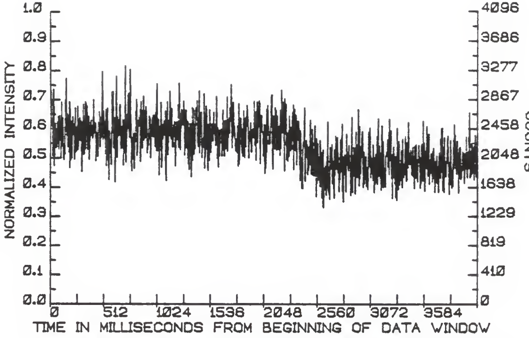

Figure 5-78. RAWPLOT of the occultation of X31590.

Figure 5-79. INTPLOT of the occultation of X31590.

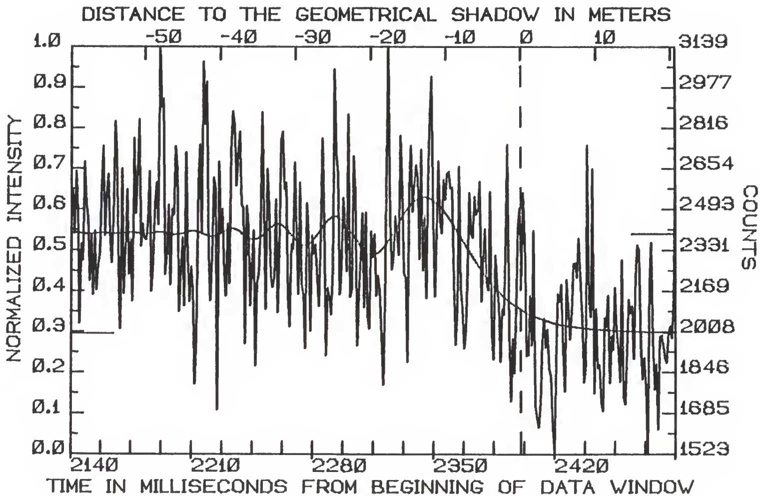

Figure 5-80. FITPLOT of the occultation of X31590.

TABLE 5-40
X31590: OBSERVATIONS, COMPUTED VALUES, AND RESIDUALS FROM BIN 2140

NUM	OBS	COMP	RESID	NUM	OBS	COMP	RESID	NUM	OBS	COMP	RESID
0	2529	2397.5	131.5	67	2719	2400.2	318.8	134	2199	2353.0	-154.0
1	2570	2398.1	171.9	68	2303	2402.3	-99.3	135	2160	2351.1	-191.1
2	2398	2398.5	-0.5	69	2128	2404.0	-276.0	136	1941	2351.0	-410.0
3	2643	2398.8	244.2	70	2267	2405.3	-138.3	137	2517	2352.6	164.4
4	2495	2398.8	96.2	71	2184	2405.8	-221.8	138	2390	2355.9	34.1
5	2041	2398.5	-357.5	72	1800	2405.6	-605.6	139	2010	2360.9	-350.9
6	2359	2398.0	-39.0	73	1981	2404.6	-423.6	140	2391	2367.3	23.7
7	2291	2397.3	-106.3	74	2600	2402.8	197.2	141	2316	2374.9	-58.9
8	2681	2396.6	284.4	75	2751	2400.5	350.5	142	2354	2383.5	-29.5
9	2517	2396.0	121.0	76	2403	2397.7	5.3	143	2218	2392.9	-174.9
10	2463	2395.5	67.5	77	3080	2394.7	685.3	144	2110	2402.7	-292.7
11	2211	2395.3	-184.3	78	2831	2391.7	439.3	145	2395	2412.7	-17.7
12	2391	2395.5	-4.5	79	3002	2389.1	612.9	146	2775	2422.4	352.6
13	2156	2395.9	-239.9	80	2317	2387.0	-70.0	147	2436	2431.7	4.3
14	2408	2396.5	11.5	81	2132	2385.7	-253.7	148	1913	2440.2	-527.2
15	2175	2397.3	-222.3	82	2303	2385.4	-82.4	149	2183	2447.8	-264.8
16	2271	2398.1	-127.1	83	2619	2386.0	233.0	150	2151	2454.1	-303.1
17	2321	2398.8	-77.8	84	2573	2387.6	185.4	151	2076	2458.9	-382.9
18	2591	2399.3	191.7	85	1699	2390.1	-691.1	152	2255	2462.3	-207.3
19	2744	2399.5	344.5	86	2681	2393.4	287.6	153	3051	2463.9	587.1
20	2388	2399.3	-11.3	87	2400	2397.3	2.7	154	2719	2463.9	255.1
21	2553	2398.8	154.2	88	2495	2401.4	93.6	155	2637	2462.2	174.8
22	2632	2398.1	233.9	89	2243	2405.5	-162.5	156	2157	2458.9	-301.9
23	2400	2397.2	2.8	90	2151	2409.3	-258.3	157	2262	2453.9	-191.9
24	2281	2396.3	-115.3	91	2436	2412.5	23.5	158	2539	2447.6	91.4
25	2455	2395.6	59.4	92	2200	2414.8	-214.8	159	2444	2439.9	4.1
26	2843	2395.1	447.9	93	2725	2416.0	309.0	160	2248	2431.1	-183.1
27	2717	2394.9	322.1	94	2883	2416.0	467.0	161	2872	2421.5	450.5
28	2256	2395.0	-139.0	95	2831	2414.7	416.3	162	2146	2411.1	-265.1
29	2019	2395.5	-376.5	96	2586	2412.3	173.7	163	2177	2400.3	-223.3
30	2655	2396.3	258.7	97	2707	2408.8	298.2	164	2706	2389.4	316.6
31	2160	2397.3	-237.3	98	2802	2404.3	397.7	165	2565	2378.4	186.6
32	2331	2398.2	-67.2	99	2515	2399.2	115.8	166	1954	2367.8	-413.8
33	2570	2399.1	170.9	100	2496	2393.8	102.2	167	2156	2357.6	-201.6
34	2236	2399.7	-163.7	101	1960	2388.4	-428.4	168	2303	2348.1	-45.1
35	2375	2400.0	-25.0	102	2507	2383.3	123.7	169	2477	2339.6	137.4
36	2131	2399.9	-268.9	103	2423	2378.9	44.1	170	2105	2332.1	-227.1
37	2777	2399.4	377.6	104	2112	2375.4	-263.4	171	2479	2325.7	153.3
38	2476	2398.7	77.3	105	2265	2373.1	-108.1	172	2070	2320.7	-250.7
39	2639	2397.7	241.3	106	2410	2372.2	37.8	173	2019	2317.1	-298.1
40	2851	2396.6	454.4	107	1872	2372.8	-500.8	174	2405	2314.9	90.1
41	2346	2395.7	-49.7	108	2203	2374.8	-171.8	175	2304	2314.2	-10.2
42	2435	2394.9	40.1	109	2239	2378.2	-139.2	176	2394	2315.0	79.0
43	2380	2394.5	-14.5	110	2423	2382.9	40.1	177	2150	2317.3	-167.3
44	2372	2394.4	-22.4	111	2881	2388.6	492.4	178	2231	2321.0	-90.0
45	2443	2394.8	48.2	112	2486	2395.1	90.9	179	2178	2326.1	-148.1
46	2644	2395.6	248.4	113	2098	2402.0	-304.0	180	1995	2332.5	-337.5
47	2169	2396.6	-227.6	114	2655	2408.9	246.1	181	1797	2340.0	-543.0
48	2280	2397.9	-117.9	115	2512	2415.6	96.4	182	2127	2348.6	-221.6
49	2516	2399.1	116.9	116	2231	2421.7	-190.7	183	2691	2358.1	332.9
50	2599	2400.1	198.9	117	2184	2426.8	-242.8	184	3139	2368.4	770.6
51	2431	2400.9	30.1	118	2219	2430.8	-211.8	185	2450	2379.4	70.6
52	3137	2401.3	735.7	119	2531	2433.3	97.7	186	2257	2390.9	-133.9
53	2900	2401.1	498.9	120	2084	2434.2	-350.2	187	2307	2402.7	-95.7
54	2933	2400.5	532.5	121	2328	2433.5	-105.5	188	2466	2414.7	51.3
55	2235	2399.4	-164.4	122	2771	2431.1	339.9	189	2396	2426.8	-30.8
56	2317	2398.1	-81.1	123	2802	2427.2	374.8	190	2313	2438.8	-125.8
57	2509	2396.5	112.5	124	2572	2421.8	150.2	191	2787	2450.6	336.4
58	2195	2395.0	-200.0	125	2600	2415.3	184.7	192	2578	2462.1	115.9
59	2495	2393.6	101.4	126	2148	2407.8	-259.8	193	2242	2473.0	-231.0
60	2471	2392.6	78.4	127	2029	2399.7	-370.7	194	2223	2483.5	-260.5
61	2743	2392.1	350.9	128	2356	2391.3	-35.3	195	1887	2493.3	-606.3
62	2654	2392.2	261.8	129	2335	2382.9	-47.9	196	2579	2502.3	76.7
63	2089	2392.9	-303.9	130	2679	2374.9	304.1	197	2746	2510.5	235.5
64	2250	2394.2	-144.2	131	2407	2367.7	39.3	198	2482	2517.8	-35.8
65	2380	2396.0	-16.0	132	2157	2361.4	-204.4	199	2589	2524.2	64.8
66	2111	2398.0	-287.0	133	2599	2356.5	242.5	200	2670	2529.6	140.4

TABLE 5-40. CONTINUED.

NUM	OBS	COMP	RESID	NUM	OBS	COMP	RESID	NUM	OBS	COMP	RESID
201	2623	2534.0	89.0	251	2075	2147.9	-72.9	301	2067	2018.7	48.3
202	2297	2537.4	-240.4	252	2383	2141.7	241.3	302	2655	2018.1	636.9
203	2730	2539.8	190.2	253	2751	2135.7	615.3	303	1765	2017.5	-252.5
204	2251	2541.1	-290.1	254	2006	2129.9	-123.9	304	2101	2016.9	84.1
205	2471	2541.4	-70.4	255	1732	2124.3	-392.3	305	1863	2016.3	-153.3
206	2143	2540.7	-397.7	256	1980	2119.0	-139.0	306	1876	2015.8	-139.8
207	2599	2539.1	59.9	257	1843	2113.9	-270.9	307	1729	2015.2	-286.2
208	2867	2536.5	330.5	258	2098	2109.0	-11.0	308	1695	2014.7	-319.7
209	3021	2532.9	488.1	259	2427	2104.3	322.7	309	2064	2014.3	49.7
210	2451	2528.6	-77.6	260	2499	2099.8	399.2	310	2029	2013.8	15.2
211	2149	2523.3	-374.3	261	2229	2095.5	133.5	311	2153	2013.4	139.6
212	2403	2517.4	-114.4	262	2559	2091.4	467.6	312	1803	2012.9	-209.9
213	2685	2510.7	174.3	263	2383	2087.4	295.6	313	1993	2012.5	-19.5
214	2445	2503.3	-58.3	264	1911	2083.7	-172.7	314	1937	2012.1	-75.1
215	2399	2495.3	-96.3	265	1915	2080.1	-165.1	315	2184	2011.8	172.2
216	2611	2486.8	124.2	266	2153	2076.6	76.4	316	2016	2011.4	4.6
217	2530	2477.7	52.3	267	1953	2073.4	-120.4	317	1934	2011.0	-77.0
218	2634	2468.2	165.8	268	2407	2070.2	336.8	318	1809	2010.7	-201.7
219	2643	2458.3	184.7	269	1715	2067.2	-352.2	319	2293	2010.4	282.6
220	2576	2448.0	128.0	270	1666	2064.4	-398.4	320	1751	2010.1	-259.1
221	2580	2437.5	142.5	271	1631	2061.6	-430.6	321	1721	2009.8	-288.8
222	2207	2426.7	-219.7	272	1727	2059.0	-332.0	322	1933	2009.5	-76.5
223	1955	2415.7	-460.7	273	1966	2056.6	-90.6	323	2137	2009.2	127.8
224	2098	2404.6	-306.6	274	2060	2054.2	5.8	324	2083	2008.9	74.1
225	2663	2393.4	269.6	275	1945	2051.9	-106.9	325	2112	2008.7	103.3
226	2184	2382.1	-198.1	276	2018	2049.8	-31.8	326	1900	2008.4	-108.4
227	2099	2370.8	-271.8	277	1861	2047.7	-186.7	327	2231	2008.2	222.8
228	1942	2359.4	-417.4	278	1835	2045.7	-210.7	328	2351	2008.0	343.0
229	2013	2348.2	-335.2	279	1626	2043.9	-417.9	329	2335	2007.7	327.3
230	2260	2337.0	-77.0	280	1535	2042.1	-507.1	330	1961	2007.5	-46.5
231	2559	2325.9	233.1	281	1884	2040.4	-156.4	331	1819	2007.3	-188.3
232	2399	2314.9	84.1	282	2159	2038.8	120.2	332	1904	2007.1	-103.1
233	2381	2304.0	77.0	283	2127	2037.2	89.8	333	1788	2006.9	-218.9
234	2544	2293.4	250.6	284	2197	2035.7	161.3	334	1523	2006.7	-483.7
235	2470	2282.9	187.1	285	1936	2034.3	-98.3	335	2201	2006.6	194.4
236	2486	2272.6	213.4	286	1772	2033.0	-261.0	336	2362	2006.4	355.6
237	2604	2262.5	341.5	287	2215	2031.7	183.3	337	1977	2006.2	-29.2
238	2128	2252.7	-124.7	288	2114	2030.5	83.5	338	1779	2006.1	-227.1
239	2302	2243.1	58.9	289	1978	2029.3	-51.3	339	1881	2005.9	-124.9
240	2416	2233.7	182.3	290	2084	2028.2	55.8	340	1621	2005.8	-384.8
241	2205	2224.6	-19.6	291	2279	2027.1	251.9	341	1988	2005.6	-17.6
242	2173	2215.8	-42.8	292	2284	2026.1	257.9	342	1992	2005.5	-13.5
243	2562	2207.2	354.8	293	2224	2025.1	198.9	343	1962	2005.3	-43.3
244	2000	2198.9	-198.9	294	2378	2024.2	353.8	344	1904	2005.2	-101.2
245	1897	2190.8	-293.8	295	2231	2023.3	207.7	345	1886	2005.1	-119.1
246	2312	2183.0	129.0	296	2069	2022.5	46.5	346	2005	2005.0	
247	2207	2175.5	31.5	297	1807	2021.6	-214.6	347	2032	2004.9	27.1
248	2115	2168.2	-53.2	298	1871	2020.9	-149.9	348	1983	2004.7	-21.7
249	1888	2161.2	-273.2	299	2747	2020.1	726.9	349	2151	2004.6	146.4
250	2099	2154.5	-55.5	300	2123	2019.4	103.6	350	2580	2004.5	575.5

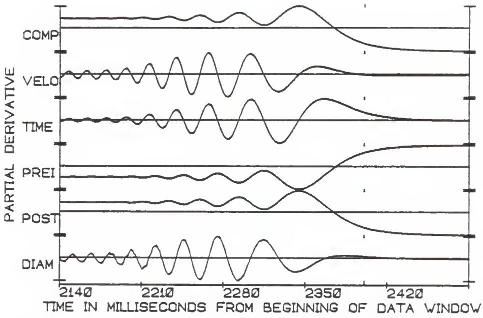

Figure 5-81. PDPLOT of the occultation of X31590.

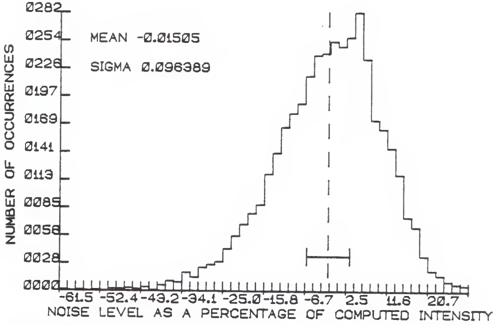

Figure 5-82. NOISEPLOT of the occultation of X31590.

TABLE 5-41
X31590: SUPPLEMENTAL STATISTICAL INFORMATION

VARIANCE/CO-VARIANCE MATRIX

DIAM	PREI	POST	TIME	VELO
3.067E¯14	3.795E¯07	-9.342E¯07	-2.879E¯08	1.217E¯10
3.795E¯07	2.716E02	2.809E01	-2.066E01	4.788E¯02
-9.342E¯07	2.809E01	8.649E02	-5.633E01	1.270E¯01
-2.879E¯08	-2.066E01	-5.633E01	2.765E01	-6.389E¯02
1.217E¯10	4.788E¯02	1.270E¯01	-6.389E¯02	1.983E¯04

CORRELATION MATRIX

	DIAM	PREI	POST	TIME	VELO
DIAM	1.000000	0.463093	-0.915775	0.629985	-0.621074
PREI	0.463093	1.000000	-0.071425	-0.330036	0.338810
POST	-0.915775	-0.071425	1.000000	-0.874404	0.868639
TIME	0.629985	-0.330036	-0.874404	1.000000	-0.999931
VELO	-0.621074	0.338810	0.868639	-0.999931	1.000000

NUMERICAL RANGES OF THE PARTIAL DERIVATIVES

	MAXIMUM	MINIMUM
DIAM	2.073E08	-2.086E08
PREI	1.367E00	1.276E¯02
POST	9.872E¯01	-3.666E¯01
TIME	1.133E01	-1.208E01
VELO	4.875E03	-5.024E03

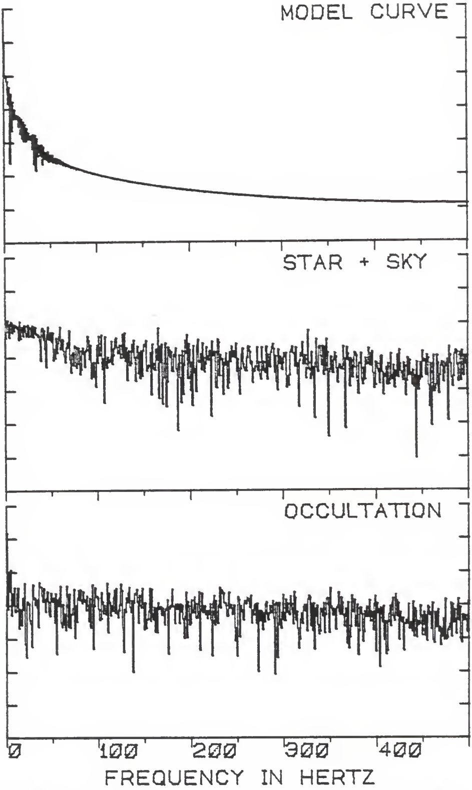

Figure 5-83. POWERPLOT of the occultation of X31590.

The distribution function of the residual intensities is shown in the NOISEPLOT, Figure 5-82. Despite the weakness of the stellar signal against the background sky, the noise characteristics of the sky itself were well behaved.

The POWERPLOT showing the usual Fourier power spectra is presented as Figure 5-83. As typical with longer duration events, the power components important to the occultation curve are shifted toward lower frequencies.

The Coordinated Universal Time of geometrical occultation was determined to be 001:02:40.703, with a relatively large one sigma uncertainty of 0.014 seconds.

ZC3458 (336 B. Aquarii)

The second occultation observed on the night of November 15, 1983 was that of the moderately bright K0 star ZC3458 (336 B. Aquarii). Even with the moon 73 percent illuminated, this event was quite promising, given the good seeing conditions which continued to prevail since the early part of the evening.

Disaster (literally, "bad star", appropriately enough), however, usually strikes at the best of times. Blow attests that observers at the University of Texas have " . . . found at least 57 ways to foul up an occultation [observation] . . ." (1983, p. 9-14). A fifty-eighth may now be contributed by the University of Florida.

The loss of a high speed photoelectric record of the ZC3458 event was due to a mechanical failure, resulting in two self-cancelling errors as far as the LODAS video strip chart display was concerned. The "0" key on the LODAS command keyboard had become mechanically sticky and electrically "bouncy". As a result, the data acquisition rate, which should have been entered as 001 samples per millisecond was entered as 010 samples per millisecond. Similarly, the video strip chart recorder display rate which was typed in as 010 display points per two acquisition times was taken as 001. Hence, the video display was updating at a rate indicative of millisecond data acquisition, while data were actually being sampled and stored at a slow rate of 100 samples per second.

The observer freely admits his error for not checking the printed observing log at the time of setting up the instrumental system. The RAWPLOT of the 40.96 seconds of data obtained (with a much-too-fast amplifier time constant of 2 KiloHertz (see Chapter 1)), is shown in Figure 5-84. The integration plot of the event, Figure 5-85, has no indication of any very widely separated components.

All, however, was not lost as the time of occultation was determined to an accuracy as well as could be obtained at this sampling rate. The

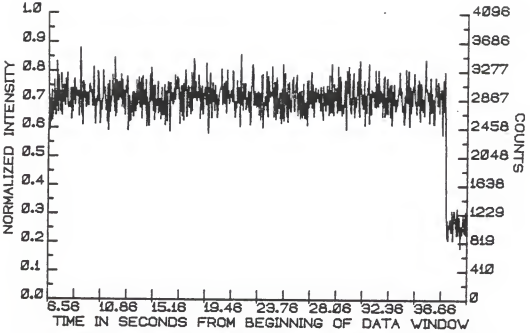

Figure 5-84. RAWPLOT of the occultation of ZC3458.

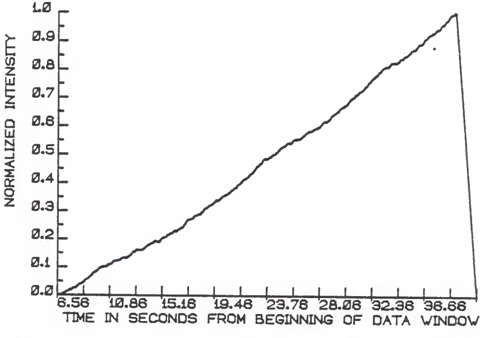

Figure 5-85. INTPLOT of the occultation of ZC3458.

Coordinated Universal Time of "geometrical" occultation was seen at 03:37:57.996 (+/- 0.006 seconds).

X01217

Four occultation disappearances were observed on the night of November 17, 1983. The first of these was the occultation of the K0 star X01217. The raw photoelectric data which was obtained is shown in Figure 5-86. The observation of this 7.7 magnitude star was made with a Johnson V filter (see Table 5-42). The integration plot of the 4096 milliseconds of acquired data, Figure 5-87, shows no indication of stellar duplicity.

Based on the predicted R-rate of 516.3 meters/second, the usual number of data points (two hundred milliseconds) were extracted for a solution determination. The preliminary run of the DC fitting procedure indicated that the actual shadow velocity was considerably slower and that the data set used was of insufficient length. As a result, the observation was re-reduced using 350 milliseconds of data. The final solution which was obtained gave an R-rate of 284.8 (+/- 16.0) meters/second. This corresponds to a moderately large local lunar limb slope of +28.3 (+/- 1.8) degrees.

The resulting best fit is shown graphically in Figure 5-88. As can be seen the observational data were rather noisy and led to a photometric S+N/N ratio of

TABLE 5-42
X01217: LUNAR OCCULTATION SUMMARY

STELLAR AND OBSERVING INFORMATION

Star: X01217, (SAO 129029, DM -00 0139)
RA: 005444 DEC: -000404 mV: 7.7 Sp: K0
Filter: V Diaphragm: I Gain: B10+ Voltage: 1200

LUNAR INFORMATION

Surface Illumination:	87 percent
Elongation from Sun:	138 degrees
Altitude Above Horizon:	42 degrees
Lunar Limb Distance:	391396 kilometers
Predicted Shadow Velocity:	516.3 meters/sec.
Predicted Angular Rate:	0.2721 arcsec/sec.

EVENT INFORMATION

Date:	November 17, 1983	UT of Event:	00:02:09
USNO V/O Code:	74	HA of Event:	-401416
Position Angle:	99.0	Cusp Angle:	52S
Contact Angle:	-44.6	Watts Angle:	121.4

MODEL PARAMETERS

Number of Data Points:	351
Number of Grid Points:	256
Number of Spectral Regions:	53
Width of Spectral Regions:	50 Angstroms
Limb Darkening Coefficient:	0.5
Effective Stellar Temperature:	5100 K

SOLUTIONS

Stellar Diameter (ams):	2.88	(4.98)
Time: (relative to Bin 0):	2091.6	(3.5)
Pre-Event Signal:	2927.6	(13.5)
Background Sky Level:	2495.6	(20.7)
Velocity (meters/sec.)	284.8	(16.0)
Lunar Limb Slope (degrees):	+28.3	(1.8)
U.T. of Occultation:	00:02:07.790	(0.004)

PHOTOMETRIC NOISE INFORMATION

Sum-of-Squares of Residuals:	14186840
Sigma (Standard Error):	201.330
Normalized Standard Error:	0.46613
Photometric (S+N)/N Ratio:	3.1453
(Change in Intensity)/Background:	0.1730
Change in Magnitude:	0.1733

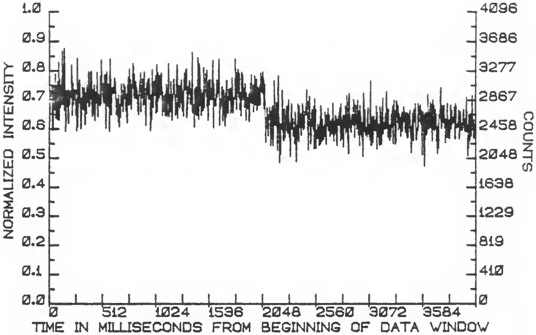

Figure 5-86. RAWPLOT of the occultation of X01217.

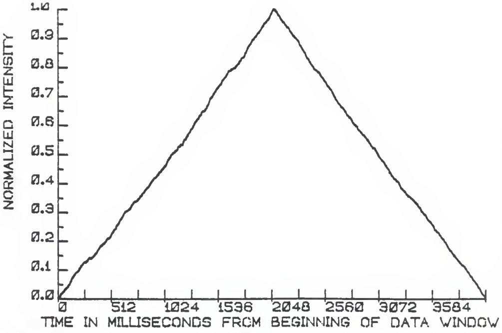

Figure 5-87. INTPLOT of the occultation of X01217.

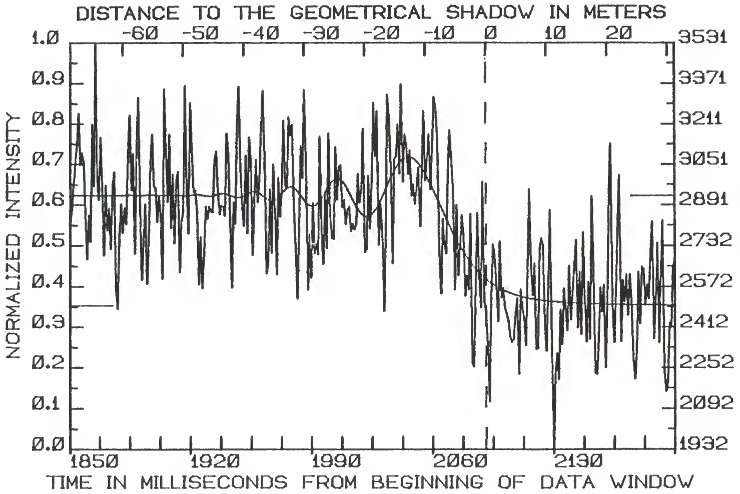

Figure 5-88. FITPLOT of the occultation of X01217.

TABLE 5-43
X01217: OBSERVATIONS, COMPUTED VALUES, AND RESIDUALS FROM BIN 1850

NUM	OBS	COMP	RESID	NUM	OBS	COMP	RESID	NUM	OBS	COMP	RESID
0	2823	2928.8	-105.8	67	3363	2927.4	435.6	134	3125	2929.2	195.8
1	2871	2928.9	-57.9	68	2951	2927.5	23.5	135	2996	2919.6	76.4
2	2964	2928.9	35.1	69	2780	2928.1	-148.1	136	3347	2910.3	436.7
3	3049	2928.9	120.1	70	3296	2928.9	367.1	137	3071	2901.8	169.2
4	3128	2928.9	199.1	71	3117	2929.8	187.2	138	2559	2894.7	-335.7
5	3253	2928.8	324.2	72	2940	2930.7	9.3	139	2777	2889.5	-112.5
6	3048	2928.7	119.3	73	2948	2931.2	16.8	140	2607	2886.5	-279.5
7	3096	2928.7	167.3	74	2863	2931.4	-68.4	141	2900	2886.0	14.0
8	3063	2928.7	134.3	75	2580	2931.1	-351.1	142	2701	2888.0	-187.0
9	2861	2928.7	-67.7	76	2767	2930.3	-163.3	143	2755	2892.5	-137.5
10	2680	2928.8	-248.8	77	2565	2929.2	-364.2	144	2697	2899.2	-202.2
11	2852	2928.9	-76.9	78	2703	2928.0	-225.0	145	3163	2908.0	255.0
12	2746	2928.9	-182.9	79	2887	2926.8	-39.8	146	2792	2918.2	-126.2
13	3211	2928.9	282.1	80	2837	2926.0	-89.0	147	2660	2929.5	-269.5
14	2966	2928.9	37.1	81	2887	2925.6	-38.6	148	2946	2941.4	4.6
15	3531	2928.8	602.2	82	2869	2925.9	-56.9	149	2723	2953.1	-230.1
16	2994	2928.7	65.3	83	2862	2926.8	-64.8	150	3175	2964.2	210.8
17	2911	2928.6	-17.6	84	3066	2928.2	137.8	151	2855	2974.1	-119.1
18	3159	2928.6	230.4	85	3104	2930.0	174.0	152	2761	2982.5	-221.5
19	2965	2928.7	36.3	86	2943	2931.9	11.1	153	2759	2988.8	-229.8
20	2694	2928.8	-234.8	87	2855	2933.5	-78.5	154	3120	2992.8	127.2
21	2969	2929.0	40.0	88	2893	2934.7	-41.7	155	2911	2994.3	-83.3
22	2791	2929.1	-138.1	89	2887	2935.1	-48.1	156	3043	2993.2	49.8
23	2879	2929.2	-50.2	90	2849	2934.7	-85.7	157	3048	2989.6	58.4
24	2720	2929.1	-209.1	91	3175	2933.4	241.6	158	2883	2983.6	-100.6
25	2966	2929.0	37.0	92	3091	2931.4	159.6	159	2911	2975.4	-64.4
26	3021	2928.7	92.3	93	2840	2928.8	-88.8	160	2815	2965.2	-150.2
27	2568	2928.5	-360.5	94	2569	2926.0	-357.0	161	2871	2953.6	-82.6
28	2484	2928.3	-444.3	95	2903	2923.4	-20.4	162	2885	2940.8	-55.8
29	2765	2928.3	-163.3	96	2817	2921.4	-104.4	163	2788	2927.4	-139.4
30	2895	2928.4	-33.4	97	3220	2920.2	299.8	164	2819	2913.8	-94.8
31	2782	2928.7	-146.7	98	3359	2920.1	438.9	165	2795	2900.4	-105.4
32	2881	2929.0	-48.0	99	3039	2921.2	117.8	166	2815	2887.7	-72.7
33	2815	2929.3	-114.3	100	2879	2923.4	-44.4	167	3015	2876.1	138.9
34	3087	2929.6	157.4	101	2809	2926.6	-117.6	168	2900	2865.9	34.1
35	3247	2929.6	317.4	102	3089	2930.5	158.5	169	2950	2857.6	92.4
36	2948	2929.5	18.5	103	2780	2934.6	-154.6	170	3193	2851.2	341.8
37	3095	2929.2	165.8	104	3159	2938.4	220.6	171	2704	2847.0	-143.0
38	2702	2928.8	-226.8	105	3069	2941.6	127.4	172	2721	2845.2	-124.2
39	3124	2928.3	195.7	106	2696	2943.7	-247.7	173	3007	2845.7	161.3
40	3317	2928.0	389.0	107	2906	2944.3	-38.3	174	2799	2848.5	-49.5
41	2890	2927.9	-37.9	108	3071	2943.5	127.5	175	2971	2853.6	117.4
42	2598	2928.1	-330.1	109	2901	2941.0	-40.0	176	3296	2860.9	435.1
43	2743	2928.4	-185.4	110	2986	2937.2	48.8	177	3083	2870.1	212.9
44	2894	2928.9	-34.9	111	3204	2932.3	271.7	178	3264	2881.0	383.0
45	2583	2929.4	-346.4	112	3343	2926.8	416.2	179	2735	2893.5	-158.5
46	2748	2929.8	-181.8	113	3073	2921.1	151.9	180	2895	2907.2	-12.2
47	3055	2930.1	124.9	114	2624	2915.9	-291.9	181	2806	2921.8	-115.8
48	3171	2930.0	241.0	115	2671	2911.7	-240.7	182	2475	2937.0	-462.0
49	2967	2929.7	37.3	116	2953	2908.9	44.1	183	2753	2952.6	-199.6
50	2959	2929.2	29.8	117	2703	2907.8	-204.8	184	3327	2968.3	358.7
51	2824	2928.6	-104.6	118	3051	2908.6	142.4	185	3245	2983.7	261.3
52	2925	2928.1	-3.1	119	2867	2911.4	-44.4	186	3039	2998.6	40.4
53	2855	2927.7	-72.7	120	2620	2916.0	-296.0	187	2663	3012.8	-349.8
54	2604	2927.6	-323.6	121	2999	2922.1	76.9	188	3071	3026.1	44.9
55	3350	2927.9	422.1	122	2844	2929.1	-85.1	189	3084	3038.2	45.8
56	3112	2928.3	183.7	123	2957	2936.7	20.3	190	3212	3049.1	162.9
57	2903	2929.0	-26.0	124	3227	2944.2	282.8	191	3015	3058.5	-43.5
58	3171	2929.6	241.4	125	2969	2951.0	18.0	192	3367	3066.3	300.7
59	2800	2930.2	-130.2	126	2960	2956.5	3.5	193	2983	3072.6	-89.6
60	3013	2930.4	82.6	127	3239	2960.3	278.7	194	3172	3077.2	94.8
61	2741	2930.4	-189.4	128	3166	2962.0	204.0	195	3135	3080.1	54.9
62	2991	2930.0	61.0	129	3209	2961.5	247.5	196	3012	3081.4	-69.4
63	3023	2929.4	93.6	130	2886	2958.7	-72.7	197	3108	3080.9	27.1
64	2629	2928.7	-299.7	131	2722	2953.7	-231.7	198	2927	3078.9	-151.9
65	2823	2928.0	-105.0	132	2524	2946.8	-422.8	199	2974	3075.3	-101.3
66	2863	2927.5	-64.5	133	2799	2938.5	-139.5	200	2895	3070.2	-175.2

TABLE 5-43. CONTINUED.

NUM	OBS	COMP	RESID	NUM	OBS	COMP	RESID	NUM	OBS	COMP	RESID
201	2971	3063.6	-92.6	251	2568	2557.5	10.5	301	2364	2503.3	-139.3
202	3039	3055.8	-16.8	252	2487	2554.3	-67.3	302	2925	2503.0	422.0
203	2807	3046.8	-239.8	253	2466	2551.3	-85.3	303	2639	2502.8	136.2
204	3007	3036.7	-29.7	254	2439	2548.5	-109.5	304	2230	2502.6	-272.6
205	3263	3025.6	237.4	255	2375	2545.8	-170.8	305	2227	2502.4	-275.4
206	2987	3013.6	-26.6	256	2351	2543.3	-192.3	306	2367	2502.2	-135.2
207	3068	3000.8	67.2	257	2363	2540.9	-177.9	307	2569	2502.0	67.0
208	3171	2987.4	183.6	258	2468	2538.7	-70.7	308	2472	2501.9	-29.9
209	2952	2973.5	-21.5	259	2524	2536.6	-12.6	309	2579	2501.7	77.3
210	3117	2959.1	157.9	260	2227	2534.6	-307.6	310	2251	2501.5	-250.5
211	3319	2944.4	374.6	261	2559	2532.7	26.3	311	2504	2501.4	2.6
212	3283	2929.4	353.6	262	2487	2530.9	-43.9	312	2944	2501.2	442.8
213	3155	2914.3	240.7	263	2451	2529.3	-78.3	313	3133	2501.1	631.9
214	2712	2899.1	-187.1	264	2340	2527.7	-187.7	314	2502	2500.9	1.1
215	2544	2883.8	-339.8	265	2639	2526.2	112.8	315	2351	2500.8	-149.8
216	2837	2868.7	-31.7	266	2954	2524.8	429.2	316	2551	2500.7	50.3
217	2743	2853.7	-110.7	267	2655	2523.5	131.5	317	2836	2500.6	335.4
218	2701	2838.9	-137.9	268	2537	2522.2	14.8	318	3010	2500.5	509.5
219	3007	2824.3	182.7	269	2663	2521.0	142.0	319	2355	2500.3	-145.3
220	3188	2810.0	378.0	270	2323	2519.9	-196.9	320	2600	2500.2	99.8
221	3088	2796.0	292.0	271	2328	2518.9	-190.9	321	2511	2500.1	10.9
222	2960	2782.3	177.7	272	2719	2517.9	201.1	322	2618	2500.0	118.0
223	2560	2769.1	-209.1	273	2762	2516.9	245.1	323	2459	2499.9	-40.9
224	2892	2756.2	135.8	274	2735	2516.0	219.0	324	2621	2499.8	121.2
225	2615	2743.8	-128.8	275	2423	2515.2	-92.2	325	2527	2499.7	27.3
226	2724	2731.7	-7.7	276	2318	2514.4	-196.4	326	2288	2499.6	-211.6
227	2851	2720.1	130.9	277	2598	2513.6	84.4	327	2208	2499.5	-291.5
228	2775	2709.0	66.0	278	2872	2512.9	359.1	328	2319	2499.4	-180.4
229	2535	2698.2	-163.2	279	2340	2512.2	-172.2	329	2631	2499.4	131.6
230	2630	2688.0	-58.0	280	1932	2511.6	-579.6	330	2426	2499.3	-73.3
231	2559	2678.1	-119.1	281	2223	2511.0	-288.0	331	2650	2499.2	150.8
232	2856	2668.7	187.3	282	2309	2510.4	-201.4	332	2640	2499.1	140.9
233	2272	2659.7	-387.7	283	2207	2509.8	-302.8	333	2507	2499.0	8.0
234	2255	2651.2	-396.2	284	2481	2509.3	-28.3	334	2581	2499.0	82.0
235	2577	2643.0	-66.0	285	2342	2508.8	-166.8	335	2525	2498.9	26.1
236	2859	2635.2	223.8	286	2564	2508.3	55.7	336	2705	2498.8	206.2
237	2615	2627.9	-12.9	287	2492	2507.8	-15.8	337	2828	2498.7	329.3
238	2489	2620.9	-131.9	288	2399	2507.4	-108.4	338	2367	2498.7	-131.7
239	2983	2614.2	368.8	289	2652	2507.0	145.0	339	2519	2498.6	20.4
240	2512	2607.9	-95.9	290	2440	2506.6	-66.6	340	2743	2498.6	244.4
241	2476	2601.9	-125.9	291	2544	2506.2	37.8	341	2351	2498.5	-147.5
242	2338	2596.3	-258.3	292	2655	2505.9	149.1	342	2653	2498.5	154.5
243	2119	2590.9	-471.9	293	2753	2505.5	247.5	343	2830	2498.4	331.6
244	2525	2585.9	-60.9	294	2408	2505.2	-97.2	344	2239	2498.4	-259.4
245	2739	2581.1	157.9	295	2631	2504.9	126.1	345	2159	2498.3	-339.3
246	2695	2576.6	118.4	296	2383	2504.6	-121.6	346	2197	2498.3	-301.3
247	2576	2572.3	3.7	297	2783	2504.3	278.7	347	2431	2498.2	-67.2
248	2433	2568.3	-135.3	298	2535	2504.0	31.0	348	2411	2498.2	-87.2
249	2749	2564.5	184.5	299	2355	2503.8	-148.8	349	2644	2498.1	145.9
250	2527	2560.9	-33.9	300	2591	2503.5	87.5	350	2684	2498.1	185.9

TABLE 5-44
X01217: SUPPLEMENTAL STATISTICAL INFORMATION

VARIANCE/CO-VARIANCE MATRIX

DIAM	PREI	POST	TIME	VELO
9.193E¯16	5.253E¯08	-8.800E¯08	-6.868E¯09	3.992E¯11
5.253E¯08	1.835E02	1.329E01	-1.093E01	4.225E¯02
-8.800E¯08	1.329E01	4.297E02	-2.321E01	8.805E¯02
-6.868E¯09	-1.093E01	-2.321E01	1.239E01	-4.798E¯02
3.992E¯11	4.225E¯02	8.805E¯02	-4.798E¯02	2.552E¯04

CORRELATION MATRIX

	DIAM	PREI	POST	TIME	VELO
DIAM	1.000000	0.609252	-0.854026	0.443445	-0.435567
PREI	0.609252	1.000000	-0.113136	-0.372319	0.378780
POST	-0.854026	-0.113136	1.000000	-0.826759	0.821489
TIME	0.443445	-0.372319	-0.826759	1.000000	-0.999956
VELO	-0.435567	0.378780	0.821489	-0.999956	1.000000

NUMERICAL RANGES OF THE PARTIAL DERIVATIVES

	MAXIMUM	MINIMUM
DIAM	1.063E09	-1.063E09
PREI	1.356E00	5.680E¯03
POST	9.943E¯01	-3.561E¯01
TIME	1.522E01	-1.567E01
VELO	3.706E03	-3.855E03

only 3.15. The solution yielded an angular diameter of of 2.88 milliseconds of arc. However, the one sigma uncertainty in this value of 4.98 milliseconds of arc is quite high, and hence, the diameter must be viewed with caution. This large formal error was partially due to the low S+N/N ratio and partially to the small dynamic range of the change in signal level in comparison to the background level (only 10.5 percent of full scale).

The 300 millisecond extract from the raw intensity data used in the DC solution, the computed intensity values, and their residuals are given in Table 5-56. The accompanying supplemental statistical information is presented in Table 5-47. Figure 5-89 shows the usual partial derivatives of the solution intensity curve. As can be seen the regions of high sensitivity to variations of each of the parameters were well covered in the 300 millisecond solution.

The noise figure of the residual amplitudes is shown on the NOISEPLOT, Figure 5-90. The usual comparative power spectra are shown in Figure 5-91. Here, one may note that even at low frequencies, the background noise is dominant over the occultation-centered data. This was another contributing factor to the large statistical uncertainty in the angular diameter determination.

The Coordinated Universal Time of geometrical occultation was 00:02:07.790 (+/- 0.004 seconds).

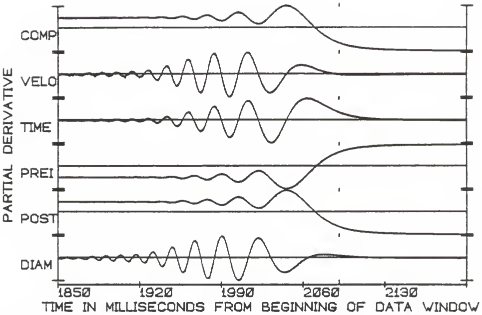

Figure 5-89. PDPLOT of the occultation of X01217.

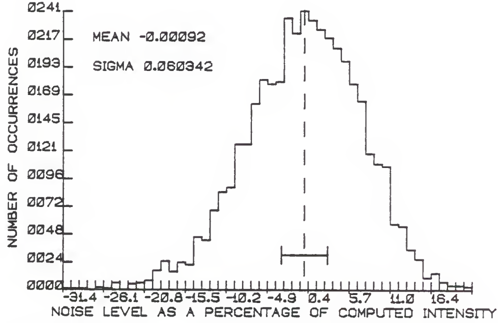

Figure 5-90. NOISEPLOT of the occultation of X01217.

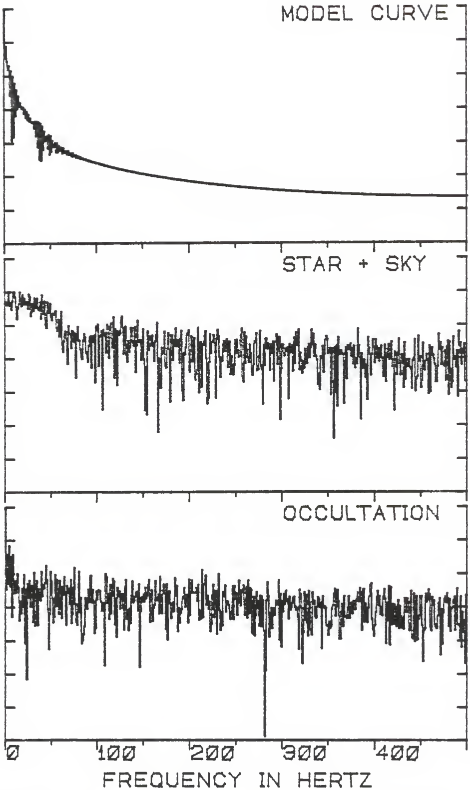

Figure 5-91. POWERPLOT of the occultation of X01217.

<u>X01246</u>

This relatively early (spectral class F0) star was occulted 78 minutes after X01217. In the intervening time, the seeing conditions improved considerably, and the "J" diaphragm was selected for this observation (as noted in the occultation summary, Table 5-45). Neither the trace of the raw intensity data (Figure 5-92) nor the integration plot (Figure 5-93) show any signs of stellar duplicity.

Three hundred milliseconds of data were used in the DC fitting process, and the best solution curve is shown in Figure 5-95. As it turned out, this was more data than was needed to be considered for a proper solution. To enable a better visualization of the fit, a detailed FITPLOT is presented as Figure 5-95. In this figure, covering only 100 milliseconds, 5-point smoothing was applied to the raw data before being plotted along with the fit to unsmoothed data.

The star was, not unexpectedly, indistinguishable from a point source. The 300 milliseconds of data subjected to DC fitting are listed (with the computed intensities and the residuals) on Table 5-46. Table 5-47 contains the variance/covariance and correlation matrices for the solution parameters, as well as the ranges of the numerical values of the partial derivatives of the intensity curve (which are shown in Figure 5-92).

TABLE 5-45
X01246: LUNAR OCCULTATION SUMMARY

STELLAR AND OBSERVING INFORMATION

Star: X01246, (SAO 109548, DM -00 0145)
RA: 005610   DEC: +002154   mV: 8.2   Sp: F0
Filter: V   Diaphragm: J   Gain: B10+   Voltage: 1200

LUNAR INFORMATION

Surface Illumination:	88 percent
Elongation from Sun:	139 degrees
Altitude Above Horizon:	55 degrees
Lunar Limb Distance:	390238 Kilometers
Predicted Shadow Velocity:	648.2 meters/sec.
Predicted Angular Rate:	0.3426 arcsec/sec.

EVENT INFORMATION

Date: November 17, 1983		UT of Event:	01:20:02
USNO V/O Code:	53	HA of Event:	-210352
Position Angle:	66.1	Cusp Angle:	85S
Contact Angle:	-15.2	Watts Angle:	88.5

MODEL PARAMETERS

Number of Data Points:	301
Number of Grid Points:	256
Number of Spectral Regions:	53
Width of Spectral Regions:	50 Angstroms
Limb Darkening Coefficient:	0.5
Effective Stellar Temperature:	7300 K

SOLUTIONS

Stellar Diameter (ams):	Point Source
Time: (relative to Bin 0):	1920.4 (3.3)
Pre-Event Signal:	2716.5 (15.9)
Background Sky Level:	2488.9 (18.2)
Velocity (meters/sec.):	688.2 (80.1)
Lunar Limb Slope (degrees):	-9.82 (7.08)
U.T. of Occultation:	01:20:01.938 (0.011)

PHOTOMETRIC NOISE INFORMATION

Sum-of-Squares of Residuals:	12365170
Sigma (Standard Error):	203.0202
Normalized Standard Error:	0.75862
Photometric (S+N)/N Ratio:	2.3182
(Change in Intensity)/Background:	0.10928
Change in Magnitude:	0.11261

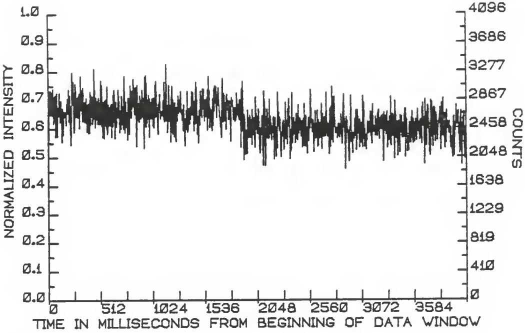

Figure 5-92. RAWPLOT of the occultation of X01246.

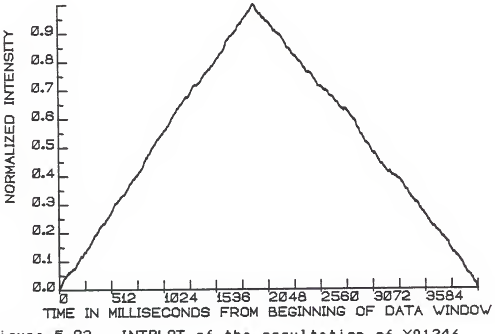

Figure 5-93. INTPLOT of the occultation of X01246.

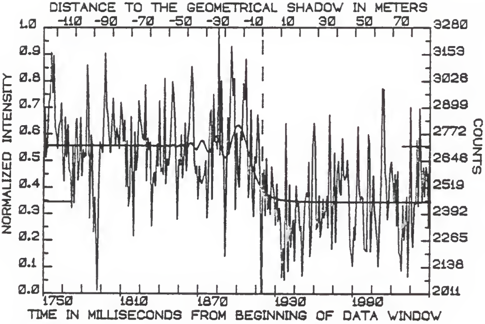

Figure 5-94. FITPLOT of the occultation of X01246.

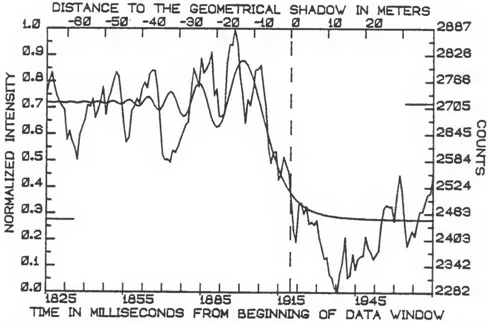

Figure 5-95. FITPLOT of the occultation of X01246 showing the raw fit to a smoothed data set.

TABLE 5-46
X01246: OBSERVATIONS, COMPUTED VALUES, AND RESIDUALS FROM BIN 1750

NUM	OBS	COMP	RESID	NUM	OBS	COMP	RESID	NUM	OBS	COMP	RESID
0	2421	2717.3	-296.3	67	2474	2717.5	-243.5	134	2735	2762.6	-27.6
1	2900	2717.3	182.7	68	2855	2717.2	137.8	135	2703	2759.2	-56.2
2	2663	2717.3	-54.3	69	2584	2717.0	-133.0	136	3280	2746.1	533.9
3	2732	2717.3	14.7	70	2288	2717.2	-429.2	137	2675	2726.3	-51.3
4	2921	2717.3	203.7	71	2782	2717.6	64.4	138	3028	2703.9	324.1
5	2944	2717.3	226.7	72	2603	2717.3	-114.3	139	2680	2683.3	-3.3
6	3161	2717.3	443.7	73	2663	2716.9	-53.9	140	2652	2668.3	-16.3
7	2972	2717.3	254.7	74	2931	2717.1	213.9	141	2191	2661.4	-470.4
8	3145	2717.3	427.7	75	2847	2717.6	129.4	142	2607	2663.7	-56.7
9	2809	2717.3	91.7	76	2807	2717.5	89.5	143	2851	2674.7	176.3
10	2771	2717.3	53.7	77	2755	2716.8	38.2	144	2680	2692.8	-12.8
11	2704	2717.3	-13.3	78	2745	2716.9	28.1	145	3023	2715.6	307.4
12	2807	2717.3	89.7	79	3007	2717.7	289.3	146	3191	2740.2	450.8
13	2835	2717.3	117.7	80	2552	2717.9	-165.9	147	2959	2764.0	195.0
14	2919	2717.3	201.7	81	2752	2717.1	34.9	148	3039	2784.8	254.2
15	2659	2717.3	-58.3	82	2703	2716.3	-13.3	149	2417	2800.8	-383.8
16	2551	2717.3	-166.3	83	2732	2717.0	15.0	150	2777	2810.9	-33.9
17	2851	2717.3	133.7	84	2335	2718.2	-383.2	151	2563	2814.6	-251.6
18	2664	2717.3	-53.3	85	2559	2718.3	-159.3	152	2524	2812.1	-288.1
19	2815	2717.3	97.7	86	2591	2716.9	-125.9	153	2786	2803.9	-17.9
20	2608	2717.3	-109.3	87	2528	2715.9	-187.9	154	2747	2790.8	-43.8
21	2587	2717.3	-130.3	88	2727	2716.8	10.2	155	3016	2773.7	242.3
22	2423	2717.3	-294.3	89	2621	2718.5	-97.5	156	2939	2753.7	185.3
23	2711	2717.2	-6.2	90	2932	2718.9	213.1	157	3131	2731.8	399.2
24	2446	2717.3	-271.3	91	2596	2717.2	-121.2	158	2776	2708.8	67.2
25	2819	2717.3	101.7	92	2610	2715.5	-105.5	159	2473	2685.7	-212.7
26	2844	2717.2	126.8	93	2581	2716.1	-135.1	160	2591	2662.9	-71.9
27	2555	2717.3	-162.3	94	3039	2718.3	320.7	161	2887	2641.0	246.0
28	2648	2717.3	-69.3	95	2539	2719.5	-180.5	162	2479	2620.4	-141.4
29	2850	2717.2	132.8	96	2654	2718.3	-64.3	163	2383	2601.2	-218.2
30	2575	2717.3	-142.3	97	2627	2715.8	-88.8	164	2666	2583.6	82.4
31	2697	2717.3	-20.3	98	2677	2714.9	-37.9	165	2639	2567.6	71.4
32	2663	2717.2	-54.2	99	2827	2716.9	110.1	166	2864	2553.3	310.7
33	2671	2717.3	-46.3	100	3023	2719.8	303.2	167	2769	2540.5	228.5
34	3103	2717.3	385.7	101	2966	2720.5	245.5	168	2559	2529.2	29.8
35	2975	2717.2	257.8	102	2841	2717.9	123.1	169	2011	2519.2	-508.2
36	2371	2717.3	-346.3	103	2575	2714.2	-139.2	170	2461	2510.4	-49.4
37	2766	2717.3	48.7	104	2367	2713.2	-346.2	171	2603	2502.8	100.2
38	2722	2717.2	4.8	105	2652	2716.3	-64.3	172	2387	2496.1	-109.1
39	2306	2717.3	-411.3	106	2627	2721.3	-94.3	173	2656	2490.3	165.7
40	2471	2717.3	-246.3	107	2768	2723.9	44.1	174	2416	2485.3	-69.3
41	2274	2717.2	-443.2	108	2567	2721.4	-154.4	175	2470	2481.0	-11.0
42	2030	2717.3	-687.3	109	2679	2715.1	-36.1	176	2392	2477.2	-85.2
43	2511	2717.3	-206.3	110	2824	2709.5	114.5	177	2618	2473.9	144.1
44	2735	2717.2	17.8	111	2600	2709.1	-109.1	178	2527	2471.1	55.9
45	2711	2717.2	-6.2	112	2752	2715.0	37.0	179	2493	2468.6	24.4
46	2687	2717.3	-30.3	113	2798	2723.9	74.1	180	2341	2466.5	-125.5
47	2872	2717.3	154.7	114	2961	2730.1	230.9	181	2536	2464.6	71.4
48	3159	2717.2	441.8	115	3096	2729.3	366.7	182	2358	2463.0	-105.0
49	2901	2717.2	183.8	116	3015	2721.1	293.9	183	2418	2461.6	-43.6
50	2867	2717.2	149.8	117	2656	2709.7	-53.7	184	2345	2460.4	-115.4
51	2752	2717.2	34.8	118	2587	2701.2	-114.2	185	2091	2459.3	-368.3
52	2685	2717.3	-32.3	119	2620	2700.6	-80.6	186	2228	2458.3	-230.3
53	2795	2717.2	77.8	120	2465	2709.1	-244.1	187	2079	2457.5	-378.5
54	2943	2717.1	225.9	121	2619	2723.0	-104.0	188	2823	2456.7	366.3
55	2800	2717.2	82.8	122	2551	2736.2	-185.2	189	2292	2456.1	-164.1
56	2719	2717.3	1.7	123	2540	2742.7	-202.7	190	2120	2455.5	-335.5
57	2801	2717.2	83.8	124	2563	2739.1	-176.1	191	2531	2454.9	76.1
58	2752	2717.1	34.9	125	2582	2726.4	-144.4	192	2236	2454.5	-218.5
59	2704	2717.3	-13.3	126	2646	2709.3	-63.3	193	2324	2454.0	-130.0
60	2923	2717.3	205.7	127	2374	2693.9	-319.9	194	2362	2453.7	-91.7
61	2860	2717.1	142.9	128	2507	2685.9	-178.9	195	2170	2453.3	-283.3
62	2738	2717.2	20.8	129	2865	2688.5	176.5	196	2527	2453.0	74.0
63	2838	2717.4	120.6	130	2888	2701.0	187.0	197	2431	2452.7	-21.7
64	2523	2717.2	-194.2	131	2465	2720.0	-255.0	198	2442	2452.5	-10.5
65	2739	2717.0	22.0	132	2964	2740.0	224.0	199	2315	2452.3	-137.3
66	2431	2717.2	-286.2	133	2740	2755.6	-15.6	200	2333	2452.1	-119.1

TABLE 5-46. CONTINUED.

NUM	OBS	COMP	RESID	NUM	OBS	COMP	RESID	NUM	OBS	COMP	RESID
201	2099	2451.9	-352.9	235	2572	2449.6	122.4	269	2607	2449.2	157.8
202	2291	2451.7	-160.7	236	2648	2449.6	198.4	270	2640	2449.2	190.8
203	2447	2451.6	-4.6	237	2516	2449.5	66.5	271	2559	2449.2	109.8
204	2495	2451.4	43.6	238	2242	2449.5	-207.5	272	2453	2449.2	3.8
205	2477	2451.3	25.7	239	2201	2449.5	-248.5	273	2583	2449.2	133.8
206	2639	2451.1	187.9	240	2146	2449.5	-303.5	274	2337	2449.1	-112.1
207	2192	2451.0	-259.0	241	2329	2449.5	-120.5	275	2596	2449.1	146.9
208	2283	2450.9	-167.9	242	2270	2449.4	-179.4	276	2210	2449.1	-239.1
209	2716	2450.8	265.2	243	2495	2449.4	45.6	277	2191	2449.1	-258.1
210	2824	2450.7	373.3	244	2809	2449.4	359.6	278	2125	2449.1	-324.1
211	2707	2450.6	256.4	245	2522	2449.4	72.6	279	2435	2449.1	-14.1
212	2321	2450.5	-129.5	246	2459	2449.4	9.6	280	2270	2449.1	-179.1
213	2331	2450.5	-119.5	247	2477	2449.4	27.6	281	2338	2449.1	-111.1
214	2480	2450.4	29.6	248	2468	2449.4	18.6	282	2476	2449.1	26.9
215	2284	2450.3	-166.3	249	2228	2449.4	-221.4	283	2095	2449.1	-354.1
216	2331	2450.3	-119.3	250	2219	2449.3	-230.3	284	2384	2449.1	-65.1
217	2464	2450.2	13.8	251	2216	2449.3	-233.3	285	2902	2449.1	452.9
218	2376	2450.2	-74.2	252	2771	2449.3	321.7	286	2294	2449.1	-155.1
219	2407	2450.1	-43.1	253	2725	2449.3	275.7	287	2235	2449.1	-214.1
220	2479	2450.1	28.9	254	2214	2449.3	-235.3	288	2446	2449.1	-3.1
221	2327	2450.0	-123.0	255	2407	2449.3	-42.3	289	2443	2449.1	-6.1
222	2864	2450.0	414.0	256	2575	2449.3	125.7	290	2744	2449.1	294.9
223	2552	2449.9	102.1	257	2415	2449.3	-34.3	291	2432	2449.1	-17.1
224	2228	2449.9	-221.9	258	2345	2449.3	-104.3	292	2895	2449.1	445.9
225	2461	2449.9	11.1	259	2262	2449.2	-187.2	293	2667	2449.1	217.9
226	2684	2449.8	234.2	260	2144	2449.2	-305.2	294	2455	2449.1	5.9
227	2260	2449.8	-189.8	261	2365	2449.2	-84.2	295	2615	2449.1	165.9
228	2585	2449.8	135.2	262	2543	2449.2	93.8	296	2479	2449.1	29.9
229	2644	2449.7	194.3	263	2993	2449.2	543.8	297	2618	2449.1	168.9
230	2507	2449.7	57.3	264	2986	2449.2	536.8	298	2576	2449.1	126.9
231	2487	2449.7	37.3	265	2593	2449.2	143.8	299	2334	2449.0	-115.0
232	2751	2449.7	301.3	266	2555	2449.2	105.8	300	2812	2449.0	363.0
233	2583	2449.6	133.4	267	2367	2449.2	-82.2				
234	2559	2449.6	109.4	268	2447	2449.2	-2.2				

TABLE 5-47
X01246: SUPPLEMENTAL STATISTICAL INFORMATION

VARIANCE/CO-VARIANCE MATRIX

DIAM	PREI	POST	TIME	VELO
3.372E¯14	2.876E¯07	-2.754E¯07	-4.922E¯08	1.347E¯09
2.876E¯07	2.534E02	5.360E00	-8.449E00	1.733E¯01
-2.754E¯07	5.360E00	3.316E02	-1.072E01	2.183E¯01
-4.922E¯08	-8.449E00	-1.072E01	1.079E01	-2.223E¯01
1.347E¯09	1.733E¯01	2.183E¯01	-2.223E¯01	6.409E¯03

CORRELATION MATRIX

	DIAM	PREI	POST	TIME	VELO
DIAM	1.000000	0.806934	-0.727659	-0.010259	0.013761
PREI	0.806934	1.000000	-0.193646	-0.481362	0.482215
POST	-0.727659	-0.193646	1.000000	-0.623821	0.619762
TIME	-0.010259	-0.481362	-0.623821	1.000000	-0.999972
VELO	0.013761	0.482215	0.619762	-0.999972	1.000000

NUMERICAL RANGES OF THE PARTIAL DERIVATIVES

	MAXIMUM	MINIMUM
DIAM	2.617E08	-2.596E08
PREI	1.367E00	6.770E¯04
POST	9.993E¯01	-3.667E¯01
TIME	2.315E01	-2.468E01
VELO	1.092E03	-1.140E03

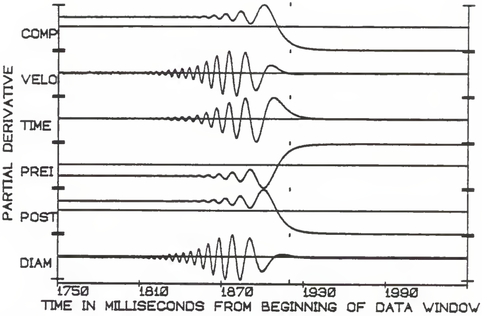

Figure 5-96. PDPLOT of the occultation of X01246.

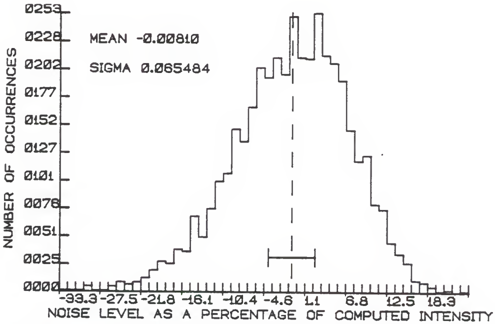

Figure 5-97. NOISEPLOT of the occultation of X01246.

The steadiness of the sky, in terms of atmospheric transparency, is attested to by the NOISEPLOT, Figure 5-97. The mean of the residual distribution is only 0.8 percent below that of the computed intensities, with a one sigma width of 6.5 percent. Despite the prevailing observing conditions, the faintness of the stellar signal in comparison to the bright sky background (10.9 percent, or 5.5 percent of full scale) led to a very low S+N/N ratio of only 2.32. This in turn was the primary cause for the large statistical uncertainties in the time of geometrical occultation (3.3 milliseconds) and the L-rate (11.6 percent of the determined value of 688.2 meters/second).

The characteristics of the comparative power spectra (Figure 5-98) are very similar to those seen for the previous occultation. The change in scale, with contributing power components more important at somewhat higher frequencies, is due to the different time-scales of the two events.

The occultation disappearance was determined to have occurred at 01:20:01.938 (+/- 0.011 seconds), Coordinated Universal Time.

ZC0126

The occultation of ZC0126 followed that of X01246 by only eight minutes. This star was of later spectral type than X01246 (G5 in comparison to F0), as well as half a magnitude brighter in V. These two differences

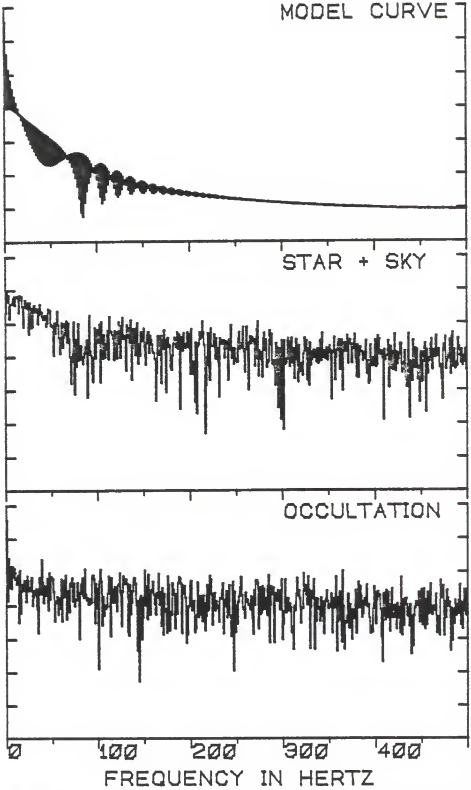

Figure 5-98. POWERPLOT of the occultation of X01246.

in characteristics led to a somewhat better occultation signal, with a S+N/N ratio of 3.45 (as noted in Table 5-48).

The raw intensity data are presented in Figure 5-99. The integration plot, Figure 5-100, suggests a possible secondary disappearance at approximately 1200 milliseconds. To see this sudden change in the integrated signal level more clearly, Figure 5-101 details the supposed secondary disappearance only. As is apparent, there is indeed a sharp decline in the integrated signal level at approximately 1205 milliseconds. No other such abrupt changes in the signal level (except, of course at the time of the primary disappearance) are seen in the data. Hence, a fainter "wide" secondary component was detected at 1205 milliseconds.

The ascending and decending branches of the integrated data, presented in Figure 5-101, were fit via least squares to linear equations. The statistical uncertainty in the intersection of the two regression lines was 0.008 seconds, which is, therefore, the uncertainty in the time of secondary disappearance.

Four hundred milliseconds of intensity data centered on the estimated time of primary occultation were fit via the DC process. This, in retrospect, was roughly 100 milliseconds longer than needed in the post-occultation portion of the data. The best fit to

TABLE 5-48
ZC0126: LUNAR OCCULTATION SUMMARY

STELLAR AND OBSERVING INFORMATION

Star: ZC0126, (SAO 109552, DM -00 0146)
RA: 005623 DEC: -001517 mV: 7.71 Sp: G5
Filter: V Diaphragm: J Gain: B10 Voltage: 1200

LUNAR INFORMATION

Surface Illumination:	88 percent
Elongation from Sun:	139 degrees
Altitude Above Horizon:	56 degrees
Lunar Limb Distance:	390149 Kilometers
Predicted Shadow Velocity:	449.8 meters/sec.
Predicted Angular Rate:	0.2378 arcsec/sec.

EVENT INFORMATION

Date: November 17, 1983		UT of Event:	01:28:05
USNO V/O Code:	64	HA of Event:	-190552
Position Angle:	98.3	Cusp Angle:	53S
Contact Angle:	-47.6	Watts Angle:	120.7

MODEL PARAMETERS

Number of Data Points:	401
Number of Grid Points:	266
Number of Spectral Regions:	53
Width of Spectral Regions:	50 Angstroms
Limb Darkening Coefficient:	0.5
Effective Stellar Temperature:	5700 K

SOLUTIONS

Stellar Diameter (ams):	Point Source
Time: (relative to Bin 0):	982.4 (2.7)
Pre-Event Signal:	2721.6 (14.0)
Background Sky Level:	2279.2 (12.6)
Velocity (meters/sec.):	322.4 (14.3)
Lunar Limb Slope (degrees):	+22.11 (1.83)
U.T. of Occultation:	01:28:01.981 (0.010)

PHOTOMETRIC NOISE INFORMATION

Sum-of-Squares of Residuals:	13087870
Sigma (Standard Error):	180.886
Normalized Standard Error:	0.40882
Photometric (S+N)/N Ratio:	3.4461
(Change in Intensity)/Background:	0.19413
Change in Magnitude:	0.19263

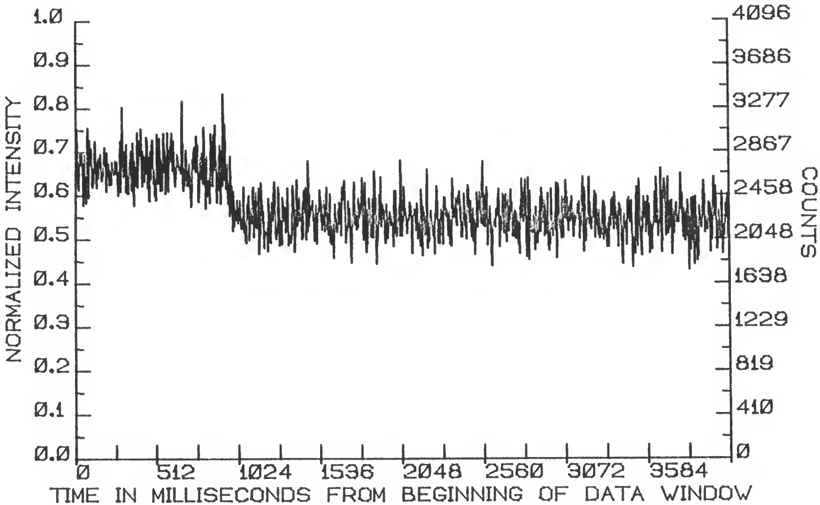

Figure 5-99. RAWPLOT of the occultation of ZC0126.

Figure 5-100. INTPLOT of the occultation of ZC0126.

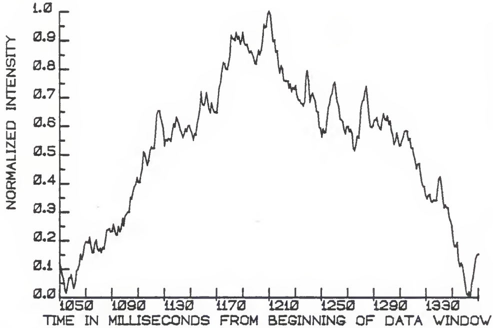

Figure 5-101. INTPLOT of the ZC0126 secondary event.

the data is shown in Figure 5-102. A detail of the disappearance is plotted, along with the data subjected to 5-point smoothing, in Figure 5-103.

The solution found ZC0126 to have no detectable disc, and hence has been classed as a point source solution. The intensity data, computed intensities and residuals are compiled in Table 5-49. The usual supplemental statistics are presented on Table 5-50.

The PDPLOT, Figure 5-104 exhibits no anomalous behavior. It does indicate, however, that a better data sample might have been selected from data points beginning roughly 50 milliseconds earlier. But, given the point source nature of the solution and the fact that the regions of sensitivity to parametric variation are well covered, this selection would not have made a significant difference in the solution.

The NOISEPLOT and the POWERPLOT for this observation are presented as Figures 5-105 and 5-106, respectively. Here, too, there is no unusual behavior.

The Coordinated Universal Time of geometrical occultation for the primary event was 01:28:01.981 (+/- 0.010 seconds). The secondary event was seen at 01:28:02.204 (+/- 0.013 seconds) C. U. T.

X01309

The last occultation observed on the night of November 17, 1983, was that of the star X01309. The observational conditions at the time of disappearance of

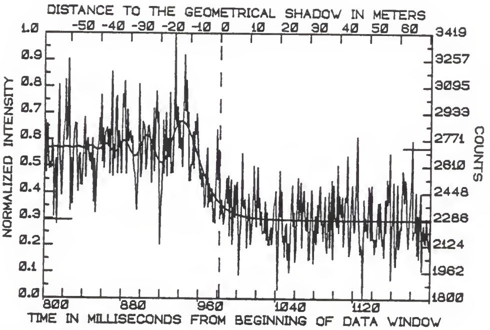

Figure 5-102. FITPLOT of the occultation of ZC0126.

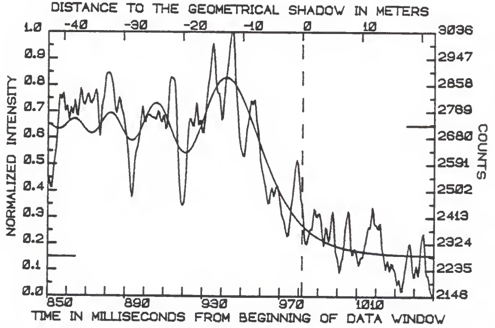

Figure 5-103. FITPLOT of the occultation of ZC0126 showing the raw fit to a smoothed data set.

TABLE 5-49
ZC0126: OBSERVATIONS, COMPUTED VALUES, AND RESIDUALS FROM BIN 800

NUM	OBS	COMP	RESID	NUM	OBS	COMP	RESID	NUM	OBS	COMP	RESID
0	2826	2724.8	101.2	67	2831	2730.9	100.1	134	2770	2808.0	-38.0
1	2883	2724.6	158.4	68	2565	2722.6	-157.6	135	3419	2824.3	594.7
2	2573	2723.8	-150.8	69	2925	2713.8	211.2	136	2905	2839.0	66.0
3	2864	2722.7	141.3	70	3183	2705.7	477.3	137	2863	2851.9	11.1
4	2703	2721.6	-18.6	71	2551	2699.3	-148.3	138	2971	2862.7	108.3
5	2595	2720.9	-125.9	72	2738	2695.5	42.5	139	2721	2871.4	-150.4
6	2628	2720.8	-92.8	73	2657	2694.8	-37.8	140	2886	2877.8	8.2
7	2597	2721.5	-124.5	74	3015	2697.4	317.6	141	2716	2882.0	-166.0
8	2767	2722.7	44.3	75	3035	2703.2	331.8	142	2779	2883.8	-104.8
9	2706	2724.0	-18.0	76	2567	2711.7	-144.7	143	2607	2883.3	-276.3
10	2303	2725.1	-422.1	77	2820	2722.0	98.0	144	2959	2880.7	78.3
11	2575	2725.6	-150.6	78	2779	2733.1	45.9	145	3287	2875.9	411.1
12	2652	2725.3	-73.3	79	2705	2743.9	-38.9	146	2949	2869.2	79.8
13	2257	2724.3	-467.3	80	2567	2753.3	-186.3	147	3132	2860.6	271.4
14	2824	2722.8	101.2	81	3047	2760.2	286.8	148	2851	2850.4	0.6
15	3103	2721.4	381.6	82	2971	2764.0	207.0	149	2936	2838.6	97.4
16	2681	2720.4	-39.4	83	3126	2764.2	361.8	150	2522	2825.5	-303.5
17	2573	2720.2	-147.2	84	2783	2760.6	22.4	151	2527	2811.2	-284.2
18	2434	2720.8	-286.8	85	2565	2753.5	-188.5	152	2619	2795.9	-176.9
19	2666	2722.1	-56.1	86	2952	2743.5	208.5	153	2619	2779.8	-160.8
20	2778	2723.7	54.3	87	2762	2731.4	30.6	154	2819	2763.1	55.9
21	2890	2725.2	164.8	88	2795	2718.1	76.9	155	2597	2745.8	-148.8
22	3134	2726.1	407.9	89	2819	2704.8	114.2	156	2882	2728.2	153.8
23	2766	2726.2	39.8	90	2751	2692.6	58.4	157	2806	2710.4	95.6
24	2788	2725.4	62.6	91	2790	2682.4	107.6	158	2928	2692.5	235.5
25	3260	2723.9	536.1	92	2645	2675.1	-30.1	159	2759	2674.6	84.4
26	2923	2722.1	200.9	93	2579	2671.4	-92.4	160	2666	2656.8	9.2
27	2339	2720.5	-381.5	94	2564	2671.4	-107.4	161	2535	2639.3	-104.3
28	2654	2719.6	-65.6	95	2395	2675.5	-280.5	162	2591	2622.0	-31.0
29	2379	2719.6	-340.6	96	2343	2683.1	-340.1	163	2487	2605.1	-118.1
30	2679	2720.6	-41.6	97	2599	2694.0	-95.0	164	2566	2588.7	-22.7
31	2831	2722.4	108.6	98	3108	2707.4	400.6	165	2505	2572.7	-67.7
32	2871	2724.5	146.5	99	2760	2722.5	37.5	166	2360	2557.2	-197.2
33	2864	2726.4	137.6	100	2545	2738.2	-193.2	167	2385	2542.2	-157.2
34	2639	2727.6	-88.6	101	2634	2753.7	-119.7	168	2602	2527.8	74.2
35	2456	2727.7	-271.7	102	2879	2767.9	111.1	169	2720	2514.0	206.0
36	2657	2726.7	-69.7	103	2859	2780.1	78.9	170	2363	2500.8	-137.8
37	2685	2724.7	-39.7	104	2826	2789.5	36.5	171	2503	2488.2	14.8
38	2497	2722.2	-225.2	105	2591	2795.5	-204.5	172	2395	2476.2	-81.2
39	2495	2719.6	-224.6	106	2622	2797.8	-175.8	173	2399	2464.7	-65.7
40	2587	2717.7	-130.7	107	2847	2796.3	50.7	174	2471	2453.8	17.2
41	2823	2716.8	106.2	108	2855	2791.1	63.9	175	2271	2443.5	-172.5
42	2904	2717.4	186.6	109	2807	2782.4	24.6	176	2350	2433.8	-83.8
43	2543	2719.4	-176.4	110	2724	2770.6	-46.6	177	2263	2424.5	-161.5
44	2731	2722.4	8.6	111	2511	2756.4	-245.4	178	2531	2415.8	115.2
45	2774	2726.0	48.0	112	2775	2740.4	34.6	179	2833	2407.6	425.4
46	2699	2729.4	-30.4	113	2963	2723.3	239.7	180	2531	2399.9	131.1
47	2636	2731.9	-95.9	114	2581	2705.9	-124.9	181	2706	2392.6	313.4
48	2682	2733.0	-51.0	115	2935	2688.9	246.1	182	2434	2385.8	48.2
49	2585	2732.3	-147.3	116	3066	2673.1	392.9	183	2316	2379.4	-63.4
50	2776	2729.7	46.3	117	2881	2659.2	221.8	184	2403	2373.3	29.7
51	2391	2725.7	-334.7	118	2935	2647.5	287.5	185	2335	2367.7	-32.7
52	2651	2720.8	-69.8	119	2389	2638.6	-249.6	186	2258	2362.4	-104.4
53	2327	2716.0	-389.0	120	2131	2632.8	-501.8	187	2307	2357.4	-50.4
54	2503	2712.1	-209.1	121	2403	2630.3	-227.3	188	2433	2352.8	80.2
55	2698	2709.7	-11.7	122	2470	2631.2	-161.2	189	2537	2348.4	188.6
56	2738	2709.4	28.6	123	2889	2635.3	253.7	190	2387	2344.3	42.7
57	2899	2711.5	187.5	124	2567	2642.6	-75.6	191	2551	2340.5	210.5
58	2739	2715.7	23.3	125	2775	2652.8	122.2	192	2184	2337.0	-153.0
59	3043	2721.5	321.5	126	2936	2665.6	270.4	193	2456	2333.6	122.4
60	2637	2728.1	-91.1	127	2551	2680.5	-129.5	194	2528	2330.5	197.5
61	2836	2734.7	101.3	128	2777	2697.2	79.8	195	2135	2327.6	-192.6
62	2600	2740.1	-140.1	129	2665	2715.1	-50.1	196	2287	2324.9	-37.9
63	2815	2743.6	71.4	130	3059	2733.9	325.1	197	2496	2322.3	173.7
64	2819	2744.4	74.6	131	2567	2753.0	-186.0	198	2300	2319.9	-19.9
65	2844	2742.5	101.5	132	2629	2772.0	-143.0	199	2499	2317.7	181.3
66	2728	2737.8	-9.8	133	2572	2790.5	-218.5	200	2514	2315.6	198.4

TABLE 5-49. CONTINUED.

NUM	OBS	COMP	RESID
201	2241	2313.7	-72.7
202	1949	2311.8	-362.8
203	2183	2310.1	-127.1
204	2255	2308.5	-53.5
205	2688	2307.0	381.0
206	2375	2305.6	69.4
207	2358	2304.3	53.7
208	2407	2303.1	103.9
209	2308	2301.9	6.1
210	2112	2300.8	-188.8
211	2265	2299.8	-34.8
212	2443	2298.8	144.2
213	2304	2297.9	6.1
214	2136	2297.1	-161.1
215	2235	2296.3	-61.3
216	2287	2295.5	-8.5
217	2611	2294.8	316.2
218	2460	2294.1	165.9
219	2319	2293.5	25.5
220	2243	2292.9	-49.9
221	2603	2292.3	310.7
222	2362	2291.8	70.2
223	2417	2291.3	125.7
224	2253	2290.8	-37.8
225	2331	2290.3	40.7
226	2199	2289.9	-90.9
227	2206	2289.5	-83.5
228	2207	2289.1	-82.1
229	2394	2288.7	105.3
230	2160	2288.4	-128.4
231	2326	2288.0	38.0
232	2130	2287.7	-157.7
233	2131	2287.4	-156.4
234	2191	2287.1	-96.1
235	2237	2286.8	-49.8
236	2135	2286.6	-151.6
237	2234	2286.3	-52.3
238	2367	2286.1	80.9
239	2412	2285.9	126.1
240	2459	2285.7	173.3
241	2070	2285.5	-215.5
242	1859	2285.3	-426.3
243	2275	2285.1	-10.1
244	2582	2284.9	297.1
245	2307	2284.8	22.2
246	2455	2284.6	170.4
247	2151	2284.4	-133.4
248	2183	2284.3	-101.3
249	2058	2284.2	-226.2
250	2235	2284.0	-49.0
251	2260	2283.9	-23.9
252	2040	2283.8	-243.8
253	2138	2283.7	-145.7
254	1965	2283.5	-318.5
255	2159	2283.4	-124.4
256	2374	2283.3	90.7
257	2495	2283.2	211.8
258	2248	2283.1	-35.1
259	2327	2283.0	44.0
260	2029	2282.9	-253.9
261	2103	2282.8	-179.8
262	2391	2282.7	108.3
263	2539	2282.6	256.4
264	2285	2282.5	2.5
265	2360	2282.4	77.6
266	2511	2282.4	228.6
267	2116	2282.3	-166.3
268	2366	2282.2	83.8
269	2463	2282.1	180.9
270	2352	2282.1	69.9
271	2231	2282.0	-51.0
272	2220	2282.0	-62.0
273	2393	2281.9	111.1
274	2040	2281.9	-241.9
275	2047	2281.8	-234.8
276	2251	2281.8	-30.8
277	2467	2281.7	185.3
278	2343	2281.7	61.3
279	2020	2281.6	-261.6
280	2175	2281.6	-106.6
281	2308	2281.5	26.5
282	2137	2281.5	-144.5
283	2376	2281.4	94.6
284	2207	2281.4	-74.4
285	2463	2281.3	181.7
286	2490	2281.3	208.7
287	2257	2281.2	-24.2
288	2279	2281.2	-2.2
289	2157	2281.1	-124.1
290	2259	2281.1	-22.1
291	2427	2281.1	145.9
292	2127	2281.1	-154.1
293	2086	2281.0	-195.0
294	2238	2281.0	-43.0
295	2455	2281.0	174.0
296	2119	2280.9	-161.9
297	2299	2280.9	18.1
298	2522	2280.9	241.1
299	2047	2280.9	-233.9
300	2495	2280.8	214.2
301	2296	2280.8	15.2
302	2295	2280.8	14.2
303	2243	2280.7	-37.7
304	2616	2280.7	335.3
305	2207	2280.7	-73.7
306	2431	2280.6	150.4
307	2360	2280.6	79.4
308	2305	2280.6	24.4
309	2424	2280.6	143.4
310	2124	2280.6	-156.6
311	2236	2280.6	-44.6
312	2423	2280.5	142.5
313	2399	2280.5	118.5
314	2672	2280.5	391.5
315	2203	2280.5	-77.5
316	2068	2280.4	-212.4
317	2118	2280.4	-162.4
318	2361	2280.4	80.6
319	2496	2280.4	215.6
320	2336	2280.4	55.6
321	2210	2280.3	-70.3
322	2237	2280.3	-43.3
323	2540	2280.3	259.7
324	2790	2280.3	509.7
325	2353	2280.3	72.7
326	2243	2280.3	-37.3
327	2076	2280.3	-204.3
328	2123	2280.2	-157.2
329	2075	2280.2	-205.2
330	1800	2280.2	-480.2
331	2407	2280.2	126.8
332	2219	2280.2	-61.2
333	2295	2280.2	14.8
334	2228	2280.2	-52.2
335	2180	2280.1	-100.1
336	2487	2280.1	206.9
337	2451	2280.1	170.9
338	2162	2280.1	-118.1
339	2493	2280.1	212.9
340	2164	2280.1	-116.1
341	2165	2280.1	-115.1
342	2079	2280.1	-201.1
343	2163	2280.1	-117.1
344	2127	2280.0	-153.0
345	2319	2280.0	39.0
346	2386	2280.0	106.0
347	2173	2280.0	-107.0
348	2391	2280.0	111.0
349	2250	2280.0	-30.0
350	2131	2280.0	-149.0
351	2164	2280.0	-116.0
352	2059	2280.0	-221.0
353	2409	2280.0	129.0
354	2211	2279.9	-68.9
355	2531	2279.9	251.1
356	2381	2279.9	101.1
357	2475	2279.9	195.1
358	2688	2279.9	408.1
359	1921	2279.9	-358.9
360	2223	2279.9	-56.9
361	2296	2279.9	16.1
362	2512	2279.9	232.1
363	2063	2279.9	-216.9
364	2003	2279.9	-276.9
365	2143	2279.9	-136.9
366	2500	2279.8	220.2
367	2111	2279.8	-168.8
368	2135	2279.8	-144.8
369	2238	2279.8	-41.8
370	2230	2279.8	-49.8
371	2581	2279.8	301.2
372	2542	2279.8	262.2
373	2393	2279.8	113.2
374	2528	2279.8	248.2
375	2463	2279.8	183.2
376	2204	2279.8	-75.8
377	2115	2279.8	-164.8
378	2223	2279.8	-56.8
379	2360	2279.8	80.2
380	2480	2279.8	200.2
381	2767	2279.7	487.3
382	2166	2279.7	-113.7
383	2208	2279.7	-71.7
384	2214	2279.7	-65.7
385	2451	2279.7	171.3
386	2071	2279.7	-208.7
387	2311	2279.7	31.3
388	2047	2279.7	-232.7
389	2337	2279.7	57.3
390	2445	2279.7	165.3
391	1975	2279.7	-304.7
392	2195	2279.7	-84.7
393	2246	2279.7	-33.7
394	2147	2279.7	-132.7
395	2137	2279.7	-142.7
396	2291	2279.7	11.3
397	2185	2279.7	-94.7
398	2128	2279.7	-151.7
399	2099	2279.7	-180.7
400	2227	2279.6	-52.6

TABLE 5-50
ZC0126: SUPPLEMENTAL STATISTICAL INFORMATION

VARIANCE/CO-VARIANCE MATRIX

DIAM	PREI	POST	TIME	VELO
3.719E¯15	1.224E¯07	-7.310E¯08	-1.376E¯08	8.217E¯11
1.224E¯07	1.970E02	5.010E00	-8.764E00	4.015E¯02
-7.310E¯08	5.010E00	1.600E02	-6.918E00	3.135E¯02
-1.376E¯08	-8.764E00	-6.918E00	7.146E00	-3.278E¯02
8.217E¯11	4.015E¯02	3.135E¯02	-3.278E¯02	2.070E¯04

CORRELATION MATRIX

	DIAM	PREI	POST	TIME	VELO
DIAM	1.000000	0.891094	-0.591950	-0.334484	0.338583
PREI	0.891094	1.000000	-0.167240	-0.663298	0.665761
POST	-0.591950	-0.167240	1.000000	-0.509287	0.504986
TIME	-0.334484	-0.663298	-0.509287	1.000000	-0.999987
VELO	0.338583	0.665761	0.504986	-0.999987	1.000000

NUMERICAL RANGES OF THE PARTIAL DERIVATIVES

	MAXIMUM	MINIMUM
DIAM	4.982E08	-4.917E08
PREI	1.367E00	1.104E¯03
POST	9.989E¯01	-3.665E¯01
TIME	1.793E01	-1.914E01
VELO	3.912E03	-3.984E03

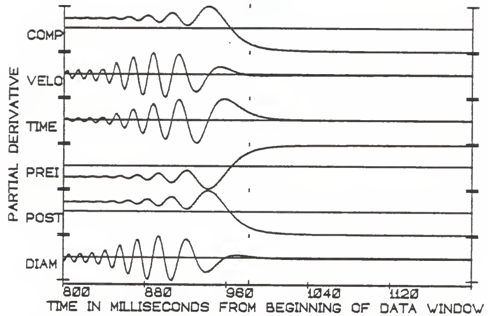

Figure 5-104. PDPLOT of the occultation of ZC0126.

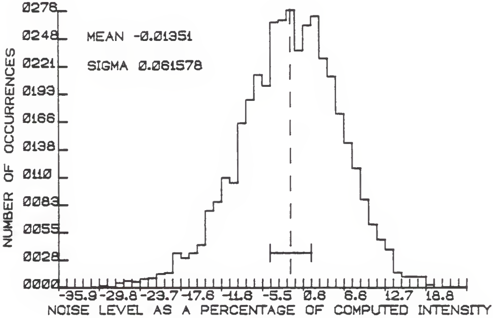

Figure 5-105. NOISEPLOT of the occultation of ZC0126.

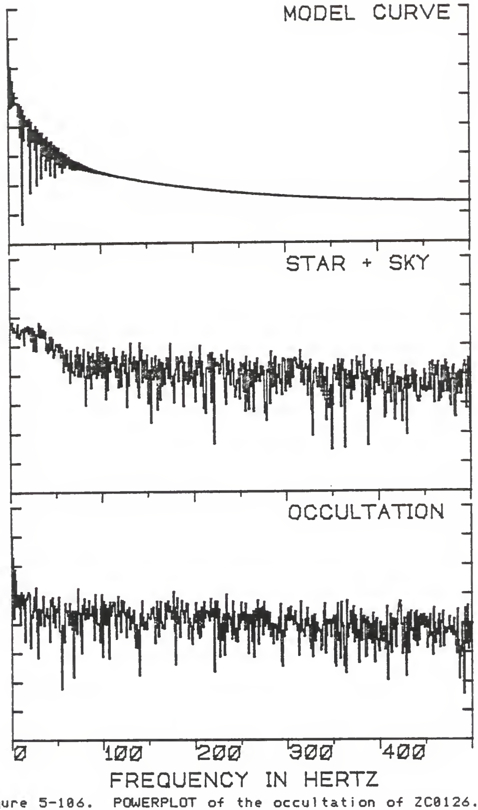

Figure 5-106. POWERPLOT of the occultation of ZC0126.

this K0 star (mV=7.8) were virtually unchanged from those which prevailed at the times of the two previous occultations. As noted on Table 5-51, the instrumental configuration was the same as that used for the ZC0126 event.

The RAWPLOT and INTPLOT (Figures 5-107 and 5-108, respectively) typify those of a single star disappearance, with no indication of stellar duplicity. A DC fit to 200 milliseconds of data was performed, and the resulting best fit is depicted in Figure 5-109. No discernible stellar disc could be detected for this star.

The observations, computed intensities and the residuals for the solution are listed in Table 5-52. The PDPLOT, Figure 5-110, shows nothing unusual in the numerical partial derivatives. Table 5-32 contains the numerical ranges of these partial derivatives along with the variance/covariance and correlation matrices of the solution parameters.

As might have been expected both the NOISEPLOT and POWERPLOT for this event (Figures 5-111, and 5-112, respectively) are very similar to those seen for the observations of ZC0126 and X01246.

The Coordinated Universal Time of geometrical occultation was 03:32:06.631 (+/- 0.005 seconds).

TABLE 5-51
X01309: LUNAR OCCULTATION SUMMARY

STELLAR AND OBSERVING INFORMATION

Star: X01309, (SAO 109577, DM +00 0159, GC1185K)
RA: 005834   DEC: +004131   mV: 7.8   Sp: K0
Filter: V   Diaphragm: J   Gain: B10   Voltage: 1200

LUNAR INFORMATION

Surface Illumination:	88 percent
Elongation from Sun:	139 degrees
Altitude Above Horizon:	59 degrees
Lunar Limb Distance:	389597 kilometers
Predicted Shadow Velocity:	384.9 meters/sec.
Predicted Angular Rate:	0.2038 arcsec/sec.

EVENT INFORMATION

Date:	November 17, 1983	UT of Event:	03:32:06
USNO V/O Code:	64	HA of Event:	+112736
Position Angle:	104.1	Cusp Angle:	47S
Contact Angle:	-54.1	Watts Angle:	126.4

MODEL PARAMETERS

Number of Data Points:	201
Number of Grid Points:	256
Number of Spectral Regions:	53
Width of Spectral Regions:	50 Angstroms
Limb Darkening Coefficient:	0.5
Effective Stellar Temperature:	5100 K

SOLUTIONS

Stellar Diameter (ams):	Point Source	
Time: (relative to Bin 0):	1954.5	(2.0)
Pre-Event Signal:	3134.6	(18.6)
Background Sky Level:	2621.9	(23.8)
Velocity (meters/sec.):	514.6	(27.7)
Lunar Limb Slope (degrees):	-20.8	(4.13)
U.T. of Occultation:	03:32:06.631	(0.005)

PHOTOMETRIC NOISE INFORMATION

Sum-of-Squares of Residuals:	7797315
Sigma (Standard Error):	197.4502
Normalized Standard Error:	0.38512
Photometric (S+N)/N Ratio:	3.59662
(Change in Intensity)/Background:	0.19555
Change in Magnitude:	0.19392

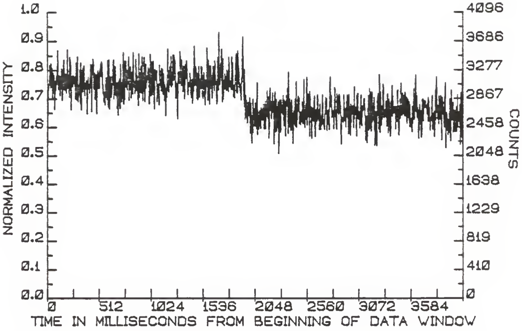

Figure 5-107. RAWPLOT of the occultation of X01309.

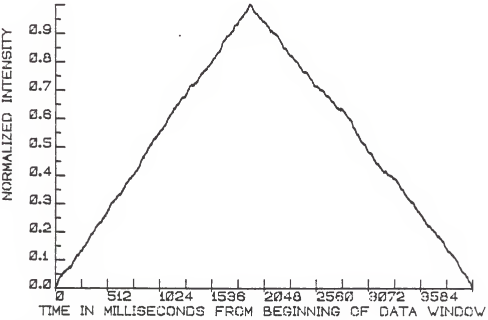

Figure 5-108. INTPLOT of the occultation of X01309.

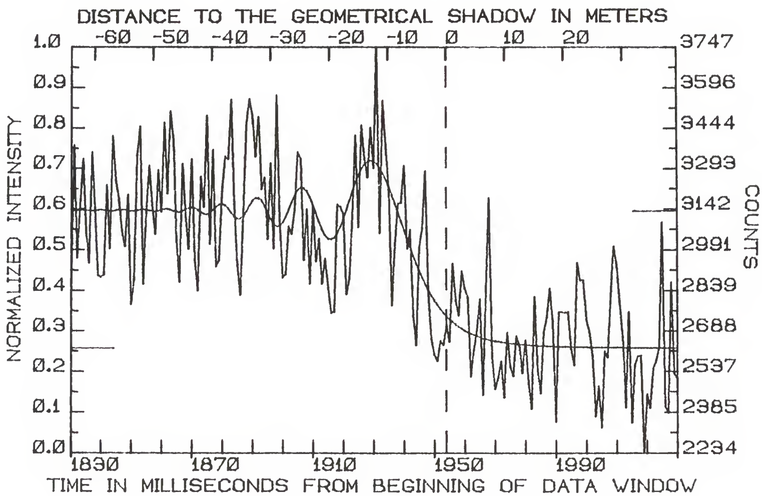

Figure 5-109. FITPLOT of the occultation of X01309.

TABLE 5-52
X01309: OBSERVATIONS, COMPUTED VALUES, AND RESIDUALS FROM BIN 1830

NUM	OBS	COMP	RESID	NUM	OBS	COMP	RESID	NUM	OBS	COMP	RESID
0	2804	3135.4	-331.4	67	2996	3087.6	-91.6	134	2689	2668.9	20.1
1	3380	3135.3	244.7	68	3568	3077.2	490.8	135	2807	2664.9	142.1
2	2960	3136.1	-176.1	69	3101	3077.9	23.1	136	2449	2661.3	-212.3
3	3155	3137.1	17.9	70	2887	3089.9	-202.9	137	2842	2658.0	184.0
4	3328	3137.2	190.8	71	2900	3111.2	-211.2	138	3183	2655.1	527.9
5	3060	3136.2	-76.2	72	3078	3138.5	-60.5	139	2592	2652.4	-60.4
6	2943	3135.0	-192.0	73	3049	3167.4	-118.4	140	2472	2650.0	-178.0
7	3353	3134.6	218.4	74	3140	3193.4	-53.4	141	2511	2647.9	-136.9
8	3144	3135.6	8.4	75	3356	3212.5	143.5	142	2575	2645.9	-70.9
9	2896	3137.3	-241.3	76	3329	3222.0	107.0	143	2439	2644.2	-205.2
10	2889	3138.2	-249.2	77	2952	3220.4	-268.4	144	2681	2642.6	38.4
11	2898	3137.4	-239.4	78	3142	3208.0	-66.0	145	2556	2641.1	-85.1
12	3231	3135.5	95.5	79	2865	3186.2	-321.2	146	2519	2639.8	-120.8
13	2996	3133.9	-137.9	80	3155	3157.8	-2.8	147	2668	2638.6	29.4
14	3414	3134.0	280.0	81	2947	3126.1	-179.1	148	2639	2637.5	1.5
15	3251	3135.9	115.1	82	3032	3094.6	-62.6	149	2530	2636.5	-106.5
16	3179	3138.2	40.8	83	2864	3066.7	-202.7	150	2655	2635.6	19.4
17	3061	3139.1	-78.1	84	2959	3045.3	-86.3	151	2495	2634.7	-139.7
18	3003	3137.9	-134.9	85	2850	3032.3	-182.3	152	2399	2633.9	-234.9
19	3195	3135.3	59.7	86	2754	3028.9	-274.9	153	2815	2633.2	181.8
20	2789	3133.4	-344.4	87	2759	3035.3	-276.3	154	2541	2632.5	-91.5
21	2879	3133.4	-254.4	88	3159	3050.9	108.1	155	2455	2631.9	-176.9
22	3340	3135.5	204.5	89	3151	3074.4	76.6	156	2683	2631.4	51.6
23	3451	3138.3	312.7	90	3126	3103.9	22.1	157	2737	2630.9	106.1
24	2863	3139.7	-276.7	91	2825	3137.4	-312.4	158	2847	2630.4	216.6
25	3128	3138.8	-10.8	92	2881	3172.6	-291.6	159	2723	2629.9	93.1
26	3303	3136.0	167.0	93	3114	3207.4	-93.4	160	2351	2629.5	-278.5
27	3157	3133.3	23.7	94	3417	3239.8	177.2	161	2759	2629.2	129.8
28	3050	3132.6	-82.6	95	3075	3268.3	-193.3	162	2759	2628.8	130.2
29	3287	3134.4	152.6	96	3455	3291.5	163.5	163	2756	2628.5	127.5
30	3131	3137.9	-6.9	97	3331	3308.6	22.4	164	2759	2628.2	130.8
31	3467	3140.8	326.2	98	3259	3319.0	-60.0	165	2622	2627.9	-5.9
32	3199	3141.1	57.9	99	3447	3322.6	124.4	166	2560	2627.7	-67.7
33	3508	3138.4	369.6	100	3294	3319.6	-25.6	167	2943	2627.4	315.6
34	3401	3134.0	267.0	101	3747	3310.3	436.7	168	2878	2627.2	250.8
35	3026	3130.3	-104.3	102	3052	3295.3	-243.3	169	2877	2627.0	250.0
36	2871	3129.8	-258.8	103	3548	3275.4	272.6	170	2732	2626.8	105.2
37	3311	3133.2	177.8	104	3379	3251.4	127.6	171	2687	2626.6	60.4
38	3120	3139.1	-19.1	105	3215	3224.0	-9.0	172	2599	2626.4	-27.4
39	2994	3144.8	-150.8	106	2783	3194.1	-411.1	173	2371	2626.2	-255.2
40	3328	3147.2	180.8	107	3006	3162.5	-156.5	174	2483	2626.0	-143.0
41	2957	3144.7	-187.7	108	3163	3129.8	33.2	175	2329	2625.8	-296.8
42	2839	3137.7	-298.7	109	3164	3096.7	67.3	176	2611	2625.7	-14.7
43	3263	3129.0	134.0	110	3303	3063.7	239.3	177	2589	2625.5	-36.5
44	3148	3122.4	25.6	111	2994	3031.3	-37.3	178	2819	2625.4	193.6
45	3492	3121.0	371.0	112	3065	2999.8	65.2	179	3003	2625.3	377.7
46	3011	3126.2	-115.2	113	2749	2969.6	-220.6	180	2936	2625.2	310.8
47	3363	3136.5	226.5	114	2635	2940.9	-305.9	181	2798	2625.1	172.9
48	2928	3148.5	-220.5	115	2998	2913.7	84.3	182	2667	2625.0	42.0
49	2951	3157.7	-206.7	116	3068	2888.3	179.7	183	2403	2624.9	-221.9
50	3207	3160.5	46.5	117	3283	2864.6	418.4	184	2760	2624.8	135.2
51	3339	3155.2	183.8	118	2832	2842.6	-10.6	185	2347	2624.7	-277.7
52	3328	3143.0	185.0	119	2659	2822.4	-163.4	186	2561	2624.6	-63.6
53	3551	3127.3	423.7	120	2600	2803.8	-203.8	187	2594	2624.5	-30.5
54	3159	3113.0	46.0	121	2575	2786.8	-211.8	188	2596	2624.4	-28.4
55	2937	3104.7	-167.7	122	2651	2771.3	-120.3	189	2234	2624.3	-390.3
56	2824	3105.4	-281.4	123	2635	2757.2	-122.2	190	2452	2624.3	-172.3
57	3126	3115.5	10.5	124	2711	2744.4	-33.4	191	2401	2624.2	-223.2
58	3458	3132.9	325.1	125	2648	2732.8	-84.8	192	2548	2624.1	-76.1
59	3555	3153.1	401.9	126	2939	2722.4	216.6	193	2575	2624.1	-49.1
60	3494	3171.1	322.9	127	2804	2713.0	91.0	194	2624	2624.0	0.0
61	3337	3182.1	154.9	128	2747	2704.5	42.5	195	3093	2624.0	469.0
62	3489	3183.1	305.9	129	2912	2696.9	215.1	196	2407	2623.9	-216.9
63	3215	3173.3	41.7	130	2848	2690.0	158.0	197	2383	2623.9	-240.9
64	3259	3154.6	104.4	131	2814	2683.9	130.1	198	2871	2623.8	247.2
65	3030	3130.8	-100.8	132	2517	2678.3	-161.3	199	2528	2623.8	-95.8
66	3312	3106.8	205.2	133	2615	2673.4	-58.4	200	2511	2623.7	-112.7

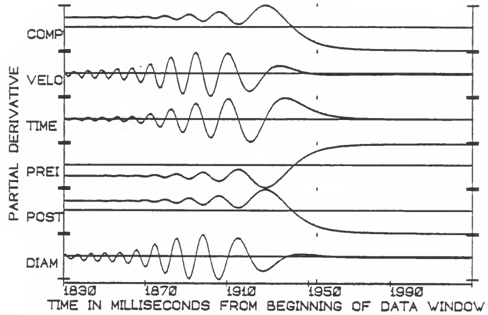

Figure 5-110. PDPLOT of the occultation of X01309.

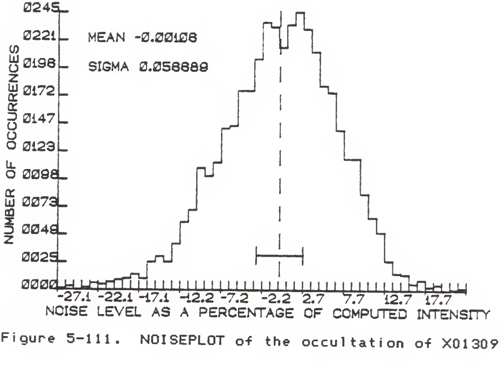

Figure 5-111. NOISEPLOT of the occultation of X01309.

TABLE 5-53
X01309: SUPPLEMENTAL STATISTICAL INFORMATION

VARIANCE/CO-VARIANCE MATRIX

DIAM	PREI	POST	TIME	VELO
3.004E¯14	4.253E¯07	-5.242E¯07	-2.350E¯08	3.963E¯10
4.253E¯07	3.435E02	1.772E01	-8.716E00	1.041E¯01
-5.242E¯07	1.772E01	5.679E02	-1.309E01	1.504E¯01
-2.350E¯08	-8.716E00	-1.309E01	4.109E00	-4.807E¯02
3.963E¯10	1.041E¯01	1.504E¯01	-4.807E¯02	7.689E¯04

CORRELATION MATRIX

	DIAM	PREI	POST	TIME	VELO
DIAM	1.000000	0.707272	-0.807680	0.275065	-0.255759
PREI	0.707272	1.000000	-0.155474	-0.463281	0.480530
POST	-0.807680	-0.155474	1.000000	-0.779561	0.767024
TIME	0.275065	-0.463281	-0.779561	1.000000	-0.999799
VELO	-0.255759	0.480530	0.767024	-0.999799	1.000000

NUMERICAL RANGES OF THE PARTIAL DERIVATIVES

	MAXIMUM	MINIMUM
DIAM	2.403E08	-2.322E08
PREI	1.367E00	3.510E¯03
POST	9.965E¯01	-3.667E¯01
TIME	3.313E01	-3.536E01
VELO	2.824E03	-2.852E03

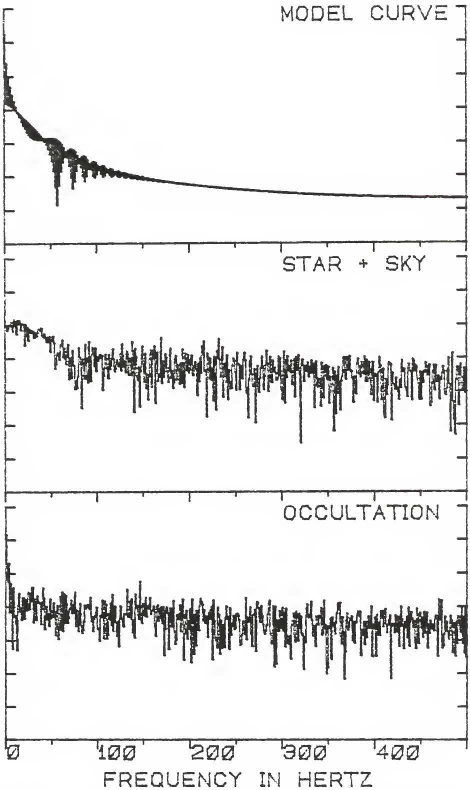

Figure 5-112. POWERPLOT of the occultation of X01309.

ZC3158 (37 Capricorni)

The bright (mV=5.79) F5 star ZC3158 was occulted under very favorable circumstances on the night of December 10, 1983. Though the event occurred early in the evening (approximately 00:07 U. T.), astronomical twilight had been over for approximately ten minutes. Thus, despite the relatively small solar elongation of 62 degrees, the event was seen in dark skies. The penalty for this was a moderately low lunar altitude, though still above two air masses. The darkened portion of the 27 percent illuminated lunar disc was quite dark, and virtually no Earthshine could be seen, even in a 6-inch finding telescope.

The seeing was unusually good for RHO and estimated at 2 seconds of arc or better. These almost extraordinary combinations of fortuitous circumstances allowed the observation to be made with the narrow bandwidth "b" filter. Though the integrated bandpass of this filter is less than 1/10 that of a Johnson B filter, the S+N/N ratio obtained for this observation (given in Table 5-54) was still a respectable 5.52.

As easily seen on the RAWPLOT, Figure 5-113, the stellar signal was highly dominant (by a factor of 6.5) over the background sky brightness. The integration plot of the 4096 milliseconds of raw data (Figure 5-114) shows no evidence of any secondary disappearances.

TABLE 5-54
ZC3158: LUNAR OCCULTATION SUMMARY

STELLAR AND OBSERVING INFORMATION

Star: ZC3158, (37 Cap, SAO 190461, DM -20 6237)
RA: 213355 DEC: -200935 mV: 5.79 Sp: F5
Filter: "b" Diaphragm: I Gain: C9+ Voltage: 1200

LUNAR INFORMATION

Surface Illumination:	27 percent
Elongation from Sun:	62 degrees
Altitude Above Horizon:	31 degrees
Lunar Limb Distance:	400741 kilometers
Predicted Shadow Velocity:	355.7 meters/sec.
Predicted Angular Rate:	0.1831 arcsec/sec.

EVENT INFORMATION

Date:	December 10, 1983	UT of Event:	00:06:42
USNO V/O Code:	59	HA of Event:	+334727
Position Angle:	118.3	Cusp Angle:	46S
Contact Angle:	-58.9	Watts Angle:	137.9

MODEL PARAMETERS

Number of Data Points:	301
Number of Grid Points:	256
Number of Spectral Regions:	5
Width of Spectral Regions:	50 Angstroms
Limb Darkening Coefficient:	0.5
Effective Stellar Temperature:	6600K

SOLUTIONS

Stellar Diameter (ams):	1.74	(1.68)
Time: (relative to Bin 0):	1521.9	(1.6)
Pre-Event Signal:	1509.9	(23.7)
Background Sky Level:	231.7	(49.3)
Velocity (meters/sec.):	269.9	(3.34)
Lunar Limb Slope (degrees):	+20.3	(0.5)
U.T. of Occultation:	00:06:39.731	(0.004)

PHOTOMETRIC NOISE INFORMATION

Sum-of-Squares of Residuals:	38293450
Sigma (Standard Error):	357.274
Normalized Standard Error:	0.2795
Photometric (S+N)/N Ratio:	4.5775
(Change in Intensity)/Background:	5.5159
Change in Magnitude:	2.0349

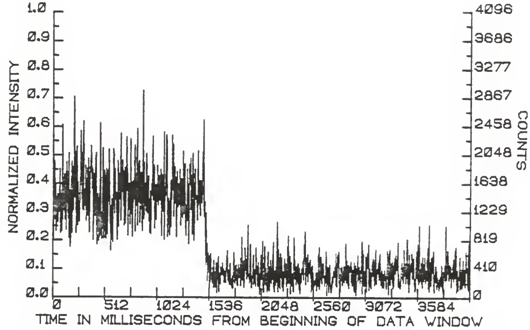

Figure 5-113. RAWPLOT of the occultation of ZC3158.

Figure 5-114. INTPLOT of the occultation of ZC3158.

Because of the somewhat slower R-rate for this event (predicted to be 0.1831 arc seconds per second), 300 milliseconds of data were used in the DC fitting process. The resulting best fit is shown graphically in Figure 5-115 and as can be seen is rather good. The slowly decaying diffraction fringes arose from the near monochromaticity of the optical bandpass. This is reflected in the PDPLOT (Figure 5-116) as well. Examination of the PDPLOT (see Table 5-56 for the ranges of numerical values in the partial derivatives) shows that the sensitivity of the solution curve to variations in the stellar diameter and velocity parameter (and to a lesser extent time of geometrical occultation) continues to be high before the start of the choosen data set. While this is true, because of the decaying amplitude of the diffraction fringes in the occultation curve itself, to include data from times earlier than considered would not be helpful. Data extracted from times before about 1280 milliseconds would be dominated by variations due to scintillation noise rather than intrinsic variations in the intensity curve.

A stellar angular diameter of 1.74 (+/- 1.68) milliseconds of arc was determined by the DC fitting procedure, for ZC3158. This star, according to Schlesinger and Jenkins (1940), has a parallax of 0.032 arc seconds, or a corresponding distance of 31 parsecs.

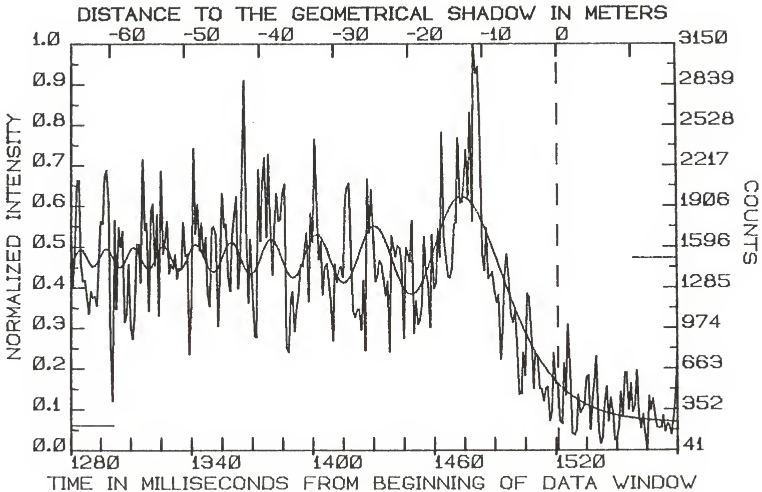

Figure 5-115. FITPLOT of the occultation of ZC3158.

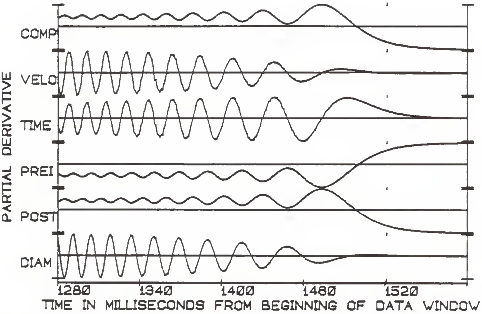

Figure 5-116. PDPLOT of the occultation of ZC3158.

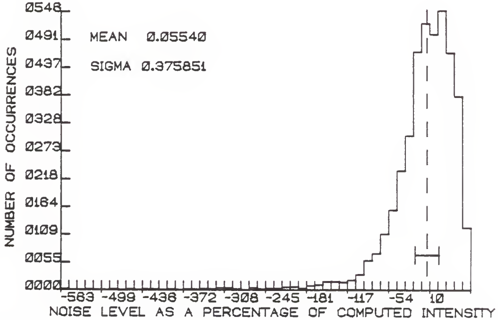

Figure 5-117. NOISEPLOT of the occultation of ZC3158.

TABLE 5-55
ZC 3158: OBSERVATIONS, COMPUTED VALUES, AND RESIDUALS FROM BIN 1280

NUM	OBS	COMP	RESID	NUM	OBS	COMP	RESID	NUM	OBS	COMP	RESID
0	1677	1466.6	210.4	67	1671	1491.4	179.6	134	1447	1332.2	114.8
1	1300	1490.2	-190.2	68	1248	1455.9	-207.9	135	1367	1323.6	43.4
2	1544	1519.5	24.5	69	1145	1427.2	-282.2	136	1955	1324.7	630.3
3	2103	1548.0	555.0	70	1735	1410.5	324.5	137	2049	1335.6	713.4
4	2103	1568.1	534.9	71	1752	1406.8	345.2	138	2083	1355.4	727.6
5	1489	1575.3	-86.3	72	1696	1416.7	279.3	139	1462	1383.6	78.4
6	1335	1566.9	-231.9	73	991	1439.7	-448.7	140	1104	1418.4	-314.4
7	1343	1545.9	-202.9	74	1346	1471.7	-125.7	141	1058	1458.2	-400.2
8	1232	1516.5	-284.5	75	2004	1510.0	494.0	142	1121	1501.4	-380.4
9	1087	1485.9	-398.9	76	1745	1548.9	196.1	143	1121	1546.0	-425.0
10	1258	1461.6	-203.6	77	1770	1584.5	185.5	144	963	1590.0	-627.0
11	1210	1449.5	-239.5	78	1378	1611.7	-233.7	145	1343	1631.6	-288.6
12	1219	1451.5	-232.5	79	1263	1628.5	-365.5	146	805	1669.3	-864.3
13	1151	1468.5	-317.5	80	1647	1631.2	15.8	147	2111	1701.2	409.8
14	1443	1496.1	-53.1	81	1832	1621.2	210.8	148	1705	1726.7	-21.7
15	1791	1527.7	263.3	82	1980	1598.6	381.4	149	2035	1744.0	291.0
16	1775	1556.8	218.2	83	1280	1566.3	-286.3	150	1680	1753.2	-73.2
17	2131	1576.8	554.2	84	1479	1528.2	-49.2	151	1335	1754.1	-419.1
18	2185	1582.6	602.4	85	2270	1488.1	781.9	152	1368	1746.1	-378.1
19	1923	1573.5	349.5	86	2871	1450.4	1420.6	153	1495	1730.6	-235.6
20	856	1551.5	-695.5	87	1759	1419.3	339.7	154	1466	1706.9	-240.9
21	422	1520.7	******	88	1170	1398.1	-228.1	155	1363	1677.0	-314.0
22	1799	1488.1	310.9	89	1654	1388.6	265.4	156	1226	1641.5	-415.5
23	1122	1460.6	-338.6	90	1311	1392.5	-81.5	157	1337	1601.5	-264.5
24	1747	1443.9	303.1	91	914	1408.5	-494.5	158	795	1558.7	-763.7
25	1595	1441.4	153.6	92	906	1435.8	-529.8	159	1684	1514.1	169.9
26	1717	1453.9	263.1	93	2183	1471.2	711.8	160	1592	1469.3	122.7
27	1023	1478.7	-455.7	94	1641	1511.2	129.8	161	1519	1425.5	93.5
28	1081	1511.0	-430.0	95	2079	1552.1	526.9	162	1604	1384.1	219.9
29	1463	1544.2	-81.2	96	2276	1590.1	685.9	163	1585	1345.9	239.1
30	991	1571.9	-580.9	97	1671	1621.4	49.6	164	1471	1312.5	158.5
31	892	1588.4	-696.4	98	2307	1643.3	663.7	165	898	1284.2	-386.2
32	1081	1590.7	-509.7	99	1740	1653.9	86.1	166	1591	1262.0	329.0
33	1619	1578.0	41.0	100	1384	1652.0	-268.0	167	1560	1246.4	313.6
34	1618	1552.9	65.1	101	1744	1638.1	105.9	168	1484	1237.3	246.7
35	1327	1519.9	-192.9	102	2003	1613.2	389.8	169	1795	1235.6	559.4
36	2263	1485.5	777.5	103	1791	1579.6	211.4	170	938	1240.5	-302.5
37	1728	1455.8	272.2	104	1804	1540.4	263.6	171	1186	1252.4	-66.4
38	1778	1436.6	341.4	105	2008	1498.6	509.4	172	1003	1270.7	-267.7
39	1109	1431.2	-322.2	106	2072	1457.8	614.2	173	1037	1294.8	-257.8
40	1875	1440.8	434.2	107	829	1421.4	-592.4	174	1172	1324.6	-152.6
41	1923	1463.7	459.3	108	789	1392.2	-603.2	175	1675	1358.9	316.1
42	1455	1495.5	-40.5	109	1189	1372.4	-183.4	176	1423	1397.3	25.7
43	1843	1531.1	311.9	110	1260	1363.7	-103.7	177	1323	1439.0	-116.0
44	1071	1564.1	-493.1	111	950	1366.5	-416.5	178	981	1483.0	-502.0
45	2176	1589.1	586.9	112	1139	1380.9	-241.9	179	1687	1528.8	158.2
46	1543	1601.2	-58.2	113	1223	1405.6	-182.6	180	1278	1575.4	-297.4
47	1631	1599.0	32.0	114	1460	1438.7	21.3	181	1327	1622.0	-295.0
48	1791	1582.5	208.5	115	1448	1477.8	-29.8	182	1733	1668.0	65.0
49	1395	1554.6	-159.6	116	1567	1520.2	46.8	183	1521	1712.6	-191.6
50	1463	1519.5	-56.5	117	1703	1562.8	140.2	184	2471	1755.2	715.8
51	1433	1483.3	-50.3	118	1179	1602.7	-423.7	185	1676	1795.2	-119.2
52	1536	1451.4	84.6	119	1851	1637.3	213.7	186	1511	1832.1	-321.1
53	1355	1429.4	-74.4	120	1633	1664.3	-31.3	187	1368	1865.4	-497.4
54	1435	1420.0	15.0	121	2424	1682.0	742.0	188	1359	1894.9	-535.9
55	1428	1425.6	2.4	122	1992	1689.3	302.7	189	1441	1920.2	-479.2
56	1781	1444.7	336.3	123	1499	1685.7	-186.7	190	1763	1941.1	-178.1
57	1527	1474.5	52.5	124	1639	1671.5	-32.5	191	1779	1957.4	-178.4
58	1544	1510.8	33.2	125	1232	1647.7	-415.7	192	2431	1969.1	461.9
59	774	1548.0	-774.0	126	1441	1615.9	-174.9	193	1928	1976.1	-48.1
60	1163	1580.6	-417.6	127	1468	1577.9	-109.9	194	1935	1978.6	-43.6
61	2350	1603.8	746.2	128	1351	1535.9	-184.9	195	2095	1976.5	118.5
62	1696	1614.8	81.2	129	1175	1492.4	-317.4	196	2338	1969.9	368.1
63	1920	1611.0	309.0	130	879	1449.9	-570.9	197	1985	1959.1	25.9
64	1570	1594.4	-24.4	131	1469	1410.7	58.3	198	2628	1944.4	683.6
65	1780	1565.5	214.5	132	1327	1376.9	-49.9	199	1791	1925.8	-134.8
66	1535	1529.9	5.1	133	1431	1350.2	80.8	200	3150	1903.7	1246.3

TABLE 5-55. CONTINUED.

NUM	OBS	COMP	RESID	NUM	OBS	COMP	RESID	NUM	OBS	COMP	RESID
201	2927	1878.3	1048.7	235	514	666.5	-152.5	269	118	312.8	-194.8
202	2975	1849.8	1125.2	236	523	644.7	-121.7	270	130	309.4	-179.4
203	2554	1818.7	735.3	237	266	623.9	-357.9	271	231	306.1	-75.1
204	1548	1785.2	-237.2	238	345	604.2	-259.2	272	487	303.0	184.0
205	1414	1749.5	-335.5	239	782	585.4	196.6	273	309	300.1	8.9
206	1744	1712.0	32.0	240	548	567.5	-19.5	274	634	297.3	336.7
207	1354	1672.9	-318.9	241	546	550.5	-4.5	275	631	294.6	336.4
208	1378	1632.6	-254.6	242	265	534.4	-269.4	276	352	292.1	59.9
209	1407	1591.2	-184.2	243	247	519.1	-272.1	277	553	289.7	263.3
210	1258	1549.1	-291.1	244	704	504.6	199.4	278	337	287.5	49.5
211	1169	1506.4	-337.4	245	461	490.8	-29.8	279	382	285.3	96.7
212	1231	1463.4	-232.4	246	999	477.8	521.2	280	651	283.3	367.7
213	736	1420.3	-684.3	247	640	465.5	174.5	281	324	281.3	42.7
214	1009	1377.3	-368.3	248	174	453.8	-279.8	282	212	279.5	-67.5
215	1379	1334.5	44.5	249	159	442.7	-283.7	283	317	277.7	39.3
216	1539	1292.1	246.9	250	193	432.2	-239.2	284	184	276.0	-92.0
217	1349	1250.2	98.8	251	463	422.3	40.7	285	41	274.4	-233.4
218	1092	1208.9	-116.9	252	330	412.9	-82.9	286	454	272.9	181.1
219	1020	1168.5	-148.5	253	356	404.1	-48.1	287	352	271.5	80.5
220	1109	1128.9	-19.9	254	380	395.7	-15.7	288	434	270.1	163.9
221	872	1090.2	-218.2	255	595	387.8	207.2	289	302	268.7	33.3
222	467	1052.5	-585.5	256	611	380.3	230.7	290	219	267.5	-48.5
223	473	1015.9	-542.9	257	200	373.2	-173.2	291	211	266.3	-55.3
224	787	980.4	-193.4	258	432	366.5	65.5	292	216	265.1	-49.1
225	610	946.0	-336.0	259	598	360.1	237.9	293	305	264.0	41.0
226	1243	912.8	330.2	260	754	354.1	399.9	294	184	263.0	-79.0
227	1215	880.7	334.3	261	199	348.5	-149.5	295	247	261.9	-14.9
228	948	849.9	98.1	262	93	343.1	-250.1	296	234	261.0	-27.0
229	517	820.2	-303.2	263	138	338.0	-200.0	297	165	260.1	-95.1
230	779	791.7	-12.7	264	401	333.2	67.8	298	294	259.2	34.8
231	757	764.4	-7.4	265	525	328.7	196.3	299	440	258.3	181.7
232	510	738.2	-228.2	266	264	324.4	-60.4	300	766	257.5	508.5
233	510	713.2	-203.2	267	439	320.3	118.7				
234	418	689.3	-271.3	268	336	316.5	19.5				

TABLE 5-56
ZC 3158: SUPPLEMENTAL STATISTICAL INFORMATION

VARIANCE/CO-VARIANCE MATRIX

DIAM	PREI	POST	TIME	VELO
4.209E¯16	1.051E¯07	-1.973E¯07	-4.960E¯10	2.342E¯12
1.051E¯07	8.947E02	8.525E01	-1.498E01	3.970E¯02
-1.973E¯07	8.525E01	2.254E03	-3.618E01	1.069E¯01
-4.960E¯10	-1.498E01	-3.618E01	3.897E00	-1.164E¯02
2.342E¯12	3.970E¯02	1.069E¯01	-1.164E¯02	4.462E¯05

CORRELATION MATRIX

	DIAM	PREI	POST	TIME	VELO
DIAM	1.000000	0.548987	-0.891538	0.642859	-0.673466
PREI	0.548987	1.000000	-0.110924	-0.283453	0.243923
POST	-0.891538	-0.110924	1.000000	-0.918646	0.933638
TIME	0.642859	-0.283453	-0.918646	1.000000	-0.999159
VELO	-0.673466	0.243923	0.933638	-0.999159	1.000000

NUMERICAL RANGES OF THE PARTIAL DERIVATIVES

	MAXIMUM	MINIMUM
DIAM	4.690E09	-4.917E09
PREI	1.367E00	2.017E¯02
POST	9.798E¯01	-3.667E¯01
TIME	4.488E01	-4.674E01
VELO	2.702E04	-2.786E04

This then gives a linear diameter for the star of approximately 6 solar radii. This is entirely consistent with the spectral and luminosity characteristics of ZC3158. Again, assuming a distance of 31 parsecs, an F5 star would have an absolute V magnitude of -0.4. This value, according to Allen (1963), would place it between luminosity classes II and III. Also, interpolating from Allen's tables, an F5 star of this luminosity class would have a diameter of roughly 8 solar diameters. Hence, a "ballpark" estimate of the anticipated diameter of the star shows the observationally determined angular diameter to be in good agreement with what might have been inferred from the previously known physical properties of ZC3158.

The NOISEPLOT of the raw data is presented as Figure 5-117. As can be seen in the RAWPLOT itself, the dispersion of the residual amplitudes about the mean intensity level is quite high. This is to be expected for photometric data whose dominant noise source is, as in this case, determined by photon arrival statistics.

The POWERPLOT of the comparative power spectra (Figure 5-118) does indeed show that the background sky level had no significant effect on the observations. The flat nature of the star-plus-sky power spectrum is typical of photon shot noise. The only low frequency components in the occultation power spectrum of any significance are due to diffraction fringing effects,

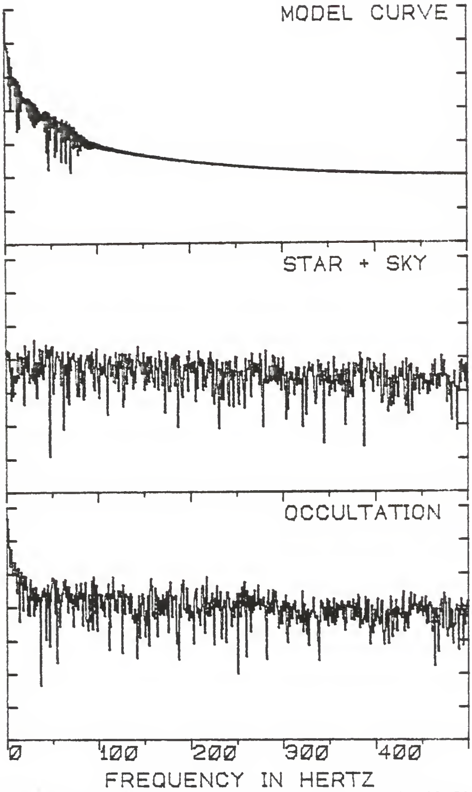

Figure 5-118. POWERPLOT of the occultation of ZC3158.

with no contributions from atmospheric scintillation or transparency variations.

The Coordinated Universal Time of geometrical occultation was 00:06:42.333 (0.004).

ZC0835

The night of March 11, 1984 U. T., gave rise to four occultations which were observed from RHO. The first of these, that of ZC0835, occurred at approximately 00:30 U. T. and hence was observed 25 minutes before the end of astronomical twilight. Though the sky was not yet completely dark, the brightness of this star (mV=6.92) led to a S+N/N ratio of 11.81 with a Johnson B filter. The seeing was quite good and enabled the use of the small "J" diaphragm, as noted in the occultation summary (Table 5-57).

The photoelectric record of the event is presented in Figure 5-119. The rather clean signal and precipitous drop are attributed to the good seeing, small background noise, and the brightness of the star. The integration plot (Figure 5-120) is remarkably clean and attests to the steadiness of the sky over time-scales of tenths of seconds to seconds. There is no indication of stellar duplicity in this figure.

The parametric solution obtained for the 200 milliseconds of observational data fit by the DC procedure, given in Table 5-58, did give rise to a value for the stellar diameter. However, the diameter determined is very close to the lower limit of detectability due to both the finite

TABLE 5-57
ZC0835: LUNAR OCCULTATION SUMMARY

STELLAR AND OBSERVING INFORMATION

Star: ZC0835, (SAO 077252, DM +24 0854)
RA: 053232 DEC: +243711 mV: 6.92 Sp: B8
Filter: B Diaphragm: J Gain: B9 Voltage: 1200

LUNAR INFORMATION

Surface Illumination:	53 percent
Elongation from Sun:	93 degrees
Altitude Above Horizon:	77 degrees
Lunar Limb Distance:	374852 kilometers
Predicted Shadow Velocity:	385.64 meters/sec.
Predicted Angular Rate:	0.2345 arcsec/sec.

EVENT INFORMATION

Date:	March 11, 1984	UT of Event:	00:39:30
USNO V/O Code:	17	HA of Event:	+130138
Position Angle:	33.7	Cusp Angle:	36N
Contact Angle:	+47.3	Watts Angle:	35.2

MODEL PARAMETERS

Number of Data Points:	201
Number of Grid Points:	256
Number of Spectral Regions:	42
Width of Spectral Regions:	50 Angstroms
Limb Darkening Coefficient:	0.5
Effective Stellar Temperature:	12000 K

SOLUTIONS

Stellar Diameter (ams):	1.08 (1.46)
Time: (relative to Bin 0):	2238.1 (0.6)
Pre-Event Signal:	2441.7 (15.0)
Background Sky Level:	791.1 (18.0)
Velocity (meters/sec.):	388.0 (5.5)
Lunar Limb Slope (degrees):	-3.15 (0.82)
U.T. of Occultation:	00:39:28.8 (0.1)

PHOTOMETRIC NOISE INFORMATION

Sum-of-Squares of Residuals:	4660483
Sigma (Standard Error):	153.6513
Normalized Standard Error:	0.092524
Photometric (S+N)/N Ratio:	11.80804
Intensity Change/Background:	2.083527
Change in Magnitude:	1.222619

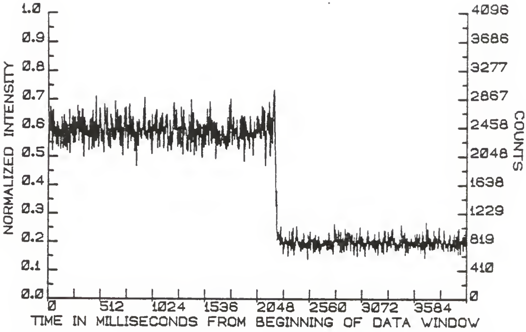

Figure 5-119. RAWPLOT of the occultation of ZC0835.

Figure 5-120. INTPLOT of the occultation of ZC0835.

TABLE 5-58
ZC0835: OBSERVATIONS, COMPUTED VALUES, AND RESIDUALS FROM BIN 2120

NUM	OBS	COMP	RESID	NUM	OBS	COMP	RESID	NUM	OBS	COMP	RESID
0	2488	2443.7	44.3	67	2487	2476.3	10.7	134	857	898.2	-41.2
1	2481	2451.3	29.7	68	2561	2392.0	169.0	135	957	890.8	66.2
2	2403	2457.7	-54.7	69	2598	2309.8	288.2	136	847	884.1	-37.1
3	2303	2459.4	-156.4	70	2472	2236.0	236.0	137	839	878.0	-39.0
4	2330	2455.3	-125.3	71	2540	2176.4	363.6	138	843	872.3	-29.3
5	2167	2447.1	-280.1	72	2413	2135.2	277.8	139	916	867.2	48.8
6	2145	2438.4	-293.4	73	2191	2115.5	75.5	140	885	862.4	22.6
7	1923	2433.4	-510.4	74	2103	2118.4	-15.4	141	1010	858.0	152.0
8	2141	2434.4	-293.4	75	2239	2143.7	95.3	142	768	854.0	-86.0
9	2021	2441.3	-420.3	76	2143	2189.8	-46.8	143	879	850.3	28.7
10	2163	2451.0	-288.0	77	2474	2253.9	220.1	144	828	846.9	-18.9
11	2123	2459.4	-336.4	78	2280	2332.4	-52.4	145	807	843.7	-36.7
12	2372	2462.8	-90.8	79	2463	2421.2	41.8	146	784	840.8	-56.8
13	2319	2459.8	-140.8	80	2907	2515.8	391.2	147	824	838.1	-14.1
14	2485	2451.7	33.3	81	2861	2611.8	249.2	148	871	835.5	35.5
15	2341	2442.2	-101.2	82	2769	2705.0	64.0	149	1007	833.2	173.8
16	2224	2435.3	-211.3	83	2794	2791.6	2.4	150	874	831.0	43.0
17	2219	2434.1	-215.1	84	2782	2868.5	-86.5	151	767	829.0	-62.0
18	2138	2439.2	-301.2	85	2855	2933.2	-78.2	152	792	827.1	-35.1
19	2472	2448.4	23.6	86	2832	2983.6	-151.6	153	712	825.3	-113.3
20	2718	2457.9	260.1	87	2905	3018.6	-113.6	154	871	823.7	47.3
21	2703	2463.5	239.5	88	2860	3037.6	-177.6	155	816	822.2	-6.2
22	2547	2462.6	84.4	89	3040	3040.6	-0.6	156	889	820.7	68.3
23	2512	2454.8	57.2	90	3144	3028.2	115.8	157	839	819.4	19.6
24	2690	2443.0	247.0	91	2997	3001.1	-4.1	158	952	818.2	133.8
25	2651	2431.4	219.6	92	2978	2960.6	17.4	159	1036	817.0	219.0
26	2837	2424.8	412.2	93	3040	2908.1	131.9	160	840	815.9	24.1
27	2672	2426.6	245.4	94	3071	2845.3	225.7	161	665	814.9	-149.9
28	2280	2437.4	-157.4	95	2846	2773.7	72.3	162	799	814.0	-15.0
29	2499	2454.7	44.3	96	2789	2695.1	93.9	163	786	813.1	-27.1
30	2520	2473.8	46.2	97	2899	2611.1	287.9	164	789	812.3	-23.3
31	2571	2488.4	82.6	98	2683	2523.3	159.7	165	862	811.5	50.5
32	2638	2493.6	144.4	99	2531	2433.0	98.0	166	840	810.8	29.2
33	2419	2486.3	-67.3	100	2160	2341.6	-181.6	167	825	810.1	14.9
34	2499	2467.2	31.8	101	1975	2250.2	-275.2	168	768	809.4	-41.4
35	2443	2439.9	3.1	102	2100	2159.8	-59.8	169	776	808.8	-32.8
36	2560	2410.8	149.2	103	2015	2071.2	-56.2	170	829	808.2	20.8
37	2549	2387.3	161.7	104	1895	1985.1	-90.1	171	861	807.6	53.4
38	2215	2376.0	-161.0	105	1768	1902.2	-134.2	172	929	807.0	122.0
39	2373	2380.7	-7.7	106	1715	1822.7	-107.7	173	888	806.5	81.5
40	2467	2402.2	64.8	107	1865	1747.0	118.0	174	1001	805.9	195.1
41	2480	2437.2	42.8	108	1955	1675.3	279.7	175	871	805.4	65.6
42	2630	2479.5	150.5	109	1746	1607.7	138.3	176	820	805.0	15.0
43	2823	2520.9	302.1	110	1529	1544.3	-15.3	177	839	804.5	34.5
44	2626	2552.9	73.1	111	1335	1485.0	-150.0	178	912	804.1	107.9
45	2647	2568.8	78.2	112	1206	1429.8	-223.8	179	802	803.7	-1.7
46	2558	2564.3	-6.3	113	1093	1378.5	-285.5	180	767	803.3	-36.3
47	2627	2539.0	88.0	114	1419	1331.0	88.0	181	680	803.0	-123.0
48	2419	2496.1	-77.1	115	1546	1287.1	258.9	182	799	802.7	-3.7
49	2473	2441.9	31.1	116	1368	1246.7	121.3	183	649	802.4	-153.4
50	2135	2384.8	-249.8	117	1238	1209.5	28.5	184	703	802.1	-99.1
51	2080	2333.7	-253.7	118	1061	1175.3	-114.3	185	673	801.8	-128.8
52	2140	2296.9	-156.9	119	1186	1144.0	42.0	186	726	801.6	-75.6
53	2240	2280.5	-40.5	120	1021	1115.3	-94.3	187	806	801.3	4.7
54	2360	2287.8	72.2	121	1047	1089.0	-42.0	188	718	801.0	-83.0
55	2060	2318.7	-258.7	122	974	1065.0	-91.0	189	858	800.8	57.2
56	2496	2370.0	126.0	123	839	1043.1	-204.1	190	899	800.5	98.5
57	2247	2435.6	-188.6	124	1001	1023.1	-22.1	191	723	800.3	-77.3
58	2193	2508.0	-315.0	125	966	1004.9	-38.9	192	665	800.0	-135.0
59	2375	2578.4	-203.4	126	954	988.2	-34.2	193	823	799.8	23.2
60	2928	2638.8	289.2	127	867	973.1	-106.1	194	953	799.6	153.4
61	2986	2682.2	303.8	128	954	959.2	-5.2	195	750	799.4	-49.4
62	2780	2703.6	76.4	129	940	946.6	-6.6	196	714	799.2	-85.2
63	2599	2700.5	-101.5	130	1113	935.1	177.9	197	838	799.0	39.0
64	2483	2672.8	-189.8	131	917	924.6	-7.6	198	746	798.9	-52.9
65	2411	2623.0	-212.0	132	1056	915.0	141.0	199	813	798.7	14.3
66	2516	2555.5	-39.5	133	938	906.2	31.8	200	711	798.6	-87.6

aperture of the telescope and the optical bandpass. This is reflected in the formal error of the determined angular diameter which was 1.08 (+/- 1.46) milliseconds of arc.

The low noise level, in comparison to the stellar signal intensity, resulted in a very good fit to the observational data. This can be seen in the FITPLOT, Figure 5-121. The PDPLOT of the solution curve, Figure 5-122, indicates that the regions of high sensitivity to parametric variation were well considered in the solution. The numerical ranges of the partial derivatives are listed, along with the other usual supplementary statistics, in Table 5-69.

The distribution function of the residual intensities is shown in the NOISEPLOT, Figure 5-21. The purely Gaussian nature of the distribution bespeaks the dominance of the stellar signal over the unimportant sky background.

The comparative power spectra, shown in Figure 5-124, are additional indicators of the quality of this observation. The frequency components of the occultation power spectrum dominates those of the star-plus-sky signal to frequencies in excess of 100 Hertz.

The determination of the Coordinated Universal Time of geometrical occultation to high precision was hampered by the inability to successfully decode the WWVB time signal, and as previously noted, this can often be a problem until well after sunset. As a result, a post-occultation calibration of the SPICA-IV/LODAS clock, nearly an hour after the time of the event, degraded the quality of the event timing. The

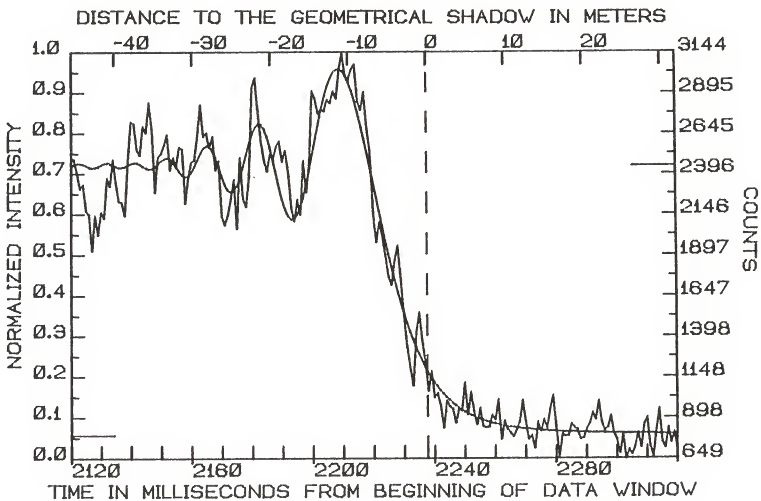

Figure 5-121. FITPLOT of the occultation of ZC0835.

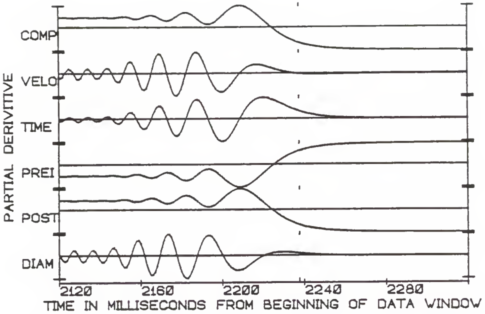

Figure 5-122. PDPLOT of the occultation of ZC0835.

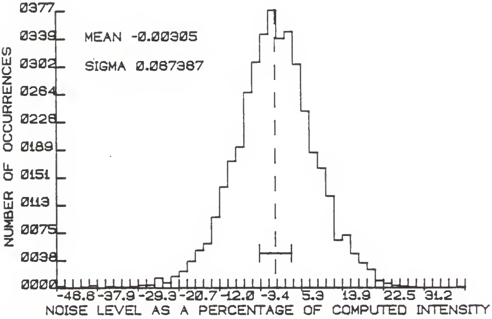

Figure 5-123. NOISEPLOT of the occultation of ZC0835.

TABLE 5-59
ZC0835: SUPPLEMENTAL STATISTICAL INFORMATION

VARIANCE/CO-VARIANCE MATRIX

DIAM	PREI	POST	TIME	VELO
5.021E¯17	1.821E¯08	-1.885E¯08	-3.245E¯10	3.783E¯12
1.821E¯08	2.259E02	1.218E01	-2.286E00	1.933E¯02
-1.885E¯08	1.218E01	3.239E02	-2.984E00	2.444E¯02
-3.245E¯10	-2.286E00	-2.984E00	3.202E¯01	-2.679E¯03
3.783E¯12	1.933E¯02	2.444E¯02	-2.679E¯03	3.033E¯05

CORRELATION MATRIX

	DIAM	PREI	POST	TIME	VELO
DIAM	1.000000	0.749272	-0.771171	0.169356	-0.150545
PREI	0.749272	1.000000	-0.156314	-0.523365	0.539440
POST	-0.771171	-0.156314	1.000000	-0.756773	0.744181
TIME	0.169356	-0.523365	-0.756773	1.000000	-0.999818
VELO	-0.150545	0.539440	0.744181	-0.999818	1.000000

NUMERICAL RANGES OF THE PARTIAL DERIVATIVES

	MAXIMUM	MINIMUM
DIAM	4.426E09	-4.589E09
PREI	1.363E00	4.073E¯03
POST	9.959E¯01	-3.630E¯01
TIME	9.160E01	-9.600E01
VELO	1.081E04	-1.121E04

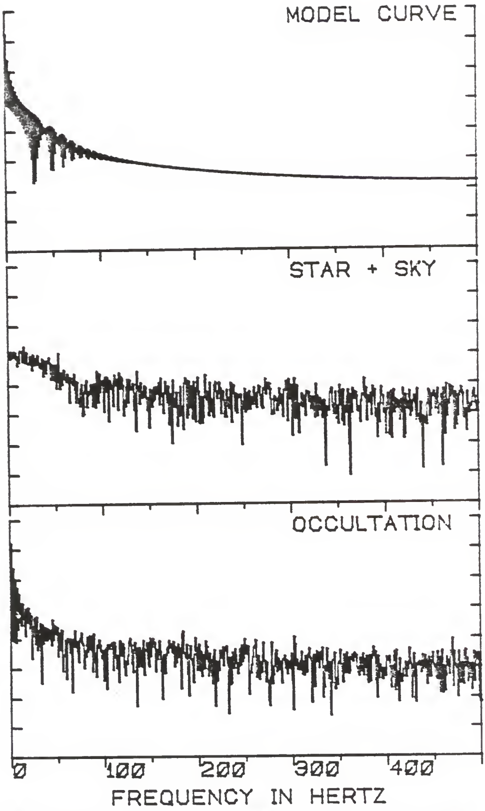

Figure 5-124. POWERPLOT of the occultation of ZC0835.

time of geometrical occultation was determined to be 00:39:28.8 (+/- 0.1 seconds) C. U. T.

X07145

The moderately bright (mV=7.4) K0 star, X07145, was occulted 49 minutes after the ZC0835 event. The good photometric conditions which were present at the time of the earlier event continued to prevail, as they did for the two events which were to follow. As a result, the plot of the raw photometric data (Figure 5-119) was extremely similar to that of ZC0835. The S+N/N ratio was not as good, since this star was roughly one half of a magnitude fainter, but was still a very substantial 7.74.

This observation was made with a Johnson V filter (as noted in Table 5-60) in accord with the spectral type of the star. The integration plot of the event (Figure 5-126) was practically free of complicating effects, which sometimes arise under noisy conditions. The linearity of the ascending and descending branches of the plotted integrated intensity function precludes the possibility of "wide" stellar duplicity.

The 200 milliseconds of data used in the DC fitting process are listed in Table 5-61, along with the computed intensities and their residuals. The FITPLOT of the observed and computed intensity curves is presented as Figure 5-127. The determined L-rate for this event of 528.9 (+/- 11.3) meters per second caused the time-scale of this event to be 56 percent faster than that of the ZC0835 event. Thus, there

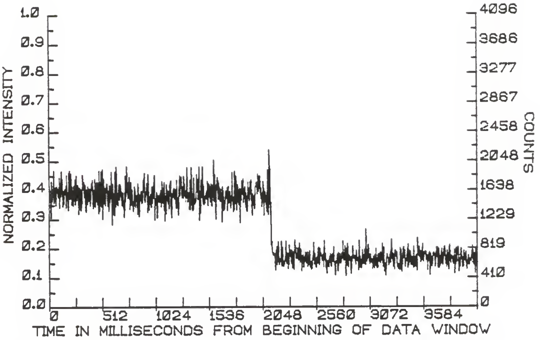

Figure 5-125. RAWPLOT of the occultation of X07145.

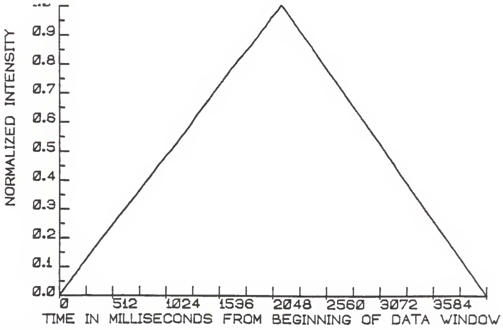

Figure 5-126. INTPLOT of the occultation of X07145.

TABLE 5-60
X07145: LUNAR OCCULTATION SUMMARY

STELLAR AND OBSERVING INFORMATION

Star: X07145 (SAO 077276, DM +24 0868)
RA: 053404 DEC: +241655 mV: 7.4 Sp: K0
Filter: V Diaphram: J Gain: B11+ Voltage: 1100

LUNAR INFORMATION

Surface Illumination:	53 percent
Elongation from Sun:	93 degrees
Altitude Above Horizon:	67 degrees
Lunar Limb Distance:	374996 kilometers
Predicted Shadow Velocity:	494.14 meters/sec.
Predicted Angular Rate:	0.2718 arcsec/sec.

EVENT INFORMATION

Date: March 11, 1984		UT of Event:	01:28:06
USNO V/O Code:	17	HA of Event:	+245103
Position Angle:	125.2	Cusp Angle:	52S
Contact Angle:	-40.7	Watts Angle:	126.6

MODEL PARAMETERS

Number of Data Points:	201
Number of Grid Points:	256
Number of Spectral Regions:	53
Width of Spectral Regions:	50 Angstroms
Limb Darkening Coefficient:	0.5
Effective Stellar Temperature:	5100K

SOLUTIONS

Stellar Diameter (ams):	Point Source	
Time: (relative to Bin 0):	2138.8	(0.8)
Pre-Event Signal:	1547.2	(13.0)
Background Sky Level:	658.7	(14.8)
Velocity (meters/sec.):	528.9	(11.3)
Lunar Limb Slope (degrees):	-10.4	(1.3)
U.T. of Occultation:	01:28:05.604	(0.006)

PHOTOMETRIC NOISE INFORMATION

Sum-of-Squares of Residuals:	3497400
Sigma (Standard Error):	131.9
Normalized Standard Error:	0.14844
Photometric (S+N)/N Ratio:	7.7369
Intensity Change/Background:	1.3491
Change in Magnitude:	0.92725

TABLE 5-61
X07145: OBSERVATIONS, COMPUTED VALUES, AND RESIDUALS FROM BIN 2025

NUM	OBS	COMP	RESID	NUM	OBS	COMP	RESID	NUM	OBS	COMP	RESID
0	1885	1549.2	335.8	67	1438	1693.5	-255.5	134	735	690.3	44.7
1	1539	1547.3	-8.3	68	1504	1699.3	-195.3	135	587	688.0	-101.0
2	1609	1547.7	61.3	69	1679	1684.0	-5.0	136	797	686.0	111.0
3	1703	1550.4	152.6	70	1928	1649.7	278.3	137	677	684.1	-7.1
4	1791	1553.1	237.9	71	1881	1601.1	279.9	138	628	682.5	-54.5
5	1680	1553.0	127.0	72	1518	1544.4	-26.4	139	655	680.9	-25.9
6	1520	1550.0	-30.0	73	1673	1486.7	186.3	140	672	679.5	-7.5
7	1527	1546.6	-19.6	74	1703	1434.9	268.1	141	819	678.2	140.8
8	1718	1545.8	172.2	75	1446	1394.7	51.3	142	597	677.0	-80.0
9	1574	1548.6	25.4	76	1409	1370.4	38.6	143	641	675.9	-34.9
10	1671	1552.8	118.2	77	1232	1364.2	-132.2	144	739	674.9	64.1
11	1347	1555.0	-208.0	78	1299	1376.7	-77.7	145	742	674.0	68.0
12	1256	1553.1	-297.1	79	1401	1406.4	-5.4	146	519	673.1	-154.1
13	1626	1548.6	77.4	80	1676	1450.8	225.2	147	675	672.3	2.7
14	1416	1545.0	-129.0	81	1560	1506.0	54.0	148	712	671.6	40.4
15	1447	1545.4	-98.4	82	1484	1567.9	-83.9	149	715	671.0	44.0
16	1511	1549.5	-38.5	83	1438	1631.9	-193.9	150	787	670.4	116.6
17	1701	1554.3	146.7	84	1433	1694.0	-261.0	151	759	669.8	89.2
18	1409	1556.1	-147.1	85	2038	1750.5	287.5	152	740	669.3	70.7
19	1359	1553.4	-194.4	86	2201	1798.3	402.7	153	574	668.8	-94.8
20	1387	1548.0	-161.0	87	2143	1835.3	307.7	154	781	668.4	112.6
21	1337	1544.0	-207.0	88	1956	1860.0	96.0	155	574	667.9	-93.9
22	1458	1544.5	-86.5	89	1516	1871.9	-355.9	156	687	667.5	19.5
23	1331	1549.5	-218.5	90	1918	1870.9	47.1	157	828	667.1	160.9
24	1555	1555.8	-0.8	91	2015	1857.8	157.2	158	847	666.8	180.2
25	1451	1558.9	-107.9	92	1937	1833.5	103.5	159	705	666.4	38.6
26	1477	1556.2	-79.2	93	1936	1799.4	136.6	160	507	666.1	-159.1
27	1571	1548.9	22.1	94	1931	1757.1	173.9	161	558	665.8	-107.8
28	1520	1541.3	-21.3	95	1783	1708.2	74.8	162	591	665.5	-74.5
29	1543	1538.4	4.6	96	1732	1654.4	77.6	163	749	665.2	83.8
30	1760	1543.0	217.0	97	1506	1597.0	-91.0	164	897	664.9	232.1
31	1552	1553.3	-1.3	98	1448	1537.7	-89.7	165	593	664.7	-71.7
32	1503	1564.0	-61.0	99	1484	1477.6	6.4	166	709	664.5	44.5
33	1589	1569.1	19.9	100	1471	1417.8	53.2	167	583	664.3	-81.3
34	1647	1564.9	82.1	101	1356	1359.2	-3.2	168	697	664.1	32.9
35	1652	1552.2	99.8	102	1455	1302.5	152.5	169	617	664.0	-47.0
36	1408	1536.5	-128.5	103	1185	1248.2	-63.2	170	728	663.8	64.2
37	1388	1525.2	-137.2	104	995	1196.8	-201.8	171	557	663.6	-106.6
38	1291	1524.5	-233.5	105	1009	1148.6	-139.6	172	675	663.4	11.6
39	1425	1535.9	-110.9	106	871	1103.5	-232.5	173	814	663.3	150.7
40	1613	1556.1	56.9	107	1079	1061.8	17.2	174	909	663.1	245.9
41	1735	1577.2	157.8	108	752	1023.4	-271.4	175	668	662.9	5.1
42	1629	1590.5	38.5	109	1160	988.2	171.8	176	613	662.8	-49.8
43	1565	1590.0	-25.0	110	909	956.1	-47.1	177	800	662.7	137.3
44	1381	1574.5	-193.5	111	891	927.0	-36.0	178	653	662.6	-9.6
45	1367	1548.3	-181.3	112	857	900.5	-43.5	179	644	662.5	-18.5
46	1507	1520.0	-13.0	113	915	876.7	38.3	180	472	662.4	-190.4
47	1363	1499.5	-136.5	114	785	855.2	-70.2	181	577	662.3	-85.3
48	1312	1494.3	-182.3	115	749	835.8	-86.8	182	597	662.2	-65.2
49	1424	1507.2	-83.2	116	864	818.5	45.5	183	622	662.1	-40.1
50	1615	1535.6	79.4	117	870	802.9	67.1	184	671	662.0	9.0
51	1927	1571.9	355.1	118	758	789.0	-31.0	185	689	661.9	27.1
52	1692	1606.0	86.0	119	772	776.6	-4.6	186	631	661.8	-30.8
53	1419	1628.1	-209.1	120	736	765.4	-29.4	187	638	661.7	-23.7
54	1544	1631.6	-87.6	121	695	755.5	-60.5	188	613	661.6	-48.6
55	1740	1614.7	125.3	122	719	746.6	-27.6	189	643	661.5	-18.5
56	1540	1580.8	-40.8	123	841	738.6	102.4	190	673	661.5	11.5
57	1401	1537.4	-136.4	124	791	731.5	59.5	191	677	661.4	15.6
58	1463	1494.4	-31.4	125	719	725.1	-6.1	192	569	661.3	-92.3
59	1481	1461.6	19.4	126	752	719.4	32.6	193	461	661.3	-200.3
60	1620	1446.5	173.5	127	595	714.3	-119.3	194	644	661.2	-17.2
61	1484	1452.7	31.3	128	717	709.7	7.3	195	595	661.1	-66.1
62	1405	1479.7	-74.7	129	712	705.6	6.4	196	731	661.1	69.9
63	1444	1522.8	-78.8	130	755	701.8	53.2	197	663	661.0	2.0
64	1721	1574.4	146.6	131	840	698.5	141.5	198	679	661.0	18.0
65	1611	1625.5	-14.5	132	603	695.5	-92.5	199	827	660.9	166.1
66	1338	1667.5	-329.5	133	829	692.8	136.2	200	661	660.9	0.1

were fewer observed points per diffraction fringe than for the previous event. Nevertheless, the fit was quite good, as an examination of the FITPLOT will reveal. The variance/covariance and correlation matrices of the solution parameters are given in Table 5-62.

The PDPLOT for this event is shown as Figure 5-128. A small amount of numerical noise was present in the computation of the partial derivative of the intensity curve with respect to the angular diameter. This numerical noise, however, was present only in the partial derivatives for times early in the solution space. At those times, as is apparent in the PDPLOT, the intensity curve was very insensitive to changes in the diameter. Hence, in this case the numerical noise which arose did not adversely affect the final solution determination.

The best fit to the observations was for the intensity curve of a point source. Thus, the angular diameter of X07145 was below the capability of detection by the occultation method.

The distribution function of the residual amplitudes, seen in Figure 5-192, is similar to that previously shown for the previous event. In this case, due to a smaller stellar signal in comparison to a slightly more variable background, a Poisson tail can be seen in the distribution function.

The POWERPLOT (Figure 5-130) indicates that the frequency components that are of most importance in the

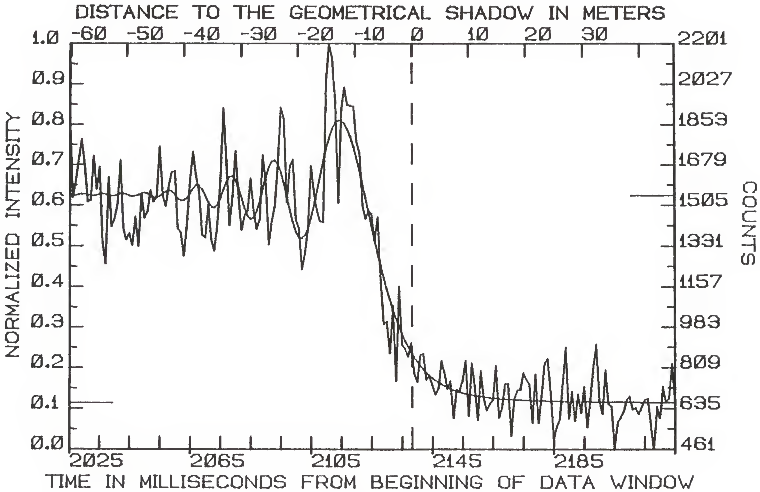

Figure 5-127. FITPLOT of the occultation of X07145.

TABLE 5-62
X07145: SUPPLEMENTAL STATISTICAL INFORMATION

VARIANCE/CO-VARIANCE MATRIX

DIAM	PREI	POST	TIME	VELO
1.430E¯16	2.593E¯08	-2.853E¯08	-4.964E¯10	8.640E¯12
2.593E¯08	1.703E02	4.570E00	-2.251E00	2.834E¯02
-2.853E¯08	4.570E00	2.231E02	-2.817E00	3.503E¯02
-4.964E¯10	-2.251E00	-2.817E00	5.799E¯01	-7.327E¯03
8.640E¯12	2.834E¯02	3.503E¯02	-7.327E¯03	1.271E¯04

CORRELATION MATRIX

	DIAM	PREI	POST	TIME	VELO
DIAM	1.000000	0.750746	-0.795461	0.161136	-0.153926
PREI	0.750746	1.000000	-0.197010	-0.523228	0.529208
POST	-0.795461	-0.197010	1.000000	-0.721394	0.716211
TIME	0.161136	-0.523228	-0.721394	1.000000	-0.999972
VELO	-0.153926	0.529208	0.716211	-0.999972	1.000000

NUMERICAL RANGES OF THE PARTIAL DERIVATIVES

	MAXIMUM	MINIMUM
DIAM	2.566E09	-2.506E09
PREI	1.365E00	2.485E¯03
POST	9.975E¯01	-3.653E¯01
TIME	6.013E01	-6.378E01
VELO	4.735E03	-4.868E03

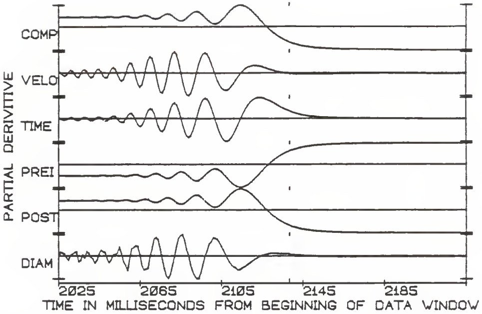

Figure 5-128. PDPLOT of the occultation of X07145.

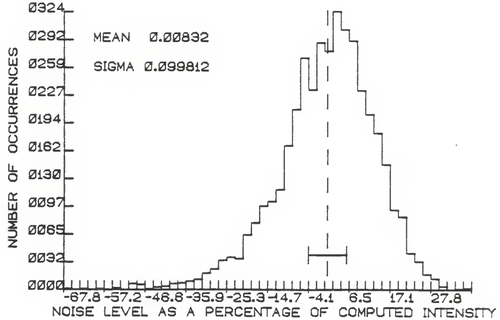

Figure 5-129. NOISEPLOT of the occultation of X07145.

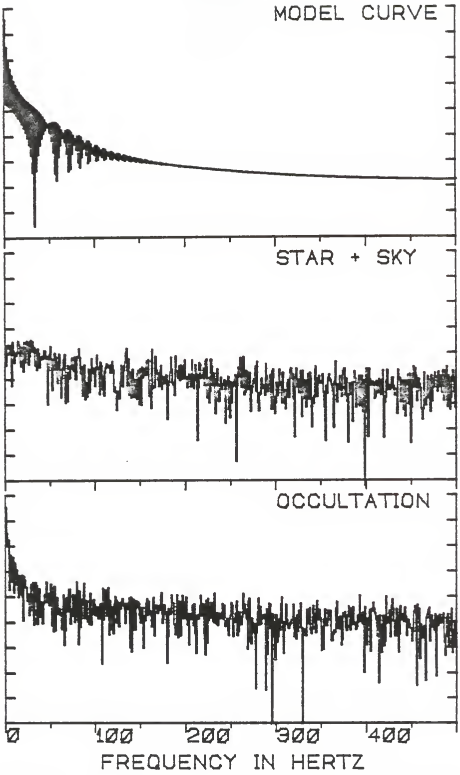

Figure 5-130. POWERPLOT of the occultation of X07145.

occultation spectral signature dominate over those in the star-plus-sky signal.

Geometrical occultation was found to have occurred at 01:28:05.604 (+/- 0.006 seconds) Coordinated Universal Time.

X07202

The third event observed on the night of March 11, 1983 U. T., was the disappearance of X07202. This K2 star was substantially fainter (mV=8.21) than either of the stars previously observed on that night. The lesser brightness of this star in comparison to either X07145 or ZC0835 and a consequently poorer S+N/N ratio of 3.07 caused the derived solution to be of lower quality.

The raw photometric data are presented in Figure 5-131. The smaller change from pre-occultation to post-occultation signal intensity is rather obvious. Although the photometric conditions throughout the night remained virtually unchanged, the ascending branch of the integration plot (see Figure 5-132) does indicate that the sky became less transparent for approximately one second just prior to the event. This behavior, however, did not seem to persist at the time of the event itself. The integration plot also shows no evidence of "wide" stellar duplicity.

The observed and computed intensity curves are shown in Figure 5-133. Two hundred milliseconds of data were used in the DC fit. This seemed appropriate given the predicted L-rate of 633.40 meters/second. The observed L-rate, determined by the fitting process to be 1132 (+/-110)

TABLE 5-63
X07202: LUNAR OCCULTATION SUMMARY

STELLAR AND OBSERVING INFORMATION

Star: X07202, (SAO 077312, DM +24 0882)
RA: 053529 DEC: +242136 mV: 8.21 Sp: K2
Filter: V Diaphragm: J Gain: C8 Voltage: 1100

LUNAR INFORMATION

Surface Illumination:	53 percent
Elongation from Sun:	94 degrees
Altitude Above Horizon:	57 degrees
Lunar Limb Distance:	375321 kilometers
Predicted Shadow Velocity:	633.40 meters/sec.
Predicted Angular Rate:	0.3481 arcsec/sec.

EVENT INFORMATION

Date:	March 11, 1984	UT of Event:	02:15:30
USNO V/O Code:	15	HA of Event:	+362114
Position Angle:	111.1	Cusp Angle:	66S
Contact Angle:	-23.7	Watts Angle:	112.4

MODEL PARAMETERS

Number of Data Points:	201
Number of Grid Points:	256
Number of Spectral Regions:	53
Width of Spectral Regions:	50 Angstroms
Limb Darkening Coefficient:	0.5
Effective Stellar Temperature:	4700 K

SOLUTIONS

Stellar Diameter (ams):	Point Source
Time: (relative to Bin 0):	2224.3 (1.6)
Pre-Event Signal:	1679.6 (18.5)
Background Sky Level:	1299.7 (18.2)
Velocity (meters/sec.):	1132.1 (110.3)
Lunar Limb Slope (degrees):	-28.1 (10.0)
U.T. of Occultation:	02:15:30.366 (0.012)

PHOTOMETRIC NOISE INFORMATION

Sum-of-Squares of Residuals:	6706927
Sigma (Standard Error):	183.1246
Normalized Standard Error:	0.4821239
Photometric (S+N)/N Ratio:	3.074155
Intensity Change/Background:	0.292238
Change in Magnitude:	0.2783562

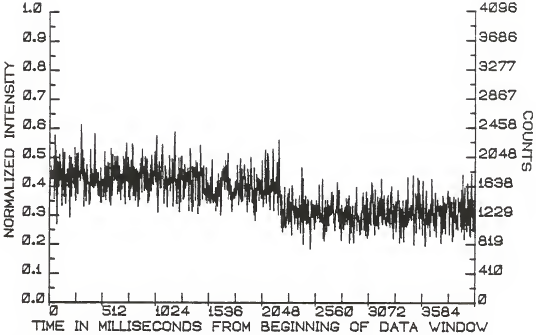

Figure 5-131. RAWPLOT of the occultation of X07202.

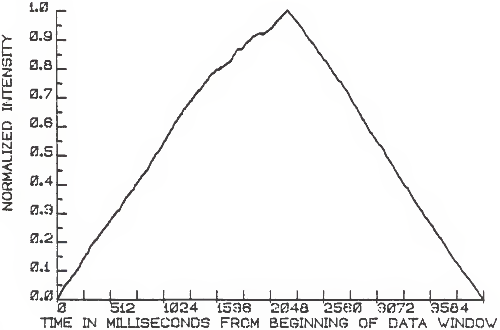

Figure 5-132. INTPLOT of the occultation of X07202.

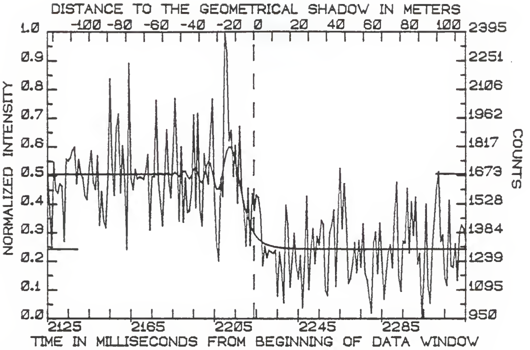

Figure 5-133. FITPLOT of the occultation of X07202.

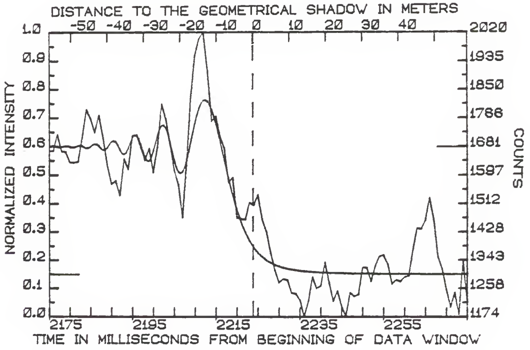

Figure 5-134. Detailed FITPLOT of the occultation of X0702 showing the raw fit to a smoothed data set.

meters/second, was considerably faster. Thus, the observed diffraction fringes were comprised of correspondingly fewer observed data points than expected. This, in addition to the lower signal intensity, was responsible for the somewhat larger statistical uncertainties in the solution parameters.

In order to allow a better visualization of the solution, the computed intensity curve is shown in detail (over 100 milliseconds only) in Figure 5-134. The observed data were subjected to 5-point smoothing before being plotted on the detailed computed curve.

As expected, no diameter was determined. The PDPLOT illustrating the partial derivatives of the computed intensity curve is shown in Figure 5-135. Unquestionably, the regions of sensitivity to parametric variation were well covered in the solution. The observed and computed intensities and the residuals are given in Table 5-64. The variance/covariance and correlation matrices of the solution parameters and the numerical ranges of the partial derivatives are contained in Table 5-65.

The NOISEPLOT (Figure 5-136), as expected, is a bit more skewed toward a Poisson distribution than that of the previous event. Also, not unexpectedly, the one sigma width of the distribution was increased to 11.98 percent.

The POWERPLOT for this event indicates that the power components of the star-plus-sky signal at low frequencies were comparable to that of the occultation signal itself. Thus, any type of Fourier smoothing was out of the question.

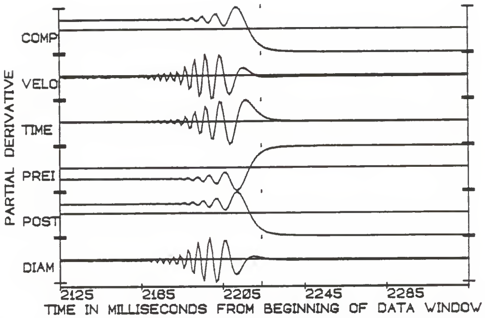

Figure 5-135. PDPLOT of the occultation of X07202.

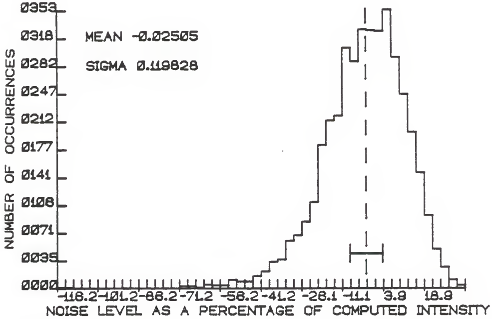

Figure 5-136. NOISEPLOT of the occultation of X07202.

TABLE 5-64
X07202: OBSERVATIONS, COMPUTED VALUES, AND RESIDUALS FROM BIN 2125

NUM	OBS	COMP	RESID	NUM	OBS	COMP	RESID	NUM	OBS	COMP	RESID
0	1684	1680.8	3.2	67	1487	1671.7	-184.7	134	1067	1300.9	-233.9
1	1513	1680.7	-167.7	68	1496	1657.0	-161.0	135	1382	1300.9	81.1
2	1321	1680.8	-359.8	69	1595	1674.3	-79.3	136	1421	1300.8	120.2
3	1740	1680.7	59.3	70	1979	1706.0	273.0	137	1499	1300.8	198.2
4	1601	1680.7	-79.7	71	1511	1714.3	-203.3	138	1112	1300.7	-188.7
5	1584	1680.7	-96.7	72	1987	1686.4	300.6	139	1453	1300.7	152.3
6	1633	1680.7	-47.7	73	1500	1648.5	-148.5	140	1708	1300.6	407.4
7	1620	1680.7	-60.7	74	1418	1637.6	-219.6	141	1405	1300.6	104.4
8	1341	1680.7	-339.7	75	1783	1666.2	116.8	142	1631	1300.5	330.5
9	1757	1680.7	76.3	76	1689	1713.0	-24.0	143	1448	1300.5	147.5
10	1747	1680.7	66.3	77	1631	1742.9	-111.9	144	1127	1300.5	-173.5
11	1763	1680.7	82.3	78	1872	1734.3	137.7	145	1151	1300.4	-149.4
12	1800	1680.7	119.3	79	2059	1692.0	367.0	146	1220	1300.4	-80.4
13	1815	1680.6	134.4	80	1556	1640.1	-84.1	147	1333	1300.4	32.6
14	1633	1680.8	-47.8	81	1325	1606.0	-281.0	148	1181	1300.4	-119.4
15	1753	1680.6	72.4	82	1241	1605.7	-364.7	149	1345	1300.3	44.7
16	1685	1680.7	4.3	83	1660	1639.1	20.9	150	1209	1300.3	-91.3
17	1664	1680.6	-16.6	84	1568	1693.4	-125.4	151	1428	1300.3	127.7
18	1571	1680.7	-109.7	85	2395	1750.6	644.4	152	1177	1300.3	-123.3
19	1552	1680.6	-128.6	86	2287	1795.0	492.0	153	1145	1300.2	-155.2
20	1711	1680.6	30.4	87	1847	1817.1	29.9	154	1059	1300.2	-241.2
21	1797	1680.7	116.3	88	1900	1814.0	86.0	155	979	1300.2	-321.2
22	1639	1680.5	-41.5	89	1669	1788.6	-119.6	156	1332	1300.2	31.8
23	1604	1680.7	-76.7	90	1825	1746.9	78.1	157	1386	1300.2	85.8
24	1771	1680.5	90.5	91	1534	1695.4	-161.4	158	1178	1300.2	-122.2
25	1423	1680.7	-257.7	92	1919	1640.5	278.5	159	1432	1300.1	131.9
26	1592	1680.6	-88.6	93	1598	1586.7	11.3	160	1252	1300.1	-48.1
27	1445	1680.6	-235.6	94	1503	1537.1	-34.1	161	1047	1300.1	-253.1
28	1410	1680.6	-270.6	95	1316	1493.5	-177.5	162	1167	1300.1	-133.1
29	1665	1680.7	-15.7	96	1608	1456.4	151.6	163	1281	1300.1	-19.1
30	2161	1680.5	480.5	97	1319	1425.6	-106.6	164	1323	1300.1	22.9
31	1728	1680.8	47.2	98	1581	1400.5	180.5	165	1206	1300.1	-94.1
32	1575	1680.5	-105.5	99	1497	1380.4	116.6	166	1479	1300.1	178.9
33	1912	1680.7	231.3	100	1575	1364.4	210.6	167	1637	1300.1	336.9
34	1983	1680.5	302.5	101	1561	1351.7	209.3	168	1157	1300.0	-143.0
35	1587	1680.7	-93.7	102	1476	1341.8	134.2	169	1088	1300.0	-212.0
36	1823	1680.4	142.6	103	1216	1333.9	-117.9	170	1343	1300.0	43.0
37	1647	1680.7	-33.7	104	1315	1327.8	-12.8	171	1331	1300.0	31.0
38	1300	1680.7	-380.7	105	1257	1322.9	-65.9	172	1607	1300.0	307.0
39	2239	1680.4	558.6	106	1295	1319.1	-24.1	173	1280	1300.0	-20.0
40	1659	1681.0	-22.0	107	1287	1316.0	-29.0	174	1539	1300.0	239.0
41	1602	1680.3	-78.3	108	1278	1313.5	-35.5	175	1370	1300.0	70.0
42	1706	1680.9	25.1	109	1295	1311.5	-16.5	176	1563	1300.0	263.0
43	1656	1680.6	-24.6	110	1064	1309.9	-245.9	177	1224	1300.0	-76.0
44	1667	1680.3	-13.3	111	1284	1308.5	-24.5	178	1278	1300.0	-22.0
45	1664	1681.5	-17.5	112	1195	1307.4	-112.4	179	950	1300.0	-350.0
46	1655	1679.9	-24.9	113	1031	1306.5	-275.5	180	1145	1300.0	-155.0
47	1696	1680.5	15.5	114	1523	1305.7	217.3	181	1526	1300.0	226.0
48	1777	1682.1	94.9	115	1428	1305.1	122.9	182	1116	1299.9	-183.9
49	1399	1679.4	-280.4	116	1109	1304.5	-195.5	183	1028	1299.9	-271.9
50	1668	1680.3	-12.3	117	1237	1304.1	-67.1	184	1301	1299.9	1.1
51	1668	1682.8	-14.8	118	1380	1303.7	76.3	185	1451	1299.9	151.1
52	2054	1679.5	374.5	119	1219	1303.3	-84.3	186	1609	1299.9	309.1
53	1652	1679.6	-27.6	120	1149	1303.0	-154.0	187	1691	1299.9	391.1
54	1543	1683.2	-140.2	121	1268	1302.7	-34.7	188	1336	1299.9	36.1
55	1419	1680.3	-261.3	122	1004	1302.4	-298.4	189	1370	1299.9	70.1
56	1652	1678.5	-26.5	123	1235	1302.2	-67.2	190	1152	1299.9	-147.9
57	1904	1683.4	220.6	124	1567	1302.1	264.9	191	1117	1299.9	-182.9
58	1649	1682.4	-33.4	125	1097	1301.9	-204.9	192	1547	1299.9	247.1
59	1561	1676.3	-115.3	126	1296	1301.7	-5.7	193	1214	1299.9	-85.9
60	1775	1680.4	94.6	127	1405	1301.6	103.4	194	1207	1299.9	-92.9
61	2063	1688.5	374.5	128	1228	1301.5	-73.5	195	1326	1299.9	26.1
62	1770	1682.0	88.0	129	1365	1301.4	63.6	196	1141	1299.9	-158.9
63	1443	1670.2	-227.2	130	1321	1301.3	19.7	197	1380	1299.9	80.1
64	1817	1676.7	140.3	131	1447	1301.2	145.8	198	1423	1299.9	123.1
65	1439	1694.9	-255.9	132	1427	1301.1	125.9	199	1405	1299.9	105.1
66	1662	1694.8	-32.8	133	1092	1301.0	-209.0	200	1349	1299.9	49.1

TABLE 5-65
X07202: SUPPLEMENTAL STATISTICAL INFORMATION

VARIANCE/CO-VARIANCE MATRIX

DIAM	PREI	POST	TIME	VELO
4.401E¯13	1.328E¯06	-8.203E¯07	-7.665E¯08	5.838E¯09
1.328E¯06	3.429E02	5.490E00	-4.822E00	2.791E¯01
-8.203E¯07	5.490E00	3.303E02	-4.658E00	2.704E¯01
-7.665E¯08	-4.822E00	-4.658E00	2.549E00	-1.489E¯01
5.838E¯09	2.791E¯01	2.704E¯01	-1.489E¯01	1.218E¯02

CORRELATION MATRIX

	DIAM	PREI	POST	TIME	VELO
DIAM	1.000000	0.886113	-0.638250	-0.216493	0.214986
PREI	0.886113	1.000000	-0.210694	-0.610273	0.607797
POST	-0.638250	-0.210694	1.000000	-0.582763	0.582383
TIME	-0.216493	-0.610273	-0.582763	1.000000	-0.999953
VELO	0.214986	0.607797	0.582383	-0.999953	1.000000

NUMERICAL RANGES OF THE PARTIAL DERIVATIVES

	MAXIMUM	MINIMUM
DIAM	6.264E08	-6.116E08
PREI	1.362E00	4.004E¯04
POST	9.996E¯01	-3.620E¯01
TIME	5.504E01	-5.869E01
VELO	9.125E02	-8.903E02

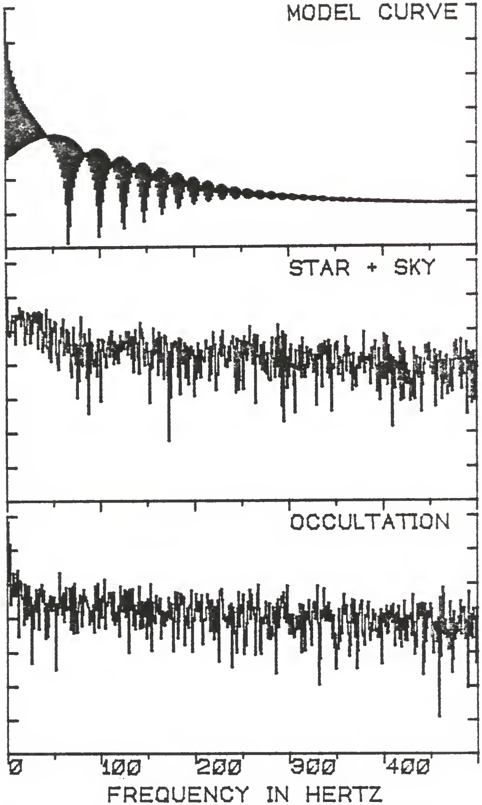

Figure 5-137. POWERPLOT of the occultation of X07202.

The determined Coordinated Universal Time of geometrical occultation was 02:15:30.366 (+/- 0.012) seconds.

X07247

The relatively faint (mV=8.9) B9 star, X07202, occulted by the moon at approximately 03:17 U. T. on March 11, 1984, was the last of the four events observed on that night. As noted in the occultation summary table (Table 5-66) a Johnson B filter was used for this observation.

The photoelectric record of the observation is shown in the RAWPLOT, Figure 5-138. On cursory examination, the integration plot (Figure 5-139) suggests a possible "wide" stellar companion roughly 150 milliseconds after the anticipated disappearance. Further detailed examination of the occultation record, however, revealed that this visual artifact in the INTPLOT was due only to the noise in the observational data. The probability of this being due to the presence of a secondary star was found to be less than 0.1.

As anticipated, given the very early spectral type of the star and its faintness, the best solution found by the DC procedure was that of a point source. This point source solution is depicted graphically in the FITPLOT, Figure 5-140. The S+N/N ratio of this observation was only 2.69. This is reflected in the obviously noisy observational data shown along with the fit. The observational data used in the DC fitting, the computed intensities and the residuals are given in Table 5-67.

TABLE 5-66
X07247: LUNAR OCCULTATION SUMMARY

STELLAR AND OBSERVING INFORMATION

Star: X07247, (SAO 077341, DM +24 0895)
RA: 053708 DEC: +241825 mV: 8.9 Sp:B9
Filter: B Diaphragm: J Gain: C7+ Voltage: 1100

LUNAR INFORMATION

Surface Illumination:	54 percent
Elongation from Sun:	94 degrees
Altitude Above Horizon:	44 degrees
Lunar Limb Distance:	375983 kilometers
Predicted Shadow Velocity:	618.7 meters/sec.
Predicted Angular Rate:	0.3394 arcsec/sec.

EVENT INFORMATION

Date:	March 11, 1984	UT of Event:	03:17:08
USNO V/O Code:	14	HA of Event:	+512416
Position Angle:	126.3	Cusp Angle:	51S
Contact Angle:	-36.1	Watts Angle:	127.5

MODEL PARAMETERS

Number of Data Points:	201
Number of Grid Points:	256
Number of Spectral Regions:	50
Width of Spectral Regions:	42 Angstroms
Limb Darkening Coefficient:	0.5
Effective Stellar Temperature:	5100 K

SOLUTIONS

Stellar Diameter (ams):	Point Source
Time: (relative to Bin 0):	1218.9 (3.4)
Pre-Event Signal:	1967.4 (15.4)
Background Sky Level:	1647.7 (31.3)
Velocity (meters/second):	444.3 (44.1)
Lunar Limb Slope (degrees):	-20.1 (7.4)
U.T. of Occultation:	03:17:07.618 (0.004)

PHOTOMETRIC NOISE INFORMATION

Sum-of-Squares of Residuals:	7116248
Sigma (Standard Error):	188.6304
Normalized Standard Error:	0.59007
Photometric (S+N)/N Ratio:	2.6937
(Change in Intensity)/Background:	0.19401
Change in Magnitude:	0.19252

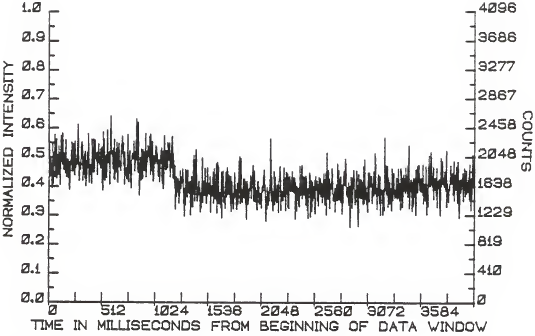

Figure 5-138. RAWPLOT of the occultation of X07247.

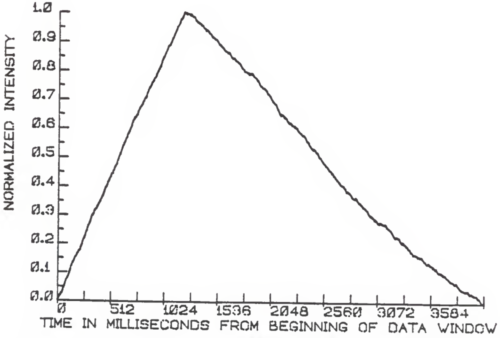

Figure 5-139. INTPLOT of the occultation of X07247.

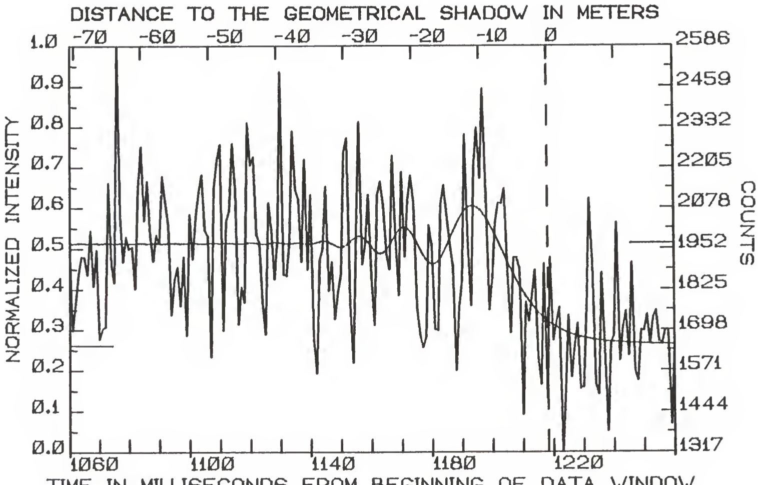

Figure 5-140. FITPLOT of the occultation of X07247.

TABLE 5-67
X07247: OBSERVATIONS, COMPUTED VALUES, AND RESIDUALS FROM BIN 1060

NUM	OBS	COMP	RESID	NUM	OBS	COMP	RESID	NUM	OBS	COMP	RESID
0	1948	1968.4	-20.4	67	2013	1969.6	43.4	134	2202	2083.5	118.5
1	1696	1968.2	-272.2	68	1856	1970.9	-114.9	135	2330	2079.3	250.7
2	1781	1968.2	-187.2	69	1981	1971.0	10.0	136	2171	2071.5	99.5
3	1872	1968.4	-96.4	70	2505	1969.8	535.2	137	2453	2060.3	392.7
4	1928	1968.4	-40.4	71	1873	1968.3	-95.3	138	2118	2046.4	71.6
5	1925	1968.2	-43.2	72	1867	1967.2	-100.2	139	1760	2030.1	-270.1
6	1872	1968.2	-96.2	73	1973	1967.2	5.8	140	1861	2012.0	-151.0
7	2009	1968.3	40.7	74	2320	1968.0	352.0	141	2032	1992.6	39.4
8	1835	1968.5	-133.5	75	2137	1969.0	168.0	142	2093	1972.4	120.6
9	1949	1968.3	-19.3	76	2107	1969.6	137.4	143	2092	1951.8	140.2
10	1669	1968.1	-299.1	77	1911	1969.1	-58.1	144	2139	1931.1	207.9
11	1701	1968.1	-267.1	78	2231	1967.9	263.1	145	1880	1910.7	-30.7
12	1708	1968.5	-260.5	79	1888	1966.7	-78.7	146	1688	1890.8	-202.8
13	2157	1968.7	188.3	80	2120	1966.4	153.6	147	1925	1871.6	53.4
14	1904	1968.4	-64.4	81	1670	1967.6	-297.6	148	1923	1853.3	69.7
15	1847	1968.0	-121.0	82	1561	1970.1	-409.1	149	1890	1835.9	54.1
16	2586	1968.0	618.0	83	1914	1973.2	-59.2	150	1433	1819.6	-386.6
17	2056	1968.4	87.6	84	1952	1975.3	-23.3	151	1785	1804.4	-19.4
18	1912	1968.8	-56.8	85	2145	1975.4	169.6	152	1724	1790.3	-66.3
19	1989	1968.6	20.4	86	1821	1972.8	-151.8	153	1805	1777.2	27.8
20	1950	1968.1	-18.1	87	1911	1968.0	-57.0	154	1885	1765.2	119.8
21	1955	1967.9	-12.9	88	1732	1962.4	-230.4	155	1611	1754.2	-143.2
22	1829	1968.2	-139.2	89	1815	1957.7	-142.7	156	1527	1744.2	-217.2
23	2141	1968.6	172.4	90	1873	1955.9	-82.9	157	1905	1735.1	169.9
24	2271	1968.6	302.4	91	2252	1957.9	294.1	158	1483	1726.8	-243.8
25	2040	1968.2	71.8	92	2297	1963.7	333.3	159	1923	1719.3	203.7
26	2163	1967.9	195.1	93	1781	1972.1	-191.1	160	1664	1712.6	-48.6
27	1995	1968.2	26.8	94	1595	1981.1	-386.1	161	1721	1706.5	14.5
28	1914	1968.6	-54.6	95	2004	1988.2	15.8	162	1768	1701.0	67.0
29	1996	1968.8	27.2	96	2348	1991.4	356.6	163	1317	1696.1	-379.1
30	1969	1968.3	0.7	97	1904	1989.4	-85.4	164	1509	1691.6	-182.6
31	2177	1967.8	209.2	98	1967	1982.4	-15.4	165	1743	1687.6	55.4
32	2100	1967.8	132.2	99	2120	1971.5	148.5	166	1550	1684.0	-134.0
33	2027	1968.4	58.6	100	1866	1958.9	-92.9	167	1646	1680.8	-34.8
34	1746	1969.1	-223.1	101	1714	1947.3	-233.3	168	1718	1677.9	40.1
35	1855	1969.1	-114.1	102	2117	1939.2	177.8	169	1514	1675.3	-161.3
36	1896	1968.3	-72.3	103	2161	1936.4	224.6	170	1519	1673.0	-154.0
37	1774	1967.5	-193.5	104	2088	1939.8	148.2	171	1769	1670.9	98.1
38	1928	1967.4	-39.4	105	1935	1949.0	-14.0	172	2107	1669.0	438.0
39	1681	1968.1	-287.1	106	1888	1962.7	-74.7	173	1907	1667.3	239.7
40	2059	1969.1	89.9	107	2242	1978.8	263.2	174	1528	1665.7	-137.7
41	1919	1969.4	-50.4	108	1988	1994.6	-6.6	175	1496	1664.4	-168.4
42	2048	1968.9	79.1	109	1807	2007.8	-200.8	176	1875	1663.1	211.9
43	2127	1968.0	159.0	110	2191	2016.2	174.8	177	1640	1662.0	-22.0
44	2182	1967.5	214.5	111	1927	2018.5	-91.5	178	1383	1660.9	-277.9
45	2011	1967.8	43.2	112	2099	2014.4	84.6	179	1653	1660.0	-7.0
46	1991	1968.5	22.5	113	2180	2004.2	175.8	180	1679	1659.2	19.8
47	1614	1969.0	-355.0	114	2096	1989.1	106.9	181	2031	1658.4	372.6
48	2143	1968.8	174.2	115	1771	1971.0	-200.0	182	1602	1657.7	-55.7
49	2227	1968.2	258.8	116	1687	1952.0	-265.0	183	1707	1657.0	50.0
50	2278	1968.0	310.0	117	1642	1934.0	-292.0	184	1756	1656.4	99.6
51	1696	1968.3	-272.3	118	1675	1919.1	-244.1	185	1617	1655.9	-38.9
52	2037	1968.9	68.1	119	2024	1908.7	115.3	186	1907	1655.4	251.6
53	2071	1969.3	101.7	120	1965	1903.8	61.2	187	1571	1654.9	-83.9
54	2280	1968.9	311.1	121	1701	1904.9	-203.9	188	1539	1654.5	-115.5
55	2141	1967.9	173.1	122	1696	1911.9	-215.9	189	1696	1654.1	41.9
56	1715	1967.1	-252.1	123	2087	1924.1	162.9	190	1695	1653.8	41.2
57	1834	1967.1	-133.1	124	2149	1940.6	208.4	191	1746	1653.4	92.6
58	1784	1968.2	-184.2	125	2059	1960.2	98.8	192	1656	1653.1	2.9
59	2347	1969.7	377.3	126	1969	1981.6	-12.6	193	1736	1652.8	83.2
60	2212	1970.7	241.3	127	1900	2003.3	-103.3	194	1759	1652.6	106.4
61	2239	1970.4	268.6	128	1571	2024.2	-453.2	195	1663	1652.3	10.7
62	1997	1969.0	28.0	129	1769	2043.0	-274.0	196	1655	1652.1	2.9
63	1971	1967.1	3.9	130	1852	2058.9	-206.9	197	1696	1651.9	44.1
64	1787	1966.0	-179.0	131	2308	2071.2	236.8	198	1696	1651.7	44.3
65	1684	1966.2	-282.2	132	1965	2079.5	-114.5	199	1402	1651.5	-249.5
66	2095	1967.7	127.3	133	1774	2083.6	-309.6	200	1640	1651.4	-11.4

The PDPLOT of the solution intensity curve (Figure 5-141) shows nothing unusual or of concern in the final numerical computations of the partial derivatives. The numerical ranges of the partial derivatives, as well as the usual supplementary statistics, are listed in Table 5-68.

The stellar signal itself was only 319.7 counts, or only 19.4 percent of the background level. Hence, the slow rise (over 4096 milliseconds) in the now strongly dominant background contribution resulted in a stronger Poisson tail in the distribution function of the residuals (see Figure 5-142).

The Coordinated Universal Time of geometrical occultation for X07247 was 03:17:07.618 (+/0.004 seconds).

The four events which occurred on this night were of progressively fainter stars, observed under similar conditions. It is of interest to compare the degradation of the solutions (in terms of the formal errors of the determined parameters), the broadening and increasing Poisson nature of the residual amplitude distributions, and the increasing dominance of the low frequency power contributions in the pre-occultation (star-plus-sky) signal. The latter can be seen for X07202 in Figure 5-143.

<u>X09514</u>

The first of two occultations observed on the night of March 12, 1984 U. T., was that of the K5 star X09514. Due to an intermittent problem in the A-to-D converter input selected for this event, approximately half of the data which

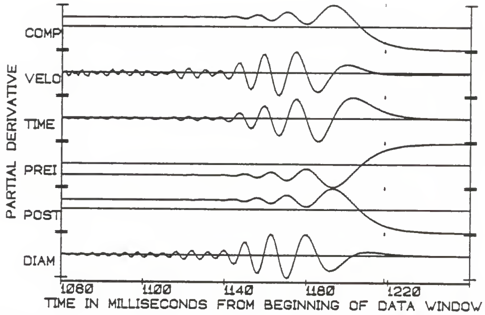

Figure 5-141. PDPLOT of the occultation of X07247.

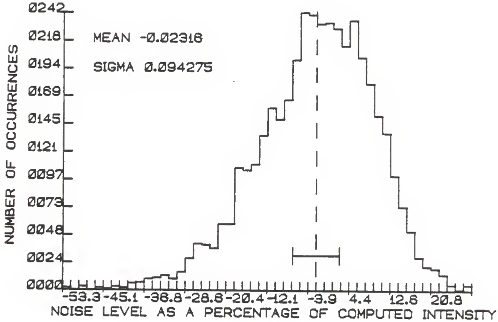

Figure 5-142. NOISEPLOT of the occultation of X07247.

TABLE 5-68
X07247: SUPPLEMENTAL STATISTICAL INFORMATION

VARIANCE/CO-VARIANCE MATRIX

DIAM	PREI	POST	TIME	VELO
1.371E¯14	2.264E¯07	-6.947E¯07	-1.822E¯08	3.630E¯10
2.264E¯07	2.457E02	2.824E01	-1.200E01	1.398E¯01
-6.947E¯07	2.824E01	1.031E03	-4.002E01	4.384E¯01
-1.822E¯08	-1.200E01	-4.002E01	1.149E01	-1.297E¯01
3.630E¯10	1.398E¯01	4.384E¯01	-1.297E¯01	1.972E¯03

CORRELATION MATRIX

	DIAM	PREI	POST	TIME	VELO
DIAM	1.000000	0.405449	-0.944025	0.762444	-0.749555
PREI	0.405449	1.000000	-0.083764	-0.242888	0.260790
POST	-0.944025	-0.083764	1.000000	-0.927240	0.919840
TIME	0.762444	-0.242888	-0.927240	1.000000	-0.999806
VELO	-0.749555	0.260790	0.919840	-0.999806	1.000000

NUMERICAL RANGES OF THE PARTIAL DERIVATIVES

	MAXIMUM	MINIMUM
DIAM	3.548E08	-3.771E08
PREI	1.363E00	1.138E¯02
POST	9.886E¯01	-3.634E¯01
TIME	2.070E01	-2.166E01
VELO	1.838E03	-1.876E03

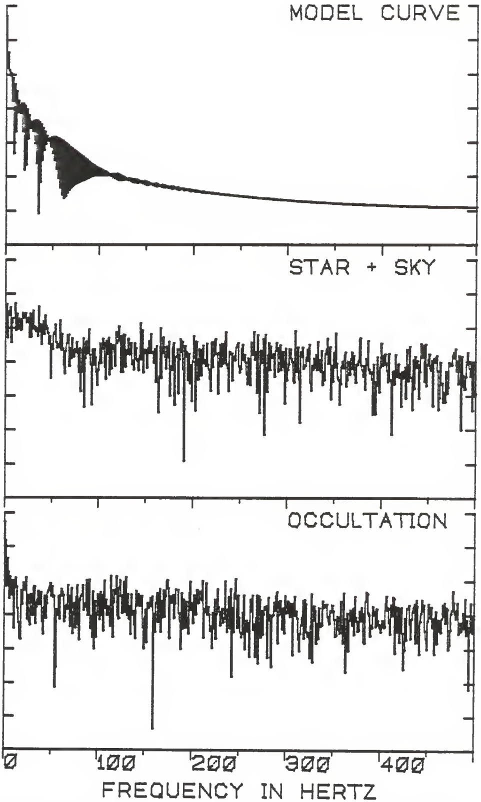

Figure 5-143. POWERPLOT of the occultation of X07247.

should have been acquired were not. This problem was not known to exist at the time of the event but came to light after the fact. Fortunately, data dropouts did not occur during the occultation event itself, and hence, did not adversely affect the solution process. The RAWPLOT (Figure 5-144) shows only that portion of the data record for which photometric data were successfully acquired.

The integration plot, Figure 5-145, (for data taken over an interval of 1920 milliseconds) shows no indication of stellar duplicity.

The best fit to the observations is shown graphically on Figure 5-146. As expected, given the poor (S+N)/N ratio (only 2.27) and an apparent V magnitude of 8.7 for the star, no angular diameter could be determined. The solution parameters are given in the occultation summary, Table 5-69. The observed and computed intensities, and the residuals are listed in Table 5-70.

Figure 5-147 shows the sensitivity of the intensity curve to variations in the solution parameters. The numerical range of the values plotted on this PDPLOT can be found on Table 5-71, along with the variance/covariance and correlation matrices of the solution parameters.

The noise figure of the residuals, taken from the 1920 milliseconds of data successfully acquired, is presented as Figure 5-148. Figure 5-149 is the POWERPLOT of the solution curve, the occultation event, and the star-plus-sky signal.

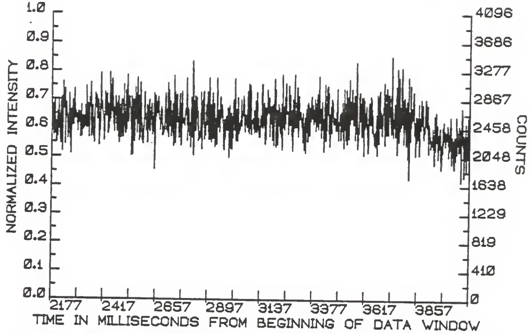

Figure 5-144. RAWPLOT of the occultation of X09514.

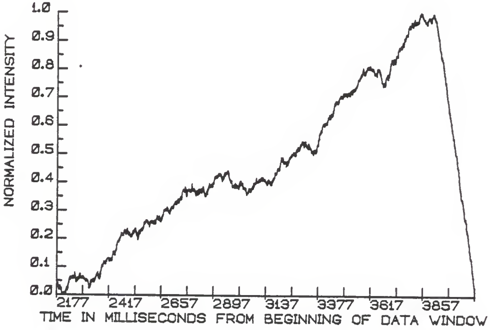

Figure 5-145. INTPLOT of the occultation of X09514.

TABLE 5-69
X09514: LUNAR OCCULTATION SUMMARY

STELLAR AND OBSERVING INFORMATION

Star: X09514, (SAO 078598, DM +25 1364)
RA: 063835   DEC: +253153   mV: 8.7   Sp: K5
Filter: B   Diaphragm: J   Gain: C7+   Voltage: 1200

LUNAR INFORMATION

Surface Illumination:	65 percent
Elongation from Sun:	107 degrees
Altitude Above Horizon:	51 degrees
Lunar Limb Distance:	369551 kilometers
Predicted Shadow Velocity:	606.3 meters/sec.
Predicted Angular Rate:	0.3384 arcsec/sec.

EVENT INFORMATION

Date:	March 12, 1984	UT of Event:	03:45:29
USNO V/O Code:	14	HA of Event:	+440653
Position Angle:	61.2	Cusp Angle:	57N
Contact Angle:	+37.1	Watts Angle:	56.4

MODEL PARAMETERS

Number of Data Points:	201
Number of Grid Points:	256
Number of Spectral Regions:	53
Width of Spectral Regions:	50 Angstroms
Limb Darkening Coefficient:	0.5
Effective Stellar Temperature:	4200 K

SOLUTIONS

Stellar Diameter (ams):	Point Source	
Time: (relative to Bin 0):	3918.4	(3.7)
Pre-Event Signal:	2596.5	(21.8)
Background Sky Level:	2305.5	(26.3)
Velocity (meters/sec.):	621.6	(77.2)
Lunar Limb Slope (degrees):	-6.36	(7.29)
U.T. of Occultation:	03:35:32.8	(0.1)

PHOTOMETRIC NOISE INFORMATION

Sum-of-Squares of Residuals:	10568390
Sigma (Standard Error):	229.8738
Normalized Standard Error:	0.78984
Photometric (S+N)/N Ratio:	2.26608
(Change in Intensity)/Background:	0.12624
Change in Magnitude:	0.12908

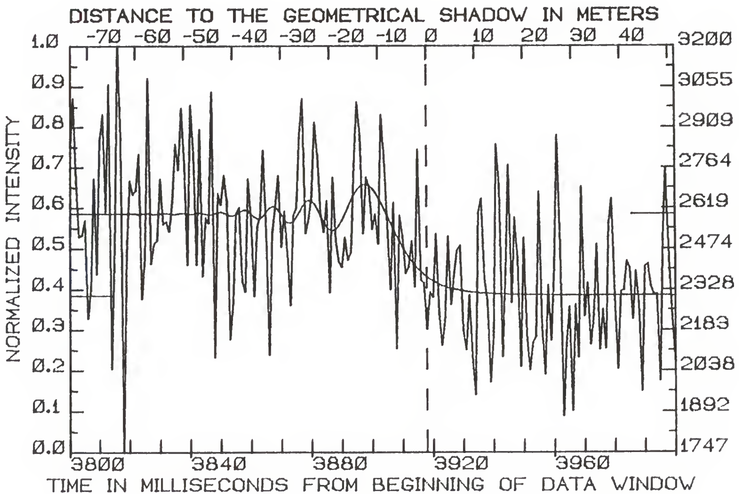

Figure 5-146. FITPLOT of the occultation of X09514.

TABLE 5-70
X09514: OBSERVATIONS, COMPUTED VALUES, AND RESIDUALS FROM BIN 3800

NUM	OBS	COMP	RESID	NUM	OBS	COMP	RESID	NUM	OBS	COMP	RESID
0	2815	2597.3	217.7	67	2529	2623.6	-94.6	134	1951	2317.1	-366.1
1	3014	2597.2	416.8	68	2623	2621.9	1.1	135	2599	2316.1	282.9
2	2716	2597.3	118.7	69	2733	2611.6	121.4	136	2651	2315.2	335.8
3	2515	2597.3	-82.3	70	2479	2595.6	-116.6	137	2368	2314.4	53.6
4	2520	2597.2	-77.2	71	2606	2579.1	26.9	138	2287	2313.7	-26.7
5	2575	2597.1	-22.1	72	2456	2567.2	-111.2	139	1996	2313.0	-317.0
6	2224	2597.3	-373.3	73	2272	2563.7	-291.7	140	2161	2312.5	-151.5
7	2327	2597.5	-270.5	74	2591	2569.9	21.1	141	2847	2311.9	535.1
8	2725	2597.3	127.7	75	2619	2584.5	34.5	142	2699	2311.5	387.5
9	2383	2597.0	-214.0	76	2883	2604.0	279.0	143	2086	2311.0	-225.0
10	2859	2597.2	261.8	77	3010	2623.6	386.4	144	2395	2310.7	84.3
11	2956	2597.5	358.5	78	2527	2638.7	-111.7	145	2772	2310.3	461.7
12	2605	2597.5	7.5	79	2578	2645.9	-67.9	146	2279	2310.0	-31.0
13	3063	2597.2	465.8	80	2659	2643.6	15.4	147	2583	2309.7	273.3
14	2044	2597.0	-553.0	81	2926	2632.2	293.8	148	2439	2309.5	129.5
15	2479	2597.4	-118.4	82	2808	2613.9	194.1	149	2052	2309.2	-257.2
16	3200	2597.6	602.4	83	2600	2591.9	8.1	150	2512	2309.0	203.0
17	2870	2597.3	272.7	84	2531	2570.1	-39.1	151	2168	2308.8	-140.8
18	1747	2596.9	-849.9	85	2643	2551.9	91.1	152	2039	2308.6	-269.6
19	2451	2597.1	-146.1	86	2317	2540.2	-223.2	153	2135	2308.5	-173.5
20	2715	2597.7	117.3	87	2728	2536.5	191.5	154	2159	2308.3	-149.3
21	2666	2597.8	68.2	88	2502	2541.4	-39.4	155	2675	2308.2	366.8
22	2680	2597.1	82.9	89	2428	2554.0	-126.0	156	2191	2308.0	-117.0
23	2811	2596.5	214.5	90	2408	2572.8	-164.8	157	2024	2307.9	-283.9
24	2295	2596.9	-301.9	91	2513	2595.7	-82.7	158	2344	2307.8	36.2
25	2439	2598.0	-159.0	92	2432	2620.4	-188.4	159	2145	2307.7	-162.7
26	3084	2598.4	485.6	93	2460	2644.5	-184.5	160	2409	2307.5	101.5
27	2420	2597.5	-177.5	94	2772	2666.1	105.9	161	2879	2307.5	571.5
28	2490	2596.3	-106.3	95	3000	2683.5	316.5	162	2476	2307.4	168.6
29	2501	2596.2	-95.2	96	2883	2695.7	187.3	163	1875	2307.3	-432.3
30	2721	2597.5	123.5	97	2527	2702.1	-175.1	164	2133	2307.2	-174.2
31	2559	2598.7	-39.7	98	2727	2702.7	24.3	165	2265	2307.2	-42.2
32	2568	2598.5	-30.5	99	2697	2697.6	-0.6	166	1894	2307.1	-413.1
33	2535	2597.1	-62.1	100	2543	2687.5	-144.5	167	2273	2307.0	-34.0
34	2639	2595.9	43.1	101	2596	2673.1	-77.1	168	2084	2307.0	-223.0
35	2849	2596.3	252.7	102	2491	2655.3	-164.3	169	2694	2306.9	387.1
36	2755	2597.9	157.1	103	2953	2635.0	318.0	170	2232	2306.8	-74.8
37	2976	2599.1	376.9	104	2798	2612.9	185.1	171	2351	2306.8	44.2
38	2775	2598.5	176.5	105	2559	2589.9	-30.9	172	2129	2306.7	-177.7
39	2416	2596.8	-180.8	106	2328	2566.7	-238.7	173	2235	2306.7	-71.7
40	2989	2595.6	393.4	107	2637	2543.7	93.3	174	2489	2306.6	182.4
41	2814	2596.4	217.6	108	2116	2521.5	-405.5	175	2112	2306.6	-194.6
42	2415	2598.4	-183.4	109	2592	2500.3	91.7	176	2256	2306.6	-50.6
43	2900	2599.8	300.2	110	2520	2480.4	39.6	177	2116	2306.5	-190.5
44	2376	2599.0	-223.0	111	2385	2461.9	-76.9	178	2562	2306.5	255.5
45	2584	2596.5	-12.5	112	2407	2445.0	-38.0	179	2651	2306.4	344.6
46	2563	2594.3	-31.3	113	2499	2429.5	69.5	180	2304	2306.4	-2.4
47	3036	2594.7	441.3	114	2337	2415.5	-78.5	181	2043	2306.4	-263.4
48	2083	2597.8	-514.8	115	2828	2403.0	425.0	182	2320	2306.4	13.6
49	2671	2601.6	69.4	116	2362	2391.8	-29.8	183	2325	2306.3	18.7
50	2630	2603.0	27.0	117	2351	2381.8	-30.8	184	2429	2306.3	122.7
51	2735	2600.5	134.5	118	2184	2373.0	-189.0	185	2405	2306.3	98.7
52	2643	2595.2	47.8	119	2319	2365.2	-46.2	186	2221	2306.3	-85.3
53	2149	2590.4	-441.4	120	2300	2358.4	-58.4	187	2394	2306.2	87.8
54	2281	2589.5	-308.5	121	2525	2352.3	172.7	188	2280	2306.2	-26.2
55	2599	2593.7	5.3	122	2244	2347.0	-103.0	189	1964	2306.2	-342.2
56	2620	2601.4	18.6	123	2127	2342.4	-215.4	190	2409	2306.2	102.8
57	2359	2608.4	-249.4	124	2227	2338.3	-111.3	191	2419	2306.1	112.9
58	2321	2610.6	-289.6	125	2517	2334.8	182.2	192	2340	2306.1	33.9
59	2722	2606.1	115.9	126	2273	2331.7	-58.7	193	2312	2306.1	5.9
60	2576	2596.5	-20.5	127	2386	2328.9	57.1	194	2311	2306.1	4.9
61	2303	2586.1	-283.1	128	2469	2326.5	142.5	195	2001	2306.1	-305.1
62	2551	2579.9	-28.9	129	2484	2324.4	159.6	196	2511	2306.1	204.9
63	2588	2581.2	6.8	130	2183	2322.6	-139.6	197	2763	2306.0	457.0
64	2825	2590.2	234.8	131	2111	2320.9	-209.9	198	2439	2306.0	133.0
65	2533	2603.7	-70.7	132	2307	2319.5	-12.5	199	2231	2306.0	-75.0
66	2092	2616.5	-524.5	133	2091	2318.2	-227.2	200	2063	2306.0	-243.0

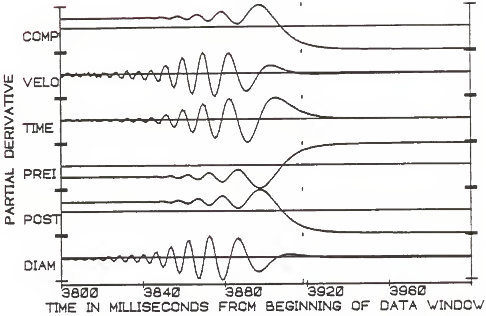

Figure 5-147. PDPLOT of the occultation of X09514.

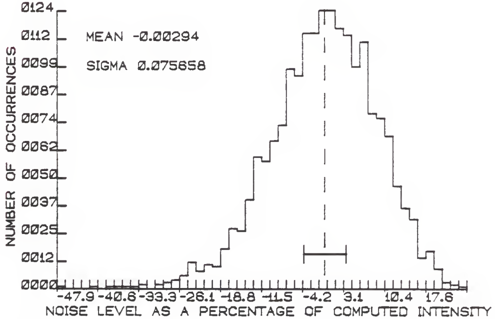

Figure 5-148. NOISEPLOT of the occultation of X09514.

TABLE 5-71
X09514: SUPPLEMENTAL STATISTICAL INFORMATION

VARIANCE/CO-VARIANCE MATRIX

DIAM	PREI	POST	TIME	VELO
3.254E¯14	5.005E¯07	-5.270E¯07	-5.312E¯08	1.290E¯09
5.005E¯07	4.841E02	1.686E01	-1.663E01	2.919E¯01
-5.270E¯07	1.686E01	6.996E02	-2.319E01	4.042E¯01
-5.312E¯08	-1.663E01	-2.319E01	1.380E01	-2.444E¯01
1.290E¯09	2.919E¯01	4.042E¯01	-2.444E¯01	5.961E¯03

CORRELATION MATRIX

	DIAM	PREI	POST	TIME	VELO
DIAM	1.000000	0.766505	-0.761986	0.128535	-0.124485
PREI	0.766505	1.000000	-0.172303	-0.479860	0.481833
POST	-0.761986	-0.172303	1.000000	-0.713209	0.709453
TIME	0.128535	-0.479860	-0.713209	1.000000	-0.999975
VELO	-0.124485	0.481833	0.709453	-0.999975	1.000000

NUMERICAL RANGES OF THE PARTIAL DERIVATIVES

	MAXIMUM	MINIMUM
DIAM	3.055E08	-3.000E08
PREI	1.365E00	1.974E¯03
POST	9.980E¯01	-3.649E¯01
TIME	2.322E01	-2.477E01
VELO	1.311E03	-1.336E03

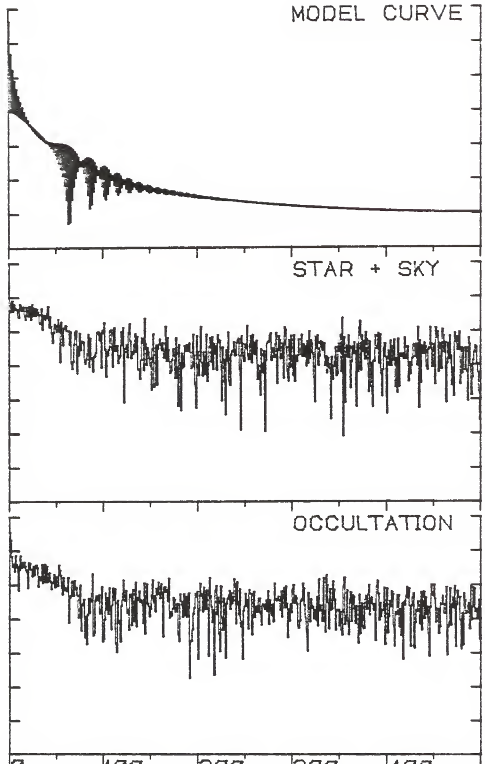

Figure 5-149. POWERPLOT of the occultation of X09514.

Unfortunately, as had occasionally happened in previously observed events, the signal strength of the WWVB time code was too low to provide a useful time reference at the time of the event. A successful post-event calibration of the SPICA-IV/LODAS clock could not be obtained until 2 hours after the event. Assuming a worst case internal clock drift of 2 seconds per day, the Coordinated Universal Time of geometrical occultation was found to be 03:35:32.8 (+/- 0.1 seconds).

ZC1030 (Epsilon Geminorum)

ZC1030 (Epsilon Geminorum, Mebsuta, BS 2473) was a prime candidate for the occultation program. This G5 supergiant (luminosity class Ib) is on the order of 6000 times as luminous as the sun. Its apparent V magnitude of 3.18 gives Epsilon Geminorum a corresponding distance of appoximately 350 parsecs. To gauge the possibility of a diameter detection for Epsilon Geminorum, Allen (1963) gives diameters of G5-I stars to be in excess of 120 solar diameters. At this distance this linear diameter corresponds to an angular diameter on the order of 3 or 4 milliseconds of arc, well above the detection threshold. On April 7, 1976, Epsilon Geminorum was occulted by Mars. This well-observed planetary occultation has been discussed by Wasserman et al. (1977).

The intermediate bandwidth "y" filter was initially selected for this observation. This star, brighter by far than any other previously observed in the occultation program, should have produced an observation with an unprecedented signal-to-noise ratio. Though X09514 had been observed under clear skies only two hours earlier, the weather conditions deteriorated rapidly. Twenty minutes before the predicted time of the event, the sky was completely covered with a heavy layer of cirrus clouds, and no stars could be seen with the unaided eye. Just prior to the event, no surface markings could be distinguished on the lunar surface. (The observing log, in fact, referred to the lunar image as "appearing like a milk bottle smeared with mayonnaise"). The star, however, was visible in the photometer viewing optics against a sky background which was chalky white. Though the clouds had attenuated the stellar signal by at least an order of magnitude, the star-plus-sky signal was still 40 percent higher than the sky background.

Under these conditions, due to adverse seeing and transparency effects, the possibility of obtaining data of sufficient quality to yield a stellar diameter was out of the question. Yet, though this fundamentally important piece of astrophysical information was to be lost, at least the time of geometrical occultation could still be obtained. The data acquisition rate was reduced to 100 points per second, while leaving the amplifier time constant at 2 kiloHertz. While this would result in severe undersampling for the purpose of stellar diameter detection, it was necessary under the poor observing conditions in order to extract a usable time of occultation. Five minutes before the predicted time of the

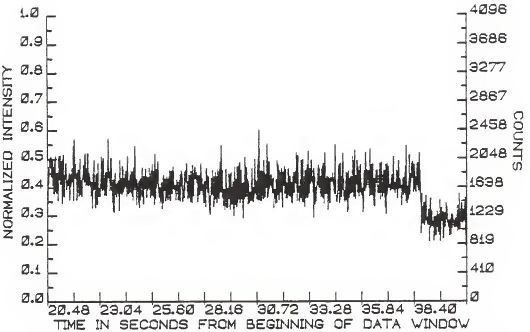

Figure 5-150. RAWPLOT of the occultation of ZC1030.

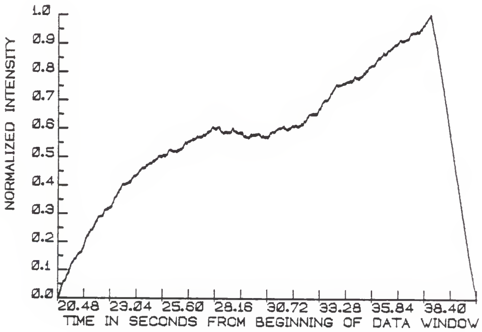

Figure 5-151. INTPLOT of the occultation of ZC1030.

event the selected filter was changed to the "b" filter, as the star-plus-sky/sky signal ratio was a approximately 10 percent higher than with the "y" filter.

The RAWPLOT of the event, Figure 5-150, shows the slowly acquired photometric data. The integration plot, Figure 5-151, is indicative of the variation in atmospheric transparency brought on by the layer of intervening clouds and haze. As can be seen, the change in signal level due to the occultation is unmistakable. No diffraction fringes are contained in the data (as expected) due to the slow data acquisition rate. The data sample corresponding to the time of disappearance was noted strictly by visual inspection. After reduction of the WWVB time code the Coordinated Universal Time of geometrical occultation was found to be 05:50:06.77 (+/- 0.01 seconds).

Under normal circumstances such an observation would have been impossible, and the presence of a layer of heavy cirrus clouds would have prevented any observing attempt. Yet, as was shown by the partial success of this observation, a bright star can yield some information (even if only the time of occultation to low precision) under adverse conditions. Occultation photometry, for chronometric and low precision astrometric work, is quite forgiving.

Summary of the Occultation Observations

The observations which have been discussed in the previous section were all made during the thirteen lunations spanning the time period from March 1983, to March 1984. During this period, 67 occultation observations were planned. Of these, photometric data were obtained for 24 occultations. The remainder, with the exception of two, were lost due to inclement weather. The two other events mentioned were not observed due to a mechanical failure in the instrumental system, which was remedied in time for the next night's observing.

Of the 24 events for which data were obtained, two (the occultations of ZC3458 and ZC1030) were observed with a data acquisition rate which was too slow to allow a complete analysis to be carried out. If the observing year discussed was typical (in terms of weather), then one might expect approximately one fruitful occultation observation for every three planned for the Rosemary Hill Observatory.

The stars ZC0916-A, X13534, and X13607 were discovered to be "close" occultation binaries. (The B component of ZC0916 was previously known to be a spectroscopic binary). Hence, though based on admittedly small number statistics, 14 percent of the 22 observations which were fully analyzed resulted in the discovery of previously unknown "close" companions. Widely separated, though much fainter, companion stars were found for ZC1221, X18067, ZC0126. Thus, 14 percent of the stars studied were revealed to have fainter "wide" components. Considering both "close" and "wide" systems, 27 percent of the stars studied turned out to have previously unknown companions. Table 5-72 summarizes the

TABLE 5-72
DERIVED QUANTITIES FOR THE OCCULTATION BINARIES

STAR	T	mV-T	mV-1	mV-2	P. S.
ZC0916-A	C	4.74	5.05	6.27	3.34
ZC0916-B	C	5.19	5.28	7.66	8.41
ZC0916-AB	W	4.30	4.74	5.19	31.5
ZC1221	W	--	--	--	440
X13534	C	8.4	8.73	9.86	6.07
X13607	C	8.2	8.58	9.52	13.15
ZC0126	W	--	--	--	38.8

Notes: 1. Type codes (T): W = wide, C = close.
2. mV-T is combined mV for both stars.
3. Projected Separation (P. S.) is milliseconds of arc.

TABLE 5-73
STELLAR ANGULAR DIAMETERS

STAR	Diam.	S.E.	S+N/N	Q
ZC0916-B1	5.89	0.84	12.680	427.6
ZC1221	2.70	2.41	9.044	62.4
X07598	5.45	2.04	4.657	22.4
ZC1462	9.27	3.69	5.666	24.9
ZC2209	12.18	1.86	9.904	43.3
X01217	2.88	4.98	3.145	1.2
ZC3158	1.74	1.68	4.578	90.3
ZC0835	1.08	1.46	11.808	265.9

Note: S.E. is the Standard Error (One Sigma).

TABLE 5-74
COORDINATED UNIVERSAL TIMES OF GEOMETRICAL OCCULTATIONS

STAR	C. U. T.	S. E.	STAR-2 C.U.T.	S. E.
ZC0916-A	02:44:33.347	0.001	02:44:33.326	0.003
ZC0916-B	02:44:33.421	0.001	02:44:33.413	0.003
ZC1221	00:44:55.877	0.012	00:44:54.731	0.018
ZC1222	01:14:46.177	0.004		
X07589	01:35:12.172	0.051		
X07598	02:12:02.030	0.005		
X13534	02:46:29.632	0.003	02:46:29.594	0.008
X13607	04:33:58.827	0.007	04:33:58.773	0.009
ZC1462	05:13:37.199	0.001		
ZC2209	03:12:53.356	0.007		
X18067	02:16:52.406	0.007		
ZC3214	03:35:43.107	0.018		
X13590	01:02:40.701	0.014		
X01217	00:02:07.790	0.004		
X01246	01:20:01.938	0.011		
ZC0126	01:28:01.981	0.010	01:28:01.753	0.010
X01309	03:32:06.631	0.005		
ZC3158	00:06:39.731	0.004		
ZC0835	00:39:28.8	0.1		
X07145	01:28:05.604	0.006		
X07202	02:15:30.366	0.012		
X07247	03:17:07.618	0.004		
X09514	03:35:32.779	0.1		
ZC1030	05:50:06.77	0.01		

Note: S. E. is the Standard Error (One Sigma) in seconds.

projected angular separations found for these double stars. In addition, the derived apparent V magnitudes are given for the "close" doubles.

Stellar angular diameters were determined for the stars ZC0916-B1, ZC1221, X07598, ZC1462, ZC2209, X01217, ZC3158, and ZC0835. However, the uncertainties in the angular diameters determined for ZC1221, ZC3158, ZC0835 and X01217 (all with angular diameters less than 3 milliseconds of arc) were rather large. In each of these cases the formal one sigma uncertainty of the diameter was nearly equal to the determined diameter itself. Indeed, in the case of X01217, the uncertainty in the diameter exceeded the angular diameter by 73 percent. The roughly 9 millisecond of arc diameter found for ZC1462 must be viewed with caution, as previously discussed. It is highly likely that, in this case, the diameter found was spurious.

Perhaps one of the two most interesting observational results obtained in the course of this investigation was the determination of the unexpectedly large angular diameter of ZC2209 (32 Librae). This determination, of approximately 12 milliseconds of arc, is quite good and cannot be easily dismissed.

Table 5-73 lists the angular diameters and their statistal uncertainties for each star for which a diameter was found. Also found on this table (as given separately in the occultation summary tables) are the photometric (S+N)/N ratios and the ratio of the pre-occultation to post-occultation signal intensities. A "quality index", denoted Q, has been assigned to each of these events. Q is defined as the product of the (S+N)/N and intensity ratios divided by the normalized standard error of the photometric O-C's. The "quality index" is not defined from any rigorous standpoint. Rather, it is designed merely to give, in a single quantity, an indication of the overall photometric conditions for a particular event. Thus, an intercomparison of Q for different events provides a relative scale for judging the quality of the observational data used in the parametric solutions.

The Coordinated Universal Times of geometrical occultation were determined for each of the 24 events. In the case of "close" doubles, the individual times of disappearance of the components were found. These times, which have been reported to the International Lunar Occultation Center (in Japan), are summarized along with their one sigma uncertainties in Table 5-74. These statistical uncertainties arise both from the internal formal error in the DC solution for the time parameter and the error inherent in edge detection of the WWVB time code.

For each individual event, the determined R and L rates depend upon the local slope of the lunar surface. In principle, for any one event the slope can assume any value. However, the likelihood of encountering an extremely large local slope should be quite small, as near-vertical protuberances are rare in comparison to the total lunar surface area which can be seen along the limb. Clearly, there should be a most likely value for a lunar slope based on the distribution function of individual slopes. This distribution function could be found by measuring the slopes of lunar surface features from the Lunar Orbiter or Apollo photographs. However, this would be a formidable task, as the lunar surface would have to be treated as a grid of no more than a few meters on a side in order to obtain a distribution function useful in the reduction and analysis of occultation observations.

If a detailed lunar slope distribution function were known, it could serve to assess the probability of a proper determination of the slopes for an individual event. In the course of this investigation, 27 local lunar slopes were determined, and the derived distribution function is shown in Figure 5-152. This figure, binned into regions 3 degrees wide, shows the occurrences of the absolute values of the determined slopes.

One would not expect a preferential alignment of lunar surface features, and hence, the mean of all slopes should average to zero. (Indeed, the mean slope angle found for the 27 observations was found to be -1.8 degrees). The mean absolute slope was approximately 15 degrees. The largest slope encountered was just in excess of 33 degrees. This distribution function is in good agreement with the distribution of lunar slopes which have been reported from observations made at McDonald Observatory over the last decade.

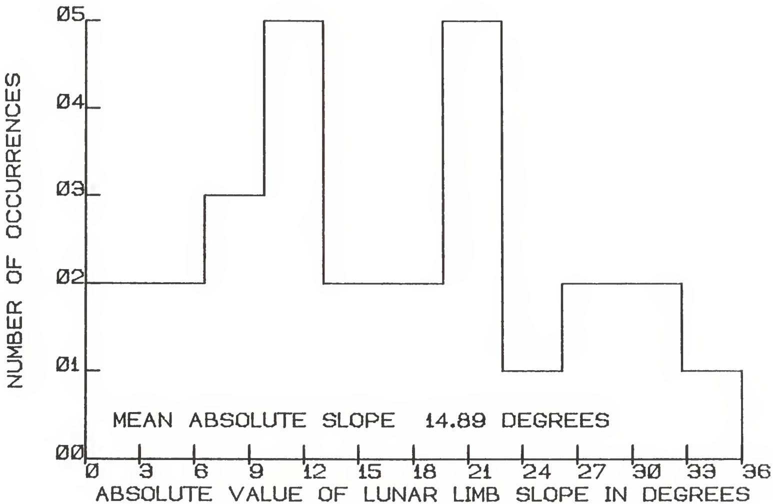

Figure 5-152. Observed distribution function of the absolute values of lunar limb slopes.

Future Directions for the Occultation Program

In order to meet the goals of the program of occultation observation discussed in Chapter 1, an instrumental system capable of obtaining fast photometric observations of lunar occultations was developed and implemented at the Rosemary Hill Observatory. Further, careful consideration of the methods available for the reduction and subsequent analyses of these observations led to improvements in the conventional numerical and computational procedures. These improvements were incorporated into a set of algorithms, implemented as APL functions, to allow a routine program of analysis to be carried out.

The systems and procedures developed have been proven viable as demonstrated by the successful determination of stellar angular diameters, the discovery of previously unsuspected multiplicity in several stellar systems, and in measuring the times of occultation events to a degree of precision useful to ongoing astrometric programs. This is not to say that there is not room for improvement. Indeed, on many levels the overall occultation program can be expanded and improved upon.

Improvements to the instrumental system at RHO could lead to the successful observation of at least twice as many occultations as are now currently possible. Specifically, all events observed to date were dark limb disappearances. For reappearance events, the star cannot be seen (as the moon is interposed between the star and the telescope prior to the event), and must one rely on the pointing accuracy of the telescope to acquire the unseen star. The 76-centimeter Tinsley reflector, however, lacks the pointing accuracy required to acquire a field typically of less than 15 arc seconds without visual reference.

A 4-inch refracting telescope with a high power eyepiece (to serve as an offset guider) was added to the 76-centimeter telescope. This was done in hope of offsetting to a nearby star, prior to the disappearance of the star under study, and observing the reappearance by guiding on the offset star. This modification, unfortunately, was unsuccessful due to differential flexure in both the telescope superstructure and the secondary mirror support. The mechanical problem of flexure is a difficult one to overcome without major modifications to the telescope structure itself.

A concerted effort to modify the drive system of the RHO 46-centimeter telescope is now beginning. New drive gears along with stepping motors for both the Right Ascension and Declination axes will allow computer control of the telescope for tracking and target acquisition. If this system is successful, the experience gained in its implementation could be used in upgrading the tracking system of the 76-centimeter telescope in a similar manner. With the ability to program differential offsets for target acquisition, the observation of dark limb reappearances becomes feasible.

Bright limb or daylight events could not be observed by the photometric system described in Chapter 2. The brightness level of the background would literally swamp the stellar signal for even the brightest of sources if observed in the visible region of the spectrum. For a number of years observations of lunar occultations of late stars in the infra-red have been made with great success (as in the case of Aldeberan as reported by White and Kreidl, 1984). While such observations are not normally as effective from low altitude sites such as RHO as at high altitude sites, K-Y Chen (1985) has indicated that infrared observations, nevertheless, can be made rather effectively. Recently, P. Chen has been testing a new infrared photometric system on the 76-centimeter telescope. Though the opportunities for infra-red observations of lunar occultations from RHO would be more restrictive than from a high altitude site, on the basis of previous work done at RHO there is reason to believe that such observations would be successful.

Clearly, the next logical step to enhance the occultation program is to move in the direction of simultaneous multicolor observations. This could be done at a minimum expense, and the gain would certainly be worth the small additional effort. The Astromechanics photometer, as previously mentioned, can be used in two channels (i.e., blue and red) simultaneously. A three channel photometer built by Flesch (1975) and used in an investigation of flare stars was recently anodized and could be used for three color observations. Use of the latter would require adding an additional input channel to the SPICA-IV/LODAS for WWVB time code detection as all three 12-bit A-to-D's would be used for acquisition of photometric data. However, the time signal could be detected with only one bit (since it is digital in nature), and this additional input could be added with little impact on the memory allocated for photometric data storage.

Multicolor observations would be advantageous from two viewpoints. First, the simultaneous solution of the residual equations resulting from multicolor observations would be more highly constrained than in the case of one single observations. The time of geometrical occultation must be the same for all colors. This condition, when enforced in the parametric solution, would result in an improved decoupling and, therefore, a more reliable determination of the solution parameters. In addition, while the diffraction fringe spacing scales linearly (in natural units) with wavelength, the effects due to irregularities on the lunar limb do not. Thus, multicolor observations would help differentiate limb effects from diffraction effects for the small number of observations where limb irregularities would otherwise hamper a meaningful solution.

In most cases, for the occultation events which were discussed, the uncertainty in the determined times of geometric occultation did not reflect the statistical uncertainty in the DC solution. Usually, the primary source of the uncertainty in the event timings arose from an inability to detect second transitions in the WWVB time code to a degree commensurable with the precision in the determination of the relative time of geometrical occultation. This situation, brought on by poor radio reception, could probably be improved with a higher gain VLF antenna. A new antenna configuration should be investigated as one of the first items considered in making continued improvements to the occultation instrumental system.

In terms of the numerical procedures used in determining the solution parameters, the consideration of second order terms in the residual equations, as suggested by Eichhorn and Clary (1974), may soon be computationally feasible. The primary reason for the linearization of the residual equations was to reduce the overall computer time necessary to acheive a convergent solution (see Chapter 3). The new generation of array processors or "supercomputers" may remove this artificial computational constraint. Indeed, at least one manufacturer (Analogics Inc, 1984) has announced an array processing computer, with effective execution speeds on the order of tem million floating point operations per second, specifically designed for APL.

The question of the distribution function of lunar limb slopes is not an idle one. Eichhorn (1977) has noted that the least squares solution process could be improved by the introduction of probabilistic constraints in the adjustments. One might reasonably assume that the distribution function of the pre-occultation and post-occultation intensities is a Gaussian (or possibly Poisson) distribution. The distribution function of the lunar limb slopes must, however, be determined empirically. As more occultation observations are made and solved, the better the knowledge of this distribution function becomes. Thus, this is a self-improving process. If one constrains the adjustment of the L-rate on the basis of the observed slope distribution function, then each newly determined slope should be added to the growing baseline data for that distribution. The inclusion of probabilistic constraints, like the consideration of second order terms, is a refinement that deserves investigation and possible future implementation.

The currently discussed observations do leave a number of questions unanswered, as pointed out earlier. As an example, the detected fourth component in the 1 Geminorum system remains a bit of an enigma. Griffin (1984) notes that the probability of non-detection by use of his photoelectric "radial velocity meter" (due to a near zero inclination of the orbital plane) is approximately one part in 800. Yet, the evidence for the existence of the A2 component is quite strong. Photoelectric radial velocity meter measurements, however, are sensitive to the spectral types of the component stars. This instrument requires that a mask be employed whose physical characteristics strongly depend on the anticipated spectral characteristics of the stars under study. The analysis of the spectra of composite stellar systems is enormously complex, and it is quite easy to imagine that a previously unsuspected component could possibly bias the interpretation of those spectra. In any event, the 1 Geminorum system is certainly one that bears further investigation.

Also lurking in the relm of unanswered questions is the unexpectedly large diameter found for ZC2209. Corroborative (or refuting) observations are most certainly needed, and observations of future occultations of this star must be planned and implemented with care.

No observational program can operate in a figurative vacuum. Lunar occultation observations, in particular, could benefit from collaborative observations from more than one site. Since the position angle of the event will vary, as seen from topocentrically different observing stations, stars which are double (or multiple) could be completely solved in terms of the positions of the components. Multiple observations at different lunar geometries will also make any possible distorting limb effects readily apparent. And, of course, multiple observations must independently yield consistent results, and hence, are essential in the confirmation of those results. Efforts should be made, if indeed the occultation program is to continue, to seek out other institutions carrying out similar programs to mount collaborative efforts.

A vacuum, however, in the literal sense, may indeed provide the ideal conditions to observe lunar occultations. As early as 1970, Nather pointed out that the moon, as seen from an orbiting spacecraft, would be stationary in Right Ascension twice each orbit. At those times the time-scale of the movement of the diffraction pattern resulting from the occultation, as projected onto the spacecraft, would be slowed enormously. From a suitably equipped orbital observing platform, data acquisition sampling rates on the order of 1 to 10 Hertz (as opposed to 1000 Hertz) could be employed with no degradation (i.e., smearing) of the diffraction pattern. Thus, from photon statistics alone, the (S+N)/N ratios could be improved by a factor of 10 to 30. This, of course, does not include the added gain of eliminating the effects of atmospheric scintillation, seeing, and transparency variation. The observed intensity curve would be adversely affected only by photon arrival statistics.

By the end of the next calendar year, the Hubble Space Telescope (HST) will be operational. The possibility of using a 94-inch orbital telescope, equipped with a high speed photometer, for spaceborne occultation observations is intriguing. There are two problems which would have to be overcome. First, normal HST operation guidelines disallow the pointing of the telescope in the vicinity of the moon due to possible damage to the various light sensitive detectors in the instruments. Second, HST requires two guide stars in different "pickles" (as described by Giacconi, 1982). The process of guide star selection might prove, in most cases, to be almost impossible. If the target star is about to be occulted then at least one and a half of the three fine guidance sensor "pickles" would be in the moon's shadow, obscuring any possible guide stars. These are technical problems which need careful study. It may indeed turn out that, despite the ideal environment for occultation observations, HST might not be suitable for a majority of candidate events.

One cannot help but reflect on the nearly mind boggling array of spaceborne and "new generation" astronomical instruments which will soon become a reality. The spectrum spanning network of the HST, the Space Infra-Red Telescope Facility, the Advanced X-Ray Astonomy Facility, the Gamma Ray Observatory, as well as UV and EUV telescopes will all be in orbit and operational in the not too distant future. New multi-meter ground-based telescopes with state of the art support equipment are being planned and will be on-line well before the turn of the century. The new 10-meter telescope to be located on the summit of Mauna Kea would be an unparalled achievement in itself, and even now, there is a glimmer of a possibility that two such instruments might be built and operated as an optical interferometer. These new instruments will open up new vistas as of yet unimagined.

Some vocal proponents of spaceborne astronomical facilities have remarked that the days of ground-based observatories are numbered. At the same time, other voices have remarked that ground-based astronomy will be accomplished only by large (greater than approximately 3 meter diameter) telescopes. With "competition" from some of the most sophisticated and finely built opto-electronic instrumentation ever to be constructed, some ask if it is now folly to plan a program for a small, ground based instrument.

The answer to both the cynics and skeptics alike is an unequivocal no. It is a fact that in terms of scientific return (expressed in the now-in-vogue units of photons per dollar), it is the small, research grade instruments which can be the most productive. Institution oriented astronomical sites, such as the University of Florida's Rosemary Hill Observatory, have the luxury of carrying out long term projects, unthinkable and misplaced on large, heavily oversubscribed instruments.

Specifically, telescopes in the 1 meter class are ideal for carrying out occultation observations in the visible and perhaps even near IR wavelengths. In the case of RHO, its other concurrent research programs require dark time, leaving moonlit nights otherwise unused. What better way to fill the unproductive hours than by adding to the knowledge of fundamental astronomical data in the measurement of stellar diameters, elucidation of the geometry and physical makeup of multiple systems, and compilation of a long term baseline of timing data for astrometric purposes?

It is to this end that this program of the observation and analysis of lunar occultations was established. It is hoped that this program will continue in full force and perhaps similar programs implemented at other small, institution oriented astronomical facilities.

APPENDIX A
LISTING OF THE 6502 PROGRAM LODAS (VERSION E07)

This appendix contains the source code for the Lunar Occultation Data Acquisition System software, which is described in Chapter 2. The revision shown here (E07) is currently in use at the Rosemary Hill Observatory.

The assembly of this program was carried out using the ASM6502 cross-assembler, available at the Northeast Regional Data Center (NERDC). The assembly directives seen in this source listing are described by NERDC (1980).

The one statement which is flagged as an error in the compilation actually is not. The ASM6502 cross-assembler has a minor "bug" which caused this valid statement to be flagged. It is assembled correctly, and the erroneous error message does not affect the generated machine code.

```
LOC   OP OPND  VALU  SOURCE STMT

                           ;
                           NAM AIM-65 LUNAR OCCULTATION DATA ACQUISITION SYSTEM
                           ;
                           ; ** LUNAR OCCULTATION DATA ACQUISITION SYSTEM **
                           ;     VERSION R65/E00
                           ;     DEVELOPMENT STARTED (VERS:A001: NOV 05,'80
                           ;     GLENN SCHNEIDER  SSRO 201
                           ;
                           ;   REVISION E06.T: FEB 10,'82
                           ;
                           ;   REVISION: E07  JAN 17,'85   ORIGIN: $0000
                           ;***************************************************************
                           ;
                           ; === SYMBOL DEFINITIONS ===
                           ;
                           ; =I/O ADDRESSING=
                           ;
               0600  OLDTAB EQU $0600    ; LAST CELL USED FOR EACH LINE OF VISUAL MEMORY
               0500  OLDTBB EQU $0500    ; LAST CELL FOR TV CHANNEL 0 (LO RESOLUTION)
               0700  TAPBUF EQU $0700    ; THIS PAGE USED FOR TAPE HEADER BUFFER
               A200  ATDCH1 EQU $A200    ; ANALOG TO DIGITAL CONVERTER CHANNEL 1, BYTE #1
               A300  ATDCH2 EQU $A300    ; ANALOG TO DIGITAL CONVERTER CHANNEL 2, BYTE #2
               A600  ATDCH3 EQU $A600    ; ANALOG TO DIGITAL CONVERTER CHANNEL 3, BYTE #3
               AF00  VIAQRB EQU $AF00    ; V.I.A. DATA OUTPUT REGISTER B
               AF01  VIAQRA EQU $AF01    ; V.I.A. DATA OUTPUT REGISTER A
               AF02  VIAQRB EQU $AF02    ; V.I.A. DATA DIRECTION REGISTER B
               AF03  VIADRA EQU $AF03    ; V.I.A. DATA DIRECTION REGISTER A
               AF0B  VIAACR EQU $AF0B    ; V.I.A. AUXILIARY CONTROL REGISTER
               AF0C  VIAPCR EQU $AF0C    ; V.I.A. PERIPHERAL CONTROL REGISTER
               AF0D  VIAIFR EQU $AF0D    ; V.I.A. INTERUPT FLAG REGISTER
               AF0E  VIAIER EQU $AF0E    ; V.I.A. INTERUPT ENABLE REGISTER
                           ;
                           ; =AIM/65 MONITOR ROUTINES=
                           ;
               EF7B  OUTDDI EQU $EF7B    ; DISPLAY ASCII CHAR IN A TO SEGMENT X
               E93C  READ   EQU $E93C    ; GET ASCII CHAR FROM KEYBOARD PUT IN A REGISTER
               EA84  PACK   EQU $EA84    ; CONVERT HEX # IN A REG TO HEXIDECIMAL ASCII
               E97A  OUTPUT EQU $E97A    ; OUTPUT ASCII CHAR OF HEX VALUE IN A REGISTER TO NEXT SEGM
               EA13  CRLOW  EQU $EA13    ; CARRIAGE RETURN LINE FEED
               E7E1  BKSP   EQU $E7E1
               EBAC  PLXY   EQU $EBAC    ; GET THE X, Y REGISTERS FROM STACK
               EB9E  PHXY   EQU $EB9E    ; PUSH THE X, Y REGISTERS ONTO STACK
               E6E1  PRITR  EQU $E6E1    ; TOGGLE PRINTER ON/OFF
                           ;
                           ; =OTHER CONSTANT ADDRESSES NEEDED=
                           ;
               A00B  UACR   EQU $A00B    ; AUXILIARY CONTROL REGISTER FOR VIA
               A00E  UIER   EQU $A00E    ; INTERUPT ENABLE REGISTER FOR VIA
               A004  UT1LL  EQU $A004    ; T1 TIMER LOW
               A005  UT1CH  EQU $A005    ; T1 TIMER HIGH
               A00D  UIFR   EQU $A00D    ; INTERUPT FLAG REGISTER
               A409  GAP    EQU $A409    ; TAPE SPEED READ/WRITE SYNCHRONIZATION
                           ;
                           ; =PAGE ZERO=
                           ;
                           ; = CONSTANT ADDRESSES NEEDED ON PAGE ZERO=
                           ;
               00EE  SVCEN  EQU $00EE    ; CODOS SVC ENABLE FLAG $80=ON,$00=OFF
                           ;
0000           0000         ORG $0000
                           ;
0000  49             ACTION FCB $49      ; ACTION CODE.
0001  0050           MSBCH1 FDB $5000    ; LOCATION TO STORE MOST SIG. BYTE OF CHNL 1 DATA
0003  0060           MSBCH2 FDB $6000    ; LOCATION TO STORE MOST SIG. BYTE OF CHNL 2 DATA
0005  0070           MSBCH3 FDB $7000    ; LOCATION TO STORE MOST SIG. BYTE OF CHNL 3 DATA
0007  00             CURSTR FCB $00      ; LEAST SIG. BYTE OF CURRENT DATA STORAGE POINTER
0008  00             MSINTC FCB $00      ; MILLISECOND INTERUPT COUNTER
0009  00             MILSEC FCB $00      ; CLOCK BUFFER MILLISECONDS (00-99)
000A  00             HUNSEC FCB $00      ; CLOCK BUFFER HUNDREDTHS OF A SECOND (00-99)
000B  00             SECOND FCB $00      ; CLOCK BUFFER SECONDS (00-59)
000C  00             MINUTE FCB $00      ; CLOCK BUFFER MINUTES (00-59)
000D  00             HOUR   FCB $00      ; CLOCK BUFFER HOURS (00-23)
```

```
LOC  OP OPND    VALU  STMT  SOURCE STMT

000E 00               0073  DAYOWK FCB $00       ; CLOCK BUFFER DAY OF WEEK (0-6)
000F 00               0074  DAYOMT FCB $00       ; CLOCK BUFFER DAY OF MONTH (01-31)
0010 00               0075  MONTH  FCB $00       ; CLOCK BUFFER (01-12)
0011 00               0076  YEAR   FCB $00       ; CLOCK BUFFER (00-99)
0012 00               0077  FRZTME FCB $00       ; STOP/FREEZE TIME DELAY INPUT BY USER
0013 01               0078  SAMRTE FCB $01       ; DATA SAMPLE RATE (MILLISECONDS PER SAMPLE)
0014 00               0079  DSPCH1 FCB $00       ; DISPLAY VALUE FOR CHANNEL 1 INTENSITY
0015 00               0080  DSPCH2 FCB $00       ; DISPLAY VALUE FOR CHANNEL 2 INTENSITY
0016 00               0081  DSPCH3 FCB $00       ; DISPLAY VALUE FOR CHANNEL 3 INTENSITY
0017 00               0082  TWREQF FCB $00       ; TAPE WRITE REQUEST FLAG
0018 00               0083  CWREQF FCB $00       ; CLOCK WRITE REQUEST FLAG
0019 00               0084  TEMP   FCB $00       ; TEMPORARY STORAGE LOCATION USED BY TBTSET
001A 00               0085  TEMPHX FCB $00       ; TEMPORARY STORAGE LOCATION USED BY HXIBCD
001B 000F             0086  TPSTRT FDB $0F00     ; START OF TAPE HEADER
001D FF7F             0087  TPEND  FDB $7FFF     ; END OF TAPE DATA
001F 00               0088  UTMDSP FCB $00       ; UPDATE TIME DISPLAY FLAG 0=NO 1=YES
0020 00               0089  UPCL   FCB $00       ; START OF MESSAGE LOCATION LOW BYTE
0021 00               0090  UPCH   FCB $00       ; START OF MESSAGE LOCATION HIGH BYTE
0022 00               0091  TMPUPD FCB $00       ; TEMPORARY LOCATION USED BY UPDATE ROUTINE
0023 00               0092  FRZFLG FCB $00       ; COUNT FREEZE FLAG 1==>COUNT AFTER ACTION=STOP
0024 00               0093  FZTMEC FCB $00       ; DECREMENTING TIME REMAINING TO END OF FREEZE
0025 00               0094  FRZCTR FCB $00       ; FREEZE COUNTER. COUNTS TENTHS OF A SECOND
0026 43               0095  OLDACT FCB $43       ; OLD ACTION CODE
0027 00               0096  AVGRL1 FCB $00       ; TEMPORARY "AVERAGING REGISTER" USED BY INTRCV
0028 00               0097  AVGRL2 FCB $00       ; DITTO
0029 00               0098  AVGRL3 FCB $00       ; DITTO
002A 00               0099  AVGRH1 FCB $00       ; DITTO
002B 00               0100  AVGRH2 FCB $00       ; DITTO
002C 00               0101  AVGRH3 FCB $00       ; DITTO
002D 00               0102  STPFLG FCB $00       ; STEP FLAG FOR INDICATING CYCLE 0,1,2 OR 3 OF INTRCV
002E 00               0103  SNPFLG FCB $00       ; SNAP FLAG. INDICATING PAGE 0 TO TAPBUF TO BE DONE
002F 00               0104  SAMPNO FCB $00       ; SAMPLE NUMBER USED BY TVDISP
0030 01               0105  SAMCTR FCB $01       ; DATA SAMPLE COUNTER (MODULUS SAMRTE)
0031 01               0106  DISRTE FCB $01       ; DISPAY RATE (EVERY DISRTE POINTS)
0032 00               0107  LINPTP FCB $00       ; LINE POINTER (0-200 DECIMAL) FOR TV DISPLAY
0033 00               0108  CHANEL FCB $00       ; CHANNEL TO BE DISPLAYED ON TV (CHANEL= CH#-1)
0034 00               0109  CHANLB FCB $00       ; LO RES TV CHANNEL
0035 00               0110  LSTPTA FCB $00       ; VALUE OF LAST CELL FOR CHANNEL A DISPLAY
0036 00               0111  LSTPTB FCB $00       ; VALUE OF LAST CELL FOR CHANNEL B DISPLAY
0037 6000             0112  LINEST FDB $0060     ; VECTOR TO FIRST CHAR POSITION OF DISPLAY LINE
0039 4080             0113  BITTAB FDB $8040     ; BIT PATTERN TABLE FOR TV DISPLAY
003B 1020             0114         FDB $2010
003D 0408             0115         FDB $0804
0040 0102             0116         FDB $0201
                      0117  ; >DISPLAY BUFFER FOR OUTPUT USING OUTDD<
0041 00               0118  DBUFF  FCB $00       ; 0=HOUR
0042 00               0119         FCB $00       ; 1=HOUR
0043 00               0120         FCB $00       ; 2=MINUTE
0044 00               0121         FCB $00       ; 3=MINUTE
0045 00               0122         FCB $00       ; 4=SECOND
0046 00               0123         FCB $00       ; 5=SECOND
0047 00               0124         FCB $00       ; 6=BLANK SPACE
0048 00               0125         FCB $00       ; 7=ACTION CODE
0049 00               0126         FCB $00       ; 8=BLANK SPACE
004A 00               0127         FCB $00       ; 9=CHANNEL 1 INTENSITY
004B 00               0128         FCB $00       ; 10=CHANNEL 1 INTENSITY
004C 00               0129         FCB $00       ; 11=CHANNEL 1 INTENSITY
004D 00               0130         FCB $00       ; 12=BLANK SPACE
004E 00               0131         FCB $00       ; 13=CHANNEL 2 INTENSITY
004F 00               0132         FCB $00       ; 14=CHANNEL 2 INTENSITY
0050 00               0133         FCB $00       ; 15=CHANNEL 2 INTENSITY
0051 00               0134         FCB $00       ; 16=BLANK SPACE
0052 00               0135         FCB $00       ; 17=CHANNEL 3 INTENSITY
0053 00               0136         FCB $00       ; 18=CHANNEL 3 INTENSITY
0054 00               0137         FCB $00       ; 19=CHANNEL 3 INTENSITY
                      0138  ;
                      0139  ;
                      0140  ;     <<<<<<<< LODAS/SPICA III MEMORY MAP >>>>>>>>
                      0141  ;
                      0142  ;     START :  USE OF THIS MEMORY REGION      : END
                      0143  ;     ======:=================================:======
                      0144  ;      $0000:                                 :
```

LOC   OP OPND   VALU   STMT   SOURCE STMT

```
:             :  PAGE ZERO.                  :
:             :                              :$00FF
:       ======:==============================:======
:       $0100:
:             :  PAGE ONE. (STACK)           :
:             :                              :$01FF
:       ======:==============================:======
:       $0200:
:             :  FREE SPACE. NOT USED.       :
:             :  USED BY FORTH               :$02FF
:       ======:==============================:======
:       $0300:
:             :  FREE SPACE. NOT USED.       :
:             :  ( MAY BE USED BY FORTH )    :$03FF
:       ======:==============================:======
:       $0400:
:             :  FREE SPACE. NOT USED.       :
:             :  ( MAY BE USED BY FORTH )    :
:             :                              :$05FF
:       ======:==============================:======
:       $0500:
:             :  OLD POINT TV SCREEN TABLE   :
:             :  FOR HI RES GRAPHICS AREA    :
:             :                              :$05FF
:       ======:==============================:======
:       $0600:
:             :  OLD POINT TV SCREEN TABLE   :
:             :  FOR LO RES GRAPHICS AREA    :
:             :                              :$06FF
:       ======:==============================:======
:       $0700:
:             :  TAPE (DISK) HEADER BUFFER   :
:             :                              :$07FF
:       ======:==============================:======
:       $0800:
:             :  CHANNEL 1 DATA STORAGE      :
:             :                              :$1FFF
:       ======:==============================:======
:       $2000:
:             :  CHANNEL 2 DATA STORAGE      :
:             :                              :$37FF
:       ======:==============================:======
:       $3800:
:             :  CHANNEL 3 DATA STORAGE      :
:             :                              :$4FFF
:       ======:==============================:======
:       $5000:
:             :  USED BY CODOS               :
:             :                              :$5FFF
:       ======:==============================:======
:       $6000:
:             :  VISIBLE MEMORY              :
:             :                              :$7FFF
:       ======:==============================:======
:       $8000:
:             :  CODOS                       :
:             :                              :$9FFF
:       ======:==============================:======
:       $A000:
:             :  INPUT/OUTPUT                :
:             :                              :$AFFF
:       ======:==============================:======
:       $B000:
:             :  FORTH ROM (Z26) MODIFIED    :
:             :  FOR <S>,<6> JUMPS TO LODAS  :
:             :                              :$BFFF
:       ======:==============================:======
:       $C000:
:             :  FORTH ROM (Z25)             :
:             :                              :$CFFF
:       ======:==============================:======
:       $D000:
```

```
LOC   OR OPND  VALU  STMT  SOURCE STMT
                     0217         :          :  LODAS F07 SVC TC CODOS   :
                     0218         :                                      :$DFFF
                     0219         :    ======:=============================:======
                     0220         :     $E000:
                     0221         :          :  AIM-65 MONITOR              :
                     0222         :          :                              :$FFFF
                     0223         :    ======:=============================:======
                     0224         :
                     0225         :
                     0226         :
                     0227         :                START OF PROGRAM
                     0228         :
                     0229         :
                     0230         :
D000           0055  0231         ORG $D000      ; ASSEMBLE AT D000. ACCESSED BY AIM-65 <N> COMMAND
                     0232         :
                     0233         ; === PROGRAM INITIALIZATION PROCEEDURE ===
                     0234         :
                     0235         ; .COLD START ENTER WITH <N> ON AIM-65 KEYBOARD
                     0236         ;            ENTER WITH <5> ON AIM-65 KEYBOARD IF MOD FORTH IN
                     0237         :
D000  4C 2DD0  D02D  0238  START5 JMP COLDST     ; GO TO COLD START ROUTINE
                     0239         :
                     0240         ; .WARM START ENTER WITH <6> ON AIM-65 KEYBOARD IF MOD FORTH IN
                     0241         :
D003  4C A3D0  D0A3  0242  START6 JMP WARMST       ; RE-ENTER FROM AIM-65 MONITOR
                     0243         :
                     0244         ; << VECTORS TO LODAS SUBROUTINES >>
                     0245         :
D006  4C 8FD2  D28F  0246  VECTBL JMP COMENT       ; VECTOR TO COMMENT ROUTINE FOR PRINTER/HEADER
D009  4C C5D2  D2C5  0247         JMP GETKEY       ; VECTOR TO KEYBOARD ENTRY WITH WAIT FOR ENTRY
D00C  4C D3D2  D2D3  0248         JMP CLEAR        ; VECTOR TO CLEAR 20 CHARACTER DISPLAY
D00F  4C EBD2  D2EB  0249         JMP PNDM         ; VECTOR TO PRINT AND DISPLAY MESSAGE
D012  4C E1D3  D3E1  0250         JMP TICSET       ; VECTOR TO SET UP TICS ON TV DISPLAY
D015  4C D9D7  D7D9  0251         JMP TVSET        ; VECTOR TO SET UP TV DISPLAY PARAMETERS
D018  4C 92D8  D892  0252         JMP TVCLEA       ; VECTOR TO CLEAR THE TV DISPLAY
D01B  4C ABD8  D8AB  0253         JMP RDCLIN       ; VECTOR TO INITIALIZE CLOCK FOR READING
D01E  4C 22D9  D922  0254         JMP DASET        ; VECTOR TO SET DATA ACQUISITION RATE
D021  4C 0AD3  D30A  0255         JMP TIMSET       ; VECTOR TO INITIALIZE CLOCK
D024  4C 56DA  DA56  0256         JMP OBHXAS       ; VECTOR TO 1-BYTE HEX TO ASCII CONVERSION
D027  4C ACD7  D7AC  0257         JMP HXIBCD       ; VECTOR TO HEX TO 2-BYTE BCD CONVERSION
D02A  4C 19D7  D719  0258         JMP KEYCK        ; VECTOR TO KEYBOARD ENTRY
                     0259         :
                     0260         ; .SET INTERUPT VECTOR ADDRESS.
                     0261         :
D02D  78             0262  COLDST SEI              ; DISABLE INTERUPTS DURING INITIALIZATION
D02E  A9 5D    D45D  0263         LDA #INTRCV      ; AIM INTERUPT AFTER MONITOR SERVICE VECTOR
*** ERROR - STMT#               263                 OUTSIDE OF RANGE
D030  8D 00A4  A400  0264         STA $A400        ; LOW ORDER BYTE
D033  A9 D4    00D4  0265         LDA #INTRCV/256
D035  8D 01A4  A401  0266         STA $A401        ; HIGH ORDER BYTE
                     0267         :
                     0268         ; .PRINT PROGRAM NAME AND VERSION NUMBER.
                     0269         :
D038  20 EBD2  D2EB  0270  LODAS0 JSR PNDM         ; PRINT AND DISPLAY MESSAGE  LODAS VERS:R65/E07
D03B  4C       L     0271         FCC LODAS
D03C  4F       O
D03D  44       D
D03E  41       A
D03F  53       S
D040  20             0272         FCB $20
D041  52       R     0273         FCC R65/E07
D042  36       6
D043  35       5
D044  2F       /
D045  45       E
D046  30       0
D047  37       7
D048  00             0274         FCB $00
D049  20 D3D2  D2D3  0275         JSR CLEAR        ; CLEAR THE DISPLAY
                     0276         :
```

```
LOC   OP OPNO  VALU  STMT  SOURCE STMT
                     0277         ; .INITIALIZE INTERUPT CONTROL REGISTERS ETC.
                     0278         ;
D04C  A9 F0    00F0  0279  SETVIA LDA #$F0      ; SET TIMER T1 FOR INTERUPTS EVERY .5 MILLISECOND
D04E  8D 04A0  A004  0280         STA UT1LL     ; $F0 IS EMPERICAL. SHOULD BE $F4
D051  A9 01    0001  0281         LCA #$01
D053  8D 05A0  A005  0282         STA UT1CH
D056  A9 40    0040  0283         LDA #$40      ; SET AUXILIARY CONTROL REGISTER FOR TIMER T1
D058  8D 0BA0  A00B  0284         STA UACR
                     0285         ;
                     0286         ; .INITIALIZE VIA (6522) FOR USE WITH EXTERNAL CLOCK.
                     0287         ;
D05B  20 8AD8  D88A  0288  CLINIT JSR WRCLIN     ; SET CLOCK CHIP FOR WRITING
D05E  A9 1F    001F  0289         LDA #$1F
D060  8D 03AF  AF03  0290         STA VIADRA
D063  A9 02    0002  0291         LDA #$02
D065  8D 0BAF  AF0B  0292         STA VIAACR
                     0293         ;
D068  A9 11    0011  0294         LDA #$11
D06A  8D 01AF  AF01  0295         STA VIAORA    ; ADDRESS FOR INTERUPT CONTROL REGISTER
D06D  A9 02    0002  0296         LDA #$02
D06F  8D 00AF  AF00  0297         STA VIAOPB    ; DATA FOR INTERUPT CONTROL REGISTER
D072  A9 82    0082  0298         LDA #$82
D074  8D 0EAF  AF0E  0299         STA VIAIER    ; INITIALIZE INTERUPT ENABLE REGISTER
D077  20 AB08  08AB  0300         JSR RDCLIN    ; SET CLOCK FOR READ
                     0301         ;
                     0302         ; .SET TAPE GAP FOR READ/WRITE SYNCHRONIZATION.
                     0303         ;
D07A  A9 20    0020  0304  SETGAP LDA #$20      ; USE 32 (DECIMAL) SYNC CHARACTERS
D07C  8D 09A4  A409  0305         STA GAP
                     0306         ;
                     0307         ; .INITIALIZE FRZTME, AND DISPLAY, TV REGIONS
                     0308         ;
D07F  A9 00    0000  0309         LDA #$00
D081  85 12    0012  0310         STA FRZTME    ; DEFAULT TO NO DELAY
D083  85 33    0033  0311         STA CHANEL    ; DEFAULT CHANNEL 1 TO TV REGION A
D085  85 14    0014  0312         STA DSPCH1    ; SET INTENSITY DISPLAY TO READ ZERO ON INITIAL QUIT
D087  85 15    0015  0313         SIA DSPCH2
D089  85 16    0016  0314         STA DSPCH3
D08B  85 35    0035  0315         STA LSTPTA    ; INITIALIZE LAST TV CELL HI RESOLUTION
D08D  85 36    0036  0316         STA LSTPTB    ; INITIALIZE LAST TV CELL LO RESOLUTION
D08F  A9 01    0001  0317         LCA #$01      ; DEFAULT CHANNEL 2 TO TV REGION B
D091  85 34    0034  0318         STA CHANLB
D093  85 13    0013  0319         SIA SAMRTE    ; INITIALIZE SAMPLE RATE (2 KHZ. PAIR AVERAGED)
D095  85 30    0030  0320         STA SAMCTR    ; INITIALIZE SAMPLE (MODULUS) COUNTER
                     0321         ;
                     0322         ; .GET USER INPUT INITIALIZATION PARAMETERS.
                     0323         ;
D097  20 22D9  D922  0324         JSR DRSET     ; INITIALIZE DATA RATE
D09A  20 9903  D399  0325         JSR FRZSET    ; INITIALIZE THE FREEZE DISPLAY
D09D  20 0907  D709  0326         JSR TVSET     ; INITIALIZE VIDEO DISPLAY FOR "GLASS CHART RCDR"
D0A0  20 0AD3  D30A  0327         JSR TIMSET    ; INITIALIZE U.T. CLOCK
                     0328         ;
                     0329         ; .INITIALIZE ACTION CODE.
                     0330         ;
D0A3  78             0331  WARMST SEI           ; DISABLE INTERUPTS
D0A4  A9 51    0051  0332         LCA #$51      ; ACTION CODE=0 (QUIT)
D0A6  85 00    0000  0333         SIA ACTION
D0A8  85 26    0026  0334         STA OLDACT
D0AA  85 48    0048  0335         STA DBUFF+7   ; STORE IN DISPLAY BUFFER
                     0336         ;
                     0337         ; .INITIALIZE COUNTERS , FLAGS, AND POINTERS.
                     0338         ;
D0AC  A9 64    0064  0339  SETCTR LDA #$64      ; INITIALIZE FREEZE COUNTER (100 MILLISECONDS)
D0AE  85 25    0025  0340         STA FRZCTR
D0B0  A9 00    0000  0341         LDA #$00
D0B2  85 EE    00EE  0342         STA $EE       ; DISABLE SERVICE CALL PROCESSOR
D0B4  85 08    0008  0343         STA MSINTC    ; 0.5 MILLISECOND INTERUPT COUNTER
D0B6  85 17    0017  0344         STA TWREOF    ; TAPE WRITE REQUEST FLAG
D0B8  85 18    0018  0345         STA CWREOF    ; CLOCK WRITE REQUEST FLAG
D0BA  85 23    0023  0346         STA FRZFLG    ; FREEZE FLAG
D0BC  85 2D    0020  0347         STA STPFLG    ; STEP FLAG (CYCLES 0,1,2,3)
D0BE  85 2F    002F  0348         STA SAMPNO    ; SAMPLE NUMBER FOR TV DISPLAY
```

```
LOC   OP DPNO   VALU  STMT  SOURCE STMT

D0C0  85 07     0007  0349         STA CURSTR      ; CURRENT STORAGE POINTER (BYTE IN PAGE)
                      0350         ;
                      0351         ; .INITIALIZE DATA STORAGE ADDRESSES.
                      0352         ;
D0C2  85 01     0001  0353  SETSTL STA MSBCH1      ; CHANNEL 1 = $0800 TO $1FFF
D0C4  85 03     0003  0354         STA MSBCH2      ; CHANNEL 2 = $2000 TO $37FF
D0C6  85 05     0005  0355         STA MSBCH3      ; CHANNEL 3 = $3800 TO $4FFF
D0C8  85 37     0037  0356         STA LINEST
D0CA  A9 08     0008  0357         LDA #$08
D0CC  85 02     0002  0358         STA MSBCH1+1
D0CE  A9 20     0020  0359         LDA #$20
D0D0  85 04     0004  0360         STA MSBCH2+1
D0D2  A9 38     0038  0361         LDA #$38
D0D4  85 06     0006  0362         STA MSBCH3+1
                      0363         ;
                      0364         ; .CLEAR CLOCK INTERUPTS AT VIA.
                      0365         ;
D0D6  A2 10     0010  0366         LDX #$10        ; ADDRESS REGISTER
D0D8  8E 01AF   AF01  0367         STX VIAADRA
D0DB  A0 00AF   AF00  0368         LDA VIAORB      ; DATA REGISTER
                      0369         ;
                      0370         ; .CLEAN UP TIMER T1 (STATE MAY BE UNKNOWN ON WARMSTART).
                      0371         ;
D0DE  A9 40     0040  0372         LDA #$40        ; DISABLE T1 INTERUPTS
D0E0  8D 0EA0   A00E  0373         STA UIER        ; INTERUPT ENABLE REGISTER
D0E3  A0 0DA0   A00D  0374         LDA UIFR        ; CLEAR INTERUPT FLAG REGISTER BY READING AND
D0E6  80 0DA0   A00D  0375         STA UIFR        ; THEN WRITING
                      0376         ;
                      0377         ; .SET UP BIT TABLE FOR TV DISPLAY.
                      0378         ;
D0E9  A0 80     0080  0379  SETBT  LDY #$80        ; INITIALIZE CELL PATTERN (I.E. '10000000')
D0EB  A2 00     0000  0380         LDX #$00        ; USE AS INDEX INTO TABLE TO BE WRITTEN
D0ED  98              0381  SETBT2 TYA             ; GET THE CURRENT PATTERN
D0EE  95 39     D039  0382         STA BITTAB,X    ; STORE IN CURRENT TABLE LOCATION
D0F0  4A              0383         LSR             ; CREATE NEW PATTERN (SHIFT RIGHT ONE BIT)
D0F1  A8              0384         TAY             ; SAVE NEW PATTERN IN Y REGISTER
D0F2  E8              0385         INX             ; INCREMENT THE TABLE POINTER
D0F3  E0 08     0008  0386         CPX #$08        ; HAVE 8 PATTERNS BEEN STORED?
D0F5  D0 F6     D0ED  0387         BNE SETBT2      ; IF NOT GO DO THE NEXT ONE
                      0388         ;
                      0389         ; .SET UP THE VIDEO DISPLAY.
                      0390         ;
D0F7  20 92D8   D892  0391         JSR TVCLEA
D0FA  20 E1C3   C3E1  0392         JSR TICSET
                      0393         ;
                      0394         ; === MAIN DRIVER ROUTINE. SCAN KEYBOARD AND WAIT FOR IRQ ===
                      0395         ;
                      0396         ; .REENABLE INTERUPTS. CHECK SNAP FLAG.
                      0397         ;
D0FD  58              0398  MAIN   CLI
                      0399         ;
                      0400         ; .SCAN KEYBOARD FOR NEW COMMAND.
                      0401         ;
D0FE  20 19D7   D719  0402  SCAN   JSR KEYCK       ; SCAN KEYBOARD RETURN ASCII CODE TO A REGISTER
                      0403         ;
                      0404         ; .NEW ACTION CODE ENTERED FROM KEYBOARD.
                      0405         ;
D101  C9 18     0018  0406         CMP #$18        ; IS THIS A CONTROL X?
D103  D0 0E     D113  0407         BNE SCAN2       ; IF NOT PROCEED NORMALLY
D105  78              0408         SEI             ; IF IT IS DISABLE INTERUPTS
D106  A0 0DA0   A00D  0409         LDA UIFR        ; CLEAR THE EXTERNAL VIA INTERUPT FLAG REGISTER
D109  8D 0DA0   A00D  0410         STA UIFR        ; BY READING AND THEN WRITING
D10C  AD 0DAF   AF0D  0411         LDA VIAIFR      ; CLEAR THE ONBOARD VIA INTERUPT FLAG REGISTER
D10F  8D 0DAF   AF0D  0412         STA VIAIFR      ; BY READING AND THEN WRITING
D112  00              0413         BRK             ; EXIT TO MONITOR
                      0414         ;
D113  C9 FF     00FF  0415  SCAN2  CMP #$FF        ; IF $FF THEN NO KEY DEPRESSED
D115  F0 72     D189  0416         BEQ ACTCHK      ; CHECK THE ACTION CODE
D117  C9 51     0051  0417         CMP #$51        ; IS THIS A 'QUIT' COMMAND?
D119  F0 43     D15E  0418         BEQ NEWCDE      ; IF SO GO TO NEW CODE ROUTINE
D11B  C9 20     0020  0419         CMP #$20        ; IS THIS A CONTROL CODE ( <$20 )?
D11D  90 12     D131  0420         BCC CONCDE      ; IF SO GO TO CONTROL CODE ROUTINE
```

```
LOC   OP OPND   VALU  STMT  SOURCE STMT

                      0421         ;
                      0422         ; .REASSIGN SYNONOMOUS KEYS IF INPUT FROM PADDLE.
                      0423         ;
D11F  C9 27     0027  0424         CMP #$27      ; IS THIS A SYNON FOR 'INTEGRATE'?
D121  D0 05     D128  0425         BNE SYNON1    ; NO. CHECK FOR NEXT SYNON
D123  A9 49     0049  0426         LDA #$49      ; REASSIGN CODE TO $49 ( 'I' )
D125  4C 5ED1   D15E  0427         JMP NEWCDE    ; GO TO NEW CODE ROUTINE
D128  C9 30     0030  0428  SYNON1 CMP #$30      ; IS THIS A SYNON FOR 'QUIT'?
D12A  D0 D2     D0FE  0429         BNE SCAN      ; INVALID ACTION CODE ENTERED. IGNORE IT
D12C  A9 51     0051  0430         LDA #$51      ; REASSIGN NEW CODE TO $51 ( 'Q' )
D12E  4C 5ED1   D15E  0431         JMP NEWCDE    ; GO TO NEW CODE ROUTINE
D131  18              0432  CONCDE CLC           ; A CONTROL CODE WAS ENTERED ADD $40 TO CONVERT
D132  69 40     0040  0433         ADC #$40      ; TO DESIRED CHARACTER FOR ACTION CODE
                      0434         ;
                      0435         ; .CHECK THAT CONTROL CODE IS VALID.
                      0436         ;
D134  C9 43     0043  0437         CMP #$43      ; IS IT A COMMENT CODE?
D136  F0 26     D15E  0438         BEQ NEWCDE    ; YES. GO TO NEW CODE ROUTINE
D138  C9 44     0044  0439         CMP #$44      ; IS IT A "DOS" CODE?
D13A  F0 22     D15E  0440         BEQ NEWCDE    ; YES. GO TO NEW CODE ROUTINE
D13C  C9 46     0046  0441         CMP #$46      ; IS IT A FILE CODE?
D13E  F0 1E     D15E  0442         BEQ NEWCDE    ; YES. GO TO NEW CODE ROUTINE
D140  C9 47     0047  0443         CMP #$47      ; IS THIS A "GO" CLOCK CODE?
D142  F0 1A     D15E  0444         BEQ NEWCDE    ; YES. GO TO NEW CODE ROUTINE
D144  C9 49     0049  0445         CMP #$49      ; IS IT AN INTEGRATE CODE?
D146  F0 16     D15E  0446         BEQ NEWCDE    ; YES. GO TO NEW CODE ROUTINE
D148  C9 50     0050  0447         CMP #$50      ; IS IT A TOGGLE PRINTER CODE?
D14A  F0 12     D15E  0448         BEQ NEWCDE    ; YES. GO TO NEW CODE ROUTINE
D14C  C9 52     0052  0449         CMP #$52      ; IS IT A SAMPLE RATE CODE?
D14E  F0 0E     D15E  0450         BEQ NEWCDE    ; YES. GO TO NEW CODE ROUTINE
D150  C9 54     0054  0451         CMP #$54      ; IS IT A TIME DELAY CODE?
D152  F0 0A     D15E  0452         BEQ NEWCDE    ; YES. GO TO NEW CODE ROUTINE
D154  C9 55     0055  0453         CMP #$55      ; IS IT A UT CLOCK CODE?
D156  F0 06     D15E  0454         BEQ NEWCDE    ; YES. GO TO NEW CODE ROUTINE
D158  C9 56     0056  0455         CMP #$56      ; IS IT A T.V. DISPLAY CODE?
D15A  F0 02     D15E  0456         BEQ NEWCDE    ; YES GO TO NEW CODE ROUTINE
D15C  D0 A0     D0FE  0457         BNE SCAN      ; NO. CODE IS INVALID IGNORE IT
                      0458         ;
D15E  48              0459  NEWCDE PHA           ; PUSH THE NEW CODE ON STACK
D15F  A5 00     0000  0460         LDA ACTION    ; GET THE OLD ACTION CODE
D161  85 26     0026  0461         STA OLDACT    ; SAVE AS THE OLD ACTION CODE
D163  68              0462         PLA           ; GET THE NEW ACTION CODE BACK
D164  85 48     0048  0463         STA DBUFF+7   ; PUT ACTION CODE IN DISPLAY BUFFER
D166  C9 51     0051  0464         CMP #$51      ; IS THIS A "Q" (QUIT) COMMAND
D168  D0 0C     D176  0465         BNE DISNCO    ; IF NOT DISPLAY THE NEW CODE
D16A  A9 01     0001  0466         LDA #$01      ; IT IS A "C" SET FREEZE FLAG
D16C  85 23     0023  0467         STA FRZFLG
D16E  A5 23     0023  0468  FZWAIT LDA FRZFLG    ; GET THE FREEZE FLAG (MAY BE RESET IN INTRCV)
D170  D0 FC     D16E  0469         BNE FZWAIT    ; FREEZE HAS NOT TIMED OUT. WAIT UNTIL IT DOES
D172  A9 51     0051  0470         LDA #$51      ; STORE A 'Q' (QUIT) IN THE ACTION CODE
D174  85 00     0000  0471         STA ACTION
D176  20 D3D2   D2D3  0472  DISNCO JSR CLEAR     ; CLEAR THE DISPLAY
D179  A2 00     0000  0473         LDX #$00      ; OUTPUT DISPLAY BUFFER TO DISPLAY AND PRINTER
D17B  B5 41     0041  0474  NEWCD1 LDA DBUFF,X   ; GET NEXT CHARACTER FROM DISPLAY BUFFER
D17D  20 7AE9   E97A  0475         JSR OUTPUT    ; OUTPUT IT
D180  E8              0476         INX           ; INCREMENT POINTER TO NEXT BUFFER POSITION
D181  8A              0477         TXA           ; GET SEGMENT COUNTER IN A REGISTER
D182  C9 14     0014  0478         CMP #20       ; SEE IF ALL CHARACTERS DISPLAYED
D184  D0 F5     D17B  0479         BNE NEWCD1    ; IF NOT GO DISPLAY NEXT CHARACTER
D186  20 13EA   EA13  0480         JSR CRLOW     ; DO A CARRIAGE RETURN LINE FEED
                      0481         ;
                      0482         ; .CHECK ACTION CODE FOR DIFFERENT POSSIBLE ROUTINES.
                      0483         ;
D189  A5 48     0048  0484  ACTCHK LDA DBUFF+7   ; GET THE NEW ACTION CODE
D18B  85 00     0000  0485         STA ACTION    ; GET THE ACTIN CODE
D18D  C9 51     0051  0486         CMP #$51      ; IS ACTION CODE 'Q' FOR QUIT?
D18F  D0 D3     D194  0487         BNE ACTCKC    ; NO. GO CHECK IF ACTION IS 'C'
D191  4C 13D2   D213  0488         JMP DISTME    ; GO UPDATE DISPLAY
D194  C9 43     0043  0489  ACTCKC CMP #$43      ; IS ACTION CODE 'C' FOR COMMENT?
D196  D0 06     D19E  0490         BNE ACTCKD    ; NO. GO CHECK IF ACTION IS 'D'
D198  20 8FD2   D28F  0491         JSR COMENT    ; ACTION IS=A GO TO COMMENT ROUTINE
D19B  4C 13D2   D213  0492         JMP DISTME    ; BACK FROM COMMENT ROUTINE. GO UPDATE DISPLAY
```

```
LOC   OP DPND   VALU  STMT  SOURCE STMT

019E  C9 44     0044  0493  ACTCKD CMP #$44       ; IS ACTION CODE 'D' FOR DOS?
01A0  D0 13     01B5  0494         BNE ACTCKU     ; NO, GO CHECK IF ACTION CODE IS 'U'
01A2  78              0495         SEI            ; DISABLE INTERUPTS
01A3  A9 8D     008D  0496         LDA #$8D       ; ENABLE SERVICE CALL PROCESSOR
01A5  85 EE     00EE  0497         STA $EE
01A7  AD 0DA0   A00D  0498         LDA UIFR       ; CLEAR THE VIA INTERUPT FLAG REGISTERS
01AA  8D 0DA0   A00D  0499         STA UIFR
01AD  AD 0DAF   AF0D  0500         LDA VIAIFR
01B0  8D 0DAF   AF0D  0501         STA VIAIFR
01B3  00              0502         BRK
01B4  00              0503         BRK
01B5  C9 55     0055  0504  ACTCKU CMP #$55       ; IS ACTION CODE='U' (U.T. CLOCK)
01B7  D0 12     01CB  0505         BNE ACTCKG     ; NO, GO CHECK IF ACTION IS 'G'
01B9  A9 01     0001  0506         LDA #$01       ; YES, SET THE CLOCK WRITE REQUEST FLAG
01BB  85 18     0018  0507         STA CWREOF
01BD  A5 18     0018  0508  CWWAIT LDA CWREOF     ; HAS COUNTDOWN TO CLOCK WRITE EXPIRED?
01BF  D0 FC     01BD  0509         BNE CWWAIT     ; TIGHT LOOP, WAIT FOR EXPIRATION
01C1  78              0510         SEI            ; DISABLE PROCESSOR INTERUPTS
01C2  20 0AD3   D30A  0511         JSR TIMSET     ; GO TO TIME SET ROUTINE
01C5  20 AED9   D9AE  0512         JSR CLENUP     ; GO TO INTERUPT DISABLE CLEAN UP ROUTINE
01C8  4C 13D2   D213  0513         JMP DISTME     ; BACK FROM TIMSET, GO UPDATE DISPLAY
01CB  C9 47     0047  0514  ACTCKG CMP #$47       ; IS ACTION CODE='G' ("GO" CLOCK COMMAND)?
01CD  D0 D6     01D5  0515         BNE ACTCKT     ; NO, GO CHECK IF ACTION IS 'T'
01CF  20 FFD8   D8FF  0516         JSR TIMGO      ; ACTION IS=G GO TO "GO" CLOCK ROUTINE
01D2  4C 13D2   D213  0517         JMP DISTME     ; BACK FROM TIMGO, GO UPDATE DISPLAY
01D5  C9 54     0054  0518  ACTCKT CMP #$54       ; IS ACTION CODE 'T' FOR TIME DELAY?
01D7  D0 06     01DF  0519         BNE ACTCKP     ; NO, GO CHECK IF ACTION IS 'P'
01D9  20 9903   0399  0520         JSR FRZSET     ; ACTION=T GO TO FREEZE/DELAY SET ROUTINE
01DC  4C 13D2   D213  0521         JMP DISTME     ; GO UPDATE DISPLAY
01DF  C9 50     0050  0522  ACTCKP CMP #$50       ; IS ACTION CODE 'P' FOR PRINTER TOGGLE
01E1  D0 06     01E9  0523         BNE ACTCKV     ; NO, GO CHECK IF ACTION CODE IS 'V'
01E3  20 8ED2   D2BE  0524         JSR TOGPRT     ; IT IS 'P', GO TOGGLE PRINTER
01E6  4C 13D2   D213  0525         JMP DISTME     ; BACK FROM TOGPRT, GO UPDATE DISPLAY
01E9  C9 56     0056  0526  ACTCKV CMP #$56       ; IS ACTION CODE 'V' FOR VIDEO DISPLAY SET?
01EB  D0 D6     01F3  0527         BNE ACTCKR     ; NO, GO CHECK IF ACTION IS 'R'
01ED  20 D907   D7D9  0528         JSR TVSET      ; ACTION=V GO SET UP VIDEO DISPLAY PARAMETERS
01F0  4C 13D2   D213  0529         JMP DISTME     ; GO UPDATE DISPLAY
01F3  C9 52     0052  0530  ACTCKR CMP #$52       ; IS ACTION CODE 'R' FOR SAMPLE RATE?
01F5  D0 06     01FD  0531         BNE ACTCKF     ; NO, GO CHECK IF ACTION CODE IS 'F'
01F7  20 2209   D922  0532         JSR ORSET      ; ACTION=R, GO SET UP DATA SAMPLING RATE
01FA  4C 13D2   D213  0533         JMP DISTME     ; GO UPDATE DISPLAY
01FD  C9 46     0046  0534  ACTCKF CMP #$46       ; IS ACTION CODE 'F' FOR FILE?
01FF  D0 0B     020C  0535         BNE DSPCHK     ; IF NO, THEN GO CHECK IF DISPLAY NEEDS UPDATING
0201  A9 01     0001  0536         LDA #$01       ; SET TAPE WRITE REQUEST FLAG
0203  85 17     0017  0537         STA TWREOF
0205  A5 17     0017  0538  TWWAIT LDA TWREOF     ; HAS COUNTDOWN TO TAPE WRITE EXPIRED?
0207  D0 FC     0205  0539         BNE TWWAIT     ; TIGHT LOOP, WAIT FOR EXPIRATION
0209  4C 6AD9   D96A  0540         JMP TAPINT     ; GO TO TAPE WRITTING ROUTINE
                      0541         ;
                      0542         ; .SEE IF DISPLAY NEEDS UPDATING.
                      0543         ;
020C  A5 1F     001F  0544  DSPCHK LDA UTMDSP     ; GET UPDATE DISPLAY FLAG
020E  D0 03     0213  0545         BNE DISTME     ; IF FLAG IS SET GO UPDATE DISPLAY
0210  4C FDD0   D0FD  0546         JMP MAIN       ; ===> GO BACK TO MAIN ===>
                      0547         ;
                      0548         ; .UPDATE DISPLAY BUFFER.
                      0549         ;
0213  A5 0D     000D  0550  DISTME LDA HOUR       ; GET THE CURRENT HOUR
0215  A2 00     0000  0551         LDX #$00       ; HOUR DISPLAY IN BUFFER POSITION 00 AND 01
0217  20 6AD2   D26A  0552         JSR PDASC2     ; STUFF 2 BYTE ASCII FOR HOUR INTO BUFFER
021A  A5 0C     000C  0553         LDA MINUTE     ; GET THE CURRENT MINUTE
021C  A2 02     0002  0554         LDX #$02       ; MINUTE DISPLAY IN BUFFER POSITION 02 AND 03
021E  20 6AD2   D26A  0555         JSR PDASC2     ; STUFF 2 BYTE ASCII FOR MINUTE INTO BUFFER
0221  A5 0B     000B  0556         LDA SECOND     ; GET THE CURRENT SECOND
0223  A2 04     0004  0557         LDX #$04       ; HOUR DISPLAY IN BUFFER POSITION 04 AND 05
0225  20 6AD2   D26A  0558         JSR PDASC2     ; STUFF 2 BYTE ASCII FOR SECOND INTO BUFFER
0228  A5 00     0000  0559         LDA ACTION     ; GET CURRENT ACTION CODE
022A  85 48     0048  0560         STA DBUFF+7    ; PUT ACTION CODE IN BUFFER POSITION 07
022C  A5 14     0014  0561         LDA DSPCH1     ; GET CURRENT CHANNEL 1 INTENSITY VALUE
022E  A2 09     0009  0562         LDX #$09       ; TO GO INTO BUFFER POSITION 09, 0A, 0B
0230  20 7FD2   D27F  0563         JSR HXASC3     ; STUFF 3 BYTE ASCII FOR CHANNEL 1 INTO BUFFER
0233  A5 15     0015  0564         LDA DSPCH2     ; GET CURRENT CHANNEL 2 INTENSITY VALUE
```

```
LOC   OP OPNO  VALU  STMT  SOURCE STMT

D235  A2 00    000D  0565         LDX #$0D       ; TO GO INTO BUFFER POSITIONS 00, 0E, 0F
D237  20 7F02  D27F  0566         JSR HXASC3     ; STUFF 3 BYTE ASCII FOR CHANNEL 2 INTO BUFFER
D23A  A5 16    0016  0567         LDA DSPCH3     ; GET CURRENT CHANNEL 3 INTENSITY VALUE
D23C  A2 11    0011  0568         LDX #$11       ; TO GO INTO BUFFER POSITIONS 11,12,13
D23E  20 7FD2  027F  0569         JSR HXASC3     ; STUFF 3 BYTE ASCII FOR CHANNEL 3 INTO BUFFER
D241  A9 20    0020  0570         LDA #$20       ; BLANK SPACES ON DISPLAY
D243  85 47    0047  0571         STA DBUFF+6
D245  85 49    0049  0572         STA DBUFF+8
D247  85 4D    004D  0573         STA DBUFF+$C
D249  85 51    0051  0574         STA DBUFF+$10
                     0575         ;
                     0576         ; .REWRITE THE DISPLAY WITH TIME, ACTION CODE, CHANNEL COUNTS
                     0577         ;
D24B  20 5502  0255  0578  DISPLY JSR DISBUF     ; OUTPUT DISPLAY BUFFER
D24E  A9 00    0000  0579         LDA #$00       ; CLEAR UPDATE TIME DISPLAY FLAG
D250  85 1F    001F  0580         STA UTMDSP
D252  4C F0D0  D0FD  0581         JMP MAIN       ; ===> GO BACK TO MAIN ===>
                     0582         ;
                     0583         ; .OUTPUT THE DISPLAY BUFFER.
                     0584         ;
D255  A2 14    0014  0585  DISBUF LDX #$14       ; INITIALIZE SEGMENT COUNTER TO ONE PAST LAST SEGMENT
D257  CA             0586  DISBF2 DEX            ; DECREMENT SEGMENT COUNTER
D258  8A             0587         TXA            ; SAVE SEGMENT COUNTER BY PUSHING IT ON STACK
D259  48             0588         PHA            ; THE OUTDDI ROUTINE CLOBBERS THE X REGISTER
D25A  B5 41    0041  0589         LDA DBUFF,X    ; LOAD THE ACCUMULATOR WITH CHARACTER TO BE OUTPUT
D25C  09 80    0080  0590         ORA #$80       ; SET HI BIT FOR DIRECT DISPLAY
D25E  20 70EF  EF70  0591         JSR OUTDDI     ; OUTPUT A REGISTER TO SEGMENT X
D261  68             0592         PLA            ; RESTORE THE SEGMENT COUNTER TO X REGISTER
D262  AA             0593         TAX
D263  D0 F2    D257  0594         BNE DISBF2     ; IF MORE TO OUTPUT GO DO IT
D265  60             0595         RTS            ; ALL DONE
                     0596         ;
                     0597         ; *PUT TWO BYTE ASCII INTO OUTPUT BUFFER*
                     0598         ;
D266  A8             0599  HXASC2 TAY            ; USE HEX VALUE OF A AS OFFSET TO DECIMAL CHAR TABLE
D267  B9 690A  0A69  0600         LDA CLCTBL,Y   ; GET THE DECIMAL VALUE
D26A  85 22    0022  0601  PDASC2 STA TMPUPD     ; SAVE PACKED DECIMAL IN TEMPORARY LOCATION TMPUPD
D26C  20 620A  0A62  0602  HIOUT  JSR LHWDFA     ; GET LEFT HALF WORD OF A REGISTER
D26F  18             0603         CLC
D270  69 30    0030  0604         ADC #$30       ; CONVERT TO ASCII
D272  95 41    0041  0605         STA DBUFF,X    ; PUT IN BUFFER POSITION X
D274  E8             0606         INX            ; SET FOR NEXT BUFFER POSITION
D275  A5 22    0022  0607         LDA TMPUPD     ; GET BACK ORIGINAL DECIMAL VALUE
D277  29 0F    000F  0608  LOWOUT AND #$0F       ; LOOK AT SECOND DECIMAL DIGIT
D279  18             0609         CLC
D27A  69 30    0030  0610         ADC #$30       ; CONVERT TO ASCII
D27C  95 41    0041  0611         STA DBUFF,X    ; PUT IN BUFFER POSITION X
D27E  60             0612         RTS
                     0613         ;
                     0614         ; *PUT THREE BYTE ASCII INTO OUTPUT BUFFER*
                     0615         ;
D27F  20 ACD7  07AC  0616  HXASC3 JSR HX1BCD     ; CONVERT HEX TO TWO BYTE DECIMAL
D282  85 22    0022  0617         STA TMPUPD     ; PUT TENS AND DIGITS IN TEMP LOCATION
D284  98             0618         TYA            ; PUT HUNDREDS DIGIT IN A REGISTER
D285  20 7702  D277  0619         JSR LOWOUT     ; PUT ASCII CHAR FOR THIS DIGIT IN DISPLAY BUFFER
D288  A5 22    0022  0620         LDA TMPUPD     ; GET TENS AND DIGITS VALUE
D28A  E8             0621         INX            ; SET NEXT DISPLAY BUFFER POSITION
D28B  20 6CD2  026C  0622         JSR HIOUT      ; PUT THESE TWO BYTES IN DISPLAY BUFFER
D28E  60             0623         RTS
                     0624         ;
                     0625         ; *ENTER COMMENTS ON PRINTER FROM JPO*
                     0626         ;
D28F  20 EBD2  02EB  0627  COMENT JSR PNDM       ; OUTPUT THE COMMENT PROMPT >
D292  3E       >     0628         FCC >
D293  00             0629         FCB $00
D294  A2 00    0000  0630         LDX #$00       ; X REGISTER USED AS CHARACTER COUNTER
D296  20 C502  02C5  0631  COMC1  JSR GETKEY     ; GET A CHARACTER FROM KEYBOARD
D299  C9 7F    007F  0632         CMP #$7F       ; IS THIS A DELETE?
D29B  D0 0B    02A8  0633         BNE COMC2      ; IF NOT GO TO COMC2
D29D  E0 00    0000  0634         CPX #$00       ; IS THIS THE FIRST CHARACTER?
D29F  F0 F5    D296  0635         BEQ COMC1      ; IT IS, GO BACK TO GET FIRST CHARACTER
D2A1  20 E1E7  E7E1  0636         JSR BKSP       ; JSR TO MONITOR BACKSPACE ROUTINE
```

```
LOC   OP OPND  VALU  STMT  SOURCE STMT

02A4  CA             0637         DEX           ; DECREMENT THE CHARACTER COUNT
02A5  18             0638         CLC
02A6  90 EE    0296  0639         BCC CONC1     ; RETURN TO GET NEXT CHARACTER
02A8  C9 0D    000D  0640  CONC2  CMP #$0D      ; IS THIS A CARRIAGE RETURN?
02AA  F0 0B    02B7  0641         BEQ CONC4     ; IF IT IS GO TO CONC4
02AC  20 7AE9  E97A  0642         JSR OUTPUT    ; OUTPUT CHARACTER
02AF  9D 2107  0721  0643         STA TAPBUF+$21,X ; SAVE IN TAPE HEADER BUFFER IN CASE NEEDED
02B2  E8             0644         INX           ; INCREMENT THE CHARACTER COUNTER
02B3  E0 27    0027  0645         CPX #$27      ; HAVE $27 CHARACTERS BEEN ENTERED?
02B5  D0 DF    0296  0646         BNE CONC1     ; GO GET NEXT CHARACTER
02B7  20 13EA  EA13  0647  CONC4  JSR CRLOW
02BA  20 CFD7  D7CF  0648         JSR ROLACT
02BD  60             0649         RTS
                     0650         ;
                     0651         ; *TOGGLE PRINTER ON/OFF*
                     0652         ;
02BE  20 E1E6  E6E1  0653  TOGPRT JSR PRITR     ; TOGGLE THE PRINTER
02C1  20 CFD7  D7CF  0654         JSR ROLACT    ; RESTORE OLD ACTION CODE
02C4  60             0655         RTS
                     0656         ;
                     0657         ; *GET A KEY PRESS, WAIT IF NO ENTRY*
                     0658         ;
02C5  20 9EE8  E89E  0659  GETKEY JSR PHXY
02C8  20 19D7  D719  0660  GETK1  JSR KEYCK
02CB  C9 FF    00FF  0661         CMP #$FF
02CD  F0 F9    02C8  0662         BEQ GETK1
02CF  20 ACE8  E8AC  0663         JSR PLXY
02D2  60             0664         RTS
                     0665         ;
                     0666         ; *CLEAR DISPLAY, FROM JPO*
                     0667         ;
02D3  48             0668  CLEAR  PHA           ; SAVE THE A REGISTER ON STACK
02D4  8A             0669         TXA           ; SAVE THE X REGISTER ON STACK
02D5  48             0670         PHA
02D6  A2 13    0013  0671         LDX #$13      ; USE X AS DISPLAY ELEMENT COUNTER $13=20
02D8  8A             0672  CLEA1  TXA
02D9  48             0673         PHA
02DA  A9 A0    00A0  0674         LDA #$A0      ; $20(SPACE) + $80 (NO CURSOR)
02DC  20 7BEF  EF7B  0675         JSR OUTDO1    ; OUTPUT BLANK TO DISPLAY AT CURRENT POSITION
02DF  68             0676         PLA
02E0  AA             0677         TAX
02E1  CA             0678         DEX           ; NEXT POSITION
02E2  10 F4    02D8  0679         BPL CLEA1     ; NOT DONE, MORE SPACES NEEDED
02E4  20 13EA  EA13  0680         JSR CRLOW     ; CARRIAGE RETURN LINE FEED
02E7  68             0681         PLA           ; RESTORE REGISTERS
02E8  AA             0682         TAX
02E9  68             0683         PLA
02EA  60             0684         RTS
                     0685         ;
                     0686         ; *PRINT AND DISPLAY MESSAGE FROM JPO*
                     0687         ;
02EB  68             0688  PNOM   PLA           ; GET ADDRESS OF CALLING ROUTINE
02EC  85 20    0020  0689         STA UPCL      ; STORE LOW BYTE
02EE  68             0690         PLA
02EF  85 21    0021  0691         STA UPCH      ; STORE HIGH BYTE
02F1  A0 00    0000  0692         LDY #$00      ; INITIALIZE OFFSET POINTER FOR FIRST CHARACTER
02F3  E6 20    0020  0693  PNOM1  INC UPCL      ; POINTER TO START OF MESSAGE
02F5  D0 02    02F9  0694         BNE PNOM2     ; IF NOT ON NEW PAGE GO TO PNOM2
02F7  E6 21    0021  0695         INC UPCH      ; SINCE IS ON NEW PAGE INCREMENT HIGH BYTE
02F9  B1 20    0020  0696  PNOM2  LDA (UPCL),Y  ; GET NEXT CHARACTER TO DISPLAY
02FB  F0 06    0303  0697         BEQ PNOM3     ; IF IS $00 THEN NO MORE
02FD  20 7AE9  E97A  0698         JSR OUTPUT    ; OUTPUT THE CHARACTER
0300  18             0699         CLC
0301  90 F0    02F3  0700         BCC PNOM1     ; GET NEXT CHARACTER
0303  A5 21    0021  0701  PNOM3  LDA UPCH      ; RESTORE LOCATION OF CALLING ROUTINE TO STACK
0305  48             0702         PHA
0306  A5 20    0020  0703         LDA UPCL
0308  48             0704         PHA
0309  60             0705         RTS
                     0706         ;
                     0707         ;
                     0708         ; *SET CLOCK TIMER, HOURS, MINUTES, SECONDS*
```

```
LOC   OP DPND  VALU  STMT  SOURCE STMT

                     0709         ;
D30A  20 D3D2  D2D3  0710  TIMSET JSR CLEAR     ; CLEAR THE DISPLAY
D30D  20 EBC2  D2EB  0711         JSR PNDM      ; PRINT THE DATE PROMPT
D310  59     Y       0712         FCC YYMMDD:
D311  59     Y
D312  4D     M
D313  4D     M
D314  44     D
D315  44     D
D316  3A     :
D317  00             0713         FCB $00
D318  20 3CE9  E93C  0714         JSR READ      ; READ KEYBOARD
D31B  C9 0D    000D  0715         CMP #13       ; IS THIS A CARRIAGE RETURN?
D31D  FD 1F    D33E  0716         BEQ TMSET2    ; IF IT IS GO SET THE TIME
D31F  20 C7D3  D3C7  0717         JSR PACK2B    ; GET NEXT CHARACTER IN YEAR
D322  85 11    0011  0718         STA YEAR      ; SAVE IN YEAR
D324  20 C4D3  D3C4  0719         JSR PACK2     ; GO GET THE MONTH
D327  05 10    0010  0720         STA MONTN     ; STORE MONTH VALUE
D329  20 D7D3  D3D7  0721         JSR DECHEX    ; CONVERT TO HEXIDECIMAL
D32C  C9 0D    000D  0722         CMP #13       ; IS MONTH ENTERED >=13?
D32E  B0 DA    D30A  0723         BCS TIMSET    ; IF SO, NO GOOD, REPROMPT INPUT
D330  20 C4D3  D3C4  0724         JSR PACK2     ; GO GET THE DAY (1-31) FROM KEYBOARD
D333  05 0F    000F  0725         STA DAYDMT    ; STORE DAY VALUE
D335  20 D7D3  D3D7  0726         JSR DECHEX    ; CONVERT TO HEXIDECIMAL
D330  F0 D0    D30A  0727         BEQ TIMSET    ; 0 INVALID REPROMPT INPUT
D33A  C9 20    0020  0728         CMP #32       ; IS DATE >=32?
D33C  B0 CC    D30A  0729         BCS TIMSET    ; IF SO, NO GOOD, REPROMPT INPUT
                     0730         ;
D33E  20 D3D2  D2D3  0731  TMSET2 JSR CLEAR     ; CLEAR THE DISPLAY
D341  20 EBD2  D2EB  0732         JSR PNDM      ; PRINT THE DAY OF WEEK PROMPT
D344  44     D       0733         FCC DAY(1=SUN):
D345  41     A
D346  59     Y
D347  20     (
D340  31     1
D349  3D     =
D34A  53     S
D34B  55     U
D34C  4E     N
D34D  29     )
D34E  3A     :
D34F  00             0734         FCB $00
D350  20 3CE9  E93C  0735         JSR READ      ; READ KEYBOARD
D353  20 7AE9  E97A  0736         JSR OUTPUT    ; OUTPUT TO DISPLAY
D356  C9 0D    000D  0737         CMP #13       ; IS THIS A CARRIAGE RETURN
D350  F0 0D    D367  0730         BEQ TMSET3    ; IF IT IS GO SET THE TIME
D35A  C9 31    0031  0739         CMP #$31      ; 0 INVALID REPROMPT INPUT
D35C  90 E0    D33E  0740         BCC TMSET2
D35E  C9 30    0030  0741         CMP #$38      ; IS DAY OF WEEK >=8?
D36D  B0 DC    D33E  0742         BCS TMSET2    ; IF SO, NO GOOD, REPROMPT INPUT
D362  10             0743         CLC           ; CONVERT TO PACKED DECIMAL
D363  29 0F    000F  0744         AND #$0F
D365  05 0E    000E  0745         STA DAYDWK    ; STORE DAY OF WEEK
                     0746         ;
D367  20 D3D2  D2D3  0747  TMSET3 JSR CLEAR     ; CLEAR THE DISPLAY
D36A  20 EBD2  D2EB  0748         JSR PNDM      ; PRINT THE TIME PROMPT
D36D  40     H       0749         FCC HNMM:
D36E  48     N
D36F  4D     M
D370  4D     M
D371  3A     :
D372  D0             0750         FCB $00
D373  20 3CE9  E93C  0751         JSR READ      ; READ KEYOCARD
D376  C9 0D    000D  0752         CMP #13       ; IS THIS A CARRIAGE RETURN?
D370  F0 18    D392  0753         BEQ TMSET4    ; IF IT IS CLEAN UP FOR EXIT
D37A  20 C7D3  D3C7  0754         JSR PACK2B    ; GET NEXT CHARACTER IN NOUR
D37D  05 0D    000D  0755         STA HOUR      ; STORE NOUR
D37F  20 D7D3  D3D7  0756         JSR DECHEX    ; CONVERT TC HEXIDECIMAL
D382  C9 18    0018  0757         CMP #24       ; IS NOUR >=24
D384  B0 E1    D367  0750         BCS TMSET3    ; IF SO, NO GOOD, REPROMPT INPUT
D306  20 C4D3  D3C4  0759         JSR PACK2     ; GET MINUTE FROM KEYBOARD
D309  05 0C    000C  0760         STA MINUTE    ; STORE MINUTE
```

```
LOC   OP DPND  VALU  STMT  SOURCE STMT

D38B  20 D7D3  D3D7  0761         JSR DECHEX    ; CONVERT TO HEXIDECIMAL
D38E  C9 3D    003D  0762         CMP #61       ; IS THIS >=61?
D390  B0 D5    D367  0763         BCS TMSET3    ; IF SO, NO GOOD, REPROMPT INPUT
D392  20 FFD8  D8FF  0764  TMSET4 JSR TIMGO     ; GO TO "GO" COMMAND FOR TIMER
D395  20 CFD7  D7CF  0765         JSR ROLACT    ; RESET OLD ACTION CODE
D398  60             0766         RTS
                     0767         ;
                     0768         ; *SET STOP/FREEZE DELAY*
                     0769         ;
D399  20 EBD2  D2EB  0770  FRZSET JSR PNDM      ; PRINT AND DISPLAY MESSAGE  DELAY 1/10 SECS:
D39C  44       D     0771         FCC DELAY
D39D  45       E
D39E  4C       L
D39F  41       A
D3A0  59       Y
D3A1  20             0772         FCB $20
D3A2  31       1     0773         FCC 1/10
D3A3  2F       /
D3A4  31       1
D3A5  30       0
D3A6  20             0774         FCB $20
D3A7  53       S     0775         FCC SECS:
D3A8  45       E
D3A9  43       C
D3AA  53       S
D3AB  3A       :
D3AC  D0             0776         FCB $00
D3AD  20 3CE9  E93C  0777         JSR READ      ; GET THE FIRST CHARACTER OF KEYBOARD ENTRY
D3B0  C9 0D    000D  0778         CMP #13       ; IS THIS A CARRIAGE RETURN?
D3B2  D0 02    D3B6  0779         BNE FRZST1    ; NO, CONTINUE SETTING DELAY TIME
D3B4  F0 0A    D3C0  0780         BEQ FRZST2    ; YES, DO NOT RESET, LEAVE EXISTING VALUE
D3B6  20 C7D3  D3C7  0781  FRZST1 JSR PACK2B    ; GET NEXT CHARACTER IN FREEZE IIME FROM KEYBOARD
D3B9  20 D7D3  D3D7  0782         JSR DECHEX    ; CONVERT TO HEXIDECIMAL
D3BC  85 12    0012  0783         STA FRZTME    ; SAVE DELAY TIME
D3BE  85 24    0024  0784         STA FZTMEC    ; SAVE IN FREEZE TIME COUNTDOWN COUNTER
D3C0  20 CFD7  D7CF  0785  FRZST2 JSR ROLACT    ; RESTORE OLD ACTION CODE
D3C3  60             0786         RTS
                     0787         ;
                     0788         ; *GET 2 DIGIT # FROM KEYBOARD, OUTPUT, AND
                     0789         ;  PUT PACKED DECIMAL IN A REGISTER*
                     0790         ;
D3C4  20 3CE9  E93C  0791  PACK2  JSR READ      ; GET FIRST DIGIT FROM KEYBOARD
D3C7  20 7AE9  E97A  0792  PACK2B JSR OUTPUT    ; DISPLAY FIRST DIGIT
D3CA  20 84EA  EA84  0793         JSR PACK      ; STORE HEX REPRESENTATION IN MSB OF A
D3CD  20 3CE9  E93C  0794         JSR READ      ; GET SECOND DIGIT FROM KEYBOARD
D3D0  20 7AE9  E97A  0795         JSR OUTPUT    ; DISPLAY SECOND DIGIT
D3D3  20 84EA  EA84  0796         JSR PACK      ; STORE HEX REPRESENTATION IN LSB OF A
D3D6  60             0797         RTS
                     0798         ;
                     0799         ; *CONVERT PACKED DECIMAL TO HEXIDECIMAL*
                     0800         ;
D3D7  A2 FF    00FF  0801  DECHEX LDX #$FF      ; INITIALIZE OFFSET POINTER, WILL BE INCREMENTED
D3D9  E8             0802         INX           ; USE X REGISTER TO SEARCH TABLE OF VALUES
D3DA  DD 69DA  DA69  0803         CMP CLCTBL,X  ; IS THE VALUE IN A SAME AS IN TABLE HERE?
D3DD  D0 FA    D3D9  0804         BNE DECHEX+2  ; IF NOT GET NEXT TABLE VALUE
D3DF  8A             0805         TXA           ; SAVE IT'S POSITION IN THE A REGISTER
D3E0  60             0806         RTS
                     0807         ;
                     0808         ; *SET UP TICS ON VIDEO DISPLAY*
                     0809         ;
D3E1  A2 00    0000  0810  TICSET LDX #$00      ; FOR UPPER PORTION OF SCREEN, START AT LINE 0
D3E3  B0 6DDB  DB6D  0811         LDA TVTBLL,X  ; SET UP LINE POINTER LO BYTE
D3E6  85 37    0037  0812         STA LINEST
D3E8  BD 35DC  DC35  0813         LDA TVTBLH,X  ; SET UP LINE POINTER HI BYTE
D3EB  85 38    0038  0814         STA LINEST+1
D3ED  AD 00    0000  0815         LDY #$00      ; OFFSET INTO CHARACTER TABLE FOR TICS
D3EF  B9 CODA  DACD  0816  TICST1 LDA TVTICS,Y  ; GET THE Y'TH CHAR IN TIC TABLE
D3F2  91 37    0037  0817         STA (LINEST),Y ; STORE IT TO THE SCREEN
D3F4  C8             0818         INY           ; INCREMENT FOR NEXT CHARACTER
D3F5  C0 A0    00A0  0819         CPY #160      ; HAVE 160 (DECIMAL) CELLS BEEN FILLED?
D3F7  D0 F6    D3EF  0820         BNE TICST1    ; IF NOT DO THE NEXT ONE
                     0821         ;
```

```
LOC   OP CPND   VALU   SOURCE STMT

D3F9  A2 C3     00C3           LDX #$C3        ; TIC MARKS FOR BOTTEM OF SCREEN
D3FB  BD 6DDB   0860           LDA TVTBLL,X    ; SEED THE LINE START VECTOR AT ONE LESS
D3FE  85 37     0037           STA LINEST      ; THAN THE LINE WANTED. WILL DRAW 3 ROWS OF TICS
D400  BD 35CC   DC35           LDA TVTBLH,X
D403  85 38     0038           STA LINEST+1
D405  A0 28     0028           LDY #$28        ; TICS START ON $28 CHAR OF TICTBL
                               ;
D407  B9 CDDA   CACD   TICST2  LDA TVTICS,Y    ; GET PATTERN FOR THE Y'TH CELL
D40A  91 37     0037           STA (LINEST),Y  ; PUT IT ON THE SCREEN
D40C  C8                       INY             ; INCREMENT FOR NEXT CELL PATTERN
D40D  C0 AD     00A0           CPY #$A0        ; SEE IF ALL CELL HAVE BEEN WRITTEN
D40F  D0 F6     0407           BNE TICST2      ; IF NOT DO THE NEXT ONE
                               ;
D411  A2 C7     00C7           LDX #$C7        ; WRITE THE TIC CHARACTERS FOR THE LAST LINE
D413  BD 6DDB   0860           LDA TVTBLL,X    ; SEED THE LINE START VECTOR
D416  85 37     0037           STA LINEST
D418  BD 35DC   DC35           LDA TVTBLH,X
D41B  85 38     0038           STA LINEST+1
D41D  A0 00     0000           LDY #$00        ; START AT THE 0'TH CHARACTER
                               ;
D41F  B9 CDDA   0ACD   TICST3  LDA TVTICS,Y    ; GET PATTERN FOR THE Y'TH CELL
D422  91 37     0037           STA (LINEST),Y  ; PUT IT ON SCREEN
D424  C8                       INY             ; INCREMENT FOR NEXT CELL
D425  C0 28     0028           CPY #$28        ; IS THE LINE FINISHED?
D427  D0 F6     D41F           BNE TICST3      ; IF NOT DO THE NEXT ONE
                               ;
                               ; . PUT 1, 2, OP 3 DASHES ABOVE CHART AREAS AS CHANNEL INDICATORS.
                               ;
D429  A2 02     0002           LDX #$02        ; PUT DASHES ON SCREEN LINE 2
D42B  BD 6DDB   0860           LDA TVTBLL,X
D42E  85 37     0037           STA LINEST
D430  BD 35DC   DC35           LDA TVTBLH,X
D433  85 38     0038           STA LINEST+1    ; SEED LINE START VECTOR
D435  A6 33     0033           LDX CHANEL      ; GET THE CHANNEL NUMBER
D437  A0 01     0001           LDY #01         ; DASHES START IN CELL 1
D439  A9 FF     00FF   CHDIS1  LDA #$FF        ; PATTERN IS $FF FOLLOWED BY $00
D43B  91 37     0037           STA (LINEST),Y  ; WRITE THE $FF TO SCREEN
D43D  C8                       INY             ; INCREMENT TO NEXT CELL POSITION
D43E  A9 00     0000           LDA #$00
D44D  91 37     0037           STA (LINEST),Y  ; WRITE THE $00 TO SCREEN
D442  8A                       TXA             ; GET THE CHANNEL NUMBER
D443  FD 04     D449           BEQ CHDIS2      ; HAVE ALL DASHES BEEN WRITTEN TO SCREEN?
D445  CA                       DEX             ; IF NOT DECREMENT
D446  C8                       INY             ; POINT TO NEXT CELL
D447  D0 F0     D439           BNE CHDIS1      ; AND WRITE NEXT DASH
D449  A6 34     0034   CHDIS2  LDX CHANLB      ; GET LO RESOLUTION CHANNEL NUMBER
D44B  A0 24     0024           LDY #$24        ; PATTERN FOR LOW RESOLUTION STARTS AT CELL $24
D44D  A9 0F     000F   CHDIS3  LDA #$0F        ; PATTERN IS SHORT DASHES ($0F)
D44F  91 37     0037           STA (LINEST),Y  ; WRITE SHORT DASH TO SCREEN
D451  8A                       TXA             ; GET THE CHANNEL NUMBER
D452  F0 04     D458           BEQ CHDIS4      ; HAVE ALL SHORT DASHES BEEN WRITTEN TO SCREEN?
D454  CA                       DEX             ; IF NOT DECREMENT
D455  C8                       INY             ; INCREMENT TO NEXT CELL POSITION
D456  D0 F5     D44D           BNE CHDIS3      ; AND WRITE NEXT SHORT DASH
                               ;
D458  A9 04     0004   CHDIS4  LDA #$04        ; SET THE LINE POINTER TO LINE A4
D45A  85 32     0032           STA LINPTR      ; (TOP OF "CHART RECORDER")
D45C  60                       RTS
                               ;
                               ;
                               ; ***LODAS VERSION: E07 INTERUPT SAMPLE ROUTINE***
                               ; . ALL CODE IN LINE TO MINIMIZE EXECUTIN TIME (NO SUBR CALLS).
                               ;
                               ; .SAVE REGISTERS A, X, Y
                               ;
D45D  48               INTRCV  PHA
D45E  8A                       TXA
D45F  48                       PHA
D460  98                       TYA
D461  48                       PHA
                               ;
                               ; .DO A SNAPSHOT (PAGE D TRANSFER TO TAPE BUFFER) IF NEEDED.
```

```
LOC   OP OPND  VALU  STMT  SOURCE STMT

                     0894         ;
0462  A5 2E    002E  0895  SNAPCK LDA SNPFLG      ; GET THE SNAP FLAG
0464  F0 11    0477  0896         BEQ ADCONV      ; IF CLEAR START A-TO-D CONVERSIONS
0466  A2 20    0020  0897         LDX #$20        ; TRANSFER PAGE 0 FROM BYTE $20 TO TAPE BUFFER
0468  B5 00    0000  0898  SNAP2  LDA 00,X        ; SAVE IN TAPE BUFFER FROM LAST BYTE DOWNWARD
046A  9D 0007  0700  0899         STA TAPBUF,X    ; STORE IN THE 'TAPE BUFFER'
046D  CA             0900         DEX             ; DECREMENT INDEX FOR PRECEEDING BYTE
046E  D0 F8    0468  0901         BNE SNAP2       ; IF NOT DONE GO TO SNAP2
0470  A9 00    0000  0902         LDA #$00        ; RESET THE SNAP FLAG
0472  85 2E    002E  0903         STA SNPFLG
0474  4C 9706  0697  0904         JMP RGET        ; PULL REGISTERS AND EXIT
                     0905         ;
                     0906         ; .START A-TO-D CONVERSIONS (35 MICROSEC MINIMUM IS REQUIRED).
                     0907         ;
0477  8D 00A2  A200  0908  ADCONV STA ATDCH1      ; WRITE TO A-TO-D CHANNEL 1 TO BEGIN CONVERSION
047A  8D 00A3  A300  0909         STA ATDCH2      ; WRITE TO A-TO-D CHANNEL 2 TO BEGIN CONVERSION
047D  8D 00A6  A600  0910         STA ATDCH3      ; WRITE TO A-TO-D CHANNEL 3 TO BEGIN CONVERSION
                     0911         ;
                     0912         ; . CHECK SOURCE OF INTERUPT.
                     0913         ;
0480  2C 00A0  A00D  0914         BIT UIFR        ; WAS IRQ FROM ONBOARD VIA?
0483  10 09    048E  0915         BPL CLCIRQ      ; IF NOT SEE IF IT WAS FROM CLOCK CHIP
0485  AD 0DA0  A00D  0916         LDA UIFR        ; CLEAR FLAG REGISTER BY FIRST READING
0488  8D 0DA0  A00D  0917         STA UIFR        ; THEN WRITTING
048B  4C CC04  04CC  0918         JMP INCMSC      ; JUMP TO INCREMENT MILLISECOND ROUTINE
                     0919         ;
048E  AD 0DAF  AF0D  0920  CLCIRQ LDA VIAIFR      ; CLEAR FLAG REGISTER BY FIRST READING
0491  8D 0DAF  AF0D  0921         STA VIAIFR      ; THEN WRITTING
0494  A2 10    0010  0922         LDX #$10        ; CLEAR INTERUPT ON CLOCK CHIP (READ STATUS REG)
0496  8E 01AF  AF01  0923         STX VIAORA      ; ADDRESS REGISTER
0499  AD 00AF  AF00  0924         LDA VIAORB      ; DATA REGISTER
049C  A9 01    0001  0925         LDA #$01        ; SET THE UPDATE DISPLAY FLAG
049E  85 1F    001F  0926         STA UTMDSP      ; (UPDATE DISPLAY EVERY 1/10 SECOND)
04A0  A5 17    0017  0927         LDA TWREQF      ; GET THE TAPE WRITE REQUEST FLAG
04A2  05 18    0018  0928         ORA CWREQF      ; LOOK AT THE CLOCK WRITE REQUEST FLAG
04A4  F0 0E    04B4  0929         BEQ RENHMI      ; IF BOTH ARE CLEAR RE-ENABLE HALF MS INTERUPTS
                     0930         ;
                     0931         ; .COUNT DOWN FOR CLOCK, TAPE WRITE SYNCHRONIZATION.
                     0932         ;
04A6  A9 02    0002  0933  CNTDWN LDA #$02        ; DISABLE 1/10 SEC INTERUPTS AT VIA
04A8  8D 0EAF  AF0E  0934         STA VIAIER
04AB  A9 00    0000  0935         LDA #$00        ; RESET TAPE WRITE REQUEST FLAG
04AD  85 17    0017  0936         STA TWREQF
04AF  85 18    0018  0937         STA CWREQF      ; AND THE CLOCK WRITE REQUEST FLAG
04B1  4C 9706  0697  0938         JMP RGET        ; PULL REGISTERS AND EXIT INTERUPT ROUTINE
                     0939         ;
                     0940         ; .REENABLE HALF MILLISECOND INTERUPTS.
                     0941         ;
04B4  A9 80    0080  0942  RENHMI LDA #$80        ; RESTART T1 TIMER. REMOVE EXTRA 100 MICROSECONDS
04B6  8D 04A0  A004  0943         STA UT1LL       ; WHICH HAVE ACCUMULATED FROM CLCIRQ PROCESSING
04B9  A9 01    0001  0944         LDA #$01        ; RESEED TIMER 1 COUNTER
04BB  8D 05A0  A005  0945         STA UT1CH       ; NOTE: LATCH IS AUTOMATICALLY RESEEDED
04BE  A9 F1    00F1  0946         LDA #$F1        ; RESTART T1 ON 'SHORT' CYCLE
04C0  8D 04A0  A004  0947         STA UT1LL
04C3  A9 C0    00C0  0948         LDA #$C0        ; SET INTERUPT ENABLE REGISTER
04C5  8D 0EA0  A00E  0949         STA UIER
04C8  A9 00    0000  0950         LDA #$00        ; RESET HALF MILLISECOND INTERUPT COUNTER
04CA  85 08    0008  0951         STA MSINTC
                     0952         ;
                     0953         ; .SEE IF HALF MILLISECOND COUNTER NEEDS INCREMENTING. DO IT.
                     0954         ;
04CC  E6 08    0008  0955  INCMSC INC MSINTC      ; INCREMENT THE HALF MILLISECOND INTERUPT COUNTER
04CE  A5 08    0008  0956         LDA MSINTC      ; GET IT
04D0  C9 C8    00C8  0957         CMP #200        ; HAVE 199 HALF MILLISECOND INTERUPTS OCCURRED?
04D2  D0 05    04D9  0958         BNE INTTST      ; NO. GO CHECK ACTION
04D4  A9 40    0040  0959         LDA #$40        ; YES. THEN DISABLE T1 INTERUPTS
04D6  8D 0EA0  A00E  0960         STA UIER
                     0961         ;
04D9  A5 00    0000  0962  INTTST LDA ACTION      ; GET THE ACTION CODE
04DB  C9 49    0049  0963         CMP #$49        ; IS IT 'INTEGRATE' ?
04DD  F0 0C    04EB  0964         BEQ SAMPLE      ; YES. GO SAMPLE
04DF  A5 08    0008  0965         LDA MSINTC      ; NO. SEE IF 1/10 SEC HAS PASSED (MSINTC RESET)
```

```
LOC   OP OPND   VALU  STMT  SOURCE STMT

D4E1  C9 01     0001  0966         CMP #$01
D4E3  D0 03     D4E8  0967         BNE INTXIT      ; IF NO EXIT INTERUPT RCUTINE
D4E5  20 EBD8   D8EB  0968         JSR ROCLCK      ; GO READ THE CLCCK
D4E8  4C 9706   0697  0969  INTXIT JMP RGET        ; RESTORE REGISTERS AND EXIT INTERUPT ROUTINE
                      0970         ;
                      0971         ; .CHECK TO SEE IF THIS POINT IS TO BE STORED.
                      0972         ;
D4EB  A5 13     0013  0973  SAMPLE LDA SAMRTE      ; GET THE DATA SAMPLE RATE
D4ED  C5 30     0030  0974         CMP SAMCTR      ; COMPARE AGAINST THE SAMPLE COUNTER
D4EF  F0 03     04F4  0975         BEQ SAMPLO      ; IF SAMPLO SHOULD BE STORED GO TO SAMPLO
D4F1  4C 9506   0695  0976         JMP STPND2      ; IF NOT EXIT AT STPND2
                      0977         ;
                      0978         ; . SELECT WHICH OF 4 DATA SAMPLING STEPS IS NEEDED.
                      0979         ;
D4F4  A9 00     0000  0980  SAMPLO LDA #00         ; REINITIALIZE THE SAMPLE COUNTER
D4F6  85 30     0030  0981         STA SAMCTR
D4F8  A5 20     0020  0982         LDA STPFLG      ; GET THE STEP FLAG IMOD 4 COUNTERI
D4FA  29 03     0003  0983         AND #$03        ; SEE WHICH OF 4 STEPS REQUIRED
D4FC  C9 01     0001  0984         CMP #$01        ; IS IT STEP1?
D4FE  F0 38     D538  0985         BEQ STEP1       ; IF IT IS GO TO STEP1
D500  C9 02     0002  0986         CMP #$02        ; IS IT STEP2?
D502  D0 03     D507  0987         BNE SAMPL2      ; IF NOT GO TO SAMPL2
D504  4C 9A05   D59A  0988         JMP STEP2       ; IF IT IS JUMP TO STEP2
D507  C9 03     0003  0989  SAMPL2 CMP #$03        ; IS IT STEP3?
D509  D0 03     D50E  0990         BNE STEP0       ; IF NOT IT MUST BE STEP0
D50B  4C E505   D5E5  0991         JMP STEP3       ; IF IT IS GO TO STEP3
                      0992         ;
                      0993         ; . PHASE 1 OF 4. SAMPLE A TO D'S. SEED LED DISPLAY. UPDATE TV.
                      0994         ;
D50E  AD 00A2   A200  0995  STEP0  LDA ATDCH1      ; READ CHANNEL 1 A-TO-D HI BYTE
D511  85 14     0014  0996         STA DSPCH1      ; STORE FOR DISPLAY USE
D513  85 2A     002A  0997         STA AVGRH1      ; STORE IN AVERAGE REGISTER HI FOR 2 BYTE AVERAGE
D515  AD 01A2   A201  0998         LDA ATDCH1+1    ; READ CHANNEL 2 A-TO-D LO BYTE
D518  85 27     0027  0999         STA AVGRL1      ; STORE IN AVERAGE REGISTER L1 FOR 2 BYTE AVERAGE
                      1000         ;
D51A  AD 00A3   A300  1001         LDA ATDCH2      ; READ CHANNEL 2 A-TO-D HI BYTE
D51D  85 15     0015  1002         STA DSPCH2      ; STORE FOR DISPLAY USE
D51F  85 2B     002B  1003         STA AVGRH2      ; STORE IN AVERAGE REGISTER HI FOR 2 BYTE AVERAGE
D521  AD 01A3   A301  1004         LDA ATDCH2+1    ; READ CHANNEL 2 A-TO-D LO BYTE
D524  85 28     0028  1005         STA AVGRL2      ; STORE IN AVERAGE REGISTER L1 FOR 2 BYTE AVERAGE
                      1006         ;
D526  AD 00A6   A600  1007         LDA ATDCH3      ; READ CHANNEL 3 A-TO-D HI BYTE
D529  85 16     0016  1008         STA DSPCH3      ; STORE FOR DISPLAY USE
D52B  85 2C     002C  1009         STA AVGRH3      ; STORE IN AVERAGE REGISTER HI FOR 2 BYTE AVERAGE
D52D  AD 01A6   A601  1010         LDA ATDCH3+1    ; READ CHANNEL 3 A-TO-D LO BYTE
D530  85 29     0029  1011         STA AVGRL3      ; STORE IN AVERAGE REGISTER L1 FOR 2 BYTE AVERAGE
                      1012         ;
D532  20 9DD6   D69D  1013         JSR TVDISP      ; PLOT POINT IIF NECESSARYI ON VIDEO DISPLAY
                      1014         ;
D535  4C 93D6   D693  1015  STEP0B JMP STPND1      ; STEP0 COMPLETED GO TO STPEND
                      1016         ;
                      1017         ; . PHASE 2 OF 4. SAMPLE A-TO-D'S. AVERAGE. STORE
                      1018         ;
D538  A4 07     0007  1019  STEP1  LDY CURSTR      ; GET THE CURRENT STORAGE POINTER IBYTE IN PAGEI
D53A  18              1020         CLC
D53B  AD 01A2   A201  1021         LDA ATDCH1+1    ; READ CHANNEL 1 A-TO-D LO BYTE
D53E  65 27     0027  1022         ADC AVGRL1      ; ADD TO PREVIOUS SAMPLE
D540  29 E0     00E0  1023         AND #$E0        ; STRIP OFF LAST BIT
D542  85 27     0027  1024         STA AVGRL1      ; STORE 2 SAMPLE AVERAGE ILOI
D544  AD 00A2   A200  1025         LDA ATDCH1      ; READ CHANNEL 1 A-TO-D HI BYTE
D547  65 2A     002A  1026         ADC AVGRH1      ; ADD TO PREVIOUS SAMPLE
D549  6A              1027         ROR             ; ROTATE RIGHT ONE BIT ISHIFT IN CARRYI
D54A  85 2A     002A  1028         STA AVGRH1      ; STORE 2 SAMPLE AVERAGE
D54C  66 27     0027  1029         ROR AVGRL1      ; ROTATE RIGHT ONE BIT ISHIFT IN CARRY)
                      1030         ;
D54E  18              1031         CLC             ; SAME PROCEEDURE AS ABOVE. FOR CHANNEL 2
D54F  AD 01A3   A301  1032         LDA ATDCH2+1
D552  65 28     0028  1033         ADC AVGRL2
D554  29 E0     00E0  1034         AND #$E0
D556  85 28     0028  1035         STA AVGRL2
D558  AD 00A3   A300  1036         LDA ATDCH2
D55B  65 2B     002B  1037         ADC AVGRH2
```

```
LOC   OP OPND   VALU  STMT  SOURCE STMT

D55D  6A              1038         ROR
D55E  85 2B     002B  1039         STA AVGRH2
D560  66 28     0028  1040         ROR AVGRL2
                      1041         ;
D562  18              1042         CLC              ; SAME PROCEEDURE AS ABOVE, FOR CHANNEL 3
D563  AD 01A6   A601  1043         LDA ATDCN3+1
D566  65 29     0029  1044         ADC AVGRL3
D568  29 E0     00E0  1045         AND #$E0
D56A  85 29     0029  1046         STA AVGRL3
D56C  AD 00A6   A600  1047         LDA ATDCN3
D56F  65 2C     002C  1048         ADC AVGRH3
D571  6A              1049         ROR
D572  85 2C     002C  1050         STA AVGRH3
D574  66 29     0029  1051         ROR AVGRL3
                      1052         ;
D576  A5 2A     002A  1053         LDA AVGRH1       ; GET CHANNEL 1 HI BYTE AVERAGE
D578  91 01     0001  1054         STA (MSBCH1),Y ; SAVE IT IN RAM
D57A  A5 2B     002B  1055         LDA AVGRH2       ; GET CHANNEL 2 HI BYTE AVERAGE
D57C  91 03     0003  1056         STA (MSBCN2),Y ; SAVE IT IN RAM
D57E  A5 2C     002C  1057         LDA AVGRH3       ; GET CHANNEL 3 HI BYTE AVERAGE
D580  91 05     0005  1058         STA (MSBCN3),Y ; SAVE IT IN RAM
                      1059         ;
D582  C8              1060         INY              ; INCREMENT THE RAM STORAGE POINTER
D583  D0 06     058B  1061         BNE STEP1C       ; IF NOT RESET TO NEXT PAGE GO TO STEP1C
                      1062         ;
D585  E6 02     0002  1063  STEP1B INC MSBCN1+1     ; INCREMENT THE STORAGE PAGE POINTERS
D587  E6 04     0004  1064         INC MSBCH2+1
D589  E6 06     0006  1065         INC MSBCH3+1
                      1066         ;
D58B  A5 27     0027  1067  STEP1C LDA AVGRL1       ; GET CHANNEL 1 LO BYTE AVERAGE
D58D  91 01     0001  1068         STA (MSBCN1),Y ; SAVE IT IN RAM
D58F  A5 28     0028  1069         LDA AVGRL2       ; GET CHANNEL 2 LO BYTE AVERAGE
D591  91 03     0003  1070         STA (MSBCN2),Y ; SAVE IT IN RAM
D593  A5 29     0029  1071         LDA AVGRL3       ; GET CHANNEL 3 LO BYTE AVERAGE
D595  91 05     0005  1072         STA (MSBCH3),Y ; SAVE IT IN RAM
D597  4C 91D6   D691  1073         JMP STPEND       ; STEP1 COMPLETED GO TO STPNDO
                      1074         ;
                      1075         ; . PHASE 3 OF 4. SAMPLE A-TO-D'S.
                      1076         ;
D59A  A5 23     0023  1077  STEP2  LDA FRZFLG       ; GET THE FREEZE FLAG
D59C  F0 23     D5C1  1078         BEQ STEP2B       ; IF CLEAR, KEEP ON SAMPLING, GO TO STEP2B
                      1079         ;
D59E  A5 12     0012  1080         LDA FRZTME       ; GET THE FREEZE TIME DELAY SET BY USER
D5A0  F0 12     05B4  1081         BEQ SETSNP       ; IF NO DELAY WANTED GO SET SNAPFLAG
D5A2  E6 25     0025  1082         INC FRZCTR       ; INCREMENT THE MILLISECOND FREEZE COUNTER
D5A4  A5 25     0025  1083         LDA FRZCTR       ; GET THE MILLISECOND FREEZE COUNTER
D5A6  C9 64     0064  1084         CMP #$64         ; HAS 1/10TH OF A SECOND PASSED?
D5A8  D0 17     D5C1  1085         BNE STEP2D       ; IF NOT KEEP ON SAMPLING
D5AA  A9 00     0000  1086         LDA #$00         ; RESET THE MILLISECOND FREEZE COUNTER
D5AC  85 25     0025  1087         STA FRZCTR
D5AE  C6 24     0024  1088         DEC FZTMEC       ; DECREMENT THE 1/10 SEC FREEZE TIME COUNTER
D5B0  A5 24     0024  1089         LDA FZTMEC       ; GET 1/10 SEC FREEZE TIME COUNTER
D5B2  D0 0D     D5C1  1090         BNE STEP2B       ; IF NOT EXPIRED KEEP ON SAMPLING
                      1091         ;
D5B4  85 23     0023  1092  SETSNP STA FRZFLG       ; CLEAR THE FREEZE FLAG
D5B6  A5 12     0012  1093         LDA FRZTME       ; GET THE FREEZE TIME SET BY USER
D5B8  85 24     0024  1094         STA FZTMEC       ; RESET THE 1/10 SEC FREEZE TIME COUNTER
D5BA  A9 01     0001  1095         LDA #$01         ; SET THE SNAP FLAG
D5BC  85 2E     002E  1096         STA SNPFLG
D5BE  4C 0FD5   D5DF  1097         JMP TIMOUT       ; PULL REGISTERS AND RTI
                      1098         ;
D5C1  A0 00A2   A200  1099  STEP2B LDA ATDCH1       ; READ CHANNEL 1 A-TO-D HI BYTE
D5C4  85 2A     002A  1100         STA AVGRH1       ; STORE IN AVERAGE REGISTER HI FOR 2 BYTE AVERAGE
D5C6  AD 01A2   A201  1101         LDA ATDCN1+1     ; READ CHANNEL 2 A-TO-D LO BYTE
D5C9  85 27     0027  1102         STA AVGRL1       ; STORE IN AVERAGE REGISTER LI FOR 2 BYTE AVERAGE
                      1103         ;
D5CB  AD 00A3   A300  1104         LDA ATDCN2       ; READ CHANNEL 2 A-TO-D HI BYTE
D5CE  85 2B     002B  1105         STA AVGRH2       ; STORE IN AVERAGE REGISTER HI FOR 2 BYTE AVERAGE
D5D0  AD 01A3   A301  1106         LDA ATDCH2+1     ; READ CHANNEL 2 A-TO-D LO BYTE
D5D3  85 28     0028  1107         STA AVGRL2       ; STORE IN AVERAGE REGISTER LI FOR 2 BYTE AVERAGE
                      1108         ;
D5D5  AD 00A6   A600  1109         LDA ATDCH3       ; READ CHANNEL 3 A-TO-D HI BYTE
```

```
LOC   OP OPNO  VALU  SOURCE STMT

05D8  85 2C    002C         STA AVGRH3    ; STORE IN AVERAGE REGISIER HI FOR 2 BYTE AVERAGE
05DA  A0 01A6  A601         LDA ATDCH3+1  ; READ CHANNEL 3 A-TO-D LC BYTE
05DD  85 29    0029         STA AVGRL3    ; STORE IN AVERAGE REGISTER LI FCR 2 BYTE AVERAGE
                            ;
05DF  20 E808  08E8  TIMOUT JSR RDCLCK    ; GO READ THE CLOCK
                            ;
05E2  4C 93D6  0693         JMP STPND1    ; STEPO COMPLETED GC TO STPEND
                            ;
                            ; .PHASE 4 OF 4. SAMPLE A-TO-D'S. AVERAGE. SHIFT. STORE.
                            ;
05E5  A4 07    0007  STEP3  LDY CURSTR    ; GET THE CURRENT STORAGE POINTER
05E7  18                    CLC
05E8  AD 01A2  A201         LDA ATDCH1+1  ; READ CHANNEL 1 A-TO-D HI BYTE
05EB  65 27    0027         ADC AVGRL1    ; ADD TC PREVIOUS SAMPLE FOP 2 BYTE AVERAGE
05ED  85 27    0027         STA AVGRL1    ; SAVE 2 SAMPLE AVERAGE
05EF  AD 00A2  A200         LDA ATDCH1    ; READ CHANNEL 1 A-TO-D HI BYTE
05F2  65 2A    002A         ADC AVGRH1    ; ADD TO PREVIOUS SAMPLE FCR 2 BYTE AVERAGE
05F4  6A                    ROR           ; SHIFT 12 BIT PLUS CARRY RIGHT 5 BITS
05F5  66 27    0027         ROR AVGRL1
05F7  4A                    LSR
05F8  66 27    0027         ROR AVGRL1
05FA  4A                    LSR
05FB  66 27    0027         ROR AVGRL1
05FD  4A                    LSR
05FE  66 27    0027         ROR AVGRL1
0600  4A                    LSR
0601  66 27    0027         ROR AVGRL1
0603  85 2A    002A         STA AVGRH1    ; STORE THE SHIFTED HI BYTE INTC AVERAGE REGISTER HI
                            ;
0605  18                    CLC
0606  AD 01A3  A301         LDA ATDCH2+1  ; READ CHANNEL 2 A-TO-D HI BYTE
0609  65 28    0028         ADC AVGRL2    ; ADD TC PREVIOUS SAMPLE FOR 2 BYTE AVERAGE
060B  85 28    0028         STA AVGRL2    ; SAVE 2 SAMPLE AVERAGE
060D  AD 00A3  A300         LDA ATDCH2    ; READ CHANNEL 1 A-TO-D HI BYTE
0610  65 2B    002B         ADC AVGRH2    ; ADD TO PREVIOUS SAMPLE FOR 2 BYTE AVERAGE
0612  6A                    ROR           ; SHIFT 12 BIT PLUS CARRY RIGHT 5 BITS
0613  66 28    0028         ROR AVGRL2
0615  4A                    LSR
0616  66 28    0028         ROR AVGRL2
0618  4A                    LSR
0619  66 28    0028         ROR AVGRL2
061B  4A                    LSR
061C  66 28    0028         ROR AVGRL2
061E  4A                    LSR
061F  66 28    0028         ROR AVGRL2
0621  85 2B    002B         STA AVGRH2    ; STORE THE SHIFTED HI BYTE INTO AVERAGE REGISTER HI
                            ;
0623  18                    CLC
0624  AD 01A6  A601         LDA ATDCH3+1  ; READ CHANNEL 3 A-TO-D HI BYTE
0627  65 29    0029         ADC AVGRL3    ; ADD TC PREVIOUS SAMPLE FOR 2 BYTE AVERAGE
0629  85 29    0029         STA AVGRL3    ; SAVE 2 SAMPLE AVERAGE
062B  AD 00A6  A600         LDA ATDCH3    ; READ CHANNEL 3 A-TO-D HI BYTE
062E  65 2C    002C         ADC AVGRH3    ; ADD TC PREVIOUS SAMPLE FOR 3 BYTE AVERAGE
0630  6A                    ROR           ; SHIFT 12 BIT PLUS CARRY RIGHT 5 BITS
0631  66 29    0029         ROR AVGRL3
0633  4A                    LSR
0634  66 29    0029         ROR AVGRL3
0636  4A                    LSR
0637  66 29    0029         ROR AVGRL3
0639  4A                    LSR
063A  66 29    0029         ROR AVGRL3
063C  4A                    LSR
063D  66 29    0029         ROR AVGRL3
                            ;
063F  11 05    0005         ORA (MSBCH3),Y ; PACK AND SAVE CHANNEL 3 HI BYTE IN RAM
0641  91 05    0005         STA (MSBCH3),Y
0643  A5 2A    002A         LDA AVGRH1     ; GET CHANNEL 1 HI BYTE, 2 SAMPLE AVERAGE
0645  11 01    0001         ORA (MSBCH1),Y ; PACK AND SAVE IN RAM
0647  91 01    0001         STA (MSBCH1),Y
0649  A5 2B    002B         LDA AVGRH2     ; GET CHANNEL 2 HI BYTE, 2 SAMPLE AVERAGE
064B  11 03    0003         ORA (MSBCH2),Y ; PACK AND SAVE IN RAM
064D  91 03    0003         STA (MSBCH2),Y
```

```
LOC   OP DPNO  VALU  STMT  SOURCE STMT

                     1182         ;
D64F  C8             1183         INY              ; INCREMENT THE RAW STORAGE POINTER
D650  D0 18    D66A  1184         BNE STEP3C       ; IF NOT RESET TO NEXT PAGE GO TO STEP1C
D652  A5 02    0002  1185         LDA MSBCH1+1     ; SEE IF 6K STORAGE REGION EXHAUSTED
D654  C9 1F    001F  1186         CMP #$1F         ; IS THIS THE LAST PAGE?
D656  D0 0C    D664  1187         BNE STEP3B       ; IF NOT GO TO STEP1B
D658  A9 07    0007  1188         LDA #$07         ; RESET ALL 3 CHANNEL STORAGE PAGE POINTERS
D65A  85 02    0002  1189         STA MSBCH1+1
D65C  A9 1F    001F  1190         LDA #$1F
D65E  85 04    0004  1191         STA MSBCH2+1
D660  A9 37    0037  1192         LDA #$37
D662  85 06    0006  1193         STA MSBCH3+1
                     1194         ;
D664  E6 02    0002  1195  STEP3B INC MSBCH1+1     ; INCREMENT THE STORAGE PAGE POINTERS
D666  E6 04    0004  1196         INC MSBCH2+1
D668  E6 06    0006  1197         INC MSBCH3+1
                     1198         ;
D66A  A5 27    0027  1199  STEP3C LDA AVGRL1     ; GET CHANNEL 1 LO BYTE AVERAGE
D66C  91 01    0001  1200         STA (MSBCH1),Y ; SAVE IT IN RAM
D66E  A5 28    0028  1201         LDA AVGRL2     ; GET CHANNEL 2 LO BYTE AVERAGE
D670  91 03    0003  1202         STA (MSBCH2),Y ; SAVE IT IN RAM
D672  A5 29    0029  1203         LDA AVGRL3     ; GET CHANNEL 3 LO BYTE AVERAGE
D674  91 05    0005  1204         STA (MSBCH3),Y ; SAVE IT IN RAM
                     1205         ;
D676  C8             1206  STPND0 INY              ; INCREMENT STORAGE POINTER
D677  D0 18    D691  1207         BNE STPEND       ; IF NOT RESET TO NEXT PAGE GO TO STPEN0
D679  A5 02    0002  1208         LDA MSBCH1+1     ; SEE IF 6K STORAGE REGION EXHAUSTED
D67B  C9 1F    001F  1209         CMP #$1F         ; IS THIS THE LAST PAGE?
D67D  D0 0C    D68B  1210         BNE STPEN2       ; IF NOT GO TO STPEN2
D67F  A9 07    0007  1211         LDA #$07         ; RESET ALL 3 CHANNEL STORAGE PAGE POINTERS
D681  85 02    0002  1212         STA MSBCH1+1
D683  A9 1F    001F  1213         LDA #$1F
D685  85 04    0004  1214         STA MSBCH2+1
D687  A9 37    0037  1215         LDA #$37
D689  85 06    0006  1216         STA MSBCH3+1
                     1217         ;
D68B  E6 02    0002  1218  STPEN2 INC MSBCH1+1     ; INCREMENT THE STORAGE PAGE POINTERS
D68D  E6 04    0004  1219         INC MSBCH2+1
D68F  E6 06    0006  1220         INC MSBCH3+1
                     1221         ;
D691  84 07    0007  1222  STPEND STY CURSTR       ; UPDATE THE STORAGE BYTE POINTER
D693  E6 2D    002D  1223  STPND1 INC STPFLG       ; INCREMENT THE STEP FLAG
D695  E6 30    0030  1224  STPND2 INC SAMCTR       ; INCREMENT THE SAMPLE COUNTER
                     1225         ;
                     1226         ;
                     1227         ; .RESTORE Y, X, AND A REGISTERS.
                     1228         ;
D697  68             1229  RGET   PLA
D698  A8             1230         TAY
D699  68             1231         PLA
D69A  AA             1232         TAX
D69B  68             1233         PLA
D69C  40             1234         RTI
                     1235         ;
                     1236         ; .DISPLAY A POINT (IF NECESSARY) ON TV DISPLAY.
                     1237         ;
D69D  E6 2F    002F  1238  TVDISP INC SAMPNO       ; INCREMENT THE SAMPLE NUMBER
D69F  A5 2F    002F  1239         LDA SAMPNO       ; GET THE INCREMENTED SAMPLE NUMBER
D6A1  C5 31    0031  1240         CMP DISRTE       ; COMPARE WITH THE DISPLAY RATE
D6A3  D0 73    0718  1241         BNE TVEXIT       ; IF NOT AN INTEGRAL VALUE OF DISRTE TVEXIT
                     1242         ;
D6A5  A4 35    0035  1243         LDY LSTPTA       ; GET THE LAST POINT CELL LOCATION FOR CHANNEL A
D6A7  B1 37    0037  1244         LDA (LINEST),Y ; GET THE VALUE OF THE INVERTED PATTERN
D6A9  49 FF    00FF  1245         EOR #$FF         ; REINVERT IT
D6AB  91 37    0037  1246         STA (LINEST),Y ; STORE IT BACK TO THE SCREEN
D6AD  A4 36    0036  1247         LDY LSTPTB       ; DO THE SAME THING FOR CHANNEL B
D6AF  B1 37    0037  1248         LDA (LINEST),Y
D6B1  49 FF    00FF  1249         EOR #$FF
D6B3  91 37    0037  1250         STA (LINEST),Y
                     1251         ;
D6B5  E6 32    0032  1252         INC LINPTR       ; INCREMENT THE LINE POINTER
D6B7  A5 32    0032  1253         LDA LINPTR       ; GET THE LINE POINTER
```

```
LOC   OP OPND  VALU  SOURCE STMT

D6B9  C9 C4    00C4         CMP #$C4      ; IS THIS THE END OF THE SCREEN?
D6BB  D0 04    D6C1         BNE TVOSP2    ; IF NOT GO TO TVOSP2
D6BD  A9 04    0004         LDA #$04      ; IF IT IS RESET TO TOP OF SCREEN
D6BF  85 32    0032         STA LINPTR    ; STORE TO LINE POINTER
                            ;
D6C1  A6 32    0032  TVOSP2 LDX LINPTR    ; GET THE LINE NUMBER ($00-$C8)
D6C3  BD 6DD8  086D         LDA TVTBLL,X  ; SET UP START OF LINE POINTER, LO BYTE
D6C6  85 37    0037         STA LINEST
D6C8  BD 35DC  0C35         LDA TVTBLH,X  ; SET UP START OF LINE POINTER, HI BYTE
D6CB  85 38    0038         STA LINEST+1
D6CD  BC 0006  0600         LDY OLDTAB,X  ; GET OLD CELL NUMBER FOR THIS LINE
D6D0  A9 00    0000         LDA #$00      ; STORE A $00 TO ERASE THE OLD POINT
D6D2  91 37    0037         STA (LINEST),Y ; ERASE AT LINE START+OLD CELL NUMBER
D6D4  BC 0005  0500         LDY OLDTBB,X  ; GET OLD CELL NUMBER FOR TV CHANNEL B
D6D7  91 37    0037         STA (LINEST),Y ; CLEAR THIS CELL
D6D9  A4 33    0033         LDY CHANEL    ; GET THE CHANNEL ASSIGNMENT TO BE DISPLAYED
D6DB  B9 14DD  0014         LDA DSPCHI,Y  ; GET THE CURRENT DATA VALUE TO BE DISPLAYED
D6DE  48                    PHA           ; SAVE IT
D6DF  4A                    LSR           ; SHIFT TO 5 BYTES TO CALCULATE NEW CELL
D6E0  4A                    LSR
D6E1  4A                    LSR
D6E2  9D 0006  0600         STA OLDTAB,X  ; SAVE CELL NUMBER FOR NEXT SCREEN ERASURE
D6E5  A8                    TAY           ; USE IT FOR PLOTTING NEW POINT
D6E6  68                    PLA           ; GET THE VALUE OF THE DATA POINT BACK
D6E7  29 07    0007         AND #07       ; USE 3 L.S. BITS FOR PATTERN TABLE LOOKUP
D6E9  AA                    TAX           ; OFFSET INTO PATTERN TABLE
D6EA  B5 39    0039         LDA BITTAB,X  ; GET THE PATTERN TO PLOT
D6EC  84 35    0035         STY LSTPTA
D6EE  49 FF    00FF         EOR #$FF
D6FD  91 37    0037         STA (LINEST),Y ; PLOT THE NEW POINT
D6F2  A4 34    0034         LDY CHANLB    ; GET THE CHANNEL ASSIGNMENT FOR TV REGION B
D6F4  B9 1400  0014         LDA DSPCHI,Y  ; GET THE DATA VALUE TO BE DISPLAYED
D6F7  48                    PHA           ; SAVE IT ON THE STACK
D6F8  4A                    LSR           ; SHIFT RIGHT 5 BITS TO GET PATTERN
D6F9  4A                    LSR
D6FA  4A                    LSR
D6FB  4A                    LSR
D6FC  4A                    LSR
D6FD  18                    CLC           ; REGION B STARTS AT CELL 32 ($20)
D6FE  69 20    0020         ADC #$20
D700  A6 32    0032         LDX LINPTR    ; GET THE LINE POINTER
D702  9D 0D05  0500         STA OLDTBB,X  ; SAVE CELL NUMBER IN OLD TABLE B
D705  A8                    TAY           ; PUT CELL NUMBER IN Y REGISTER
D706  68                    PLA           ; GET THE DATA VALUE BACK
D707  4A                    LSR           ; FIGURE OUT WHICH PATTERN TO USE
D708  4A                    LSR
D709  29 07    D007         AND #$07
D70B  AA                    TAX           ; USE AS OFFSET TO PATTERN TABLE
D70C  B5 39    0039         LDA BITTAB,X
D70E  84 36    0036         STY LSTPTB
D710  49 FF    00FF         EOR #$FF
D712  91 37    0037         STA (LINEST),Y ; PLOT THE TV REGION B POINT
D714  A9 00    000D         LDA #$00      ; RESET SAMPLE NUMBER TO ZERO
D716  85 2F    002F         STA SAMPND
D718  60             TVEXIT RTS
                            ;
                            ; *KEYBOARD ROUTINE FROM AIM-65 MONITOR*
                            ;
D719  20 EFEC  ECEF  KEYCK  JSR $ECEF           ;RDONEK
D71C  20 2AED  E02A  KEYCO  JSR $ED2A           ;DEBKEY
D71F  A9 8F    008F         LDA #$8F
D721  8D 80A4  A480         STA $A480
D724  AD 82A4  A482         LDA $A482
D727  4A                    LSR
D728  B0 20    D74A         BCS KEYCK1
D72A  A2 03    0003         LDX #$03
D72C  A9 7F    007F         LDA #$7F
D72E  38             KEYCKD SEC
D72F  6A                    ROR
D730  48                    PHA
D731  20 08ED  ED08         JSR $ED08           ;ONEK2
D734  AD 82A4  A482         LDA $A482
```

```
LOC  OP DPND  VALU  STMT  SOURCE STMT

D737 4A             1326         LSR
D738 90 06    0740  1327         BCC KEYC00
D73A 68             1328         PLA
D73B CA             1329         DEX
D73C D0 FD    D72E  1330         BNE KEYCK0
D73E F0 CC    071C  1331         BEQ KEYC0
D740 68             1332  KEYC00 PLA
D741 AD 28A4  A428  1333         LDA $A428
D744 49 FF    00FF  1334         EOR #$FF
D746 AA             1335         TAX
D747 EE 2AA4  A42A  1336         INC $A42A
D74A 20 05ED  E005  1337  KEYCK1 JSR $ED05          ;DNEKEY
D74D 88             1338         DEY
D74E D0 09    D759  1339         BNE KEYC1B
D750 AD 28A4  A428  1340         LDA $A428
D753 C9 F7    00F7  1341         CMP #$F7
D755 B0 04    075B  1342         BCS KEYCK2
D757 90 C3    071C  1343         BCC KEYC0
D759 30 47    D7A2  1344  KEYC1B BMI KEYC11
D75B 20 2CED  E02C  1345  KEYCK2 JSR $ED2C          ;DEBK1
D75E 98             1346         TYA
D75F 0A             1347         ASL
D760 0A             1348         ASL
D761 0A             1349         ASL
D762 A8             1350         TAY
D763 AD 28A4  A428  1351         LDA $A428
D766 4A             1352  KEYCK3 LSR
D767 90 D3    076C  1353         BCC KEYCK4
D769 C8             1354         INY
D76A D0 FA    0766  1355         BNE KEYCK3
D76C B9 21F4  F421  1356  KEYCK4 LDA $F421,Y
D76F 48             1357         PHA
D770 8A             1358         TXA
D771 F0 24    0797  1359         BEQ KEYCK7
D773 29 10    0010  1360         AND #$10
D775 F0 06    077D  1361         BEQ KEYCK5
D777 68             1362         PLA
D778 29 3F    003F  1363         AND #$3F
D77A 4C 9807  0798  1364         JMP KEYCK8
D77D 68             1365  KEYCK5 PLA
D77E 48             1366         PHA
D77F 29 40    0040  1367         AND #$40
D781 DD 14    D797  1368         BNE KEYCK7
D783 68             1369         PLA
D784 48             1370         PHA
D785 29 0F    000F  1371         AND #$0F
D787 F0 DE    0797  1372         BEQ KEYCK7
D789 C9 DC    000C  1373         CMP #$DC
D78B B0 05    D792  1374         BCS KEYCK6
D78D 68             1375         PLA
D78E 29 EF    00EF  1376         AND #$EF
D790 DD 06    D798  1377         BNE KEYCK8
D792 68             1378  KEYCK6 PLA
D793 D9 10    0010  1379         ORA #$10
D795 D0 01    D798  1380         BNE KEYCK8
D797 68             1381  KEYCK7 PLA
D798 C9 60    0060  1382  KEYCK8 CMP #$6D
D79A DD D6    D7A2  1383         BNE KEYC11
D79C E0 0D    0000  1384         CPX #$DD
D79E F0 03    07A3  1385         BEQ KEYC10
D7A0 29 4F    004F  1386         AND #$4F
D7A2 60             1387  KEYC11 RTS
D7A3 A9 00    0000  1388  KEYC10 LDA #$00
D7A5 8D 77A4  A477  1389         STA $A477
D7A8 20 50F0  F050  1390         JSR $F050
D7AB 60             1391         RTS
                    1392         ;
                    1393         ; *CONVERT HEX BYTE TO 2 BYTE BCD. BYTE TO BE CONVERTED IN
                    1394         ;   A REGISTER. RESULT: MSB IN Y REGISTER, LSB IN A REGISTER*
                    1395         ;
D7AC 18             1396  HX1BCD CLC           ; CLEAR THE CARRY BIT
D7AD A0 00    0000  1397         LDY #$00      ; ASSUME THAT VALUE IS <100
```

```
LOC   OP DPND  VALU  STMT  SOURCE STMT

D7AF  C9 C8    00C8  1398         CMP #$C8       ; IS VALUE =>200 (DECIMAL)?
D7B1  B0 06    D7B9  1399         BCS GTE200     ; IF IT IS GO TO GTE200
D7B3  C9 64    0064  1400         CMP #$64       ; IS VALUE => 100 (DECIMAL) ? (PUT < 200)
D7B5  B0 DA    D7C1  1401         BCS GTE100     ; IF IT IS THEN GO TO GTE100
D7B7  90 0D    D7C6  1402         BCC HBSAVE+1   ; VALUE IS < 100
D7B9  C8             1403  GTE200 INY            ; STORE $02 IN Y REGISTER
D7BA  C8             1404         INY
D7BB  38             1405         SEC
D7BC  E9 C8    00C8  1406         SBC #$C8       ; SUBTRACT 200 (DECIMAL) FROM VALUE
D7BE  4C C5D7  D7C5  1407         JMP HBSAVE     ; GO SAVE APPROPRIATE VALUES
D7C1  C8             1408  GTE100 INY            ; STORE $01 IN Y REGISTER
D7C2  38             1409         SEC            ; SUBTRACT 100 (DECIMAL) FROM VALUE
D7C3  E9 64    0064  1410         SBC #$64
D7C5  18             1411  HBSAVE CLC            ; CLEAR THE CARRY BIT
D7C6  86 1A    001A  1412         STX TEMPHX     ; SAVE THE X REGISTER (OUTDD) POINTER)
D7C8  AA             1413         TAX            ; A REGISTER IS HEX VALUE OF DECIMAL 0 TO 99
D7C9  BD 69DA  DA69  1414         LDA CLCTBL,X   ; USE AS OFFSET TO GET DECIMAL CHAR FROM TABLE
D7CC  A6 1A    001A  1415         LDX TEMPHX     ; RESTORE THE X REGISTER (OUTDD) POINTER)
D7CE  60             1416         RTS
                     1417  ;
                     1418  ; *CLEAR DISPLAY AND RESTORE OLD ACTION CODE*
                     1419  ;
D7CF  20 D3D2  D2D3  1420  ROLACT JSR CLEAR      ; CLEAR THE DISPLAY
D7D2  A5 26    0026  1421         LDA OLDACT     ; GET THE OLD ACTION CODE
D7D4  85 00    0000  1422         STA ACTION     ; STORE BACK AS THE NEW ACTION CODE
D7D6  85 48    0048  1423         STA DBUFF+7    ; PUT IN THE DISPLAY BUFFER
D7D8  60             1424         RTS
                     1425  ;
                     1426  ; *SETUP VIDEO DISPLAY PARAMETERS*
                     1427  ;
D7D9  20 D3D2  D2D3  1428  TVSET  JSR CLEAR      ; CLEAR THE DISPLAY
D7DC  20 EBC2  D2EB  1429         JSR PNDM       ; PRINT PROMPT FOR DISPLAY CHANNEL ENTRY
D7DF  44       D     1430         FCC DISPLAY
D7E0  49       I
D7E1  53       S
D7E2  50       P
D7E3  4C       L
D7E4  41       A
D7E5  59       Y
D7E6  20             1431         FCB $20
D7E7  43       C     1432         FCC CHANNEL
D7E8  48       H
D7E9  41       A
D7EA  4E       N
D7EB  4E       N
D7EC  45       E
D7ED  4C       L
D7EE  20             1433         FCB $20
D7EF  41       A     1434         FCC A:
D7F0  3A       :
D7F1  0D             1435         FCB $0D
D7F2  20 3CE9  E93C  1436         JSR READ       ; READ KEYBOARD
D7F5  C9 0D    000D  1437         CMP #$0D       ; IS FIRST CHARACTER A CARRIAGE RETURN?
D7F7  F0 16    D80F  1438         BEQ TVSETB     ; IF IT IS GO TO TVSETB
D7F9  20 7AE9  E97A  1439         JSR OUTPUT     ; IF NOT OUTPUT IT
D7FC  C9 31    0031  1440         CMP #$31       ; WAS CHANNEL 1 SELECTED?
D7FE  F0 08    D808  1441         BEQ TVSET1     ; IF SO GO TO TVSET1
D800  C9 32    0032  1442         CMP #$32       ; WAS CHANNEL 2 SELECTED?
D802  F0 04    D808  1443         BEQ TVSET1     ; IF SO GO TO TVSET1
D804  C9 33    0033  1444         CMP #$33       ; WAS CHANNEL 3 SELECTED?
D806  D0 D1    D7D9  1445         BNE TVSET      ; IF NOT, ILLEGAL CHANNEL, REPROMPT
                     1446  ;
D808  29 0F    000F  1447  TVSET1 AND #$0F       ; GET HEX VALUE OF CHANNEL
D80A  38             1448         SEC
D80B  E9 01    0001  1449         SBC #$01       ; DECREMENT BY 1
D80D  85 33    0033  1450         STA CHANEL     ; SAVE AS DATA CHANNEL OFFSET
                     1451  ;
D80F  20 D3D2  D2D3  1452  TVSETB JSR CLEAR      ; CLEAR THE DISPLAY
D812  20 EBD2  D2EB  1453         JSR PNDM       ; PRINT PROMPT FOR DISPLAY CHANNEL ENTRY
D815  44       D     1454         FCC DISPLAY
D816  49       I
D817  53       S
```

```
LOC   OP OPND  VALU  STMT  SOURCE STMT

D818  50    P
D819  4C    L
D81A  41    A
D81B  59    Y
D81C  20          1455         FCB $20
D81D  43    C     1456         FCC CHANNEL
D81E  48    H
D81F  41    A
D820  4E    N
D821  4E    N
D822  45    E
D823  4C    L
D824  20          1457         FCB $20
D825  42    B     1458         FCC B:
D826  3A    :
D827  00          1459         FCB $00
D828  20 3CE9  E93C 1460         JSR READ      ; READ KEYBOARD
D82B  C9 0D    000D 1461         CMP #$0D      ; IS FIRST CHARACTER A CARRIAGE RETURN?
D82D  F0 16    D845 1462         BEQ TVSET3    ; IF IT IS GO TO TVSET3
D82F  20 7AE9  E97A 1463         JSR OUTPUT    ; IF NOT OUTPUT IT
D832  C9 31    0031 1464         CMP #$31      ; WAS CHANNEL 1 SELECTED?
D834  F0 08    D83E 1465         BEQ TVSET2    ; IF SO GO TO TVSET2
D836  C9 32    0032 1466         CMP #$32      ; WAS CHANNEL 2 SELECTED?
D838  F0 04    D83E 1467         BEQ TVSET2    ; IF SO GO TO TVSET2
D83A  C9 33    0033 1468         CMP #$33      ; WAS CHANNEL 3 SELECTED?
D83C  D0 D1    D80F 1469         BNE TVSET8    ; IF NOT, ILLEGAL CHANNEL, REPROMPT
                    1470         ;
D83E  29 0F    000F 1471  TVSET2 AND #$0F      ; GET HEX VALUE OF CHANNEL
D840  38            1472         SEC
D841  E9 01    0001 1473         SBC #$01      ; DECREMENT BY 1
D843  85 34    0034 1474         STA CHANLB    ; SAVE AS DATA CHANNEL OFFSET
                    1475         ;
D845  A9 00    0000 1476  TVSET3 LDA #$00      ; TEMP WILL BE USED IN THIS SUBROUTINE
D847  85 19    0019 1477         STA TEMP
D849  20 D302  02D3 1478         JSR CLEAR     ; CLEAR THE DISPLAY
D84C  20 E802  02E8 1479         JSR PNDM      ; PRINT PROMPT FOR CHART RATE ENTRY
D84F  28    (     1480         FCC (DATA
D850  44    D
D851  41    A
D852  54    T
D853  41    A
D854  20          1481         FCB $20
D855  52    R     1482         FCC RATE)/PT:
D856  41    A
D857  54    T
D858  45    E
D859  29    )
D85A  2F    /
D85B  50    P
D85C  54    T
D85D  3A    :
D85E  00          1483         FCB $00
D85F  20 3CE9  E93C 1484         JSR READ      ; GET FIRST OF THREE DIGITS ( VALUE <256 )
D862  C9 0D    000D 1485         CMP #$0D      ; WAS A CARRIAGE RETURN ENTERED?
D864  F0 22    D888 1486         BEQ TVSETX    ; IF SO EXIT
D866  20 7AE9  E97A 1487         JSR OUTPUT    ; OUTPUT FIRST DIGIT ENTERED
D869  C9 30    0030 1488         CMP #$30      ; WAS FIRST DIGIT A ZERO?
D86B  F0 10    D87D 1489         BEQ TVSET6    ; IF SO GO TO TVSET6
D86D  C9 31    0031 1490         CMP #$31      ; WAS FIRST DIGIT A 1?
D86F  F0 08    D879 1491         BEQ TVSET4    ; IF SO GO TO TVSET4
D871  C9 32    0032 1492         CMP #$32      ; WAS FIRST DIGIT A 2?
D873  D0 D0    D845 1493         BNE TVSET3    ; ILLEGAL FIRST DIGIT, REPROMPT
                    1494         ;
D875  A9 C8    00C8 1495         LDA #200      ; SET TO 200 (DECIMAL) AND GO TO TVSET5
D877  D0 02    087B 1496         BNE TVSET5
D879  A9 64    0064 1497  TVSET4 LDA #100      ; SET TO 100 (DECIMAL)
D87B  85 19    0019 1498  TVSET5 STA TEMP      ; STORE IN TEMP
                    1499         ;
D87D  20 C4D3  D3C4 1500  TVSET6 JSR PACK2     ; INPUT NEXT 2 DIGITS
D880  20 D7D3  D3D7 1501         JSR DECHEX    ; CONVERT TO HEXIDECIMAL
D883  18            1502         CLC           ; ADD 1X100 DECIMAL AS NEEDED
D884  65 19    0019 1503         ADC TEMP
```

```
LOC   OP OPND  VALU  STMT  SOURCE STMT

D886  85 31    0031  1504         STA DISRTE     ; SAVE THE DISPLAY RATE
D888  20 92D8  D892  1505  TVSFTX JSR TVCLEA     ; GO CLEAR THE VIDEO DISPLAY
D88B  20 E1D3  D3E1  1506         JSR TICSET     ; DRAW TICS ON THE NOW CLEARED SCREEN
D88E  20 CF07  07CF  1507         JSR ROLACT     ; RESTORE THE OLD ACTION CODE
D891  60             1508         RTS
                     1509         ;
                     1510         ; *CLEAR THE VIDEO DISPLAY*
                     1511         ;
D892  A9 60    0060  1512  TVCLEA LDA #$60       ; VISABLE MEMORY RUNS FROM $6000 TO $7FFF
D894  85 1A    001A  1513         STA TEMP+1     ; USE DESTRUCTABLE PAGE ZERO TEMP REGISTERS
D896  A9 00    0000  1514         LDA #$00
D898  85 19    0019  1515         STA TEMP
D89A  A8             1516         TAY            ; INITIAL CELL IS SET UP. Y REGISTER IS PAGE OFFSET
D89B  A9 00    0000  1517  TVCL1  LDA #$00       ; STORING $00 WILL CLEAR THAT CELL
D89D  91 19    0019  1518         STA (TEMP),Y   ; CLEAR IT
D89F  C8             1519         INY            ; NEXT BYTE
D8A0  D0 F9    D89B  1520         BNE TVCL1      ; FIRST BYTE OF NEW PAGE?
D8A2  E6 1A    001A  1521         INC TEMP+1     ; YES. INCREMENT PAGE
D8A4  A5 1A    001A  1522         LDA TEMP+1     ; ALL VISUAL MEMORY PAGES CLEARED?
D8A6  C9 80    0080  1523         CMP #$80
D8A8  D0 F1    D89B  1524         BNE TVCL1      ; IF NOT. KEEP ON GOING
D8AA  60             1525         RTS
                     1526         ;
                     1527         ; *INITIALIZE CLOCK FOR READING*
                     1528         ;
D8AB  48             1529  RDCLIN PHA
D8AC  A9 00    0000  1530         LDA #$00
D8AE  8D 02AF  AF02  1531         STA VIADRB
D8B1  A9 18    0018  1532         LDA #$18       ; TRIGGER ON UPWARD TRANSITION OF CLOCK
D8B3  8D 0CAF  AF0C  1533  RDCL12 STA VIARCR
D8B6  68             1534         PLA
D8B7  60             1535         RTS
D8B8  68             1536         PLA
D8B9  60             1537         RTS
                     1538         ;
                     1539         ; * INITIALIZE CLOCK FOR WRITING*
                     1540         ;
D8BA  48             1541  WRCLIN PHA
D8BB  A9 FF    00FF  1542         LDA #$FF
D8BD  8D 02AF  AF02  1543         STA VIADRB
D8C0  A9 9F    009F  1544         LDA #$9F
D8C2  D0 EF    D8B3  1545         BNE RDCL12
                     1546         ;
                     1547         ; *WRITE TO CLOCK (START OUTBOARD TIMER)*
                     1548         ;
D8C4  20 BAD8  D8BA  1549  GOCLCK JSR WRCLIN     ; SET CLOCK FOR WRITING
D8C7  A9 10    0010  1550         LDA #$10       ; SET FOR 10 SECONDS
D8C9  A2 02    0002  1551         LDX #$02       ; SELECT SECONDS WORD
D8CB  8E 01AF  AF01  1552         STX VIADRA
D8CE  8D 00AF  AF00  1553         STA VIADRB
D8D1  A2 07    0007  1554         LDX #$07       ; INDEX TO CLOCK BUFFER
D8D3  B5 09    0009  1555  GOCLC2 LDA MILSEC,X   ; GET EACH VALUE
D8D5  8E 01AF  AF01  1556         STX VIADRA     ; SELECT DATA WORD TO BE WRITTEN
D8D8  8D 00AF  AF00  1557         STA VIADRB     ; WRITE DATA WORD
D8DB  CA             1558         DEX            ; GET NEXT VALUE
D8DC  E0 02    0002  1559         CPX #$02
D8DE  D0 F3    D8D3  1560         BNE GOCLC2
D8E0  A9 15    0015  1561         LDA #$15       ; SEND "GO" COMMAND TO CLOCK CHIP
D8E2  8D 01AF  AF01  1562         STA VIADRA     ; RESET SECS.XXX=00.000
D8E5  8D 00AF  AF00  1563         STA VIADRB
D8E8  20 ABD8  D8AB  1564         JSR RDCLIN     ; RESET CLOCK FOR READING
                     1565         ;
                     1566         ; *READ FROM CLOCK*
                     1567         ;
D8EB  48             1568  RDCLCK PHA            ; SAVE THE A AND X REGISTERS ON STACK
D8EC  8A             1569         TXA
D8ED  48             1570         PHA
D8EE  A2 07    0007  1571         LDX #$07       ; INDEX POINTER TO DATA WORD (M,D1,D2,H,M...)
D8F0  8E 01AF  AF01  1572  RDCLC2 STX VIADRA     ; SELECT WORD TO BE READ
D8F3  AD 00AF  AF00  1573         LDA VIADRB
D8F6  95 09    0009  1574         STA MILSEC,X   ; STORE DATA IN CLOCK BUFFER
D8F8  CA             1575         DEX            ; GET NEXT DATA WORD FROM CLOCK
```

```
LOC   OP CPND  VALU  STMT  SOURCE STMT

D8F9  10 FS    D8F0  1576         BPL RDCLC2
D8FB  68             1577         PLA            ; RESTORE REGISTERS
D8FC  AA             1578         TAX
D8FD  68             1579         PLA
D8FE  60             1580         RTS
                     1581         ;
                     1582         ; *START THE CLOCK FROM KEYBOARD COMMAND*
                     1583         ;
D8FF  20 D302  02D3  1584  TIMGD  JSR CLEAR      ; CLEAR THE DISPLAY
D902  20 EBC2  D2EB  1585         JSR PNOM       ; PRINT AND DISPLAY CLOCK START PROMPT
D905  53       S     1586         FCC START=ANY
D906  54       T
D907  41       A
D908  52       R
D909  54       T
D90A  30       =
D90B  41       A
D90C  4E       N
D90D  59       Y
D90E  20             1587         FCB $20
D90F  45       E     1588         FCC EXIT=CR
D910  58       X
D911  49       I
D912  54       T
D913  30       =
D914  43       C
D915  52       R
D916  00             1589         FCB $00
D917  20 3CE9  E93C  1590         JSR READ       ; GET KEYBOARD ENTRY
D91A  C9 0D    000D  1591         CMP #13        ; IS IT A CARRIAGE RETURN?
D91C  F0 03    0921  1592         BEQ TIMGD2     ; IF IT IS THEN RTS
D91E  20 C408  08C4  1593         JSR GOCLCK     ; GO WRITE TO THE CLOCK
D921  60             1594  TIMGD2 RTS
                     1595         ;
D922  A9 00    0000  1596  ORSET  LDA #$00       ; TEMP WILL BE USED IN THIS SUBROUTINE
D924  85 19    0019  1597         STA TEMP
D926  20 D302  0203  1598         JSR CLEAR      ; CLEAR THE DISPLAY
D929  20 EBC2  02EB  1599         JSR PNOM       ; PRINT PROMPT FOR DATA RATE ENTRY
D92C  44       D     1600         FCC DATA
D92D  41       A
D92E  54       T
D92F  41       A
D930  20             1601         FCB $20
D931  52       R     1602         FCC RATE
D932  41       A
D933  54       T
D934  45       E
D935  20             1603         FCB $20
D936  4D       M     1604         FCC MS/PT:
D937  53       S
D938  2F       /
D939  50       P
D93A  54       T
D93B  3A       :
D93C  00             1605         FCB $00
D93D  20 3CE9  E93C  1606         JSR READ       ; GET FIRST OF THREE DIGITS ( VALUE <256 )
D940  C9 0D    000D  1607         CMP #$0D       ; WAS A CARRIAGE RETURN ENTERED?
D942  F0 22    D966  1608         BEQ DRSETX     ; IF SO EXIT
D944  20 7AE9  E97A  1609         JSR OUTPUT     ; OUTPUT FIRST DIGIT ENTERED
D947  C9 30    0030  1610         CMP #$30       ; WAS FIRST DIGIT A ZERO?
D949  F0 10    095B  1611         BEQ DRSET6     ; IF SO GO TO DRSET6
D94B  C9 31    0031  1612         CMP #$31       ; WAS FIRST DIGIT A 1?
D94D  F0 08    D957  1613         BEQ DRSET4     ; IF SO GO TO DRSET4
D94F  C9 32    0032  1614         CMP #$32       ; WAS FIRST DIGIT A 2?
D951  D0 CF    0922  1615         BNE DRSET      ; ILLEGAL FIRST DIGIT, REPROMPT
                     1616         ;
D953  A9 C8    00C8  1617         LDA #200       ; SET TO 200 (DECIMAL) AND GO TO DRSET5
D955  D0 02    0959  1618         BNE DRSET5
D957  A9 64    0064  1619  DRSET4 LDA #100       ; SET TO 100 (DECIMAL)
D959  85 19    0019  1620  ORSET5 STA TEMP       ; STORE IN TEMP
                     1621         ;
D95B  20 C4D3  D3C4  1622  ORSET6 JSR PACK2      ; INPUT NEXT 2 DIGITS
```

```
LOC    OP DPND   VALU  STMT  SOURCE STMT

D95E   20 D7D3   D3D7  1623          JSR DECHEX     ; CONVERT TO HEXIDECIMAL
D961   18              1624          CLC            ; ADD IXIDD DECIMAL AS NEEDED
D962   65 19     0019  1625          ADC TEMR
D964   85 13     0013  1626          STA SAMRTE     ; SAVE THE DISPLAY RATE
D966   20 CFD7   D7CF  1627  ORSETX  JSR ROLACT     ; RESTORE THE OLD ACTION CODE
D969   60              1628          RTS
                       1629          ;
                       1630          ; === SYMBOL NAMES FOR TARE ROUTINE ===
                       1631          ;
                       1632          ; =DUMP AND MONITOR PARAMETERS AND FLAGS=
                       1633          ;
                 0106  1634  S2      EDU $0106      ; VERTICAL COUNT
                 A413  1635  DUTFLG  EDU $A413      ; DUTRUT DEVICE FLAG
                 A415  1636  CURPD2  EDU $A415      ; DISRLAY POINTER
                 A419  1637  COUNT   EDU $A419      ; COUNTER 100-991
                 A41A  1638  SI      EQU $A41A      ; START ADDRESS CF AREA
                 A41C  1639  ADDR    EDU $A41C      ; ENDING ADDRESS OF AREA
                 A41E  1640  CKSUM   EDU $A41E      ; CHECK SUM
                       1641          ;
                       1642          ; =AIM-65 MONITOR ROUTINES=
                       1643          ;
                 E2CD  1644  NXTADD  EQU $E2CD      ; ADD Y REGISTER TO ADDR+1, ADDR
                 E531  1645  DUTCKS  EQU $E531      ; GET CHARACTER SPECIFIED BY START ADDR (SI)
                 E538  1646  DUTCK   ECU $E538      ; ADD TC CHECKSUM AND RRINT
                 E538  1647  DUTCKI  EDU $E538      ; DUTCK AFTER CHECKSUM ROUTINE
                 E55D  1648  ADDSI   EDU $E55D      ; ADD DNE TO ADDR (SI)
                 E566  1649  INCS2   EDU $E566      ; INCREMENT VERTICAL COUNT
                 E56F  1650  DUMPTA  EDU $E56F      ; DREN A FILE FCR OUTPUT
                 E8C5  1651  TAP3Z   EDU $E8C5      ; SET IN/DUT FLAG
                 E8CF  1652  NAMD    EQU $E8CF      ; GET FILE NAME
                 E98A  1653  SEMI    EDU $E98A      ; WRITE A ";" TO DUTPUT DEVICE
                 E9FD  1654  CRLF    EDU $E9FD      ; OUTPUT A CRLF TO ANY DEVICE
                 EB4D  1655  CLCRK   EQU $EB4D      ; CLEAR CHECKSUM
                       1656          ;
                       1657          ; *TAPE WRITE INITIALIZATION*
                       1658          ;
                       1659          ; .GET STARTING AND ENDING ADDRESSES.
                       1660          ;
D96A   78              1661  TAPINT  SEI            ; DISABLE RROCESSOR INTERUPTS
D96B   A9 00     0000  1662          LDA #00        ; FOR NOW ALWAYS START AT $0700
D96D   85 1B     001B  1663          STA TPSTRT
D96F   A9 07     0007  1664          LDA #$07
D971   85 1C     001C  1665          STA TPSTRT+1
D973   A9 FF     00FF  1666          LDA #$FF       ; FOR NOW ALWAYS END AT $4FFF
D975   85 1D     001D  1667          STA TPEND
D977   A9 4F     004F  1668          LDA #$4F
D979   85 1E     001E  1669          STA TPEND+1
                       1670          ;
                       1671          ; .GET TAPE HEADER COMMENT. MAXIMUM 40 CHARACTERS.
                       1672          ;
D97B   A2 08     0008  1673          LDX #$08       ; STARTING ROINT IN TAPE HEADER FOR COMMENT
D97D   20 8FD2   D28F  1674          JSR COMENT     ; GO TO COMMENT ROUTINE
                       1675          ;
                       1676          ; *WRITE CONTIGUDUS BLOCK OF DATA TO TAPE*
                       1677          ;
D980   20 EBC2   D2EB  1678          JSR PNDM       ; PROMPT FOR FILE NAME
D983   46         F    1679          FCC FILE
D984   49         I
D985   4C         L
D986   45         E
D987   2D              1680          FCB #$2D
D988   4E         N    1681          FCC NAME
D989   41         A
D98A   4D         M
D98B   45         E
D98C   00              1682          FCB #$00
D98D   20 C3D9   D9C3  1683          JSR WRTAPE     ; GO WRITE THE TAPE
                       1684          ;
                       1685          ; .CLEAN UP AFTER WRITING TARE.
                       1686          ;
D990   20 EBC2   D2EB  1687          JSR PNDM       ; ACKNOWLEDGE TARE WRITE COMPLETE
D993   54         T    1688          FCC TAPE
```

```
LOC   OP OPNO  VALU  STMT  SOURCE STMT

D994  41     A
D995  50     P
D996  45     E
D997  20            1689         FCB #$20
D998  57     W      1690         FCC WRITE
D999  52     R
D99A  49     I
D99B  54     T
D99C  45     E
D99D  20            1691         FCB #$20
D99E  43     C      1692         FCC COMPLETED
D99F  4F     O
D9A0  4D     M
D9A1  50     P
D9A2  4C     L
D9A3  45     E
D9A4  54     T
D9A5  45     E
D9A6  44     D
D9A7  00            1693         FCB #$00
D9A8  20 AED9 D9AE  1694         JSR CLENUP     ; CLEAR THEN RE-ENABLE 1/10 SECOND INTERUPTS AT VIA
D9AB  4C FD00 00F0  1695         JMP MAIN       ; ==> GO TO MAIN ==>
                    1696         ;
                    1697         ; *RESET MSINTC, CLEAR INTERUPTS, ENABLE 1/10 SEC INTERUPTS*
                    1698         ;
D9AE  A9 C7   00C7  1699  CLENUP LDA #199       ; RESET HALF MS. INTERUPT COUNTER
D9B0  85 08   0008  1700         STA MSINTC
D9B2  A2 10   0010  1701         LDX #$10       ; CLEAR INTERUPTS BEFORE RE-ENABLING
D9B4  8E 01AF AF01  1702         STX VIAORA     ; V.I.A. ADDRESS REGISTER
D9B7  AD 00AF AF00  1703         LDA VIAORB     ; V.I.A. DATA REGISTER
D9BA  A9 82   0082  1704         LDA #$82       ; ENABLE 1/10 SECOND INTERUPTS AT VIA
D9BC  8D 0EAF AF0E  1705         STA VIAIER
D9BF  20 CF07 07CF  1706         JSR ROLACT     ; RESTORE OLD ACTION CODE
D9C2  60            1707         RTS
                    1708         ;
                    1709         ; *TRANSFER CONTIGUOUS BLOCK OF DATA TO TAPE*
                    1710         ;
D9C3  A9 54   0054  1711  WRTAPE LDA #$54       ; SET OUTPUT DEVICE CODE='T' (TAPE)
D9C5  8D 13A4 A413  1712         STA OUTFLG
                    1713         ;
                    1714         ; .TRANSFER ENDING AND STARTING ADDRESSES TO ADDR AND S1.
                    1715         ;
D9C8  A5 1D   001D  1716         LDA TPEND      ; GET LO BYTE OF ENDING ADDRESS
D9CA  8D 1CA4 A41C  1717         STA ADDR       ; STORE BYTE OF ENDING ADDRESS USED BY WRTAPE
D9CD  A5 1B   001B  1718         LDA TPSTRT     ; GET LO BYTE OF STARTING ADDRESS
D9CF  8D 1AA4 A41A  1719         STA S1         ; LO BYTE OF STARTING ADDRESS USED BY WRTAPE
D9D2  A5 1E   001E  1720         LDA TPEND+1    ; GET HI BYTE OF ENDING ADDRESS
D9D4  8D 1DA4 A41D  1721         STA ADDR+1     ; STORE HI BYTE OF ENDING ADDRESS FOR TAPEWR
D9D7  A5 1C   001C  1722         LDA TPSTRT+1   ; GET HI BYTE OF STARTING ADDRESS
D9D9  8D 1BA4 A41B  1723         STA S1+1       ; STORE HI BYTE OF ENDING ADDRESS FOR TAPEWR
                    1724         ;
D9DC  20 CFE8 E8CF  1725         JSR NAMO       ; GET THE FILE NAME
                    1726         ;
D9DF  A2 01   0001  1727         LDX #01        ; SET IN/OUT FLAG=1 ( TAPE OUTPUT )
D9E1  20 C5E8 E8C5  1728         JSR TAP3Z      ; SAVE I/O FLAG AND WAIT FOR USER RESPONCE
D9E4  20 6FE5 E56F  1729         JSR DUMPTA     ; OPEN A FILE FOR OUTPUT TO TAPE BY BLOCKS
D9E7  20 13EA EA13  1730         JSR CRLOW      ; CARRIAGE RETURN LINE FEED TO DISPLAY
                    1731         ;
D9EA  A9 00   0000  1732         LDA #00        ; CLEAR THE RECORD COUNT
D9EC  8D 0601 0106  1733         STA S2
D9EF  8D 0701 0107  1734         STA S2+1
                    1735         ;
D9F2  A0 01   0001  1736         LDY #01        ; OUTPUT ONE MORE BYTE
D9F4  20 C0E2 E2C0  1737         JSR NXTADD     ; ADD Y TO ADDR+1 AND ADDR
                    1738         ;
D9F7  20 F0E9 E9F0  1739  DU2    JSR CRLF       ; CR/LF TO ANY OUTPUT DEVICE (TAPE)
                    1740         ;
                    1741         ; .CALCULATE NUMBER OF BYTES YET TO BE DUMPED.
                    1742         ;
D9FA  20 40E8 E840  1743         JSR CLCRK      ; CLEAR CHECKSUM
D9FD  AD 1CA4 A41C  1744         LDA ADDR       ; ENDING ADDRESS - CURRENT ADDRESS
DA00  38            1745         SEC
```

```
LOC   OP OPNO  VALU         SOURCE STMT

0A01  E0 1AA4  A41A                SBC S1
0A04  48                           PHA                 ; NUMBER OF BYTES LO
0A05  AD 1DA4  A41D                LDA ADDR+1
0A08  E0 1BA4  A41B                SBC S1+1
0A0B  D0 09    0A16                BNE OU6             ; NUMBER OF BYTES HI
                                   ;
                                   ; .SEE IF 24 OR MORE BYTES LEFT.
                                   ;
0A0D  68                           PLA
0A0E  F0 42    0A52                BEQ OU10Z           ; NUMBER OF BYTES HI WAS ZERO
0A10  C9 24    0024                CMP #$24            ; DONE
0A12  90 05    0A19                BCC OU8             ; IS THE NUMBER OF BYTES > 24T
0A14  B0 01    0A17                BCS OU7             ; NO, ONLY OUTPUT REMAINING BYTES
                                   ;                   ; YES, 24 BYTES IN NEXT RECORD
0A16  68                    OU6    PLA
                                   ;
0A17  A9 24    0024         OU7    LDA #$24
                                   ;
0A19  48                    OU8    PHA
0A1A  20 BAE9  E9BA                JSR SEMI            ; OUTPUT ";", NUMBER OF BYTES, AND PUSH A REGISTER
0A1D  68                           PLA
0A1E  8D 19A4  A419                STA COUNT           ; SET NUMBER OF BYTES
0A21  20 3BE5  E53B                JSR OUTCK           ; OUTPUT NUMBER OF BYTES
0A24  AD 1BA4  A41B                LDA S1+1            ; OUTPUT ADDRESS
0A27  20 3BE5  E53B                JSR OUTCK
0A2A  AD 1AA4  A41A                LDA S1
0A2D  20 3BE5  E53B                JSR OUTCK
                                   ;
                                   ; .OUTPUT DATA.
                                   ;
0A30  20 31E5  E531         OU9    JSR OUTCKS          ; GET CHARACTER SPECIFIED BY S1
0A33  A9 00    0000                LDA #00             ; CLEAR DISPLAY POINTER
0A35  8D 15A4  A415                STA CURPO2
0A38  20 5DE5  E55D                JSR ADDS1           ; INCREMENT S1+1, AND S1
0A3B  CE 19A4  A419                DEC COUNT           ; DECREMENT BYTE COUNT
0A3E  D0 F0    0A30                BNE OU9             ; NOT DONE WITH THIS RECORD
                                   ;
                                   ; .OUTPUT THE CHECKSUM.
                                   ;
0A40  AD 1FA4  A41F                LDA CKSUM+1
0A43  20 3BE5  E53B                JSR OUTCK1          ; CHECKSUM LO BYTE
0A46  AD 1EA4  A41E                LDA CKSUM
0A49  20 3BE5  E53B                JSR OUTCK1          ; CHECKSUM HI BYTE
0A4C  20 66E5  E566                JSR INCS2           ; INCREMENT VERTICAL COUNT
0A4F  4C F709  09F7                JMP OU2             ; NEXT RECORD
0A52  20 E0E4  E4EB         OU10Z  JSR $E4EB           ; OUTPUT LAST RECORD. LET MONITOR CLEAN UP
0A55  60                           RTS                 ; ALL DONE
                                   ;
                                   ; *CONVERT ONE BYTE HEX (00-0F) TO ASCII (30 TO 4T)
                                   ;
0A56  C9 0A    000A         OBHXAS CMP #$0A
0A58  90 04    0A5E                BCC LT10            ; IF <10 GO TO LT10
0A5A  18                           CLC
0A5B  69 37    0037                ADC #$37            ; ADD 37 FOR $41 ETC.
0A5D  60                           RTS
0A5E  18                    LT10   CLC
0A5F  69 30    0030                ADC #$30            ; ADD 30 FOR $30 ETC.
0A61  60                           RTS
                                   ;
                                   ; *MOVE LEFT HALF WORD OF A REGISTER INTO RIGHT HALF WORD.
                                   ;   THEN ZERO OUT THE LEFT HALF WORD*
                                   ;
0A62  29 F0    00F0         LHWOFA AND #$F0            ; ZERO RIGHT HALF WORD
0A64  4A                           LSR                 ; SHIFT LEFT HALF WORD TO RIGHT HALF WORD
0A65  4A                           LSR
0A66  4A                           LSR
0A67  4A                           LSR
0A68  60                           RTS
                                   ;
                                   ; .DECIMAL CHARACTER TABLE USED IN CLOCK AND DISPLAY ROUTINES.
                                   ;
0A69  00                    CLCTBL FCB $00
```

```
LOC   OP OPND   VALU   STMT   SOURCE STMT

DA6A  01               1818          FCB $01
DA6B  02               1819          FCB $02
DA6C  03               1820          FCB $03
DA6D  04               1821          FCB $04
DA6E  05               1822          FCB $05
DA6F  06               1823          FCB $06
DA70  07               1824          FCB $07
DA71  08               1825          FCB $08
DA72  09               1826          FCB $09
DA73  10               1827          FCB $10
DA74  11               1828          FCB $11
DA75  12               1829          FCB $12
DA76  13               1830          FCB $13
DA77  14               1831          FCB $14
DA78  15               1832          FCB $15
DA79  16               1833          FCB $16
DA7A  17               1834          FCB $17
DA7B  18               1835          FCB $18
DA7C  19               1836          FCB $19
DA7D  20               1837          FCB $20
DA7E  21               1838          FCB $21
DA7F  22               1839          FCB $22
DA80  23               1840          FCB $23
DA81  24               1841          FCB $24
DA82  25               1842          FCB $25
DA83  26               1843          FCB $26
DA84  27               1844          FCB $27
DA85  28               1845          FCB $28
DA86  29               1846          FCB $29
DA87  30               1847          FCB $30
DA88  31               1848          FCB $31
DA89  32               1849          FCB $32
DA8A  33               1850          FCB $33
DA8B  34               1851          FCB $34
DA8C  35               1852          FCB $35
DA8D  36               1853          FCB $36
DA8E  37               1854          FCB $37
DA8F  38               1855          FCB $38
DA90  39               1856          FCB $39
DA91  40               1857          FCB $40
DA92  41               1858          FCB $41
DA93  42               1859          FCB $42
DA94  43               1860          FCB $43
DA95  44               1861          FCB $44
DA96  45               1862          FCB $45
DA97  46               1863          FCB $46
DA98  47               1864          FCB $47
DA99  48               1865          FCB $48
DA9A  49               1866          FCB $49
DA9B  50               1867          FCB $50
DA9C  51               1868          FCB $51
DA9D  52               1869          FCB $52
DA9E  53               1870          FCB $53
DA9F  54               1871          FCB $54
DAA0  55               1872          FCB $55
DAA1  56               1873          FCB $56
DAA2  57               1874          FCB $57
DAA3  58               1875          FCB $58
DAA4  59               1876          FCB $59
DAA5  60               1877          FCB $60
DAA6  61               1878          FCB $61
DAA7  62               1879          FCB $62
DAA8  63               1880          FCB $63
DAA9  64               1881          FCB $64
DAAA  65               1882          FCB $65
DAAB  66               1883          FCB $66
DAAC  67               1884          FCB $67
DAAD  68               1885          FCB $68
DAAE  69               1886          FCB $69
DAAF  70               1887          FCB $70
DAB0  71               1888          FCB $71
DAB1  72               1889          FCB $72

LOC   OP OPND   VALU   STMT   SOURCE STMT

DAB2  73               1890          FCB $73
DAB3  74               1891          FCB $74
DAB4  75               1892          FCB $75
DAB5  76               1893          FCB $76
DAB6  77               1894          FCB $77
DAB7  78               1895          FCB $78
DAB8  79               1896          FCB $79
DAB9  80               1897          FCB $80
DABA  81               1898          FCB $81
DABB  82               1899          FCB $82
DABC  83               1900          FCB $83
DABD  84               1901          FCB $84
DABE  85               1902          FCB $85
DABF  86               1903          FCB $86
DAC0  87               1904          FCB $87
DAC1  88               1905          FCB $88
DAC2  89               1906          FCB $89
DAC3  90               1907          FCB $90
DAC4  91               1908          FCB $91
DAC5  92               1909          FCB $92
DAC6  93               1910          FCB $93
DAC7  94               1911          FCB $94
DAC8  95               1912          FCB $95
DAC9  96               1913          FCB $96
DACA  97               1914          FCB $97
DACB  98               1915          FCB $98
DACC  99               1916          FCB $99
                       1917   ;
                       1918   ; ** CHARACTER TABLE FOR VIDEC TIC MARKS **
                       1919   ;
DACD  FFFF             1920   TVTICS FDB $FFFF
DAD0  FFFF             1921          FDB $FFFF
DAD1  FFFF             1922          FDB $FFFF
DAD3  FFFF             1923          FDB $FFFF
DAD5  FFFF             1924          FDB $FFFF
DAD7  FFFF             1925          FDB $FFFF
DAD9  FFFF             1926          FCB $FFFF
DADB  FFFF             1927          FDB $FFFF
DADD  FFFF             1928          FDB $FFFF
DAE0  FFFF             1929          FDB $FFFF
DAE1  FFFF             1930          FDB $FFFF
DAE3  FFFF             1931          FDB $FFFF
DAE5  FFFF             1932          FDB $FFFF
DAE7  FFFF             1933          FCB $FFFF
DAE9  FFFF             1934          FDB $FFFF
DAEB  FFFF             1935          FDB $FFFF
DAED  FFFF             1936          FDB $FFFF
DAF0  FFFF             1937          FDB $FFFF
DAF1  FFFF             1938          FDB $FFFF
DAF3  FFFF             1939          FDB $FFFF
DAF5  8000             1940          FDB $0080
DAF7  0000             1941          FDB $0000
DAF9  0000             1942          FDB $0000
DAFB  0001             1943          FDB $0100
DAFD  0000             1944          FDB $0000
DB00  0000             1945          FDB $0000
DB01  0000             1946          FDB $0000
DB03  0001             1947          FDB $0100
DB05  0000             1948          FDB $0000
DB07  0000             1949          FDB $0000
DB09  0000             1950          FDB $0000
DB0B  0001             1951          FDB $0100
DB0D  0000             1952          FDB $0000
DB10  0000             1953          FDB $0000
DB11  0000             1954          FDB $0000
DB13  0001             1955          FDB $0100
DB15  8000             1956          FDB $0080
DB17  0001             1957          FCB $0100
DB19  0000             1958          FDB $0000
DB1B  0001             1959          FDB $0100
DB1D  8000             1960          FDB $0080
DB20  0000             1961          FDB $0000
```

```
LOC   OP OPNO  VALU  STMT  SOURCE STMT

DB21  0000           1962          FDB $0000
DB23  0001           1963          FCB $0100
DB25  0000           1964          FDB $0000
DB27  0000           1965          FCB $0000
DB29  0000           1966          FDB $0000
DB2B  0001           1967          FDB $0100
DB2D  0000           1968          FDB $0000
DB2F  0000           1969          FDB $0000
DB31  0000           1970          FDB $0000
DB33  0001           1971          FDB $0100
DB35  0000           1972          FCB $0000
DB37  0000           1973          FDB $0000
DB39  0000           1974          FDB $0000
DB3B  0001           1975          FDB $0100
DB3D  8000           1976          FDB $0080
DB3F  0001           1977          FDB $0100
DB41  0000           1978          FCB $0000
DB43  0001           1979          FCB $0100
DB45  8000           1980          FDB $0080
DB47  0000           1981          FDB $0000
DB49  0000           1982          FDB $0000
DB4B  0001           1983          FDB $0100
DB4D  0000           1984          FDB $0000
DB4F  0000           1985          FDB $0000
DB51  0000           1986          FDB $0000
DB53  0001           1987          FDB $0100
DB55  0000           1988          FDB $0000
DB57  0000           1989          FDB $0000
DB59  0000           1990          FDB $0000
DB5B  0001           1991          FDB $0100
DB5D  0000           1992          FDB $0000
DB5F  0000           1993          FDB $0000
DB61  0000           1994          FDB $0000
DB63  0001           1995          FDB $0100
DB65  8000           1996          FDB $0080
DB67  0001           1997          FDB $0100
DB69  0000           1998          FDB $0000
DB6B  0001           1999          FDB $0100
                     2000          ;
                     2001          ; .LO BYTE VIDEO LINE START ADDRESS.
                     2002          ;
DB6D  00             2003  TVTBLL  FCB $00
DB6E  28             2004          FCB $28
DB6F  50             2005          FCB $50
DB70  78             2006          FCB $75
DB71  A0             2007          FCB $A0
DB72  C8             2008          FCB $C8
DB73  F0             2009          FCB $F0
DB74  18             2010          FCB $18
DB75  40             2011          FCB $40
DB76  68             2012          FCB $68
DB77  90             2013          FCB $90
DB78  B8             2014          FCB $B8
DB79  E0             2015          FCB $E0
DB7A  08             2016          FCB $08
DB7B  30             2017          FCB $30
DB7C  58             2018          FCB $58
DB7D  80             2019          FCB $80
DB7E  A8             2020          FCB $A8
DB7F  D0             2021          FCB $D0
DB80  F8             2022          FCB $F8
DB81  20             2023          FCB $20
DB82  48             2024          FCB $48
DB83  70             2025          FCB $70
DB84  98             2026          FCB $98
DB85  C0             2027          FCB $C0
DB86  E8             2028          FCB $E8
DB87  10             2029          FCB $10
DB88  38             2030          FCB $38
DB89  60             2031          FCB $60
DB8A  88             2032          FCB $88
DB8B  B0             2033          FCB $B0
```

```
LOC   OP OPNO  VALU  STMT  SOURCE STMT

DB8C  D8             2034          FCB $D8
DB8D  00             2035          FCB $00
DB8E  28             2036          FCB $28
DB8F  50             2037          FCB $50
DB90  78             2038          FCB $78
DB91  A0             2039          FCB $A0
DB92  C8             2040          FCB $C8
DB93  F0             2041          FCB $F0
DB94  18             2042          FCB $18
DB95  40             2043          FCB $40
DB96  68             2044          FCB $68
DB97  90             2045          FCB $90
DB98  B8             2046          FCB $B8
DB99  E0             2047          FCB $E0
DB9A  08             2048          FCB $08
DB9B  30             2049          FCB $30
DB9C  58             2050          FCB $58
DB9D  80             2051          FCB $80
DB9E  A8             2052          FCB $A8
DB9F  D0             2053          FCB $D0
DBA0  F8             2054          FCB $F8
DBA1  20             2055          FCB $20
DBA2  48             2056          FCB $48
DBA3  70             2057          FCB $70
DBA4  98             2058          FCB $98
DBA5  C0             2059          FCB $C0
DBA6  E8             2060          FCB $E8
DBA7  10             2061          FCB $10
DBA8  38             2062          FCB $38
DBA9  60             2063          FCB $60
DBAA  88             2064          FCB $88
DBAB  B0             2065          FCB $B0
DBAC  D8             2066          FCB $D8
DBAD  00             2067          FCB $00
DBAE  28             2068          FCB $28
DBAF  50             2069          FCB $50
DBB0  78             2070          FCB $78
DBB1  A0             2071          FCB $A0
DBB2  C8             2072          FCB $C8
DBB3  F0             2073          FCB $F0
DBB4  18             2074          FCB $18
DBB5  40             2075          FCB $40
DBB6  68             2076          FCB $68
DBB7  90             2077          FCB $90
DBB8  B8             2078          FCB $B8
DBB9  E0             2079          FCB $E0
DBBA  08             2080          FCB $08
DBBB  30             2081          FCB $30
DBBC  58             2082          FCB $58
DBBD  80             2083          FCB $80
DBBE  A8             2084          FCB $A8
DBBF  D0             2085          FCB $D0
DBC0  F8             2086          FCB $F8
DBC1  20             2087          FCB $20
DBC2  48             2088          FCB $48
DBC3  70             2089          FCB $70
DBC4  98             2090          FCB $98
DBC5  C0             2091          FCB $C0
DBC6  E8             2092          FCB $E8
DBC7  10             2093          FCB $10
DBC8  38             2094          FCB $38
DBC9  60             2095          FCB $60
DBCA  88             2096          FCB $88
DBCB  B0             2097          FCB $B0
DBCC  D8             2098          FCB $D8
DBCD  00             2099          FCB $00
DBCE  28             2100          FCB $28
DBCF  50             2101          FCB $50
DBD0  78             2102          FCB $78
DBD1  A0             2103          FCB $A0
DBD2  C8             2104          FCB $C8
DBD3  F0             2105          FCB $F0
```

```
LOC   OP OPND  VALU  STMT  SOURCE STMT

0BD4  18             2106         FCB $18
0BD5  40             2107         FCB $40
0BD6  68             2108         FCB $68
0BD7  90             2109         FCB $90
0BD8  B8             2110         FCB $B8
0BD9  E0             2111         FCB $E0
0BDA  08             2112         FCB $08
0BDB  30             2113         FCB $30
0BDC  58             2114         FCB $58
0BDD  80             2115         FCB $80
0BDE  A8             2116         FCB $A8
0BDF  D0             2117         FCB $D0
0BE0  F8             2118         FCB $F8
0BE1  20             2119         FCB $20
0BE2  48             2120         FCB $48
0BE3  70             2121         FCB $70
0BE4  98             2122         FCB $98
0BE5  C0             2123         FCB $C0
0BE6  E8             2124         FCB $E8
0BE7  10             2125         FCB $10
0BE8  38             2126         FCB $38
0BE9  60             2127         FCB $60
0BEA  88             2128         FCB $88
0BEB  B0             2129         FCB $B0
0BEC  D8             2130         FCB $D8
0BED  00             2131         FCB $00
0BEE  28             2132         FCB $28
0BEF  50             2133         FCB $50
0BF0  78             2134         FCB $78
0BF1  A0             2135         FCB $A0
0BF2  C8             2136         FCB $C8
0BF3  F0             2137         FCB $F0
0BF4  18             2138         FCB $18
0BF5  40             2139         FCB $40
0BF6  68             2140         FCB $68
0BF7  90             2141         FCB $90
0BF8  B8             2142         FCB $B8
0BF9  E0             2143         FCB $E0
0BFA  08             2144         FCB $08
0BFB  30             2145         FCB $30
0BFC  58             2146         FCB $58
0BFD  80             2147         FCB $80
0BFE  A8             2148         FCB $A8
0BFF  D0             2149         FCB $D0
0C00  F8             2150         FCB $F8
0C01  20             2151         FCB $20
0C02  48             2152         FCB $48
0C03  70             2153         FCB $70
0C04  98             2154         FCB $98
0C05  C0             2155         FCB $C0
0C06  E8             2156         FCB $E8
0C07  10             2157         FCB $10
0C08  38             2158         FCB $38
0C09  60             2159         FCB $60
0C0A  88             2160         FCB $88
0C0B  B0             2161         FCB $B0
0C0C  D8             2162         FCB $D8
0C0D  00             2163         FCB $00
0C0E  28             2164         FCB $28
0C0F  50             2165         FCB $50
0C10  78             2166         FCB $78
0C11  A0             2167         FCB $A0
0C12  C8             2168         FCB $C8
0C13  F0             2169         FCB $F0
0C14  18             2170         FCB $18
0C15  40             2171         FCB $40
0C16  68             2172         FCB $68
0C17  90             2173         FCB $90
0C18  B8             2174         FCB $B8
0C19  E0             2175         FCB $E0
0C1A  08             2176         FCB $08
0C1B  30             2177         FCB $30

LOC   OP OPND  VALU  STMT  SOURCE STMT

0C1C  58             2178         FCB $58
0C1D  80             2179         FCB $80
0C1E  A8             2180         FCB $A8
0C1F  D0             2181         FCB $D0
0C20  F8             2182         FCB $F8
0C21  20             2183         FCB $20
0C22  48             2184         FCB $48
0C23  70             2185         FCB $70
0C24  98             2186         FCB $98
0C25  C0             2187         FCB $C0
0C26  E8             2188         FCB $E8
0C27  10             2189         FCB $10
0C28  38             2190         FCB $38
0C29  60             2191         FCB $60
0C2A  88             2192         FCB $88
0C2B  B0             2193         FCB $B0
0C2C  D8             2194         FCB $D8
0C2D  00             2195         FCB $00
0C2E  28             2196         FCB $28
0C2F  50             2197         FCB $50
0C30  78             2198         FCB $78
0C31  A0             2199         FCB $A0
0C32  C8             2200         FCB $C8
0C33  F0             2201         FCB $F0
0C34  18             2202         FCB $18
                     2203         *
                     2204         * HI BYTE VIDEO LINE START.
                     2205         *
0C35  60             2206  TVTBLH FCB $60
0C36  60             2207         FCB $60
0C37  60             2208         FCB $60
0C38  60             2209         FCB $60
0C39  60             2210         FCB $60
0C3A  60             2211         FCB $60
0C3B  60             2212         FCB $60
0C3C  61             2213         FCB $61
0C3D  61             2214         FCB $61
0C3E  61             2215         FCB $61
0C3F  61             2216         FCB $61
0C40  61             2217         FCB $61
0C41  61             2218         FCB $61
0C42  62             2219         FCB $62
0C43  62             2220         FCB $62
0C44  62             2221         FCB $62
0C45  62             2222         FCB $62
0C46  62             2223         FCB $62
0C47  62             2224         FCB $62
0C48  62             2225         FCB $62
0C49  63             2226         FCB $63
0C4A  63             2227         FCB $63
0C4B  63             2228         FCB $63
0C4C  63             2229         FCB $63
0C4D  63             2230         FCB $63
0C4E  63             2231         FCB $63
0C4F  64             2232         FCB $64
0C50  64             2233         FCB $64
0C51  64             2234         FCB $64
0C52  64             2235         FCB $64
0C53  64             2236         FCB $64
0C54  64             2237         FCB $64
0C55  65             2238         FCB $65
0C56  65             2239         FCB $65
0C57  65             2240         FCB $65
0C58  65             2241         FCB $65
0C59  65             2242         FCB $65
0C5A  65             2243         FCB $65
0C5B  65             2244         FCB $65
0C5C  66             2245         FCB $66
0C5D  66             2246         FCB $66
0C5E  66             2247         FCB $66
0C5F  66             2248         FCB $66
0C60  66             2249         FCB $66
```

```
LOC   OP OPND  VALU  STMT  SOURCE STMT

DC61  66             2250         FCB $66
DC62  67             2251         FCB $67
DC63  67             2252         FCB $67
DC64  67             2253         FCB $67
DC65  67             2254         FCB $67
DC66  67             2255         FCB $67
DC67  67             2256         FCB $67
DC68  67             2257         FCB $67
DC69  68             2258         FCB $68
DC6A  68             2259         FCB $68
DC6B  68             2260         FCB $68
DC6C  68             2261         FCB $68
DC6D  68             2262         FCB $68
DC6E  68             2263         FCB $68
DC6F  69             2264         FCB $69
DC70  69             2265         FCB $69
DC71  69             2266         FCB $69
DC72  69             2267         FCB $69
DC73  69             2268         FCB $69
DC74  69             2269         FCB $69
DC75  6A             2270         FCB $6A
DC76  6A             2271         FCB $6A
DC77  6A             2272         FCB $6A
DC78  6A             2273         FCB $6A
DC79  6A             2274         FCB $6A
DC7A  6A             2275         FCB $6A
DC7B  6A             2276         FCB $6A
DC7C  6B             2277         FCB $6B
DC7D  6B             2278         FCB $6B
DC7E  6B             2279         FCB $6B
DC7F  6B             2280         FCB $6B
DC80  6B             2281         FCB $6B
DC81  6B             2282         FCB $6B
DC82  6C             2283         FCB $6C
DC83  6C             2284         FCB $6C
DC84  6C             2285         FCB $6C
DC85  6C             2286         FCB $6C
DC86  6C             2287         FCB $6C
DC87  6C             2288         FCB $6C
DC88  6C             2289         FCB $6C
DC89  6D             2290         FCB $6D
DC8A  6D             2291         FCB $6D
DC8B  6D             2292         FCB $6D
DC8C  6D             2293         FCB $6D
DC8D  6D             2294         FCB $6D
DC8E  6D             2295         FCB $6D
DC8F  6E             2296         FCB $6E
DC90  6E             2297         FCB $6E
DC91  6E             2298         FCB $6E
DC92  6E             2299         FCB $6E
DC93  6E             2300         FCB $6E
DC94  6E             2301         FCB $6E
DC95  6F             2302         FCB $6F
DC96  6F             2303         FCB $6F
DC97  6F             2304         FCB $6F
DC98  6F             2305         FCB $6F
DC99  6F             2306         FCB $6F
DC9A  6F             2307         FCB $6F
DC9B  6F             2308         FCB $6F
DC9C  70             2309         FCB $70
DC9D  70             2310         FCB $70
DC9E  70             2311         FCB $70
DC9F  70             2312         FCB $70
DCA0  70             2313         FCB $70
DCA1  70             2314         FCB $70
DCA2  71             2315         FCB $71
DCA3  71             2316         FCB $71
DCA4  71             2317         FCB $71
DCA5  71             2318         FCB $71
DCA6  71             2319         FCB $71
DCA7  71             2320         FCB $71
DCA8  71             2321         FCB $71
```

```
LOC   OP OPND  VALU  STMT  SOURCE STMT

DCA9  72             2322         FCB $72
DCAA  72             2323         FCB $72
DCAB  72             2324         FCB $72
DCAC  72             2325         FCB $72
DCAD  72             2326         FCB $72
DCAE  72             2327         FCB $72
DCAF  73             2328         FCB $73
DCB0  73             2329         FCB $73
DCB1  73             2330         FCB $73
DCB2  73             2331         FCB $73
DCB3  73             2332         FCB $73
DCB4  73             2333         FCB $73
DCB5  74             2334         FCB $74
DCB6  74             2335         FCB $74
DCB7  74             2336         FCB $74
DCB8  74             2337         FCB $74
DCB9  74             2338         FCB $74
DCBA  74             2339         FCB $74
DCBB  74             2340         FCB $74
DCBC  75             2341         FCB $75
DCBD  75             2342         FCB $75
DCBE  75             2343         FCB $75
DCBF  75             2344         FCB $75
DCC0  75             2345         FCB $75
DCC1  75             2346         FCB $75
DCC2  76             2347         FCB $76
DCC3  76             2348         FCB $76
DCC4  76             2349         FCB $76
DCC5  76             2350         FCB $76
DCC6  76             2351         FCB $76
DCC7  76             2352         FCB $76
DCC8  76             2353         FCB $76
DCC9  77             2354         FCB $77
DCCA  77             2355         FCB $77
DCCB  77             2356         FCB $77
DCCC  77             2357         FCB $77
DCCD  77             2358         FCB $77
DCCE  77             2359         FCB $77
DCCF  78             2360         FCB $78
DCD0  78             2361         FCB $78
DCD1  78             2362         FCB $78
DCD2  78             2363         FCB $78
DCD3  78             2364         FCB $78
DCD4  78             2365         FCB $78
DCD5  79             2366         FCB $79
DCD6  79             2367         FCB $79
DCD7  79             2368         FCB $79
DCD8  79             2369         FCB $79
DCD9  79             2370         FCB $79
DCDA  79             2371         FCB $79
DCDB  79             2372         FCB $79
DCDC  7A             2373         FCB $7A
DCDD  7A             2374         FCB $7A
DCDE  7A             2375         FCB $7A
DCDF  7A             2376         FCB $7A
DCE0  7A             2377         FCB $7A
DCE1  7A             2378         FCB $7A
DCE2  7B             2379         FCB $7B
DCE3  7B             2380         FCB $7B
DCE4  7B             2381         FCB $7B
DCE5  7B             2382         FCB $7B
DCE6  7B             2383         FCB $7B
DCE7  7B             2384         FCB $7B
DCE8  7B             2385         FCB $7B
DCE9  7C             2386         FCB $7C
DCEA  7C             2387         FCB $7C
DCEB  7C             2388         FCB $7C
DCEC  7C             2389         FCB $7C
DCED  7C             2390         FCB $7C
DCEE  7C             2391         FCB $7C
DCEF  7D             2392         FCB $7D
DCF0  7D             2393         FCB $7D
```

```
LOC   OP OPND  VALU  STMT  SOURCE STMT

DCF1  7D             2394         FCB $7D
DCF2  7D             2395         FCB $7D
DCF3  7D             2396         FCB $7D
DCF4  7D             2397         FCB $7D
DCF5  7E             2398         FCB $7E
DCF6  7E             2399         FCB $7E
DCF7  7E             2400         FCB $7E
DCF8  7E             2401         FCB $7E
DCF9  7E             2402         FCB $7E
DCFA  7E             2403         FCB $7E
DCFB  7E             2404         FCB $7E
DCFC  7F             2405         FCB $7F
```

SYMBOL	VALU	DEFN	REFERENCES
ACTCHK	D189	0484	0416
ACTCKC	D194	0489	0487
ACTCKD	D19E	0493	0490
ACTCKF	D1FD	0534	0531
ACTCKG	D1C8	0514	0505
ACTCKP	D1DF	D522	0519
ACTCKR	D1F3	0530	0527
ACTCKT	D1D5	0518	0515
ACTCKU	D1B5	0504	0494
ACTCKV	D1E9	0526	0523
ACTION	D000	0062	0333 0460 0471 0485 0559 0962 1422
ADCONV	D477	0908	0896
ADDR	A41C	1639	1717 1721 1744 1748
ADDSI	E55D	1648	1779
ATDCH1	A200	0021	0908 0995 0998 1021 1025 1099 1101 1122 1125
ATDCH2	A300	0022	0909 1001 1004 1032 1036 1104 1106 1140 1143
ATDCH3	A600	0023	0910 1007 1010 1043 1047 1109 1111 1158 1161
AVGRH1	002A	D099	0997 1026 1028 1053 1100 1126 1137 1176
AVGRH2	D02B	0100	1003 1037 1039 1055 1105 1144 1155 1179
AVGRH3	002C	0101	1009 1048 1050 1057 1110 1162
AVGRL1	0027	0096	0999 1022 1024 1029 1067 1102 1123 1124 1128 1130 1132 1134 1136 1199
AVGRL2	0028	0097	1005 1033 1035 1040 1069 1107 1141 1142 1146 1148 1150 1152 1154 1201
AVGRL3	0029	0098	1011 1044 1046 1051 1071 1112 1159 1160 1164 1166 1168 1170 1172 1203
BITTAB	D039	0113	0382 1280 1302
BKSP	E7E1	0040	0636
CHANEL	0033	D108	0311 0855 1269 1450
CHANLB	0034	0109	0318 0867 1284 1474
CHDIS1	D439	0857	0866
CHDIS2	D449	0867	0863
CHDIS3	D44D	0869	0875
CHDIS4	D458	0877	0872
CKSUM	A41E	1640	1765 1787
CLCIRQ	D48E	0920	0915
CLCRK	E84D	1655	1743
CLCTBL	DA69	1817	0600 0803 1414
CLEAR	D2D3	0668	0710 0731 0747 1420 1428 1452 1478 1584 1598 0248 0275 0472
CLEA1	D2D8	0672	0679
CLENUP	D9AE	1699	0512 1694
CLINIT	D058	0288	
CNTDWN	D4A6	D533	
COLDST	D02D	D262	0238
CDMC1	D29E	0631	0635 0639 0646
CDMC2	D2A8	0640	0633
CDMC4	D287	0647	0641
CDMENT	D28F	0627	1674 0246 0491
CONCDE	D131	0432	0420
COUNT	A419	1637	1767 1780
CRLF	E9F0	1654	1739
CRLOW	EA13	0039	0480 0647 0680 1730
CURPD2	A415	1636	1778
CURSTR	0007	0066	0349 1019 1120 1222
CWREOF	D018	0083	0345 0507 0508 0528 0937
CWWAIT	D180	0508	0509
DAYDMT	000F	0074	0725
DAYDWK	D00E	0073	0745
DBUFF	D041	0118	0335 0463 0474 0484 0560 0571 0572 0573 0574 0589 0605 0611 1423
DECHEX	D3D7	0801	0804 1501 1623 0721 0726 0756 0761 0782
DISBF2	D257	0586	0594
DISBUF	D255	0585	0578
DISNCD	D176	0472	0465
DISPLY	D248	0578	
DISRTE	D031	0106	1240 1504
DISTME	D213	0550	0488 0492 D513 D517 D521 0525 0529 0533 0545
DRSET	D922	1556	1615 0254 0324 D532
DRSETX	D966	1627	1608
DRSET4	D957	1619	1613
DRSET5	D959	1620	1618
DRSET6	D958	1622	1611
DSPCHK	D20C	0544	0535
DSPCH1	0014	0079	0312 D561 0996 1270 1285
DSPCH2	D015	0080	0313 0564 1002
DSPCH3	0016	0081	0314 0567 1008

SYMBOL	VALU	DEFN	REFERENCES
DUMPTA	E56F	1650	1729
DU10Z	0A52	1791	1755
DU2	09F7	1739	1790
DU6	0A16	1760	1750
DU7	0A17	1762	1758
DU8	DA19	1764	1757
DU9	DA30	1776	1781
FRZCTR	0025	0094	0340 1082 1083 1087
FRZFLG	0023	0092	0346 0467 0468 1077 1092
FRZSET	D399	0770	0325 0520
FRZST1	D386	0781	0779
FRZST2	03C0	0785	0780
FRZTME	0012	0077	0310 0783 1080 1093
FZTMEC	0024	0093	0784 1088 1089 1094
FZWAIT	016E	0468	0469
GAP	A409	0052	0305
GETKEY	D2C5	0659	0247 0631
GETK1	D2C8	0660	0662
GOCLCK	D8C4	1549	1593
GOCLC2	D803	1555	1560
GTE100	D7C1	1408	1401
GTE200	D789	1403	1399
HBSAVE	D7C5	1411	1402 1407
HIDUT	D26C	0602	0622
HOUR	0000	0072	0550 0755
HUNSEC	000A	0069	
HXASC2	D266	0599	
HXASC3	D27F	0616	0563 0566 0569
HX1BCD	D7AC	1396	0257 0616
INCMSC	D4CC	0955	0918
INCS2	E566	1649	1789
INTRCV	045D	0887	0263 0265
INTTST	D409	0962	0958
INTXIT	D4E8	0969	0967
KEYCK	0719	1312	0258 0402 0660
KEYCK0	D72E	1321	1330
KEYCK1	D74A	1337	1318
KEYCK2	D758	1345	1342
KEYCK3	D766	1352	1355
KEYCK4	D76C	1356	1353
KEYCK5	D770	1365	1361
KEYCK6	D792	1378	1374
KEYCK7	D797	1381	1359 1369 1372
KEYCK8	D798	1382	1364 1377 1380
KEYC0	D71C	1313	1331 1343
KEYC00	D740	1332	1327
KEYC18	D759	1344	1339
KEYC10	D7A3	1388	1385
KEYC11	D7A2	1387	1344 1383
LHWDFA	DA62	1808	0602
LINEST	0037	0112	0356 0812 0814 0817 0824 0826 0830 0837 0839 0843 0852 0854 0858 0861 0870 1244 1246 1248 1250 1261 1263 1266 1268 1283 1305
LINPTR	0032	0107	0878 1252 1253 1257 1259 1294
LODA50	D038	0270	
LDWDUT	0277	0608	0619
LSTPTA	0035	0110	0315 1243 1281
LSTPTB	0036	0111	0316 1247 1303
LT10	DA5E	1801	1797
MAIN	00F0	0398	0546 0581 1695
MILSEC	0009	0068	1555 1574
MINUTE	000C	0071	0553 0760
MONTH	0010	0075	0720
MSBCH1	0001	0063	0353 0358 1054 1063 1068 1177 1178 1185 1189 1195 1200 1208 1212 1218
MSBCH2	0003	0064	0354 0360 1056 1064 1070 1180 1181 1191 1196 1202 1214 1219
MSBCH3	0005	0065	0355 0362 1058 1065 1072 1174 1175 1193 1197 1204 1216 1220
MSINTC	0008	0067	0343 0951 0955 0956 0965 1700
NAMD	E8CF	1652	1725
NEWCDE	D15E	0459	0418 0427 0431 0438 0440 0442 0444 0446 0448 0450 0452 0454 0456
NEWCD1	D178	0474	0479
NXTADD	E2C0	1644	1737
OBHXAS	DA56	1796	0256
OLDACT	0026	0095	0334 0461 1421

SYMBOL	VALU	DEFN	REFERENCES
OLDTAB	0600	0018	1264 1275
OLDTBB	0500	0019	1267 1295
OUTCK	E538	1646	1768 1770 1772
OUTCKS	E531	1645	1776
OUTCK1	E53B	1647	1786 1788
OUTDD1	EF7B	0035	0591 0675
OUTFLG	A413	1635	1712
OUTPUT	E97A	0038	0475 0642 0698 0736 0792 0795 1439 1463 1487 1609
PACK	EA84	0037	0793 0796
PACK2	D3C4	0791	1500 1622 0719 0724 0759
PACK2B	D3C7	0792	0717 0754 0781
PDASC2	D26A	0601	0552 0555 0558
PHXY	EB9E	0042	0659
PLXY	EBAC	0041	0663
PNDM	D2E8	0688	0711 0732 0748 0770 1429 1453 1479 1585 1599 1678 1687 0249 0270 0627
PNDM1	D2F3	0693	0700
PNDM2	D2F9	0696	0694
PNDM3	D303	0701	0697
PRITR	E6E1	0043	0653
RDCLCK	D8E8	1568	0968 1114
RDCLC2	D8F0	1572	1576
RDCLIN	D8AE	1529	1564 0253 0300
RDCLI2	D8B3	1533	1545
READ	E93C	0036	0714 0735 0751 0777 0791 0794 1436 1460 1484 1590 1606
RENHM1	D4B4	0942	0929
RGET	DC97	1229	0904 0938 0969
RDLACT	D7CF	1420	1507 1627 1706 0648 0654 0765 0785
SAMCTR	0030	0105	0320 0974 0981 1224
SAMPLE	D4E8	0973	0964
SAMPL0	D4F4	0980	0975
SAMPL2	D507	0989	0987
SAMPNO	002F	0104	0348 1238 1239 1307
SAMRTE	0013	0078	0319 0973 1626
SCAN	D0FE	0402	0429 0457
SCAN2	D113	0415	0407
SECOND	000E	0070	0556
SEM1	E9BA	1653	1765
SETBT	D0E9	0379	
SETBT2	D0ED	0381	0387
SETCTR	D0AC	0339	
SETGAP	D07A	0304	
SETSNP	D5B4	1092	1081
SETSTL	D0C2	0353	
SETVIA	D04C	0279	
SNAPCK	D462	0895	
SNAP2	D468	0898	0901
SNPFLG	002E	0103	0895 0903 1096
START5	D000	0238	
START6	D003	0242	
STEP0	D50E	0995	0990
STEP0B	D535	1015	
STEP1	D538	1019	0985
STEP1B	D585	1063	
STEP1C	D588	1067	1061
STEP2	D59A	1077	0988
STEP2B	D5C1	1099	1078 1085 1090
STEP3	D5E5	1120	0991
STEP3B	D664	1195	1187
STEP3C	D66A	1199	1184
STPEND	D691	1222	1073 1207
STPEN2	D688	1218	1210
STPFLG	002D	0102	0347 0982 1223
STPND0	D676	1206	
STPND1	D693	1223	1015 1116
STPND2	D695	1224	0976
SVCEN	00EE	0058	
SYNON1	D128	0428	0425
S1	A41A	1638	1719 1723 1746 1749 1769 1771
S2	0106	1634	1733 1734
TAPBUF	0700	0020	0643 0899
TAPINT	096A	1661	0540
TAP3Z	E8C5	1651	1728

```
SYMBOL   VALU  DEFN  REFERENCES

TEMP     0019  0084  1477 1498 1503 1513 1515 1518 1521 1522 1597 1620 1625
TEMPHX   001A  0085  1412 1415
TICSET   D3E1  0810  1506 0250 0392
TICST1   D3EF  0816  0820
TICST2   D407  0829  0833
TICST3   041F  0842  0846
TIMGD    08FF  1584  0516 0764
TIMGD2   D921  1594  1592
TIMDUT   050F  1114  1097
TIMSET   D30A  0710  0723 0727 0729 0255 0327 0511
TMPUPD   0022  0091  0601 0607 0617 0620
TMSET2   033E  0731  0740 0742 0716
TMSET3   D367  0747  0758 0763 0738
TMSET4   0392  0764  0753
TOGPRT   D28E  0653  0524
TPEND    0010  0087  1667 1669 1716 1720
TPSTRT   0018  0086  1663 1665 1718 1722
TVCLEA   D892  1512  0252 0391 1505
TVCL1    D898  1517  1520 1524
TVDISP   D69D  1238  1013
TVDSP2   D6C1  1259  1255
TVEXIT   D718  1308  1241
TVSET    D709  1428  1445 0251 0326 0520
TVSET8   D80F  1452  1469 1438
TVSETX   D888  1505  1486
TVSET1   D808  1447  1441 1443
TVSET2   D83E  1471  1465 1467
TVSET3   D845  1476  1493 1462
TVSET4   D879  1497  1491
TVSET5   D878  1458  1496
TVSET6   D870  1500  1489
TVTBLH   DC35  2206  0813 0825 0838 0853 1262
TVTBLL   D86D  2003  0811 0823 0836 0851 1260
TVTICS   DAC0  1920  0816 0829 0842
TWREOF   0017  0082  0344 0537 0538 0927 0936
TWWAIT   0205  0538  0539
UACR     A008  0047  0284
UIER     A00E  0048  0373 0949 0960
UIFR     A000  0051  0374 0375 0409 0410 0498 0499 0914 0916 0917
UPCH     0021  0090  0691 0695 0701
UPCL     0020  0089  0689 0693 0696 0703
UTMDSP   001F  0088  0544 0580 0926
UTICH    A005  0050  0282 0545
UTILL    A004  0049  0280 0943 0947
VECTBL   D006  0246
VIAACR   AF08  0028  0292
VIADRA   AF03  0027  0290
VIADRB   AF02  0026  1531 1543
VIAIER   AF0E  0031  0299 0934 1705
VIAIFR   AF00  0030  0411 0412 0500 0501 0920 0921
VIADRA   AF01  0025  0295 0367 0923 1552 1556 1562 1572 1702
VIADRB   AF00  0024  0297 0368 0924 1553 1557 1563 1573 1703
VIAPCR   AF0C  0029  1533
WARMST   D0A3  0331  0242
WRCLIN   D8BA  1541  1549 0288
WRTAPE   09C3  1711  1683
YEAR     0011  0076  0718

 1 STATEMENTS FLAGGED IN THIS ASSEMBLY
```

APPENDIX B
LISTING OF THE 6502 PROGRAM OCCTRANS

This appendix contains an assembly language source code listing for the 6502 machine language program called OCCTRANS. This program is discussed in Chapter 4. This program was assembled with the ASM6502 cross-assembler mentioned in the introduction to Appendix A.

```
                     ;*************************************************************
                     ;
                     NAM  SPICA-IV/CODOS FILE TRANSFER & TERMINAL PROGRAM: DCCTPANS
                     ;
                     ; PROGRAMMING STARTED: FEBRUARY 10, 1984
                     ; LAST REVISION: FEBRUARY 12, 1984
                     ; REVISION NUMBER: A01
                     ;
                     ; GLENN SCHNEIDER    1-904-392-2058
                     ; SPACE SCIENCES RESEARCH BUILDING - 211
                     ; DEPARTMENT OF ASTRONOMY
                     ; UNIVERSITY OF FLORIDA
                     ; GAINESVILLE, FLORIDA 32611  U.S.A.
                     ;
                     ;*************************************************************
                     ;
                     ; THIS PROGRAM IS USED TO DOWNLOAD A CODOS DISK FILE ON A SPICA-IV
                     ; SYSTEM WITH AN ACIA TO ANOTHER COMPUTER.  THE COMMUNICATION
                     ; PROTOCOL IN PLACE IS FOR THE HARRIS-500 COMPUTER AT CIMAR.
                     ; THE ONLY VALID USER COMMANDS ARE:
                     ;  CTRL-F  TO ENTER THE FILE NAME TO BE TRANSMITTED
                     ;  CTRL-T  TO BEGIN DATA TRANSMISSION
                     ; THE PROGRAM WILL PRODUCE THE FOLLOWING OUTPUT ON THE 20
                     ; CHARACTER ALPHANUMERIC DISPLAY:
                     ;  FN?    PROMPT FOR ENTRY OF A FILE NAME
                     ;  EOF    INDICATES END-OF-FILE ENCOUNTED, TRANSMISSION COMPLETE
                     ;  *NF*   FILE SPECIFIED NOT FOUND ON DISK
                     ; RECORDS OF 36 BYTES, FORMATTED AS 72 ASCII CHARACTERS ARE
                     ; TRANSMITTED, AND TERMINATED WITH A CR ($0D).  THE NEXT RECORD
                     ; IS TRANSMITTED AFTER THE RECEIPT OF AN LF ($0A).  THE LAST
                     ; RECORD MAY BE SHORT.  THE FIRST 10 BYTES (20 ASCII CHARACTERS)
                     ; TRANSMITTED ARE THE CODOS INTERNAL FILE HEADER AND ARE NOT
                     ; PART OF THE OBSERVING DATA.  THE ONLY HANDSHAKING IS BY THE
                     ; SENDING OF A CR, AND AWAITING A LF.  WAITING IS DONE IN A
                     ; SOFT LOOP, INTERRUPTS ARE NOT USED.  DTR, CTS, RTS, AND DSP
                     ; RS-232 SIGNALS ARE IGNORED.
                     ;
                     ;*************************************************************
                     ;
                     ; <<< PAGE ZERO LOCATIONS >>>
                     ;
0000           0000          ORG $00
0000  00             HIBYTE  FCB $00        ; LEFT HALF WORD OF ASCII BYTE
0001  00             LOBYTE  FCB $00        ; RIGHT HALF WORD OF ASCII BYTE
                     ;
0086           0002          ORG $86
0086  0002           PREGU3  FDB $0200      ; CODOS P-REGISTER U3 (FILE NAME SPECIFICATION)
                     ;
00EE           0088          ORG $EE
00EE  80             SVCENB  FCB $80        ; CODOS SERVICE CALL PROCESSOR ENABLE BYTE
                     ;
                     ; <<< I/O ADDRESSING>>>
                     ;
               AA00  ACIA0   EQU $AA00      ; ACIA COMMAND, CONTROL AND STATUS
               AA01  ACIA1   EQU $AA01      ; ACIA DATA
                     ;
                     ; <<<AIM-65 MONITOR ROUTINES>>>
                     ;
               E704  QM      EQU $E704      ; PRINT AND DISPLAY A QUESTION MARK
               E907  RCHEK   EQU $E907      ; SCAN KEYBOARD, IF KEYDOWN PUT ASCII IN A-REG ELSE $FF
               E97A  OUTPUT  EQU $E97A      ; OUTPUT ONE CHARACTER TO PRINTER/DISPALY
               EA13  CRLOW   EQU $EA13      ; OUTPUT A CR/LF TO PRINTER DISPLAY
               EA46  NUMA    EQU $EA46      ; CONVERTS 2 HEX #'S IN <A> TO ASCII AND OUTPUT
               EA51  NOUT    EQU $EA51      ; CONVERTS 1 HEX # IN <A> TO ASCII AND OUTPUT
               FE96  REDI    EQU $FE96      ; INPUT 1 CHAR FROM KEYBOARD, PUT ASCII IN A-REG
                     ;
0300           00EF          ORG $0300      ; RAM SPACE $0300
                     ;
                     ; **** COLD START PROGRAM INITIALIZATION ****
                     ;
0300  78             CSTART  SEI            ; DISABLE INTERRUPTS ON THE MICROPROCESSOR BUS
0301  D8                     CLD            ; CLEAR DECIMAL MODE
```

```
LOC   OP OPND   VALU  STMT  SOURCE STMT

0302  A9 00     0000  0073         LDA #00       ; FILE NAME TO BE STORED AT $0200
0304  85 B6     00B6  0074         STA PREGU3
0306  A9 02     0002  0075         LDA #$02
0308  85 B7     00B7  0076         STA PREGU3+1
                      0077         ;
                      0078         ; .SET UP ACIA FOR BAUD RATE, STOP BITS, PARITY.
                      0079         ;
030A  A9 03     0003  0080  ACIAIN LDA #$03
030C  8D 00AA   AA00  0081         STA ACIAO
030F  A9 11     0011  0082         LDA #$11
0311  8D 00AA   AA00  0083         STA ACIAO
0314  A9 80     0080  0084         LDA #$80
0316  8D 00AA   AA00  0085         STA ACIAO
                      0086         ;
0319  A9 80     0080  0087  SVCIN  LDA #$80      ; ENABLE THE CODOS SERVICE CALL PROCESSOR
031B  85 FE     00FE  0088         STA SVCENB
                      0089         ;
                      0090         ; .CHECK KEYBOARD COMMAND.
                      0091         ;
031D  20 96FE   FE96  0092  CMDCHK JSR RED1      ; READ A CHARACTER FROM THE KEYBOARD
0320  C9 14     0014  0093  CMDCK2 CMP #$14      ; IS IT A CTRL-T (TRANSMIT DATA FILE)?
0322  F0 F9     031D  0094         BEQ CMDCHK    ; IF SO WAIT UNTIL FILE TRANSMISSION COMPLETED
                      0095         ;
0324  C9 06     0006  0096         CMP #$06      ; IS IT A CTRL-F (SPECIFY FILE NAME)
0326  F0 1F     0347  0097         BEQ FNAME     ; IF SO GET FILE NAME
0328  C9 0D     0000  0098         CMP #$0D      ; IS IT A CARRIAGE RETURN?
032A  D0 F1     031D  0099         BNE CMDCHK    ; IF NOT THEN CHECK KEY CLOSURE AGAIN
                      0100         ;
032C  20 13EA   EA13  0101         JSR CRLOW     ; DO A CR/LF
                      0102         ;
032F  20 0D03   030D  0103  READLP JSR RDACIA    ; GET A CHARACTER FROM THE ACIA
0332  C9 0A     000A  0104         CMP #$0A      ; IS IT A LINE FEED (RECORD TERMINATOR)?
0334  D0 F9     032F  0105         BNE READLP    ; IF NOT GET NEXT ACIA CHARACTER
                      0106         ;
0336  A9 5E     005E  0107         LDA #$5E      ; ASCII ^ CHARATER
0338  20 7AE9   E97A  0108         JSR OUTPUT    ; OUTPUT TO DISPLAY (LINE END INDICATION)
033B  20 96FE   FE96  0109         JSR RED1      ; READ A CHARACTER FROM KEYBOARD
033E  20 13EA   EA13  0110         JSR CRLOW     ; DO A CR/LF
0341  20 7AE9   E97A  0111         JSR OUTPUT    ; OUTPUT CHARACTER READ
0344  4C 2003   0320  0112         JMP CMDCK2    ; CHECK FOR USER ENTRY
                      0113         ;
0347  A9 46     0046  0114  FNAME  LDA #$46      ; PRINT PROMPT 'FN?'
0349  20 7AE9   E97A  0115         JSR OUTPUT
034C  A9 4E     004E  0116         LDA #$4E
034E  20 7AE9   E97A  0117         JSR OUTPUT
0351  20 D4E7   E7D4  0118         JSR OM
                      0119         ;
0354  A2 00     0000  0120         LDX #00       ; FILE NAME BUFFER POINTER
0356  20 96FE   FE96  0121  GETNAM JSR RED1      ; GET NEXT CHARACTER OF FILE NAME
0359  9D 0002   0200  0122         STA $0200,X   ; STORE IN BUFFER
035C  E8              0123         INX           ; POINT TO NEXT CHARACTER POSITION
035D  C9 0D     000D  0124         CMP #$0D      ; WAS A CR ENTERED?
035F  D0 F5     0356  0125         BNE GETNAM    ; IF NOT GET NEXT CHARACTER IN NAME
0361  20 13EA   EA13  0126         JSR CRLOW     ; DO A CRLF
                      0127         ;
0364  A2 05     0005  0128         LDX #$05      ; SEED CHANNEL NUMBER FOR CODOS
0366  00              0129         BRK           ; NOT A BREAK  ISSUANCE OF SVC #$15
0367  15              0130         FCB #$15      ; ASSIGN CHANNEL #5 TO NAMED FILE
0368  10 2E     0398  0131         BPL NOFILE    ; HANDLE ERROR IF FILE NOT FOUND
                      0132         ;
036A  A0 00     0000  0133  CCOUNT LDY #$00      ; CHARACTER COUNTER
036C  00              0134  GETBYT BRK           ; NOT A BREAK  ISSUANCE OF SVC #$03
036D  03              0135         FCB #$03      ; INPUT BYTE FROM ASSIGNED CHANNEL
036E  B0 42     03B2  0136         BCS EOF       ; HANDLE END-OF-FILE CONDITION
                      0137         ;
0370  20 0404   0404  0138         JSR HXASC     ; CONVERT HEX TO ASCII
0373  A5 00     0000  0139         LDA HIBYTE    ; GET ASCII REPRESENTATION OF HI PART OF BYTE
0375  20 CB03   03CB  0140         JSR XMIT      ; TRANSMIT IT TO THE HARRIS COMPUTER
0378  A5 01     0001  0141         LDA LOBYTE    ; GET ASCII REPRESENTATION OF LO PART OF BYTE
037A  20 CB03   03CB  0142         JSR XMIT      ; TRANSMIT IT TO THE HARRIS
                      0143         ;
037D  C8              0144         INY           ; INCREMENT CHARACTER COUNT BY 2
```

```
LOC   OP OPND  VALU  SOURCE STMT

037E  C8                    INY
037F  C0 48    0048         CPY #$48      ; HAVE 72 (DECIMAL) CHARACTERS BEEN SENT?
0381  D0 E9    036C         BNE GETBYT    ; GET AND SEND NEXT BYTE
0383  A9 00    0000         LDA #$00      ; SEND A CR TO THE HARRIS (END OF LINE)
0385  20 CB03  03CB         JSR XMIT
                            ;
0388  20 D003  03D0  WAITHS JSR RDACIA    ; HANDSHAKE ON RECEIPT OF CR BY HARRIS
038B  C9 0A    000A         CMP #$0A      ; DID SPICA GET A LF BACK FROM HARRIS?
038D  D0 F9    0388         BNE WAITHS    ; IF NOT WAIT FOR HANDSHAKE
038F  20 13EA  EA13         JSR CRLOW     ; DO A CR/LF
0392  20 F103  03F1         JSR DELAY     ; WAIT > 3 MILLISECONDS
0395  4C 6A03  036A         JMP CCOUNT    ; START NEXT DATA RECORD
                            ;
                            ; .CODOS FILE ERROR CONDITION - FILE NOT FOUND.
                            ;
0398  A9 2A    002A  NOFILE LDA #$2A      ; PRINT '*NF*'
039A  20 7AE9  E97A         JSR OUTPUT
039D  A9 4E    004E         LDA #$4E
039F  20 7AE9  E97A         JSR OUTPUT
03A2  A9 46    0046         LDA #$46
03A4  20 7AE9  E97A         JSR OUTPUT
03A7  A9 2A    002A         LDA #$2A
03A9  20 7AE9  E97A         JSR OUTPUT
03AC  20 13EA  EA13         JSR CRLOW     ; DO A CR/LF
03AF  4C 1003  0310         JMP CMDCHK    ; CHECK FOR USER COMMAND
                            ;
                            ; .END-OF-FILE ENCOUNTERED.
                            ;
03B2  A9 45    0045  EOF    LDA #$45      ; PRINT 'EOF'
03B4  20 7AE9  E97A         JSR OUTPUT
03B7  A9 4F    004F         LDA #$4F
03B9  20 7AE9  E97A         JSR OUTPUT
03BC  A9 46    0046         LDA #$46
03BE  20 7AE9  E97A         JSR OUTPUT
03C1  A2 05    0005         LDX #05       ; CODOS CHANNEL NUMBER
03C3  00                    BRK           ; NOT A BREAK  CODOS SERVICE CALL
03C4  16                    FCB #$16      ; FREE THE ASSIGNED CHANNEL
                            ;
03C5  20 13EA  EA13         JSR CRLOW     ; DO A CR/LF
03C8  4C 1003  0310         JMP CMDCHK    ; CHECK FOR USER COMMAND
                            ;
                            ; * TRANSMIT AN ASCII BYTE IN THE A-REGISTER *
                            ;
03CB  48             XMIT   PHA           ; SAVE THE A-REGISTER ON THE STACK
03CC  AD 00AA  AA00  XMITW  LDA ACIA0     ; GET THE ACIA STATUS REGISTER
03CF  29 02    0002         AND #$02      ; CHECK TO SEE IF TRANSMIT REGISTER IS EMPTY
03D1  C9 02    0002         CMP #$02
03D3  D0 F7    03CC         BNE XMITW     ; IF NOT WAIT UNTIL IT IS
03D5  20 F103  03F1         JSR DELAY     ; WAIT > 3 MILLISECONDS
                            ;
03D8  68                    PLA           ; GET THE HEX BYTE
03D9  8D 01AA  AA01         STA ACIA1     ; PUT IT IN THE ACIA TRANSMIT REGISTER
03DC  60                    RTS
                            ;
                            ; * READ AN ASCII BYTE FROM THE ACIA RECEIVE REGISTER *
                            ;
03D0  AD 00AA  AA00  RDACIA LDA ACIA0     ; GET ACIA STATUS REGISTER
03E0  29 01    0001         AND #$01      ; CHECK RECEIVE BIT
03E2  F0 F9    03D0         BEQ RDACIA    ; IF EMPTY WAIT UNTIL CHARACTER RECEIVED
                            ;
03E4  AD 01AA  AA01         LDA ACIA1     ; GET THE CHARACTER FROM ACIA DATA REGISTER
03E7  29 7F    007F         AND #$7F      ; CONVERT TO 7-BIT CODE
03E9  C9 0A    000A         CMP #$0A      ; SEE IF IT WAS A LF
03EB  F0 03    03F0         BEQ RDEXIT    ; IF IT WAS EXIT WITHOUT OUTPUT
03ED  20 7AE9  E97A         JSR OUTPUT    ; OUTPUT RECEIVED CHARACTER TO DISPLAY
03F0  60             RDEXIT RTS
                            ;
                            ; * WAIT IN A DELAY LOOP (5865 MICROSECONDS) *
                            ;
03F1  A2 FF    00FF  DELAY  LDX #$FF      ; DELAY LOOP COUNTER
03F3  6E FFFF  FFFF  DELAY2 ROR $FFFF     ; 6-MICROSECOND INSTRUCTION $FFFF IS ROM
03F6  6E FFFF  FFFF         ROR $FFFF
```

```
LOC   OP UPND  VALU  STMT  SOURCE STMT

03F9  6E FFFF  FFFF  0217         ROR $FFFF
03FC  CA             0218         DEX              ; DECREMENT LOOP COUNTER
03FD  E0 00    0000  0219         CPX #$00         ; ZERO CHECK WITH 2-MICROSEC INSTRUCTION
03FF  D0 F2    03F3  0220         BNE DELAY2
0401  A2 05    0005  0221         LDX #$05         ; RESTORE CODOS CHANNEL NUMBER
0403  60             0222         RTS
                     0223         ;
                     0224         ; * CONVERT HEX TO ASCII AND SAVE IN HIBYTE/LOBYTE *
                     0225         ;
0404  48             0226  HXASC  PHA              ; SAVE HEX BYTE ON STACK
0405  29 F0    00F0  0227         AND #$F0         ; GET LEFT HW
0407  4A             0228         LSR              ; SHIFT TO RIGHT HW
0408  4A             0229         LSR
0409  4A             0230         LSR
040A  4A             0231         LSR
040B  20 51EA  EA51  0232         JSR NOUT         ; CONVERT TO ASCII AND OUTPUT
040E  85 00    0000  0233         STA HIBYTE       ; SAVE AS HIBYTE
                     0234         ;
0410  68             0235         PLA              ; GET HEX BYTE FROM STACK
0411  29 0F    000F  0236         AND #$0F         ; GET RIGHT HW
0413  20 51EA  EA51  0237         JSR NOUT         ; CONVERT TO ASCII AND OUTPUT
0416  85 01    0001  0238         STA LOBYTE       ; SAVE AS LO BYTE
0418  60             0239         RTS


SYMBOL   VALU  DEFN  REFERENCES

ACIAIN   030A  0080
ACIAO    AA00  0054  0081 0083 0085 0189 0201
ACIAI    AA01  0055  0196 0205
CCOUNT   036A  0133  0156
CMDCHK   0310  0092  0094 0099 0169 0184
CMDCK2   0320  0093  0112
CHLOW    EA13  0062  0101 0110 0126 0154 0168 0183
CSTART   0300  0071
DELAY    03F1  0214  0155 0193
DELAY2   03F3  0215  0220
EOF      0382  0173  0136
FNAME    0347  0114  0097
GETBYT   036C  0134  0147
GETNAM   0356  0121  0125
HIBYTE   0000  0043  0139 0233
HXASC    0404  0226  0138
LOBYTE   0001  0044  0141 0238
NOFILE   0398  0160  0131
NOUT     EA51  0064  0232 0237
NUMA     EA46  0063
OUTPUT   E97A  0061  0108 0111 0115 0117 0161 0163 0165 0167 0174 0176 0178 0209
PREGU3   0006  0047  0074 0076
OM       E7D4  0059  0118
RCHEK    E907  0060
RDACIA   03DD  0201  0203 0103 0151
RDEXIT   03F0  0210  0208
READLP   032F  0103  0105
REDI     FE96  0065  0092 0109 0121
SVCENB   00EE  0050  0088
SVCIN    0319  0087
WAITHS   0388  0151  0153
XMIT     03CB  0188  0140 0142 0149
XMITW    03CC  0189  0192

NO STATEMENTS FLAGGED
```

APPENDIX C
LISTING OF THE APL WORKSPACE OCCPREP

```
   ∇ Y←BIT12 X
[1]  ⍝UNPACKS 12 BIT BIT-PACKED LODAS DATA
[2]  Y←2⊥⍉(⌽12,.6666666667×⍴X)⍴⍉(8⍴2)⊤X
    ∇

   ∇ IDENT
[1]  ' '
[2]  ' *** LUNAR OCCULTATION DATA PREPARATION WORKSPACE **
    *'
[3]  '      VERSION: A02/HARRIS'
[4]  '      REVISION DATE 18 JUNE 1984'
[5]  '      NOTE: ⎕IO←0'
[6]  ' '
[7]   ⍝ GLENN SCHNEIDER  DEPARTMENT OF ASTRONOMY
[8]   ⍝ UNIVERSITY OF FLORIDA  GAINESVILLE, FL 32611
    ∇

   ∇ READ;Y
[1]  ⍝READS IN A LODAS DATA FILE FROM A SPICA-IV/CODOS DIS
    K
[2]  ⍝THE SPICA-IV MUST RUN THE PROGRAM ¨HARRISTERM¨
[3]  ⍝THE DOWNLOADED FILE IS IN THE TEXT VARIABLE ¨DATA¨
[4]  DATA←⍳0
[5]  L1:' '
[6]  →(∨/(2 3⍴'∊⊤⌊END')∧.=3↑Y←⍞)/L2
[7]  →L1,⍴DATA←DATA,Y,(72-⍴Y)⍴'*'
[8]  L2:ERRS←'*'+.=DATA
    ∇

   ∇ TRANSLATE X;D;Q;M;A;C;F;Y;⎕IO
[1]  ⍝PREPARES A DOWNLOADED LODAS FILE FOR APL USE
[2]  ⎕IO←0
[3]  'TIMESTAMP: ',(TS X),'  DATA SET LENGTH: ',(⍕⍴X),' BY
    TES.'
[4]  D←256↑Y←16 16⊥⍉((.5×⍴X),2)⍴'0123456789ABCDEF'⍳20↓X
[5]  F←1+⌊(¯2048+D[2 7]+.×256 1)÷1.5
[6]  Q←1↓,⊖' ',9 2⍴(HEADER←512↑20↓X)[18+⍳18]
[7]  M←12 3⍴'JANFEBMARAPRMAYJUNJULAUGSEPOCTNOVDEC'
[8]  ⎕←DATE←Q[6 7],' ',M[¯1+⍎Q[3 4];],' 19',2↑Q
```

```
 [9]  ⎕←TIME←,Q[4 2ρ12 13 15 16 18 19 21 22],4 1ρ'::.',Q[24
     ]
[10]  A←'ABCDEFGHIJKLMNOPQRSTUVWXYZ0123456789.!/+- '
[11]  C←'⍺⊥∩⌊∊_∇∆⍳∘'''⎕|⊤○⋆?ρ⌈~↓∪⍵⊃↑⊂0123456789.¨/÷+'
[12]  ⎕←COMS←A[C⍳⎕AV[D[33+⍳39]]]
[13]  CH1←FΦBIT12 CH1←6144↑Y←256↓Y
[14]  CH2←FΦBIT12 CH2←6144↑Y←6144↓Y
[15]  CH3←FΦBIT12 CH3←6144↑6144↓Y
     ∇

    ∇ Y←TS D
 [1]  ⍝EXTRACTS THE TIME STAMP FROM A LODAS FILE HEADER
 [2]  Y←,(⊖8 2ρ¯16↑56↑⍕D),' '
     ∇
```

APPENDIX D
LISTING OF THE APL WORKSPACE: OCCRED

```
    ∇ B←W BBDY L
[1]   ⍝B=NORMALIZED RADIATED BLACKBODY POWER CONTRIBUTION
[2]   ⍝L[1]=ASSUMED EFFECTIVE COLOR TEMPERATURE OF THE STAR
[3]   ⍝L[2]=NUMBER OF TERMS USED IN THE NUMERICAL INTERGATI
      ON
[4]   ⍝ W=WAVELENGTH LIST
[5]   B←B÷+/B←+/.000037412÷(W*5)××¯1+1.43879÷L[1]×W←.000000
      01×W∘.+(0,ιL[2])-L[2]÷2
    ∇

    ∇ R←CM X;V
[1]   ⍝CORRELATION MATRIX FOR THE MATRIX <X>
[2]   V←(V∘.×V←1 1⍉R←(⍉R)+.×R←X-(ρX)ρ(+⌿X)÷1↑ρX)*.5
[3]   ⍝PATCH FOR DIVISION SCALING PROBLEM ON THE HARRIS
[4]   V[1;1]←R[1;1]
[5]   R←R÷V
    ∇

    ∇ DC P;DI;CVEC;ITER;N;I;X;V;D;R;Y;S
[1]   ⍝DIFFERENTIAL CORRECTIONS PROCEDURE FOR LUNAR OCCULTA
      TIONS
[2]   ⍝FIVE PARAMETER MODEL, FIXED LIMB DARKENING AND TEMPE
      RATURE
[3]   SOLS←1 14ρP,SSE←0ρDI←(5ρ0),1.02,(4ρ1.0003),1
[4]   CVEC←¯1⌽N←5+ι5+ITER←0
[5]   R←R÷+/R←(⍎FILT)[;2]×(⍎FILT)[;1]BBDY P[4],(1↑-⌿⊖2 2ρ⍎F
      ILT)÷5
[6]   S←+/2×P[11]LDARKEN GRID P[5]
[7]   L0:X←(2↑P[3])ρ0
[8]   +5↓SOL←P,0ρSSE←SSE,⎕←(Y←OBS-COMP←P[8]+(-/P[7 8])×R WI
      DE P)+.*2
[9]   DI[6]←1.02++/(P[6]<1 2 3×○÷180×3600000)/.2 .12 .06
[10]  L1:P[I]←DI[I]×1E¯12⌈P[I←1↑CVEC←1⌽CVEC]
[11]  D←-COMP-P[8]+(-/P[7 8])×R WIDE P
[12]  ⍝ →((5,(P[12]>ITER)/3)∧.≠1↓ρX←X,D÷-/(DI[I],1)×1E¯12⌈(
      P←SOL)[I])/L1
[13]  →(5≠1↓ρX←X,D÷-/(DI[I],1)×1E¯12⌈(P←SOL)[I])/L1
[14]  →(P[12]<ITER←ITER+1)/L2
[15]  P[N]←(LIMS[1;ι5]⌊P[N]+P[14]×Y⌹X)⌈LIMS[2;ι5]
```

```
[16]  →L0,,SOLS←SOLS,[1]P
[17]  L2:'SOLUTION HISTORY: '
[18]  ⍞SOLS←(0,⍳P[12]),((⍋SSE)⍳⍳1↑⍴SSE),SSE,SOLS
[19]  'STANDARD ERRORS: ',⍕ER←(1 1⍉COV←(((,Y-X+.×Y⌹X)+.*2)÷
     -/⍴X)×HINV(⍉X)+.×DI←X)*.5
[20]  PDER←X
     ∇

    ∇ P2 DC2 P;DI;CVEC;ITER;N;I;X;V;D;R;Y;AD;S
 [1]  ⍝DIFFERENTIAL CORRECTIONS PROCEDURE FOR LUNAR OCCULTA
     TIONS
 [2]  ⍝NINE PARAMETER MODEL, FIXED LIMB DARKENING AND TEMPE
     RATURE
 [3]  SOLS2←SOLS←1 14⍴P,SSE←0⍴DI←DI2←(5⍴0),1.02 1.0003,1.00
     1,(2⍴1.0003),1
 [4]  CVEC←¯1⌽N←5+⍳5+ITER←0
 [5]  R←R÷+/R←(⍎FILT)[;2]×(⍎FILT)[;1]BBDY P[4],(1↑-⌿⊖2 2⍴⍎F
     ILT)÷5
 [6]  R2←R2÷+/R2←(⍎FILT)[;2]×(⍎FILT)[;1]BBDY P2[4],(1↑-⌿⊖2
     2⍴⍎FILT)÷5
 [7]  S←+/2×P[11]⌊DARKEN GRID P[5]
 [8]  L0:X←X2←(2↑P[3])⍴0
 [9]  SSE←SSE,⎕←(Y←OBS-COMP←P[8]+(P2[7]×R2 WIDE P2)+P[7]×R
     WIDE P)+.*2
[10]  →5↓SOL2←P2,0⍴⎕←5↓SOL←P
[11]  DI[6]←1.02++/(P[6]<1 2 3×○÷180×3600000)/.2 .12 .06
[12]  DI2[6]←1.02++/(P2[6]<1 2 3×○÷180×3600000)/.2 .12 .06
[13]  L1:P[I]←DI[I]×1E¯12⌈P[I←1↑CVEC←1⌽CVEC]
[14]  D←-COMP-P[8]+(P2[7]×R WIDE P2)+P[7]×R WIDE P
[15]  →(5>1↓⍴X←X,D÷-/(DI[I],1)×1E¯12⌈(P←SOL)[I])/L1
[16]  ⍝⍝ P[N]←(LIMS[1;⍳5]⌊P[N]+P[14]×Y⌹X)⌈LIMS[2;⍳5]
[17]  CVEC←¯1⌽N
[18]  L1B:P2[I]←DI2[I]×1E¯12⌈P2[I←1↑CVEC←1⌽CVEC]
[19]  →(I=8)/L1B
[20]  D←-COMP-P[8]+(P2[7]×R WIDE P2)+P[7]×R WIDE P
[21]  →(9>1↓⍴X←X,D÷-/(DI2[I],1)×1E¯12⌈(P2←SOL2)[I])/L1B ⍝⍝
[22]  ⍝⍝ →(4>1↓⍴X2←X2,D÷-/(DI2[I],1)×1E¯12⌈(P2←SOL2)[I])/L1
     B
[23]  P[N]←(LIMS[1;⍳5]⌊P[N]+5↑AD←P[14]×Y⌹X)⌈LIMS[2;⍳5] ⍝⍝
[24]  P2[5+S]←(LIMS2[1;S]⌊P2[5+S]+¯4↑AD)⌈LIMS2[2;S←1 2 4 5]
     ⍝⍝
[25]  ⍝⍝ P2[5+S]←(LIMS2[1;S]⌊P2[5+S]+P[14]×Y⌹X2)⌈LIMS2[2;S←
     1 2 4 5]
[26]  →(P[12]<ITER←ITER+1)/L2
[27]  →L0,,SOLS←SOLS,[1]P,0⍴SOLS2←SOLS2,[1]P2
[28]  L2:'SOLUTION HISTORY: '
[29]  ⍞SOLS←(0,⍳P[12]),((⍋SSE)⍳⍳1↑⍴SSE),SSE,SOLS,SOLS2[;5+S
     ]
[30]  'STANDARD ERRORS: ',⍕ER←(1 1⍉COV←(((,Y-X+.×Y⌹X)+.*2)÷
     -/⍴X)×HINV2(⍉X)+.×DI←X←X,X2)*.5
[31]  PDER←X
     ∇

    ∇ Z←FFT X;T;I;G;N;Q;⎕IO
```

```
 [1]  ⍝FAST FOURIER TRANSFORM OF X; FROM RGS
 [2]  ⍝X VECTOR OF REALS OR X[;0]=REAL X[;1]=IMAGINARY
 [3]  ⎕IO←0
 [4]  →(2=ρρX)/L0
 [5]  X←X,[.5]0
 [6]  L0:T←2⊥⊖(Gρ2)⊤⍳I←2*G←⌈2⍟1↑ρX
 [7]  X←((N←I÷2),2 2)ρ((I,2)↑X÷I*.5)[T;]
 [8]  T←⍉2 1∘.○○(N↑T)÷2×N
 [9]  Z←(+/[1]X),[.5]-/[I←1]X
[10]  LA:Z←((N←N÷2),(2×I←I×2),2)ρZ
[11]  X←(0,I,0)↓Z
[12]  Z←(0,-I,0)↓Z
[13]  Z←(Z+Q),Z-Q←(+/Q×X),[1.5]-/(Q←(N,I,2)ρ(I,2)↑T)×⌽X
[14]  →(1<N)/LA
[15]  Z←((2×I,1)ρZ)[2⊥⊖(Gρ2)⊤⍳2*G;]
     ∇

    ∇ Z←FFTI X;T;I;G;N;Q;⎕IO
 [1]  ⍝FAST INVERSE FOURIER TRANSFORM OF X; FROM RGS
 [2]  ⍝X IS VECTOR OF REALS, OR X[;0]=REAL X[;1]=IMAGINARY
 [3]  ⎕IO←0
 [4]  →(2=ρρX)/L0
 [5]  X←X,[0.5] 0
 [6]  L0:T←2⊥⊖(Gρ2)⊤⍳I←2*G←⌈2⍟1↑ρX
 [7]  X←((N←I÷2),2 2)ρ((I,2)↑X÷I*.5)[T;]
 [8]  T←⍉2 1∘.○○(N↑T)÷¯2×N
 [9]  Z←(+/[1]X),[.5]-/[I←1]X
[10]  LA:Z←((N←N÷2),(2×I←I×2),2)ρZ
[11]  X←(0,I,0)↓Z
[12]  Z←(0,-I,0)↓Z
[13]  Z←(Z+Q),Z-Q←(+/Q×X),[1.5]-/(Q←(N,I,2)ρ(I,2)↑T)×⌽X
[14]  →(1<N)/LA
[15]  Z←((2×I,1)ρZ)[2⊥⊖(Gρ2)⊤⍳2*G;]
     ∇

    ∇ W←FNOS P;T
 [1]  W←((P[10]×P[9]-⍳P[3])∘.+(P[2]×1000×3○P[6]÷2)÷2×T÷¯.5-
     T-⍳2×T←P[5])×(÷.0000000001 500×.×2↑P)*.5
     ∇

    ∇ F←N FRESNEL W;⎕IO
 [1]  ⍝W IS VECTOR OF FRESNEL NUMBERS
 [2]  ⍝N IS NUMBER OF TERMS IN NUMERICAL INTEGRATION
 [3]  F←.5×+⌿(.5+(1 1∘.×W)×(2÷N)×+/1 2∘.○○.5×((W÷N)∘.×¯1+2×
     ⍳.5×N)*2)*2
     ∇

    ∇ F FTSMOOTH X;⎕IO;T
 [1]  ⍝FOURIER SMOOTHING OF OBSERVATIONAL DATA
 [2]  ⍝F IS THE CUTOFF FREQUENCY IN HERTZ
 [3]  ⍝X[0] IS THE BIN NUMBER OF OCCULTATION
 [4]  ⍝X[1] IS LENGTH OF SMOOTHED DATA SET
 [5]  ⍝CHI MUST BE RESIDENT IN THE WS
 [6]  ⎕IO←0
```

```
      OBS←FFT 1024↑(¯512+514⌈X[0]⌊3595)↓CH1)*2
      OBS←FFTI 1024 2↑(F,2)↑OBS
      OBS←X[1]↑(512-⌊.5×X[1])↓OBS
     ∇

     ∇ Y←GRID N;R;R2;X
      ⍝NORMALIZED RADIAL GRID AREA DISTRIBUTION (2D) SPHERI
      CAL STAR
      ⍝N=SQUARE ROOT OF NUMBER OF GRID POINTS PER QUADRANT
      X←(⍳R),[.5]¯1+⍳R←1↑⍴Y←(2⍴N)⍴0
      L1:R2←(X×((R*2)-X*2)*.5)+R×R×¯1○X÷R
      Y[;1+R]←N⍴-⌿R2-((X×((R*2)-X*2)*.5)+R×R×¯1○(X←(0 ¯1+⍴X
      )↑X)÷R←R-1),0
      →L1×⍳1≠1↓⍴R2
      Y←Y÷4×+/+/Y←(1-⍳N)⌽⌽Y×(⍳N)∘.≤⍳N
     ∇

     ∇ Y←HINV X;C
      ⍝PATCH FOR PROBLEM WITH MONADIC ⌹ IN HARRIS APL
      C←10*.5×10⍟X[1;1]
      X[;1]←X[;1]÷C
      X[1;]←X[1;]÷C
      Y←⌹X
      Y[1;]←Y[1;]÷C
      Y[;1]←Y[;1]÷C
     ∇

     ∇ Y←HINV2 X;C
      ⍝PATCH FOR PROBLEM WITH MONADIC ⌹ IN HARRIS APL
      C←10*.5×10⍟⌈/⌈/X
      X[;1 6]←X[;1 6]÷C
      X[1 6;]←X[1 6;]÷C
      Y←⌹X
      Y[1 6;]←Y[1 6;]÷C
      Y[;1 6]←Y[;1 6]÷C
     ∇

     ∇ IDENT
      ' '
      ' *** LUNAR OCCULTATION DATA REDUCTION WORKSPACE ***'
      '      VERSION C03/HARRIS BATCH'
      '      REVISION DATE: 29 APRIL 1985'
      '      NOTE: THIS WORKSPACE IS ⎕IO←1'
      ' '
       ⍝ GLENN SCHNEIDER  DEPARTMENT OF ASTRONOMY
       ⍝ UNIVERSITY OF FLORIDA  GAINESVILLE, FL 32611
     ∇

     ∇ INPUT2 X;PR;C
      ⍝X IS RAW OBSERVING DATA (I.E. CH1)
      ⍝CONVERSATIONAL ENTRY OF INITIAL DC2 PARAMETERS
      NAME←32↓⍞,0⍴⍞←'NAME OR CATALOG NUMBER OF STAR: '
      DATE←27↓⍞,0⍴⍞←'U. T. DATE OF OBSERVATION: '
      COMN←28↓⍞,0⍴⍞←'ANY COMMENTS TO BE PRINTED: '
```

```
[6]  PV←⎕,0ρ⍞←'ENTER THE MONOCHROMATIC WAVELENGTH, OR ENTE
    R 0 TO USE FILTER TABLE'
[7]  ⍎(PV≠0)/'FILT←''MONO''',0ρMONO←1 2ρPV,1
[8]  →(PV≠0)/I0
[9]  'ENTER THE NAME OF THE FILTER TABLE TO BE USED:'
[10] FILT←⍞
[11] I0:PV←PV,⎕,0ρ⍞←'ENTER THE DISTANCE TO THE LUNAR LIMB
    IN KILOMETERS'
[12] BIN←⎕,0ρ⍞←'ENTER STARTING BIN NUMBER OF DATA TO BE US
    ED'
[13] PV←PV,⎕,0ρ⍞←'ENTER NUMBER OF DATA POINTS TO BE USED'
[14] OBS←(¯1↑PV)↑(BIN-1)↓X
[15] PV←PV,⎕,0ρ⍞←'ENTER THE EFFECTIVE COLOR TEMPERATURE OF
     THE STAR'
[16] PV←PV,⎕,0ρ⍞←'ENTER THE SQUARE ROOT OF THE NUMBER OF G
    RID PTS./QUADRANT'
[17] PV←PV,⎕÷C←206264806.2,0ρ⍞←'ENTER ESTIMATED DIAMETER I
    N ARC-MILLISECONDS'
[18] LIMS←⎕÷C,0ρ⍞←PR←'  ENTER UPPER AND LOWER LIMIT'
[19] PV←PV,⎕,0ρ⍞←'ENTER INTENSITY (COUNTS) FOR FIRST STAR'
[20] LIMS←LIMS,⎕,0ρ⍞←PR
[21] PV←PV,⎕,0ρ⍞←'ENTER BACKGROUND SKY-LIGHT CONTRIBUTION'
[22] LIMS←LIMS,⎕,0ρ⍞←PR
[23] PV←PV,⎕-BIN,0ρ⍞←'ENTER ESTIMATED BIN NUMBER OF GEOMET
    RICAL OCCULTATION FOR STAR 1'
[24] LIMS←LIMS,,(¯1↑PV)∘.+1 ¯1×⎕,0ρ⍞←' PLUS OR MINUS HOW M
    ANY MILLISECONDS?'
[25] PV←PV,(PV[2]×¯3○⎕÷206265),0ρ⍞←'ENTER SHADOW VELOCITY
    IN A-SEC/SEC'
[26] LIMS←LIMS,(PV[2]×¯3○⎕÷206265),0ρ⍞←PR
[27] PV←PV,⎕,0ρ⍞←'ENTER ASSUMED LIMB DARKENING CO-EFFICIEN
    T'
[28] LIMS←⍉6 2ρLIMS,⎕,0ρ⍞←PR
[29] PV←1E¯12⌈PV,⎕,0ρ⍞←'ENTER MAXIMUM NUMBER OF ITERATIONS
     FOR DC PROCEEDURE'
[30] PV←PV,|1↑-/2 2↑⍎FILT
[31] PV←PV,⎕,0ρ⍞←'ENTER FRACTIONAL ADJUSTMENT TO BE USED (
    0 TO 1)'
[32] PV2←PV,0ρLIMS2←LIMS
[33] PV2[4]←⎕,0ρ⍞←'ENTER TEMPERATURE OF THE SECOND STAR'
[34] PV2[6]←⎕÷C,0ρ⍞←'ENTER DIAMETER ESTIMATE FOR SECOND ST
    AR'
[35] LIMS2[;1]←⎕÷C,0ρ⍞←PR
[36] PV2[7]←⎕,0ρ⍞←'ENTER INTENSITY (COUNTS) FOR SECOND STA
    R'
[37] LIMS2[;2]←⎕,0ρ⍞←PR
[38] PV2[9]←⎕-BIN,0ρ⍞←'ENTER TIME OF GEOMETRICAL OCCULTATI
    ON (BIN) FOR STAR 2'
[39] LIMS2[;4]←(¯1↑PV2)∘.+1 ¯1×⎕,0ρ⍞←'PLUS OR MINUS HOW MA
    NY MILLISECONDS?'
    ∇

   ∇ INPUT X;PR;C
[1]   ⍝X IS RAW OBSERVING DATA (I.E. CH1)
```

```
[2]   ⍝CONVERSATIONAL ENTRY OF INITIAL DC PARAMETERS
[3]  NAME←32↑⍞,0⍴⍞←'NAME OR CATALOG NUMBER OF STAR: '
[4]  DATE←27↑⍞,0⍴⍞←'U. T. DATE OF OBSERVATION: '
[5]  COMN←28↑⍞,0⍴⍞←'ANY COMMENTS TO BE PRINTED: '
[6]  PV←⎕,0⍴⎕←'ENTER THE MONOCHROMATIC WAVELENGTH, OR ENTE
     R 0 TO USE FILTER TABLE'
[7]  ⍎(PV≠0)/'FILT←''MONO''',0⍴MONO←1 2⍴PV,1
[8]  →(PV≠0)/I0
[9]  'ENTER THE NAME OF THE FILTER TABLE TO BE USED:'
[10] FILT←⍞
[11] I0:PV←PV,⎕,0⍴⎕←'ENTER THE DISTANCE TO THE LUNAR LIMB
     IN KILOMETERS'
[12] BIN←⎕,0⍴⎕←'ENTER STARTING BIN NUMBER OF DATA TO BE US
     ED'
[13] PV←PV,⎕,0⍴⎕←'ENTER NUMBER OF DATA POINTS TO BE USED'
[14] OBS←(¯1↑PV)↑(BIN-1)↓X
[15] PV←PV,⎕,0⍴⎕←'ENTER THE EFFECTIVE COLOR TEMPERATURE OF
     THE STAR'
[16] PV←PV,⎕,0⍴⎕←'ENTER THE SQUARE ROOT OF THE NUMBER OF G
     RID PTS./QUADRANT'
[17] PV←PV,⎕÷C←206264806.2,0⍴⎕←'ENTER ESTIMATED DIAMETER I
     N ARC-MILLISECONDS'
[18] LIMS←⎕÷C,0⍴⎕←PR←'  ENTER UPPER AND LOWER LIMIT'
[19] PV←PV,⎕,0⍴⎕←'ENTER PRE-EVENT LEVEL OF STAR+SKY SIGNAL
     '
[20] LIMS←LIMS,⎕,0⍴⎕←PR
[21] PV←PV,⎕,0⍴⎕←'ENTER POST-EVENT LEVEL OF LIMB+SKY SIGNA
     L'
[22] LIMS←LIMS,⎕,0⍴⎕←PR
[23] PV←PV,⎕-BIN,0⍴⎕←'ENTER ESTIMATED BIN NUMBER OF GEOMET
     RICAL OCCULTATION'
[24] LIMS←LIMS,,(¯1↑PV)∘.+1 ¯1×⎕,0⍴⎕←' PLUS OR MINUS HOW M
     ANY MILLISECONDS?'
[25] PV←PV,(PV[2]×¯3○⎕÷206265),0⍴⎕←'ENTER SHADOW VELOCITY
     IN A-SEC/SEC'
[26] LIMS←LIMS,(PV[2]×¯3○⎕÷206265),0⍴⎕←PR
[27] PV←PV,⎕,0⍴⎕←'ENTER ASSUMED LIMB DARKENING CO-EFFICIEN
     T'
[28] LIMS←⍉6 2⍴LIMS,⎕,0⍴⎕←PR
[29] PV←1E¯12⌈PV,⎕,0⍴⎕←'ENTER MAXIMUM NUMBER OF ITERATIONS
     FOR DC PROCEEDURE'
[30] PV←PV,|1↑-/2 2↑⍎FILT
[31] PV←PV,⎕,0⍴⎕←'ENTER FRACTIONAL ADJUSTMENT TO BE USED (
     0 TO 1)'
     ∇

   ∇ Y←X LDARKEN G;T
[1]   ⍝Y=NORMALIZED GRID DISTRIBUTION OF LIMB DARKENED STA
     R
[2]   ⍝G=STELLAR GRID QUADRANT TO BE LIMB DARKENED (GENERA
     TED BY: GRID)
[3]   ⍝X=LIMB DARKENING COEFFICIENT
[4]   ⍝RESULT OBTAINED FROM A LINEAR LIMB DARKENING LAW
[5]  Y←Y÷4×+/+/Y←G×(T∘.≤T)×(1-T)⌽⌽(⍴G)⍴(1-X)+X×2○¯1○(T-.5)
```

```
      ÷ρT←ι1↑ρG
      ∇

    ∇ Y←NPOL V;T;I;⎕CT
[1]    ⍝INTERPOLATION OF FRESNEL INTENSITY VALUE FOR FRESNE
      L NUMBER <V>
[2]   Y←FREN[I]+(-⌿FREN[¯1 0∘.+I←(1+.5×ρFREN)-100×T])×100×V
      -T←.01×⌊.5+V×100
      ∇

    ∇ OUTPUT2;S;T;PM;CT;W;Q
[1]   ⍝FORMATTED OUTPUT FOR DC2 SOLUTION
[2]   (20ρ' '),'OCCULTATION OF: ',NAME
[3]   (20ρ' '),DATE,' U. T.'
[4]   (20ρ' '),COMN
[5]   ' '
[6]   '  INPUT PARAMETERS:'
[7]   ' '
[8]   'CENTRAL WAVELENGTH OF PASSBAND:',(0⍕+/×/⍉FILT),' ANG
      STROMS'
[9]   'LUNAR LIMB DISTANCE (KM):        ',6 0⍕SOL[2]
[10]  'EFFECTIVE TEMPERATURE STAR-1  : ',⍕SOL[4]
[11]  'EFFECTIVE TEMPERATURE STAR-2  : ',⍕SOL2[4]
[12]  'LIMB DARKENING COEFFICIENT STAR-1: ',⍕SOL[11]
[13]  'LIMB DARKENING COEFFICIENT STAR-2: ',⍕SOL2[11]
[14]  ' '
[15]  '  MODEL PARAMETERS:'
[16]  ' '
[17]  'NUMBER OF DATA POINTS: ',⍕SOL[3]
[18]  'NUMBER OF GRID POINTS: ',⍕(SOL[5]×2)*2
[19]  'NUMBER OF SPECTRAL REGIONS: ',⍕1↑ρ⍉FILT
[20]  'WIDTH OF SPECTRAL REGIONS:  ',(⍕-/⌽(⍉FILT)[1,2⌊1↑ρ⍉F
      ILT;1]),' ANGSTROMS'
[21]  'NUMBER OF ITERATIONS:  ',⍕SOL[12]
[22]  ' '
[23]  '  SOLUTIONS FOR STAR-1:'
[24]  ' '
[25]  PM←' +/-'
[26]  'STELLAR DIAMETER (ARC-MILLISECONDS): ',(6 2⍕SOL[6]×2
      06264806),PM,6 2⍕ER[1]×206264806
[27]  'BIN OF GEOMETRICAL OCCULTATION:         ',(7 1⍕SOL[9]+B
      IN),PM,4 1⍕ER[4]
[28]  'SIGNAL LEVEL OF STAR-1 (COUNTS)         ',(6 1⍕SOL[7]),
      PM,5 1⍕ER[2]
[29]  ST←×1-T←SOL[10]÷PV[10]
[30]  'OBSERVED LUNAR SHADOW VELOCITY:      ',(7 5⍕SOL[10]),
      PM,(7 5⍕ER[5]),' KM/SEC'
[31]  'PREDICTED LUNAR SHADOW VELOCITY:     ',(7 5⍕PV[10]),'
       KM/SEC'
[32]  T←'LOCAL SLOPE OF LUNAR LIMB:          ','- +'[ST+2],,
      (6 2⍕.5×+/S←(180÷○1)×¯2○T←T⌊÷T),' DEG'
[33]  T,PM,5 3⍕|.5×-/Q⌊|Q←(÷○÷180)×(SOL[10]∘.+1 ¯1×ER[5])÷P
      V[10]
[34]  2 1ρ' '
```

```
[35]  '  SOLUTIONS FOR STAR-2:'
[36]  ' '
[37]  'STELLAR DIAMETER (ARC-MILLISECONDS): ',(6 2⍕SOL2[6]×
      206264806),PM,6 2⍕ER[6]×206264806
[38]  'BIN OF GEOMETRICAL OCCULTATION:        ',(7 1⍕SOL2[9]+
      BIN),PM,4 1⍕ER[8]
[39]  'SIGNAL LEVEL OF STAR-2 (COUNTS)        ',(6 1⍕SOL2[7])
      ,PM,4 1⍕ER[7]
[40]  'POST-EVENT LIMB+SKY SIGNAL LEVEL:      ',(6 1⍕SOL[8]),
      PM,4 1⍕ER[3]
[41]  'OBSERVED LUNAR SHADOW VELOCITY:      ',(7 5⍕SOL2[10])
      ,PM,(7 5⍕ER[9]),' KM/SEC'
[42]  ST←×1-T←SOL2[10]÷PV[10]
[43]  T←'LOCAL SLOPE OF LUNAR LIMB:           ','- +'[ST+2],,
      (6 2⍕.5×+/S←(180÷○1)×¯2○T←T⌊÷T),' DEG'
[44]  T,PM,6 3⍕|.5×-/Q⌊|Q←(÷○÷180)×(SOL2[10]∘.+1 ¯1×ER[9])÷
      PV[10]
[45]  2 1⍴' '
[46]  '  OTHER PARAMETERS AND DERIVED SOLUTIONS:'
[47]  ' '
[48]  'POST-EVENT LIMB+SKY SIGNAL LEVEL:      ',(6 1⍕SOL[8]),
      PM,4 1⍕ER[3]
[49]  'TEMPORAL SEPARATION OF THE STARS:   ',(6 1⍕|SOL[9]-S
      OL2[9]),PM,(4 1⍕(ER[4 8]+.*2)*.5),' MS.'
[50]  'WEIGHTED MEAN L-RATE: ',(6 4⍕W←((SOL[10],SOL2[10])+.
      ÷ER[5 9])÷+/÷ER[5 9]),' KM/SEC'
[51]  'SPATIAL SEPARATION FROM R-RATES WHICH ARE:'
[52]  T←' PREDICTED (',(⍕Q),' ARC SEC/SEC):  ',6 2⍕(|SOL2[9
      ]-SOL[9])×Q←206265×3○÷/PV[10 2]
[53]  T,' MILLISECONDS OF ARC'
[54]  T←' WEIGHTED MEAN (',(6 4⍕Q),' ARC SEC/SEC):  ',6 2⍕(
      |SOL2[9]-SOL[9])×Q←206265×3○W÷PV[2]
[55]  T,' MILLISECONDS OF ARC'
[56]  'BRIGHTNESS RATIO (BRIGHTER/FAINTER): ',6 4⍕T←÷/(SOL[
      7],SOL2[7])[⍒SOL[7],SOL2[7]]
[57]  'MAGNITUDE DIFFERENCE:                    ',6 4⍕(100*.2)⍟T
[58]  2 1⍴' '
[59]  '  PHOTOMETRIC STATISTICS:'
[60]  ' '
[61]  'SUM OF SQUARES OF RESIDUALS: ',⍕S←(OBS-COMP)+.*2
[62]  'SIGMA (STANDARD ERROR):       ',⍕S←(S÷¯1+⍴OBS)*.5
[63]  'NORMALIZED STANDARD ERROR:    ',⍕S←S÷SOL[7]+SOL2[7]
[64]  'PHOTOMETRIC (SIGNAL+NOISE)/NOISE RATIO:  ',⍕(1+S)÷S
[65]  '(INTENSITY CHANGE)/BACKGROUND:     ',⍕S←(SOL[7]+SOL2[
      7])÷SOL[8]
[66]  'CHANGE IN MAGNITUDE:                   ',⍕-(÷100*÷5)⍟1+S
[67]  2 1⍴' '
[68]  '  SUPPLEMENTAL STATISTICS: '
[69]  ' '
[70]  'VARIANCE/CO-VARIANCE MATRIX:'
[71]  CT←9 11⍴1↓⎕←' DIAMETER1  INTENSITY1 SKY INTS   OCC TI
      ME1  L-RATE1    DIAMETER2  INTENSITY2 OCC TIME2  L-RAT
[72]  'M⍞-⍞E11.4' ⎕FMT COV
[73]  ' '
```

```
[74]  (13ρ' '),,CT
[75]  ((1⊥⍉∧\CT=' ')⌽CT),'M⍞-⍞F11.6' ⎕FMT CM COV
[76]  RESTAB
    ∇

    ∇ OUTPUT;S;T;PM;CT
 [1]  ⍝PRODUCES A FORMATTED REPORT ON THE STELLAR SOLUTION
 [2]  (20ρ' '),'OCCULTATION OF: ',NAME
 [3]  (20ρ' '),DATE,' U. T.'
 [4]  (20ρ' '),COMN
 [5]  ' '
 [6]  ' INPUT PARAMETERS:'
 [7]  ' '
 [8]  'CENTRAL WAVELENGTH OF PASSBAND:',(0⍕+/×/⍎FILT),' ANG
      STROMS'
 [9]  'LUNAR LIMB DISTANCE (KM):        ',6 0⍕SOL[2]
[10]  'EFFECTIVE TEMPERATURE (KELVIN): ',⍕SOL[4]
[11]  'LIMB DARKENING COEFFICIENT:      ',⍕SOL[11]
[12]  ' '
[13]  'MODEL PARAMETERS:'
[14]  ' '
[15]  'NUMBER OF DATA POINTS: ',⍕SOL[3]
[16]  'NUMBER OF GRID POINTS: ',⍕(SOL[5]×2)*2
[17]  'NUMBER OF SPECTRAL REGIONS: ',⍕1↑ρ⍎FILT
[18]  'WIDTH OF SPECTRAL REGIONS:  ',(⍕-/⌽(⍎FILT)[1,2⌊1↑ρ⍎F
      ILT;1]),' ANGSTROMS'
[19]  'NUMBER OF ITERATIONS:  ',⍕SOL[12]
[20]  ' '
[21]  ' SOLUTIONS:'
[22]  ' '
[23]  PM←' +/-'
[24]  'STELLAR DIAMETER (ARC-MILLISECONDS): ',(6 2⍕SOL[6]×2
      06264806),PM,6 2⍕ER[1]×206264806
[25]  'BIN OF GEOMETRICAL OCCULTATION:        ',(7 1⍕SOL[9]+B
      IN),PM,4 1⍕ER[4]
[26]  'PRE-EVENT STAR+SKY SIGNAL LEVEL:       ',(6 1⍕SOL[7]),
      PM,4 1⍕ER[2]
[27]  'POST-EVENT LIMB+SKY SIGNAL LEVEL:      ',(6 1⍕SOL[8]),
      PM,4 1⍕ER[3]
[28]  ST←×1-T←SOL[10]÷PV[10]
[29]  'OBSERVED LUNAR SHADOW VELOCITY:      ',(7 5⍕SOL[10]),
      PM,(7 5⍕ER[5]),' KM/SEC'
[30]  'PREDICTED LUNAR SHADOW VELOCITY:     ',(7 5⍕PV[10]),'
       KM/SEC'
[31]  T←'LOCAL SLOPE OF LUNAR LIMB:            ','- +'[ST+2],,
      (6 2⍕.5×+/S←(180÷○1)×¯2○T←T⌊÷T),' DEG'
[32]  T,PM,5 3⍕|.5×-/Q⌊|Q←(÷○÷180)×(SOL[10]∘.+1 ¯1×ER[5])÷P
      V[10]
[33]  2 1ρ' '
[34]  'VARIANCE-COVARIANCE MATRIX:'
[35]  'M⍞-⍞F12.5' ⎕FMT COV
[36]  2 1ρ' '
[37]  'CORRELATION MATRIX:'
[38]  ¯60↑,CT←5 10ρ' DIAMETER   *+LIMB  LIMB+SKY  TIME OC
```

```
    C  VELOCITY  '
[39]  ((1⊥⍉∧\CT=' ')⌽CT),'M⍞-⍞F10.5' ⎕FMT CM COV
[40]  2 1⍴' '
[41]  'SUM OF SQUARES OF RESIDUALS: ',⍕S←(OBS-COMP)+.*2
[42]  'SIGMA (STANDARD ERROR):        ',⍕S←(S÷¯1+⍴OBS)*.5
[43]  'NORMALIZED STANDARD ERROR:    ',⍕S←S÷-/SOL[7 8]
[44]  'PHOTOMETRIC (SIGNAL+NOISE)/NOISE RATIO:  ',⍕(1+S)÷S
[45]  '(INTENSITY CHANGE)/BACKGROUND:     ',⍕S←(-/SOL[7 8])÷
     SOL[8]
[46]  'CHANGE IN MAGNITUDE:                  ',⍕-(÷100*÷5)⍟1+S
[47]  RESTAB
    ∇

    ∇ RESTAB;Q;N
[1]   ⍝PRODUCES A TABLE OF OBS, COMP, AND RESIDUALS
[2]   4 1⍴' '
[3]   (29↑' '),'TABLE 5-XXX'
[4]   '  ',NAME,': OBSERVATIONS, COMPUTED VALUES, AND RESID
     UALS  FROM BIN ',⍕BIN
[5]   ' '
[6]   72⍴'='
[7]   'NUM OBS  COMP   RESID    NUM OBS  COMP   RESID    NU
     M OBS  COMP   RESID'
[8]   '--- ---- ------ ------   --- ---- ------ ------   --
     - ---- ------ ------'
[9]   Q←((3×N←⌈(⍴OBS)÷3),4)↑(¯1+⍳⍴OBS),OBS,COMP,[1.5]OBS-CO
     MP
[10]  Q←Q[⍳N;],((N,0)↑(-N,0)↓Q),(2×N,0)↓Q
[11]  '3(BI3,X1,BI4,X1,BF6.1,X1,M⍞-⍞BF6.1,X3)' ⎕FMT Q
[12]  72⍴'='
    ∇

    ∇ START
[1]   ⍝OVERALL CONTROL FUNCTION FOR DC EXECUTION
[2]   'REDUCTION RUN FOR THE STAR: ',NAME
[3]   DC PV
[4]   DC PV←(¯3↓3↓,SOLS[SOLH←SOLS[;2]⍳1;]),10,PV[13],.5
[5]   DC(¯3↓3↓,SOLS[SOLF←SOLS[;2]⍳1;]),0,PV[13],.5
[6]   OUTPUT
    ∇

    ∇ START2
[1]   ⍝OVERALL CONTROL FUNCTION FOR DC2 EXECUTION
[2]   'REDUCTION RUN FOR THE STAR ',NAME
[3]   PV2 DC2 PV
    ∇

    ∇ Y←R WIDE P;I;T
[1]   ⍝COMPUTATION OF WIDEBAND FRESNEL PATTERN
[2]   ⍝P IS THE CURRENT PARAMETER VECTOR (PV)
[3]   ⍝R=CONVOLVED SYSTEM RESPONCE AND SOURCE SPECTRAL ENER
     GY CURVES
[4]   I←1↑Y←P[3]⍴0
[5]   ⍝S←+/2×P[11]LDARKEN GRID P[5]
```

```
[6]  W0:Y←Y+R[I]×(NPOL FNOS P←(⍎FILT)[I←I+1;1],1↓P)+.×(⌽T)
     ,T←S
[7]  →(I≠1↑⍴⍎FILT)/W0
     ∇
```

NAME: VFILTER
SHAPE: 53 2

4450	0.0001294
4500	0.0002588
4550	0.0003881
4600	0.0005175
4650	0.0006469
4700	0.0007763
4750	0.0011644
4800	0.0016820
4850	0.0023289
4900	0.0047872
4950	0.0112563
5000	0.0208306
5050	0.0296287
5100	0.0380386
5150	0.0450252
5200	0.0513650
5250	0.0548583
5300	0.0555052
5350	0.0553759
5400	0.0545996
5450	0.0534351
5500	0.0507181
5550	0.0481304
5600	0.0452840
5650	0.0426963
5700	0.0398499
5750	0.0364860
5800	0.0337689
5850	0.0307931
5900	0.0282055
5950	0.0252297
6000	0.0225126
6050	0.0194074
6100	0.0166904
6150	0.0142321
6200	0.0122914
6250	0.0104800
6300	0.0087980
6350	0.0071161
6400	0.0054341
6450	0.0041403
6500	0.0029758
6550	0.0024583
6600	0.0020701
6650	0.0016820
6700	0.0014232
6750	0.0012938
6800	0.0010351
6850	0.0007763
6900	0.0006469
6950	0.0003881
7000	0.0002588
7050	0.0001294

NAME: BFILTER
SHAPE: 42 2

3600	0.0000953
3650	0.0004767
3700	0.0013347
3750	0.0023834
3800	0.0044809
3850	0.0115359
3900	0.0207837
3950	0.0397559
4000	0.0469063
4050	0.0489084
4100	0.0499571
4150	0.0505291
4200	0.0511965
4250	0.0513872
4300	0.0514825
4350	0.0510058
4400	0.0497664
4450	0.0473830
4500	0.0451902
4550	0.0427114
4600	0.0400419
4650	0.0376585
4700	0.0347984
4750	0.0331776
4800	0.0295548
4850	0.0271713
4900	0.0244065
4950	0.0219277
5000	0.0192583
5050	0.0164935
5100	0.0137287
5150	0.0111545
5200	0.0085804
5250	0.0058156
5300	0.0034322
5350	0.0020974
5400	0.0015254
5450	0.0008580
5500	0.0004767
5550	0.0002860
5600	0.0001907
5650	0.0000953

NAME: NARROWV
SHAPE: 5 2

5295	0.0621118
5345	0.2251553
5395	0.4487578
5445	0.2251553
5495	0.0388199

NAME: NARROWB
SHAPE: 5 2

4600	0.0658106
4650	0.2247191
4700	0.4558587
4750	0.2247191
4800	0.0288925

APPENDIX E

LISTING OF THE APL WORKSPACE OCCPLOTS

```
    ∇ Y←N BIN D;⎕IO;T
[1]   ⍝BIN DATA FOR INTO CLASSES FOR HISTOGRAM
[2]   ⍝D IS DATA VECTOR; N IS NUMBER OF CLASSES
[3]   ⎕IO←1
[4]   Y←(T+D[1]-.5×1↑T),[1.5]+/(¯1+⍳N)∘.=+⌿((1↑D)+T←+\Nρ((⌈
     /D)-⌊/D)÷N)∘.<D←D[⍋D]
     ∇

    ∇ D CENTER S;R
[1]   ⍝CENTER TEXT LABEL
[2]   R←S[0]+.5×S[1]-(ρD)×8÷53
[3]   ((1,ρD)ρD)LABELD 1 3ρR,¯2↑S
     ∇

    ∇ Y←N ESMOOTH D;⎕IO;T;V
[1]   ⍝N-POINT WEIGHTED SMOOTHING OF THE VECTOR D
[2]   ⍝(1↓N) IS NUMBER OF TERMS TO USE NUMERICALLY IN E SMO
     OTHING
[3]   ⍝(1↑N) IS THE 1/E FOLDING SPACING WRT THE DATA SPACIN
     G
[4]   ⎕IO←0
[5]   Y←((V←⌊.5+.5×1↑N)ρ1↑Y),Y←(T÷+/T←*-(÷1↑N)×⍳1↓N)+.×(⍳1↓
     N)⌽(1↓N,ρD)ρD
[6]   Y←(¯3×V)↓Y
[7]   Y←(ρD)ρY,(2×V)ρ(+/(-1↓N)↑D)÷1↓N
     ∇

    ∇ Z←FFT X;T;I;G;N;Q;⎕IO
[1]   ⍝FAST FOURIER TRANSFORM OF X; FROM RGS
[2]   ⍝X VECTOR OF REALS OR X[;0]=REAL X[;1]=IMAGINARY
[3]   ⎕IO←0
[4]   →(2=ρρX)/L0
[5]   X←X,[.5]0
[6]   L0:T←2⊥⊖(Gρ2)⊤⍳I←2*G←⌈2⍟1↑ρX
[7]   X←((N←I÷2),2 2)ρ((I,2)↑X÷I*.5)[T;]
[8]   T←⍉2 1∘.○○(N↑T)÷2×N
[9]   Z←(+/[1]X),[.5]-/[I←1]X
[10]  LA:Z←((N←N÷2),(2×I←I×2),2)ρZ
[11]  X←(0,I,0)↓Z
```

```
[12]  Z←(0,-I,0)↓Z
[13]  Z←(Z+Q),Z-Q←(+/Q×X),[1.5]-/(Q←(N,I,2)ρ(I,2)↑T)×⌽X
[14]  →(1<N)/LA
[15]  Z←((2×I,1)ρZ)[2⊥⊖(Gρ2)⊤⍳2*G;]
    ∇

    ∇ Z←FFTI X;T;I;G;N;Q;⎕IO
[1]   ⍝FAST INVERSE FOURIER TRANSFORM OF X; FROM RGS
[2]   ⍝X IS VECTOR OF REALS, OR X[;0]=REAL X[;1]=IMAGINARY
[3]   ⎕IO←0
[4]   →(2=ρρX)/L0
[5]   X←X,[0.5] 0
[6]   L0:T←2⊥⊖(Gρ2)⊤⍳I←2*G←⌈2⍟1↑ρX
[7]   X←((N←I÷2),2 2)ρ((I,2)↑X÷I*.5)[T;]
[8]   T←⍉2 1∘.○(N↑T)÷¯2×N
[9]   Z←(+/[1]X),[.5]-/[I←1]X
[10]  LA:Z←((N←N÷2),(2×I←I×2),2)ρZ
[11]  X←(0,I,0)↓Z
[12]  Z←(0,-I,0)↓Z
[13]  Z←(Z+Q),Z-Q←(+/Q×X),[1.5]-/(Q←(N,I,2)ρ(I,2)↑T)×⌽X
[14]  →(1<N)/LA
[15]  Z←((2×I,1)ρZ)[2⊥⊖(Gρ2)⊤⍳2*G;]
    ∇

    ∇ FITPLOT X;⎕IO;ZRO;SPA;XPOS;STV;NUMN;N
[1]   ⍝PLOT OF THE FITTED OCCULTATION CURVE
[2]   ⍝X=STARTING BIN NUMBER; OBS, COMP, SOL MUST BE GLOBAL
[3]   ⎕IO←0
[4]   X←X,(X+SOL[2]),(X+SOL[8]),SOL[9],SOL[5]×206264810
[5]   START
[6]   PLOTSET ¯.3 0
[7]   AXISD 2 1.75 7 0 .35 .15
[8]   AXISD 2 1.75 7 0 1.4 ¯.05
[9]   AXISD 2 1.75 4.75 90 .475 ¯.15
[10]  AXISD 2,(1.75+4.75÷20),4.275 90,(4.75÷10),¯.08
[11]  AXISD 9 1.75 4.75 90 .475 .15
[12]  AXISD 9,(1.75+4.75÷20),4.275 90 .475 .08
[13]  ZRO←2+(-/X[2 0])×7÷-/X[1 0]
[14]  SPA←10×÷X[3]×(-/X[1 0])÷7
[15]  AXISD ZRO,6.5,(ZRO-2),180,SPA,.15
[16]  AXISD ZRO,6.5,(9-ZRO),0,SPA,¯.15
[17]  ('ZF3.1' ⎕FMT .1×⍳11)LABELD 1.55,(1.75+.475×⍳11),[.5]
      0
[18]  ('LI4' ⎕FMT(⌊/OBS)+((⌈/OBS)-⌊/OBS)×.1×⍳11)LABELD 9.05
      ,(1.75+.475×⍳11),[.5]0
[19]  ('LI4' ⎕FMT X[0]+(⍳5)×.2×¯1+-/X[1 0])LABELD(2+1.4×⍳5)
      ,1.55,[.5]5ρ0
[20]  XPOS←ZRO-SPA×⌊(ZRO-2)÷SPA
[21]  STV←¯10×⌊(ZRO-2)÷SPA
[22]  NUMM←(⌊(ZRO-2)÷SPA)+⌊(9-ZRO)÷SPA
[23]  ('M⎕-⎕LI4' ⎕FMT STV+10×⍳NUMM)LABELD((XPOS+NUMM↑+\0,NU
      MMρSPA),[.5]6.55),0
[24]  'TIME IN MILLISECONDS FROM BEGINNING OF DATA WINDOW'
      CENTER 1 9 1.3 0
```

```
[25]  'ANGULAR SEPARATION IN MILLISECONDS OF ARC' CENTER 1
      9 6.75 0
[26]  (1 20ρ'NORMALIZED INTENSITY')LABELD 1 3ρ1.4 2.8 90
[27]  (1 6ρ'COUNTS')LABELD 1 3ρ9.8 4.9 270
[28]  N←0
[29]  L1:AXISD ZRO,(2+.475×N),(.475÷2),270
[30]  →(10≠N←N+1)/L1
[31]  1 SPLINE(2+7×(ιρOBS)÷¯1+ρOBS),1.75+4.75×(OBS-⌊/OBS)÷⌈
      /OBS-⌊/OBS
[32]  1 SPLINE(2+7×(ιρCOMP)÷¯1+ρCOMP),1.75+4.75×(COMP-⌊/OBS
      )÷⌈/OBS-⌊/OBS
[33]  AXISD 8.5,(1.75+4.75×(SOL[6]-⌊/OBS)÷(⌈/OBS)-⌊/OBS),.5
      0
[34]  AXISD 2,(1.75+4.75×(SOL[7]-⌊/OBS)÷(⌈/OBS)-⌊/OBS),.5 0
[35]  AXISD ZRO,6.32,(X[4]×.1×SPA),0
[36]  PLOTEND
      ∇

    ∇ FITPLOT2 X;⎕IO;ZRO;SPA;XPOS;STV;NUMN;N
 [1]  ⍝PLOT OF THE FITTED TWO-STAR OCCULTATION CURVE
 [2]  ⍝X=STARTING BIN NUMBER; OBS, COMP, SOL MUST BE GLOBAL
 [3]  ⎕IO←0
 [4]  X←X,(X+SOL[2]),(SOL[8]+X2←X),SOL[9],SOL[5]×206264810
 [5]  START
 [6]  PLOTSET ¯.3 0
 [7]  AXISD 2 1.75 7 0 .35 .15
 [8]  AXISD 2 1.75 7 0 1.4 ¯.05
 [9]  AXISD 2 1.75 4.75 90 .475 ¯.15
[10]  AXISD 2,(1.75+4.75÷20),4.275 90,(4.75÷10),¯.08
[11]  AXISD 9 1.75 4.75 90 .475 .15
[12]  AXISD 9,(1.75+4.75÷20),4.275 90 .475 .08
[13]  ZRO←2+(-/X[2 0])×7÷-/X[1 0]
[14]  SPA←10×÷X[3]×(-/X[1 0])÷7
[15]  AXISD ZRO,6.5,(ZRO-2),180,SPA,.15
[16]  AXISD ZRO,6.5,(9-ZRO),0,SPA,¯.15
[17]  ('ZF3.1' ⎕FMT .1×ι11)LABELD 1.55,(1.75+.475×ι11),[.5]
      0
[18]  ('LI4' ⎕FMT(⌊/OBS)+((⌈/OBS)-⌊/OBS)×.1×ι11)LABELD 9.05
      ,(1.75+.475×ι11),[.5]0
[19]  ('LI4' ⎕FMT X[0]+(ι5)×.2×¯1+-/X[1 0])LABELD(2+1.4×ι5)
      ,1.55,[.5]5ρ0
[20]  XPOS←ZRO-SPA×⌊(ZRO-2)÷SPA
[21]  STV←¯10×⌊(ZRO-2)÷SPA
[22]  NUMM←(⌊(ZRO-2)÷SPA)+⌊(9-ZRO)÷SPA
[23]  ('M⎕-⎕LI4' ⎕FMT STV+10×ιNUMM)LABELD((XPOS+NUMM↑+\0,NU
      MMρSPA),[.5]6.55),0
[24]  'TIME IN MILLISECONDS FROM BEGINNING OF DATA WINDOW'
      CENTER 1 9 1.3 0
[25]  'ANGULAR SEPARATION IN MILLISECONDS OF ARC' CENTER 1
      9 6.75 0
[26]  (1 20ρ'NORMALIZED INTENSITY')LABELD 1 3ρ1.4 2.8 90
[27]  (1 6ρ'COUNTS')LABELD 1 3ρ9.8 4.9 270
[28]  N←0
[29]  L1:AXISD ZRO,(2+.475×N),(.475÷2),270
```

```
 →(10≠N←N+1)/L1
 1 SPLINE(2+7×(⍳⍴OBS)÷¯1+⍴OBS),1.75+4.75×(OBS-⌊/OBS)÷⌈
  /OBS-⌊/OBS
 1 SPLINE(2+7×(⍳⍴COMP)÷¯1+⍴COMP),1.75+4.75×(COMP-⌊/OBS
  )÷⌈/OBS-⌊/OBS
 AXISD 8.5,(1.75+4.75×((SOL[7]+SOL2[6]+SOL[6])-⌊/OBS)÷
  (⌈/OBS)-⌊/OBS),.5 0
 AXISD 2,(1.75+4.75×(SOL[7]-⌊/OBS)÷(⌈/OBS)-⌊/OBS),.5 0
 AXISD ZRO,6.32,(X[4]×.1×SPA),0
 X←X2,(X2+SOL2[2]),(X2+SOL2[8]),SOL2[9],SOL2[5]×206264
  810
 N←0×1↑ZRO←2+(-/X[2 0])×7÷-/X[1 0]
 SPA←10×÷X[3]×(-/X[1 0])÷7
 L2:AXISD ZRO,(2+.475×N),(.475÷2),270
 →(10≠N←N+1)/L2
 AXISD ZRO,6.32,(X[4]×.1×SPA),0
 PLOTEND
∇

∇ R←FT Y;M;N;⎕IO
 ⍝DISCRETE FOURIER TRANSFORMATION OF EVENLY SPACED REA
 L DATA
 ⎕IO←0
 M←(⍳2×N)×○÷N←(⍴Y)÷2
 R←1 2⍴⌽,(+/Y)÷2×N
 L1:R←R,[0](÷N)×+/(1 1∘.×Y)×2 1∘.○(1↑⍴R)×M
 →(N>¯1+1↑⍴R)/L1
 R[N;]←.5 0×,¯1 2↑R
∇

∇ FTPREP X;⎕IO;T
 ⍝SETS UP GLOBAL FOR POWER SPECTRA ANALYSIS
 ⍝X IS CENTER OF TRANSFORM WINDOW FROM DATA SET
 ⎕IO←0
 FTOBS←.5×+/(FFT FTDATA←1024↑(¯512+514⌈X⌊3595)↓CH1)*2
 ⍎(3595≥X+1512)/'FTOUT←¯1012↑(X+1512)↑CH1'
 ⍎(3595<X+1512)/'FTOUT←¯1012↑(X-510)↑CH1'
 FTOUT←.5×(FFT FTOUT)+.*2
 T←¯1↓SOL[6]+(COMP[0]-SOL[6])×T÷⌈/T←T-⌊/T←+\+\⍳1+⌊.5×1
 024-⍴COMP
 FTMOD←T,COMP
 FTMOD←FTMOD,1↓SOL[7]+(-SOL[7]-¯1↑FTMOD)×⌽T÷⌈/T←T-⌊/T←
 +\+\⍳1+⌊1024-⍴FTMOD
 FTMOD←.5×(FFT FTMOD)+.*2
∇

∇ IDENT
 '   ***LUNAR OCCULTATION PLOTTING WORKSPACE***'
 '       VERSION: B01/HARRIS'
 '       WSID: DISPLOT'
 '       LAST REVISION: 10 APRIL 85'
 ' '
 '       NOTE: THIS WORKSPACE IS ⎕IO←0'
∇
```

```
    ∇ INTPLOT X;⎕IO
[1]   ⍝INTEGRATION PLOT OF THE DATA VECTOR X
[2]   ⎕IO←0
[3]   START
[4]   AXISD 2 1.75 7 0 .4375 ¯.15
[5]   AXISD 2 1.75 7 0 .875 ¯.05
[6]   AXISD 2 1.75 4.75 90 .475 ¯.15
[7]   AXISD 2,(1.75+4.75÷20),4.275 90,(4.75÷10),¯.08
[8]   ('ZF3.1' ⎕FMT .1×⍳11)LABELD 1.55,(1.75+.475×⍳11),[.5]
     0
[9]   ('LI4' ⎕FMT((⍴X)÷8)×⍳8)LABELD(2+.875×⍳8),1.55,[.5]8⍴0
[10]  'TIME IN MILLISECONDS FROM BEGINNING OF DATA WINDOW'
     CENTER 1 9 1.3 0
[11]  (1 20⍴'NORMALIZED INTENSITY')LABELD 1 3⍴1.25 3.22 90
[12]  X←-(⌊/X)-X←+\X-(+/X)÷⍴X←X[2 3],2↓X
[13]  1 SPLINE (2+7×(⍳⍴X)÷¯1+⍴X),1.75+4.75×X÷⌈/X
[14]  PLOTEND
    ∇

    ∇ F←X INVFT R;⎕IO
[1]   ⍝INVERSE FOURIER TRANSFORMATION FROM COEFFICIENT MATR
     IX
[2]   ⎕IO←0
[3]   X←2 0 1⍉2 1∘.○X∘.×1↓⍳1↑⍴R
[4]   F←,(1 1↑R)++/+/((⍴X)⍴1 0↓R)×X
    ∇

    ∇ NOISEPLOT X;OC;PD;R;MEAN;SIGMA;Y;BR;N
[1]   ⍝NOISE FIGURE FOR LUNAR OCCULTATION
[2]   ⍝X IS BIN NUMBER OF START OF DATA USED IN SOLUTION
[3]   ⍝MUST HAVE SOL OBS AND COMP AS GLOBAL VARIABLES
[4]   OBS∧.=SOL[2]↑(X-1)↓CH1
[5]   ⍝X[1]=FIRST BIN OF DATA X[2]=LENGTH OF DATA
[6]   OC←((X-1)↑CH1)-SOL[6]
[7]   OC←OC,(OBS-COMP),((¯1+SOL[2]+X)↓CH1)-SOL[7]
[8]   PD←BR←⍉50 BIN OC←2↓OC÷CH1
[9]   PD[0;]←PD[0;]-PD[0;0]
[10]  PD←PD×⍉(⌽⍴PD)⍴7 4.75÷⌈/PD
[11]  X←2+1↓¯1↓,(7×(⍳51)÷50)∘.×1 1
[12]  Y←1.75+,PD[1;]∘.×1 1
[13]  START
[14]  PLOTSET ¯.1 0
[15]  AXISD 2 1.75 7 0 .14 ¯.15
[16]  AXISD 2 1.75 7 0 .7 ¯.05
[17]  AXISD 2 1.75 4.75 90 .475 ¯.15
[18]  ('ZI4' ⎕FMT .1×(⍳11)×0 1/R←(⌈/BR)-⌊/BR)LABELD 1.38,(1
     .75+.475×⍳11),[.5]0
[19]  ('M⍞-⍞LF5.1' ⎕FMT 100×(1↑⌊/BR)+.1×(⍳10)×1↑R)LABELD(2+
     .7×⍳10),1.55,[.5]10⍴0
[20]  1 SPLINE X,[¯.5]Y
[21]  'NOISE LEVEL AS A PERCENTAGE OF COMPUTED INTENSITY' C
     ENTER 1 9 1.3 0
[22]  (1 20⍴'NUMBER OF OCCURANCES')LABELD 1 3⍴1.2 2.8 90
```

```
[23]  MEAN←(+/2↓OC)÷4094
[24]  SIGMA←((OC*2)+.*.5)÷4093
[25]  N←0
[26]  L1:AXISD(2+7×(MEAN-1↑⌊/BR)÷1↑R),(2+.475×N),.2375 90
[27]  →(10≠N←N+1)/L1
[28]  AXISD T←(2+7×((MEAN-.5×SIGMA)-1↑⌊/BR)÷1↑R),2.35,T,0,(
     T←7×SIGMA÷1↑R),.15
[29]  AXISD T×(5ρ1),¯1
[30]  (1 20ρ20↑,'MEAN ',,'M⍞-⍞F8.5' ⎕FMT MEAN)LABELD 1 3ρ2.
     5 6 0
[31]  (1 20ρ20↑,'SIGMA ',,'F8.6' ⎕FMT SIGMA)LABELD 1 3ρ2.5
     5.5 0
[32]  PLOTEND
     ∇

    ∇ PDPLOT S;X;N;⎕IO
 [1]  ⍝PLOT OF THE NORMALIZED FIRST DERIVATIVES OF INTENSIT
     Y
 [2]  ⍝S IS STARTING BIN NUMBER
 [3]  ⎕IO←0
 [4]  X←.75×X÷(ρX)ρ⌈/X←X-(ρX)ρ⌊/X←PDER,COMP
 [5]  X←X+(ρX)ρ1.82+.78×⍳6
 [6]  X←X,[.5]2+((7÷ρCOMP)×⍳ρCOMP)∘.×6ρ1
 [7]  N←0
 [8]  START
 [9]  L1:1 SPLINE,⍉⌽X[;;N]
[10]  AXISD 2,(1.82+N×.78),.75 90 .75 .1
[11]  AXISD 2,(1.82+N×.78),.75 90 .75 ¯.1
[12]  AXISD 9,(1.82+N×.78),.75 90 .75 .1
[13]  AXISD 9,(1.82+N×.78),.75 90 .75 ¯.1
[14]  AXISD(2+7×SOL[8]÷ρCOMP),(2.56+N×.78),.04 90
[15]  AXISD 2,(2.21+N×.78),7 0
[16]  →(6≠N←N+1)/L1
[17]  AXISD(2+7×SOL[8]÷ρCOMP),1.75 .07 90
[18]  AXISD 2 1.75 7 0 1.4 .05
[19]  AXISD 2 1.75 7 0 1.4 ¯.05
[20]  'TIME IN MILLISECONDS FROM BEGINNING OF DATA WINDOW'
     CENTER 1 9 1.3 0
[21]  (⊖6 4ρ'COMPVELOTIMEPREIPOSTDIAM')LABELD 1.35,(2.02+.7
     8×⍳6),[.5]6ρ0
[22]  (1 18ρ'PARTIAL DERIVATIVES')LABELD 1 3ρ1.2 2.8 90
[23]  ('LI4' ⎕FMT S+(⍳5)×.2×¯1+ρCOMP)LABELD(2+1.4×⍳5),1.55,
     [.5]5ρ0
[24]  PLOTEND
     ∇

    ∇ PDPLOT2 S;X;N;⎕IO
 [1]  ⍝PLOT OF NORMALIZED FIRST DERIVATIVES OF INTENSITY
 [2]  ⍝FOR TWO-STAR (DC2) SOLUTION
 [3]  ⍝S IS STARTING BIN NUMBER
 [4]  ⎕IO←0
 [5]  X←.52×X÷(ρX)ρ⌈/X←X-(ρX)ρ⌊/X←(1 1 0 1 1 1 1 1 1/PDER),
     COMP
 [6]  X←X+(ρX)ρ1.82+.52×⍳9
```

```
 [7]  X←X,[.5]2+((7÷ρCOMP)×ιρCOMP)∘.×9ρ1
 [8]  N←0
 [9]  START
[10]  L1:1 SPLINE,⍉⌽X[;;N]
[11]  AXISD 2,(1.82+N×.52),.5 90 .5 .1
[12]  AXISD 2,(1.82+N×.52),.5 90 .5 ¯.1
[13]  AXISD 9,(1.82+N×.52),.5 90 .5 .1
[14]  AXISD 9,(1.82+N×.52),.5 90 .5 ¯.1
[15]  AXISD(2+7×SOL2[8]÷ρOBS),(2.56+N×.52),.04 90
[16]  AXISD(2+7×SOL[8]÷ρOBS),(2.56+N×.52),.04 90
[17]  AXISD 2,(2.08+N×.52),7 0
[18]  →(9≠N←N+1)/L1
[19]  AXISD(2+7×SOL[8]÷ρOBS),1.75 .07 90
[20]  AXISD(2+7×SOL2[8]÷ρOBS),1.75 .07 90
[21]  AXISD 2 1.75 7 0 1.4 .05
[22]  AXISD 2 1.75 7 0 1.4 ¯.05
[23]  'TIME IN MILLISECONDS FROM BEGINNING OF DATA WINDOW'
     CENTER 1 9 1.3 0
[24]  (⊖9 4ρ'COMPVEL2TIM2INT2DIA2VEL1TIM1INT1DIA1')LABELD 1
     .35,(2.02+.52×ι9),[.5]9ρ0
[25]  (1 18ρ'PARTIAL DERIVATIVES')LABELD 1 3ρ1.2 2.8 90
[26]  ('LI4' ⎕FMT S←(ι5)×.2×¯1+ρCOMP)LABELD(2+1.4×ι5),1.55,
     [.5]5ρ0
[27]  PLOTEND
     ∇

    ∇ POWERPLOT;R;X;I;⎕IO
 [1]  ⍝POWER SPECTRA OF MODEL CURVE, STAR+SKY, AND OCCULTAT
     ION
 [2]  ⍝EXECUTE FTPREP IN BEFORE POWERPLOT
 [3]  ⎕IO←0
 [4]  START
 [5]  PLOTSET ¯.3 0
 [6]  AXISD 2 1 5 90 1 .1
 [7]  AXISD 2 1.5 4 90 1 .05
 [8]  AXISD 4.66 1 5 90 1 .1
 [9]  AXISD 4.66 1.5 4 90 1 .05
[10]  AXISD 7.32 1 5 90 1 .1
[11]  AXISD 7.32 1.5 4 90 1 .05
[12]  X←(500↑1↓FTOBS),(500↑1↓FTOUT),500↑1↓FTMOD
[13]  R←10*0 ¯1+⌈10⍟(⌈/X),⌊/X
[14]  X←(10⍟X)÷10⍟R[0]
[15]  I←1↓¯1↓,(5×÷500)×(ι501)∘.×1 1
[16]  1 SPLINE(2+2.5×,(500↑X)∘.×1 1),1+⌽I
[17]  1 SPLINE(4.66+2.5×,(500↓1000↑X)∘.×1 1),1+⌽I
[18]  1 SPLINE(7.32+2.5×,(1000↓X)∘.×1 1),1+⌽I
[19]  AXIS 2 1 2.5 0,(2.5÷-/10⍟R),.1
[20]  AXIS 4.66 1 2.5 0,(2.5÷-/10⍟R),.1
[21]  AXIS 7.32 1 2.5 0,(2.5÷-/10⍟R),.1
[22]  AXIS 2 6 2.5 0,(2.5÷-/10⍟R),¯.1
[23]  AXIS 4.66 6 2.5 0,(2.5÷-/10⍟R),¯.1
[24]  AXIS 7.32 6 2.5 0,(2.5÷-/10⍟R),¯.1
[25]  ('LI3' ⎕FMT 100×ι5)LAXISD 1.8 6 1 270
[26]  (1 18ρ'FREQUENCY IN HERTZ')LABELD 1 3ρ1.5 4.95 271
```

```
[27]  (1 11⍴'OCCULTATION')LAXISD 4.36 3 0 271
[28]  (1 10⍴'STAR + SKY')LAXISD 7.02 3 0 271
[29]  (1 11⍴'MODEL CURVE')LAXISD 9.68 3 0 271
[30]  PLOTEND
     ∇

    ∇ RAWPLOT X;⎕IO;ZRO;SPA;NEG;POS;XPOS;STV;NUMM;N
 [1]  ⍝PLOT OF THE RAW DATA, X (EVERY 4 POINTS)
 [2]  ⎕IO←0
 [3]  START
 [4]  PLOTSET ¯.4 0
 [5]  AXISD 2 1.75 7 0 .4375 .15
 [6]  AXISD 2 1.75 7 0 .875 ¯.05
 [7]  AXISD 2 1.75 4.75 90 .475 ¯.15
 [8]  AXISD 2,(1.75+4.75÷20),4.275 90,(4.75÷10),¯.08
 [9]  AXISD 9 1.75 4.75 90 .475 .15
[10]  AXISD 9,(1.75+4.75÷20),4.275 90 .475 .08
[11]  ('ZF3.1' ⎕FMT .1×⍳11)LABELD 1.55,(1.75+.475×⍳11),[.5]
     0
[12]  ('LI4' ⎕FMT 4096×.1×⍳11)LABELD 9.05,(1.75+.475×⍳11),[
     .5]0
[13]  ('LI4' ⎕FMT 512×⍳8)LABELD(2+.875×⍳8),1.55,[.5]8⍴0
[14]  'TIME IN MILLISECONDS FROM BEGINNING OF DATA WINDOW'
     CENTER 1 9 1.3 0
[15]  (1 20⍴'NORMALIZED INTENSITY')LABELD 1 3⍴1.4 2.8 90
[16]  (1 6⍴'COUNTS')LABELD 1 3⍴9.8 4.9 270
[17]  1 SPLINE(8192⍴0 0 1 0)/(2+7×(⍳4096)÷4095),1.75+4.75×X
     ÷4095
[18]  PLOTEND
     ∇

    ∇ Y←N SMOOTH D;⎕IO
 [1]  ⍝N-POINT UNWEIGHTED SMOOTHING OF THE VECTOR D
 [2]  ⎕IO←0
 [3]  Y←(⍴D)⍴((⌊.5×N)↑D),((-N)↓(+⌿(⍳N)⌽(N,⍴D)⍴D)÷N),(-⌈.5×N
     )↑D
     ∇
```

LIST OF REFERENCES

Abt, H. A., and Kallarakal, V. V., 1963. Astrophys. J., 138, 140.

Allen, C. W., 1963, Astrophysical Quantities (London: Athlone Press), p. 170.

Analogics Incorporated, 1984, The APL Machine (Danvers, MA: Author).

Astronomical Time Mechanisms, 1980, Model 240 fast photometer amplifier operating instructions (Gainesville, FL: Author).

Barnes, T. G., and Evans, D. S., 1976, Mon. Not. Roy. Astron. Soc., 174, 489.

Bender, David F., 1979, in Asteroids, ed. T. Gehrels (Tucson: University of Arizona Press), p. 1014.

Bevington, P. R., 1969, Data Reduction and Analysis for the Physical Sciences (New York: McGraw-Hill Book Company), p. 127.

Blow, Graham L., 1983, in Solar System Photometry Handbook, ed. R. M. Genet (Richmond: Willmann-Bell, Inc.). p. 9-14.

Bowker, D. E., and Hughes, J. K., 1971, Lunar Orbiter Photographic Atlas of the Moon, NASA SP-206 (Washington: NASA).

Bracewell, R., 1965, The Fourier Transform and Its Applications (New York: McGraw-Hill Book Company), p. 296.

Brenner, Norman, 1982, APL Quote Quad, 13-1, 57.

Brown, D. C., 1955, Ballistic Research Laboratories Report, 937 (Aberdeen Proving Ground, MD: Ballistic Research Laboratories).

Brown, R. H., 1968, in Annual Reviews of Astronomy and Astrophysics, 6, 13.

Brown, R. H., 1980, in Optical Telescopes of the Future. ESO Conference, eds. E. Pacini, W. Ricter and R. N. Wilson (Geneva: ESO), p. 391.

Campbell, W. W., and Moore, J. H., 1907, Astrophys. J., 25, 54.

Caton, D. B., 1981, Ph.D. Dissertation, University of Florida.

Chen, K-Y, 1985, private communication.

Chen, K-Y, and Rekenthaler, D. A., 1966, Quarterly Journal of the Florida Academy of Sciences, 29, 1.

Department of the Army, 1953, Antennas and Radio Propagation, TM 11-666 (Washington, DC: U. S. Government Printing Office), 17.

Dunham, E. W., Baron, R. L., Conner, S., Dunham, D. W., Dunham, J. B., Schneider, G., Cohen, H. L., Helms III, V. T., Croom, M., and Safko, J., 1984, A. J., 89, 1755.

Dunham, D. W., Evans, D. S., McGraw, J. T., Sandmann, W. H., and Wells, D. C., 1973, A. J., 78, 482.

Eddington, A. E., 1909, Mon. Not. Roy. Astron. Soc., 69, 178.

Eggen, O. J., 1965, Astrophys. J., 70, 19.

Eichhorn, H., 1977, Mon. Not. Roy. Astron. Soc., 182, 355.

Eichhorn, H., and Clary, W. G., 1974, Mon. Not. Roy. Astron. Soc., 166, 425.

Evans, D. S., 1951, Mon. Not. Roy. Astron. Soc., 111, 64.

------------, 1959, Mon. Not. Roy. Astron. Soc. S. Africa, 18, 158.

------------, 1968, Q. J. Roy. Astr. Soc., 9, 388.

------------, 1970, A. J., 75, 589.

------------, 1971, A. J., 76, 1107.

Evans, D. S., Africano, J. L., Fekel, F. C., Montemayor, T., Palm, C., Silverberg, E., Citters, W. V., Wiant, J., 1977, A. J., 82, 495.

Falkoff, A. D., and Iverson, K. E., 1968, Symposium on Interactve Systems for Experimental Applied Mathematics, eds. M. Klerer and J. Reinfelds (New York: Academic Press).

Falkoff, A. D., and Iverson, K. E., 1970, APL/360 User's Guide (GH20-0683-1) (Poughkeepsie, NY: IBM).

Falkoff, A. D., and Orth, D. L., 1979, APL Quote Quad, 9-4, 409.

Finsen, W. S., and Worley, C. E., 1970, Republic Observatory Johannesburg, Circulars, 7-129, 203.

Flesch, T., 1975, Ph.D. Dissertation, University of Florida.

Giacconi, R., 1982, in The Space Telescope Observatory, ed. D. N. B. Hall, NASA CP-2244 (Washington: NASA), p. 1.

Gillman, L., and Rose, A. J., 1974, APL: An Interactive Approach, Second Edition, Revised Printing (New York: John Wiley and Sons, Inc.).

Griffin, R. F., 1980, Sky and Telescope, 58, 19.

Griffin, R. F., and Radford, G. A., 1976, Observatory, 96, 188.

Henden, A. A., and Kaitchuck, R. H., 1982, Astronomical Photometry (New York: Van Nostrand Reinhold Company), p. 371.

Iverson, K. E., 1962, A Programming Language (New York: John Wiley and Sons, Inc.).

Kamas, G., 1977, Time and Frequency User's Manual-NBS Technical Note, 695, 118.

Keenan, P. C., and McNeil, R. C., 1976, An Atlas of Spectra of the Cooler Stars: Types G, K, M, S and C (Columbus: Ohio State University Press), Plates 19, 21 and 23.

Kuiper, G. P., 1948, Astrophys. J., 108, 542.

Lohmann, A. W., and Weigelt, G. P., 1980, in Optical Telescopes of the Future. ESO Conference, eds. E. Pacini, W. Richter and R. N. Wilson (Geneva: ESO), p. 489.

Lukac, M., 1983, U. S. N. O. Lunar Occultation Predictions for 1983, private communication.

---------, 1984, U. S. N. O. Lunar Occultation Predictions for 1984, private communication.

MacMahon, P. A., 1909, Mon. Not. Astron. Soc. S. Africa, 69, 126.

Meyer, S. L., 1975, Data Analysis for Scientists and Engineers, (New York: John Wiley and Sons, Inc.), p. 399.

Micro Technology Unlimited, 1979, K-1016 16K Byte Memory 6502 System Low Power Memory (Raleigh: Author).

-------------------------, 1980a, K-1013 Double Density Disk Controler for KIM/MTU Bus Systems (Raleigh: Author).

-------------------------, 1980b, K-1008 Visible Memory (Raleigh: Author).

-------------------------, 1980c, K-1020 Prototyping Board (Raleigh: Author).

-------------------------, 1980d, K-1005 Card File and 5-Slot Motherboard for Expansion of 6502 Based Microcomputers Using the KIM/MTU Bus (Raleigh: Author).

-------------------------, 1981, Channel-Oriented Disk Operating System Release 1.2 User Manual (Raleigh: Author).

Mihalas, D., and Binney, J., 1981, Galactic Astronomy Structure and Kinematics (San Francisco: W. H. Freeman and Company), p. 107.

Morbey, C. L., 1972, Pub. Dom. Ap. Obs., 14, 45.

Muller, P., 1961, I.A.U. Commission des Etoiles Doubles Circulaire d'Information, 24.

Murdin, P., 1971, Astrophys. J., 169, 615.

Nather, R. E., and Evans, D. S., 1970, A. J., 75, 575.

Nather, R. E. and McCants, M. M., 1970, A. J., 84, 872.

NERDC, 1980, MINIS & MICROS, (Gainesville, FL: University of Florida), p. 18.

Oliver, J. P., 1976, Rev. Sci. Instrum., 47, 581.

Pakin, S., and Polvka, R. P., 1975, APL: The Language and Its Usage, (Englewood Cliffs, NJ: Prentice-Hall).

Parise, R., 1978, Master's Thesis, University of Florida.

Pollock, J. T., 1981, private communication.

Rigdway, S. T., 1977, A. J., 82, 511.

Robertson, J. R., 1940, Astronomical Papers Prepared for the Use of the American Ephemeris And Nautical Almanac: Catalog of 3539 Zodiacal Stars for the Equinox of 1950.0, 10-2 (Washington: USNO).

Rockwell International, 1978, AIM-65 Microcomputer User's Guide (Anaheim, CA: Author), p. 7-45.

Schlesinger, F., and Jenkins, L. F., 1940, Yale University Observatory Catalog of Bright Stars, (New Haven, CT: The New Haven Printing Company), p. 66.

Schmidtke, Paul C., and Africano, John L., 1984, A. J., 89, 663.

Schneider, G., 1981, APL Quote Quad, 11-4, 23.

Schneider, G., and Brown, R. G., 1976, Warner Computer Systems APL Technical Notes, 47, 28.

Selfridge, Ralph G., 1983, CIMAR Plotting, private communication.

------------------, 1984, private communication.

Smillie, K. W., 1976, in APL76 Conference Proceedings, ed. G. T. Hunter (Ottawa, Canada: Association for Computing Machinery), p. 401.

Tassoul, J. L., 1978, Theory of Rotating Stars, ed. J. P. Ostriker (Princeton, NJ: Princeton University Press), p. 28.

Taylor, Jr., J. H., 1966, Nature, 210, 1105.

True Time Instruments, 1974, Operating and Service Manual WWVB Time Code Receiver (Santa Rosa, CA: Author), p. 45.

Van Flandern, T. C., 1973, USNO Occultation Predictions Format, (Washington: USNO) p. 3.

------------------, 1974, Bull. A. Astron. Soc., 6, 206.

------------------, 1975, Occultation Newsletter, 1, 28.

Wasserman, L. H., Millis, R. L., and Williamson, R. M., 1977, A. J., 82, 506.

White, M. W., and Slettebak, A., 1980, A. J., 85, 257.

White, N. M., and Kreidl, T. J., 1984, A. J., 89, 424.

Whitford, A. E., 1939, Astrophys. J., 89, 472.

Williams, J. D., 1939, Astrophys. J., 89, 467.

Wilson, R. E., 1976, Astron. and Astrophys., 48, 349.

Worley, C. E., 1984, Washington Double Star Catalog (USNO), private communication.

Young, R. K., 1919, Pub. Dom. Ap. Obs., 1 ,119.

BIOGRAPHICAL SKETCH

Glenn H Schneider (no "." after the H, please note) was born to Elaine and Ira G. Schneider on October 12, 1955, an otherwise un-noteworthy day, except perhaps for the fact that it marked the 463rd anniversary of the discovery of America, as commonly reckoned. At the tender age of three he received his first telescope (Sears, 40X!), and learned early in life the meaning of light pollution.

He attended public school 97 and J.H.S. 135 (also known as the Frank D. Whalen Junior High School, though no one ever knew who Frank D. Whalen was) in New York City. Thanks to the closing of the school during the summer of 1969 he was permitted to retain possession of the school library's copies of <u>The Larousse Encyclopedia of Astronomy</u> and <u>Norton's Star Atlas</u>. Later that year he became a member of the Amateur Observers' Society of New York. These two events forever influenced his life and started him on the path to a career in astronomy.

He graduated from The Bronx High School of Science in June of 1972. Shortly thereafter, he organized an international solar eclipse expedition, in hopes of observing his second total solar eclipse. The clouds which hung ominously over the Gaspé Peninsula that day served to reinforce his devotion to shadow chasing.

In June of 1976, he earned a Bachelor of Science degree in physics from the New York Institute of Technology. Before entering the graduate program in astronomy at the University of Florida in September of 1977, he worked as an APL technical analyst for Warner Computer Systems, Inc.

After eight years, two trips to the South Pole, seemingly endless commuting between Gainesville, Paris, Noordwijc and Bristol, statistically improbable stretches of cloudy weather during scheduled observing runs, and being thwarted at every turn by wayward computers (micro and macro), he expects, finally, to receive the degree of Doctor of Philosophy in August of 1985. He has accepted a position at the Space Telescope Science Institute, working for the Computer Sciences Corporation as a Science and Mission Operations Astronomer.

He has observed every total solar eclipse since March, 1970, and intends to keep chasing the moon's shadow well into the future. He has a definite preference for Dr. Brown's Celery Tonic (now called Cel-Ray Soda, alas), and egg creams made with Fox's U-Bet chocolate syrup and Good-Health seltzer.

At the moment he is single, but this malady is expected to be cured on June 7, 1985.

I certify that I have read this study and that in my opinion it conforms to acceptable standards of scholarly presentation and is fully adequate, in scope and quality, as a dissertation for the degree of Doctor of Philosophy.

John P. Oliver, Chairman
Associate Professor of Astronomy

I certify that I have read this study and that in my opinion it conforms to acceptable standards of scholarly presentation and is fully adequate, in scope and quality, as a dissertation for the degree of Doctor of Philosophy.

Heinrich Eichhorn
Professor of Astronomy

I certify that I have read this study and that in my opinion it conforms to acceptable standards of scholarly presentation and is fully adequate, in scope and quality, as a dissertation for the degree of Doctor of Philosophy.

Howard L. Cohen
Associate Professor of Astronomy

I certify that I have read this study and that in my opinion it conforms to acceptable standards of scholarly presentation and is fully adequate, in scope and quality, as a dissertation for the degree of Doctor of Philosophy.

Heywood C. Smith
Associate Professor of Astronomy

I certify that I have read this study and that in my opinion it conforms to acceptable standards of scholarly presentation and is fully adequate, in scope and quality, as a dissertation for the degree of Doctor of Philosophy.

Ralph G. Selfridge
Professor of Computer and
Information Sciences

This dissertation was submitted to the Graduate Faculty of the Department of Astronomy in the College of Liberal Arts and Sciences and to the Graduate School and was accepted as partial fulfillment of the requirements for the degree of Doctor of Philosophy.

August 1985 Dean, Graduate School

```
[2]   ⍝CONVERSATIONAL ENTRY OF INITIAL DC PARAMETERS
[3]   NAME←32↑⍞,0ρ⍞←'NAME OR CATALOG NUMBER OF STAR: '
[4]   DATE←27↑⍞,0ρ⍞←'U. T. DATE OF OBSERVATION: '
[5]   COMN←28↑⍞,0ρ⍞←'ANY COMMENTS TO BE PRINTED: '
[6]   PV←⎕,0ρ⎕←'ENTER THE MONOCHROMATIC WAVELENGTH, OR ENTE
     R 0 TO USE FILTER TABLE'
[7]   ⍎(PV≠0)/'FILT←''MONO''',0ρMONO←1 2ρPV,1
[8]   →(PV≠0)/I0
[9]   'ENTER THE NAME OF THE FILTER TABLE TO BE USED:'
[10]  FILT←⍞
[11]  I0:PV←PV,⎕,0ρ⎕←'ENTER THE DISTANCE TO THE LUNAR LIMB
     IN KILOMETERS'
[12]  BIN←⎕,0ρ⎕←'ENTER STARTING BIN NUMBER OF DATA TO BE US
     ED'
[13]  PV←PV,⎕,0ρ⎕←'ENTER NUMBER OF DATA POINTS TO BE USED'
[14]  OBS←(¯1↑PV)↑(BIN-1)↓X
[15]  PV←PV,⎕,0ρ⎕←'ENTER THE EFFECTIVE COLOR TEMPERATURE OF
     THE STAR'
[16]  PV←PV,⎕,0ρ⎕←'ENTER THE SQUARE ROOT OF THE NUMBER OF G
     RID PTS./QUADRANT'
[17]  PV←PV,⎕÷C←206264806.2,0ρ⎕←'ENTER ESTIMATED DIAMETER I
     N ARC-MILLISECONDS'
[18]  LIMS←⎕÷C,0ρ⎕←PR←'  ENTER UPPER AND LOWER LIMIT'
[19]  PV←PV,⎕,0ρ⎕←'ENTER PRE-EVENT LEVEL OF STAR+SKY SIGNAL
     '
[20]  LIMS←LIMS,⎕,0ρ⎕←PR
[21]  PV←PV,⎕,0ρ⎕←'ENTER POST-EVENT LEVEL OF LIMB+SKY SIGNA
     L'
[22]  LIMS←LIMS,⎕,0ρ⎕←PR
[23]  PV←PV,⎕-BIN,0ρ⎕←'ENTER ESTIMATED BIN NUMBER OF GEOMET
     RICAL OCCULTATION'
[24]  LIMS←LIMS,,(¯1↑PV)∘.+1 ¯1×⎕,0ρ⎕←' PLUS OR MINUS HOW M
     ANY MILLISECONDS?'
[25]  PV←PV,(PV[2]×¯3○⎕÷206265),0ρ⎕←'ENTER SHADOW VELOCITY
     IN A-SEC/SEC'
[26]  LIMS←LIMS,(PV[2]×¯3○⎕÷206265),0ρ⎕←PR
[27]  PV←PV,⎕,0ρ⎕←'ENTER ASSUMED LIMB DARKENING CO-EFFICIEN
     T'
[28]  LIMS←⍉6 2ρLIMS,⎕,0ρ⎕←PR
[29]  PV←1E¯12⌈PV,⎕,0ρ⎕←'ENTER MAXIMUM NUMBER OF ITERATIONS
     FOR DC PROCEEDURE'
[30]  PV←PV,|1↑-⌿2 2↑⍎FILT
[31]  PV←PV,⎕,0ρ⎕←'ENTER FRACTIONAL ADJUSTMENT TO BE USED (
     0 TO 1)'
     ∇

    ∇ Y←X LDARKEN G;T
[1]   ⍝Y=NORMALIZED GRID DISTRIBUTION OF LIMB DARKENED STA
     R
[2]   ⍝G=STELLAR GRID QUADRANT TO BE LIMB DARKENED (GENERA
     TED BY: GRID)
[3]   ⍝X=LIMB DARKENING COEFFICIENT
[4]   ⍝RESULT OBTAINED FROM A LINEAR LIMB DARKENING LAW
[5]   Y←Y÷4×+/+/Y←G×(T∘.≤T)×(1-T)⌽⌽(ρG)ρ(1-X)+X×2○¯1○(T-.5)
```

```
    ÷⍴T←⍳1↑⍴G
    ∇

   ∇ Y←NPOL V;T;I;⎕CT
[1]   ⍝INTERPOLATION OF FRESNEL INTENSITY VALUE FOR FRESNE
    L NUMBER <V>
[2]  Y←FREN[I]+(-⌿FREN[¯1 0∘.+I←(1+.5×⍴FREN)-100×T])×100×V
    -T←.01×⌊.5+V×100
    ∇

   ∇ OUTPUT2;S;T;PM;CT;W;Q
[1]  ⍝FORMATTED OUTPUT FOR DC2 SOLUTION
[2]  (20⍴' '),'OCCULTATION OF: ',NAME
[3]  (20⍴' '),DATE,' U. T.'
[4]  (20⍴' '),COMN
[5]  ' '
[6]  '  INPUT PARAMETERS:'
[7]  ' '
[8]  'CENTRAL WAVELENGTH OF PASSBAND:',(0⍕+/×/⍉FILT),' ANG
    STROMS'
[9]  'LUNAR LIMB DISTANCE (KM):         ',6 0⍕SOL[2]
[10] 'EFFECTIVE TEMPERATURE STAR-1  : ',⍕SOL[4]
[11] 'EFFECTIVE TEMPERATURE STAR-2  : ',⍕SOL2[4]
[12] 'LIMB DARKENING COEFFICIENT STAR-1: ',⍕SOL[11]
[13] 'LIMB DARKENING COEFFICIENT STAR-2: ',⍕SOL2[11]
[14] ' '
[15] '  MODEL PARAMETERS:'
[16] ' '
[17] 'NUMBER OF DATA POINTS: ',⍕SOL[3]
[18] 'NUMBER OF GRID POINTS: ',⍕(SOL[5]×2)*2
[19] 'NUMBER OF SPECTRAL REGIONS: ',⍕1↑⍴⍉FILT
[20] 'WIDTH OF SPECTRAL REGIONS:  ',(⍕-/⌽(⍉FILT)[1,2⌊1↑⍴⍉F
    ILT;1]),' ANGSTROMS'
[21] 'NUMBER OF ITERATIONS:  ',⍕SOL[12]
[22] ' '
[23] '  SOLUTIONS FOR STAR-1:'
[24] ' '
[25] PM←' +/-'
[26] 'STELLAR DIAMETER (ARC-MILLISECONDS): ',(6 2⍕SOL[6]×2
    06264806),PM,6 2⍕ER[1]×206264806
[27] 'BIN OF GEOMETRICAL OCCULTATION:        ',(7 1⍕SOL[9]+B
    IN),PM,4 1⍕ER[4]
[28] 'SIGNAL LEVEL OF STAR-1 (COUNTS)       ',(6 1⍕SOL[7]),
    PM,5 1⍕ER[2]
[29] ST←×1-T←SOL[10]÷PV[10]
[30] 'OBSERVED LUNAR SHADOW VELOCITY:      ',(7 5⍕SOL[10]),
    PM,(7 5⍕ER[5]),' KM/SEC'
[31] 'PREDICTED LUNAR SHADOW VELOCITY:     ',(7 5⍕PV[10]),'
     KM/SEC'
[32] T←'LOCAL SLOPE OF LUNAR LIMB:          ','- +'[ST+2],,
    (6 2⍕.5×+/S←(180÷○1)×¯2○T←T⌊÷T),' DEG'
[33] T,PM,5 3⍕|.5×-/Q⌊|Q←(÷○÷180)×(SOL[10]∘.+1 ¯1×ER[5])÷P
    V[10]
[34] 2 1⍴' '
```

```
[35]  '  SOLUTIONS FOR STAR-2:'
[36]  ' '
[37]  'STELLAR DIAMETER (ARC-MILLISECONDS): ',(6 2⍕SOL2[6]×
      206264806),PM,6 2⍕ER[6]×206264806
[38]  'BIN OF GEOMETRICAL OCCULTATION:       ',(7 1⍕SOL2[9]+
      BIN),PM,4 1⍕ER[8]
[39]  'SIGNAL LEVEL OF STAR-2 (COUNTS)       ',(6 1⍕SOL2[7])
      ,PM,4 1⍕ER[7]
[40]  'POST-EVENT LIMB+SKY SIGNAL LEVEL:    ',(6 1⍕SOL[8]),
      PM,4 1⍕ER[3]
[41]  'OBSERVED LUNAR SHADOW VELOCITY:     ',(7 5⍕SOL2[10])
      ,PM,(7 5⍕ER[9]),' KM/SEC'
[42]  ST←×1-T←SOL2[10]÷PV[10]
[43]  T←'LOCAL SLOPE OF LUNAR LIMB:           ','- +'[ST+2],,
      (6 2⍕.5×+/S←(180÷○1)×¯2○T←T⌊÷T),' DEG'
[44]  T,PM,6 3⍕|.5×-/Q⌊|Q←(÷○÷180)×(SOL2[10]∘.+1 ¯1×ER[9])÷
      PV[10]
[45]  2 1⍴' '
[46]  '  OTHER PARAMETERS AND DERIVED SOLUTIONS:'
[47]  ' '
[48]  'POST-EVENT LIMB+SKY SIGNAL LEVEL:    ',(6 1⍕SOL[8]),
      PM,4 1⍕ER[3]
[49]  'TEMPORAL SEPARATION OF THE STARS:   ',(6 1⍕|SOL[9]-S
      OL2[9]),PM,(4 1⍕(ER[4 8]+.*2)*.5),' MS.'
[50]  'WEIGHTED MEAN L-RATE: ',(6 4⍕W←((SOL[10],SOL2[10])+.
      ÷ER[5 9])÷+/÷ER[5 9]),' KM/SEC'
[51]  'SPATIAL SEPARATION FROM R-RATES WHICH ARE:'
[52]  T←' PREDICTED (',(⍕Q),' ARC SEC/SEC):  ',6 2⍕(|SOL2[9
      ]-SOL[9])×Q←206265×3○÷/PV[10 2]
[53]  T,' MILLISECONDS OF ARC'
[54]  T←' WEIGHTED MEAN (',(6 4⍕Q),' ARC SEC/SEC):  ',6 2⍕(
      |SOL2[9]-SOL[9])×Q←206265×3○W÷PV[2]
[55]  T,' MILLISECONDS OF ARC'
[56]  'BRIGHTNESS RATIO (BRIGHTER/FAINTER): ',6 4⍕T←÷/(SOL[
      7],SOL2[7])[⍒SOL[7],SOL2[7]]
[57]  'MAGNITUDE DIFFERENCE:                    ',6 4⍕(100*.2)⍟T
[58]  2 1⍴' '
[59]  '  PHOTOMETRIC STATISTICS:'
[60]  ' '
[61]  'SUM OF SQUARES OF RESIDUALS: ',⍕S←(OBS-COMP)+.*2
[62]  'SIGMA (STANDARD ERROR):      ',⍕S←(S÷¯1+⍴OBS)*.5
[63]  'NORMALIZED STANDARD ERROR:   ',⍕S←S÷SOL[7]+SOL2[7]
[64]  'PHOTOMETRIC (SIGNAL+NOISE)/NOISE RATIO:  ',⍕(1+S)÷S
[65]  '(INTENSITY CHANGE)/BACKGROUND:     ',⍕S←(SOL[7]+SOL2[
      7])÷SOL[8]
[66]  'CHANGE IN MAGNITUDE:                    ',⍕-(÷100*÷5)⍟1+S
[67]  2 1⍴' '
[68]  '  SUPPLEMENTAL STATISTICS: '
[69]  ' '
[70]  'VARIANCE/CO-VARIANCE MATRIX:'
[71]  CT←9 11⍴1↓⎕←' DIAMETER1  INTENSITY1 SKY INTS   OCC TI
      ME1  L-RATE1    DIAMETER2  INTENSITY2 OCC TIME2  L-RAT
[72]  'M⍞-⍞E11.4' ⎕FMT COV
[73]  ' '
```

```
[74]  (13ρ' '),,CT
[75]  ((1⊥⌽∧\CT=' ')⌽CT),'M⎕-⎕F11.6' ⎕FMT CM COV
[76]  RESTAB
    ∇

    ∇ OUTPUT;S;T;PM;CT
 [1]  ⍝PRODUCES A FORMATTED REPORT ON THE STELLAR SOLUTION
 [2]  (20ρ' '),'OCCULTATION OF: ',NAME
 [3]  (20ρ' '),DATE,' U. T.'
 [4]  (20ρ' '),COMN
 [5]  ' '
 [6]  ' INPUT PARAMETERS:'
 [7]  ' '
 [8]  'CENTRAL WAVELENGTH OF PASSBAND:',(0⍕+/×/⍎FILT),' ANG
     STROMS'
 [9]  'LUNAR LIMB DISTANCE (KM):        ',6 0⍕SOL[2]
[10]  'EFFECTIVE TEMPERATURE (KELVIN): ',⍕SOL[4]
[11]  'LIMB DARKENING COEFFICIENT:     ',⍕SOL[11]
[12]  ' '
[13]  'MODEL PARAMETERS:'
[14]  ' '
[15]  'NUMBER OF DATA POINTS: ',⍕SOL[3]
[16]  'NUMBER OF GRID POINTS: ',⍕(SOL[5]×2)*2
[17]  'NUMBER OF SPECTRAL REGIONS: ',⍕1↑ρ⍎FILT
[18]  'WIDTH OF SPECTRAL REGIONS:  ',(⍕-/⌽(⍎FILT)[1,2⌊1↑ρ⍎F
     ILT;1]),' ANGSTROMS'
[19]  'NUMBER OF ITERATIONS:  ',⍕SOL[12]
[20]  ' '
[21]  ' SOLUTIONS:'
[22]  ' '
[23]  PM←' +/-'
[24]  'STELLAR DIAMETER (ARC-MILLISECONDS): ',(6 2⍕SOL[6]×2
     06264806),PM,6 2⍕ER[1]×206264806
[25]  'BIN OF GEOMETRICAL OCCULTATION:        ',(7 1⍕SOL[9]+B
     IN),PM,4 1⍕ER[4]
[26]  'PRE-EVENT STAR+SKY SIGNAL LEVEL:       ',(6 1⍕SOL[7]),
     PM,4 1⍕ER[2]
[27]  'POST-EVENT LIMB+SKY SIGNAL LEVEL:      ',(6 1⍕SOL[8]),
     PM,4 1⍕ER[3]
[28]  ST←×1-T←SOL[10]÷PV[10]
[29]  'OBSERVED LUNAR SHADOW VELOCITY:       ',(7 5⍕SOL[10]),
     PM,(7 5⍕ER[5]),' KM/SEC'
[30]  'PREDICTED LUNAR SHADOW VELOCITY:      ',(7 5⍕PV[10]),'
     KM/SEC'
[31]  T←'LOCAL SLOPE OF LUNAR LIMB:            ','- +'[ST+2],,
     (6 2⍕.5×+/S←(180÷○1)×¯2○T←T⌊÷T),' DEG'
[32]  T,PM,5 3⍕|.5×-/Q⌊|Q←(÷○÷180)×(SOL[10]∘.+1 ¯1×ER[5])÷P
     V[10]
[33]  2 1ρ' '
[34]  'VARIANCE-COVARIANCE MATRIX:'
[35]  'M⎕-⎕F12.5' ⎕FMT COV
[36]  2 1ρ' '
[37]  'CORRELATION MATRIX:'
[38]  ¯60↑,CT←5 10ρ' DIAMETER    *+LIMB  LIMB+SKY  TIME OC
```

```
     C  VELOCITY  '
[39]  ((1⊥⍉∧\CT=' ')⌽CT),'M⎕-⎕F10.5' ⎕FMT CM COV
[40]  2 1⍴' '
[41]  'SUM OF SQUARES OF RESIDUALS: ',⍕S←(OBS-COMP)+.*2
[42]  'SIGMA (STANDARD ERROR):        ',⍕S←(S÷¯1+⍴OBS)*.5
[43]  'NORMALIZED STANDARD ERROR:   ',⍕S←S÷-/SOL[7 8]
[44]  'PHOTOMETRIC (SIGNAL+NOISE)/NOISE RATIO:  ',⍕(1+S)÷S
[45]  '(INTENSITY CHANGE)/BACKGROUND:     ',⍕S←(-/SOL[7 8])÷
     SOL[8]
[46]  'CHANGE IN MAGNITUDE:                   ',⍕-(÷100*÷5)⍟1+S
[47]  RESTAB
     ∇

    ∇ RESTAB;Q;N
 [1]   ⍝PRODUCES A TABLE OF OBS, COMP, AND RESIDUALS
 [2]  4 1⍴' '
 [3]  (29↑' '),'TABLE 5-XXX'
 [4]  '  ',NAME,': OBSERVATIONS, COMPUTED VALUES, AND RESID
     UALS  FROM BIN ',⍕BIN
 [5]  ' '
 [6]  72⍴'='
 [7]  'NUM OBS  COMP   RESID    NUM OBS  COMP   RESID    NU
     M OBS  COMP   RESID'
 [8]  '--- ---- ------ ------   --- ---- ------ ------   --
     - ---- ------ ------'
 [9]  Q←((3×N←⌈(⍴OBS)÷3),4)↑(¯1+⍳⍴OBS),OBS,COMP,[1.5]OBS-CO
     MP
[10]  Q←Q[⍳N;],((N,0)↓(-N,0)↓Q),(2×N,0)↓Q
[11]  '3(BI3,X1,BI4,X1,BF6.1,X1,M⎕-⎕BF6.1,X3)' ⎕FMT Q
[12]  72⍴'='
     ∇

    ∇ START
 [1]  ⍝OVERALL CONTROL FUNCTION FOR DC EXECUTION
 [2]  'REDUCTION RUN FOR THE STAR: ',NAME
 [3]  DC PV
 [4]  DC PV←(¯3↓3↓,SOLS[SOLH←SOLS[;2]⍳1;]),10,PV[13],.5
 [5]  DC(¯3↓3↓,SOLS[SOLF←SOLS[;2]⍳1;]),0,PV[13],.5
 [6]  OUTPUT
     ∇

    ∇ START2
 [1]  ⍝OVERALL CONTROL FUNCTION FOR DC2 EXECUTION
 [2]  'REDUCTION RUN FOR THE STAR ',NAME
 [3]  PV2 DC2 PV
     ∇

    ∇ Y←R WIDE P;I;T
 [1]  ⍝COMPUTATION OF WIDEBAND FRESNEL PATTERN
 [2]  ⍝P IS THE CURRENT PARAMETER VECTOR (PV)
 [3]  ⍝R=CONVOLVED SYSTEM RESPONCE AND SOURCE SPECTRAL ENER
     GY CURVES
 [4]  I←1↑Y←P[3]⍴0
 [5]  ⍝S←+/2×P[11]LDARKEN GRID P[5]
```

```
[6]  W0:Y←Y+R[I]×(NPOL FNOS P←(⍎FILT)[I←I+1;1],1↓P)+.×(⌽T)
     ,T←S
[7]  →(I≠1↑ρ⍎FILT)/W0
     ∇
```

NAME: VFILTER
SHAPE: 53 2

4450	0.0001294
4500	0.0002588
4550	0.0003881
4600	0.0005175
4650	0.0006469
4700	0.0007763
4750	0.0011644
4800	0.0016820
4850	0.0023289
4900	0.0047872
4950	0.0112563
5000	0.0208306
5050	0.0296287
5100	0.0380386
5150	0.0450252
5200	0.0513650
5250	0.0548583
5300	0.0555052
5350	0.0553759
5400	0.0545996
5450	0.0534351
5500	0.0507181
5550	0.0481304
5600	0.0452840
5650	0.0426963
5700	0.0398499
5750	0.0364860
5800	0.0337689
5850	0.0307931
5900	0.0282055
5950	0.0252297
6000	0.0225126
6050	0.0194074
6100	0.0166904
6150	0.0142321
6200	0.0122914
6250	0.0104800
6300	0.0087980
6350	0.0071161
6400	0.0054341
6450	0.0041403
6500	0.0029758
6550	0.0024583
6600	0.0020701
6650	0.0016820
6700	0.0014232
6750	0.0012938
6800	0.0010351
6850	0.0007763
6900	0.0006469
6950	0.0003881
7000	0.0002588
7050	0.0001294

NAME: BFILTER
SHAPE: 42 2

3600	0.0000953
3650	0.0004767
3700	0.0013347
3750	0.0023834
3800	0.0044809
3850	0.0115359
3900	0.0207837
3950	0.0397559
4000	0.0469063
4050	0.0489084
4100	0.0499571
4150	0.0505291
4200	0.0511965
4250	0.0513872
4300	0.0514825
4350	0.0510058
4400	0.0497664
4450	0.0473830
4500	0.0451902
4550	0.0427114
4600	0.0400419
4650	0.0376585
4700	0.0347984
4750	0.0331776
4800	0.0295548
4850	0.0271713
4900	0.0244065
4950	0.0219277
5000	0.0192583
5050	0.0164935
5100	0.0137287
5150	0.0111545
5200	0.0085804
5250	0.0058156
5300	0.0034322
5350	0.0020974
5400	0.0015254
5450	0.0008580
5500	0.0004767
5550	0.0002860
5600	0.0001907
5650	0.0000953

NAME: NARROWV
SHAPE: 5 2

5295	0.0621118
5345	0.2251553
5395	0.4487578
5445	0.2251553
5495	0.0388199

NAME: NARROWB
SHAPE: 5 2

4600	0.0658106
4650	0.2247191
4700	0.4558587
4750	0.2247191
4800	0.0288925

APPENDIX E
LISTING OF THE APL WORKSPACE OCCPLOTS

```
    ∇ Y←N BIN D;⎕IO;T
 [1]  ⍝BIN DATA FOR INTO CLASSES FOR HISTOGRAM
 [2]  ⍝D IS DATA VECTOR; N IS NUMBER OF CLASSES
 [3]  ⎕IO←1
 [4]  Y←(T+D[1]-.5×1↑T),[1.5]+/(¯1+⍳N)∘.=+⌿((1↑D)+T←+\Nρ((⌈
     /D)-⌊/D)÷N)∘.<D←D[⍋D]
     ∇

    ∇ D CENTER S;R
 [1]  ⍝CENTER TEXT LABEL
 [2]  R←S[0]+.5×S[1]-(ρD)×8÷53
 [3]  ((1,ρD)ρD)LABELD 1 3ρR,¯2↑S
     ∇

    ∇ Y←N ESMOOTH D;⎕IO;T;V
 [1]  ⍝N-POINT WEIGHTED SMOOTHING OF THE VECTOR D
 [2]  ⍝(1↓N) IS NUMBER OF TERMS TO USE NUMERICALLY IN E SMO
     OTHING
 [3]  ⍝(1↑N) IS THE 1/E FOLDING SPACING WRT THE DATA SPACIN
     G
 [4]  ⎕IO←0
 [5]  Y←((V←⌊.5+.5×1↑N)ρ1↑Y),Y←(T÷+/T←*-(÷1↑N)×⍳1↓N)+.×(⍳1↓
     N)⌽(1↓N,ρD)ρD
 [6]  Y←(¯3×V)↓Y
 [7]  Y←(ρD)ρY,(2×V)ρ(+/(-1↓N)↑D)÷1↓N
     ∇

    ∇ Z←FFT X;T;I;G;N;Q;⎕IO
 [1]  ⍝FAST FOURIER TRANSFORM OF X; FROM RGS
 [2]  ⍝X VECTOR OF REALS OR X[;0]=REAL X[;1]=IMAGINARY
 [3]  ⎕IO←0
 [4]  →(2=ρρX)/L0
 [5]  X←X,[.5]0
 [6]  L0:T←2⊥⊖(Gρ2)⊤⍳I←2*G←⌈2⍟1↑ρX
 [7]  X←((N←I÷2),2 2)ρ((I,2)↑X÷I*.5)[T;]
 [8]  T←⍉2 1∘.○○(N↑T)÷2×N
 [9]  Z←(+/[1]X),[.5]-/[I←1]X
[10]  LA:Z←((N←N÷2),(2×I←I×2),2)ρZ
[11]  X←(0,I,0)↓Z
```

```
[12]  Z←(0,-I,0)↓Z
[13]  Z←(Z+Q),Z-Q←(+/Q×X),[1.5]-/(Q←(N,I,2)ρ(I,2)↑T)×⌽X
[14]  →(1<N)/LA
[15]  Z←((2×I,1)ρZ)[2⊥⊖(Gρ2)⊤⍳2*G;]
    ∇

    ∇ Z←FFTI X;T;I;G;N;Q;⎕IO
[1]   ⍝FAST INVERSE FOURIER TRANSFORM OF X; FROM RGS
[2]   ⍝X IS VECTOR OF REALS, OR X[;0]=REAL X[;1]=IMAGINARY
[3]   ⎕IO←0
[4]   →(2=ρρX)/L0
[5]   X←X,[0.5] 0
[6]   L0:T←2⊥⊖(Gρ2)⊤⍳I←2*G←⌈2⍟1↑ρX
[7]   X←((N←I÷2),2 2)ρ((I,2)↑X÷I*.5)[T;]
[8]   T←⍉2 1∘.○(N↑T)÷¯2×N
[9]   Z←(+/[1]X),[.5]-/[I←1]X
[10]  LA:Z←((N←N÷2),(2×I←I×2),2)ρZ
[11]  X←(0,I,0)↓Z
[12]  Z←(0,-I,0)↓Z
[13]  Z←(Z+Q),Z-Q←(+/Q×X),[1.5]-/(Q←(N,I,2)ρ(I,2)↑T)×⌽X
[14]  →(1<N)/LA
[15]  Z←((2×I,1)ρZ)[2⊥⊖(Gρ2)⊤⍳2*G;]
    ∇

    ∇ FITPLOT X;⎕IO;ZRO;SPA;XPOS;STV;NUMN;N
[1]   ⍝PLOT OF THE FITTED OCCULTATION CURVE
[2]   ⍝X=STARTING BIN NUMBER; OBS, COMP, SOL MUST BE GLOBAL
[3]   ⎕IO←0
[4]   X←X,(X+SOL[2]),(X+SOL[8]),SOL[9],SOL[5]×206264810
[5]   START
[6]   PLOTSET ¯.3 0
[7]   AXISD 2 1.75 7 0 .35 .15
[8]   AXISD 2 1.75 7 0 1.4 ¯.05
[9]   AXISD 2 1.75 4.75 90 .475 ¯.15
[10]  AXISD 2,(1.75+4.75÷20),4.275 90,(4.75÷10),¯.08
[11]  AXISD 9 1.75 4.75 90 .475 .15
[12]  AXISD 9,(1.75+4.75÷20),4.275 90 .475 .08
[13]  ZRO←2+(-/X[2 0])×7÷-/X[1 0]
[14]  SPA←10×÷X[3]×(-/X[1 0])÷7
[15]  AXISD ZRO,6.5,(ZRO-2),180,SPA,.15
[16]  AXISD ZRO,6.5,(9-ZRO),0,SPA,¯.15
[17]  ('ZF3.1' ⎕FMT .1×⍳11)LABELD 1.55,(1.75+.475×⍳11),[.5]
     0
[18]  ('LI4' ⎕FMT(⌊/OBS)+((⌈/OBS)-⌊/OBS)×.1×⍳11)LABELD 9.05
     ,(1.75+.475×⍳11),[.5]0
[19]  ('LI4' ⎕FMT X[0]+(⍳5)×.2×¯1+-/X[1 0])LABELD(2+1.4×⍳5)
     ,1.55,[.5]5ρ0
[20]  XPOS←ZRO-SPA×⌊(ZRO-2)÷SPA
[21]  STV←¯10×⌊(ZRO-2)÷SPA
[22]  NUMM←(⌊(ZRO-2)÷SPA)+⌊(9-ZRO)÷SPA
[23]  ('M⍞-⍞LI4' ⎕FMT STV+10×⍳NUMM)LABELD((XPOS+NUMM↑+\0,NU
     MMρSPA),[.5]6.55),0
[24]  'TIME IN MILLISECONDS FROM BEGINNING OF DATA WINDOW'
     CENTER 1 9 1.3 0
```

```
[25]  'ANGULAR SEPARATION IN MILLISECONDS OF ARC' CENTER 1
     9 6.75 0
[26]  (1 20⍴'NORMALIZED INTENSITY')LABELD 1 3⍴1.4 2.8 90
[27]  (1 6⍴'COUNTS')LABELD 1 3⍴9.8 4.9 270
[28]  N←0
[29]  L1:AXISD ZRO,(2+.475×N),(.475÷2),270
[30]  →(10≠N←N+1)/L1
[31]  1 SPLINE(2+7×(⍳⍴OBS)÷¯1+⍴OBS),1.75+4.75×(OBS-⌊/OBS)÷⌈
     /OBS-⌊/OBS
[32]  1 SPLINE(2+7×(⍳⍴COMP)÷¯1+⍴COMP),1.75+4.75×(COMP-⌊/OBS
     )÷⌈/OBS-⌊/OBS
[33]  AXISD 8.5,(1.75+4.75×(SOL[6]-⌊/OBS)÷(⌈/OBS)-⌊/OBS),.5
     0
[34]  AXISD 2,(1.75+4.75×(SOL[7]-⌊/OBS)÷(⌈/OBS)-⌊/OBS),.5 0
[35]  AXISD ZRO,6.32,(X[4]×.1×SPA),0
[36]  PLOTEND
     ∇

    ∇ FITPLOT2 X;⎕IO;ZRO;SPA;XPOS;STV;NUMN;N
 [1]  ⍝PLOT OF THE FITTED TWO-STAR OCCULTATION CURVE
 [2]  ⍝X=STARTING BIN NUMBER; OBS, COMP, SOL MUST BE GLOBAL
 [3]  ⎕IO←0
 [4]  X←X,(X+SOL[2]),(SOL[8]+X2←X),SOL[9],SOL[5]×206264810
 [5]  START
 [6]  PLOTSET ¯.3 0
 [7]  AXISD 2 1.75 7 0 .35 .15
 [8]  AXISD 2 1.75 7 0 1.4 ¯.05
 [9]  AXISD 2 1.75 4.75 90 .475 ¯.15
[10]  AXISD 2,(1.75+4.75÷20),4.275 90,(4.75÷10),¯.08
[11]  AXISD 9 1.75 4.75 90 .475 .15
[12]  AXISD 9,(1.75+4.75÷20),4.275 90 .475 .08
[13]  ZRO←2+(-/X[2 0])×7÷-/X[1 0]
[14]  SPA←10×÷X[3]×(-/X[1 0])÷7
[15]  AXISD ZRO,6.5,(ZRO-2),180,SPA,.15
[16]  AXISD ZRO,6.5,(9-ZRO),0,SPA,¯.15
[17]  ('ZF3.1' ⎕FMT .1×⍳11)LABELD 1.55,(1.75+.475×⍳11),[.5]
     0
[18]  ('LI4' ⎕FMT(⌊/OBS)+((⌈/OBS)-⌊/OBS)×.1×⍳11)LABELD 9.05
     ,(1.75+.475×⍳11),[.5]0
[19]  ('LI4' ⎕FMT X[0]+(⍳5)×.2×¯1+-/X[1 0])LABELD(2+1.4×⍳5)
     ,1.55,[.5]5⍴0
[20]  XPOS←ZRO-SPA×⌊(ZRO-2)÷SPA
[21]  STV←¯10×⌊(ZRO-2)÷SPA
[22]  NUMM←(⌊(ZRO-2)÷SPA)+⌊(9-ZRO)÷SPA
[23]  ('M⍞-⍞LI4' ⎕FMT STV+10×⍳NUMM)LABELD((XPOS+NUMM↑+\0,NU
     MM⍴SPA),[.5]6.55),0
[24]  'TIME IN MILLISECONDS FROM BEGINNING OF DATA WINDOW'
     CENTER 1 9 1.3 0
[25]  'ANGULAR SEPARATION IN MILLISECONDS OF ARC' CENTER 1
     9 6.75 0
[26]  (1 20⍴'NORMALIZED INTENSITY')LABELD 1 3⍴1.4 2.8 90
[27]  (1 6⍴'COUNTS')LABELD 1 3⍴9.8 4.9 270
[28]  N←0
[29]  L1:AXISD ZRO,(2+.475×N),(.475÷2),270
```

```
[30]  →(10≠N←N+1)/L1
[31]  1 SPLINE(2+7×(⍳⍴OBS)÷¯1+⍴OBS),1.75+4.75×(OBS-⌊/OBS)÷⌈
     /OBS-⌊/OBS
[32]  1 SPLINE(2+7×(⍳⍴COMP)÷¯1+⍴COMP),1.75+4.75×(COMP-⌊/OBS
     )÷⌈/OBS-⌊/OBS
[33]  AXISD 8.5,(1.75+4.75×((SOL[7]+SOL2[6]+SOL[6])-⌊/OBS)÷
     (⌈/OBS)-⌊/OBS),.5 0
[34]  AXISD 2,(1.75+4.75×(SOL[7]-⌊/OBS)÷(⌈/OBS)-⌊/OBS),.5 0
[35]  AXISD ZRO,6.32,(X[4]×.1×SPA),0
[36]  X←X2,(X2+SOL2[2]),(X2+SOL2[8]),SOL2[9],SOL2[5]×206264
     810
[37]  N←0×1↑ZRO←2+(-/X[2 0])×7÷-/X[1 0]
[38]  SPA←10×÷X[3]×(-/X[1 0])÷7
[39]  L2:AXISD ZRO,(2+.475×N),(.475÷2),270
[40]  →(10≠N←N+1)/L2
[41]  AXISD ZRO,6.32,(X[4]×.1×SPA),0
[42]  PLOTEND
     ∇

    ∇ R←FT Y;M;N;⎕IO
 [1]  ⍝DISCRETE FOURIER TRANSFORMATION OF EVENLY SPACED REA
     L DATA
 [2]  ⎕IO←0
 [3]  M←(⍳2×N)×○÷N←(⍴Y)÷2
 [4]  R←1 2⍴⌽,(+/Y)÷2×N
 [5]  L1:R←R,[0](÷N)×+/(1 1∘.×Y)×2 1∘.○(1↑⍴R)×M
 [6]  →(N>¯1+1↑⍴R)/L1
 [7]  R[N;]←.5 0×,¯1 2↑R
     ∇

    ∇ FTPREP X;⎕IO;T
 [1]  ⍝SETS UP GLOBAL FOR POWER SPECTRA ANALYSIS
 [2]  ⍝X IS CENTER OF TRANSFORM WINDOW FROM DATA SET
 [3]  ⎕IO←0
 [4]  FTOBS←.5×+/(FFT FTDATA←1024↑(¯512+514⌈X⌊3595)↓CH1)*2
 [5]  ⍎(3595≥X+1512)/'FTOUT←¯1012↑(X+1512)↑CH1'
 [6]  ⍎(3595<X+1512)/'FTOUT←¯1012↑(X-510)↑CH1'
 [7]  FTOUT←.5×(FFT FTOUT)+.*2
 [8]  T←¯1↓SOL[6]+(COMP[0]-SOL[6])×T÷⌈/T←T-⌊/T←+\+\⍳1+⌊.5×1
     024-⍴COMP
 [9]  FTMOD←T,COMP
[10]  FTMOD←FTMOD,1↓SOL[7]+(-SOL[7]-¯1↑FTMOD)×⌽T÷⌈/T←T-⌊/T←
     +\+\⍳1+⌊1024-⍴FTMOD
[11]  FTMOD←.5×(FFT FTMOD)+.*2
     ∇

    ∇ IDENT
 [1]  '   ***LUNAR OCCULTATION PLOTTING WORKSPACE***'
 [2]  '       VERSION: B01/HARRIS'
 [3]  '       WSID: DISPLOT'
 [4]  '       LAST REVISION: 10 APRIL 85'
 [5]  ' '
 [6]  '       NOTE: THIS WORKSPACE IS ⎕IO←0'
     ∇
```

```
    ∇ INTPLOT X;⎕IO
 [1]  ⍝INTEGRATION PLOT OF THE DATA VECTOR X
 [2]  ⎕IO←0
 [3]  START
 [4]  AXISD 2 1.75 7 0 .4375 ¯.15
 [5]  AXISD 2 1.75 7 0 .875 ¯.05
 [6]  AXISD 2 1.75 4.75 90 .475 ¯.15
 [7]  AXISD 2,(1.75+4.75÷20),4.275 90,(4.75÷10),¯.08
 [8]  ('ZF3.1' ⎕FMT .1×ι11)LABELD 1.55,(1.75+.475×ι11),[.5]
     0
 [9]  ('LI4' ⎕FMT((ρX)÷8)×ι8)LABELD(2+.875×ι8),1.55,[.5]8ρ0
[10]  'TIME IN MILLISECONDS FROM BEGINNING OF DATA WINDOW'
     CENTER 1 9 1.3 0
[11]  (1 20ρ'NORMALIZED INTENSITY')LABELD 1 3ρ1.25 3.22 90
[12]  X←-(⌊/X)-X←+\X-(+/X)÷ρX←X[2 3],2↓X
[13]  1 SPLINE (2+7×(ιρX)÷¯1+ρX),1.75+4.75×X÷⌈/X
[14]  PLOTEND
     ∇

    ∇ F←X INVFT R;⎕IO
 [1]  ⍝INVERSE FOURIER TRANSFORMATION FROM COEFFICIENT MATR
     IX
 [2]  ⎕IO←0
 [3]  X←2 0 1⍉2 1∘.○X∘.×1↓ι1↑ρR
 [4]  F←,(1 1↑R)++/+/((ρX)ρ1 0↓R)×X
     ∇

    ∇ NOISEPLOT X;OC;PD;R;MEAN;SIGMA;Y;BR;N
 [1]  ⍝NOISE FIGURE FOR LUNAR OCCULTATION
 [2]  ⍝X IS BIN NUMBER OF START OF DATA USED IN SOLUTION
 [3]  ⍝MUST HAVE SOL OBS AND COMP AS GLOBAL VARIABLES
 [4]  OBS∧.=SOL[2]↑(X-1)↓CH1
 [5]  ⍝X[1]=FIRST BIN OF DATA X[2]=LENGTH OF DATA
 [6]  OC←((X-1)↑CH1)-SOL[6]
 [7]  OC←OC,(OBS-COMP),((¯1+SOL[2]+X)↓CH1)-SOL[7]
 [8]  PD←BR←⍉50 BIN OC←2↓OC÷CH1
 [9]  PD[0;]←PD[0;]-PD[0;0]
[10]  PD←PD×⍉(⌽ρPD)ρ7 4.75÷⌈/PD
[11]  X←2+1↓¯1↓,(7×(ι51)÷50)∘.×1 1
[12]  Y←1.75+,PD[1;]∘.×1 1
[13]  START
[14]  PLOTSET ¯.1 0
[15]  AXISD 2 1.75 7 0 .14 ¯.15
[16]  AXISD 2 1.75 7 0 .7 ¯.05
[17]  AXISD 2 1.75 4.75 90 .475 ¯.15
[18]  ('ZI4' ⎕FMT .1×(ι11)×0 1/R←(⌈/BR)-⌊/BR)LABELD 1.38,(1
     .75+.475×ι11),[.5]0
[19]  ('M⍞-⍞LF5.1' ⎕FMT 100×(1↑⌊/BR)+.1×(ι10)×1↑R)LABELD(2+
     .7×ι10),1.55,[.5]10ρ0
[20]  1 SPLINE X,[¯.5]Y
[21]  'NOISE LEVEL AS A PERCENTAGE OF COMPUTED INTENSITY' C
     ENTER 1 9 1.3 0
[22]  (1 20ρ'NUMBER OF OCCURANCES')LABELD 1 3ρ1.2 2.8 90
```

```
[23]  MEAN←(+/2↓OC)÷4094
[24]  SIGMA←((OC*2)+.*.5)÷4093
[25]  N←0
[26]  L1:AXISD(2+7×(MEAN-1↑⌊/BR)÷1↑R),(2+.475×N),.2375 90
[27]  →(10≠N←N+1)/L1
[28]  AXISD T←(2+7×((MEAN-.5×SIGMA)-1↑⌊/BR)÷1↑R),2.35,T,0,(
      T←7×SIGMA÷1↑R),.15
[29]  AXISD T×(5ρ1),¯1
[30]  (1 20ρ20↑,'MEAN ',,'M⍞-⍞F8.5' ⎕FMT MEAN)LABELD 1 3ρ2.
      5 6 0
[31]  (1 20ρ20↑,'SIGMA ',,'F8.6' ⎕FMT SIGMA)LABELD 1 3ρ2.5
      5.5 0
[32]  PLOTEND
      ∇

    ∇ PDPLOT S;X;N;⎕IO
 [1]  ⍝PLOT OF THE NORMALIZED FIRST DERIVATIVES OF INTENSIT
      Y
 [2]  ⍝S IS STARTING BIN NUMBER
 [3]  ⎕IO←0
 [4]  X←.75×X÷(ρX)ρ⌈/X←X-(ρX)ρ⌊/X←PDER,COMP
 [5]  X←X+(ρX)ρ1.82+.78×⍳6
 [6]  X←X,[.5]2+((7÷ρCOMP)×⍳ρCOMP)∘.×6ρ1
 [7]  N←0
 [8]  START
 [9]  L1:1 SPLINE,⍉⌽X[;;N]
[10]  AXISD 2,(1.82+N×.78),.75 90 .75 .1
[11]  AXISD 2,(1.82+N×.78),.75 90 .75 ¯.1
[12]  AXISD 9,(1.82+N×.78),.75 90 .75 .1
[13]  AXISD 9,(1.82+N×.78),.75 90 .75 ¯.1
[14]  AXISD(2+7×SOL[8]÷ρCOMP),(2.56+N×.78),.04 90
[15]  AXISD 2,(2.21+N×.78),7 0
[16]  →(6≠N←N+1)/L1
[17]  AXISD(2+7×SOL[8]÷ρCOMP),1.75 .07 90
[18]  AXISD 2 1.75 7 0 1.4 .05
[19]  AXISD 2 1.75 7 0 1.4 ¯.05
[20]  'TIME IN MILLISECONDS FROM BEGINNING OF DATA WINDOW'
      CENTER 1 9 1.3 0
[21]  (⊖6 4ρ'COMPVELOTIMEPREIPOSTDIAM')LABELD 1.35,(2.02+.7
      8×⍳6),[.5]6ρ0
[22]  (1 18ρ'PARTIAL DERIVATIVES')LABELD 1 3ρ1.2 2.8 90
[23]  ('LI4' ⎕FMT S+(⍳5)×.2×¯1+ρCOMP)LABELD(2+1.4×⍳5),1.55,
      [.5]5ρ0
[24]  PLOTEND
      ∇

    ∇ PDPLOT2 S;X;N;⎕IO
 [1]  ⍝PLOT OF NORMALIZED FIRST DERIVATIVES OF INTENSITY
 [2]  ⍝FOR TWO-STAR (DC2) SOLUTION
 [3]  ⍝S IS STARTING BIN NUMBER
 [4]  ⎕IO←0
 [5]  X←.52×X÷(ρX)ρ⌈/X←X-(ρX)ρ⌊/X←(1 1 0 1 1 1 1 1 1/PDER),
      COMP
 [6]  X←X+(ρX)ρ1.82+.52×⍳9
```

```
 [7]  X←X,[.5]2+((7÷⍴COMP)×⍳⍴COMP)∘.×9⍴1
 [8]  N←0
 [9]  START
[10]  L1:1 SPLINE,⍉⌽X[;;N]
[11]  AXISD 2,(1.82+N×.52),.5 90 .5 .1
[12]  AXISD 2,(1.82+N×.52),.5 90 .5 ¯.1
[13]  AXISD 9,(1.82+N×.52),.5 90 .5 .1
[14]  AXISD 9,(1.82+N×.52),.5 90 .5 ¯.1
[15]  AXISD(2+7×SOL2[8]÷⍴OBS),(2.56+N×.52),.04 90
[16]  AXISD(2+7×SOL[8]÷⍴OBS),(2.56+N×.52),.04 90
[17]  AXISD 2,(2.08+N×.52),7 0
[18]  →(9≠N←N+1)/L1
[19]  AXISD(2+7×SOL[8]÷⍴OBS),1.75 .07 90
[20]  AXISD(2+7×SOL2[8]÷⍴OBS),1.75 .07 90
[21]  AXISD 2 1.75 7 0 1.4 .05
[22]  AXISD 2 1.75 7 0 1.4 ¯.05
[23]  'TIME IN MILLISECONDS FROM BEGINNING OF DATA WINDOW'
     CENTER 1 9 1.3 0
[24]  (⊖9 4⍴'COMPVEL2TIM2INT2DIA2VEL1TIM1INT1DIA1')LABELD 1
     .35,(2.02+.52×⍳9),[.5]9⍴0
[25]  (1 18⍴'PARTIAL DERIVATIVES')LABELD 1 3⍴1.2 2.8 90
[26]  ('LI4' ⎕FMT S←(⍳5)×.2×¯1+⍴COMP)LABELD(2+1.4×⍳5),1.55,
     [.5]5⍴0
[27]  PLOTEND
     ∇

    ∇ POWERPLOT;R;X;I;⎕IO
 [1]  ⍝POWER SPECTRA OF MODEL CURVE, STAR+SKY, AND OCCULTAT
     ION
 [2]  ⍝EXECUTE FTPREP IN BEFORE POWERPLOT
 [3]  ⎕IO←0
 [4]  START
 [5]  PLOTSET ¯.3 0
 [6]  AXISD 2 1 5 90 1 .1
 [7]  AXISD 2 1.5 4 90 1 .05
 [8]  AXISD 4.66 1 5 90 1 .1
 [9]  AXISD 4.66 1.5 4 90 1 .05
[10]  AXISD 7.32 1 5 90 1 .1
[11]  AXISD 7.32 1.5 4 90 1 .05
[12]  X←(500↑1↓FTOBS),(500↑1↓FTOUT),500↑1↓FTMOD
[13]  R←10*0 ¯1+⌈10⍟(⌈/X),⌊/X
[14]  X←(10⍟X)÷10⍟R[0]
[15]  I←1↓¯1↓,(5×÷500)×(⍳501)∘.×1 1
[16]  1 SPLINE(2+2.5×,(500↑X)∘.×1 1),1+⌽I
[17]  1 SPLINE(4.66+2.5×,(500↓1000↑X)∘.×1 1),1+⌽I
[18]  1 SPLINE(7.32+2.5×,(1000↓X)∘.×1 1),1+⌽I
[19]  AXIS 2 1 2.5 0,(2.5÷-/10⍟R),.1
[20]  AXIS 4.66 1 2.5 0,(2.5÷-/10⍟R),.1
[21]  AXIS 7.32 1 2.5 0,(2.5÷-/10⍟R),.1
[22]  AXIS 2 6 2.5 0,(2.5÷-/10⍟R),¯.1
[23]  AXIS 4.66 6 2.5 0,(2.5÷-/10⍟R),¯.1
[24]  AXIS 7.32 6 2.5 0,(2.5÷-/10⍟R),¯.1
[25]  ('LI3' ⎕FMT 100×⍳5)LAXISD 1.8 6 1 270
[26]  (1 18⍴'FREQUENCY IN HERTZ')LABELD 1 3⍴1.5 4.95 271
```

```
[27]  (1 11ρ'OCCULTATION')LAXISD 4.36 3 0 271
[28]  (1 10ρ'STAR + SKY')LAXISD 7.02 3 0 271
[29]  (1 11ρ'MODEL CURVE')LAXISD 9.68 3 0 271
[30]  PLOTEND
     ∇

    ∇ RAWPLOT X;⎕IO;ZRO;SPA;NEG;POS;XPOS;STV;NUMM;N
 [1]  ⍝PLOT OF THE RAW DATA, X (EVERY 4 POINTS)
 [2]  ⎕IO←0
 [3]  START
 [4]  PLOTSET ¯.4 0
 [5]  AXISD 2 1.75 7 0 .4375 .15
 [6]  AXISD 2 1.75 7 0 .875 ¯.05
 [7]  AXISD 2 1.75 4.75 90 .475 ¯.15
 [8]  AXISD 2,(1.75+4.75÷20),4.275 90,(4.75÷10),¯.08
 [9]  AXISD 9 1.75 4.75 90 .475 .15
[10]  AXISD 9,(1.75+4.75÷20),4.275 90 .475 .08
[11]  ('ZF3.1' ⎕FMT .1×⍳11)LABELD 1.55,(1.75+.475×⍳11),[.5]
     0
[12]  ('LI4' ⎕FMT 4096×.1×⍳11)LABELD 9.05,(1.75+.475×⍳11),[
     .5]0
[13]  ('LI4' ⎕FMT 512×⍳8)LABELD(2+.875×⍳8),1.55,[.5]8ρ0
[14]  'TIME IN MILLISECONDS FROM BEGINNING OF DATA WINDOW'
     CENTER 1 9 1.3 0
[15]  (1 20ρ'NORMALIZED INTENSITY')LABELD 1 3ρ1.4 2.8 90
[16]  (1 6ρ'COUNTS')LABELD 1 3ρ9.8 4.9 270
[17]  1 SPLINE(8192ρ0 0 1 0)/(2+7×(⍳4096)÷4095),1.75+4.75×X
     ÷4095
[18]  PLOTEND
     ∇

    ∇ Y←N SMOOTH D;⎕IO
 [1]  ⍝N-POINT UNWEIGHTED SMOOTHING OF THE VECTOR D
 [2]  ⎕IO←0
 [3]  Y←(ρD)ρ((⌊.5×N)↑D),((-N)↓(+⌿(⍳N)⌽(N,ρD)ρD)÷N),(-⌈.5×N
     )↑D
     ∇
```

LIST OF REFERENCES

Abt, H. A., and Kallarakal, V. V., 1963. Astrophys. J., 138, 140.

Allen, C. W., 1963, Astrophysical Quantities (London: Athlone Press), p. 170.

Analogics Incorporated, 1984, The APL Machine (Danvers, MA: Author).

Astronomical Time Mechanisms, 1980, Model 240 fast photometer amplifier operating instructions (Gainesville, FL: Author).

Barnes, T. G., and Evans, D. S., 1976, Mon. Not. Roy. Astron. Soc., 174, 489.

Bender, David F., 1979, in Asteroids, ed. T. Gehrels (Tucson: University of Arizona Press), p. 1014.

Bevington, P. R., 1969, Data Reduction and Analysis for the Physical Sciences (New York: McGraw-Hill Book Company), p. 127.

Blow, Graham L., 1983, in Solar System Photometry Handbook, ed. R. M. Genet (Richmond: Willmann-Bell, Inc.). p. 9-14.

Bowker, D. E., and Hughes, J. K., 1971, Lunar Orbiter Photographic Atlas of the Moon, NASA SP-206 (Washington: NASA).

Bracewell, R., 1965, The Fourier Transform and Its Applications (New York: McGraw-Hill Book Company), p. 296.

Brenner, Norman, 1982, APL Quote Quad, 13-1, 57.

Brown, D. C., 1955, Ballistic Research Laboratories Report, 937 (Aberdeen Proving Ground, MD: Ballistic Research Laboratories).

Brown, R. H., 1968, in Annual Reviews of Astronomy and Astrophysics, 6, 13.

Brown, R. H., 1980, in Optical Telescopes of the Future. ESO Conference, eds. E. Pacini, W. Ricter and R. N. Wilson (Geneva: ESO), p. 391.

Campbell, W. W., and Moore, J. H., 1907, Astrophys. J., 25, 54.

Caton, D. B., 1981, Ph.D. Dissertation, University of Florida.

Chen, K-Y, 1985, private communication.

Chen, K-Y, and Rekenthaler, D. A., 1966, Quarterly Journal of the Florida Academy of Sciences, 29, 1.

Department of the Army, 1953, Antennas and Radio Propagation, TM 11-666 (Washington, DC: U. S. Government Printing Office), 17.

Dunham, E. W., Baron, R. L., Conner, S., Dunham, D. W., Dunham, J. B., Schneider, G., Cohen, H. L., Helms III, V. T., Croom, M., and Safko, J., 1984, A. J., 89, 1755.

Dunham, D. W., Evans, D. S., McGraw, J. T., Sandmann, W. H., and Wells, D. C., 1973, A. J., 78, 482.

Eddington, A. E., 1909, Mon. Not. Roy. Astron. Soc., 69, 178.

Eggen, O. J., 1965, Astrophys. J., 70, 19.

Eichhorn, H., 1977, Mon. Not. Roy. Astron. Soc., 182, 355.

Eichhorn, H., and Clary, W. G., 1974, Mon. Not. Roy. Astron. Soc., 166, 425.

Evans, D. S., 1951, Mon. Not. Roy. Astron. Soc., 111, 64.

------------, 1959, Mon. Not. Roy. Astron. Soc. S. Africa, 18, 158.

------------, 1968, Q. J. Roy. Astr. Soc., 9, 388.

------------, 1970, A. J., 75, 589.

------------, 1971, A. J., 76, 1107.

Evans, D. S., Africano, J. L., Fekel, F. C., Montemayor, T., Palm, C., Silverberg, E., Citters, W. V., Wiant, J., 1977, A. J., 82, 495.

Falkoff, A. D., and Iverson, K. E., 1968, Symposium on Interactve Systems for Experimental Applied Mathematics, eds. M. Klerer and J. Reinfelds (New York: Academic Press).

Falkoff, A. D., and Iverson, K. E., 1970, APL/360 User's Guide (GH20-0683-1) (Poughkeepsie, NY: IBM).

Falkoff, A. D., and Orth, D. L., 1979, APL Quote Quad, 9-4, 409.

Finsen, W. S., and Worley, C. E., 1970, Republic Observatory Johannesburg, Circulars, 7-129, 203.

Flesch, T., 1975, Ph.D. Dissertation, University of Florida.

Giacconi, R., 1982, in The Space Telescope Observatory, ed. D. N. B. Hall, NASA CP-2244 (Washington: NASA), p. 1.

Gillman, L., and Rose, A. J., 1974, APL: An Interactive Approach, Second Edition, Revised Printing (New York: John Wiley and Sons, Inc.).

Griffin, R. F., 1980, Sky and Telescope, 58, 19.

Griffin, R. F., and Radford, G. A., 1976, Observatory, 96, 188.

Henden, A. A., and Kaitchuck, R. H., 1982, Astronomical Photometry (New York: Van Nostrand Reinhold Company), p. 371.

Iverson, K. E., 1962, A Programming Language (New York: John Wiley and Sons, Inc.).

Kamas, G., 1977, Time and Frequency User's Manual-NBS Technical Note, 695, 118.

Keenan, P. C., and McNeil, R. C., 1976, An Atlas of Spectra of the Cooler Stars: Types G, K, M, S and C (Columbus: Ohio State University Press), Plates 19, 21 and 23.

Kuiper, G. P., 1948, Astrophys. J., 108, 542.

Lohmann, A. W., and Weigelt, G. P., 1980, in Optical Telescopes of the Future. ESO Conference, eds. E. Pacini, W. Richter and R. N. Wilson (Geneva: ESO), p. 489.

Lukac, M., 1983, U. S. N. O. Lunar Occultation Predictions for 1983, private communication.

---------, 1984, U. S. N. O. Lunar Occultation Predictions for 1984, private communication.

MacMahon, P. A., 1909, Mon. Not. Astron. Soc. S. Africa, 69, 126.

Meyer, S. L., 1975, Data Analysis for Scientists and Engineers, (New York: John Wiley and Sons, Inc.), p. 399.

Micro Technology Unlimited, 1979, K-1016 16K Byte Memory 6502 System Low Power Memory (Raleigh: Author).

-------------------------, 1980a, K-1013 Double Density Disk Controler for KIM/MTU Bus Systems (Raleigh: Author).

-------------------------, 1980b, K-1008 Visible Memory (Raleigh: Author).

-------------------------, 1980c, K-1020 Prototyping Board (Raleigh: Author).

-------------------------, 1980d, K-1005 Card File and 5-Slot Motherboard for Expansion of 6502 Based Microcomputers Using the KIM/MTU Bus (Raleigh: Author).

-------------------------, 1981, Channel-Oriented Disk Operating System Release 1.2 User Manual (Raleigh: Author).

Mihalas, D., and Binney, J., 1981, Galactic Astronomy Structure and Kinematics (San Francisco: W. H. Freeman and Company), p. 107.

Morbey, C. L., 1972, Pub. Dom. Ap. Obs., 14, 45.

Muller, P., 1961, I.A.U. Commission des Etoiles Doubles Circulaire d'Information, 24.

Murdin, P., 1971, Astrophys. J., 169, 615.

Nather, R. E., and Evans, D. S., 1970, A. J., 75, 575.

Nather, R. E. and McCants, M. M., 1970, A. J., 84, 872.

NERDC, 1980, MINIS & MICROS, (Gainesville, FL: University of Florida), p. 18.

Oliver, J. P., 1976, Rev. Sci. Instrum., 47, 581.

Pakin, S., and Polvka, R. P., 1975, APL: The Language and Its Usage, (Englewood Cliffs, NJ: Prentice-Hall).

Parise, R., 1978, Master's Thesis, University of Florida.

Pollock, J. T., 1981, private communication.

Rigdway, S. T., 1977, A. J., 82, 511.

Robertson, J. R., 1940, Astronomical Papers Prepared for the Use of the American Ephemeris And Nautical Almanac: Catalog of 3539 Zodiacal Stars for the Equinox of 1950.0, 10-2 (Washington: USNO).

Rockwell International, 1978, AIM-65 Microcomputer User's Guide (Anaheim, CA: Author), p. 7-45.

Schlesinger, F., and Jenkins, L. F., 1940, Yale University Observatory Catalog of Bright Stars, (New Haven, CT: The New Haven Printing Company), p. 66.

Schmidtke, Paul C., and Africano, John L., 1984, A. J., 89, 663.

Schneider, G., 1981, APL Quote Quad, 11-4, 23.

Schneider, G., and Brown, R. G., 1976, Warner Computer Systems APL Technical Notes, 47, 28.

Selfridge, Ralph G., 1983, CIMAR Plotting, private communication.

------------------, 1984, private communication.

Smillie, K. W., 1976, in APL76 Conference Proceedings, ed. G. T. Hunter (Ottawa, Canada: Association for Computing Machinery), p. 401.

Tassoul, J. L., 1978, Theory of Rotating Stars, ed. J. P. Ostriker (Princeton, NJ: Princeton University Press), p. 28.

Taylor, Jr., J. H., 1966, Nature, 210, 1105.

True Time Instruments, 1974, Operating and Service Manual WWVB Time Code Receiver (Santa Rosa, CA: Author), p. 45.

Van Flandern, T. C., 1973, USNO Occultation Predictions Format, (Washington: USNO) p. 3.

------------------, 1974, Bull. A. Astron. Soc., 6, 206.

------------------, 1975, Occultation Newsletter, 1, 28.

Wasserman, L. H., Millis, R. L., and Williamson, R. M., 1977, A. J., 82, 506.

White, M. W., and Slettebak, A., 1980, A. J., 85, 257.

White, N. M., and Kreidl, T. J., 1984, A. J., 89, 424.

Whitford, A. E., 1939, Astrophys. J., 89, 472.

Williams, J. D., 1939, Astrophys. J., 89, 467.

Wilson, R. E., 1976, Astron. and Astrophys., 48, 349.

Worley, C. E., 1984, Washington Double Star Catalog (USNO), private communication.

Young, R. K., 1919, Pub. Dom. Ap. Obs., 1 ,119.

BIOGRAPHICAL SKETCH

Glenn H Schneider (no "." after the H, please note) was born to Elaine and Ira G. Schneider on October 12, 1955, an otherwise un-noteworthy day, except perhaps for the fact that it marked the 463rd anniversary of the discovery of America, as commonly reckoned. At the tender age of three he received his first telescope (Sears, 40X!), and learned early in life the meaning of light pollution.

He attended public school 97 and J.H.S. 135 (also known as the Frank D. Whalen Junior High School, though no one ever knew who Frank D. Whalen was) in New York City. Thanks to the closing of the school during the summer of 1969 he was permitted to retain possession of the school library's copies of The Larousse Encyclopedia of Astronomy and Norton's Star Atlas. Later that year he became a member of the Amateur Observers' Society of New York. These two events forever influenced his life and started him on the path to a career in astronomy.

He graduated from The Bronx High School of Science in June of 1972. Shortly thereafter, he organized an international solar eclipse expedition, in hopes of observing his second total solar eclipse. The clouds which hung ominously over the Gaspé Peninsula that day served to reinforce his devotion to shadow chasing.

In June of 1976, he earned a Bachelor of Science degree in physics from the New York Institute of Technology. Before entering the graduate program in astronomy at the University of Florida in September of 1977, he worked as an APL technical analyst for Warner Computer Systems, Inc.

After eight years, two trips to the South Pole, seemingly endless commuting between Gainesville, Paris, Noordwijc and Bristol, statistically improbable stretches of cloudy weather during scheduled observing runs, and being thwarted at every turn by wayward computers (micro and macro), he expects, finally, to receive the degree of Doctor of Philosophy in August of 1985. He has accepted a position at the Space Telescope Science Institute, working for the Computer Sciences Corporation as a Science and Mission Operations Astronomer.

He has observed every total solar eclipse since March, 1970, and intends to keep chasing the moon's shadow well into the future. He has a definite preference for Dr. Brown's Celery Tonic (now called Cel-Ray Soda, alas), and egg creams made with Fox's U-Bet chocolate syrup and Good-Health seltzer.

At the moment he is single, but this malady is expected to be cured on June 7, 1985.

I certify that I have read this study and that in my opinion it conforms to acceptable standards of scholarly presentation and is fully adequate, in scope and quality, as a dissertation for the degree of Doctor of Philosophy.

John P. Oliver, Chairman
Associate Professor of Astronomy

I certify that I have read this study and that in my opinion it conforms to acceptable standards of scholarly presentation and is fully adequate, in scope and quality, as a dissertation for the degree of Doctor of Philosophy.

Heinrich Eichhorn
Professor of Astronomy

I certify that I have read this study and that in my opinion it conforms to acceptable standards of scholarly presentation and is fully adequate, in scope and quality, as a dissertation for the degree of Doctor of Philosophy.

Howard L. Cohen
Associate Professor of Astronomy

I certify that I have read this study and that in my opinion it conforms to acceptable standards of scholarly presentation and is fully adequate, in scope and quality, as a dissertation for the degree of Doctor of Philosophy.

Heywood C. Smith
Associate Professor of Astronomy

I certify that I have read this study and that in my opinion it conforms to acceptable standards of scholarly presentation and is fully adequate, in scope and quality, as a dissertation for the degree of Doctor of Philosophy.

Ralph G. Selfridge
Professor of Computer and
Information Sciences

This dissertation was submitted to the Graduate Faculty of the Department of Astronomy in the College of Liberal Arts and Sciences and to the Graduate School and was accepted as partial fulfillment of the requirements for the degree of Doctor of Philosophy.

August 1985

Dean, Graduate School